



**Center for Doctoral Studies
Sciences and Techniques and Medical Sciences**

NATIONAL SCHOOL OF APPLIED SCIENCES OF TANGIER

Doctoral program: Sciences and Engineering Techniques

DOCTORAL THESIS

**Presented by
Mr. Yassir BOULAAMANE**

Discipline: Biology, Pharmacology

Specialty: Cheminformatics, Biochemistry, Microbiology

Title

**Data-driven discovery of bioactive natural products:
Application to neurodegenerative and infectious diseases**

Defense scheduled for **20/07/2024** in front of the jury composed of:

Name	Grade	Institution	Title
Prof. Rachid BELFKIH	PES	FMPT, UAE, Tetouan, Morocco	President
Prof. Abdelkader Jalil EL HANGOUCHÉ	PES	FMPT, UAE, Tetouan, Morocco	Reviewer
Prof. Samir CHTITA	MCH/PH	FSBM, UH2, Casablanca, Morocco	Reviewer
Prof. Jaouad EL HARTI	PES	FMPR, UM5, Rabat, Morocco	Reviewer
Prof. Naima GHAILANI NOUROUTI	PES	FSTT, UAE, Tetouan, Morocco	Examiners
Prof. Mohamed CHABBI	PES	FSTT, UAE, Tetouan, Morocco	Examiners
Prof. Younes SMANI	PES	CABD, UPO, Seville, Spain	Guest
Prof. Amal MAURADY	PH	FSTT, UAE, Tetouan, Morocco	Doctoral Supervisor

Host research structure: Laboratory of Innovative Technologies, National School of Applied Sciences of Tangier, Abdelmalek Essaadi University, Tetouan, Morocco

ABSTRACT

Neurodegenerative disorders and infectious diseases are major public health challenges, requiring innovative approaches to discover new therapies. Natural products, rich in structural diversity and beneficial biological activities such as antioxidant, anti-inflammatory, and antibacterial properties, have been exploited in the treatment of various conditions. However, despite their potential, the vast chemical space of natural products remains unexplored. This thesis proposes a data-driven methodology, combining machine learning and molecular modelling, to identify and prioritize promising compounds for neurodegenerative and infectious diseases. In the case of neurodegenerative diseases, we explored multi-target ligands that modulate proteins involved in the pathophysiological mechanisms of Parkinson's disease, such as monoamine oxidase B, acetylcholinesterase, adenosine A_{2A} receptors, glutamate receptors, and α-synuclein. Through quantitative structure-activity relationship (QSAR) models, pharmacophore modelling, and molecular docking, we identified potential antioxidant activity in natural derivatives of coumarins, diarylheptanoids, and dihydrochalcones. Additionally, a cinnamic acid derivative shows promise in modulating α-synuclein aggregation by stabilizing its monomers. Regarding infectious diseases caused by *Acinetobacter baumannii*, an integrated virtual screening strategy combining QSAR modelling and molecular docking on the outer membrane protein, OmpW, identified Demethoxycurcumin, a natural curcuminoid product. Molecular dynamics simulations elucidated the binding stability and interaction profiles of the identified compounds with their respective targets, while pharmacokinetic/toxicity predictions confirmed their favorable drug-likeness. Experimental validation studies demonstrated that Demethoxycurcumin exhibited potent antibacterial activity against colistin-resistant strains of *A. baumannii*. The discovery of these promising new biomolecules demonstrates the potential of data-driven approaches to accelerate the discovery of bioactive natural products, offering a versatile framework to explore various pathological contexts and develop innovative therapies.

Keywords: Natural products, Parkinson's disease, oxidative stress, monoamine oxidase B, acetylcholinesterase, adenosine A_{2A} receptors, glutamate receptors, α-synuclein, *Acinetobacter baumannii*, outer membrane protein W, quantitative structure-activity relationships, molecular dynamics simulations, pharmacokinetics, toxicity, prediction, antibacterial activity.

RÉSUMÉ

Les troubles neurodégénératifs et les maladies infectieuses sont des défis majeurs en santé publique, nécessitant des approches innovantes pour découvrir de nouvelles thérapies. Les produits naturels, riches en diversité structurelle et en activités biologiques bénéfiques telles que les propriétés antioxydantes, anti-inflammatoires et antibactériennes, ont été exploités dans le traitement de diverses affections. Cependant, malgré leur potentiel, l'intégralité de l'espace chimique des produits naturels reste inexplorée. Cette thèse propose une méthodologie basée sur les données, combinant l'apprentissage automatique et la modélisation moléculaire, pour identifier et prioriser les composés prometteurs pour les maladies neurodégénératives et infectieuses. Dans le cas des maladies neurodégénératives, nous avons exploré les ligands multi-cibles qui modulent les protéines impliquées dans les mécanismes physiopathologiques de la maladie de Parkinson, telles que les monoamines oxydases, l'acétylcholinestérase, les récepteurs A_{2A} de l'adénosine et l' α -synucléine. Grâce à des modèles de relation quantitative structure-activité (QSAR), à la modélisation de pharmacophores et à l'amarrage moléculaire, nous avons identifié une activité potentielle contre le stress oxydatif dans les dérivés naturels de la coumarine, les diarylheptanoïdes et les dihydrochalcones. En outre, un dérivé de l'acide cinnamique s'avère prometteur pour moduler l'agrégation de l' α -synucléine en stabilisant ses monomères. Concernant les maladies infectieuses causées par *Acinetobacter baumannii*, une stratégie de criblage virtuel intégrée combinant la modélisation QSAR et l'amarrage moléculaire sur la protéine de la membrane externe, OmpW, a permis d'identifier la déméthoxycurcumine, un produit naturel curcuminoïde. Des études de validation expérimentale ont montré que la déméthoxycurcumine présentait une activité antibactérienne puissante contre les souches d'*Acinetobacter baumannii* résistantes aux antibiotiques. La découverte de ces nouvelles biomolécules prometteuses démontre le potentiel des approches basées sur les données pour accélérer la découverte de produits naturels bioactifs, offrant un cadre polyvalent pour explorer divers contextes pathologiques et développer des thérapies innovantes.

Mots-clés : Produits naturels, maladie de Parkinson, stress oxydatif, monoamine oxydase B, acétylcholinestérase, récepteurs d'adénosine A_{2A}, récepteurs de glutamate, α -synucléine, *Acinetobacter baumannii*, protéine de membrane externe W, relations quantitatives de structure-activité, simulations de dynamique moléculaire, pharmacocinétique, toxicité, prédition, activité antibactérienne.

نبذة مختصرة

تعتبر اضطرابات الأمراض العصبية والأمراض المعدية مصدر قلق صحي عالمي ملح، مما يتطلب استراتيجيات مبتكرة للعلاجات الجديدة. لطالما كانت المنتجات الطبيعية، بتنوعها الهيكلي و سلالاتها الفريدة، مصدراً قيماً لاكتشاف الأدوية. ومع ذلك، لا يزال الفضاء الكيميائي الهائل للمنتوجات الطبيعية غير مستغل إلى حد كبير. تقدم هذه الأطروحة إطاراً قائماً على البيانات يستخدم أساليب التعلم الآلي والنماذج الجزيئية لاستكشاف وترتيب مرشحات المنتوجات الطبيعية الراغبة للأمراض العصبية والأمراض المعدية. من خلال استكشاف قواعد بيانات المنتوجات الطبيعية على نطاق واسع بشكل منهجي، يحدد هذا الإطار المركبات ذات الأنشطة البيولوجية المرغوبة. بالنسبة لاضطرابات الأمراض العصبية ، يركز الاهتمام على روابط متعددة الأهداف التي تنظم البروتينات ذات الصلة بمرض الشلل الرعاشي « Parkinosn's disease » مثل إنزيمات monoamine oxidase B ، إنزيم acetylcholinesterase ، مستقبلات الأبيوسين A_{2A} ، مستقبلات α -synuclein . باستخدام نماذج العلاقة الكمية بين التركيب والنشاط، ونمذجة السمات الدوائية، والربط الجزيئي، لقد حددنا النشاط المحتمل ضد الإجهاد التأكسدي في مشقات الكومارين، ثانيات أريلهبتانويد، وثنائيات هيدروكالكونات. بالإضافة إلى ذلك، تظهر مشقة حمض السيناميك وعداً في كبح تراكم α -synuclein عن طريق استقرار مفرادتها. في سياق الأمراض المعدية، حددت استراتيجية فرز اقتراضية متكاملة تجمع بين نمذجة العلاقة الكمية بين التركيب والنشاط، والربط القائم على التركيب ضد الهدف البكتيري OmpW ، وهو بروتين الغشاء الخارجي، المركب ديميثوكسي كوركيومين، وهو منتج طبيعي من الكوركومين، كمرشح واعد. وضحت محاكاة الديناميكا الجزيئية استقرار الربط وملفات تفاعل المركبات المحددة مع أهدافها، بينما أكدت التنبؤات الحركية الدوائية/السمية على خصائصها المرغوبة الشبيهة بالدواء. أظهر ديميثوكسي كوركيومين نشاطاً قوياً مضاداً للبكتيريا ضد سلالات *Acinetobacter baumannii* المقاومة لمضادات ميكروبات متعددة في دراسات التحقق التجريبية. ظهر هذه الأطروحة قوة النهج القائمة على البيانات في تسريع اكتشاف المنتوجات الطبيعية النشطة بيولوجياً، وتقدم إطاراً متعدد الاستخدامات لاستكشاف سياقات الأمراض المختلفة وتطوير علاجات مبتكرة.

الكلمات المفتاحية: α -synuclein، *Acinetobacter baumannii*، محاكاة الديناميكيات الجزيئية، المنتوجات الطبيعية، بروتين الغشاء الخارجي W، الإجهاد التأكسدي، مرض باركنسون، العلاقات الكمية بين البنية والنشاط، الفحص الاقتراضي، نشاط مضاد للجراثيم.

ACKNOWLEDGMENTS

First and foremost, I would like to express my sincere gratitude to my supervisor, Prof. Amal MAURADY, for her invaluable guidance, unwavering support, and constant encouragement throughout my PhD journey. Her expertise, dedication, and mentorship have been pivotal in shaping my research and personal growth.

I am deeply indebted to Prof. Mohammed Reda BRITEL for hosting me at the laboratory of innovative technologies. The multidisciplinary nature of the lab provided me with a rich environment to collaborate with colleagues from diverse backgrounds and learn from their experiences, which significantly broadened my perspective.

I extend my heartfelt appreciation to Prof. Younes SMANI for welcoming me into the Andalusian Center for Developmental Biology. His warm hospitality, mentorship, and the invaluable opportunity to contribute to his lab's projects significantly enriched my skills and knowledge, enabling me to explore new frontiers in my research.

I am grateful to Prof. George TSIAMIS for hosting me at the laboratory of Systems Microbiology and Applied Genomics. The training and supervision I received there were instrumental in developing my research capabilities.

I would also like to express my sincere thanks to Prof. Achraf EL ALLALI, Prof. Mahmoud A. A. IBRAHIM, and my co-authors for providing the necessary resources and support for conducting the extensive computational work required for this research.

Special thanks to my colleagues and friends, Badr-Edine, Iman, and Soukayna for their invaluable support and companionship during my tenure in the program.

I would like to extend my heartfelt appreciation to my family for their unwavering support and understanding during the demanding and time-consuming process of completing this thesis. Their constant encouragement and belief in me were a source of strength and motivation throughout this journey.

Finally, I would like to thank all those who have directly or indirectly contributed to the successful completion of this thesis. Your support and assistance have been invaluable, and I am truly grateful for the opportunity to learn and grow with your help.

LIST OF FIGURES

Figure 1. Distribution of NPs in each kingdom of life. [19].	8
Figure 2. Classification of NPs in organic chemistry [25].	9
Figure 3. Chemical structures and natural sources of some examples of approved NPs as drugs.	11
Figure 4. Biosynthesis and catabolism of DA [43].	13
Figure 5. Dopamine processing in a synapse. After release dopamine can either be taken up again by the presynaptic terminal or broken down by enzymes [44].	13
Figure 6. The synthesis of MPPP involves several steps that can lead to contamination by MPTP [64].	16
Figure 7. Global epidemiology of carbapenem-resistant <i>Acinetobacter</i> strains [155].	29
Figure 8. The key virulence factors in <i>A. baumannii</i> [157].	30
Figure 9. An overview of the main steps involved in the drug discovery process.	44
Figure 10. Schematic representation of the QSAR modelling workflow [315].	46
Figure 11. Dopamine and its molecular graph. Different types of nodes according to atomic elements and different types of edges depending on the chemical bond in the molecule [319].	48
Figure 12. A) Function and symbol of each ASCII character used in SMILES representation. B) 2D chemical structure and SMILES representation of DA.	48
Figure 13. SMARTS patterns and their visualization across three MACCS fingerprints using SMARTS PLUS [322].	49
Figure 14. Representation of the connection tables for DA within an SDF file.	50
Figure 15. The different types of molecular descriptors [326].	50
Figure 16. Generating an ECFP molecular fingerprint. The maximum allowed diameter here is 4, the successive circles have diameters of 0, 2 and 4. The presence of the obtained substructures is stored in a bit vector, here of length 8 [329].	51
Figure 17. General workflow of a machine learning algorithm.	52
Figure 18. The architecture of a convolutional neural network [349].	55
Figure 19. The architecture of an artificial neural network.	56
Figure 20. Presentation of the first pharmacophores to have been published. Beckett's model (a) from 1963 defines approximate distances between Zone 1, a negatively charged anionic cavity for accommodating a quaternary amine, Zone 2, a positively charged point for binding to acetylcholine and its analogues, and Zone 3, charged to interact with the OH of muscarine, the C-O of acetylcholine and its analogues, or the double bond of furanic analogues of muscarine [369]. Kier's model (b) proposes calculated distances between 3 key atoms common to acetylcholine, muscarine, and muscarone [370].	63
Figure 21. Methods to obtain the 3D structure of a biological target of interest include experimental approaches such as X-ray crystallography and NMR spectroscopy, as well as de novo methods such as structure prediction by homology.	64
Figure 22. Molecular docking software classification.	66
Figure 23. Flowchart of a molecular docking experiment.	68
Figure 24. Evolution of the reasons for failure of drug candidates in clinical phases between 1991 and 2000 [400].	68
Figure 25. Commonly used physicochemical properties and their drug-likeness rules.	69
Figure 26. Visual diagram of key ADMET parameters for evaluating the safety of drug candidates during development stages.	70
Figure 27. Geometric constraints of a hydrogen bond [421].	76
Figure 28. Chemical structures of proposed NPs against Parkinson's disease and <i>A. baumannii</i> infections.	164

LIST OF TABLES

Table 1. List of some flavonoids and their reported pharmacological activities in literature.....	25
Table 2. List of bioactive NPs against <i>A. baumannii</i> (modified from [294]).	42
Table 3. List of popular open access chemical bioactivity databases used in drug discovery.....	46
Table 4. Comparison between different connections tables formats.....	49
Table 5. Comprehensive list of natural product libraries suitable for high-throughput virtual screening studies.	60
Table 6. List of open-source and commercial molecular docking programs.	66
Table 7. Comparison of Classical MD, ab initio simulations, and Monte Carlo simulations.....	72
Table 8. Comparison of force fields in MD simulations.....	72
Table 9. Description of commonly used software packages for MD simulations.....	79
Table 10. Proposed lead candidates from NPs through in silico approaches for Parkinson's disease and their reported activities from the literature.	162
Table 11. Proposed lead candidate against <i>A. baumannii</i> infections and its previously reported activities.....	164

LIST OF ABBREVIATIONS

AA _{2A} R: Adenosine A _{2A} receptor	LRRK2: Leucine-rich repeat kinase 2
AChE: Acetylcholinesterase	MAO: Monoamine oxidase
AD: Alzheimer's disease	MD: Molecular dynamics
AHL: acyl-homoserine lactone	MDR: Multi-drug resistant
AMR: Antimicrobial resistance	MIC: Minimal inhibitory concentration
API: Application programming interface	ML: Machine learning
AUC: Area under the curve	NIH: National Institute of Health
BBB: Blood-brain barrier	NMDAR: N-methyl-D-aspartate receptor
CDC: Centers for Disease Control and Prevention	NPs: Natural products
CNN: Convolutional neural network	OM: Outer membrane
CNS: Central nervous system	OMPs: Outer membrane proteins
CRAB: Carbapenem-resistant <i>A. baumannii</i>	OMVs: Outer membrane vesicles
DA: Dopamine	PD: Parkinson's disease
DFT: Density functional theory	P-gp: P-glycoprotein
DL: Deep learning	pIC ₅₀ : Predicted half maximal inhibitory concentration
ECFP: Extended-connectivity fingerprints	QS: Quorum-sensing
ET: Extra Trees	QSAR: Quantitative structure-activity relationship
FDA: Food and Drug Administration	QSPR: Quantitative structure-property relationship
GI: Gastrointestinal	RF: Random Forest
IC ₅₀ : Half maximal inhibitory concentration	ROC: Receiving operating characteristic
ICU: Intensive care unit	ROS: Reactive oxygen species
K _d : Dissociation constant	SBVS: Structure-based virtual screening
K _i : Inhibitor constant	SNpc: Substantia nigra pars compacta
KNN: K-Nearest Neighbors	SVM: Support Vector Machine
LBVS: Ligand-based virtual screening	Tc: Tanimoto coefficient
LOS: Lipooligosaccharides	WHO: World Health Organization
LPS: Lipopolysaccharides	XDR: Extensive-drug resistant

TABLE OF CONTENTS

ABSTRACT	i
RÉSUMÉ.....	ii
نبذة مختصرة.....	iii
ACKNOWLEDGMENTS.....	iv
LIST OF FIGURES.....	v
LIST OF TABLES	vi
LIST OF ABBREVIATIONS	vii
TABLE OF CONTENTS	viii
CHAPTER I: INTRODUCTION	1
1 Background and motivation.....	2
2 Research objectives.....	4
3 Thesis outline	5
CHAPTER II: LITERATURE REVIEW	6
1 Natural products in drug discovery.....	7
1.1 Definition of natural products.....	7
1.2 Classification of natural products	7
1.2.1 Primary metabolites.....	8
1.2.2 Secondary metabolites.....	8
1.3 Therapeutic applications of natural products	9
1.3.1 Challenges and opportunities	9
1.3.2 Natural products as sources of new drugs.....	10
2 Overview of Parkinson's disease	12
2.1 History and epidemiology.....	12
2.2 Neuropathology.....	12
2.2.1 Dopaminergic impairment.....	12
2.2.2 Lewy bodies	14
2.3 Symptomatology	14
2.3.1 Motor symptoms	14
2.3.2 Non-motor symptoms.....	15
2.4 Etiology.....	15
2.4.1 Genetic forms	15
2.4.2 Sporadic forms	16
2.5 Pathogenesis.....	17
2.5.1 Oxidative stress	17

TABLE OF CONTENTS

2.5.2	α -synuclein	18
2.6	Therapeutic approaches	19
2.6.1	Dopaminergic drugs	19
2.6.2	Non-dopaminergic drugs.....	21
2.7	Novel approaches in development.....	22
2.7.1	α -synuclein modulators	23
2.7.2	LRRK2 inhibitors.....	23
2.7.3	Repurposed drugs.....	23
2.7.4	Neurotrophic factors.....	24
2.7.5	Multi-target drugs.....	24
2.8	Natural products in treating Parkinson's disease.....	25
3	Overview of <i>Acinetobacter baumannii</i>	28
3.1	History and epidemiology of <i>A. baumannii</i>	28
3.2	Virulence factors and pathogenesis of <i>A. baumannii</i>	29
3.2.1	Outer membrane proteins	30
3.2.2	Capsular polysaccharides	31
3.2.3	Phospholipase.....	31
3.2.4	Biofilm formation.....	31
3.2.5	Quorum-sensing	32
3.2.6	Metal acquisition system.....	32
3.2.7	Outer membrane vesicles	32
3.2.8	Protein secretion systems	32
3.3	Clinical impact of <i>A. baumannii</i> infections	33
3.3.1	Most frequent clinical manifestations	33
3.3.2	The challenge of antimicrobial resistance	35
3.4	Treatment of <i>A. baumannii</i> infections	36
3.4.1	Current treatment and drugs.....	36
3.4.2	Novel and future treatment options.....	38
3.5	Natural products in treating <i>A. baumannii</i> infections	42
4	Computational methods in drug discovery	44
4.1	Overview of the drug discovery process.....	44
4.2	Cheminformatics in drug discovery.....	45
4.2.1	Quantitative structure-activity relationships	45
4.2.2	Chemical bioactivity databases	46
4.2.3	Molecular representations	47

TABLE OF CONTENTS

4.2.4	Artificial intelligence in drug discovery.....	52
4.2.5	Performance evaluation.....	57
4.3	Molecular modelling.....	59
4.3.1	Chemical libraries	60
4.3.2	Ligand-based virtual screening	61
4.3.3	Structure-based virtual screening	63
4.3.4	Pharmacokinetics and toxicity filters	68
4.3.5	Molecular dynamics simulations.....	71
4.3.6	MD simulations workflow	73
4.3.7	MD trajectory data analysis.....	75
4.3.8	Free energy calculations.....	77
4.3.9	MD simulations software	78
CHAPTER III:	CHEMICAL LIBRARY DESIGN, QSAR AND MOLECULAR DYNAMICS SIMULATIONS OF NATURALLY OCCURRING COUMARINS AS DUAL INHIBITORS OF MAO-B AND ACHE	80
CHAPTER IV:	EXPLORING NATURAL PRODUCTS AS MULTI-TARGET-DIRECTED DRUGS FOR PARKINSON'S DISEASE: AN IN-SILICO APPROACH INTEGRATING QSAR, PHARMACOPHORE MODELLING, AND MOLECULAR DYNAMICS SIMULATIONS	101
CHAPTER V:	PROBING THE MOLECULAR MECHANISMS OF A-SYNUCLEIN INHIBITORS UNVEILS PROMISING NATURAL CANDIDATES THROUGH MACHINE-LEARNING QSAR, PHARMACOPHORE MODELING, AND MOLECULAR DYNAMICS SIMULATIONS	122
CHAPTER VI:	ANTIBIOTIC DISCOVERY WITH ARTIFICIAL INTELLIGENCE FOR THE TREATMENT OF <i>ACINETOBACTER BAUMANNII</i> INFECTIONS.....	141
CHAPTER VII:	GENERAL DISCUSSION.....	159
CHAPTER VIII:	CONCLUSION AND PERSPECTIVES	165
REFERENCES.....		167
LIST OF PUBLICATIONS		195
LIST OF COMMUNICATIONS		196
DECLARATION OF AUTHORSHIP		197
ANNEXES		198

CHAPTER I: INTRODUCTION

1 Background and motivation

Natural products (NPs) have long been recognized as a rich and invaluable source of bioactive molecules with immense therapeutic potential [1]. Throughout history, NPs have played a pivotal role in drug discovery, contributing to numerous clinically approved medications across various therapeutic areas [2]. Their structural diversity, accumulated through millions of years of evolutionary processes, offers a unique chemical space for exploring novel bioactivities and pharmacological targets [3]. Despite their proven track record and the vast diversity of NP repositories, the exploration and exploitation of this chemical space remain a formidable challenge [4]. The traditional approaches of bioactivity-guided fractionation and isolation are often laborious, time-consuming, and resource-intensive, hindering the efficient identification of bioactive NP scaffolds [5].

In response to the growing volume of biomedical data in chemistry and biology, there is a need for new methods and approaches for analyzing it [6]. *In silico* and data-driven approaches offer a more efficient and cost-effective alternative to traditional experimental methods. These computational techniques, including quantitative structure-activity relationships (QSAR), pharmacophore modelling, molecular docking, and molecular dynamics (MD) simulations, can quickly screen vast chemical libraries to identify potential leads [7]. Chemical libraries serve as crucial databases for virtual drug screening, providing scientists with access to diverse chemical compounds with varying properties and structures, enabling exploration of a broad range of potential drug candidates [8]. Additionally, the accumulation of large databases enables improved integration of machine learning (ML) and artificial intelligence (AI) techniques, facilitating the development and integration of more precise models for predicting the bioactivity and pharmacokinetics of novel drugs [9]. The application of ML and AI algorithms to vast chemical and biological data can uncover intricate patterns and relationships, accelerating the discovery process and enhancing the accuracy of predictions.

Neurodegenerative diseases, such as Alzheimer's, Parkinson's, and Huntington's disease, are characterized by the progressive loss of neuronal structure and function, leading to cognitive, motor, and behavioral impairments [10]. Despite significant advances in our understanding of the underlying pathological mechanisms, there is an unmet need for effective "disease-modifying" therapies. While current dopaminergic therapies can provide symptomatic relief, they are associated with significant side effects and lose efficacy over the long term as the disease progresses, necessitating the development of novel therapeutic interventions [11].

On the other hand, infectious diseases, exacerbated by the alarming rise of antimicrobial resistance (AMR), pose a severe global health threat [12]. The emergence of multidrug-resistant (MDR) pathogens like *Acinetobacter baumannii* has rendered many conventional antibiotics ineffective, necessitating the discovery of novel antimicrobial agents with distinct mechanisms of action to combat these evolving infectious agents [13], [14].

To address these challenges, this doctoral thesis harnesses the power of computational approaches to navigate the vast chemical space of NPs efficiently. By integrating data-driven methodologies with experimental validation, this research aims to accelerate the discovery of bioactive NPs with potential therapeutic applications in alleviating oxidative stress and protein aggregation, the primary hallmarks of Parkinson's disease (PD), as well as combating infectious diseases caused by MDR pathogens like *A. baumannii* by targeting the virulence factor OmpW.

2 Research objectives

To rationalize the discovery of NPs for combating PD and *A. baumannii* infections, data-driven approaches were utilized to efficiently screen the extensive chemical space within publicly available databases. The aim was to uncover novel NPs as lead drug candidates for experimental studies. This research thesis comprised the following objectives:

Objective 1: Coumarins have been extensively studied as dual inhibitors of monoamine oxidase B (MAO-B) and acetylcholinesterase (AChE) for the treatment of PD, the potential of naturally occurring coumarins in this context remains largely untapped. Thus, we designed CoumarinDB, a manually curated library containing chemical information on all naturally occurring coumarins in literature. A multi-stage virtual screening, incorporating QSAR regression models and molecular docking against MAO-B and AChE, was conducted to identify new potentially active coumarin derivatives from medicinal plants with neuroprotective effects against oxidative stress.

Objective 2: Subsequently, our exploration for natural remedies against neurodegeneration and oxidative stress in PD led us to uncover structural similarities between a dual-acting drug on MAO-B, adenosine A_{2A} receptor AA_{2A}R, and the reference N-methyl-D-aspartate receptor (NMDAR) antagonist, Ifenprodil. This observation inspired the development of QSAR models based on classification algorithms to predict the bioactivity of natural molecules within the largest NP database, COCONUT. Molecular modelling studies were then employed to discover novel natural multi-target agents against MAO-B, AA_{2A}R, and NMDAR.

Objective 3: The investigation delved into the disease-modifying potential of the α -synuclein pathway. A literature search revealed the promising clinical candidate Anle138b, along with other drugs sourced from ChEMBL. To elucidate the molecular mechanisms of α -synuclein modulators, QSAR models were developed followed by molecular modelling. The objective was to identify potential natural candidates from the LOTUS database, which offers superior molecule annotations compared to COCONUT, capable of modulating α -synuclein fibrillation and aggregation.

Objective 4: Shifting the focus to infectious diseases caused by *A. baumannii*, this objective aimed to expand the investigation by applying a similar methodology to explore the potential of NPs sourced from the Ambinter chemical library. Specifically, the goal was to identify compounds that could serve as inhibitors of OmpW, with the aim of addressing the challenge posed by MDR strains.

3 Thesis outline

This thesis begins by establishing its background and research objectives, then delves into exploring NPs as potential treatments for neurodegenerative diseases, with a focus on PD, and addressing the pressing need for effective therapies against infectious diseases like those caused by *A. baumannii*. The subsequent chapters are structured as follows:

Chapter II conducts a thorough Literature Review, emphasizing the importance of NPs in drug discovery, providing an overview of neurodegenerative diseases, particularly PD, and discussing the challenges of antimicrobial resistance, especially in *A. baumannii* infections. It also introduces *in silico* methods in drug discovery, explaining the crucial role of cheminformatics, chemometrics, and molecular modelling techniques in expediting the identification and optimization of potential drug candidates. This chapter lays the groundwork for the subsequent empirical investigations.

Chapters III through VI focus on specific applications of *in silico* methodologies in NP research. Chapter III centers on chemical library design, QSAR analysis, and MD simulations targeting MAO-B and AChE inhibition using naturally occurring coumarins. Chapter IV extends this inquiry by exploring the entire chemical space of NPs as multi-target-directed drugs to combat oxidative stress in PD. Chapter V utilizes machine learning-based QSAR and MD simulations to study α -synuclein aggregation inhibitors and identify potential natural alternatives.

In Chapter VI, the focus shifts to antibiotic discovery, employing artificial intelligence techniques to discover novel therapeutic strategies against *A. baumannii* infections, bridging computational chemistry and microbiology.

Chapter VII offers a General Discussion synthesizing the findings from the preceding chapters, providing insights into the potential applications of NPs in drug discovery, addressing challenges and opportunities in the field, and proposing future research directions.

Finally, Chapter VIII concludes the thesis by summarizing key findings, reflecting on their implications for the scientific community, and outlining potential research directions. This structured approach aims to contribute to advancing therapeutic interventions against neurodegenerative diseases and infectious pathogens in the fields of NP research and drug discovery.

CHAPTER II: LITERATURE REVIEW

1 Natural products in drug discovery

NPs have a rich history of use in traditional medicines and herbal remedies, remaining a significant source of inspiration for modern small-molecule drug discovery [2]. In fact, approximately two-thirds of all small-molecule drugs approved between 1981 and 2019 are linked, to varying degrees, to NPs. While only 5% of drugs introduced during this period are unaltered NPs, 28% are derivatives of NPs, and 35% either mimic or contain a pharmacophore derived from NPs [2]. The notable recognition of the importance of NP research for public health was exemplified by the awarding of the 2015 Nobel Prize in Physiology or Medicine to William C. Campbell, Satoshi Omura, and Youyou Tu for their discovery of two NPs (avermectin and artemisinin), which significantly advanced the treatment of diseases caused by parasites [2].

1.1 Definition of natural products

NPs are chemical compounds or substances produced by a living organism, which are found in nature. Thanks to the development of new technologies (high-throughput screening programs, separation, and isolation techniques), the number of NPs discovered at the beginning of the 21st century exceeds one million. More than 50% of these compounds are produced by plants [15]. In organic chemistry, the definition of NPs is limited to primary and secondary metabolites, which are purified organic compounds isolated from natural sources [16]. NPs sometimes have a beneficial therapeutic effect as traditional medicines for the treatment of diseases, thus providing knowledge to derive active principles as “lead” molecules for drug discovery.

1.2 Classification of natural products

NPs can be classified according to their biological function, biosynthetic pathway, or source as illustrated in Figure 1. These products include natural and organic foods, as well as compounds produced by living organisms such as plants, animals, fungi, and bacteria. Within the field of medicinal chemistry, NPs are often further restricted to secondary metabolites, which are not essential for survival but provide organisms that produce them with an evolutionary advantage [17].

- **Classification by Biological Function:** NPs can be classified based on their role in the organism’s survival and reproduction. Primary metabolites, such as carbohydrates, proteins, lipids, and nucleic acids, play an important and primary role in metabolic reactions. Secondary metabolites, on the other hand, do not seem to have any obvious

metabolic or evolutionary function and may be formed as a result of a “metabolic accident” or are by-products of the synthesis machinery of the cellular enzymes [18].

- **Classification by Biosynthetic Pathway:** NPs can be classified based on the biosynthetic pathway they follow. For example, terpenes are a class of NPs that are synthesized from a common precursor, isopentenyl pyrophosphate [18].
- **Classification by Source:** NPs can be classified according to the organism from which they are derived. For example, NPs from plants are often referred to as “phytochemicals”, while those from fungi are known as “mycotoxins”. NPs from animals are often used in the pharmaceutical industry, with examples including antibiotics produced by bacteria [17]

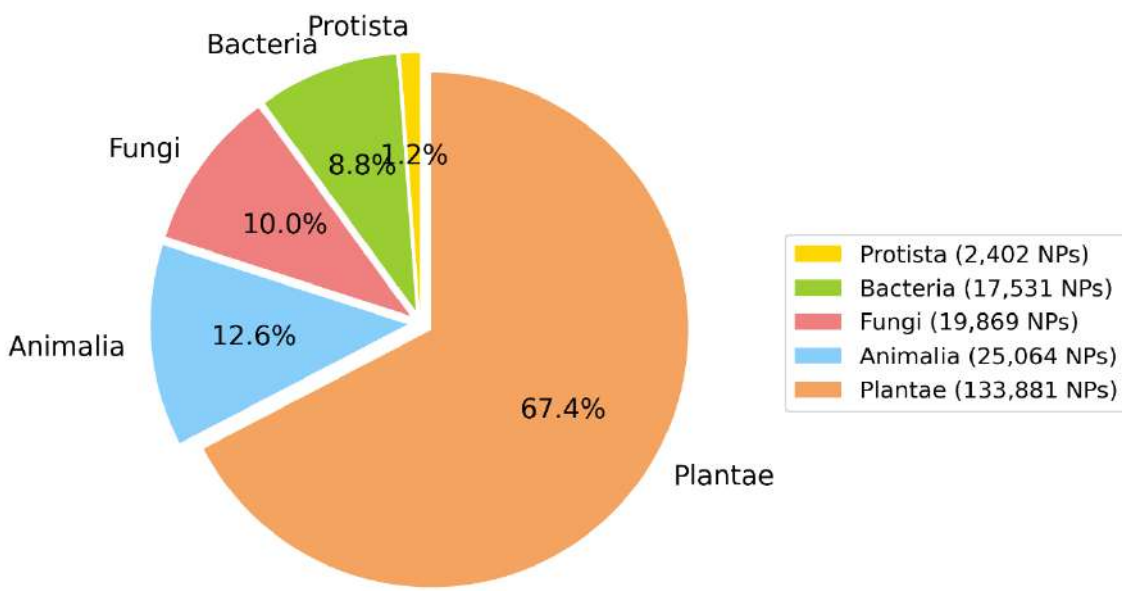


Figure 1. Distribution of NPs in each kingdom of life. [19].

1.2.1 Primary metabolites

A primary metabolite is a type of metabolite that is essential for the growth, development, and normal reproduction of an organism or cell. This chemical compound is involved in maintaining the physiological functions of that organism. They are the intermediate products of anabolic metabolism, which are used by cells to form essential macromolecules. Amino acids, vitamins, and alcohol are some of the primary metabolites produced industrially [20].

1.2.2 Secondary metabolites

Secondary metabolites are compounds produced by organisms that are not necessary for primary metabolic processes [21]. However, they can be important in an ecological or other sense. Secondary metabolites are considered the end products of primary metabolites because

they are derived through pathways in which primary metabolites are involved. More than 2,140,000 secondary metabolites are known and are classified based on their wide diversity in structure, function, and biosynthesis [22]. There are three main classes of secondary metabolites such as terpenoids, nitrogen-containing compounds, and phenolic compounds (Figure 2) [23].

The main functions of secondary metabolites, including antibiotics, are to confer a selective advantage to the organism. For example, they can serve as defense by secreting toxins against herbivores and insects, or conversely, attract certain beneficial species such as pollinators [24].

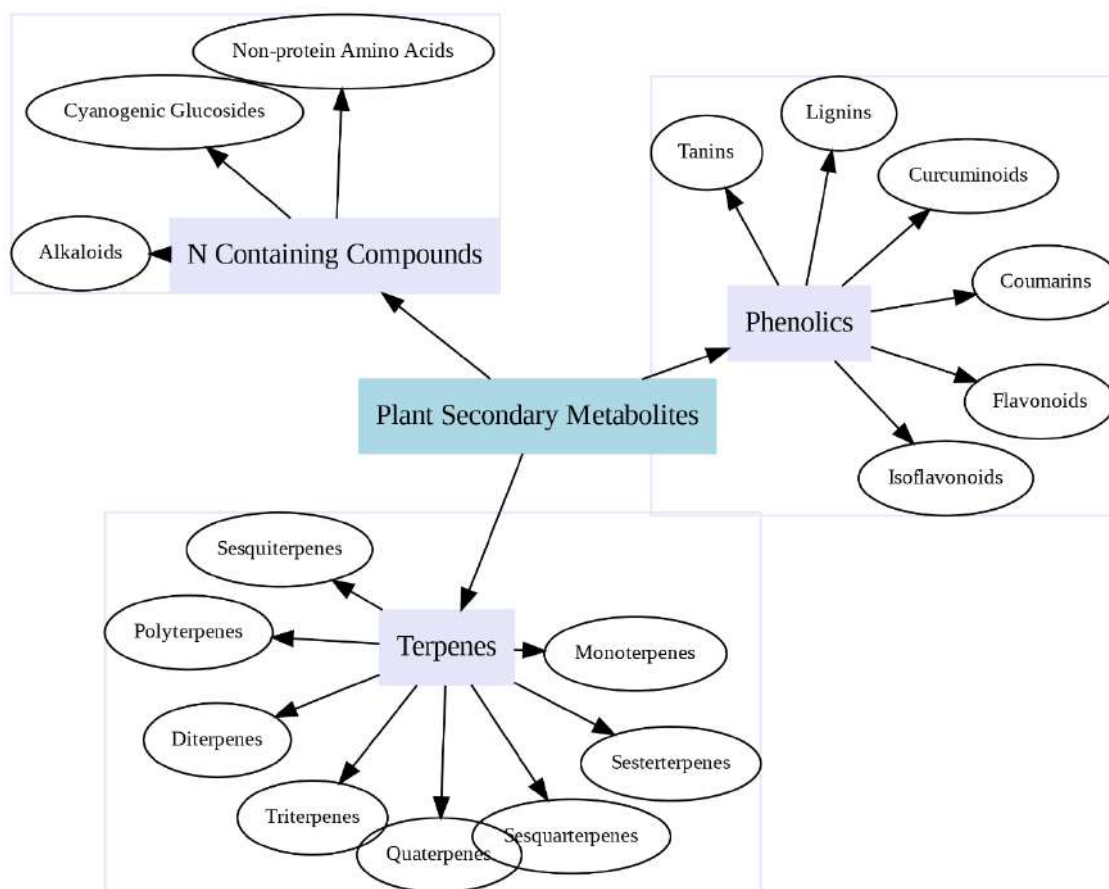


Figure 2. Classification of NPs in organic chemistry [25].

1.3 Therapeutic applications of natural products

1.3.1 Challenges and opportunities

NPs have historically made a major contribution to pharmacotherapy, particularly for cancer, infectious diseases, and neurodegenerative diseases. However, NPs also present challenges for drug discovery, such as technical barriers to screening, isolation, characterization, and optimization, which have contributed to a decline in their pursuit by the pharmaceutical industry since the 1990s [26]. The primary bottleneck in NP-based drug discovery lies in the availability of materials for testing. The sourcing process can be lengthy, and costly, with legal challenges

often arising during transportation across borders. Once materials reach their destination, the process involves production of extracts, in vitro testing for bioactivity, identification, and isolation of bioactive compounds from complex mixtures, determination of mode of action, and resupply of compounds of interest through partial or total chemical synthesis. Additionally, profiling their pharmacological, pharmacokinetic, and toxicological properties requires expertise, substantial efforts, time, and funds, with success not guaranteed.

In recent years, several technological and scientific developments, including better AI integration and improved analytical tools, are addressing these challenges, and opening new opportunities. As a result, interest in NPs as drugs is being revitalized, particularly for combating infectious diseases whose microbial resistance requires the constant discovery of new alternatives and neurodegenerative diseases whose pathophysiological mechanisms are multiple and complex [27].

1.3.2 Natural products as sources of new drugs

NPs have been a significant source of new drugs, with many being derived from plants. These compounds have played a crucial role in drug discovery and design, as they often contain unique and structurally diverse chemical components that can serve as templates for the development of novel therapeutic agents [28].

Some notable examples of NPs used in drug discovery include morphine, a potent analgesic derived from the opium poppy (*Papaver somniferum*), and codeine, a milder analgesic/cough suppressant from the same source [29], [30]. Penicillin, the revolutionary antibiotic produced by *Penicillium fungus*, remains a vital drug despite the development of modified versions [31]. Additionally, artemisinin, a sesquiterpene lactone derived from the plant *Artemisia annua*, is a cornerstone of malaria treatment, with derivatives developed to enhance its effectiveness and explore potential antitumor activity, such as Artesunate, as illustrated in Figure 3 [32]. Topotecan, a derived compound from the plant *Camptotheca acuminata*, is a chemotherapy drug used to treat ovarian and lung cancer [33]. Galantamine, an acetylcholinesterase (AChE) inhibitor approved for the treatment of Alzheimer's disease, is derived from the bulbs and flowers of the *Galanthus nivalis* (common snowdrop) and *Galanthus woronowii* (Caucasian snowdrop) plants [34], [35]. Other promising NPs include capsaicin, the active compound in *Capsicum* plants (chili peppers), used for pain and inflammation management, and Brintellix (vortioxetine), an antidepressant medication, derived from the fungus *Aspergillus*, used to treat major depressive disorder. [36], [37].

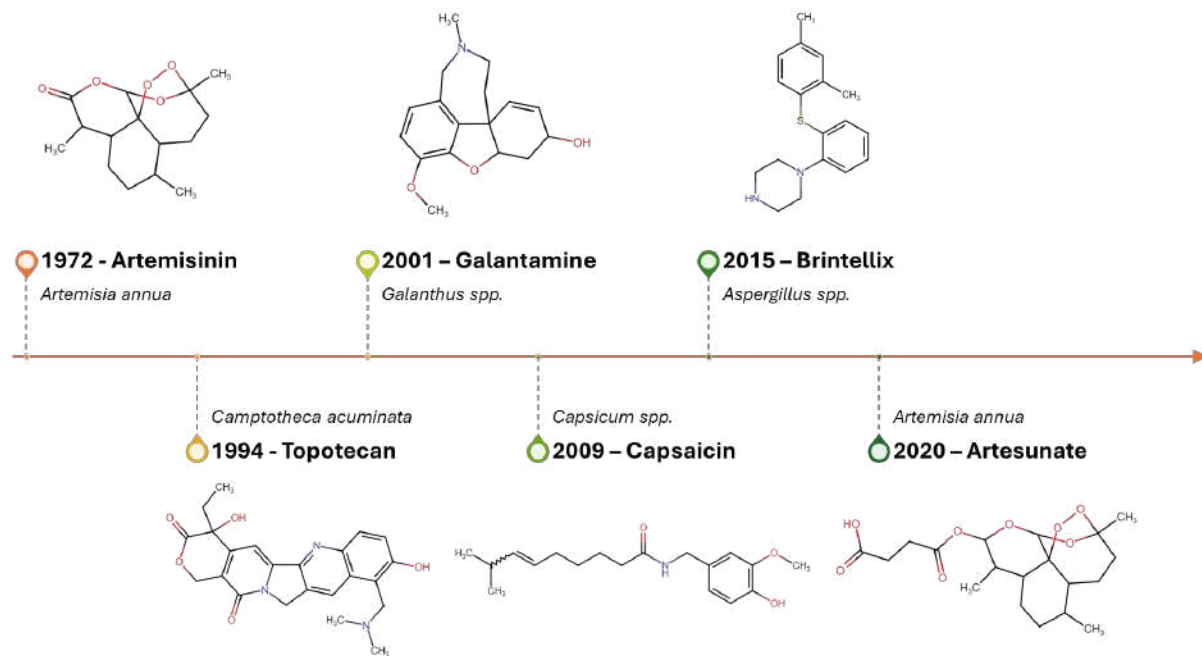


Figure 3. Chemical structures and natural sources of some examples of approved NPs as drugs.

2 Overview of Parkinson's disease

2.1 History and epidemiology

PD is a progressive neurodegenerative disease first described by James Parkinson in his work “An Essay on the Shaking Palsy” in 1817 as the association of a resting tremor in a context of muscle deficit without intellectual deficit [38]. Later, rigidity was mentioned and considered by Troussseau (1865) and Charcot (1885). Then Wernicke (1906) recognized the notion of akinesia by separating it from rigidity [39]. More than two centuries later, there is no cure for PD. However, in recent decades, research has revealed the molecular mechanisms of neurodegeneration, which is bringing us closer to designing therapies that can change the course of these neurodegenerative diseases. PD is the second most common neurodegenerative disease after Alzheimer’s disease [40]. Worldwide, it is estimated to affect 6 million people with a prevalence of about 150 per 100,000 inhabitants in the general population, rising to 1.5% beyond 65 years of age [41].

In Morocco, the prevalence of PD is not well documented, however it's estimated in 2015 that 34,803 people are affected by this disease according to a study published in 2020 in the Journal of Parkinson's Disease [42].

2.2 Neuropathology

From a pathological standpoint, PD is a progressive disorder characterized by the loss of dopaminergic neurons in the substantia nigra *pars compacta* (SNpc). It is associated with the formation of abnormal protein clumps called Lewy bodies; abnormal cytoplasmic inclusions that contain aggregates of a fibrillary protein called α -synuclein.

2.2.1 Dopaminergic impairment

2.2.1.1 Dopamine metabolism

Dopamine (DA) belongs to the family of catecholamines, organic compounds that act as neurotransmitters and are synthesized from the amino acid tyrosine. The hydroxylation of the phenyl ring of tyrosine by the enzyme, tyrosine hydroxylase, leads to dihydroxyphenylalanine (DOPA). DA is then obtained by decarboxylation of DOPA by DOPA-decarboxylase (Figure 4).

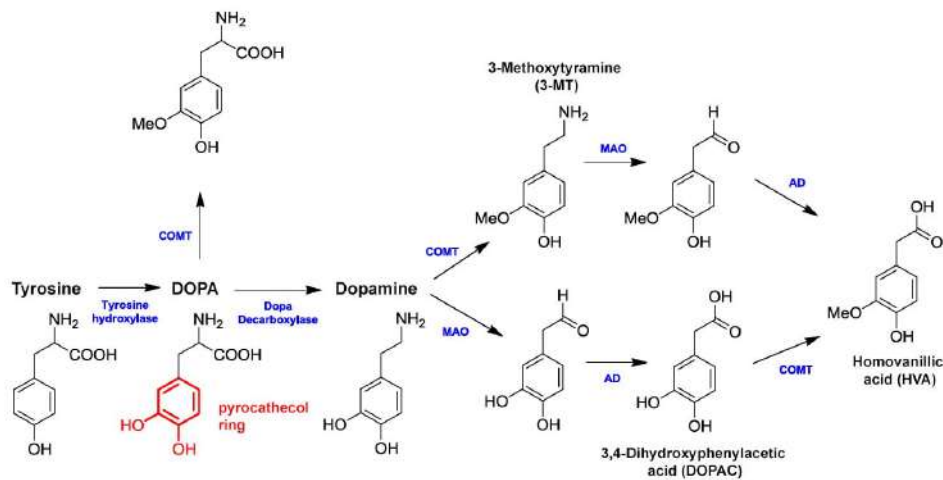


Figure 4. Biosynthesis and catabolism of DA [43].

After being produced in the presynaptic terminals, DA is stored in synaptic vesicles, and released into the synapse through exocytosis (Figure 5). It binds to and activates dopamine receptors, which can be located on postsynaptic dendrites or presynaptic receptors. After being released, dopamine molecules quickly become unbound from their receptors and are reabsorbed back into the presynaptic cell through reuptake. The level of extracellular dopamine is modulated by two mechanisms: phasic and tonic transmission. Phasic release is triggered by action potentials, while tonic release is regulated by other neurons and the rate of dopamine reuptake.

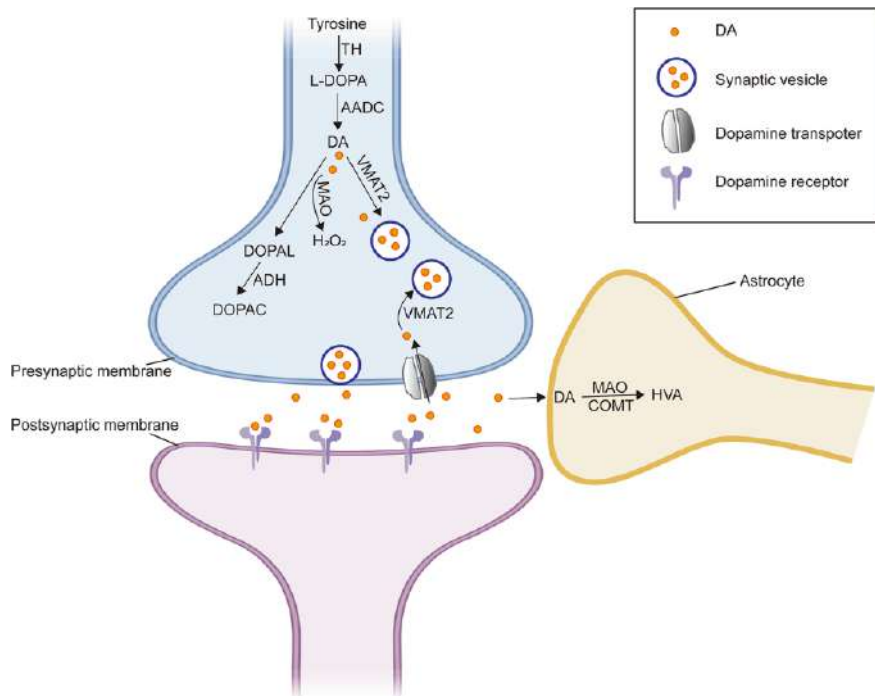


Figure 5. Dopamine processing in a synapse. After release dopamine can either be taken up again by the presynaptic terminal or broken down by enzymes [44].

2.2.1.2 Dopamine lesion

Dopamine (DA) is a crucial neurotransmitter that regulates various functions such as movement, motivation, reward, and hormone secretion [45]. Dopaminergic neurons are found in specific brain areas like the SNpc, ventral tegmental area, and others, collectively known as the dopamine system. This system plays a role in motor function, reward/motivation, and hormone secretion like prolactin. In PD, there is degeneration and death of dopaminergic neurons, particularly in the nigrostriatal pathway connecting the SNpc and striatum. This causes a deficiency in dopamine levels, disrupting the balance with acetylcholine [46]. The rate of neurodegeneration is twice as fast in PD compared to normal aging [47]. PD is characterized by a lesion in the nigrostriatal dopaminergic pathway, resulting in a decrease in striatal dopamine levels [48]. Even when 50-60% of dopaminergic neurons in the SNpc have degenerated and striatal dopamine is reduced by 70%, PD motor symptoms like tremors, muscle stiffness, and loss of coordination start appearing [49], [50].

2.2.2 Lewy bodies

During anatomical studies on the SNpc of PD patients, Friedrich Lewy observed cytoplasmic inclusions called Lewy bodies in 1913 [51]. Post-mortem examinations revealed these Lewy bodies in the cytoplasm of most degenerating dopaminergic neurons in PD patients [52]. Lewy bodies are circular intraneuronal cytoplasmic inclusions measuring 5-25 micrometers in diameter. Their exact composition is not well-defined, but they contain proteins like ubiquitin, parkin, and α -synuclein, which is the main component and is phosphorylated at serine-129 within Lewy bodies [53]. The origin and implications of Lewy bodies are uncertain, but they may play a protective role by sequestering toxic insoluble forms of α -synuclein and other proteins, supported by the presence of proteins involved in degradation pathways within them [52]. In PD, the presence of Lewy bodies coincides with the specific loss of dopaminergic neurons and glial cell activation in the SNpc, with more severe damage in the ventrolateral region compared to the relatively preserved dorsomedial region (ventral tegmental area). Striatal degeneration is uneven, with the ventral putamen more affected than the dorsal caudate nucleus [54]. The recurrent finding of Lewy bodies in PD patients has led to their use as histopathological markers of the disease.

2.3 Symptomatology

2.3.1 Motor symptoms

From a symptomatic point of view, PD is characterized by motor disturbances such as progressive asymmetric rest tremor, motor rigidity, and bradykinesia, which are related to the

loss of dopaminergic neurons in the SN_{pc}, resulting in a DA deficit in the striatum, responsible for the onset of characteristic motor symptoms of the disease. These clinical symptoms appear when about 60-80% of striatal dopaminergic terminals and about 40-50% of cell bodies in the SN_{pc} have disappeared [55], [56]. Although these motor symptoms are improved by medication at the beginning of treatment, complications corresponding to motor fluctuations and dyskinesias occur in all patients after 5 to 10 years of evolution.

2.3.2 Non-motor symptoms

Initially defined as an exclusively motor pathology, PD is in fact a complex condition that includes non-motor symptoms that have a significant impact on the quality of life of patients [57]. These manifestations can represent the main complications in some patients who do not show severe motor disorders. Understanding these non-motor disturbances now appears to be a critical factor for better patient management. In fact, some non-motor signs can represent true predictive markers of PD. Non-motor disturbances include olfactory disturbances in 80% of cases, orthostatic hypertension, gastrointestinal (GI) and urinary sphincter disturbances in more than 70% of cases, but also a cognitive deficit related to subcortical frontal dysexecutive syndrome or thought and memory disorders. Mood disorders and visual difficulties have also been reported [58]. Most Parkinson's subjects suffer from chronic pain either musculoskeletal, neuropathic, or related to dystonia or central akinesia [59]. Finally, the deregulation of wake/sleep cycles is among the most frequent and disabling non-motor disorders found in PD patients. These various symptoms and disorders reflect an alteration of all dopaminergic pathways even if the nigrostriatal pathway remains the most affected. However, deficits regarding mesolimbic and mesocortical dopaminergic pathways can also play a role in the development of cognitive and even motor disorders [60]. Similarly dopaminergic neurons in the nigrostriatal pathway projecting to the dorsolateral motor regions of the striatum are more affected than those projecting to the more cognitive ventral regions. These alterations become more accentuated with the progression of neurodegeneration, which is estimated to be a loss of 1% of dopaminergic neurons per year, while it is twice as low in healthy subjects [61].

2.4 Etiology

2.4.1 Genetic forms

While most of the PD cases are sporadic, approximately 5% are familial, meaning they are hereditary and linked to mutations in specific genes with either dominant or recessive inheritance patterns. The discovery in 1997 of mutations in the SNCA gene, which codes for the α -synuclein protein, and their involvement in a rare form of PD, sparked significant interest

in studying the genetic factors contributing to the etiology of the disease. Subsequently, mutations in several other genes have been identified as causative for hereditary forms of PD. These include genes coding for proteins such as PARK2, ubiquitin C-terminal hydrolase L1 (UCH-L1), DJ-1, PINK1, and LRRK2. The identification of these genetic mutations has provided valuable insights into the molecular mechanisms underlying PD pathogenesis and has facilitated the development of potential therapeutic strategies targeting specific genetic factors [62]. PD can be inherited in an autosomal dominant pattern if the LRRK2 or SNCA gene is involved, where the presence of a single copy of the altered gene in each cell is sufficient to cause the disease, and an affected individual typically has one parent who also has the disease; or in an autosomal recessive pattern when the PARK7, PINK1, or PRKN gene is implicated, requiring two copies of the altered gene in each cell for the disease to manifest, with the parents of an individual with this form of autosomal recessive PD often being carriers who possess one copy of the altered gene but do not exhibit signs or symptoms themselves.

2.4.2 Sporadic forms

2.4.2.1 Historical background

In 1976, Barry Kidston, a chemistry student from Maryland, synthesized and injected an analogue of meperidine: 1-methyl-4-phenyl-4-propionoxypiperidine (MPPP). Three days after the injection, he developed symptoms of PD. Later, the National Institute of Health (NIH) found traces of N-methyl-4-phenyl-1, 2, 3, 6-tetrahydropyridine (MPTP) and other meperidine analogues in his laboratory. Tested on rats, the substances were found to have no effect. This would later be explained by the tolerance of these rodents to this type of neurotoxin. The patient was successfully treated with L-DOPA but died 18 months later from a cocaine overdose. His autopsy revealed significant destruction of dopaminergic neurons in the SN [63]. It should be noted that this choice for MPPP is explained by the powerful analgesic properties of this compound and its ease of synthesis from unregulated chemicals. MPPP is obtained in two steps from N-methyl-4-piperidone (NMP). Treated with phenyl lithium, it is first transformed into 4-hydroxy-4-phenyl-N-methylpiperidine (HPMP). This alcohol is then esterified by propionic anhydride to finally lead to MPPP. However, a secondary dehydration reaction can occur during this last step, causing contamination of MPPP by MPTP (Figure 6).

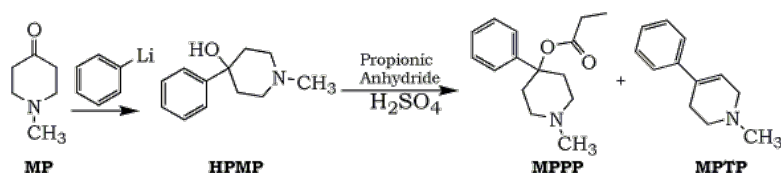


Figure 6. The synthesis of MPPP involves several steps that can lead to contamination by MPTP [64].

In 1979, Davis et al., suggested that the use of batches containing a mixture of HPMP, MPPP and MPTP was the origin of the Parkinsonism observed in Barry Kidston [65]. Later, in 1982, new cases of Parkinsonian syndrome were described in seven drug users, again following the injection of MPPP. Recovered by neurologist J. W. Langston, a sample of the incriminated substance could be studied by the chemist I. Irwin from Stanford University. Mass spectrometry analysis identified among the different meperidine analogues, a common compound with those previously identified by the NIH: MPTP [63]. Logically, the hypothesis that MPTP was the origin of the Parkinsonian syndrome developed by drug users was proposed. Later, J. W. Langston, in collaboration with the NIH, confirmed through studies not on rats but on primates, that MPTP intoxication was indeed the cause of the PD observed in drug users [23], [25].

2.4.2.1.2 Toxins exposure

Later, several chemicals used in the composition of herbicides, pesticides, and insecticides and which had the same target as MPTP, were suspected of being involved in the genesis of PD. It should be recalled that in more than 90% of cases, PD manifests itself sporadically and would therefore result from environmental factors such as exposure to toxins [67], [68], [69]. This hypothesis is supported by several epidemiological studies showing a higher prevalence of PD in areas of intensive agriculture using significant amounts of pesticides, herbicides, and insecticides. Similarly, chronic exposure to certain heavy metals such as copper, manganese or lead could form a risk factor [70].

2.5 Pathogenesis

While etiology refers to the factors that initiate the process of a disease, pathogenesis - and in the case of PD - refers to the actual mechanisms leading to the loss of dopaminergic neurons. In terms of the pathogenesis of PD, there are currently two major theories that are not necessarily antagonistic. The first theory suggests that the misfolding and toxic accumulation of insoluble forms of α -synuclein are key to the neurodegenerative process. The second theory suggests that the mitochondrial dysfunction and resulting oxidative stress are the cause.

2.5.1 Oxidative stress

Several studies have shown that oxidative stress is involved in the mechanisms of cell death in neurodegenerative diseases [71]. In these diseases, markers of oxidative stress are at a high level. Although the sequence of deleterious events leading to cell death is not clarified for these degenerative disorders, there are many arguments involving oxidative stress in the processes of neurodegeneration [72]. These data have led to the development of antioxidant therapeutic

strategies whose effects have been evaluated in therapeutic trials, mostly controlled, with variable results depending on the pathologies implicated. In both the idiopathic and genetic forms of PD, oxidative stress has been identified as the underlying common mechanism that leads to cellular dysfunction [73]. Thus, the SN of PD patients shows increased levels of oxidized lipids, proteins, and DNA [74], and reduced levels of glutathione [75].

Oxidative stress occurs when there is an imbalance between the production of ROS and cellular antioxidant activity. Due to the presence of enzymes whose activity generates ROS such as tyrosine hydroxylase and monoamine oxidase (MAO), dopaminergic neurons are particularly susceptible to oxidative stress. In addition, dopaminergic nigral neurons contain iron, which catalyzes the Fenton reaction, in which superoxide radicals and hydrogen peroxide can contribute to additional oxidative stress [76]. Due to this intrinsic sensitivity to reactive species, moderate oxidative stress can trigger a cascade of events that leads to cellular degeneration. The main sources of this oxidative stress are the ROS produced during dopamine metabolism, mitochondrial dysfunction and neuroinflammation.

2.5.2 α -synuclein

Two elements support the hypothesis that α -synuclein is involved in the pathogenesis of PD. The first is the presence of this protein in the histopathological markers of PD, which are defined as Lewy bodies. The second element comes from the etiology of the disease. In fact, it has been shown that mutations in the gene encoding α -synuclein are involved in genetic forms of PD [62]. α -synuclein is a small protein composed of 140 amino acids in its native state and is expressed ubiquitously in the brain but is mainly localized in presynaptic terminals where it associates with membranes and vesicular structures [77]. Although its biological role is not yet fully understood, many studies suggest that it is involved in regulating and maintaining dopaminergic homeostasis in the cell, particularly by inhibiting the activity of tyrosine hydroxylase, thereby reducing dopamine biosynthesis [78]. Its ability to bind to many endogenous and exogenous molecules, such as proteins or various metal ions, makes it complex to identify its physiological role. In 2000, a pathological nonsense mutation affecting the SNCA gene encoding α -synuclein was identified in patients with PD [79]. This is a point mutation in which a single nucleotide base is changed, resulting in a stop codon. The mutated gene produces a truncated protein due to premature translation termination, rendering it mostly non-functional. In the SNCA gene, this occurs at codon "53", where an alanine residue is replaced by threonine (A53T) [80]. Other point mutations have been discovered subsequently such as the substitution of an alanine at codon "30" with a proline (A30P) [39], and that of a glutamic acid at codon

“46” with a lysine (E46K) [82]. Except for hereditary cases of PD that are accompanied by either an increase in the α -synuclein gene or by specific mutations (A30P, A53T, and E46K), the cause of α -synuclein accumulation and the formation of Lewy bodies remains unclear. Recently, the idea of dysfunction in intracellular degradation systems for α -synuclein has regained interest. Studies have described cathepsin D as the main enzyme that degrades α -synuclein, thereby preventing its aggregation and toxicity. This is in line with more recent studies showing that increasing cathepsin D activity would inhibit α -synuclein aggregation and its toxicity [83], [84]. Therefore, this self-amplifying loop of α -synuclein aggregation that promotes neuron degeneration and disease progression appears to be a promising target for the development of new therapeutic approaches.

2.6 Therapeutic approaches

The available treatments for PD do not cure the disease, but often provide a significant improvement in symptoms by attempting to compensate for the dopamine deficiency in the striatum. This compensation can be achieved by administering a dopamine precursor or a dopamine agonist, or by inhibiting dopamine metabolism. This explains the resistance encountered during dopamine treatment and the efforts to develop neuroprotective treatments that can slow neurodegenerative processes. However, the limited understanding of the molecular mechanisms of the disease remains the main barrier to therapeutic innovation. In recent years, with the evolution of brain imaging techniques, there has been renewed interest in neurosurgery. Nevertheless, all existing treatments are symptomatic, and the therapeutic strategy will be considered based on the clinical form and stage of the disease.

2.6.1 Dopaminergic drugs

2.6.1.1 L-DOPA

The most used medication treatment to compensate for the dopamine deficiency caused by neuronal loss in PD is L-DOPA (also known as levodopa, and l-3,4-dihydroxyphenylalanine), a synthetic precursor of DA that can cross the blood-brain barrier (BBB). The use of L-DOPA as a DA replacement treatment is highly effective in improving the symptoms of the disease and remains the standard medication [85]. L-DOPA is used in combination with peripheral decarboxylase inhibitors (PDIs). PDIs will prevent the transformation of L-DOPA into DA at the peripheral level and therefore, will only be metabolized into DA after crossing the BBB. In addition, PDIs are unable to cross the BBB and do not interfere with DA production in the brain.

2.6.1.2 DA agonists

Although the DA precursor, L-DOPA, remains the reference symptomatic treatment, other medications such as DA agonists have been proven effective in treating PD symptoms in the early and advanced stages of the disease. One of the advantages of these medications compared to L-DOPA is a lower risk of developing dyskinesia and motor fluctuations. DA agonists act by directly binding to DA receptors in the central nervous system (CNS). They are most used in combination with L-DOPA to limit motor fluctuations and abnormal movements caused by L-DOPA, while still benefiting from its positive effects on the disease. However, DA agonists can also cause some unwanted side effects. Some of the most common side effects include nausea, vomiting, dizziness, headache, and confusion. Other side effects include constipation, dry mouth, and changes in libido. A serious potential adverse effect of DA agonists is impulse control disorder which can manifest as compulsive gambling, increased sexual behavior, binge eating, compulsive shopping or hyperphagia. Another potential adverse effect is augmentation, which is the most common long-term side effect affecting 7% of patients per year who are on DA agonist therapy [86]. It's a phenomenon where DA agonists can cause the symptoms to worsen or to appear earlier in the day than before.

2.6.1.3 MAO-B inhibitors

The preclinical development of the first MAO-B inhibitor began in the 1960s with the molecule L-Deprenyl, which was later renamed selegiline [87]. It was shown that selegiline does not induce any side effects associated with tyramine metabolism due to its selectivity for MAO-B. A little later, a new molecule was marketed, rasagiline, which is ten times more selective for MAO-B than selegiline. It has shown its efficacy as monotherapy in early forms or in combination with other treatments in fluctuating forms. More recently, safinamide was approved in Europe in 2015 and in the United States and Canada in 2017 and 2019, respectively. It is a highly selective and reversible inhibitor for MAO-B. It is used in the treatment of motor fluctuations as a complement to L-DOPA or as monotherapy in the early stages of the disease. These MAO inhibitors work by inhibiting the reuptake of catecholamines, which allows to make up for the DA deficit. Their interest in PD lies in the possibility of reinforcing the action of L-DOPA by increasing and prolonging plasma DA levels. Their indication is in the improvement of motor fluctuations as a complement to L-DOPA. In addition, safinamide also acts through non-dopaminergic mechanisms by blocking voltage-dependent sodium and calcium channels and, consequently, inhibiting neuronal release of glutamate, which plays a role in dyskinesia [88].

2.6.1.4 COMT inhibitors

Catechol-O-methyltransferase (COMT) is an enzyme that catalyzes the methylation of catechol substrates using S-adenosyl-L-methionine (SAM) as a methyl donor [89]. COMT substrates include catecholamines, their hydroxylated metabolites, catechol estrogens, ascorbic acid, dietary phytochemicals, and medicinal compounds [89]. The major physiological role of COMT is the elimination of biologically active or toxic catechols, such as L-DOPA in PD patients. COMT also plays a role in modulating prefrontal DA neurotransmission.

COMT inhibitors were first discovered in the 1950s but had limited success due to poor activity and selectivity [90]. In the late 1980s, a new generation of potent and selective COMT inhibitors were discovered, consisting of disubstituted catechols with electron-withdrawing groups such as nitro groups, carbonyl groups, or carbon-carbon double bonds [91]. These inhibitors showed three orders of magnitude higher potency in inhibiting COMT activity compared to the earlier generation of inhibitors.

Some examples of COMT inhibitors include entacapone and tolcapone [92]. Like MAO-B inhibitors, they are often used in combination with L-DOPA, to enhance the effect of these drugs. However, COMT inhibitors are not suitable for everyone and may have side effects such as nausea, diarrhea, and other GI symptoms [93].

2.6.2 Non-dopaminergic drugs

Recently, other drugs have been developed for the treatment of PD involving different neural pathways such as those involved in the release of adenosine, glutamate, and acetylcholinesterase. Experimental studies on nerve cells and animal models have shown that inhibition of these pathways can limit the release of free radicals and reduce neuronal apoptosis, suggesting a neuroprotective potential for drugs acting through these non-dopaminergic mechanisms [94], [95].

2.6.2.1 AA₂AR antagonists

The AA₂AR represents one of the three subtypes of adenosine receptors, which are G protein-coupled receptors formed by seven transmembrane α helices, with the endogenous ligand adenosine [96]. The activation of these receptors by the agonist, adenosine, leads to a cascade of reactions that eventually activates adenylate cyclase, increasing the cAMP synthesis rate. The link between the AA₂AR and PD stems from the link in which activation of the AA₂AR counteracts the actions of DA, a key neurotransmitter in motor control. Therefore, blocking the AA₂AR by administering its antagonists could help alleviate the motor symptoms of PD.

Furthermore, oral administration of AA_{2A}R antagonists in experimental models has prevented the death of dopaminergic neurons, suggesting their neuroprotective properties [97]. A caffeine derivative called Istradefylline was the first AA_{2A}R antagonist approved in Japan in 2013 and in the United States in 2019 as an adjunctive treatment to L-DOPA in Parkinson's patients with motor fluctuations [98], [99].

2.6.2.2 NMDAR antagonists

NMDAR is a type of glutamatergic ionotropic receptor found on neurons and involved in the transmission of nerve impulses and synaptic plasticity[100]. It represents one of three types of ionotropic glutamate receptors, along with AMPA and kainate receptors. The NMDAR plays an important role in memory and learning, as it allows the transmission of nerve impulses between neurons when synapses are repeatedly activated. It is also involved in the regulation of neuronal excitability and apoptosis [101]. The NMDAR is activated by the neurotransmitter glutamate and requires the simultaneous presence of glutamate and glycine to be activated. When activated, it allows the entry of calcium and sodium ions into the cell, which can lead to changes in neuronal excitability and nerve impulse transmission [102]. The NMDAR is a potential target for PD treatment because of its role in neuroprotection [103]. Studies have shown that glutamate, an excitatory neurotransmitter, plays a role in PD and that PD patients have higher levels of glutamate than healthy individuals. NMDAR antagonists have been shown to improve motor symptoms, reduce dyskinesia caused by levodopa, and slow neurodegeneration in PD models, making NMDAR a promising target for a non-dopaminergic treatment option that can address the severe motor complications of current dopamine replacement strategies [104].

2.6.2.3 AChE inhibitors

AChE inhibitors are drugs that prevent acetylcholine metabolism, a neurotransmitter involved in the transmission of nerve impulses between neurons. AChE inhibitors, primarily used to treat AD, may also be effective in improving cognitive impairment and dementia in PD patients according to a clinical study [60]. A recent meta-analysis of randomized controlled trials investigated the effects of AChE inhibitors on major PD symptoms and found that rivastigmine was effective for PD dementia [105].

2.7 Novel approaches in development

There are new drug approaches called “disease-modifying” for the treatment of PD that aim to slow down, stop, or reverse the underlying degenerative process that causes PD, rather than just

managing the symptoms of the disease [106], [107]. These approaches are still in their early stages and require further research to determine their effectiveness and safety.

2.7.1 α -synuclein modulators

α -synuclein modulators are a class of disease-modifying therapies that target the accumulation of α -synuclein protein in the brain, which is thought to play a key role in the development and progression of PD [108]. These therapies aim to inhibit or reduce the aggregation of α -synuclein, thereby slowing down or reversing the degenerative process that leads to PD. There are different types of α -synuclein modulators in development, including monoclonal antibodies, small molecules, and gene therapies. Anle138b and NPT200-11 are two such molecules that are being evaluated for their effectiveness and safety in clinical trials for PD [108], [109]. However, these therapies are still in development and may require further research to determine their safety and effectiveness in treating PD.

2.7.2 LRRK2 inhibitors

Leucine-rich repeat kinase 2 (LRRK2) is a protein that is involved in the regulation of cell growth, survival, and movement. Mutations in the gene that codes for LRRK2 are the most common genetic cause of PD and are thought to contribute to the development and progression of the disease by altering the activity of the protein [110].

LRRK2 has been linked to PD through Genome-wide association studies (GWAS) and its most common mutation, G2019S, increases kinase activity. Inhibitors of LRRK2 could be useful for treating PD [111]. LRRK2 inhibitors are a class of disease-modifying therapies that aim to reduce the activity of the LRRK2 protein by binding to and inhibiting the enzyme. A study discovered a series of potent LRRK2 inhibitors and optimized them through a surrogate crystallography approach. One highly potent, selective and brain penetrant inhibitor, 14 (PF-06447475), was identified and further studied for safety and efficacy *in vivo* [112].

2.7.3 Repurposed drugs

Repurposing drugs involves using already approved drugs to treat a disease different from the one for which they were originally developed. This can be done by using existing scientific and clinical data on the drug, as well as knowledge of the biology of the targeted disease. Repurposing drugs can be a promising approach to the development of new treatments, as it allows to take advantage of drugs that have already been proven and approved for clinical use [113]. Several drugs have been repurposed in the treatment of PD. For example, temazepam, a drug used to treat hypertension, has been tested as an adjunctive treatment for PD patients.

Preclinical studies have shown that temazepam could protect dopamine neurons from cell death and improve Parkinsonian symptoms in animal models. Clinical studies have also shown that temazepam could improve PD symptoms in patients with the disease [114].

Other studies have suggested that certain antidiabetic drugs could have a beneficial effect on PD symptoms. For example, insulin and glucagon-like peptide-1 (GLP-1) receptor agonists have been studied as a potential treatment for PD. Preclinical studies have shown that insulin and GLP-1 receptor agonists could protect dopamine neurons from cell death and improve PD symptoms in animal models. Clinical studies have also shown that these drugs could improve PD symptoms in patients with the disease [115].

2.7.4 Neurotrophic factors

Neurotrophic factors are proteins that play an important role in the survival and development of neurons. They are involved in many brain functions, including neuronal plasticity, interneuronal communication, and neuron regeneration. Several neurotrophic factors have been studied for their potential in the treatment of PD, including neurotrophin-3 (NT-3) and nerve growth factor (NGF) [116], [117]. However, they are still on clinical trials, so they are not commonly employed in PD treatment yet.

2.7.5 Multi-target drugs

In 2005, Morphy and Rankovic reviewed more than 300 reports in drug discovery and development journals about compounds designed as multi-target drugs for neurodegenerative diseases [118]. The development of these drugs is challenging due to the need for balancing the affinities of one drug molecule for multiple targets and obtaining appropriate physicochemical properties [119]. Lead generation strategies for these diseases are based on the discovery of disease gene products and brain enzymes, but the design of multiple ligands is made difficult by the lack of clear evolutionary relationships among the potential protein targets [120]. To overcome these obstacles, molecular biology, and genomics approaches, combined with computational resources are being used to accelerate the discovery of credible drug targets in the design of these drugs.

There are several multi-target drugs that are in development for the treatment of PD [121]. These drugs are designed to target multiple pathways and mechanisms involved in the disease, with the goal of improving symptom management and slowing disease progression [122]. One example of a multi-target drug for PD is Istradefylline [123]. This drug is an antagonist of AA_{2A}R that has been shown to improve motor function in people with PD. It works by blocking

the action of adenosine, a chemical messenger that can inhibit the activity of neurons releasing dopamine in the brain. It also increases the dopamine levels by inhibiting MAO-B, key enzyme for dopamine degradation. Other multi-target drugs that are in development for PD include compounds that target G protein-coupled receptors, enzymatic systems, and other signaling pathways involved in the disease. These drugs are currently at different stages of development and more research is needed to determine their safety and efficacy.

2.8 Natural products in treating Parkinson's disease

NPs derived from plants, including flavonoids, coumarins, curcuminoids, and alkaloids, hold significant promise for the treatment of PD. These bioactive phytochemicals offer potent antioxidant and anti-inflammatory properties, promote mitochondrial function, and enhance cognitive abilities [124]. Additionally, they can act as inhibitors for α -synuclein aggregation, and monoamine oxidase production, while also acting as agonists for dopaminergic neurons [125], [126]. Given the socioeconomic burden and undesirable side effects associated with many synthetic drugs, these natural remedies provide a compelling alternative for PD management.

Herbs, fruits, vegetables, and spices offer a rich source of neuroprotective NPs. Key compounds include flavonoids, alkaloids, xanthones, saponins, catechins, coumarins, and curcuminoids. Their potential in combating PD lies in their diverse mechanisms of action and potential to address the complex pathology of the disease.

Flavonoids can be classified into different groups such as anthocyanidins, chalcones, flavonols, flavanones, flavanonols, flavones and isoflavonoids. Additionally, flavonoids can be found in plants in the free form (aglycones) or linked to sugars (glycosides). The form linked to the glycoside is the most common flavone and flavonol consumed in food. Flavonoids possess several pharmacological activities such as antiparkinsonian, anti-ulcer, spasmolytic, antidepressant, antibacterial, anti-hypertensive, anti-diabetic, anti-inflammatory, and anticancer properties. The antiparkinsonian activity of the most common flavonoids is depicted in Table 1.

Table 1. List of some flavonoids and their reported pharmacological activities in literature.

Chemical class	Compound	Antiparkinsonian activity	Reference
Flavones	Baicalein	Inhibits the formation of α -synuclein oligomers and prevents their fibrillation.	[127]
	Luteolin	Inhibits the inflammation mediators and modulates microglial activation.	[128]
	Apigenin		

	Nobiletin	Inhibits microglial activation and activates intracellular survival pathways, involved in neuronal survival and protection.	[129]
Flavonols	Tangeretin Quercetin	Increases striatal dopamine, neuronal survival, and antioxidant enzyme levels, suggesting its neuroprotective effects.	[130]
	Rutin Isoquercetin	Protects against neurotoxicity induced by 6-hydroxydopamine (6-OHDA)	[131], [132]
	Kaempferol	Exhibits antioxidant activity leading to improved motor function and increased dopamine levels. Protects against acute toxicity induced by rotenone and preserves striatal glutamatergic response in rat brain	[133]
Flavanones	Naringenin	Anti-apoptotic effects in animal models of PD Protects nigrostriatal projections from neurotoxicity induced by 6-OHDA	[134]
Isoflavones	Genistein	Protects dopaminergic neurons against neurotoxicity induced by lipopolysaccharides by inhibiting microglial activation.	[135]

Geiparvarin, a natural coumarin derivative isolated from *Geijera parviflora* has shown inhibitory effects on MAO-B. Several of its analogues have been prepared and evaluated as inhibitors of the two MAO isoforms, MAO-A and MAO-B. The 6-demethyl congener of Geiparvarin proved to be a potent and selective inhibitor of MAO-B. X-ray crystallography and molecular modelling studies helped to understand the observed structure-activity relationships [136].

Additionally, experimental studies on potential impact factors of PD have firmly established that the purine alkaloid, caffeine, the most consumed dietary factor, can exert not only neuroprotective effects but also improve motor and non-motor symptoms in PD [137]. These multiple benefits of caffeine in PD are supported by the convergence of epidemiological and animal evidence. At least six large prospective epidemiological studies have firmly established a relationship between increasing caffeine consumption and decreasing the risk of developing PD [138]. Furthermore, animal studies have also demonstrated that caffeine confers neuroprotection against dopaminergic neurodegeneration using Parkinsonian models induced by mitochondrial toxins such as MPTP [139]. Although caffeine has complex pharmacological profiles, studies in genetic knock-out mice have clearly revealed that caffeine's action is

mediated by the brain's AA_{2A}R and confers neuroprotection by modulating neuroinflammation, excitotoxicity, and mitochondrial function. Recent studies have highlighted new emerging mechanisms, including caffeine modulation of α -synuclein degradation with improved autophagy and caffeine modulation of gut microbiome and gut-brain axis in Parkinsonian models. Moreover, since the first clinical trial in 2003, the Food and Drug Administration (FDA) of the United States finally approved the clinical use of a caffeine derivative, Istradefylline, for the treatment of PD in September 2019 [140].

Moreover, curcumin, a polyphenolic compound isolated from the rhizomes of *Curcuma longa* has been studied for its neuroprotective effects in PD [141]. The turmeric rhizome contains a set of substances, curcuminoids, of which curcumin is the most abundant [142]. Chemically, these substances have marked antioxidant properties, as well as anti-inflammatory properties. In addition, curcumin has shown, in cell cultures, the ability to block the multiplication of several types of cancer cells. However, due to poor intestinal absorption, blood curcumin concentrations of the order used in these studies cannot be obtained orally. Studies have shown that a substance derived from pepper, piperine, significantly increases curcumin absorption. But it acts by increasing the overall permeability of the intestinal wall, which can be a source of health problems. More recently, new forms of turmeric have appeared, theoretically more absorbable by the intestine (nanoparticles, phospholipids). But there is a lack of clinical data on their efficacy and potential toxicity. It has been shown to have potent anti-inflammatory, antioxidant, limiting the production of free radicals, mitochondrial protection, and iron chelation effects. Curcumin is considered a promising therapeutic agent for the treatment of PD [141].

3 Overview of *Acinetobacter baumannii*

Infectious diseases pose a significant global health threat, exacerbated by the alarming rise of AMR among pathogenic microorganisms [143]. The emergence and rapid dissemination of MDR strains have rendered many conventional antibiotics ineffective, compromising our ability to combat these infectious agents effectively [144]. *A. baumannii*, a notorious gram-negative bacterium, has emerged as a major cause of nosocomial infections worldwide, particularly in intensive care units and among immunocompromised patients [145]. This bacterium belongs to the ESKAPE group of pathogens known for their ability to “escape” the effects of antibiotics due to multidrug resistance mechanisms [146]. The remarkable ability of *A. baumannii* to acquire resistance mechanisms against multiple classes of antibiotics, coupled with its ability to persist in harsh environments, has made it a formidable pathogen and a significant public health concern [146]. The increasing prevalence of MDR *A. baumannii* infections highlights the urgent need for the development of novel antimicrobial agents with distinct mechanisms of action to circumvent the existing resistance mechanisms [147]. Traditional antibiotic discovery approaches have struggled to keep pace with the rapid evolution of resistance, necessitating the exploration of alternative sources and strategies for identifying new antimicrobial leads [148]. NPs, with their structural diversity and unique biosynthetic origins, offer a rich reservoir for the discovery of novel antimicrobial compounds with innovative mechanisms of action [149].

3.1 History and epidemiology of *A. baumannii*

The history of *A. baumannii* dates to the early 20th century when it was first discovered by Dutch microbiologist Martinus Willem Beijerinck in 1911 [150]. Initially classified as a non-motile bacterium, it was later reclassified by Paul Baumann in 1968, who proposed the name *Acinetobacter* for the genus, as it could not be further sub-classified into different species. *A. baumannii* was initially susceptible to common antibiotics but has since evolved into a multidrug-resistant bacterium, capable of acquiring resistance genes [151]. One of the first antibiotic-resistant strains of *A. baumannii*, called carbapenem-resistant *A. baumannii* (CRAB), was isolated in 1991 (Figure 7) [151].

A. baumannii has become increasingly important as a nosocomial infection, affecting people with compromised immune systems. It is known to survive on artificial surfaces and resist desiccation, which allows it to remain and possibly infect new patients for some time [152], [153].

The escalating levels of AMR in *A. baumannii* have led to substantial morbidity and mortality rates in the USA, ranging from 26% to 68%, as documented by the Centers for Disease Control and Prevention (CDC). In Morocco, the epidemiology of *A. baumannii* infections has been a focus of research. A recent study examining antimicrobial resistance among Global Antimicrobial Resistance and Use Surveillance System (GLASS) pathogens in Morocco revealed that both *A. baumannii* and *Staphylococcus aureus* are prevalent opportunistic pathogens responsible for community and nosocomial infections in the country. Imipenem resistance in *A. baumannii* was reported to have a median rate of 74.5% in the context of antimicrobial resistance data in Morocco [154]. These findings emphasize the widespread presence of antimicrobial resistance in *A. baumannii* strains within the country, highlighting a significant public health concern regarding the management of infections caused by this pathogen.

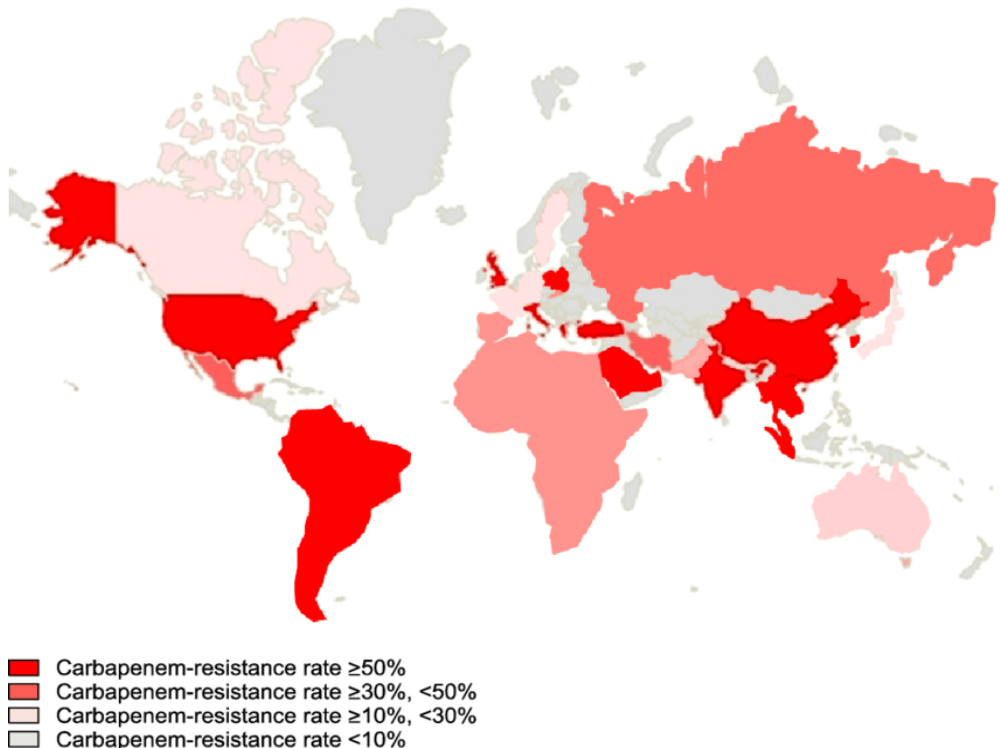


Figure 7. Global epidemiology of carbapenem-resistant *Acinetobacter* strains [155].

3.2 Virulence factors and pathogenesis of *A. baumannii*

A. baumannii is a highly adaptable and virulent pathogen that can cause a range of infections, including pneumonia, urinary tract infections, and bloodstream infections. Its ability to form biofilms on various surfaces, including medical devices and host cells, contributes to its persistence and resistance to antibiotics [156]. The following are the key virulence factors and mechanisms of *A. baumannii* (Figure 8).

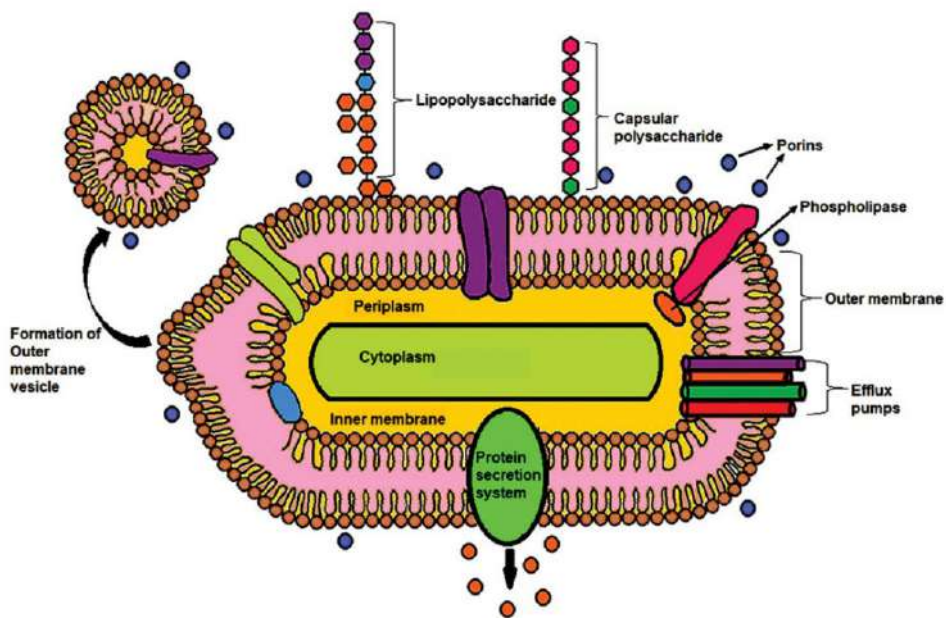


Figure 8. The key virulence factors in *A. baumannii* [157].

3.2.1 Outer membrane proteins

A. baumannii possesses a double membrane comprising an outer membrane (OM) and an inner membrane, providing protection and essential nutrients for viability. The OM serves as the primary interface between the bacterium and its external environment, acting as a barrier against the entry of various toxic molecules, including antibiotics, while facilitating the influx of necessary nutrients [158]. This membrane exhibits a unique lipid composition, with phospholipids predominantly in the inner leaflet and lipopolysaccharides (LPS) in the outer leaflet [159].

Integral to the OM are outer membrane proteins (OMPs), including OmpA, OmpW, and Omp33-36, which play pivotal roles in nutrient uptake, cell adhesion, signaling, and waste export [160]. Structurally, OMPs form closed toroidal structures composed of antiparallel β -barrel sheets spanning the lipid bilayer. These proteins are implicated in antimicrobial resistance and virulence, contributing to functions such as biofilm formation, cell invasion, and evasion of host defenses [159].

OmpA, a highly conserved OMP, is abundant in *A. baumannii* and is associated with various pathogenic traits, including biofilm formation, epithelial cell adhesion, invasion, and induction of apoptosis [161], [162]. Similarly, OmpW is involved in the transport of hydrophobic molecules across the OM and plays a role in iron homeostasis [163]. Omp33-36 induces apoptosis and modulates autophagy in human cells, affecting bacterial adherence, invasion, and cytotoxicity [164], [165].

Moreover, reduced expression of porins CarO and OprD-like has been linked to attenuated virulence in multidrug-resistant *A. baumannii* strains, highlighting the importance of these OMPs in pathogenesis [166]. While CarO is extensively characterized for its role in antimicrobial resistance, its contribution to virulence remains to be fully elucidated.

3.2.2 Capsular polysaccharides

Capsular polysaccharides in *A. baumannii* play a crucial role in antimicrobial resistance and are targeted for defensive passive immunization. Mutants lacking these polysaccharides show reduced intrinsic resistance to peptide antibiotics, while antibiotic exposure triggers their hyperproduction, leading to increased virulence in murine models [167]. The transcriptional upregulation of the K-locus gene, primarily regulated by the BfmRS two-component system, contributes to this hyperproduction [168], [169]. Specifically, bfmR aids in lung persistence during pneumonia, while bfmS is involved in biofilm formation, cell adherence, and resistance to serum [168]. While historically considered essential for OM stability, *A. baumannii* strains lacking lipopolysaccharides (LPS) have been identified, although defects in LPS biosynthesis clearly impact virulence [170]. LPS plays diverse roles, including in cell motility, adhesion, immune response stimulation, and resistance to antimicrobial agents and opsonophagocytic killing. Recent studies suggest that *A. baumannii* strains may form only lipooligosaccharides (LOS) instead of traditional LPS, with LOS lacking the O-antigen domain present in LPS [171], [172].

3.2.3 Phospholipase

Phospholipase, an enzyme involved in phospholipid metabolism, serves as a virulence factor in *A. baumannii* [173]. This enzyme exists in three classes: A, C, and D [173]. Phospholipase C enhances the bacterium's adhesion, invasion ability, and cytolytic activity [174]. Disruption of phospholipase D in *A. baumannii* results in decreased serum survival, reduced invasion of epithelial cells, and diminished pathogenesis in murine pneumonia models [175].

3.2.4 Biofilm formation

Biofilm formation in *A. baumannii* involves microorganisms embedded in a self-produced matrix, enabling survival in harsh conditions, hindering antibiotic effectiveness, and aiding immune evasion [176]. The process encompasses stages such as surface adhesion, quorum sensing (QS) for coordinated biofilm formation, and subsequent dispersion for colonization [177]. Key factors in biofilm formation include pilus formation, regulated by the BfmRS system, and the production of poly-beta-1,6-N-acetylglucosamine, crucial for biofilm integrity

and immune evasion [178]. The biofilm-associated protein Bap contributes to biofilm maturation and maintenance [179].

3.2.5 Quorum-sensing

QS is a bacterial communication system crucial for coordinating various biological processes and regulating virulence factors like surface motility and biofilm formation [180]. Recent research suggests that QS in *A. baumannii* may influence the development of secondary bacteremia in pneumonia patients [181]. QS involves the production of small diffusible signaling molecules, such as acyl-homoserine lactones (AHLs) [182]. Once a threshold concentration of AHLs is reached, these molecules bind to their receptors, initiating molecular cascades mediated by transcriptional activators like AbaR [183]. This leads to the synthesis of more AHL molecules by the AHL-synthase AbaI, facilitating bacterial survival and proliferation [183].

3.2.6 Metal acquisition system

Many aerobic bacteria, including *A. baumannii*, combat iron limitation in their environment by producing siderophores – high-affinity molecules that scavenge iron [184]. Acinetobactin, a key siderophore produced by *A. baumannii*, plays a critical role in pathogenesis; it functions as a virulence factor by facilitating bacterial survival within epithelial cells, contributing to cellular damage, and increasing mortality in infection models [185]. Beyond acinetobactin, other metal acquisition systems also contribute to *A. baumannii*'s virulence [186], [187]. These include the NfuA Fe-S scaffold protein, mechanisms to sequester iron from the host protein calprotectin, and the ZnuABC zinc acquisition system [186], [188].

3.2.7 Outer membrane vesicles

Outer membrane vesicles (OMVs) are spherical nanovesicles released by the outer membrane of different Gram-negative pathogenic bacteria [189]. They consist of components such as LPS, OMPs, phospholipids, and nucleic acids [190]. OMVs serve as vehicles for transporting virulence factors like OmpA, contributing to biofilm formation, and potentially participating in QS and the transfer of antimicrobial resistance genes [191].

3.2.8 Protein secretion systems

A. baumannii utilizes multiple protein secretion systems to mediate its virulence. Notably, the type II secretion system (T2SS), type VI secretion system (T6SS), and type V autotransporter Ata have been implicated in this pathogen's pathogenicity [156]. The T2SS is responsible for translocating various proteins, including lipases and proteases, from the periplasmic space to

the outer membrane or extracellular environment [192]. Its functionality is essential for full virulence in *A. baumannii*. Conversely, the T6SS acts as a secretion machine to inject effector proteins, aiding in bacterial competition or enhancing colonization during host infection [193]. *A. baumannii* utilizes its T6SS for bacterial competition, albeit in a strain-specific manner. Finally, the type V autotransporter Ata is a membrane protein involved in biofilm formation, adherence to extracellular matrix, and in vivo virulence [194]

3.3 Clinical impact of *A. baumannii* infections

The clinical impact of *A. baumannii* infections is significant, particularly in healthcare settings. *A. baumannii* infections, especially those caused by MDR strains, have been associated with substantial mortality rates, high hospital costs, and increased morbidity in vulnerable patients [195]. The most common clinical manifestations of *A. baumannii* infections include pneumonia and bacteremia. Infections due to MDR *A. baumannii*, particularly carbapenem-resistant strains, pose a serious challenge in healthcare settings due to their association with high mortality rates and limited treatment options [195].

The risk factors for acquiring multidrug-resistant *A. baumannii* isolates include recent exposure to antimicrobial agents, the use of invasive devices like catheters, severity of illness, prolonged hospital stays, and recent surgeries [196]. The transmission of *A. baumannii* can occur through contaminated hospital surfaces, medical equipment, and close contact between affected patients or colonizers [195]. Additionally, *A. baumannii* can be part of the normal skin microbiota, with a significant percentage of healthy individuals being colonized by it [195].

3.3.1 Most frequent clinical manifestations

Acinetobacter's ability to colonize various human epithelial surfaces allows it to be found in a wide range of biological samples, including respiratory secretions, wound surfaces, and urine. However, the presence of *Acinetobacter* in these samples does not always indicate an active infection. In a multicenter cohort study in Spain involving 221 clinical isolates of *Acinetobacter*, only 52.9% of isolates were found to be causative agents of infection, while the rest were considered colonization [197]. *Acinetobacter* infections can affect any system or organ in the body, particularly in individuals undergoing invasive procedures that disrupt natural defense barriers. Although community-acquired infections by *Acinetobacter* have been reported, the majority are healthcare-associated, predominantly occurring in intensive care units [198]. The most common infections caused by *Acinetobacter* include respiratory tract infections, bacteremia, urinary tract infections, surgical wound infections, and postsurgical

meningitis [197]. This study primarily focuses on ventilator-associated pneumonia (VAP), the most prevalent infection caused by *Acinetobacter*, along with the associated bacteremia [198].

3.3.1.1 Respiratory infections

Respiratory tract infections, particularly pneumonia and tracheobronchitis, are among the most common nosocomial infections caused by *A. baumannii* [199]. In regions where *A. baumannii* is prevalent, it is often the primary pathogen isolated from patients with hospital-acquired pneumonia (HAP), accounting for over 36% of cases in Asia [200]. However, in some countries, it is responsible for a smaller proportion, ranging from 1% to 2% of nosocomial pneumonia cases [201]. Risk factors for nosocomial pneumonia caused by *A. baumannii* include orotracheal intubation, tracheostomy, prior antibiotic therapy, prolonged intensive care unit (ICU) stays, recent surgery, underlying chronic lung disease, and aspiration of secretions [201]. These infections typically involve multiple lobes and can lead to complications such as parapneumonic pleural effusion, cavitation, and bronchopleural fistula. Additionally, approximately 12% of cases are accompanied by bacteremia, with pneumonia being the most common clinical focus [202]. Tracheobronchitis due to *A. baumannii* is also prevalent in the nosocomial setting, particularly among ventilated patients. While the diagnostic criteria for tracheobronchitis are not universally agreed upon, its clinical impact often leads to the development of pneumonia [203].

3.3.1.2 Bacteremia

Bacteremia, the second most common nosocomial infection caused by *A. baumannii*, often manifests with pneumonia as the primary clinical focus, followed by intravenous catheters [204]. Less common origins include urinary tract, skin and soft tissue infections, nosocomial meningitis, or intra-abdominal infections. Additionally, the source of bacteremia remains unknown in up to 44% of cases. *A. baumannii* is responsible for over 12% of hospital-acquired bloodstream infections (BSI) in ICUs globally, with varying prevalence across different regions [205]. Patients at high risk for *A. baumannii* bacteremia include those admitted to ICUs, especially those with a Charlson comorbidity index > 3 , previous hospitalizations, total parenteral nutrition, chemotherapy, or recent antibiotic therapy, particularly β -lactams or carbapenems [206]. The presence of invasive devices or procedures such as mechanical ventilation, intravascular catheters, bladder catheters, or nasogastric tubes are significant risk factors for *A. baumannii* bacteremia [207].

3.3.2 The challenge of antimicrobial resistance

A. baumannii presents a diverse array of resistance mechanisms against antimicrobial agents, leading to strains highly resilient to most clinically available antibiotics [14]. Alarmingly, certain European nations have reported that over half of *Acinetobacter spp.* isolates exhibit resistance to all monitored antimicrobial categories, including carbapenems, fluoroquinolones, and aminoglycosides [208]. In response to this urgent need, Tacconelli et al. (2017) compiled a catalog of antibiotic-resistant “priority pathogens”, highlighting 12 bacterial families posing the most substantial threat to human health and demanding immediate development of novel antibiotics [209]. Within this framework, CRAB is designated as “priority 1” [209].

3.3.2.1 Carbapenem resistance in *A. baumannii*

Carbapenems have long been considered the primary treatment for infections caused by MDR *A. baumannii*. However, there has been a concerning rise in carbapenem resistance among *A. baumannii* isolates, particularly associated with prior carbapenem use. A global study spanning from 2005 to 2009, involving 5127 *Acinetobacter spp.* isolates from 140 hospitals across 32 countries, revealed an overall nonsusceptibility rate to imipenem and meropenem of 45.9% and 48.2%, respectively. Notably, there was a significant increase in nonsusceptibility percentages from 27.8% and 37.5% (for imipenem and meropenem, respectively) in 2005 to 62.4% and 64.4% in 2009 [210]. Additionally, data from six countries collecting resistance data in 2009, particularly from microorganisms associated with ICU-acquired infections, reported CRAB isolates at rates of up to 80% [211]. More recently, a study based on the Magic Bullet clinical trial found that 97% of *A. baumannii* isolates collected from patients in Greece, Italy, and Spain between 2012 and 2015 were resistant to imipenem, with the resistance always associated with acquired carbapenemases, such as OXA-23 (80%), OXA-24/40 (4.6%), OXA-58 (1.5%), or OXA-23/58 (1.5%) [212].

Carbapenem resistance in *A. baumannii* is primarily mediated by synergistic mechanisms, including the production of antimicrobial-degrading enzymes, efflux pumps, and porin mutations [213]. Enzymatic degradation by carbapenemases, notably carbapenem-hydrolyzing class D β -lactamases (CHDLs) such as OXA-type enzymes, along with class B β -lactamases and class A β -lactamase KPC, is the most prevalent mechanism [214]. Additionally, overexpression of efflux pumps, particularly AdeABC, reduces antibiotic accumulation [215], [216], [217]. *A. baumannii*'s inherent lower number and size of porins, such as CarO, contribute to OM impermeability, further reducing antibiotic penetration. Reduced expression of porins

like CarO and Omp33-36 diminishes antibiotic entry, aiding in carbapenem resistance [218], [219].

3.3.2.2 Colistin resistance in *A. baumannii*

Colistin resistance in *A. baumannii* is a growing concern due to the increasing prevalence of multidrug-resistant strains. A meta-analysis found a low prevalence of colistin resistance among *A. baumannii* isolates worldwide from 2000 to 2023, with an increase from 2% (95% CI 1–4%) in 2009 to 6% (95% CI 3–11%) in 2023 1. The highest rates of resistance were found in western Europe (7%) and South America (6%) [220]. The LPS loss or its modification is more commonly associated with colistin resistance 3. Previous colistin treatment is a primary risk factor for colistin-resistant *A. baumannii* colonization and infection [170], [220].

The molecular characterization of colistin-resistant *A. baumannii* strains has shown that all strains belonged to PFGE-A, ST-281, and had a very similar acquired resistome, indicating that colistin resistance emerges in clinical settings from colistin susceptible strains [221]. The transcriptome plays a role in bacterial physiology and antimicrobial resistance mechanisms, and some publications have described the transcriptome contribution in the colistin resistance mechanism [221]. Intrinsic colistin tolerance mechanisms are also associated with more than 30 genes mainly associated with LPS biosynthesis and regulation [170]. Higher levels of RamA cause LPS modulations and hence increased colistin resistance [221]. The loss of LPS results in colistin resistance in *A. baumannii* [170].

3.4 Treatment of *A. baumannii* infections

Carbapenems have been the primary treatment for infections caused by MDR *A. baumannii* since their discovery in 1985 [222]. However, widespread use of these drugs has led to the rapid emergence of resistant strains worldwide. This escalating antimicrobial resistance has outpaced the development of new antibiotics, prompting the implementation of antimicrobial stewardship programs such as the Antibiotic Stewardship Toolkit designed by the CDC [223]. Additionally, there's been a resurgence of old antibiotics, either alone or in combination, and increased focus on exploring new therapeutic strategies to address infections caused by MDR *A. baumannii* strains.

3.4.1 Current treatment and drugs

3.4.1.1 Carbapenems

Carbapenems (imipenem, meropenem, and doripenem) remain the preferred treatment for multidrug-resistant (MDR) *A. baumannii* when the bacteria remain susceptible [224]. To

maximize their effectiveness, prolonged infusion strategies are often used to optimize the time the antibiotic concentration remains above the minimum inhibitory concentration (MIC) [225]. Imipenem shows strong *in vitro* activity against *A. baumannii*, while meropenem is preferred due to its stability in extended infusion and lower seizure risk [226]. However, rising meropenem MICs decrease the likelihood of optimal pharmacokinetic/pharmacodynamic (PK/PD) index attainment, necessitating combination therapy [227]. Doripenem offers a potential alternative for strains resistant to imipenem, but clinical experience remains limited. Therefore, empirical carbapenem use, especially in monotherapy, is not recommended for severe infections in areas with high carbapenem resistance rates [228].

3.4.1.2 Polymyxins

Polymyxin B and colistin (polymyxin E) are the only polymyxins commonly used in clinical practice, with colistin being the most extensively utilized [229]. Initially overshadowed due to reports of nephrotoxicity and neurotoxicity, colistin has re-emerged as a last-resort treatment for multidrug-resistant Gram-negative pathogens [230]. However, the emergence of colistin-resistant strains, including hetero-resistant isolates, is concerning, necessitating a cautious approach to its use [231]. Genetic alterations in the PmrAB two-component system and lipid A biosynthesis genes were initially linked to colistin resistance, but recent studies have identified plasmid-mediated resistance genes in *A. baumannii* isolates from various regions [232]. Despite advancements in understanding colistin's pharmacokinetics, challenges persist in establishing optimal dosing regimens and specific guidelines due to a lack of standardized dose units and pharmacodynamic studies. The area under the curve (AUC)/MIC ratio is considered the best indicator of colistin efficacy, with plasma concentrations of approximately 2 µg/mL recommended for effectiveness against susceptible *A. baumannii* [233]. Higher doses of colistin have been adopted to overcome resistance, but definitive consensus on dosing remains elusive [234]. While studies suggest potential benefits of high-dose colistin, its empirical use may not always be warranted, especially considering its comparable efficacy but higher nephrotoxicity compared to other antibiotics in certain contexts [235]. Further research is needed to explore higher doses of colistin and their impact on efficacy and toxicity, particularly in critically ill patients.

3.4.1.3 Tetracyclines

Minocycline, doxycycline, and tigecycline exhibit both *in vitro* and *in vivo* activity against *A. baumannii*, including CRAB, and MDR strains [236], [237], [238]. These antibiotics can show synergistic effects when combined with other antimicrobials. Minocycline, with its existing

intravenous formulation, has demonstrated promising clinical success rates and tolerability in treating MDR or CRAB infections [239]. Similarly, doxycycline has been used successfully to treat ventilator-associated pneumonia (VAP) caused by MDR *A. baumannii* [240]. Tigecycline, a newer tetracycline derivative, also offers a valuable option for treating multidrug-resistant infections due to its activity against strains resistant to other classes of antibiotics [241].

3.4.1.4 Combination therapy

Combination therapy is a common approach in treating *A. baumannii* infections, particularly when dealing with MDR strains [242]. The rationale behind using multiple antibiotics is to exploit the synergistic effect of different classes and improve treatment outcomes. However, most data regarding antimicrobial combinations are based on *in vitro* or animal studies, raising doubts about their translation into clinical practice [243]. Even identical antimicrobial combinations have shown varying results, further complicating their clinical application [243], [244]. One study found that colistin-based combination therapy, such as colistin and carbapenem or colistin and tigecycline, did not significantly improve overall clinical response, ICU mortality, length of stay, or nephrotoxicity compared to colistin alone [245], [246]. However, the colistin-based combination therapy was shown to increase the microbiological response [247], [248]. Another study evaluated the synergistic effects of sulbactam in combination with ampicillin, carbapenem, or cefoperazone against *A. baumannii* species and found a synergistic effect when sulbactam was combined with ampicillin, carbapenem, or cefoperazone [249], [250]. *In vitro* studies have shown synergistic effects between tigecycline and sulbactam, but no synergistic interaction was observed with ciprofloxacin [251]. However, there was a small antagonistic effect (6.66% (2/30)) when sulbactam was combined with colistin, which prompted a reconsideration of the usefulness of this combination [251].

A systematic review and meta-analysis of 12 controlled studies found no compelling evidence to suggest that combination therapy of polymyxins is superior to monotherapy [246]. Consequently, many experts advocate for further research to elucidate the potential benefits and drawbacks of combination therapy for *A. baumannii* infections [245].

3.4.2 Novel and future treatment options

3.4.2.1 New antibiotics

New antibiotics against *A. baumannii* are being developed to combat the increasing resistance to traditional antibiotics. Some of these new antibiotics and their mechanisms of action include:

- **Eravacycline:** Eravacycline is a novel aminomethylcycline antibiotic that has shown activity against *A. baumannii*, including strains with carbapenem resistance [252], [253]
- **Cefiderocol:** Cefiderocol is a siderophore cephalosporin that has shown activity against *A. baumannii*, including strains with carbapenem resistance [254], [255]
- **Beta-lactamase inhibitors:** These agents, such as avibactam and vaborbactam, are used in combination with beta-lactam antibiotics to inhibit beta-lactamase enzymes produced by *A. baumannii*, thereby increasing the effectiveness of the antibiotics [256], [257].
- **Lipopeptides:** Lipopeptides, such as daptomycin, have shown activity against *A. baumannii*, although their clinical use is limited due to the development of resistance [258].

The mechanism of action for these new antibiotics varies, including targeting bacterial cell walls, inhibiting protein synthesis, and disrupting bacterial membranes. The development of these new antibiotics is crucial in the fight against antibiotic resistance in *A. baumannii* infections.

3.4.2.2 Anti-virulence drugs

There exists a wide range of factors contributing to the pathogenesis of *A. baumannii*, suggesting that targeting these mechanisms could be a viable strategy for novel antimicrobial agents [259]. By inhibiting the virulence factors of *A. baumannii*, we could potentially reduce its pathogenicity and revert it to its previous role as an opportunistic and seldom pathogenic bacterium. Since this approach does not rely on bactericidal action, the emergence of new resistant strains may not pose a limitation [260]. Combining this strategy with traditional antimicrobial agents could allow for a potent combination. Experimental findings demonstrating the effectiveness of drugs capable of blocking virulence factors, known as “anti-virulence drugs”, are promising, as are the potential benefits of non-antimicrobial approaches. However, careful consideration and further extensive studies are necessary to fully understand the potential use of these new molecules as therapeutic alternatives [261].

3.4.2.2.1 OMPs inhibitors

Many Gram-negative pathogens, including *A. baumannii*, exploit the externally exposed loops of certain OMPs to interact with hosts, induce virulence factors, invade tissues, and evade the immune system through mutation [262], [263], [264]. Consequently, targeting OMPs has emerged as a promising strategy against such pathogens. Specifically, OmpA and OmpW have been identified as potential drug targets. Research efforts have led to the development of OmpA inhibitors like the cyclic hexapeptide AOA-2, which demonstrated efficacy in inhibiting

bacterial adherence to host cells, reducing host cell death, and inhibiting biofilm formation [265]. *In vivo* studies showed significant reductions in bacterial concentrations and mortality in *A. baumannii* infections, particularly when used in combination with colistin [266]. Similarly, novel inhibitors targeting *A. baumannii* OmpW were developed using *in silico* screening, resulting in promising antibacterial activity against various clinical isolates of *A. baumannii* strains for several compounds. These findings suggest that targeting OMPs could offer new avenues for combating *A. baumannii* infections [267].

3.4.2.2.2 LPS synthesis inhibitors

Another potential treatment approach for *A. baumannii* infections involves inhibiting the bacterial synthesis of LPS by blocking *lpx* genes [268]. LpxC inhibition, achieved by compounds like LpxC-1, effectively disrupts LPS biosynthesis, preventing *A. baumannii* from triggering sepsis and enhancing bacterial killing by the immune system. Studies have shown that LpxC-1 can provide complete protection against lethal infections in mice without inducing cross-resistance [269]. Additionally, the development of novel LpxC inhibitors, such as LpxC-4, has shown promise as potent broad-spectrum agents with low rates of spontaneous resistance emergence. Furthermore, recent advancements in understanding the structures of LpxA and LpxD pave the way for exploring them as potential targets for new antibacterial agents [270], [271].

3.4.2.2.3 Biofilm formation inhibitors

Numerous strategies have been explored to inhibit biofilm formation by *A. baumannii*. These include using garlic ointment and gaseous nitric oxide to prevent biofilm formation in wounds, as well as employing DispersinB, an antibiofilm enzyme, either alone or in combination with the KSL-W antimicrobial peptide, to disperse preformed biofilms and inhibit their formation in chronic wound infections [272], [273], [274]. Additionally, a 2-aminoimidazole compound has been developed to target BfmR, a regulator involved in biofilm development, while a potent anti-biofilm peptide inhibits biofilm formation and eradicates preformed biofilms by blocking guanosine pentaphosphate (pppGpp) and tetraphosphate (ppGpp), a crucial signal in biofilm development [275], [276]. Furthermore, chimeric peptides have been found to prevent biofilm formation by *A. baumannii* clinical isolates, exhibiting significant antibacterial effects superior to several conventional antibiotics [277].

3.4.2.2.4 QS inhibitors

The interception of QS has emerged as a promising strategy for combating bacterial infections, including those caused by *A. baumannii* [182], [261]. QS, which controls virulence in many

bacterial pathogens, involves the use of signal molecules like AHLs and receptors like AbaR [261]. To disrupt QS in *A. baumannii*, various compounds have been developed to block the AbaR receptor. These compounds, including non-native AHLs and unsaturated fatty acids, have shown potent antagonistic effects against AbaR, leading to reduced motility and biofilm formation in *A. baumannii* [278], [279].

3.4.2.2.5 Iron chelators

Iron plays a crucial role as a cofactor in various bacterial processes, prompting exploration into iron chelators and competitors as potential alternatives or supplements to antibiotics. Several iron chelators such as deferoxamine, deferiprone, Apo6619, VK28 dihydrochloride, and 2,2'-dipyridyl (DIP) have been developed, with varying degrees of effectiveness against *A. baumannii*. Among them, DIP exhibited the highest antibacterial activity, albeit dependent on the growth medium used [280]. In terms of iron competitors, gallium (Ga^{+3}) has been extensively studied for its potential against *A. baumannii*. Gallium, possessing similar properties to iron (Fe^{+3}), competes for binding to iron-requiring enzymes and proteins. This competition inhibits bacterial components essential for growth, as gallium lacks the ability to undergo oxidation-reduction cycles [281]. Promising results from *in vitro* and *in vivo* studies have been reported, particularly when gallium is used alone or in combination with colistin against *A. baumannii* isolates [282], [283]. However, like iron chelators, the effectiveness of gallium treatment depends on the growth medium used [282].

3.4.2.2.6 Repurposed drugs

Drug repurposing as an alternative strategy to treat MDR *A. baumannii* infections is gaining traction due to several advantages. These drugs already have extensive pharmacological data from preclinical and clinical trials, which can expedite their evaluation for new therapeutic application. Several studies have identified non-antibiotic compounds that can inhibit the growth of MDR *A. baumannii* strains. For example, a drug repurposing screen using a bacterial growth assay led to the identification and confirmation of 43 active compounds, including seven approved drugs or pharmacologically active compounds for non-antimicrobial indications [284]. These drugs, such as 5-fluorouracil, fluspirilene, and Bay 11-7082, can resensitize MDR *A. baumannii* strains to antibiotics like azithromycin and colistin in a two-drug combination format [284]. Tamoxifen, a drug originally developed for the treatment of breast cancer, has shown potential in combating infections caused by MDR *A. baumannii*. The drug has been found to increase survival and decrease bacterial burden in animal models of infection with MDR *A. baumannii*, *Pseudomonas aeruginosa*, and *Escherichia coli* [285]. Other drug families,

including anthelmintics, antifungals, anti-inflammatory/immunomodulatory drugs, and statins, have been explored as potential candidates [286], [287], [288], [289]. Although preclinical studies have shown promising results, further safety testing in a broader human population is necessary before repurposed drugs can be clinically used to combat infections caused by MDR *A. baumannii* [290].

3.5 Natural products in treating *A. baumannii* infections

The increasing resistance of *A. baumannii* to various antibiotics has led researchers to explore alternative therapeutic options, including NPs like medicinal plants, honey, or bee propolis [291], [292]. These NPs are being investigated as potential sources of antimicrobial agents due to their diverse chemical structures, which may offer unique mechanisms of action against resistant bacteria. Additionally, NPs may have fewer side effects compared to traditional antibiotics and align with a more natural approach to medicine. For instance, a study found that Lebanese herbal compounds, such as thymol, carvacrol, and eugenol, have potential *in silico* activity against CRAB [293]. Additionally, herbal compounds like tannic acid and ellagic acid have been shown to enhance the activity of rifampicin, coumermycin, fusidic acid, novobiocin, and chlorobiocin against *A. baumannii* [294]. A comprehensive list of bioactive compounds and their plant sources is presented in Table 2.

Table 2. List of bioactive NPs against *A. baumannii* (modified from [294]).

Compound	Source	Antibacterial assay method	MIC ($\mu\text{g/mL}$)	References
Hexahydroxy diphenoyl ester vescalagin	<i>Lythrum salicaria</i>	Agar well diffusion test	n/a	[295], [296]
Ellagic acid	<i>Rosa rugosa</i>	MIC, MBC	250	[297]
Terchebulin	<i>Terminalia chebula</i>	MIC, MBC	500	[297]
Chebulagic acid			1000	
Chebulinic acid			62.5	
Corilagin			1000	
Norwogonin	<i>Scutellaria baicalensis</i>	MIC, MBC	128	[298]
Eugenol	<i>Syzygium aromaticum</i>	MIC, CFU	1250	[299]
Trans-cinnamaldehyde	<i>Cinnamomum zeylanicum</i>	MIC, CFU	310	[300]
Carvacrol	<i>Oreganum vulgare</i>	MIC, CFU	310	[301]
Thymol	<i>Thymus</i>	CFU	n/a	[302]

Overview of *Acinetobacter baumannii*

Epigallocatechin gallate	<i>Camellia sinensis</i>	MIC, time kill assay, FIC index, CFU	312–625	[303]
Epicatechin	<i>Camellia sinensis</i>	Disk diffusion assay	n/a	[303]
α -elemene, δ -elemene, furanosesquiterpenes	<i>Commiphora molmol</i>	Disk diffusion assay, CFU, MIC	2500	[304]
p-Coumaric acid, ascorbic acid, pyrocatechol, cinnamic acid	<i>Aloe vera</i>	Agar well diffusion technique	n/a	[305]
Allyl methyl disulfide, Diallylsulfide, Diallyltrimulfide, Allyl methyl trisulfide, Diallyldisulfide, Diallyltetrasulfide	<i>Allium sativum</i>	MIC	3120	[306]

4 Computational methods in drug discovery

4.1 Overview of the drug discovery process

The drug discovery process is a multifaceted journey that typically consists of several key stages. It often begins with a pre-discovery phase, where basic research is conducted to understand the mechanisms underlying diseases and identify potential targets, such as proteins [307]. Subsequently, the drug discovery stage involves the search for molecules, with a focus on small compounds that can modulate these targets. This process can involve the use of computer-aided drug design (CADD) approaches to identify and optimize potential drug candidates. CADD encompasses a range of theoretical and computational methods that are part of modern drug discovery, including structure-based drug design (SBDD) and ligand-based drug design (LBDD). These approaches employ mathematical tools and software packages to manipulate and quantify the properties of potential drug candidates, enabling the analysis of macromolecular structures and the prediction of their properties [308], [309]. CADD has become an indispensable part of drug discovery, offering faster and more efficient drug design, a higher chance of success for improving drug efficacy, and a reduction in experimental costs [310]. The drug discovery process is a lengthy and rigorous endeavor, typically taking 10-15 years for a new drug to be approved. Throughout this process, various stages, such as target discovery, lead compound identification, and preclinical and clinical research, are undertaken to ensure the safety and effectiveness of potential drug candidates (Figure 9). The application of CADD in drug discovery has become increasingly important, offering valuable insights and guidance in the identification, optimization, and evaluation of potential drug candidates.

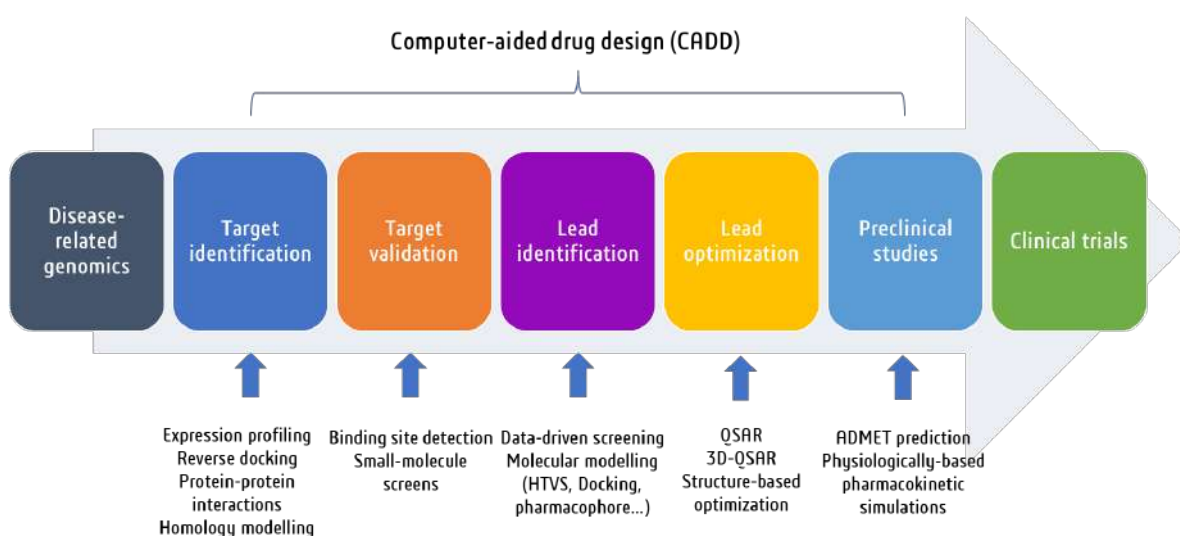


Figure 9. An overview of the main steps involved in the drug discovery process.

4.2 Cheminformatics in drug discovery

Cheminformatics emerged as an active field in the 1970s, initially in academia and later adopted by the pharmaceutical industry. The term was formally defined for drug discovery applications by F.K. Brown in 1998 [311]. It is an interdisciplinary field combining chemistry, computer science, and information science principles to solve chemical problems. Cheminformatics plays a pivotal role in drug discovery by aiding the design of compound libraries, chemical data storage, virtual screening, and quantitative structure-activity relationship (QSAR) modelling [312]. Data-driven drug discovery is an approach within cheminformatics that relies on analyzing large datasets to identify new therapeutic targets, optimize drug candidates, and improve drug discovery efficiency. It employs advanced computational techniques like ML and deep learning (DL) algorithms, and cheminformatics tools to process and extract insights from diverse data sources. This data-driven analysis aims to uncover intricate relationships between compound activity and chemical information, guiding and accelerating drug discovery efforts that would be challenging to achieve through traditional methods alone.

4.2.1 Quantitative structure-activity relationships

QSAR is the process by which a chemical structure is correlated with a well-determined effect, such as biological activity or pharmacokinetic property [313]. Thus, biological activity can be expressed quantitatively, such as the concentration of a substance required to achieve a certain biological response. Additionally, when physical and chemical properties or structures are expressed numerically, a mathematical relationship, or quantitative structure-activity relationship, can be proposed between them [313]. The mathematical expression obtained can then be used as a predictive means of the biological response for similar structures. QSAR models are constructed using ML algorithms, such as neural networks or decision trees (Figure 10). These algorithms are trained on known molecule data with measured biological activities, to predict the biological activity of new molecules [314]. QSAR models are often used in combination with other techniques, such as molecular modelling, to achieve better prediction accuracy. They can also be used to identify patterns in the data that can be used to understand the underlying mechanisms of biological activity. QSAR models are very useful for saving time and money by allowing for the prediction of biological activity of molecules before they are synthesized and tested *in vitro* or *in vivo*. However, they also have limitations and cannot always predict biological activity with high accuracy. Therefore, they should be used with caution and in combination with other techniques to achieve accurate results.

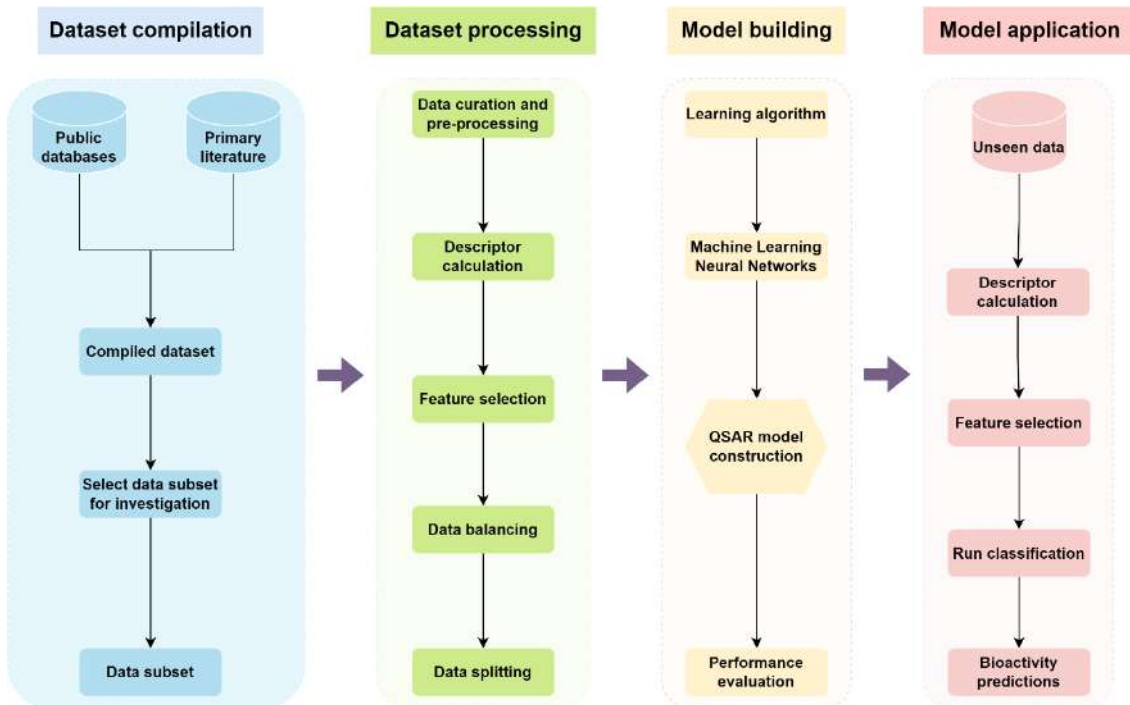


Figure 10. Schematic representation of the QSAR modelling workflow [315].

4.2.2 Chemical bioactivity databases

Chemical bioactivity databases such as ChEMBL, BindingDB, PubChem Bioassays, PDBbind, and BRENDA Enzyme Database play a crucial role in modern chemical biology research (Table 3). These databases contain curated data on experimental bioactive molecules including their chemical structures, bioactivity data (such as K_i , K_d , IC_{50} , % of inhibition, and EC_{50}), and interactions with macromolecules such as proteins and enzymes. These databases facilitate data-driven drug discovery approaches, such as applying ML methodologies to identify relationships in large datasets.

Table 3. List of popular open access chemical bioactivity databases used in drug discovery.

Database	Advantages	Number of bioactivities	Website
ChEMBL	<ul style="list-style-type: none"> - Manually curated database of bioactive molecules ensuring high quality data - Comprehensive chemical and bioactivity data - Advanced filtering and analysis options 	>2.4 million compounds and >20 million activities	https://www.ebi.ac.uk/chembl/
BindingDB	<ul style="list-style-type: none"> - Offers a public repository of experimental binding affinity data for protein-ligand interactions - Provides virtual screening tools to predict targets and identify potential drug candidates - Supports programmatic access and data downloads for integration into research workflows 	>1 million binding data points for >2,500 protein targets and ~500,000 small molecules	https://www.bindingdb.org/

PubChem Bioassays	<ul style="list-style-type: none"> - Vast repository of chemical and biological data, including structures, bioactivities, and screening results - Search for molecules flexibly using names, SMILES codes, or chemical structures - Integrated analysis tools for exploring data patterns and relationships 	<ul style="list-style-type: none"> >1.5 million assay records, >115 million compounds and >290 million bioactivity data points 	https://pubchem.ncbi.nlm.nih.gov/
PDBbind	<ul style="list-style-type: none"> - Provides experimentally measured binding affinity data for protein-ligand complexes - Links energetic and structural information for detailed analysis of protein-ligand interactions - Requires free registration for full access to database, ensuring data security and access control 	Binding affinities for 23,496 biomolecular complexes in PDB, including protein-ligand (19,443), protein-protein (2,852), protein-nucleic acid (1,052), and nucleic acid-ligand complexes (149)	http://www.pdbbind.org.cn/
BRENDA Enzyme Database	<ul style="list-style-type: none"> - Database focused on enzyme functions, providing comprehensive information on enzyme nomenclature, reactions, specificity, structure, and references - Offers data directly from primary literature, ensuring reliable and up-to-date information 	<ul style="list-style-type: none"> >330,000 enzyme synonyms, and >295,000 inhibitors, and >22,000 reactions 	https://www.brenda-enzymes.org/

4.2.3 Molecular representations

The technological progress of the last century, marked by the computer revolution and the advent of high-throughput screening technologies in drug discovery, paved the way for computer analysis and visualization of bioactive molecules. To achieve this, it became necessary to represent molecules in a syntax that is readable by computers and understandable by scientists from various disciplines. Many chemical representations have been developed over the years, the number of which is due to the rapid development of computers and the complexity of producing a representation that encompasses all structural and chemical characteristics.

4.2.3.1 Graph representation

A molecular graph representation is a mapping of the atoms and bonds that make up a molecule into sets of nodes and edges. Typically, nodes are represented by circles or spheres, and edges by lines (Figure 11). In molecular graph representations, nodes are often represented using letters indicating the type of atom (like in the periodic table), or simply as the intersections of bonds (for carbon atoms) [316]. Formally, a molecular graph representation is a 2D object that can be used to represent 3D information (such as atomic coordinates, bond angles, and chirality). However, all spatial relationships between nodes must be encoded as node and/or edge attributes, as nodes in a graph (the mathematical object) do not formally have spatial

positions, only pairwise relationships [317]. Both 2D and 3D representations of graphs can be easily visualized using various software programs, including UCSF Chimera, Avogadro, PyMOL, and VMD [318]

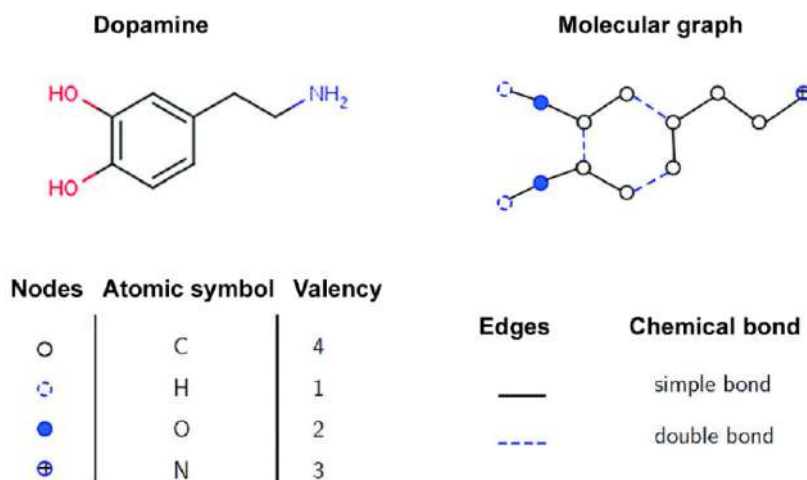


Figure 11. Dopamine and its molecular graph. Different types of nodes according to atomic elements and different types of edges depending on the chemical bond in the molecule [319].

4.2.3.2 SMILES format

SMILES (Simplified Molecular Input Line Entry Specification) is a line notation language used to represent chemical structures as a string of ASCII characters (Figure 12). The language is designed to be simple, compact, and machine-readable, making it ideal for use in computer databases and for representing structures in computer programs [320]. SMILES can be used to store and analyze large amounts of molecular data, such as information about the structure of potential drug candidates. Additionally, SMILES can be used in conjunction with molecular modelling software to generate 2D and 3D representations of molecules, allowing researchers to perform molecular docking studies. These simulations can provide valuable information about the physical properties of potential drug candidates, such as their binding affinity, solubility, and stability [321].

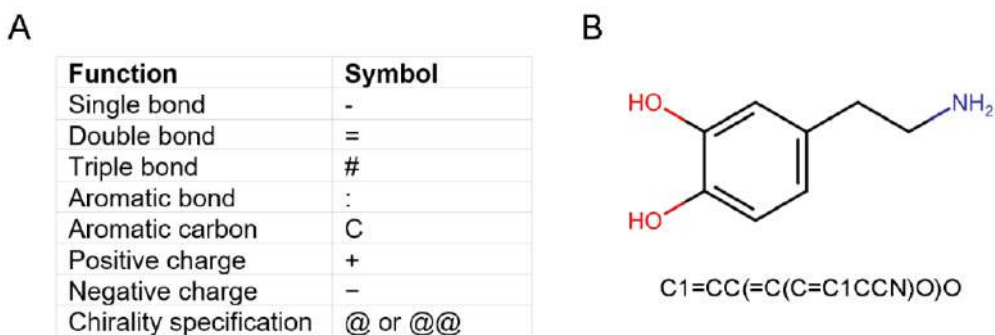


Figure 12. A) Function and symbol of each ASCII character used in SMILES representation. B) 2D chemical structure and SMILES representation of DA.

4.2.3.3 SMARTS format

SMARTS (SMILES arbitrary target specification) is a language used in cheminformatics to specify substructures in molecules. It is an extension of SMILES and allows for flexible and efficient substructure-search specifications in terms that are meaningful (Figure 13). SMARTS uses atomic and bond symbols to specify a graph, and the labels for the graph's nodes and edges are used to say what type of atom each node represents and what type of bond each edge represents [322].

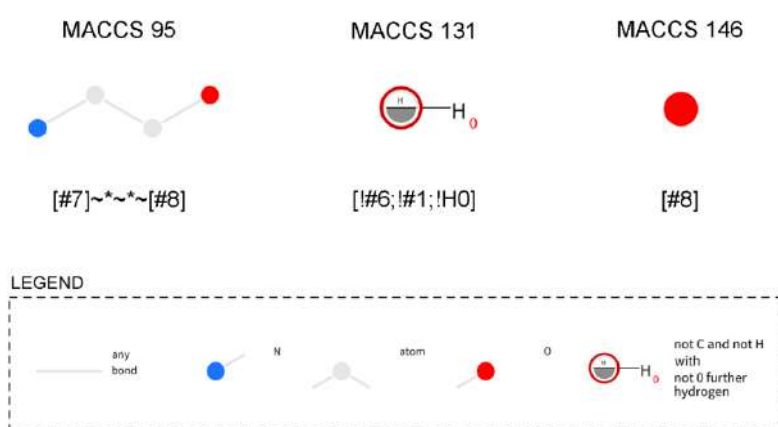


Figure 13. SMARTS patterns and their visualization across three MACCS fingerprints using SMARTS PLUS [322].

4.2.3.4 Connection tables

The MOL file format, created by MDL Information Systems, is part of the CT file family, also known as chemical table files (Figure 14). These files use connection tables to describe molecular structures, making them highly versatile and widely used for transferring chemical information. The MOL file format encapsulates the connection table and can be enclosed within a structure/data (SD) file, which includes not only structural information but also additional property data for multiple molecules. Other formats in the CT file family include the RXN file, which describes individual reactions, the RD file, which stores reactions or molecules along with their associated data, the RG file, designed for handling queries, and the XD file, an XML-based format for transferring structures or reactions with their metadata (Table 4) [323].

Table 4. Comparison between different connections tables formats.

MOL format	MOL2 format	SDF format	RXN format
Can only store one molecule per file.	Store multiple records such as MOLECULE, ATOM, BOND,	Can store multiple chemical structures in one file.	Used to store information on chemical reactions.
Cannot store complex information.	SUBSTRUCTURE, and SET.	Can store other information (e.g. chemical properties).	
Need more storage space.			
Lack of explicit atom types.			
Lack of standardization.			

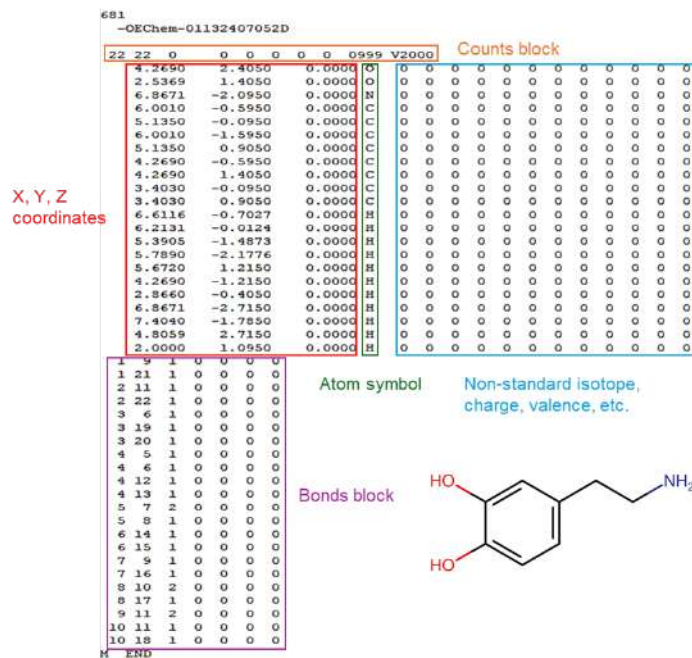


Figure 14. Representation of the connection tables for DA within an SDF file.

4.2.3.5 Molecular descriptors

A molecular descriptor in chemistry is a mathematical representation for characterizing a molecule that allows comparison of different molecules and searching for related molecules in a database [324]. These descriptors are classified into three categories: physicochemical, topological, or electronic, and are mostly characteristics of the 2D, or 3D structure of the molecule (Figure 15). The concept of “molecular descriptor” is closely related to the molecular structure and properties of an observable experimental molecule. The numerical values expressing the molecular descriptors can be obtained from the experimental physicochemical properties of the molecules or through theoretical mathematical formulas and computational algorithms [325].

1D	2D	3D
Chemical formula Molecular weight Number of atoms Number of bonds Number of rings Polar surface area LogP	Substructure 2D fingerprint 	Structure Pharmacophores Shape

Figure 15. The different types of molecular descriptors [326].

Molecular fingerprints are descriptors specifically optimized for complex computational calculations, such as predictions of new properties using ML. These descriptors are encoded in 1D as bit vectors. The information represented by these bits can come from an initial 2D or 3D representation. In this work, we will focus on 2D molecular fingerprints, which are used to estimate the similarity between two molecules. These molecular fingerprints encode in each of their bits the presence or absence of certain substructures in the molecule. These fragments can be predefined or obtained from each molecule which is considered as a template. The Molecular ACCess System (MACCS) fingerprint is an example using predefined fragments. It consists of 166 substructures that can effectively distinguish between molecules [327]. The extended connectivity fingerprint (ECFP) is designed to capture the molecular features using a circle with an increasing diameter to obtain substructures representative of the molecule. The generation of an ECFP is illustrated in Figure 16. For example, the fingerprint has a length of 8 bits and the circles go up to a diameter of 4 atoms, taking the diameters of 0, 2 and 4 atoms. This diameter is commonly used for similarity search or molecule clustering. ML methods sometimes require higher diameters, up to 8 atoms. The length of the bit vector is usually much larger than the one used for the illustration, with a size of 1024 or 2048 bits [328].

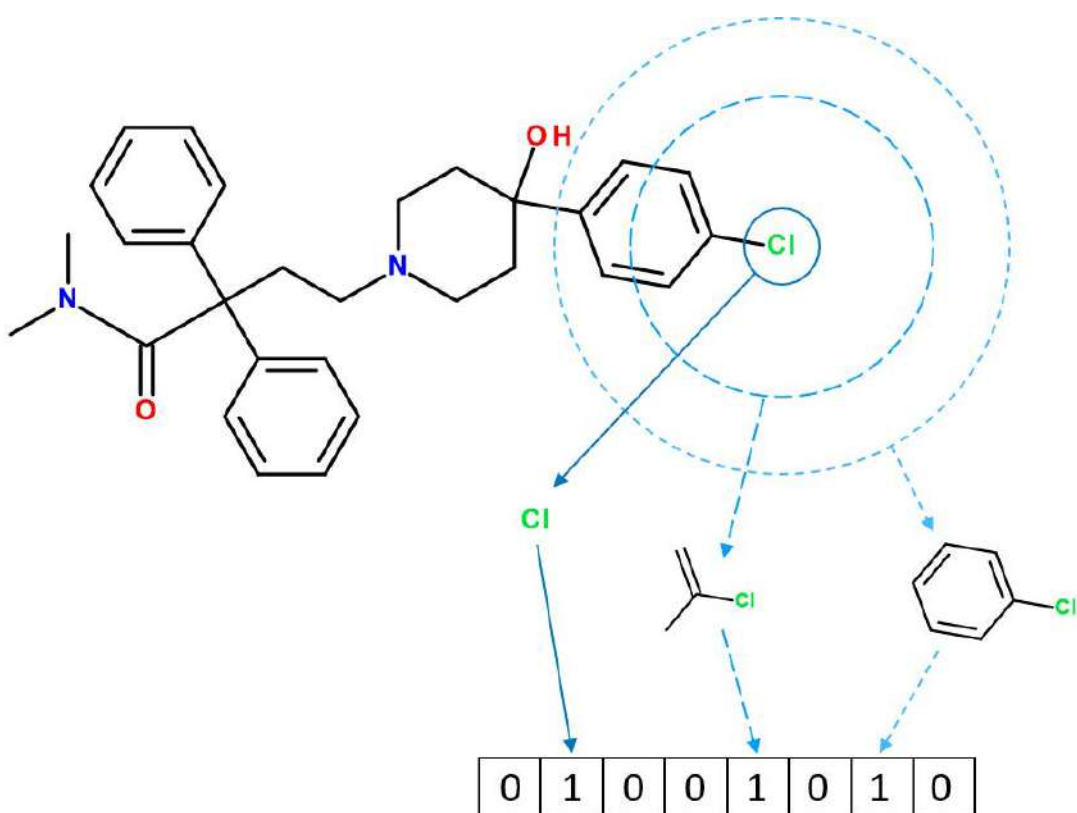


Figure 16. Generating an ECFP molecular fingerprint. The maximum allowed diameter here is 4, the successive circles have diameters of 0, 2 and 4. The presence of the obtained substructures is stored in a bit vector, here of length 8 [329].

4.2.4 Artificial intelligence in drug discovery

4.2.4.1 Machine learning

ML models are increasingly being used to develop QSAR models, as they can handle large and complex datasets and can be used to identify patterns and relationships in the data that traditional statistical methods may not be able to detect (Figure 17). There are various ML models used in QSAR, such as Random Forest (RF), Support Vector Machine (SVM), k-Nearest Neighbors (KNN), and XGBoost (XGB) [330]. Among these, RF and SVM are considered the most widely used in drug discovery. RF is a type of ensemble learning method that combines multiple decision trees to improve the accuracy and stability of the model. It is particularly useful for handling high-dimensional and noisy data. SVM is a supervised learning algorithm that can be used for both classification and regression problems. It is particularly useful for handling small datasets with many features.

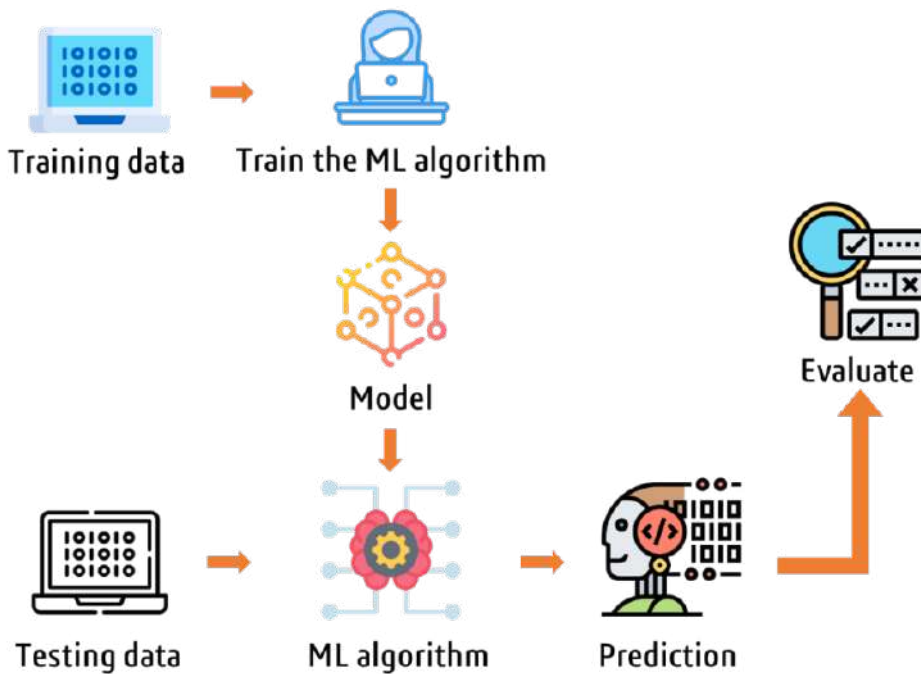


Figure 17. General workflow of a machine learning algorithm.

4.2.4.1.1 Random Forest

RF, developed by Leo Breiman in 2001, is an ensemble learning method used for classification, regression, and other tasks [331]. It operates by constructing multiple decision trees at training time, with each tree trained on a different subset of the data and using a random subset of features at each split [331]. The predictions of the individual trees are then combined to make the final prediction [332]. RF is known for its ability to handle overfitting by creating multiple

trees, each trained slightly differently, which helps to reduce overfitting and improve the generalization performance of the model [333].

4.2.4.1.2 Support Vector Machine

SVM, firmly established by Vladimir Vapnik's pioneering work and theoretical contributions, is a supervised learning algorithm specifically designed to identify a hyperplane that maximizes the margin between two distinct classes of data [334], [335]. The margin is defined as the distance between the hyperplane and the nearest data points from each class [336]. These data points, which are near the hyperplane, are referred to as support vectors. Mathematically, the hyperplane is defined by the following equation (Eq. 1):

$$w^T \times x + b = 0 \quad (1)$$

Where w is the normal vector to the hyperplane, x is a data point, and b is the bias term.

4.2.4.1.3 K-Nearest Neighbors

In 1919, Evelyn Fix proposed a nearest neighbor rule for estimating probability densities which was followed by progressive refinements culminating in its present-day prominence as a robust and versatile ML tool [337]. KNN algorithm is a non-parametric instance-based learning approach that classifies a new data point by examining the k nearest data points in the training set [338]. The label assigned to the new data point is determined by the most frequent class among its k nearest neighbors [339]. In most cases, the distance between two data points, x and y , is computed using the Euclidean distance metric (Eq. 2):

$$d(x, y) = \sqrt{\sum_i (x_i - y_i)^2} \quad (2)$$

Where x_i and y_i are the i -th components of the data points x and y , respectively.

4.2.4.1.4 Gaussian Naïve Bayes

GNB is a classification technique used in ML based on a probabilistic approach and Gaussian distribution. It was developed by applying Bayes' theorem with strong independence assumptions, making it an extension of the Naïve Bayes classifier [340]. GNB supports continuous-valued features and models each feature as conforming to a Gaussian distribution [341]. The mathematical representation of GNB is given by (Eq. 3):

$$P(c|x) = \frac{(P(c) \times \prod_i P(x_i|c))}{P(x)} \quad (3)$$

Where $P(c|x)$ is the probability of a data point (x) belonging to a specific class (c), given its features, $P(c)$ is the prior probability of class (c) being encountered, calculated from the overall frequency of class (c) in the dataset, $P(x_i|c)$ is the likelihood of observing a particular feature

value (x_i) in data point (x) given that it belongs to class (c), and $P(x)$ is the overall probability of observing the data point (x), often calculated as a normalization factor to ensure probabilities sum to 1.

4.2.4.1.5 XGBoost

XGB, known as Extreme Gradient Boosting, represents a tree-based ensemble learning algorithm that operates within the framework of gradient boosting [342]. In 2014, Tianqi Chen's vision set the spark for XGB, and thanks to Carlos Guestrin's fine-tuning, it evolved into a powerhouse in the real world, boosting performance and pushing boundaries in the ML landscape [342]. This algorithm constructs a sequence of decision trees, with each subsequent tree trained to minimize the errors of its predecessors [342]. To mitigate overfitting, the trees undergo pruning. The predictions generated by an XGB model are the cumulative sum of the predictions made by all the trees within the ensemble (Eq. 4):

$$\hat{y} = \sum_t f_t(x) \quad (4)$$

Where $f_t(x)$ is the prediction of the t -th tree for the data point x .

4.2.4.2 Deep learning

DL is a subset of ML that uses artificial neural networks with multiple layers to learn from large amounts of data and solve complex problems. It is based on the idea of representation learning and abstraction, where simple but non-linear modules transform the representation at one slightly more abstract level. DL models can create new features on their own and can be used to analyze various types of data, including images, voice, and text. DL has been increasingly applied to QSAR and quantitative structure-property relationship (QSPR) modelling, as it can handle complex data structures and interactions, and has shown promising results in predicting various properties of molecules [343].

4.2.4.2.1 Convolutional neural networks

A convolutional neural network (CNN) is a type of DL neural network that is designed to process data that has a grid-like topology, such as an image (Figure 18). CNNs are particularly useful for image recognition and classification tasks, as well as for natural language processing and speech recognition. In the context of drug discovery, CNNs can be used to develop QSAR/QSPR models. There are three main types of QSAR models that can be developed using CNNs: graph-based, image-based, and fingerprints-based models [344].

Graph-based QSAR models use the chemical structure of a compound represented as a graph, where atoms are nodes and chemical bonds are edges. CNNs can be used to learn the structural features of the compound from the graph representation [345].

For image-based QSAR models, CNNs can automatically extract relevant features and relationships from the molecular images. The convolutional layers enable the network to recognize spatial hierarchies of features, capturing important structural characteristics. This approach proves valuable in predicting the activity of compounds for drug discovery without the need for labor-intensive experiments.

In fingerprints-based QSAR models use the chemical structure of a compound represented as a binary fingerprint, where each bit corresponds to the presence or absence of a specific structural feature. CNNs can be used to learn the structural features of the compound from the fingerprint representation. Both types of models can be useful for drug discovery as they can predict the activity of compounds without the need for expensive and time-consuming experiments.

Several studies have explored the application of CNNs in QSAR modelling. For instance, a study published in the Journal of Cheminformatics introduced a molecular property prediction model based on the CNN framework, demonstrating the potential of deep learning in predicting molecular properties [346]. Additionally, a paper in the BMC Bioinformatics journal presented a learning-based method, CNN-DDI, for predicting drug-drug interactions using CNNs [347]. Furthermore, a study in Molecular Diversity journal discussed the potential of deep learning in improving QSAR models, highlighting the effectiveness of deep neural networks in learning directly from low-level encoded data without the need for computing molecular descriptors [348].

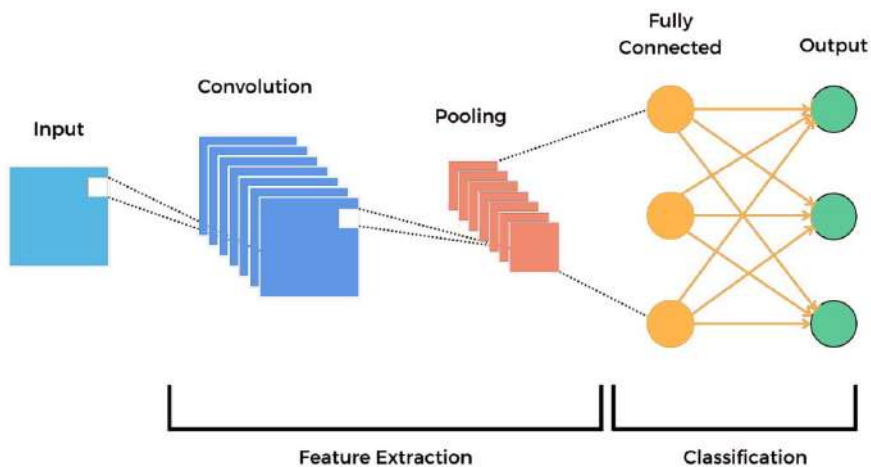


Figure 18. The architecture of a convolutional neural network [349]

4.2.4.2.2 Artificial neural networks

Artificial neural networks (ANNs) are a type of ML algorithm that mimics the capacity of the human brain in terms of recognizing underlying relationships and patterns, mimicking the way the human brain processes information (Figure 19) [350]. ANNs can identify rules from samples and accurately describe the relationships between independent variables and dependent variables, and the training of ANNs resembles the process of approximating the formulas [351]. [352]. ANNs have been used in various drug discovery stages, including target identification, lead optimization, and toxicity prediction [352]. ANNs have also been used to develop QSAR models, which can predict the activity of compounds without the need for expensive and time-consuming experiments [352], [353]. ANNs have been applied to drug discovery in various ways, such as predicting drug-related features, including bioactivities and drug-drug interactions, and accelerating the drug discovery process [344]. ANNs are crucial in medicinal chemistry for predicting and designing new molecules. They streamline drug discovery by enabling faster and more efficient drug design, increasing the likelihood of improving drug efficacy, and reducing experimental costs. [344], [352], [353].

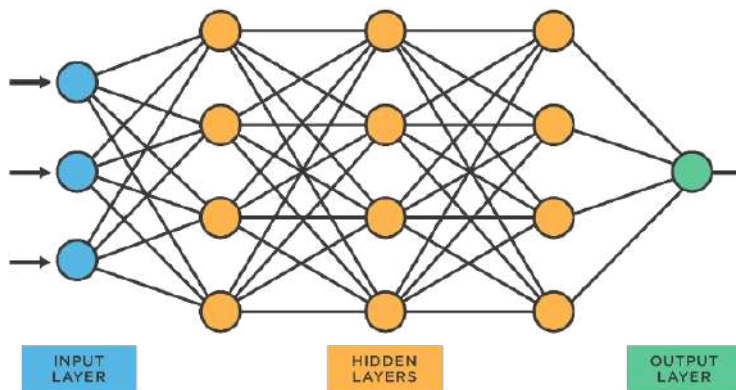


Figure 19. The architecture of an artificial neural network.

4.2.4.2.3 Recurrent neural networks

Recurrent neural networks (RNNs) have been successfully applied in drug discovery for *de novo* drug design, generating focused molecule libraries, and optimizing multiple traits collectively [354]. RNNs can learn the interrelationships between elements of the input over a protracted length of the input series, and they can capture sequential dependencies and generate new sequences based on learned patterns. According to recent research, Memory Augmented RNNs have been used for *de novo* drug design [355]. The study proposed three RNN-based architectures augmented with external memory for de-novo generation of small molecules. These architectures include a refactoring of a stack augmented RNN, adaptations of two

recurrent neural network architectures, the Neural Turing Machine (NTM), and the Differentiable Neural Computer (DNC), with external memory to support random access, an advantage over the first-in-last-out access imposed by a stack and establishing their efficacy [355]. The study also compared the performance of these architectures with simpler recurrent neural networks (Long Short-Term Memory and Gated Recurrent Unit) without an external memory component to explore the impact of augmented memory in the task. The results showed that the proposed memory-augmented RNN architectures outperformed the baseline models in terms of the diversity and novelty of the generated molecules [355].

4.2.5 Performance evaluation

4.2.5.1 Regression metrics

In QSAR modelling, regression metrics are used to evaluate the performance of a regression model that predicts continuous numerical values, such as biological activity or property values, based on chemical features or descriptors of molecules.

4.2.5.1.1 Coefficient of determination

The coefficient of determination (R^2) is a measure of how well the regression model fits the data. It represents the proportion of the variance in the dependent variable that is predictable from the independent variable. The formula (Eq. 5) quantifies the proportion of the total variance in the dependent variable that is explained by the regression model. R^2 values range from 0 to 1, where 1 indicates a perfect fit (the model explains all the variability), and values closer to 0 indicate poorer model fit.

$$R^2 = 1 - \left(\frac{SSres}{SStot} \right) \quad (5)$$

Where $SSres$ is the sum of squared residuals, also known as the residual sum of squares (RSS). It measures the total variance that is not explained by the regression model. $SStot$ is the total sum of squares, which represents the total variance in the dependent variable y around its mean.

4.2.5.1.2 Mean Squared Error

The average squared difference between the predicted values and the actual values. It measures the overall prediction error of the model (Eq. 6).

$$MSE = \left(\frac{1}{n} \right) \sum_{i=1}^n (y_i - \hat{y}_i)^2 \quad (6)$$

Where n is the number of samples or observations. y_i represents the actual observed value for the i -th sample. \hat{y}_i represents the predicted value for the i -th sample.

4.2.5.1.3 Mean Absolute Error

The average absolute difference between the predicted values and the actual values (Eq. 7). It provides a more intuitive understanding of the prediction error than MSE.

$$MAE = \left(\frac{1}{n}\right) \sum_{i=1}^n |y_i - \hat{y}_i| \quad (7)$$

4.2.5.1.4 Root Mean Squared Error

The square root of the MSE. It has the same units as the dependent variable, making it easier to interpret than MSE (Eq. 8).

$$RMSE = \sqrt{\left(\frac{1}{n}\right) \sum_{i=1}^n (y_i - \hat{y}_i)^2} \quad (8)$$

4.2.5.2 Classification metrics

Classification metrics are used to evaluate the performance of models that predict categorical outcomes, such as the activity or toxicity of a molecule. These metrics assess how well the model predicts the class labels of the samples based on their chemical features or descriptors.

4.2.5.2.1 Sensitivity

Sensitivity, also known as true positive rate or recall, measures the proportion of actual positive instances (true positives) that are correctly identified by the model as positive (Eq. 9). In other words, sensitivity quantifies the model's ability to correctly detect or capture positive instances from the entire pool of positive instances in the dataset.

$$SE = \frac{TP}{(TP + FN)} \quad (9)$$

Where True Positives (TP) are the instances that are correctly classified as positive by the model. False Negatives (FN) are the instances that are actually positive but are incorrectly classified as negative by the model.

4.2.5.2.2 Specificity

Specificity measures the proportion of true negative predictions (correctly predicted negatives) out of all actual negative instances in the dataset (Eq. 10).

$$SP = \frac{TN}{(TN + FP)} \quad (10)$$

Where True Negatives (TN) are the instances that are correctly classified as negative by the model. False Positives (FP) are the instances that are actually negative but are incorrectly classified as positive by the model.

4.2.5.2.3 Accuracy

Accuracy measures the proportion of correctly classified instances out of the total number of instances (Eq. 11).

$$ACC = \frac{(TP + TN)}{(TP + TN + FP + FN)} \quad (11)$$

4.2.5.2.4 F1 Score

The F1 score is the harmonic mean of precision and recall. It provides a single metric that balances both precision and recall (Eq. 12).

$$F1 = \frac{2TP}{(2TP + FP + FN)} \quad (12)$$

4.2.5.2.5 Matthews' correlation coefficient

Matthews' correlation coefficient (MCC) is a metric commonly used to evaluate the performance of binary classification models, including those used in QSAR studies (Eq. 13). MCC considers true positives, true negatives, false positives, and false negatives, providing a balanced measure of classification performance, especially in imbalanced datasets.

$$MCC = \frac{(TP \times TN - FP \times FN)}{\sqrt{((TP + FP) \times (TP + FN) \times (TN + FP) \times (TN + FN))}} \quad (13)$$

4.3 Molecular modelling

Molecular modelling is a computational technique used to predict the properties and behavior of molecules. It encompasses various methods, theoretical and computational, that help researchers understand molecular systems and their processes [356]. The principles used in molecular modelling can be categorized into three main types: *ab initio*, empirical, and semi-empirical [357].

- ***Ab initio* methods:** This approach is based on fundamental principles, which are derived from quantum mechanics. *Ab initio* MD is a type of *ab initio* molecular modelling that simulates the behavior of molecules in real time [358]. This method allows for the study of chemical processes in condensed phases with greater accuracy and fewer biases [358]. Density functional theory (DFT) is an example of *ab initio* calculations, instrumental in both *de novo* drug design and molecular geometry optimization [359]. In drug design, DFT aids in predicting stable structures, analyzing electronic properties, and assessing binding energies. For molecular geometry, DFT is used for optimization, transition state analysis, and vibrational studies, providing accurate insights into molecular behavior and interactions [360].

- **Empirical methods:** This approach involves the use of force fields to describe the interactions between atoms in a molecule. The force fields are derived from experimental data, such as bond lengths, angles, and thermodynamic properties [361]. Empirical molecular modelling is often used in conjunction with MD simulations to study the conformational changes of proteins and the binding of ligands [361].
- **Semi-empirical methods:** This approach combines the principles of quantum mechanics (QM) with experimental data to describe the electronic structure of molecules. Semi-empirical methods make approximations and use parameters fitted to experimental data, making them less computationally expensive than *ab initio* methods. While less fundamentally rigorous than *ab initio*, they can still provide reasonably accurate descriptions of molecular properties [357].

Molecular modelling techniques have been applied in various fields, including computational chemistry, drug design, computational biology, and materials science, to study molecular systems ranging from small chemical compounds to large biomolecules. These techniques have been instrumental in advancing our understanding of molecular processes and designing new molecules for therapeutic purposes [357].

4.3.1 Chemical libraries

Chemical libraries are collections of chemical compounds that are synthesized experimentally or isolated from natural sources such as plants, animals, and microorganisms. These compounds are often of interest for their potential medicinal properties, and many have been used for centuries in traditional medicine [362], [363]. NP libraries can be created by isolating and purifying compounds from natural sources, or by synthesizing compounds that are structurally like those found in nature. These libraries can be used in a variety of applications, including drug discovery, material design, and chemical synthesis [364]. Chemical libraries are becoming increasingly important as a resource for drug discovery and development, as they can be used to screen large numbers of compounds for potential activity against specific targets. Table 5 presents a comprehensive compilation of publicly accessible libraries of NPs designed for virtual screening.

Table 5. Comprehensive list of natural product libraries suitable for high-throughput virtual screening studies.

Database	Number of NPs	Description	Link
COCONUT	406,747	Contains curated, standardized data on natural product structures, bioactivities, origins, and references.	https://coconut.naturalproducts.net/

LOTUS	276,518	Provides detailed information on NPs with known bioactivities and isolation information.	https://lotus.naturalproducts.net/
ZINC20	80,617	Includes both natural and synthetic compounds, ideal for virtual screening and cheminformatics research.	https://zinc20.docking.org/
NPASS	94,413	Offers extensive data on natural product bioactivities, origins, and literature references.	https://bidd.group/NPASS/index.php
Cannabis Compound Database	6,172	Comprehensive resource for cannabinoids, terpenes, and other chemicals found in Cannabis sativa.	https://cannabisdatabase.ca/
SuperNatural III	449,058	Features curated data on NPs with reported bioactivities and isolation details.	https://bioinf-applied.charite.de/supernatural_3/
FooDB	70,926	Includes naturally occurring compounds found in food, particularly bioactive molecules.	https://foodb.ca/
NANPDB	4,928	Focuses on NPs and traditional medicine knowledge from North African plants.	https://african-compounds.org/about/nanpdb/
EANPDB	1,871	Focuses on NPs and traditional medicine knowledge from East African plants.	https://african-compounds.org/about/eanpdb/
SANCDB	1,017	Focus on natural compounds isolated from the plant and marine life in and around South Africa	https://sanfdb.rubi.ru.ac.za/
CMNPD	31,561	Extensive resource for marine-derived NPs, including structures, bioactivities, and isolation sources.	https://www.cmnpd.org/
SistematX	8,593	Provides data on plant secondary metabolites, including alkaloids, terpenoids, and phenolics.	https://sistematx.ufpb.br/
Eximed	5,096	Features Natural-Product-Based Library with potential for drug development.	https://eximedlab.com/Screening-Compounds.html
CoumarinDB	905	Specialized database dedicated to coumarins, a class of NPs with diverse bioactivities.	https://yboulaamane.github.io/CoumarinDB/
Ambinter	11,648	Comprehensive collection of NPs with structural and bioactivity information.	https://www.ambinter.com/

4.3.2 Ligand-based virtual screening

Ligand-based virtual screening is a method for predicting potential new active molecules based on the knowledge of at least one known active ligand. This approach relies on the principle that structurally similar molecules often exhibit similar bioactivity profiles. It proves particularly valuable in cases where the therapeutic target is unknown or lacks an experimentally resolved crystallographic structure. Furthermore, ligand-based virtual screening offers computational efficiency compared to structure-based approaches, enabling the screening of millions of

compounds. The most employed methods include similarity search, pharmacophore modelling, and QSAR models. Additionally, 3D-QSAR, which incorporates knowledge of bioactive conformations for descriptor calculation, features techniques such as Comparative Molecular Field Analysis (CoMFA) and Comparative Molecular Similarity Indices Analysis (CoMSIA). These techniques aim to elucidate the spatial and steric requirements crucial for ligand-receptor interactions, optimizing molecular designs for enhanced bioactivity.

4.3.2.1 Similarity search

Similarity search is the method to use when very few ligands have been reported for the chosen biological target. A similarity search can be conducted as soon as an active ligand is known [365]. This method is based on the use of descriptors and similarity metrics to compare molecules to be screened against one or more reference ligands to predict their activity profile. Tanimoto similarity, also known as Tanimoto coefficient (T_c), is a similarity metric commonly used in cheminformatics to quantify the similarity between two molecular fingerprints. It is calculated as the ratio of the number of common bits (features) between two fingerprints to the total number of bits present in both fingerprints (Eq. 14). The Tanimoto index ranges from 0 (no common bits) to 1 (identical fingerprints). Several studies have shown that the Tanimoto index is a popular and effective choice for fingerprint-based similarity calculations [366].

$$Tc_{(A,B)} = \frac{N(A \cap B)}{(N(A)+N(B)- N(A \cap B))} \quad (14)$$

Where $N(A)$ is the number of bits set to 1 in molecule A's fingerprint, $N(B)$ is the number of bits set to 1 in molecule B's fingerprint, and $N(A \cap B)$ is the number of bits set to 1 in both molecule A and B's fingerprints.

4.3.2.2 Pharmacophore modelling

The concept of pharmacophore was developed by Ehrlich in the late 19th century [367]. At that time, although the term pharmacophore was not used, Ehrlich developed the idea that certain chemical groups in a molecule are responsible for its biological or pharmacological action. The first modern definition of pharmacophore, using the term “abstract features” instead of “chemical groups”, dates to 1960 [368]. The first pharmacophore model identifying orders of magnitude of distance between the features constituting the pharmacophore (Figure 20a) was published in 1963 for muscarinic agents [369]. Kier also published the first pharmacophore model with precise distances measured between the different groups constituting the pharmacophore, referred to as the “proposed receptor pattern” (Figure 20b) [370].

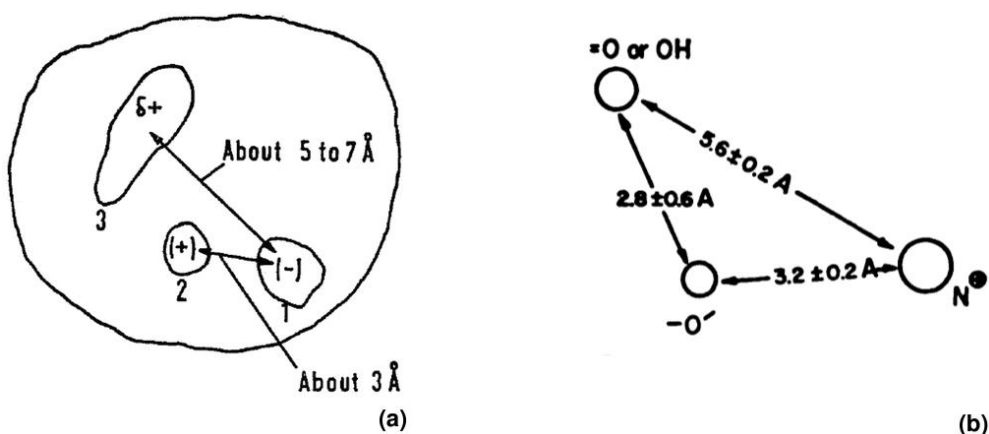


Figure 20. Presentation of the first pharmacophores to have been published. Beckett's model (a) from 1963 defines approximate distances between Zone 1, a negatively charged anionic cavity for accommodating a quaternary amine, Zone 2, a positively charged point for binding to acetylcholine and its analogues, and Zone 3, charged to interact with the OH of muscarine, the C-O of acetylcholine and its analogues, or the double bond of furanic analogues of muscarine [369]. Kier's model (b) proposes calculated distances between 3 key atoms common to acetylcholine, muscarine, and muscarone [370]

The official definition of International Union of Pure and Applied Chemistry (IUPAC) from 1998 states that a pharmacophore consists of the entire steric and electronic properties of a molecule that are necessary for optimal supramolecular interactions with a specific biological target, resulting in either generation or blocking of a biological response [371]. According to this definition, molecules sharing the same pharmacophore for a given target should bind to the receptor in an identical manner and exhibit similar activity profiles. The generated pharmacophore is then used to screen a chemical library for molecules that overlay with this pharmacophore. One of the major characteristics of this type of method is that a pharmacophore is defined by complementary pharmacophoric points, which are functional groups rather than groups of atoms. The different pharmacophoric points sought after include hydrogen bond donors and acceptors, positively charged groups that form electrostatic interactions with negatively charged groups and vice versa, and aromatic groups, considered separately from the larger class of hydrophobic groups from which they originate, and both are complementary to other hydrophobic groups [372].

4.3.3 Structure-based virtual screening

When the 3D structure of the biological target of interest is available, methods known as structure-based approaches can be used for virtual screening (Figure 21) [373]. These 3D structures can be obtained through two primary experimental methods:

- **X-ray crystallography:** This technique involves crystallizing the protein and then bombarding it with X-rays to reveal its atomic structure.

- **Nuclear magnetic resonance (NMR):** This method probes the protein's structure in solution using magnetic fields and radio waves.

The resolution of a protein structure is a critical parameter in structural biology that describes the level of detail and precision with which the positions of atoms are determined.

A vast repository of experimentally determined 3D structures is freely accessible through the RCSB Protein Data Bank (PDB), a global resource housing over 200,000 structures to date [374]. Resolution is expressed in units of angstroms (\AA) and is inversely related to the quality of the data. A lower resolution value indicates higher quality data, meaning that the crystallographers were able to obtain more detailed information about the atomic positions.

However, when experimental structures are unavailable, computational methods for structure prediction have become increasingly powerful:

- **Sequence homology modelling:** This approach utilizes structural data from related proteins with known structures to construct a model of the target protein.
- **AlphaFold:** This groundbreaking AI system, developed by DeepMind, has transformed structure prediction by achieving remarkable accuracy, often contrasting experimental methods [375]. AlphaFold (<https://alphafold.ebi.ac.uk/>) has generated over 200 million protein structures with high confidence, significantly expanding the structural coverage of the protein universe.

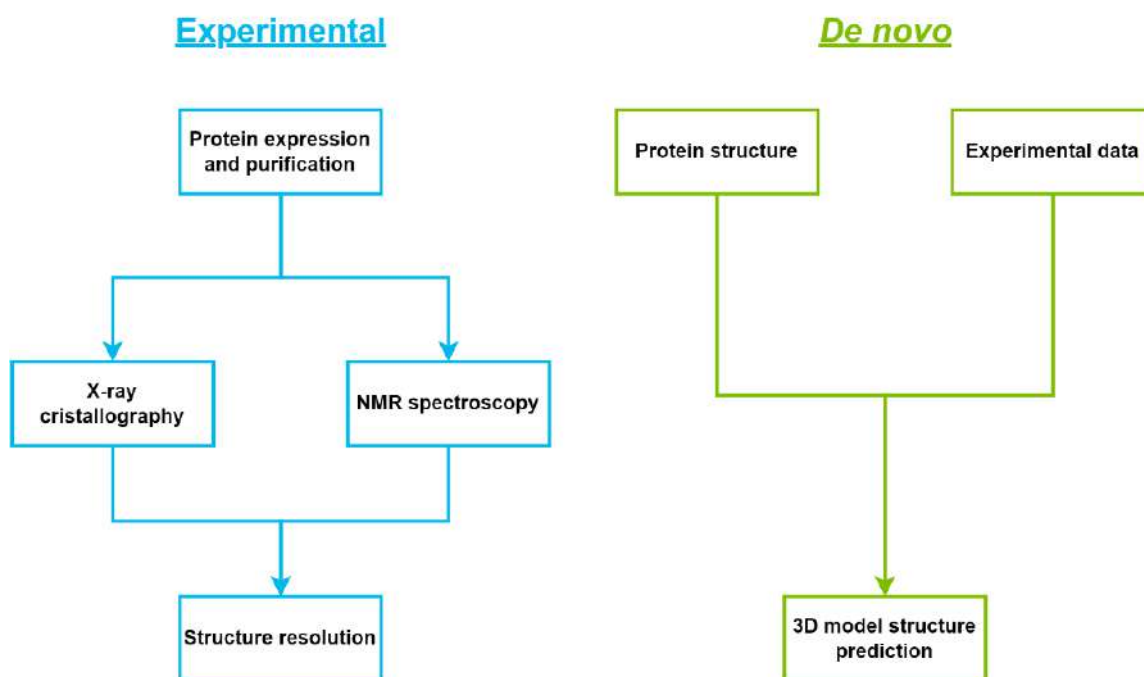


Figure 21. Methods to obtain the 3D structure of a biological target of interest include experimental approaches such as X-ray crystallography and NMR spectroscopy, as well as de novo methods such as structure prediction by homology.

4.3.3.1 Concept of molecular docking

Over time, molecular docking has become an integral part of the drug discovery process. Since its initial development in the 1980s, advancements in computer hardware and the accessibility of small molecule and protein structures have contributed to the refinement of docking methods, resulting in its widespread adoption in both industrial and academic research [376]. The aim of molecular docking is to predict whether a molecule can bind to the active site of a protein based on the prediction of the conformation and orientation of the molecule during its binding to the receptor. To achieve this, docking methods combine the use of a search algorithm to generate putative binding modes or “poses” of the ligand in the receptor, and a scoring function used to rank the different poses according to a predicted affinity score. Docking methods aim to identify potential ligands of the protein target among all the molecules studied, and determine the correct poses or conformations adopted by the ligands during binding to the receptor.

4.3.3.2 Classification of molecular docking

For decades, the “lock-and-key” model dominated our understanding of ligand-receptor binding, leading to the development of rigid docking methods [377]. These early algorithms treated molecules as static entities, attempting to replicate the perfect key-hole fit [378]. In this approach, the ligand is positioned in the binding site through translation and rotation. For example, the software FRED enumerates all rotations and translations for a ligand inside the binding site as its first step[379]. Then, a negative image of the binding site is used to eliminate poses that are incompatible with the active site (due to clashes or distance). Finally, the selected poses are scored, and the best ones are optimized. However, this static view fails to capture the inherent dynamism of biomolecular interactions [379]. Figure 22 summarizes the differences between the three types of molecular docking.

Driven by the need for increased accuracy, semi-flexible docking emerged. This approach acknowledges the inherent conformational flexibility of both ligands and receptors, allowing limited conformational changes during the docking process [380]. Consequently, semi-flexible docking offers a more nuanced picture of binding by exploring a wider range of poses [381].. One common approach is to use a rotamer library to represent the possible conformations of the ligand [381]. The software then samples different combinations of rotamers and positions the ligand in the binding site. Another approach is to use a normal mode analysis to identify the most flexible regions of the ligand and the receptor [382]. The software then allows these regions to move during the docking simulation. However, for highly flexible systems, even semi-flexible approaches may fall short [383]. While computationally demanding, flexible

docking provides unmatched accuracy, enabling the prediction of binding modes for complex and dynamic systems. One common approach is to use a protein structure prediction method to generate a library of receptor conformations [384]. The software then docks the ligand to each of these conformations and scores the resulting poses. Another approach is to use a MD simulation to simulate the binding process [385]. This allows the software to observe the ligand and receptor as they move and interact with each other.

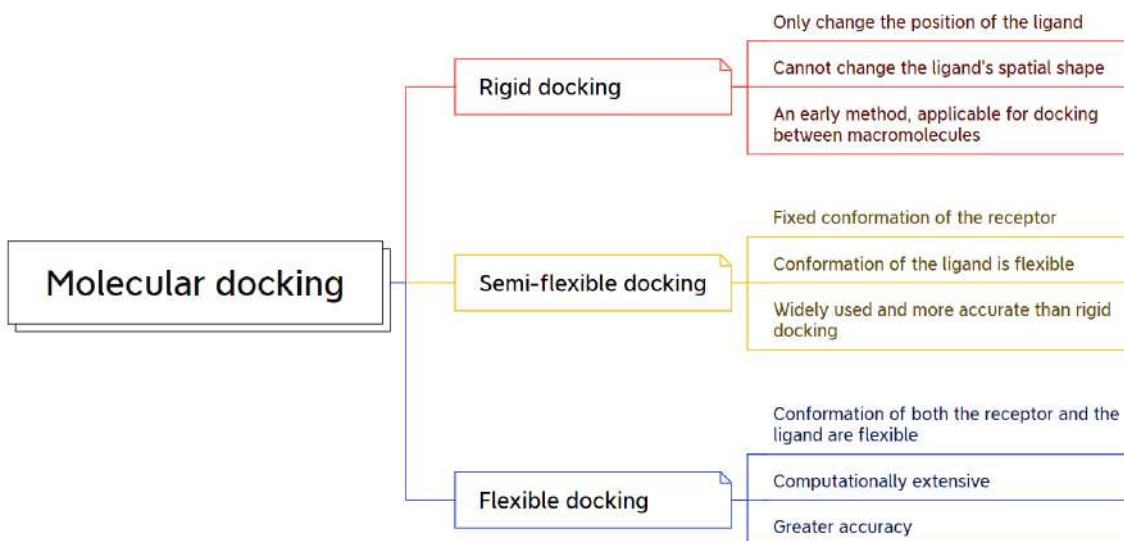


Figure 22. Molecular docking software classification.

4.3.3.3 Molecular docking programs

Molecular docking programs play a pivotal role in drug discovery, predicting the binding of small molecules to biomolecular targets. Through advanced algorithms, they simulate interactions and identify favorable binding modes, guiding the discovery of potent and selective drugs [386]. Virtual screening, enabled by molecular docking, efficiently prioritizes potential drug candidates from vast compound libraries, streamlining the drug discovery process. Continuous advancements, including refined force fields and flexibility considerations, further enhance docking programs, accelerating the path to new therapies. Table 6 provides information about different molecular docking programs, highlighting key aspects of each program.

Table 6. List of open-source and commercial molecular docking programs.

Program	Licence	Docking Type	Scoring function	Reference
AutoDock Vina	Open-source	Flexible	Semi-empirical, force field-based, knowledge-based potentials	[387]
DOCK 4.0	Open-source	Rigid, Semi-flexible	Empirical, force field-based scoring (grid-based)	[388]
GOLD	Commercial Academic	Flexible	Empirical (ChemScore, GoldScore, ChemPLP), knowledge-based function (ASP)	[389]

Glide	Commercial	Flexible	Empirical (GlideScore, Ligand conformer (Emodel)	[390]
MOE	Commercial	Flexible	Empirical: London dG (fast and efficient, suitable for virtual screening), GBVI/WSA dG (more accurate, suitable for lead optimization)	[391]
AutoDock	Open-source	Flexible	Uses Lamarckian genetic algorithm. Semi-empirical, force field-based	[392]
FlexX	Commercial	Flexible	Empirical	[393]
FRED	Academic	Rigid	Shape-based scoring, Chemgauss4 scoring	[394]
Surflex-Dock	Commercial	Flexible	Empirical scoring function	[395]
Molegro4	Commercial	Flexible	Combines empirical, knowledge-based and force field scoring	[396]
Molegro5	Open-source	Semi-flexible		

4.3.3.4 Docking screens protocol

High-throughput virtual screening (HTVS) is a computational technique that can rapidly sift through vast chemical libraries to identify a select number of molecules exhibiting desirable biological activity. HTVS enables the rapid evaluation of millions of compounds against target receptors. By assessing predicted binding affinities and modes, HTVS prioritizes candidate molecules with the highest potential for success, significantly narrowing the scope for subsequent wet-lab experimentation and optimizing resource allocation. This targeted approach not only enhances hit rates, but also mitigates the financial burden associated with late-stage clinical trial failures, which often stem from suboptimal lead compound selection.

The successful discovery of drugs heavily relies on the meticulous preparation of both the target protein and the candidate ligand for docking simulations (Figure 23). The protein structure undergoes necessary modifications including the addition of polar hydrogens and the removal of extraneous water molecules. Similarly, the ligand undergoes several preparations, including the addition of polar hydrogens, Gasteiger charge calculation, and the merging of non-polar atoms. Subsequently, the ligand is converted into a compatible format depending on the employed software. To define the search space for the binding site, a grid map is created. The docking run then evaluates various ligand poses within the binding site using a scoring function. The top-ranked candidates, typically within the top 10 %, are prioritized for further experimental validation and visualization with tools like Schrödinger's PyMOL or UCSF Chimera.

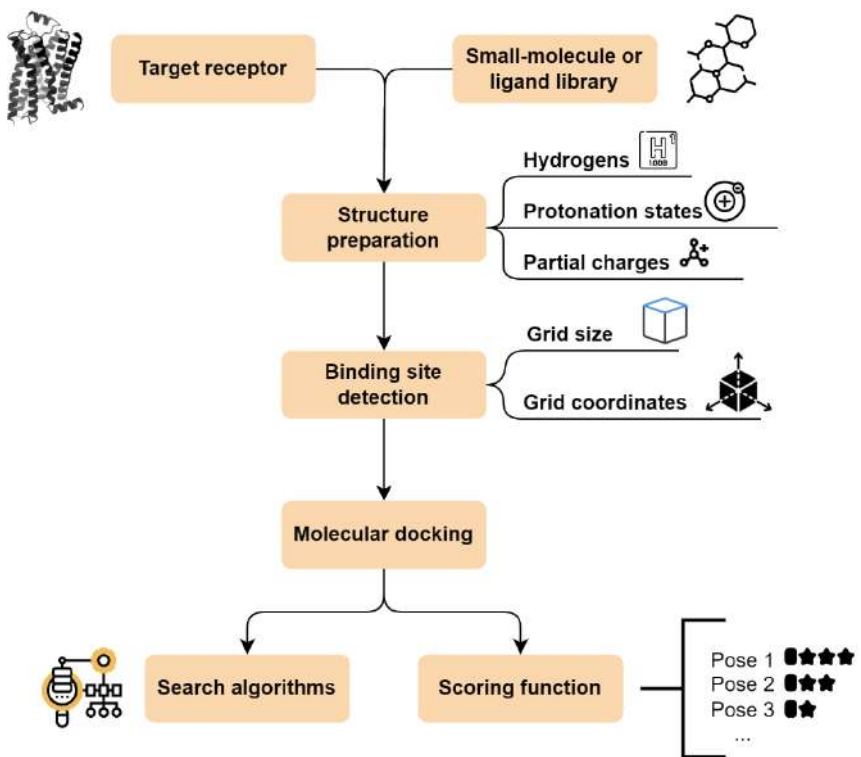


Figure 23. Flowchart of a molecular docking experiment.

4.3.4 Pharmacokinetics and toxicity filters

An estimated 40% of small-molecule drug candidates failing clinical trials in the 1990s suffered from poor bioavailability and pharmacokinetic properties, hindering their ability to reach target sites, and be effectively eliminated from the body (Figure 24) [397].

In the era of bioinformatics and cheminformatics, predictive tools have revolutionized drug discovery by allowing early prediction of drug-likeness and absorption, distribution, metabolism, elimination, and toxicity (ADMET) profiles of drug candidates. Despite the high costs associated with drug development, the pharmaceutical industry still faces a staggering 90% failure rate during the transition from preclinical to clinical trials [398], [399].

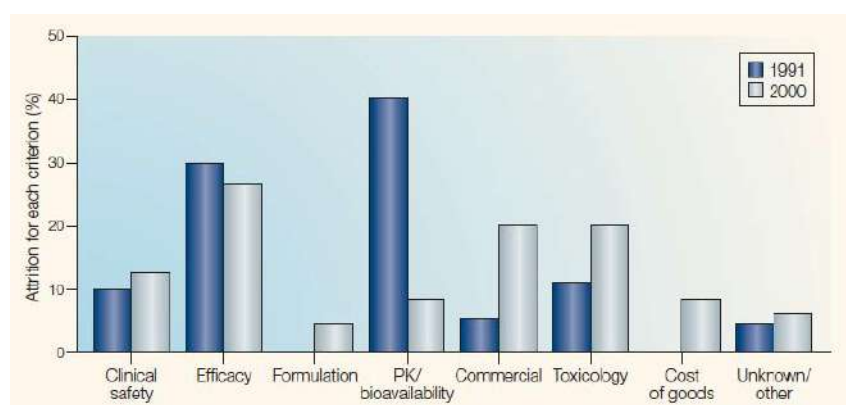


Figure 24. Evolution of the reasons for failure of drug candidates in clinical phases between 1991 and 2000 [400].

4.3.4.1 Physicochemical properties

Physicochemical properties are essential for understanding the probability of a drug candidate's success and are used to filter compounds with unfavorable properties and poor development potential. Drug-likeness scores, which are based on physicochemical properties as shown in Figure 25, are used to assess a compound's potential to succeed in clinical trials and are essential for economizing research costs. They are also a key element in raising the success of drug candidates during preclinical development. Physicochemical properties are related to interactions with different structural and physicochemical properties of drug candidates, and they are used to optimize drug-like properties of lead candidates. Certain physicochemical properties, such as molecular weight, are considered intrinsic properties of a molecule, meaning their values remain consistent regardless of the software used for their calculation. Other properties, however, are classified as predicted values and may exhibit slight variations between different software packages [401]. For example, Osiris Property Explorer and Marvin Suite water employ fragment-based methods to assign pre-calculated logS values to individual chemical fragments within the molecule and sum them up, accounting for bond adjustments and interactions. Other web servers like SwissADME use training datasets of known molecules and their logS values to statistically generate predictive QSPR models for calculating logS of new compounds.

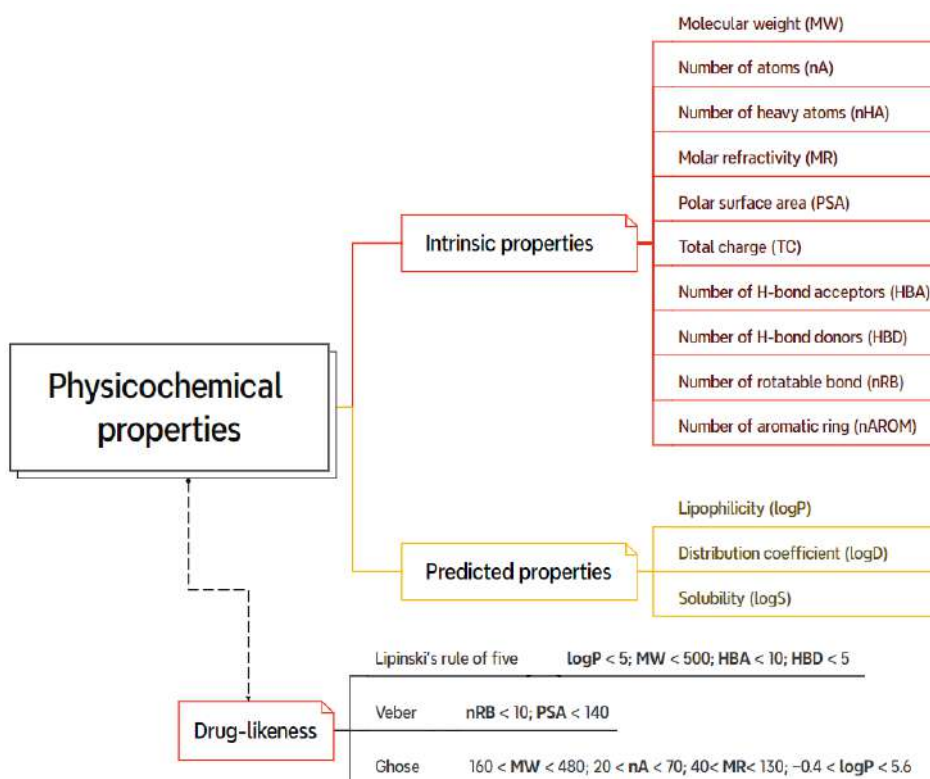


Figure 25. Commonly used physicochemical properties and their drug-likeness rules.

4.3.4.2 ADMET properties

The integration of ADMET profiling into early-stage drug synthesis represents a paradigm shift in the pharmaceutical landscape. Proactive optimization of these critical parameters has the potential to mitigate the risks and financial burdens associated with late-stage clinical trial failures, which often stem from suboptimal ADMET profiles. This shift is further empowered by the emergence of ML and AI-based QSPR models. These models, trained on extensive datasets of experimental ADMET data and molecular descriptors, enable the precise prediction of ADMET properties for novel drug candidates. This invaluable predictive power allows researchers to prioritize compounds with optimal absorption, distribution, metabolism, excretion, and toxicity profiles, streamlining the drug discovery process and boosting the success rate of promising therapeutics.

Furthermore, as detailed in Figure 26, specific physicochemical properties play a pivotal role in determining the *in vivo* fate and efficacy of drugs. Understanding these intricate relationships equips researchers with the knowledge to rationally design drug candidates with favourable ADMET characteristics, thereby accelerating the path towards safe and effective therapeutics for patients in need.

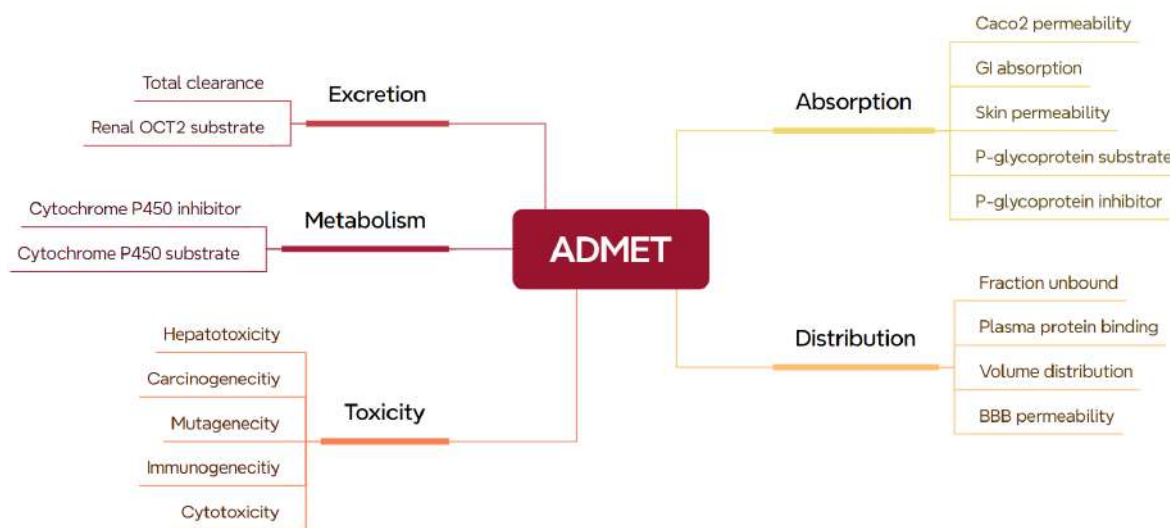


Figure 26. Visual diagram of key ADMET parameters for evaluating the safety of drug candidates during development stages.

4.3.4.3 *In silico* ADMET prediction tools

In silico ADMET tools are computational tools that can predict the ADMET properties of drug candidates using different mathematical models and algorithms, such as regression, classification, and neural networks [401]. *In silico* ADMET tools can predict various ADMET endpoints, such as Caco-2 permeability, BBB penetration, CYP450 interaction, and

hepatotoxicity [402]. While *in silico* ADMET prediction tools have made significant progress, the accuracy and applicability of these tools depend on the quality and availability of experimental data, the validity and relevance of the models, and the user's expertise and interpretation of the results. Some popular *in silico* ADMET tools include ADMETlab, SwissADME, and pkCSM, among others [403], [404], [405].

4.3.5 Molecular dynamics simulations

MD has emerged as an indispensable computational method, providing unprecedented insights into the dynamic behavior and intricate interactions of molecules. The field of structural biology has traditionally focused on capturing static snapshots of molecules, akin to frozen frames in a film. However, the essence of life lies in the dynamic interplay of atoms and molecules. MD serves as a bridge, simulating the time-dependent behavior of these microscopic entities and transforming static structures into dynamic systems.

4.3.5.1 Classical mechanics

Classical molecular mechanics (MM) forms the foundation of MD simulations, which are used to understand the motion and interactions of atoms and molecules. These simulations rely on the equations of classical mechanics, such as Newton's laws of motion, to predict the positions and velocities of atoms at successive time steps. The basic principles of classical mechanics, like the conservation of energy and momentum, guide simulation dynamics. MD simulations are useful for studying large systems with a high number of particles, including protein-ligand complexes in drug discovery [406]. In comparison, Monte Carlo simulations provide an alternative approach. Unlike classical MD, Monte Carlo simulations use random sampling to explore the conformational space of molecules, focusing on thermodynamic ensembles and statistical probabilities [407]. This method is adept at studying systems with significant conformational changes, offering a statistical, thermodynamic perspective on the energetically favorable states of a system. Classical MD simulations have limitations stemming from the fact that they do not account for quantum effects and may not accurately represent the interactions between particles. Non-classical MD simulations, which uses forces obtained from electronic structure theory calculations (typically DFT) to evolve the system's dynamics in time, can provide a more accurate representation of certain systems [408]. Despite these limitations, classical MD remains a valuable tool for investigating a wide range of biological and chemical phenomena, providing insights into the dynamic nature of molecular systems. Table 7 provides a comparative overview of Classical MD, ab initio simulations, and Monte Carlo simulations based on their underlying principles, representation of particles, time evolution approach,

consideration of quantum effects, accuracy, typical applications, computational cost, and limitations.

Table 7. Comparison of Classical MD, ab initio simulations, and Monte Carlo simulations.

Aspect	Classical MD	Ab Initio	Monte Carlo
Underlying Principles	Classical Mechanics	Quantum Mechanics	Statistical Mechanics
Particle Representation	Point masses for atoms and molecules	Explicit consideration of electron cloud	Statistical ensembles for molecular states
Time Evolution	Time-dependent trajectories of particles	Quantum mechanical evolution of wavefunctions	Statistical sampling of conformational space
Quantum Effects	Neglects quantum effects	Explicitly considers quantum effects	Does not consider quantum effects directly
Accuracy	Efficient for large systems, less accurate	High accuracy but computationally expensive	Statistical accuracy, less detailed trajectory
Applications	Macroscopic dynamics, large molecular systems	Small to medium-sized molecular systems	Wide range, especially for conformational studies
Computational Cost	Computationally efficient	Computationally expensive	Moderate computational cost
Typical Use Cases	Protein folding, ligand binding	Small molecules, electronic structure	Thermodynamics, conformational exploration
Limitations	Limited accuracy in capturing quantum effects	Computationally intensive for large systems	Limited in capturing detailed dynamic behavior

4.3.5.2 Force fields

At the core of MD lies the concept of force fields, mathematical models that encapsulate the intricate web of interactions between atoms (Table 8). Force fields are vital in classical MD, defining a system's potential energy surface and describing atomic and molecular interactions. These interactions include bonded terms (bond stretching, angle bending) and non-bonded terms (van der Waals forces, electrostatic interactions) [409], [410]. Force field parameters are calibrated using experimental data and quantum calculations, influencing simulation outcomes [411]. Ongoing developments in force field refinement aim to address challenges like solvent effects and improve accuracy, enhancing the predictive capabilities of classical MD in capturing complex molecular system dynamics [412].

Table 8. Comparison of force fields in MD simulations.

Force Field	Potential Energy Terms included	Description	Reference
AMBER	Bonded and non-bonded interactions	Biomolecules, proteins. Reproduces biomolecular structures well. Limited accuracy for some non-biological systems.	[413]
GAFF2	Bonded and non-bonded interactions	Organic molecules, ligands. Improved accuracy for small organic molecules. May not be as accurate for large biomolecules and complex systems.	[414]
CHARMM36	Bonded and non-bonded interactions	Biomolecules, lipids. Captures protein dynamics and lipid behavior. May require parameterization for non-standard molecules.	[415]

GROMOS	Bonded and non-bonded interactions	Biomolecules, small molecules. Efficient for small to medium-sized systems. Limited transferability to diverse molecular systems.	[416]
OPLS3e	Bonded and non-bonded interactions	Broad range of molecules. Balanced accuracy across various molecular types. Parameterization may be required for specific cases.	[417]
MARTINI	Coarse-grained representation	Lipids, polymers. Efficient for large-scale simulations, captures mesoscale behavior. Loss of atomic details, suitable for specific types of simulations.	[418]
AMOEBA	Many-body interactions, polarizability	Various molecular systems. Accurate representation of electrostatic and polar interactions. Computationally demanding, particularly for large systems.	[419]

4.3.6 MD simulations workflow

Preparing and running MD simulation for a protein-ligand complex involves several key steps from system preparation to MD trajectory production.

4.3.6.1 System preparation

Each system is meticulously prepared to conform to the requirements of the selected force field. The nomenclature of atomic types and residue names is force field-specific, typically differing from that of the PDB. Notably, force fields exhibit distinctions in the protonation states of histidine, which are not explicitly captured in the PDB format. These states include charged state, neutral τ tautomer, anionic τ tautomer, and anionic π tautomer. Subsequently, any missing hydrogens are systematically added, and the hydrogen bonding network undergoes optimization. This optimization involves the rotation of the side chains of asparagine, glutamine, and histidine residues, or the adjustment of the protonation state in the case of histidines [420].

4.3.6.2 System solvation

Each protein-ligand complex is placed within a water box, which may take the form of a cubic, rectangular, triclinic, or orthorhombic shape. This configuration ensures a minimum water layer of at least 10 Å surrounds the complex. The choice of a water model, such as Single Point Charge (SPC) or Transferable Intermolecular Potential 3 Point (TIP3P), is crucial for accurately representing the behavior of water molecules in the simulation.

4.3.6.3 System neutralization

Additionally, the overall charge of the complex must be neutralized, this is achieved by adding Na^+ and Cl^- ions to the solvent. The electrostatic potential is computed at multiple points on a grid that spans the volume of the system, accounting for the positions of ions.

4.3.6.4 Energy minimization

The energy minimization step aims to optimize the molecular structure and reach a more stable starting configuration. It relieves steric clashes, corrects bond distortions, and allows the system to settle into a local energy minimum. During this step, an iterative optimization algorithm like steepest descent or conjugate gradient is used to adjust the atomic coordinates and minimize the potential energy of the system. Forces on atoms are calculated and positions are adjusted in each iteration until convergence criteria like an energy threshold or maximum iterations are met. The goal is to guide the system to a local minimum on the potential energy surface, where forces on each atom are near zero. After minimization, the stability and quality of the minimized structure are assessed by checking bond parameters, examining the overall structure, and ensuring no major clashes or unrealistic distortions remain. This step is crucial for obtaining a reasonable starting point for further calculations or simulations.

4.3.6.5 Equilibration

Following energy minimization, the equilibration step involves adjusting the system's temperature and pressure, allowing solvent molecules to properly interact with the biomolecular components.

- **NVT Equilibration (Constant Number of Particles, Volume, and Temperature):**
In the first equilibration phase, the system is allowed to evolve at a constant temperature (NVT ensemble). This involves applying a thermostat to control the temperature and adjusting atomic velocities accordingly. The duration of this phase allows the system to reach a thermal equilibrium, where the temperature fluctuations stabilize.
- **NPT Equilibration (Constant Number of Particles, Pressure, and Temperature):**
Subsequently, the system undergoes equilibration at a constant temperature and pressure (NPT ensemble). This phase includes the application of a barostat to control pressure and may involve adjusting box dimensions to achieve the desired pressure. The system is allowed to equilibrate under these conditions, ensuring that both temperature and pressure fluctuations reach a stable state.

4.3.6.6 Production MD

Following NVT and NPT equilibration, the system transitions to the production MD run, where the dynamics of the protein-ligand complex are observed over an extended period. This phase is critical for obtaining meaningful data on the system's behavior.

4.3.7 MD trajectory data analysis

In the analysis phase of the MD simulation, various techniques are employed to extract meaningful insights from the obtained trajectory data.

4.3.7.1 Root-Mean-Square Deviation

The Root-Mean-Square Deviation (RMSD) is a measure of the similarity between two structures. The RMSD between two structures v and w of n atoms each (or n points) is calculated with the following formula (Eq. 15):

$$RMSD_{v,w} = \sqrt{\frac{1}{n} \sum_{i=1}^n \|v_i - w_i\|^2} \quad (15)$$

RMSD is used to compare protein structures. It is typically applied to the C α atoms of the protein. In MD analysis, it is used to observe the deviation of the system from the initial structure. The system is equilibrated when the RMSD reaches a plateau. Other analyses are typically performed on the stabilized portion of the trajectory.

4.3.7.2 Root-Mean-Square Fluctuation

While RMSD is an average calculated over all atomic coordinates of the system at each step of the trajectory. The Root-Mean-Square Fluctuation (RMSF) corresponds to an average calculated over all steps of the trajectory for each atom (Eq. 16).

$$RMSF_i = \sqrt{\frac{1}{T} \sum_{t=0}^{t=T} (x_i^t - \bar{x}_i)^2} \quad (16)$$

Here, $RMSF_i$ represents the fluctuation of atom i calculated over a trajectory of T steps. It is determined by taking the square root of the average squared distance between the position of the atom at time t (x_i^t) and the average position of the atom (\bar{x}_i). This analysis provides valuable insights into stable regions within protein structures.

4.3.7.3 Radius of gyration

The radius of gyration (Rg) is a measure of the compactness or spread of a molecular structure around its center of mass. Changes in Rg may indicate structural transitions, such as protein folding/unfolding or conformational changes induced by ligand binding or unbinding. Mathematically, the Rg can be expressed as (Eq. 17):

$$Rg = \sqrt{\frac{1}{N} \sum_{i=1}^N m_i r_i^2} \quad (17)$$

Where N is the total number of atoms, m_i is the mass of atom i , r_i is the distance of atom i from the centre of mass.

4.3.7.4 Solvent-accessible surface area

Solvent Accessible Surface Area (SASA) provides insights into the accessibility of a protein's surface to its surrounding solvent environment. SASA quantifies the extent to which atoms on the protein surface are accessible to solvent molecules, influencing various biological processes, including ligand binding. Changes in SASA during protein-ligand interactions can indicate alterations in the protein's conformation, accessibility of binding sites, and the potential impact on ligand binding affinity.

The Shrake-Rupley algorithm is widely employed for SASA calculations due to its computational efficiency. It involves rolling a probe sphere over the molecular surface and determining the solvent-accessible points, allowing for an estimation of the accessible surface area of the biomolecule.

4.3.7.5 Hydrogen bond analysis

Hydrogen bonds play a crucial role in maintaining the structure of proteins. The energy required to break a hydrogen bond ranges from 5 to 30 kJ/mol, making it stronger than van der Waals interactions but weaker than ionic or covalent bonds. Hydrogen bonds involve an electronegative atom such as oxygen, nitrogen, or fluorine, and a hydrogen atom covalently bonded to another electronegative atom.

The formation of a hydrogen bond depends on the relative position and the types of atoms in the donor (D) and acceptor (A). In MD simulations, observations on hydrogen bonds include the average number of bonds, which can be used to compare interactions between atom groups, and an analysis of occupancy or presence, providing information on stable regions within a molecule. Parameters such as the angle (θ) between the DH and DA vectors and the distance (d) between D and A are crucial, with θ being less than 40° and d less than 3.5 \AA for effective hydrogen bonding as illustrated in Figure 27 [421].

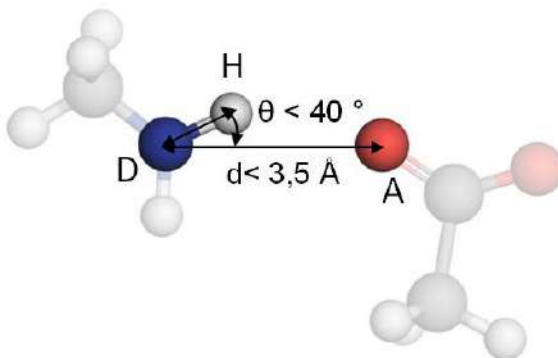


Figure 27. Geometric constraints of a hydrogen bond [421].

4.3.7.6 Principal component analysis

Principal component analysis (PCA) is a powerful statistical method that aims to reduce the dimensionality of a dataset while retaining the essential features and variability present in the original data. In the context of MD simulations of biomolecular systems, PCA is particularly valuable for identifying dominant motions, describing structural variations, and uncovering the principal components governing the system's dynamics.

- **Covariance Matrix:** PCA begins by constructing the covariance matrix from the atomic positional fluctuations obtained during the MD simulation.
- **Eigen decomposition:** The covariance matrix is then diagonalized, yielding eigenvectors and eigenvalues.
- **Principal Components:** The eigenvectors represent the principal components, and the eigenvalues indicate the magnitude of the variance along each principal component.

4.3.8 Free energy calculations

4.3.8.1 Molecular mechanics/Generalized Born Surface Area

Molecular mechanics/Generalized Born Surface Area (MM/GBSA) is a computational approach used to estimate free energy changes in biomolecular systems, particularly for studying binding affinities of ligands to proteins [422]. The MM/GBSA method was developed by Peter Kollman and his group at the University of California, San Diego (UCSD) in the late 1990s [423]. It combines MM calculations, which describe the bonded and non-bonded interactions within the system, with a continuum solvation model based on the Generalized Born (GB) theory to account for solvent effects [424]. The binding free energy of a ligand to a protein receptor is calculated as the thermodynamic difference between the individual free energies of the free protein (P), the free ligand (L), and the formed complex (PL) in solvent (Eq. 18):

$$\Delta G_{bind} = G_{PL} - (G_P + G_L) \quad (18)$$

The binding free energy can be decomposed into the vacuum potential energy, ΔE_{MM} , which includes the energy of both bonded as well as non-bonded interactions (Eq. 19), and it is calculated based on the MM force-field parameters [425], [426].

$$\Delta E_{MM} = \Delta E_{bonded} + \Delta E_{nonbonded} = \Delta E_{bonded} + (\Delta E_{ele} + \Delta E_{vdw}) \quad (19)$$

Where ΔE_{bonded} represents bonded interactions encompassing bond, angle, dihedral, and improper interactions. $\Delta E_{nonbonded}$ represents nonbonded interactions comprising both

electrostatic (ΔE_{ele}) and van der Waals (ΔE_{vdw}) interactions, modeled through Coulomb and Lennard-Jones potential functions, respectively. In the single trajectory approach, the conformation of the protein and ligand in both the bound and unbound forms is assumed to be identical. Consequently, ΔE_{bonded} is consistently considered as zero [427].

This binding free energy can be further described to account for the free energy of solvation (Eq. 20):

$$\Delta G_{bind} = \Delta E_{ele} + \Delta E_{vdw} + \Delta G_{GB} + \Delta G_{SASA} - T\Delta S \quad (20)$$

The equation incorporates the solvation energy (ΔG_{GB}) accounting for polar solvation effects using an implicit solvation GB model, and the SASA solvation energy (ΔG_{SASA}) capturing nonpolar solvation effects based on the approximation of SASA [428]. The conformational entropy term ($-T\Delta S$) which is calculated by normal-mode analysis, is usually neglected due to the high computational cost and technical errors associated with its calculation [429].

4.3.8.2 Molecular mechanics/Poisson-Boltzmann Surface Area

Like MM/GBSA, Molecular mechanics/Poisson-Boltzmann Surface Area (MM/PBSA) is a computational method used for the estimation of free energy changes in biomolecular systems, especially for studying ligand binding to proteins. MM/PBSA combines MM calculations with a continuum solvation model as described in MM/GBSA (Eq. 21), but it uses the computationally time-consuming Poisson-Boltzmann (PB) equation to describe the electrostatic solvation effects (ΔG_{solv}) [430].

$$\Delta G_{bind} = \Delta E_{ele} + \Delta E_{vdw} + \Delta G_{solv} + \Delta G_{SASA} - T\Delta S \quad (21)$$

4.3.9 MD simulations software

There are several software packages available for MD simulations. Some popular options include GROMACS, AMBER, Desmond, LAMMPS, and NAMD. These software packages are widely used for MD simulations and offer various features suitable for different research needs. GROMACS is a free and open-source software suite for high-performance MD and output analysis [431], while AMBER is a suite of programs for MD simulations of proteins and nucleic acids [432]. Desmond is a high-performance MD simulation software package developed at D. E. Shaw Research. It is designed to perform MD simulations of biological systems on conventional computer clusters and can also be used for absolute and relative free energy calculations, such as free energy perturbation [433]. LAMMPS is a classical MD code with a focus on materials modelling [434]. NAMD is a powerful, parallel MD simulation software package [435]. The choice of software depends on specific research requirements, user

expertise, and the nature of the simulations to be performed. Table 9 details some of the commonly used MD simulation software packages.

Table 9. Description of commonly used software packages for MD simulations.

Program	Licence	Description	Reference
GROMACS	Open-source (GPLv2)	A versatile package to perform MD, scalable and efficient in performing large-scale simulations	[431]
AMBER	Open-source (Artistic License 2.0)	A suite of biomolecular simulation programs that includes several force fields for the simulation of proteins, nucleic acids, and carbohydrates.	[432]
Desmond	Commercial and academic	Developed by Schrödinger, Desmond is a high-performance MD simulation program with a focus on drug discovery.	[433]
LAMMPS	Open-source (GPLv2)	A classical MD simulation code, designed to run efficiently on parallel computers.	[434]
NAMD	Open-source (NAMD License, like GPL)	A parallel MD code designed for high-performance simulation of large biomolecular systems.	[435]

**CHAPTER III: CHEMICAL LIBRARY
DESIGN, QSAR AND MOLECULAR
DYNAMICS SIMULATIONS OF
NATURALLY OCCURRING
COUMARINS AS DUAL INHIBITORS
OF MAO-B AND ACHE**

CHAPTER III: CHEMICAL LIBRARY DESIGN, QSAR AND MOLECULAR DYNAMICS
SIMULATIONS OF NATURALLY OCCURRING COUMARINS AS DUAL INHIBITORS OF
MAO-B AND AChE

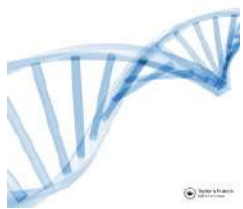
Following our previous work on coumarins (refer to Annex 1), we have compiled a chemical library to consolidate information on naturally occurring coumarins. Employing a multi-stage virtual screening approach, incorporating QSAR modelling, molecular docking, and ADMET prediction, we targeted MAO-B and AChE—known for their neuroprotective and “disease-modifying” potential in Parkinson’s and Alzheimer’s diseases. Ten coumarin derivatives with potential dual-target action against MAO-B and AChE were identified. Molecular docking highlighted CDB0738 and CDB0046 as promising candidates with favourable interactions and suitable ADMET profiles. MD simulations over 100 ns demonstrated the stability of CDB0738, indicating its potential as a dual inhibitor of MAO-B and AChE. However, experimental studies are required to validate their bioactivity. These findings highlighted the potential of naturally occurring coumarins as candidates against relevant targets, encouraging further virtual screening studies against the chemical library.

The details of this work are reported in the following publication.

Boulaamane, Y., Kandpal, P., Chandra, A., Britel, M. R., & Maurady, A. (2023). Chemical library design, QSAR modelling and molecular dynamics simulations of naturally occurring coumarins as dual inhibitors of MAO-B and AChE. *Journal of Biomolecular Structure and Dynamics*, 1-18. (Reprinted with permission)

Available at: <https://doi.org/10.1080/07391102.2023.2209650>

Conceptualization: Y.B. A.M; Methodology: Y.B., A.M.; Investigation: Y.B., A.M.; Visualization: Y.B., I.A., H.P.; Supervision: M.R.B., A.M.; Writing—original draft: Y.B.; Writing—review & editing: Y.B., A.M.



Chemical library design, QSAR modeling and molecular dynamics simulations of naturally occurring coumarins as dual inhibitors of MAO-B and AChE

Yassir Boulaamane, Pallavi Kandpal, Anshuman Chandra, Mohammed Reda Britel & Amal Maurady

To cite this article: Yassir Boulaamane, Pallavi Kandpal, Anshuman Chandra, Mohammed Reda Britel & Amal Maurady (2023): Chemical library design, QSAR modeling and molecular dynamics simulations of naturally occurring coumarins as dual inhibitors of MAO-B and AChE, *Journal of Biomolecular Structure and Dynamics*, DOI: [10.1080/07391102.2023.2209650](https://doi.org/10.1080/07391102.2023.2209650)

To link to this article: <https://doi.org/10.1080/07391102.2023.2209650>



Published online: 18 May 2023.



Submit your article to this journal [↗](#)



View related articles [↗](#)



View Crossmark data [↗](#)



Chemical library design, QSAR modeling and molecular dynamics simulations of naturally occurring coumarins as dual inhibitors of MAO-B and AChE

Yassir Boulaamane^a, Pallavi Kandpal^b, Anshuman Chandra^c, Mohammed Reda Britel^a and Amal Maurady^{a,d} 

^aLaboratory of Innovative Technologies, National School of Applied Sciences of Tangier, Abdelmalek Essaadi University, Tetouan, Morocco;

^bProteinInsights, New Delhi, India; ^cICMR-National Institute of Malaria Research, New Delhi, India; ^dFaculty of Sciences and Techniques of Tangier, Abdelmalek Essaadi University, Tetouan, Morocco

Communicated by Ramaswamy H. Sarma

ABSTRACT

Coumarins are a highly privileged scaffold in medicinal chemistry. It is present in many natural products and is reported to display various pharmacological properties. A large plethora of compounds based on the coumarin ring system have been synthesized and were found to possess biological activities such as anticonvulsant, antiviral, anti-inflammatory, antibacterial, antioxidant as well as neuroprotective properties. Despite the wide activity spectrum of coumarins, its naturally occurring derivatives are yet to be investigated in detail. In the current study, a chemical library was created to assemble all chemical information related to naturally occurring coumarins from the literature. Additionally, a multi-stage virtual screening combining QSAR modeling, molecular docking, and ADMET prediction was conducted against monoamine oxidase B and acetylcholinesterase, two relevant targets known for their neuroprotective properties and 'disease-modifying' potential in Parkinson's and Alzheimer's disease. Our findings revealed ten coumarin derivatives that may act as dual-target drugs against MAO-B and AChE. Two coumarin candidates were selected from the molecular docking study: CDB0738 and CDB0046 displayed favorable interactions for both proteins as well as suitable ADMET profiles. The stability of the selected coumarins was assessed through 100 ns molecular dynamics simulations which revealed promising stability through key molecular interactions for CDB0738 to act as dual inhibitor of MAO-B and AChE. However, experimental studies are necessary to evaluate the bioactivity of the proposed candidate. The current results may generate an increasing interest in bioprospecting naturally occurring coumarins as potential candidates against relevant macromolecular targets by encouraging virtual screening studies against our chemical library.

ARTICLE HISTORY

Received 19 February 2023

Accepted 5 April 2023

KEYWORDS

Coumarin; monoamine oxidase B; acetylcholinesterase; molecular docking; ADMET prediction; molecular dynamics simulations; QSAR modeling

1. Introduction

Neurodegenerative disorders such as Alzheimer's and Parkinson's disease remains the most frequent neurological diseases in the world (Barnham et al., 2004). Neurodegenerative diseases are characterized by the progressive loss of neuronal cells in the brain because of different factors contributing to its progression such as the deposition of amyloid fibrils, oxidative stress, mitochondrial dysfunction, and metal accumulation (Dugger & Dickson, 2017). Parkinson's disease (PD) is the second most frequent neurological disorder in the world that is described by the loss of dopaminergic neurons in the midbrain causing striatal dopamine deficiency (Poewe et al., 2017). It is estimated to affect six million people worldwide with an increasing prevalence expected to reach 2- to 3-fold by 2030 (Lee & Gilbert, 2016; Poewe & Mahlknecht, 2020). The most frequent motor symptoms are dyskinesia, shaking, and difficulty moving (Xia & Mao, 2012). Other non-motor symptoms may appear earlier such as depression, insomnia, and constipation (National Institute for Clinical Excellence, 2006). There is accumulating evidence indicating that oxidative damage and mitochondrial

imbalance contribute to the cascade of events leading to the degeneration of the dopaminergic neurons (Dias et al., 2013). Thus, there is an increasing need for novel 'disease-modifying' therapies (Kalia et al., 2015). Current therapeutic strategies for PD treatment include L-DOPA therapy which remains the gold standard for controlling PD motor symptoms, other dopaminergic treatments include dopamine agonists, monoamine oxidase B (MAO-B) inhibitors and catechol-O-methyl transferase (COMT) inhibitors (Kaakkola, 2010; Lang & Marras, 2014). Non-dopaminergic treatments have also been proven to be effective for alleviating PD symptoms and slowing down neuronal damage such as adenosine A_{2A} receptor and N-methyl-D-aspartate (NMDA) receptor antagonists (Bara-Jimenez et al., 2003; Bibbiani et al., 2003). While acetylcholinesterase (AChE) inhibitors are mainly used to treat Alzheimer's disease, a clinical study has shown that AChE inhibitors may be efficacious for improving cognitive impairment and dementia in PD patients (Van Laar et al., 2011). Another recent meta-analysis included randomized controlled trials to investigate the effects of AChE inhibitors on PD's major symptoms, it was found that rivastigmine was effective for PD dementia (Chen et al., 2021). There's a great

deal of literature outlining the dual-activity of coumarin derivatives against MAO-B and AChE. Brühlmann et al. (2001) conducted an experimental study of a set of 17 coumarins with known inhibition against MAO enzymes against AChE, all the compounds inhibited AChE with values in the micromolar range (3 – 100 µM) (Brühlmann et al., 2001). Another study reported the structural requirements of coumarins as dual inhibitors of MAO-B and AChE through molecular docking and structure-activity relationship analysis (Yusufzai et al., 2018). More recently, Ekström et al. (2022) synthetized a series of coumarins against MAO-B and AChE, the most potent compounds were bearing the N-methylbenzylamine moiety at position C7 and the N-benzylpiperidine moiety that is found in Donepezil, a reference AChE inhibitor that is prescribed to AD patients (Ekström et al., 2022).

Structural analysis of the crystallographic structure of MAO-B (PDB ID: 2V61) revealed that the latter is a dimer formed by a globular domain attached to the membrane through a C-terminal helix (Binda et al., 2007). The substrate fixing domain, located near the FAD cofactor binding domain, contains the active site of the enzyme. This active site is comprised of two cavities: an entrance cavity covered by the residues Pro-102, Pro-104, Leu164, Phe-168, Leu-171, and Ile-198, and a substrate cavity formed by Tyr-60, Cys-172, Tyr-188, Gln-206, Phe-343, Tyr-398, and Tyr-435 (Boulaamane et al., 2023). The residues Ile-199 and Tyr-326 act as 'gating' residues for the substrate cavity, playing a crucial role in determining substrate and inhibitor specificity for MAO-B (Milczek et al., 2011).

Meanwhile, the analysis of AChE crystal structure (PDB ID: 4EY7) revealed the presence of a dimer like MAO-B. The binding cavity is divided into the peripheral anionic site (PAS) formed by the residues: Trp-286, Tyr-337 and Phe-338; and the catalytic anionic site (CAS) which consists of the residues: Trp-86, Glu-202, Tyr-337 and Phe-338 (Pourshojaei et al., 2019). A study conducted with single and multiple site-specific mutants of mouse AChE revealed three distinct regions that confer selectivity for AChE inhibitors over butyrylcholinesterase (BChE). The first domain is defined by the acyl pocket dimensions, where the side chains of Phe-295 and Phe-297 primarily outline the acyl pocket dimensions. By replacing these phenylalanine side chains with the aliphatic residues found in BChE, the enzyme can catalyze larger substrates and accommodate selective BChE inhibitors. The second domain is found near the lip of the active center gorge defined by two tyrosines, Tyr-72 and Tyr-124, and by Trp-286. This region is crucial for the selectivity of bisquaternary inhibitors, such as BW284C51. The third domain is responsible for choline binding and defined by Tyr-337 [23]. The 3D structures of MAO-B and AChE along with their respective active sites are shown in Figure 1.

Despite the accumulating studies reporting the multi-target potential of synthetic drugs, the use of natural products against multiple therapeutic targets is yet to be investigated in detail (Lu et al., 2012). Numerous studies have reported the potency of natural products from medicinal plants, fruits, and vegetables to act as antiparkinsonian agents such as alkaloids, glycosides, flavonoids, caffeine, xanthones,

catechins and coumarins which demonstrated neuroprotective properties associated with strong antioxidant and monoamine oxidase inhibitory activity (Carradori et al., 2014; Khanam et al., 2021; Singla et al., 2021).

Coumarins are phenolic compounds formed by fused benzene and α -pyrone rings (Garrard, 2014). Benzopyrones such as coumarins and flavonoids are present in many vegetables, fruit, seeds, nuts, coffee, tea, and wine (Lacy & O'Kennedy, 2004). Thus, dietary exposure to benzopyrones is considerable, which explains why extensive research into their pharmacological and therapeutic properties is underway over many years (Venugopala et al., 2013). A wide variety of coumarin derivatives have shown anticonvulsant, antiviral, anti-inflammatory, antibacterial, antioxidant and monoamine oxidase inhibitory activities (Stefanachi et al., 2018).

The growing volume of biomedical data in chemistry and biology requires development of new methods and approaches for their analysis (Tetko & Engkvist, 2020). *In silico* and data-driven approaches are much more time and cost effective compared to traditional experimental approaches (Zhao et al., 2020). They can rapidly screen large chemical libraries to identify promising leads (Pasrija et al., 2022). In fact, chemical libraries are essential databases for virtual drug screening. They consist of vast collections of chemical compounds with diverse structures and properties, allowing scientists to explore a wide range of potential drug candidates (Fukunishi & Lintuluoto, 2010). Furthermore, *in silico* methods allow for the generation of targeted libraries that focus on specific biological targets, chemical classes, or geographical regions. An illustrative example is the Benzylisoquinoline Alkaloids database (BIAdb), which encompasses over 800 plant-derived compounds of this chemical class enabling users to explore and obtain comprehensive information on these compounds (Singla et al., 2010).

Herein, we aimed to construct a chemical library of all available naturally occurring coumarins with their natural sources from which they were isolated to allow users to identify potential lead compounds and their source prior to their synthesis through high-throughput virtual screening. Furthermore, the chemical library was subject to a multi-stage virtual screening using quantitative structure-activity relationships (QSAR) models, molecular docking and ADMET evaluation to explore the potency of natural coumarins to act as dual inhibitors against MAO-B and AChE. Finally, the lead compounds were subject to 100 ns molecular dynamics simulations to further assess their stability over time.

2. Materials and methods

2.1. Data collection and chemical library design

PubMed search engine (<https://pubmed.ncbi.nlm.nih.gov/>) was employed to retrieve the available literature reporting the chemical data on coumarin containing compounds identified from natural sources using 'natural coumarins' as a search query. Our search revealed three book sections and one review article published in Progress in the Chemistry of Organic Natural Products in 1952, 2002, and 2017 and Journal of Pharmaceutical Sciences in 1964 respectively

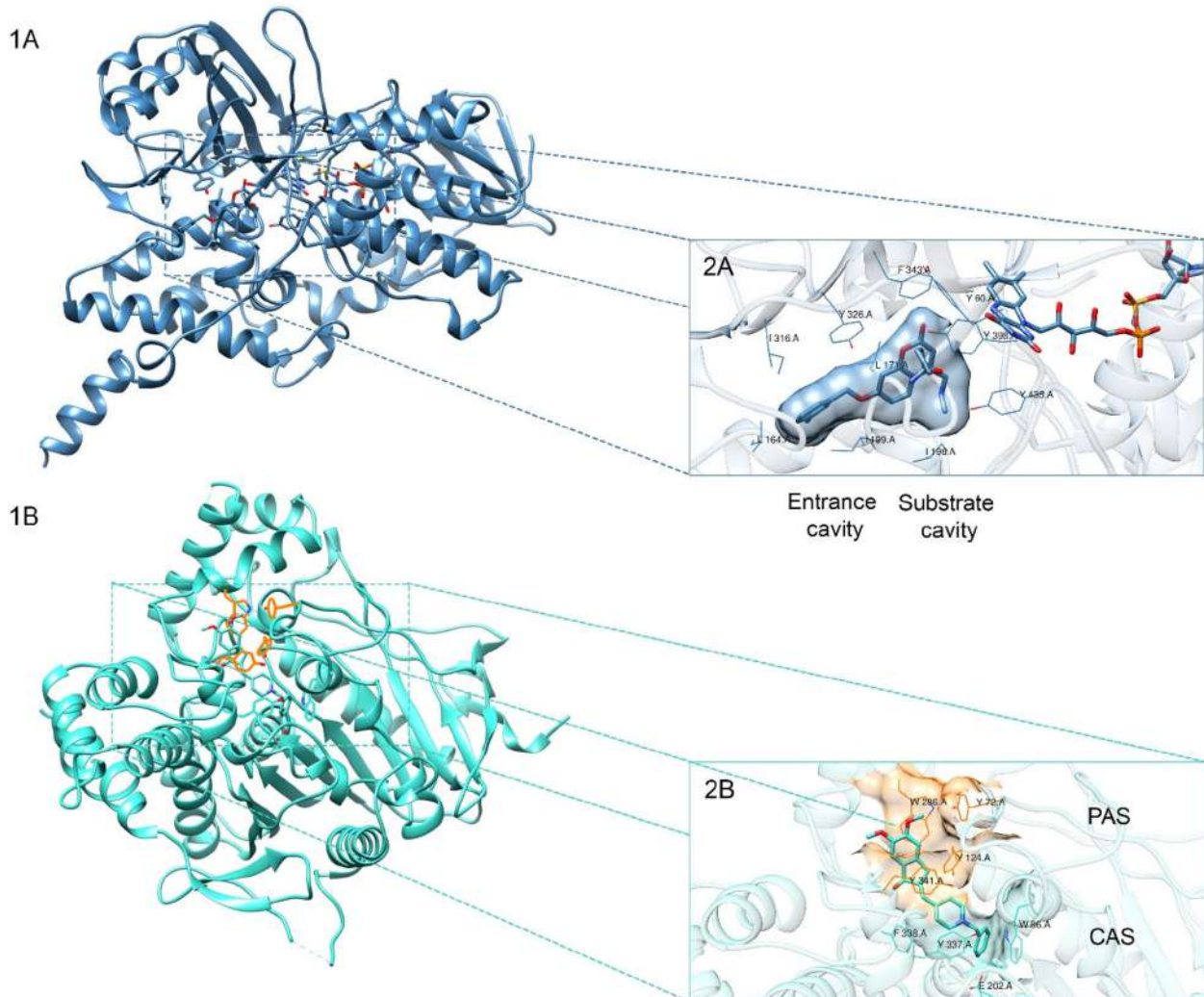


Figure 1. (1A) Crystal structure of MAO-B (PDB ID: 2V61) in complex with 7-(3-chlorobenzylxy)-4-(methylamino)methyl-coumarin. (2A) Active site residues of MAO-B. (1B) Crystal structure of AChE (PDB ID: 4EY7) in complex with Donepezil. (2B) Active residues of the peripheral anionic site (PAS) and the catalytic anionic site (CAS) of AChE.

(Dean, 1952; Murray, 2002; Sarker & Nahar, 2017; Soine, 1964). The first step consisted of extracting the compound's names, chemical class, and natural sources. Subsequently, we searched the PubChem database to retrieve the PubChem IDs and chemical structures of all the compounds in SMILES format. OSIRIS DataWarrior software was used to generate unique chemical identifiers InChI Keys for all the molecules (Sander et al., 2015). Duplicate compounds were removed resulting in 905 unique natural coumarins. Furthermore, physicochemical properties such as lipophilicity, molecular weight, water solubility, number of hydrogen bond donors/acceptors, rotatable bonds, and polar surface area were computed as shown in Figure 2. All chemical information of the compounds can be found in CoumarinDB (<https://yboloualame.github.io/CoumarinDB/>).

2.2. QSAR modeling

From ChEMBL database (<https://www.ebi.ac.uk/chembl/>), we retrieved two datasets containing chemical structures that were classified according to their calculated activity,

including 5066 MAO-B inhibitors and 8846 AChE inhibitors with reported half maximal inhibitory concentration (IC_{50}) values (Mendez et al., 2019). The datasets were manually curated, duplicate compounds were removed when multiple bioactivity values were reported for a given compound by calculating the mean value of the 'Standard Value' column in the pandas DataFrame grouped by the 'Molecule ChEMBL ID' column. The resulting mean values are added to a new column in the DataFrame called 'mean_value'. Thereafter, the DataFrame.drop_duplicates function included in the Pandas library (McKinney, 2011) was used to identify and remove duplicate rows in the dataset based on the values in the 'Molecule ChEMBL ID' column to keep only one occurrence.

Logarithmic transformation was applied to all the activity values to better determine the potency of the compounds (Burggraaff et al., 2020; Tarasova et al., 2015). The workflow of QSAR modeling is shown in Figure 3.

The datasets were then converted to SMILES format, RDKit cheminformatics software was used to generate molecular descriptors using Morgan fingerprints (Ding et al., 2021; Landrum, 2013). The IC_{50} values were converted to

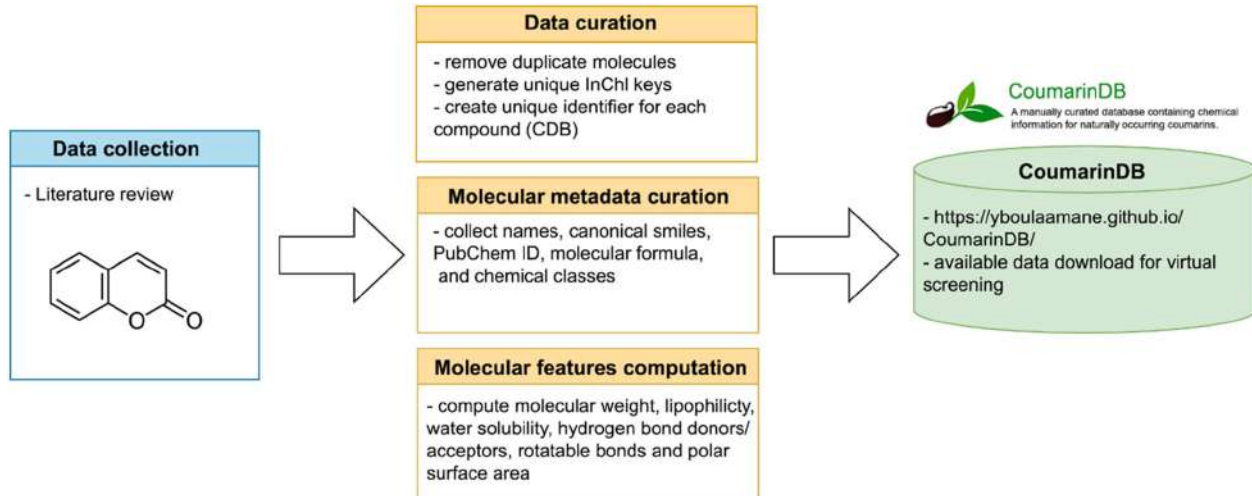


Figure 2. Chemical library construction and curation of CoumarinDB.

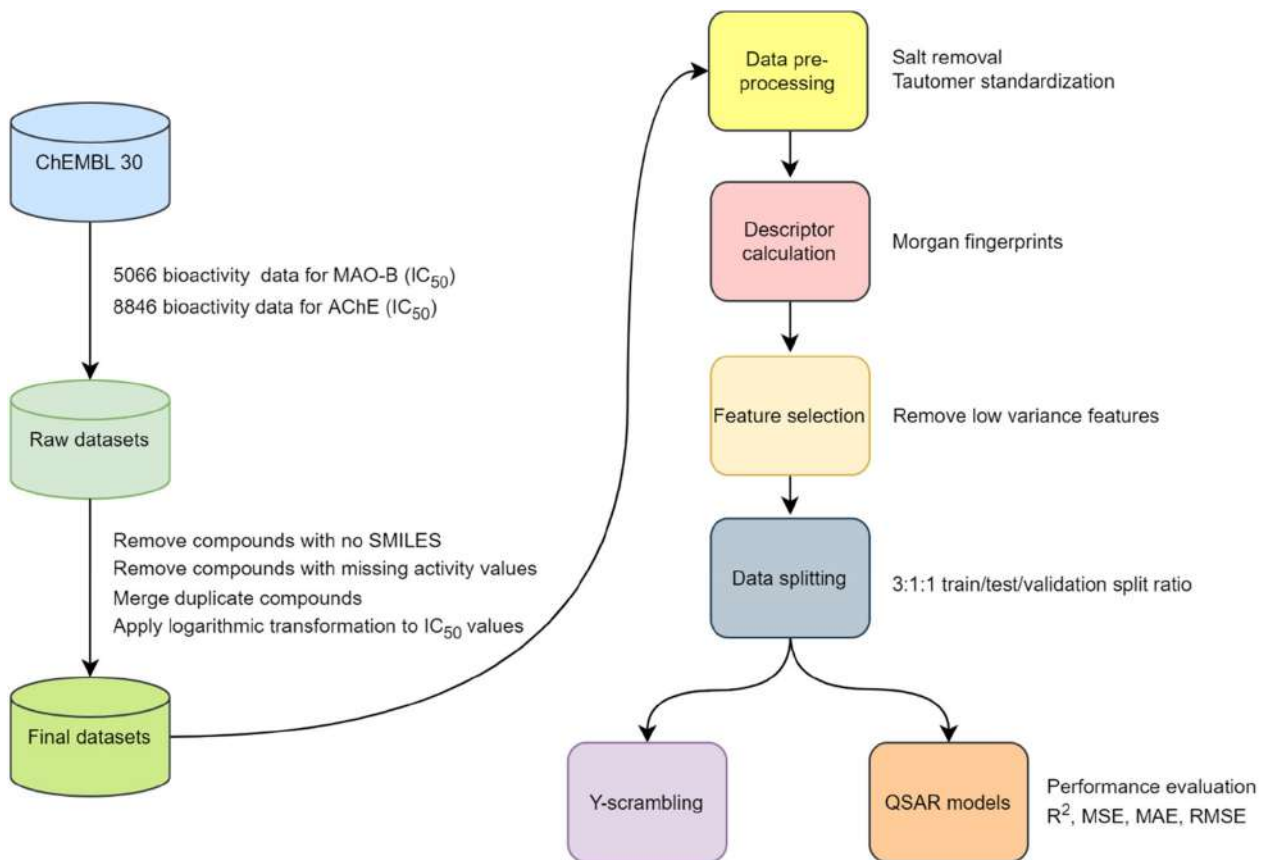


Figure 3. QSAR workflow for modelling the bioactivity prediction of MAO-B and AChE.

Table 1. Distribution of the molecules in the training, testing and validation dataset.

Dataset	Train set	Test set	Validation set	Total dataset
Number of Molecules in MAO-B dataset	2526	842	843	4211
Number of Molecules in AChE dataset	2618	873	873	4363

pIC_{50} for ease of handling. The dataset was split into a 3:1:1 ratio of training, testing and validation sets. The number of molecules in each of them is listed in Table 1.

Machine learning algorithms like multiple linear regression (MLR), random forest (RF), decision trees (DT), support vector

regression (SVR), AdaBoost and extreme gradient boosting (XGB) were used for building the model (Wu et al., 2021). These models were built with all the hyperparameters set to default and were assessed using validation metrics such as the coefficient of determination (R^2), mean squared error

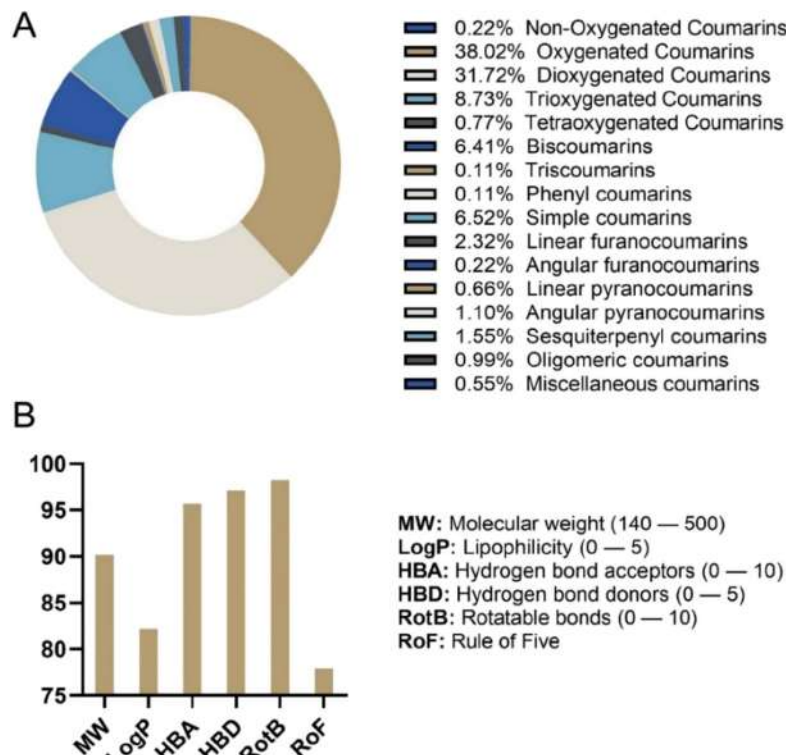


Figure 4. (A) Chemical class distribution of naturally occurring coumarins. (B) Percentage of compounds in the recommended range for each physicochemical parameter of the rule of five.

(MSE), mean absolute error (MAE) and root mean squared error (RMSE). The QSAR workflow is illustrated represented in Figure 3.

2.3. Preparation of ligand structures

The designed library of coumarins was found to contain mostly oxygenated and deoxygenated coumarins as shown in Figure 4A. Primary filtration was conducted based on Lipinski's rule of five. 706 out of 905 (78%) molecules were retained for the present study as drug-like compounds (Figure 4B). OSIRIS DataWarrior cheminformatics program was used to generate an SDF file for all the ligands (Sander et al., 2015). Thereafter, the OpenBabel toolbox was used to split the compounds and optimize the chemical structures using MMFF94 force field (Halgren, 1996; O'Boyle et al., 2011). Partial charges and atom types were computed for the molecular docking study.

2.4. Molecular docking

https://www.rcsb.org/) (Binda et al., 2007). Alternatively, crystal structure of AChE (PDB ID: 4EY7, resolution = 2.3 Å) in complex with Donepezil (E20) was selected for the molecular docking (Cheung et al., 2012). Native ligands and crystal water molecules were removed to make computations easier and clear the binding pocket of

possible water molecules that would distort the pose search. Chain B was removed from both protein dimers and only one chain was kept for the molecular docking along with the FAD cofactor in MAO-B as it plays an important role in the proper functioning of the enzyme in catalyzing the deamination of monoamines (Edmondson & Newton-Vinson, 2001). Residues with missing atoms were fixed using the CHARMM-GUI web server (Jo et al., 2008). Polar hydrogen and Kollman charges were added using AutoDockTools (Huey & Morris, 2008). Finally, the native ligands were used to define the grid box parameters to cover the entire binding sites residues. The grid box was generated largely enough to fit all the active site residues of MAO-B and AChE (24 × 24 × 24 Å) in x, y and z directions, respectively. The grid box was placed in a way to cover both cavities in the selected targets and to allow larger molecules to dock properly (51.2 × 155.5 × 28.7 Å and -14.1 × -43.8 × 27.7 Å for MAO-B and AChE respectively). Molecular docking was performed using AutoDock Vina with an exhaustiveness = 8 and num_modes = 10 (representing 10 conformations) (Trott & Olson, 2010).

2.5. ADME/tox prediction

Forty percent of drug candidates fail in clinical trials due to unfavorable pharmacokinetic properties (Lin et al., 2003). *In silico* open access tools for predicting Absorption, Distribution, Metabolism, Excretion and Toxicity (ADMET) parameters have emerged as a cost-efficient approach in the early phases of drug development (Gola et al., 2006). The pharmacokinetics and toxicity parameters for the selected

Table 2. The validation metrics of the algorithms used at default hyperparameters.

Algorithm	MAO-B Dataset				AChE Dataset			
	R ²	MSE	MAE	RMSE	R ²	MSE	MAE	RMSE
MLR	0.19	2.96	4.68	4.54	-0.24	10.3	2.13	3.21
RF	0.72	0.65	0.58	0.81	0.67	1.11	0.70	1.05
DT	0.30	1.14	0.71	1.07	0.52	1.58	0.77	1.26
SVR	0.59	0.68	0.59	0.82	0.70	1.01	0.67	1.00
AdaBoost	0.20	1.32	0.95	1.15	0.34	2.19	1.27	1.48
XGB	0.60	0.65	0.58	0.81	0.69	1.01	0.69	1.01

coumarins such as water solubility, intestinal absorption, blood-brain barrier permeability, drug-drug interactions, Ames toxicity and hepatotoxicity were computed using pkCSM online calculation tool (<http://biosig.unimelb.edu.au/pkcs/>) (Pires et al., 2015).

2.6. Molecular dynamics workflow

Two compounds which demonstrated great affinity towards MAO-B and AChE as well as great pharmacokinetics properties were selected from the molecular docking study to perform MD simulations to study the stability of the protein-ligand complexes over time. Desmond module of Schrödinger's suite (2020-3) was used to run 100 ns MD simulation (Bowers et al., 2006). The water-soaked solvated system was created in Desmond using the System Builder panel. OPLS2005 force field was selected, and Single Point Charge (SPC) was used as a solvent model with a 10 Å orthorhombic box for both proteins (Shivakumar et al., 2010). The system was neutralized by randomly adding enough counter-ions (Na⁺ and Cl⁻) and isosmotic state was maintained by adding 0.15 M NaCl. The solvated model system was subjected to energy minimization using OPLS2005 force field parameters as the default protocol associated with Desmond (Boulaamane et al., 2023). Then, the system was equilibrated throughout the simulation time via NPT ensemble at a constant 300 K temperature and 1 atm pressure using the Nose-Hoover thermostat algorithm and Martyna-Tobias-Klein barostat algorithm, respectively (Melchionna et al., 1993; Möller et al., 1992). A total of 100 ns simulations were carried out, during which 1000 frames were recorded. Finally, MD simulation trajectory was analyzed using the Simulation Interaction Diagram (SID) tool (Katari et al., 2016).

3. Results and discussion

3.1. QSAR models validation

The performance of the generated machine learning models is presented in **Table 2**. The MLR algorithm performed the worst of all on the MAO-B dataset with a very low value (0.19) and on the AChE dataset with a negative R² and a corresponding high error rate. AdaBoost performed better than MLR on both the datasets, however R² was still below 0.5, and MSE value was high. A better performance was observed by the SVR, XGB and RF algorithm with an R² value of 0.59, 0.60, and 0.61 respectively, on the MAO-B dataset. Moreover, a better metric was obtained using these algorithms on the

Table 3. The grid parameters of SVR algorithm used in GridSearchCV*.

Dataset	Hyperparameter	Values
MAO-B	n_estimators	200–2000, step = 10
	max_features	'auto,' 'sqrt'
	max_depth	10–110, step = 11
	min_sample_split	2, 5, 10
	min_sample_leaf	1, 2, 4
	bootstrap	'True,' 'False'
	kernel	'linear,' 'rbf,' 'sigmoid', 'poly'
	tolerance	1e-3, 1e-4, 1e-5, 1e-6
	C	1, 1.5, 2, 2.5, 3
	degree	1, 2, 3, 4, 5, 6
AChE	gamma	'scale,' 'auto'

*The acronyms for the various parameters are as mentioned in the scikit-learn documentation.

AChE dataset. However, the best model amongst all was RF with an R² value of 0.72 and MSE of 0.65, for the MAO-B dataset and for the AChE dataset, it was SVR with an R² value of 0.70 and MSE of 1.01.

Since the best of all the algorithms used was RF for the MAO-B dataset and SVR for the AChE dataset, the hyperparameters were set to be optimized using the GridSearchCV function in Scikit-Learn. The algorithm was extensively searched using the RepeatedKFold, where number of folds was set to 10 with 3 repeats and with parameters as presented in **Table 3**.

The best model of all the parameters for the SVR was found to be with kernel: rbf, C:3, tol: 1e-0.5, gamma: 'scale' and degree: 3. The model was improved and an r² value of 0.74 and MSE of 0.86 was obtained. For the MAO-B dataset, the best RF parameters were found to be at n_estimators = 800, min_samples_split = 5, min_samples_leaf = 1, max_features = 'sqrt', max_depth = 90, bootstrap = False. The model was found to show an r² value of 0.65 and MSE of 0.58. These models were also applied to the validation set (for their respective datasets). The evaluation metrics for the test and validation set are given in **Table 4**.

To ascertain that the evaluation metrics obtained were not obtained by-chance correlation, a y-scrambling was performed for five times, where the associated pIC₅₀ values for the molecules in the training set were jumbled, the model was 'fit' using them and predicted for the test set. The goal was to check if the model performs worse, indicating that there is no chance correlation in the model. The results are presented in **Table 5**. All the 5 models generated performed poorly, with high error metrics and a negative correlation value, thereby indicating that the model used here is robust.

The models with the best hyperparameters of RF and SVR algorithm were applied to the dataset of the naturally occurring coumarins (having 706 molecules) to identify potential leads for biological evaluation. The top molecules are presented in **Figure 5**.

3.2. Molecular docking results

The molecular docking protocol implemented in AutoDock Vina was validated by redocking the crystal ligands of MAO-B and AChE against their respective binding sites (Mateev et al., 2022; Trott & Olson, 2010). Co-crystallized ligands were downloaded from PubChem database and prepared using

the same parameters for the tested ligands (Kim et al., 2019). The root-mean-square deviation (RMSD) was calculated by superposing both docked and native ligands, the latter was used as a reference. The results yielded values of 0.87 Å for MAO-B and 0.98 Å for AChE demonstrating a good accuracy of the docking program (Figure 6).

The top scoring, common molecules predicted by both the datasets were then docked into the active site of MAO-B and AChE using AutoDock Vina (Trott & Olson, 2010). The best conformations of the docked compounds were selected based on their binding affinity and their similarity to the co-crystallized ligands by means of superposition. Hydrogen bonds and nearby hydrophobic interactions were visualized using DS Visualizer (Biovia, 2017). Docking scores and hydrogen bonds of the best candidates along with the reference inhibitors are displayed in Table 6.

Molecular interactions analysis was conducted for the two highest-scoring candidates (Figures 7 and 8). CDB0738 revealed the presence of a hydrogen bond involving Gln-206 which is known to act as a hydrogen bond acceptor for

most MAO-B inhibitors (Boulaamane et al., 2022). Another hydrogen bond was found to involve Tyr-435 of the aromatic cage. A π - π stacking interaction was observed between the pyrone ring of the coumarin scaffold and Tyr-326, a key aromatic residue, suggesting potential selectivity for MAO-B over MAO-A where this residue is replaced by the aliphatic amino acid, Ile-335. Meanwhile, CDB0046 formed a hydrogen bond with Pro-102, a rigid residue located at the extremity of the entrance cavity of the MAO-B binding pocket. This interaction may be attributed to the larger size of the compound, potentially conferring selectivity for MAO-B over MAO-A, as the latter has a smaller cavity and cannot accommodate bulkier compounds. An additional hydrogen bond was observed between CDB0046 and Cys-172, a residue located in the catalytic site of MAO-B. It's important to note that this residue is not conserved in both isoenzymes. In MAO-A, Cys-172 is replaced by Asn-171, and Cys-323 is in the opposite side of the binding pocket, further adding to the potential selectivity of the studied coumarin (Di Paolo et al., 2019).

On the other hand, CDB0738 formed a hydrogen bond with Glu-202 located in the choline binding site of AChE. This interaction plays an essential role in maintaining the critical hydrogen bond network required to support the catalytic triad of AChE (Wang et al., 2022). CDB0738 also exhibited two additional π - π stacking interactions involving the aromatic amino acids Trp-86 and Tyr-341 known for stabilizing AChE inhibitors (Ranjan et al., 2015). In contrast, CDB0046 formed four hydrogen bonds with Tyr-72, a residue known to be critical for the selectivity of bisquaternary inhibitors (Radic et al., 1993). The 3-hydroxy-3-(hydroxymethyl)-5-

Table 4. The evaluation metrics using the best model generated from hyper-parameter tuning.

Dataset	Algorithm	R ²	MSE	MAE	RMSE
MAO-B	Test Set	0.78	0.58	0.56	0.76
	Validation Set	0.75	0.60	0.58	0.78
AChE	Test Set	0.74	0.86	0.62	0.93
	Validation Set	0.76	0.79	0.59	0.89

Table 5. The highest values obtained for r² and MSE for the y-scrambled dataset.

Dataset	y-scrambled models	R ²	MSE	MAE	RMSE
MAO-B (Using the RF with best parameters)	Y_1	-0.25	2.05	1.15	1.43
	Y_2	-0.19	1.97	1.11	1.40
	Y_3	-0.16	1.91	1.11	1.38
	Y_4	-0.08	1.78	1.07	1.33
	Y_5	-0.15	1.90	1.10	1.38
AChE (Using the SVR with best parameters)	Y_1	-0.14	3.76	1.62	1.94
	Y_2	-0.14	3.76	1.60	1.94
	Y_3	-0.25	4.12	1.69	2.03
	Y_4	-0.19	3.94	1.62	1.98
	Y_5	-0.24	4.08	1.65	2.02

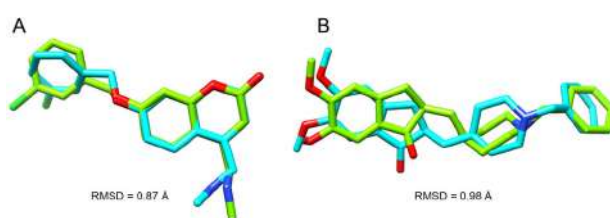


Figure 6. RMSD values and Superimposition of native co-crystallized (cyan color) and docked ligands (chartreuse color) for MAO-B (A) and AChE (B).

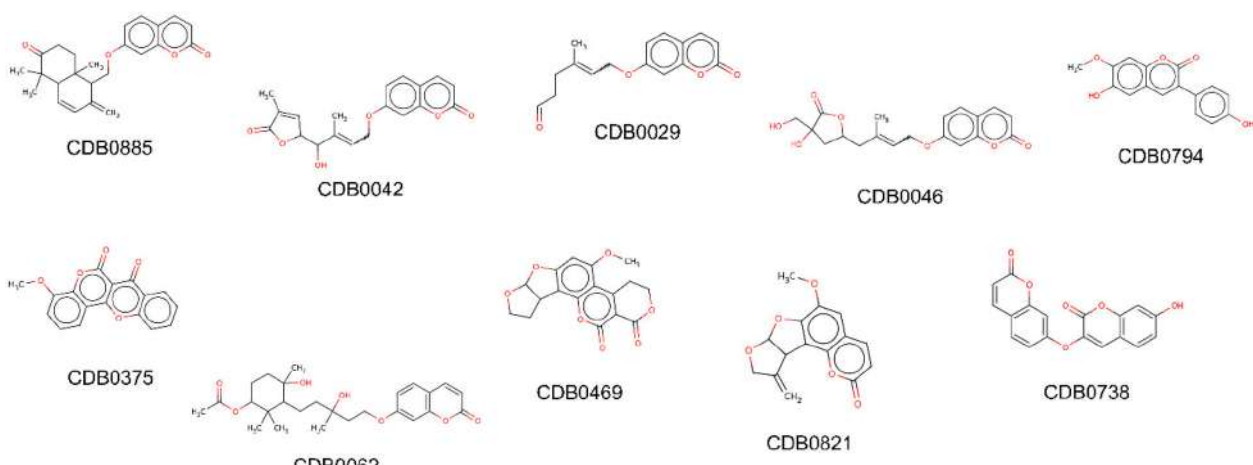
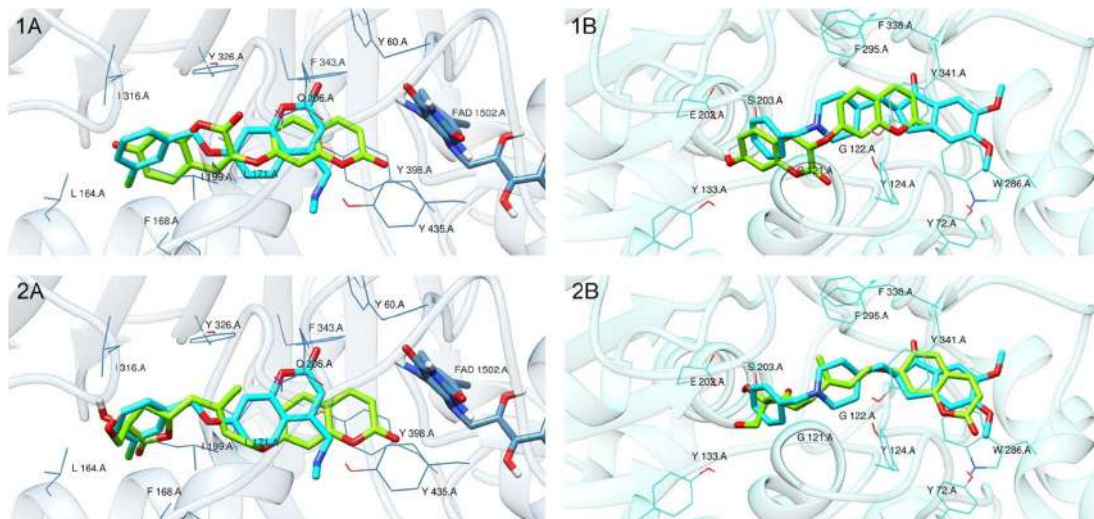


Figure 5. Top ranked molecules with predicted $pIC_{50} > 6$ by the RF and SVR models created using MAO-B and AChE respectively.

Table 6. Molecular docking results of the selected naturally occurring coumarins against MAO-B and AChE.

Compound	Natural source	Docking score (kcal/mol)		Hydrogen bonds		$\pi-\pi$ interactions	
		MAO-B	AChE	MAO-B	AChE	MAO-B	AChE
C18 ^a	—	-9.8	-10.5	Cys-172	Ser-125 His-447	Tyr-326 Tyr-398	Trp-286 Phe-338 Tyr-341
E20 ^b	—	-7.9	-11.3	—	Phe-295	Phe-343	Trp-86 Tyr-341
CDB0738	<i>Edgeworthia chrysanth</i>	-12.7	-12.4	Gln-206 Tyr-435	Glu-202	Tyr-326 Tyr-398	Trp-86 Tyr-341
CDB0046	<i>Clausena excavata</i>	-9.7	-11.1	Pro-102 Cys-172	Tyr-72 Gly-121 Glu-202 Ser-203	Tyr-398	Trp-286
CDB0042	<i>Clausena excavata</i>	-9.9	-10.9	Tyr-188 Ile-199	Tyr-72 Gly-121 Ser-203	Tyr-398	Trp-286
CDB0885	<i>Ferula narthex</i>	-7.5	-12.6	Tyr-435	Tyr-72	Tyr-398	Trp-286 Tyr-341
CDB0794	<i>Nicotiana tabacum</i>	-9.3	-10.3	Cys-172 Tyr-435	—	Tyr-326	Tyr-337 Tyr-341
CDB0029 CDB0375	<i>Aegle marmelos</i> <i>Polygala fruticosa</i>	-9.3 -7.9	-9.4 -10.2	Tyr-435	—	Tyr-398	Tyr-341
CDB0062	<i>Ferula polyantha</i>	-5.8	-10.8	—	Gly-121 Ser-203	Tyr-398	Trp-286
CDB0469	<i>Aspergillus flavus</i>	-5.8	-10.5	—	Tyr-124 Tyr-133	Tyr-435 Leu-171	Trp-86
CDB0821	<i>Micromelum minutum</i>	-5.5	-9.2	—	Tyr-124	Tyr-326 Tyr-398	Tyr-337

^a7-(3-chlorobenzoyloxy)-4-(methylamino)methyl-coumarin; ^bDonepezil.**Figure 7.** Docking conformations of the selected coumarin candidates (chartreuse color) superposed to reference ligands (cyan color). (1A) CDB0738-MAO-B complex; (2A) CDB0046-MAO-B complex; (1B) CDB0738-AChE complex; (2B) CDB0046-AChE complex.

methyloxolan-2-one moiety linked to the coumarin scaffold was responsible for the other observed hydrogen bonds involving Gly-121, Glu-202, and Ser-203. Moreover, the coumarin scaffold formed two $\pi-\pi$ stacking interactions with Trp-286 located in the PAS of AChE. Trp-286 is thought to play a crucial role in the allosteric modulation of human AChE activity by binding to ligands at the entrance of the active site gorge. Mutations of Trp-286 have been shown to result in a significant decrease in binding affinity of PAS ligands, indicating its importance in the ligand recognition (Barak et al., 1994).

3.3. ADME/tox prediction results

ADME and toxicity prediction results for the selected coumarins are shown in Table 7. pkCSM predicted water solubility show that all the compounds have values ranging between -3.2 and -5.5 which are within the recommended range (-6.5 to 0.5) where 95% of similar values for known drugs fall inside (Ntie-Kang, 2013). Predicted intestinal absorption shows that all the selected coumarins have great oral absorption and thus greater bioavailability. Moreover, all the drugs displayed good blood-brain barrier permeability values which is a necessary parameter to consider for developing

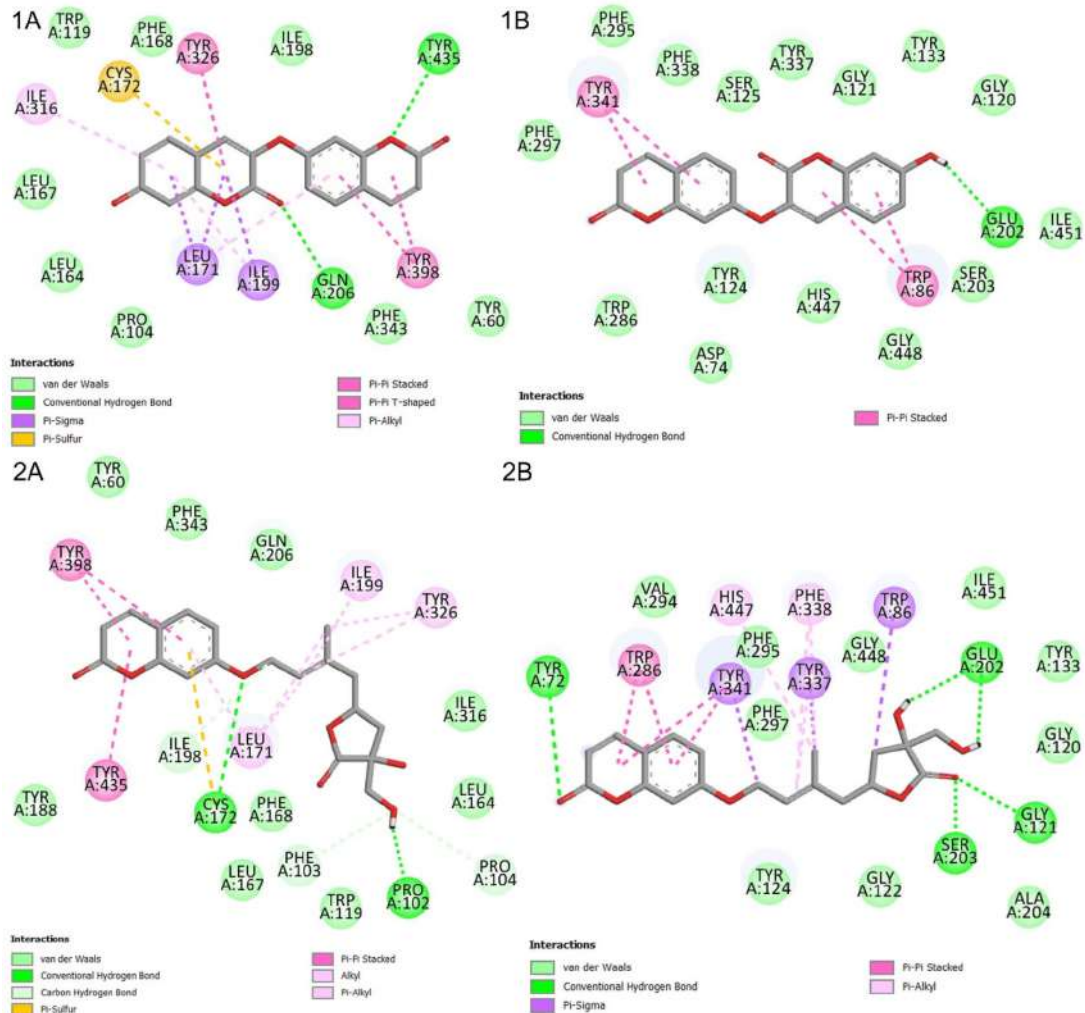


Figure 8. Protein-ligand interaction diagrams of the selected coumarin candidates. (1A) CDB0738-MAO-B complex; (2A) CDB0046-MAO-B complex; (1B) CDB0738-AChE complex; (2B) CDB0046-AChE complex.

Table 7. ADMET prediction results of the selected coumarins.

Compound	Water solubility	Intestinal absorption	BBB permeability	CNS permeability	CYP2D6 interaction	Ames toxicity	Liver toxicity
C18	-4.2	93.7	0.2	-2.1	Yes	Yes	Yes
E20	-4.6	93.7	0.2	-1.5	Yes	No	Yes
CDB0738	-5.5	99.4	-0.2	-1.7	No	No	No
CDB0046	-3.6	97.3	-0.5	-2.9	No	No	No
CDB0042	-3.9	96.7	-0.3	-2.4	No	Yes	No
CDB0885	-3.4	78.2	-0.9	-3.4	No	Yes	Yes
CDB0794	-3.3	94.2	-0.2	-2.2	No	Yes	No
CDB0029	-3.4	100	-0.5	-2.1	No	Yes	Yes
CDB0375	-4.3	92.5	-0.7	-2.9	No	No	Yes
CDB0062	-3.5	100	-0.8	-3.1	No	No	No
CDB0469	-3.4	100	-0.1	-2.9	No	Yes	No
CDB0821	-4.4	95.2	-0.6	-1.9	No	No	No

brain-acting drugs. CNS permeability is another parameter that takes the blood-brain permeability surface (\log_{10} PS) as a factor. Most of the selected coumarins are considered to penetrate the CNS while some others have average permeability, CDB0885 and CDB0062 are considered unable to penetrate the CNS due to their low \log_{10} PS values (< -3.0). Furthermore, all compounds, excluding the reference ligands, were identified as non-inhibitors of CYP2D6, which is particularly necessary for drugs acting on the brain since the expression of CYP2D6 is higher in the brain and is involved

in metabolizing endogenous neural compounds suggesting its neuroprotective properties. Ames toxicity revealed that six coumarins including the reference MAO-B inhibitor are predicted as mutagenic. Hepatotoxicity also predicted three coumarins in addition to the reference ligands as positive for inducing liver related injuries.

Water solubility: Solubility of the molecule in water at 25 °C (\log_{10} mol/L); Intestinal absorption: Percentage that will be absorbed through the human intestine; BBB permeability: Logarithmic ratio of brain to plasma drug concentrations.

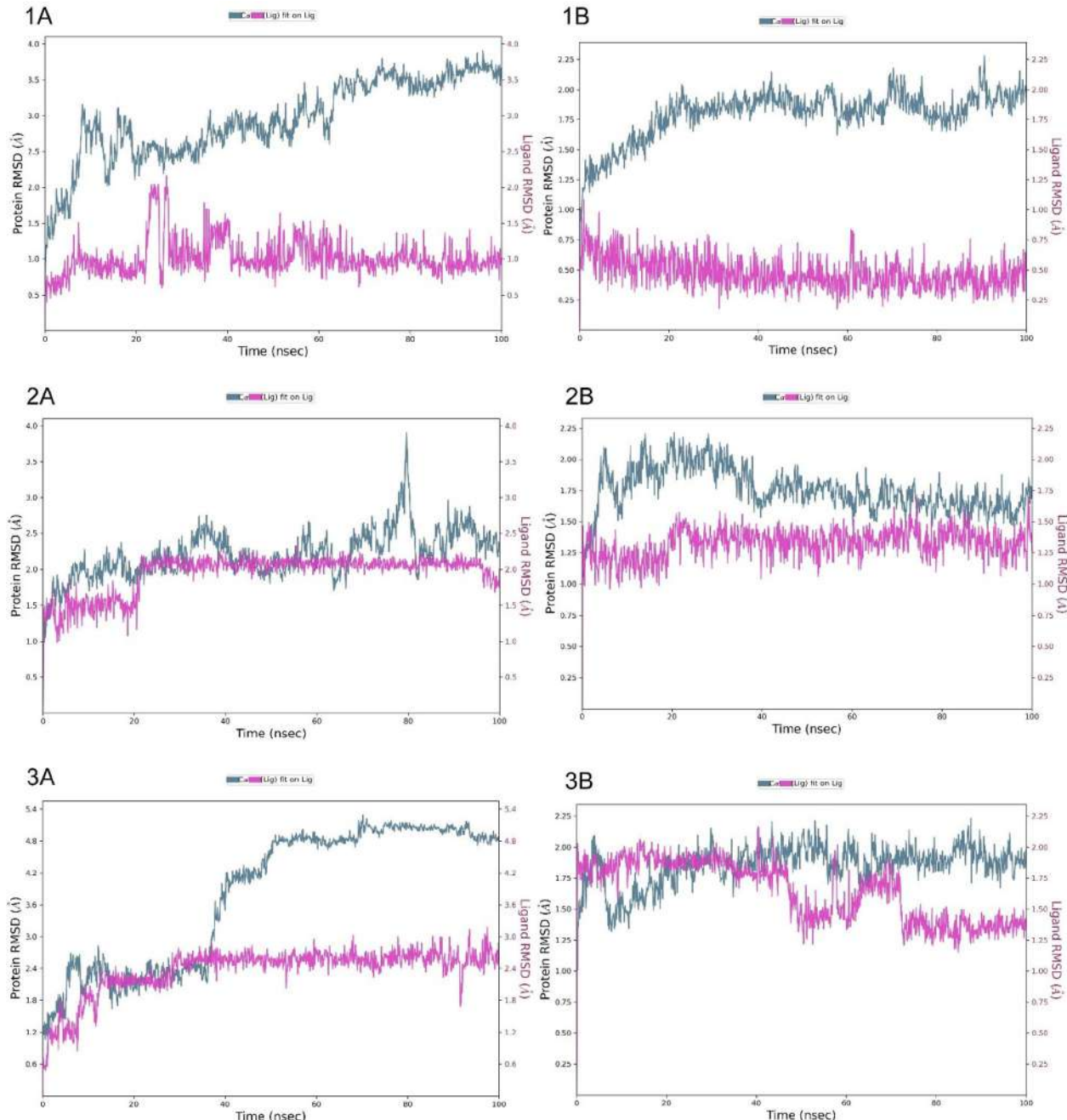


Figure 9. Time-dependent protein–ligand root-mean square deviation (RMSD) plots of MAO-B in complex with reference inhibitor (C18) (1A), CDB00738 (2A), CDB0046 (3A) and AChE in complex with reference inhibitor (donepezil) (1B), CDB00738 (2B), CDB0046 (3B).

(logBB > 0.3 is considered to cross the BBB while molecules with logBB<-1 are poorly distributed to the brain; CNS permeability: Compounds with a logPS>-2 are considered to penetrate CNS, while those with logPS<-3 are considered as unable to penetrate the CNS; Ames toxicity: A positive prediction indicates that the compound is mutagenic and therefore may act as a carcinogen; Liver toxicity: Drug-induced liver injury.

3.5. Molecular dynamics simulations

The best coumarin candidates namely, CDB0738 and CDB0046 in complex with MAO-B and AChE were selected from the

molecular docking study in addition to the reference protein–ligand complexes to perform molecular dynamics simulations and assess their stability over time. Various molecular dynamics analyses were conducted such as root-mean square deviation (RMSD), root-mean square fluctuation (RMSF), protein–ligand interactions and ligand properties variation with respect to the simulation period.

3.5.1. Root-mean square deviation

The RMSD plots of the selected coumarin candidates and the reference inhibitors in complex with MAO-B and AChE are shown in Figure 9. The RMSD values indicate how much the

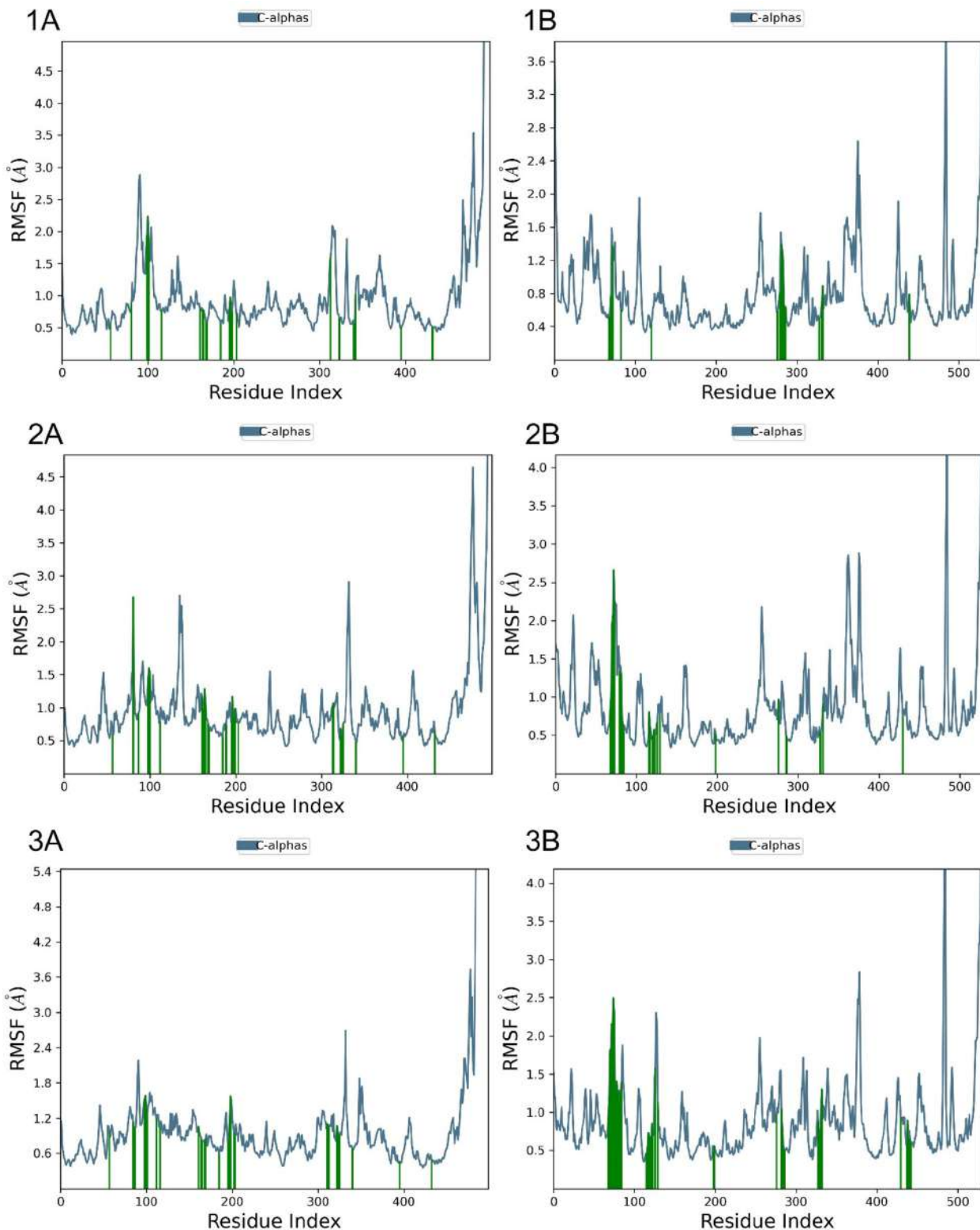


Figure 10. Time-dependent protein–ligand root-mean square fluctuation (RMSF) plots of MAO-B in complex with reference inhibitor (C18) (1A), CDB00738 (2A), CDB0046 (3A) and AChE in complex with reference inhibitor (donepezil) (1B), CDB00738 (2B), CDB0046 (3B).

protein and ligand have moved from their starting positions and how stable the complex is as a result.

The CDB0738-MAOB complex showed low RMSD values of around 2.5 Å, which is acceptable for protein-ligand

complexes (Ahmad et al., 2022). This suggests that the complex is relatively stable and that the protein and ligand have only moved slightly from their initial positions. The CDB0046-MAOB complex, however, showed larger RMSD values of

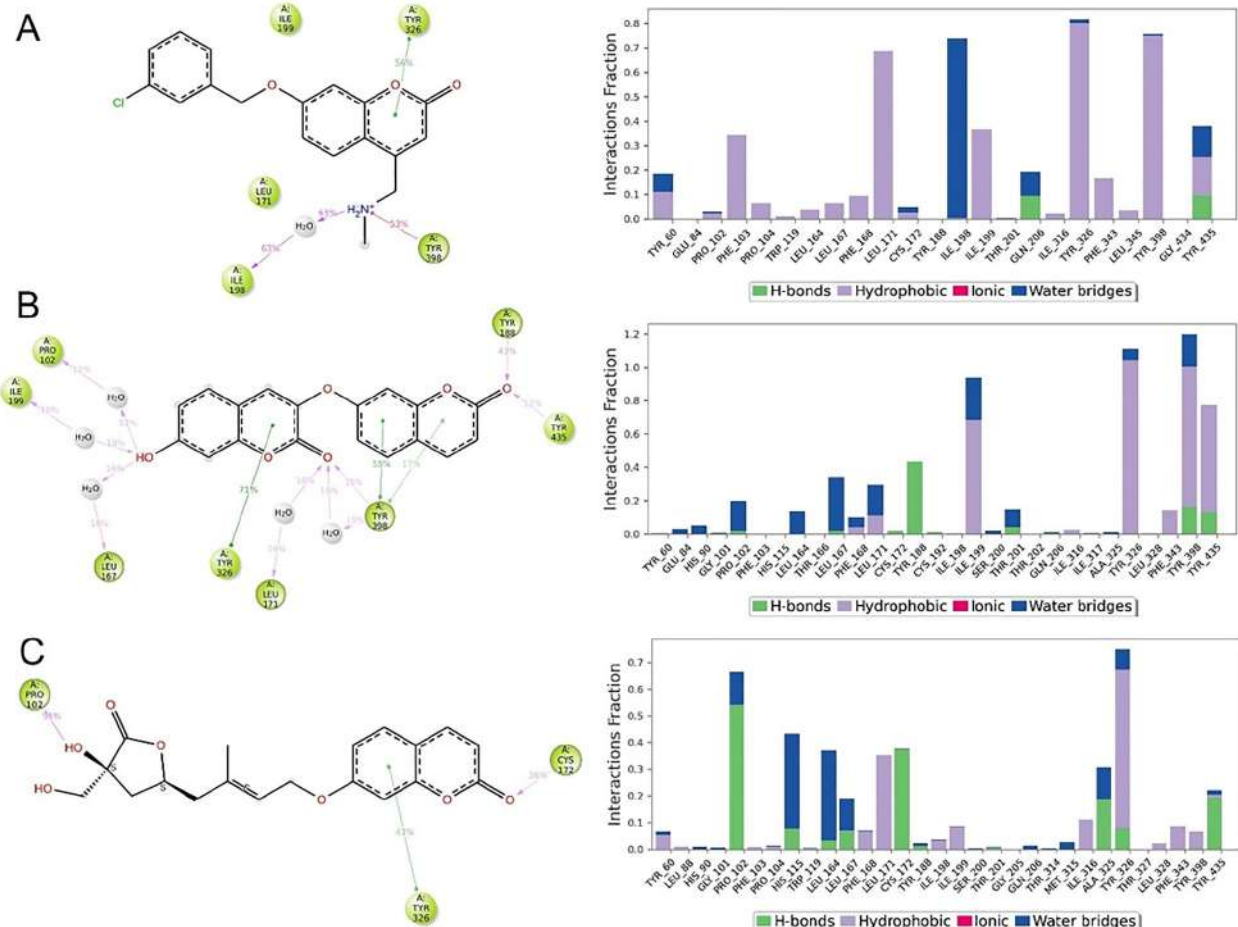


Figure 11. Simulation interaction diagrams and histograms of C18 (A), CDB0738 (B) and CDB0046 (C) in complex with MAO-B. Residues involved in the interactions are presented in the x axis, the y axis presents the normalized value of the temporal length of the interactions during the simulation.

around 4 Å, indicating that the complex is less stable and that the protein has moved significantly over time. This could be due to the bulky size of the CDB0046 molecule inducing structural changes to the protein. This is also noted in the ligand RMSD which revealed deviations around 1, 2, and 2.4 Å for the reference inhibitor, CDB0738 and CDB0046 respectively.

For the AChE complex, the reference complex displayed RMSD values of around 2 Å, which is also considered acceptable (Kua et al., 2002). The CDB0738-AChE complex exhibited even lower RMSD values of around 1.75 Å, indicating that the complex is more stable than the reference complex. The CDB0046-AChE complex showed similar RMSD values to the reference complex, around 2 Å. Regarding the ligand RMSD values, Donepezil showed very low values ranging between 0.25 and 0.75 Å with respect to the protein, indicating that it is highly stable in the protein cavity. CDB0738 showed slightly higher values of around 1.25 and 1.5 Å, while CDB0046 was the least stable with values around 2 Å during the first 75 ns but stabilized to around 1.25 and 1.5 Å for the rest of the simulation.

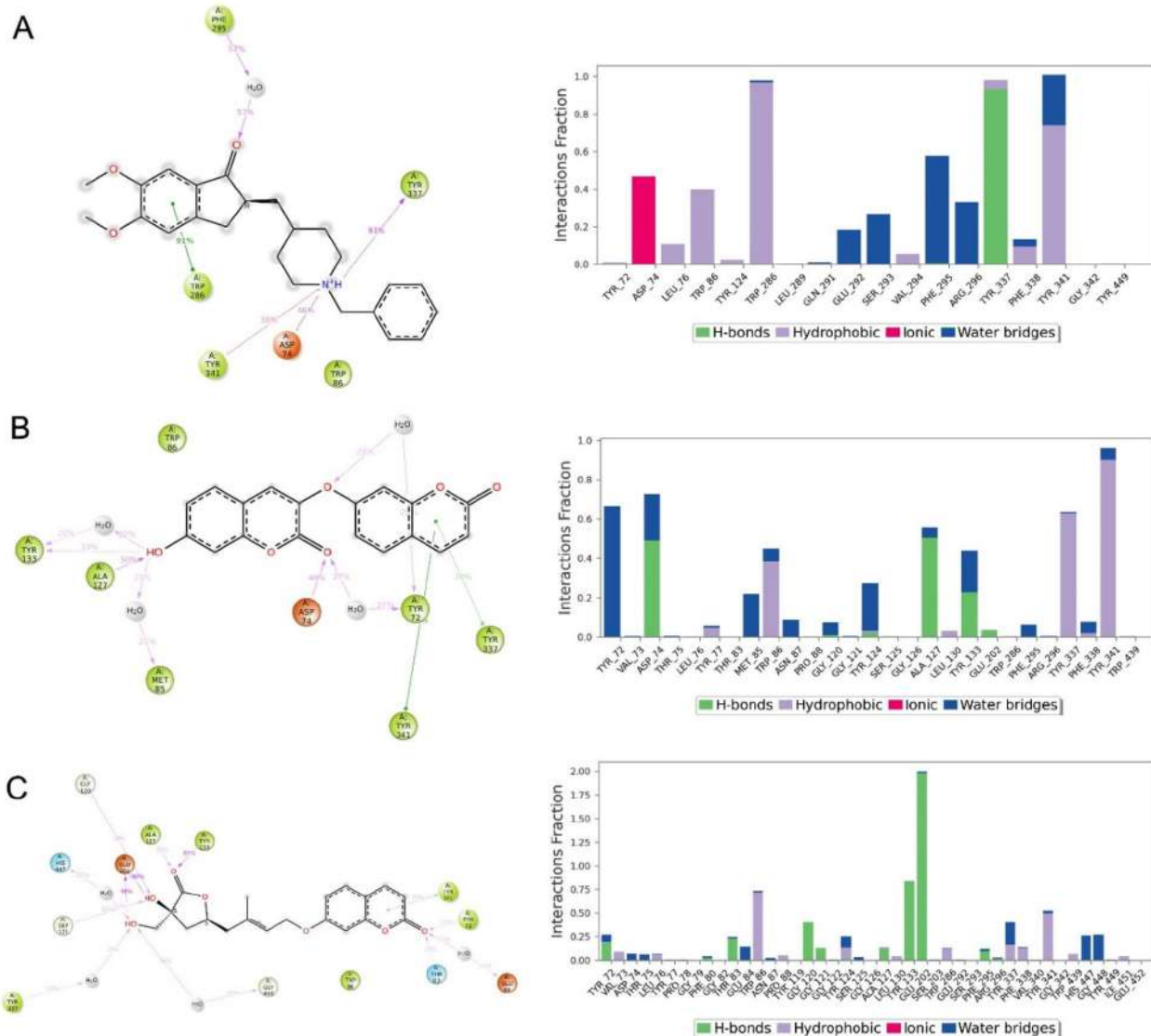
Overall, the RMSD results suggest that CDB0738 may be a more suitable candidate for inhibition of MAO-B and AChE than the reference inhibitors and CDB0046 due to its stability in the protein cavity.

3.5.2. Root-mean square fluctuation

The RMSF is a valuable tool in analyzing the fluctuations of individual atoms along the protein chain during molecular dynamics simulations (Martínez, 2015). The RMSF plots shown in Figure 10 display the fluctuations in the protein structure, with peaks indicating areas of the protein that show the highest amount of movement. It is common to see that the ends (N-terminal and C-terminal) of the protein fluctuate more than any other part of the protein structure. On the other hand, secondary structure elements like α -helices and β -strands tend to be more rigid and less flexible compared to loop regions, and thus, exhibit lower levels of fluctuation. In addition, protein residues that interact with the ligand are identified on the RMSF plot by green-colored vertical bars, highlighting the specific areas of the protein that are involved in binding with the ligand.

Figure 10 shows the residues of the MAO-B enzyme in complex with the selected coumarins remained stable throughout the simulation. The results indicate the highest fluctuations were at 5 Å for all three MAO-B complexes, but these fluctuating residues are not involved in ligand binding as they are in the C-terminal region, indicating slight conformational change.

For AChE, the RMSF analysis displays some high fluctuations around 3 Å, however, the ligand-binding regions are



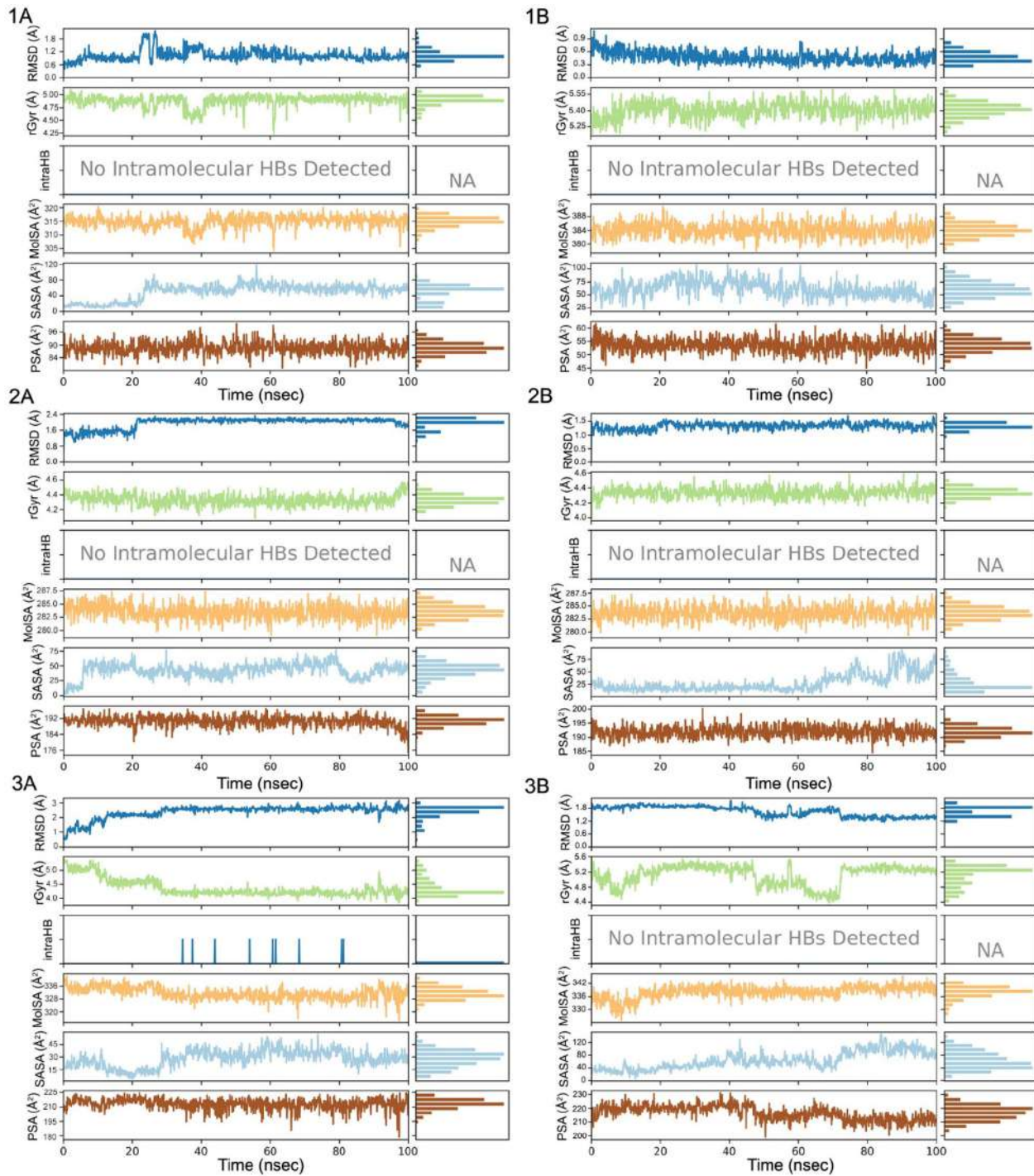


Figure 13. Variation in the ligand properties (RMSD, rGyr, intraHB, MoISA, SASA and PSA) with respect to the simulation time. (1A) The reference MAO-B inhibitor, C18; (2A) CDB0738; (3A) CDB0046; (1B) the reference AChE inhibitor, Donepezil; (2B) CDB0738; (3B) CDB0046.

throughout the simulation, as supported by several studies in the literature (Daoud et al., 2018; Shen et al., 2002). Donepezil, the reference inhibitor, has been shown to form a hydrogen bond with Tyr-337 in the PAS. This amino acid is known to bind the quaternary trimethylammonium tail group of acetylcholine and may therefore play a crucial role in inhibiting AChE activity (Messaad et al., 2022; Zhou et al., 2010). The ionic interaction with Asp-74 in the PAS has also been shown to play a role in the specificity of cationic organophosphonates as it acts as a proton acceptor (Barak

et al., 1994; Sugimoto et al., 2000). The hydrophobic interactions with Trp-86, Trp-286, and Tyr-341 in both the CAS and PAS have been shown to stabilize the ligand in the binding pocket and contribute to the inhibition (Hosea et al., 1996).

For CDB0738, the three hydrogen bonds with Asp-74, Ala-127, and Tyr-133 in the PAS have been shown to play a critical role in inhibition (Dhananjayan et al., 2013). CDB0046 has important hydrogen bonds with Tyr-133 in the PAS and Glu-202 in the CAS, as well as hydrophobic interactions with Trp-86 and Tyr-341 in both anionic sites.



3.5.4. Ligand properties variation

To assess the stability of the selected compounds in the cavities of MAO-B and AChE, five molecular properties namely, ligand RMSD, radius of gyration (rGyr), molecular surface area (MolSA), solvent accessible surface area (SASA), and polar surface area (PSA) were analyzed over a 100 ns simulation period, as depicted in Figure 13. The ligand RMSD measures the deviation of a ligand's conformation relative to a reference conformation, usually the first frame (Krishnaveni, 2015). The RMSD values of all compounds remained below 2 Å throughout the simulation for AChE. As for MAO-B, CDB0738 showed fluctuations at 2.4 Å before stabilizing at 2 Å at the end of the simulation, meanwhile CDB0046 exhibited some deviations around 3 Å through all the simulation. The radius of gyration, which measures the 'extendedness' of a ligand and is equivalent to its principal moment of inertia, remained constant and ranged from 4 to 5 Å for the selected compounds which is due to the size of the ligands and their flexibility resulting in more mobility, thus reducing their compactness. The MolSA was calculated using a probe radius of 1.4 Å and represents the van der Waals surface area. The SASA area reflects the surface area accessible to water molecules, and the polar surface area represents the solvent-accessible surface area that is contributed by only oxygen and nitrogen atoms. Despite the exposure and rotational flexibility of the protein and the ligand, deviations in the surface area (MolSA, SASA and PSA) were found to be higher in CDB0046 when compared to CDB0738 indicating a higher degree of charged surface area in the former which can affect the solubility and stability of a molecule in polar solvents, such as water. For MolSA and SASA, the size of the molecule and the specific solvent used can affect the values obtained. For example, larger molecules will generally have larger MolSA and SASA values, while smaller molecules will have smaller values. Similarly, different solvents may lead to different MolSA and SASA values, depending on the size and properties of the solvent molecules (Ferdausi et al., 2022).

4. Conclusion

MAO-B and AChE are considered relevant targets when developing neuroprotective drugs against Parkinson's and Alzheimer's disease. Coumarins and their derivatives have been synthetized for decades and extensively evaluated against neurodegenerative diseases, however natural coumarins are yet to be investigated. The present study aimed to collect all available naturally occurring coumarins with their corresponding natural sources. A chemical library was designed to bioprospect novel coumarin candidates as neuroprotective agents. QSAR models were generated using all available MAO-B and AChE inhibitors with their reported experimental activity to screen for potential MAO-B and AChE inhibitors from natural coumarins. Our results revealed ten coumarins with pIC_{50} values > 6 . The selected coumarins were subjected for molecular docking study to assess their binding affinities and molecular interactions. CDB0738 and CDB0046 showed potential as inhibitors for MAO-B and AChE. Both compounds showed promising interactions with

critical amino acids involved in the stability and the specificity of MAO-B and AChE, indicating their potential affinity and selectivity towards these enzymes. Molecular dynamics were performed to analyze the stability of the protein-ligand complexes over 100 ns simulation period. Our results indicated that CDB0738 had the lowest RMSD values, around 2.5 Å for MAO-B and 1.75 Å for AChE, indicating that it was the most stable complex among the candidates. Moreover, RMSF analysis showed typical fluctuations in the N- and C-terminal residues, however the ligand-binding regions were less fluctuating. Analysis of molecular interactions revealed the presence of key hydrogen bonds and highlighted the importance of hydrophobic interactions as reported in the literature. For AChE, the two coumarin candidates, CDB0738 and CDB0046, formed critical interactions with residues from the CAS and the PAS in a similar manner to the reference inhibitor, Donepezil. Finally, the *in silico* ADMET parameters of the screened coumarins were found to be acceptable and within the suitable range for human use. This study provides renewed hope that naturally occurring products, especially coumarins could potentially lead to the development of a new neuroprotective drug for the treatment of Parkinson's and Alzheimer's disease. However, additional *in vitro* and *in vivo* studies are needed to confirm their effectiveness.

Acknowledgments

We would like to thank Francisco Javier Luque Garriga, Professor in the Department of Chemical Physics, University of Barcelona, Spain, for his assistance. His contribution is sincerely appreciated and gratefully acknowledged.

Disclosure statement

No potential conflict of interest was reported by the authors.

Funding

The authors gratefully acknowledge ProteinsInsights, Nangal Raya, New Delhi, India, for providing the computational resources essential for the successful completion of this research.

ORCID

Amal Maurady <http://orcid.org/0000-0001-9298-717X>

References

- Ahmad, I., Kumar, D., & Patel, H. (2022). Computational investigation of phytochemicals from *Withania somnifera* (Indian ginseng/ashwagandha) as plausible inhibitors of GluN2B-containing NMDA receptors. *Journal of Biomolecular Structure & Dynamics*, 40(17), 7991–8003. <https://doi.org/10.1080/07391102.2021.1905553>
- Azam, F., Madi, A. M., & Ali, H. I. (2012). Molecular docking and prediction of pharmacokinetic properties of dual mechanism drugs that block MAO-B and adenosine A2A receptors for the treatment of Parkinson's disease. *Journal of Young Pharmacists: JYP*, 4(3), 184–192. <https://doi.org/10.4103/0975-1483.100027>
- Bara-Jimenez, W., Sherzai, A., Dimitrova, T., Favit, A., Bibbiani, F., Gillespie, M., Morris, M. J., Mouradian, M. M., & Chase, T. N. (2003).

- Adenosine A2A receptor antagonist treatment of Parkinson's disease. *Neurology*, 61(3), 293–296. <https://doi.org/10.1212/01.wnl.0000073136.00548.d4>
- Barak, D., Kronman, C., Ordentlich, A., Ariel, N., Bromberg, A., Marcus, D., Lazar, A., Velan, B., & Shafferman, A. (1994). Acetylcholinesterase peripheral anionic site degeneracy conferred by amino acid arrays sharing a common core. *Journal of Biological Chemistry*, 269(9), 6296–6305. [https://doi.org/10.1016/S0021-9258\(17\)37371-4](https://doi.org/10.1016/S0021-9258(17)37371-4)
- Barnham, K. J., Masters, C. L., & Bush, A. I. (2004). Neurodegenerative diseases and oxidative stress. *Nature Reviews. Drug Discovery*, 3(3), 205–214. <https://doi.org/10.1038/nrd1330>
- Bibbiani, F. O. H. J. D., Oh, J. D., Petzer, J. P., Castagnoli, N., Jr, Chen, J. F., Schwarzschild, M. A., & Chase, T. N. (2003). A2A antagonist prevents dopamine agonist-induced motor complications in animal models of Parkinson's disease. *Experimental Neurology*, 184(1), 285–294. [https://doi.org/10.1016/s0014-4886\(03\)00250-4](https://doi.org/10.1016/s0014-4886(03)00250-4)
- Binda, C., Wang, J., Pisani, L., Caccia, C., Carotti, A., Salvati, P., Edmondson, D. E., & Mattevi, A. (2007). Structures of human monoamine oxidase B complexes with selective noncovalent inhibitors: Safinamide and coumarin analogs. *Journal of Medicinal Chemistry*, 50(23), 5848–5852. <https://doi.org/10.1021/jm070677y>
- Biovia, D. S. (2017). *Discovery studio visualizer*. 936.
- Boulaamane, Y., Ahmad, I., Patel, H., Das, N., Britel, M. R., & Maurady, A. (2023). Structural exploration of selected C6 and C7-substituted coumarin isomers as selective MAO-B inhibitors. *Journal of Biomolecular Structure and Dynamics*, 41(6), 2326–2340. <https://doi.org/10.1080/07391102.2022.2033643>
- Boulaamane, Y., Ibrahim, M. A., Britel, M. R., & Maurady, A. (2022). In silico studies of natural product-like caffeine derivatives as potential MAO-B inhibitors/A2AR antagonists for the treatment of Parkinson's disease. *Journal of Integrative Bioinformatics*, 19(4), 16–17. <https://doi.org/10.1515/jib-2021-0027>
- Bowers, K. J., Chow, E., Xu, H., Dror, R. O., Eastwood, M. P., Gregersen, B. A., ... Shaw, D. E. (2006). Scalable algorithms for molecular dynamics simulations on commodity clusters [Paper presentation]. In Proceedings of the 2006 ACM/IEEE Conference on Supercomputing, November). (pp. 84–es). <https://doi.org/10.1145/1188455.1188544>
- Brühlmann, C., Ooms, F., Carrupt, P. A., Testa, B., Catto, M., Leonetti, F., Altomare, C., & Carotti, A. (2001). Coumarins derivatives as dual inhibitors of acetylcholinesterase and monoamine oxidase. *Journal of Medicinal Chemistry*, 44(19), 3195–3198. <https://doi.org/10.1021/jm010894d>
- Burggraaff, L., van Vlijmen, H. W. T., IJzerman, A. P., & van Westen, G. J. P. (2020). Quantitative prediction of selectivity between the A1 and A2A adenosine receptors. *Journal of Cheminformatics*, 12(1), 33. <https://doi.org/10.1186/s13321-020-00438-3>
- Carradori, S., D'Ascenzo, M., Chimenti, P., Secci, D., & Bolasco, A. (2014). Selective MAO-B inhibitors: A lesson from natural products. *Molecular Diversity*, 18(1), 219–243. <https://doi.org/10.1007/s11030-013-9490-6>
- Chaudhuri, K. R., Healy, D. G., & Schapira, A. H. National Institute for Clinical Excellence. (2006). Non-motor symptoms of Parkinson's disease: Diagnosis and management. *The Lancet. Neurology*, 5(3), 235–245. [https://doi.org/10.1016/S1474-4422\(06\)70373-8](https://doi.org/10.1016/S1474-4422(06)70373-8)
- Chen, J. H., Huang, T. W., & Hong, C. T. (2021). Cholinesterase inhibitors for gait, balance, and fall in Parkinson disease: A meta-analysis. *Npj Parkinson's Disease*, 7(1), 1–7. <https://doi.org/10.1038/s41531-021-00251-1>
- Cheung, J., Rudolph, M. J., Burshteyn, F., Cassidy, M. S., Gary, E. N., Love, J., Franklin, M. C., & Height, J. J. (2012). Structures of human acetylcholinesterase in complex with pharmacologically important ligands. *Journal of Medicinal Chemistry*, 55(22), 10282–10286. <https://doi.org/10.1021/jm300871x>
- Daoud, I., Melkemi, N., Salah, T., & Ghalem, S. (2018). Combined QSAR, molecular docking and molecular dynamics study on new Acetylcholinesterase and Butyrylcholinesterase inhibitors. *Computational Biology and Chemistry*, 74, 304–326. <https://doi.org/10.1016/j.compbiochem.2018.03.021>
- Dean, F. M. (1952). Naturally occurring coumarins. *Fortschritte der Chemie Organischer Naturstoffe/Progress in the Chemistry of Organic Natural Products/Progrès Dans La Chimie Des Substances Organiques Naturelles*, 225–291.
- Dhananjayan, K., Sumathy, A., & Palanisamy, S. (2013). Molecular docking studies and in-vitro acetylcholinesterase inhibition by terpenoids and flavonoids. *Asian Journal of Research in Chemistry*, 6(11), 1011–1017.
- Di Paolo, M. L., Cozza, G., Milelli, A., Zonta, F., Sarno, S., Minniti, E., Ursini, F., Rosini, M., & Minarini, A. (2019). Benextramine and derivatives as novel human monoamine oxidases inhibitors: An integrated approach. *The FEBS Journal*, 286(24), 4995–5015. <https://doi.org/10.1111/febs.14994>
- Dias, V., Junn, E., & Mouradian, M. M. (2013). The role of oxidative stress in Parkinson's disease. *Journal of Parkinson's Disease*, 3(4), 461–491. <https://doi.org/10.3233/JPD-130230>
- Ding, Y., Chen, M., Guo, C., Zhang, P., & Wang, J. (2021). Molecular fingerprint-based machine learning assisted QSAR model development for prediction of ionic liquid properties. *Journal of Molecular Liquids*, 326, 115212. <https://doi.org/10.1016/j.molliq.2020.115212>
- Dugger, B. N., & Dickson, D. W. (2017). Pathology of neurodegenerative diseases. *Cold Spring Harbor Perspectives in Biology*, 9(7), a028035. <https://doi.org/10.1101/cshperspect.a028035>
- Edmondson, D. E., & Newton-Vinson, P. (2001). The covalent FAD of monoamine oxidase: Structural and functional role and mechanism of the flavinylation reaction. *Antioxidants & Redox Signaling*, 3(5), 789–806. <https://doi.org/10.1089/15230860152664984>
- Ekström, F., Gottinger, A., Forsgren, N., Catto, M., Iacovino, L. G., Pisani, L., & Binda, C. (2022). Dual Reversible Coumarin Inhibitors Mutually Bound to Monoamine Oxidase B and Acetylcholinesterase Crystal Structures. *ACS Medicinal Chemistry Letters*, 13(3), 499–506. <https://doi.org/10.1021/acsmmedchemlett.2c00001>
- Ferdausi, N., Islam, S., Rimti, F. H., Quayum, S. T., Arshad, E. M., Ibnat, A., Islam, T., Arefin, A., Ema, T. I., Biswas, P., Dey, D., & Azad, S. A. (2022). Point-specific interactions of isovitexin with the neighboring amino acid residues of the hACE2 receptor as a targeted therapeutic agent in suppressing the SARS-CoV-2 influx mechanism. *Journal of Advanced Veterinary and Animal Research*, 9(2), 230–240. <https://doi.org/10.5455/javar.2022.i588>
- Fukunishi, Y., & Lintuluoto, M. (2010). Development of chemical compound libraries for in silico drug screening. *Current Computer-Aided Drug Design*, 6(2), 90–102. <https://doi.org/10.2174/15734091091202450>
- Garrard, A. (2014). Coumarins. In *Encyclopedia of Toxicology*. (pp. 1052–1054). Elsevier. <https://doi.org/10.1016/B978-0-12-386454-3.00798-3>
- Gola, J., Obrezanova, O., Champness, E., & Segall, M. (2006). ADMET property prediction: The state of the art and current challenges. *QSAR & Combinatorial Science*, 25(12), 1172–1180. <https://doi.org/10.1002/qsar.200610093>
- Halgren, T. A. (1996). Merck molecular force field. I. Basis, form, scope, parameterization, and performance of MMFF94. *Journal of Computational Chemistry*, 17(5–6), 490–519. [https://doi.org/10.1002/\(SICI\)1096-987X\(199604\)17:5/6<490::AID-JCC1>3.0.CO;2-P](https://doi.org/10.1002/(SICI)1096-987X(199604)17:5/6<490::AID-JCC1>3.0.CO;2-P)
- Hosea, N. A., Radić, Ž., Tsigelny, I., Berman, H. A., Quinn, D. M., & Taylor, P. (1996). Aspartate 74 as a primary determinant in acetylcholinesterase governing specificity to cationic organophosphonates. *Biochemistry*, 35(33), 10995–11004. <https://doi.org/10.1021/bi9611220>
- Huey, R., & Morris, G. M. (2008). *Using AutoDock 4 with AutoDocktools: A tutorial*. The Scripps Research Institute. 8, 54–56.
- Jo, S., Kim, T., Iyer, V. G., & Im, W. (2008). CHARMM-GUI: A web-based graphical user interface for CHARMM. *Journal of Computational Chemistry*, 29(11), 1859–1865. <https://doi.org/10.1002/jcc.20945>
- Kakkola, S. (2010). Problems with the present inhibitors and a relevance of new and improved COMT inhibitors in Parkinson's disease. *International Review of Neurobiology*, 95, 207–225.
- Kalia, L. V., Kalia, S. K., & Lang, A. E. (2015). Disease-modifying strategies for Parkinson's disease. *Movement Disorders: Official Journal of the Movement Disorder Society*, 30(11), 1442–1450. <https://doi.org/10.1002/mds.26354>
- Katari, S. K., Natarajan, P., Swargam, S., Kanipakam, H., Pasala, C., & Umamaheswari, A. (2016). Inhibitor design against JNK1 through e-pharmacophore modeling docking and molecular dynamics

- simulations. *Journal of Receptor and Signal Transduction Research*, 36(6), 558–571. <https://doi.org/10.3109/10799893.2016.1141955>
- Khanam, S., Subitsha, A. J., & Sabu, S. (2021). Plants as a promising source for the treatment of parkinson disease: A systematic review. *IP International Journal of Comprehensive and Advanced Pharmacology*, 5(4), 158–166. <https://doi.org/10.18231/j.ijcaap.2020.032>
- Kim, S., Chen, J., Cheng, T., Gindulyte, A., He, J., He, S., Li, Q., Shoemaker, B. A., Thiessen, P. A., Yu, B., Zaslavsky, L., Zhang, J., & Bolton, E. E. (2019). PubChem 2019 update: Improved access to chemical data. *Nucleic Acids Research*, 47(D1), D1102–D1109. <https://doi.org/10.1093/nar/gky1033>
- Krishnaveni, M. (2015). Docking, simulation studies of desulphosinigrin-cyclin dependent kinase 2, an anticancer drug target. *Int. J. Pharm. Sci. Rev. Res.*, 30(2), 115–118.
- Kua, J., Zhang, Y., & McCammon, J. A. (2002). Studying enzyme binding specificity in acetylcholinesterase using a combined molecular dynamics and multiple docking approach. *Journal of the American Chemical Society*, 124(28), 8260–8267. <https://doi.org/10.1021/ja0204291>
- Lacy, A., & O'Kennedy, R. (2004). Studies on Coumarins and Coumarin-Related Compounds to Determine their Therapeutic Role in the Treatment of Cancer. *Current Pharmaceutical Design*, 10(30), 3797–3811. <https://doi.org/10.2174/1381612043382693>
- Landrum, G. (2013). RDKit: A software suite for cheminformatics, computational chemistry, and predictive modeling.
- Lang, A. E., & Marras, C. (2014). Initiating dopaminergic treatment in Parkinson's disease. *Lancet (London, England)*, 384(9949), 1164–1166. [https://doi.org/10.1016/S0140-6736\(14\)60962-4](https://doi.org/10.1016/S0140-6736(14)60962-4)
- Lee, A., & Gilbert, R. M. (2016). Epidemiology of Parkinson disease. *Neurologic Clinics*, 34(4), 955–965. <https://doi.org/10.1016/j.ncl.2016.06.012>
- Lin, J., Sahakian, D. C., De Morais, S. M., Xu, J. J., Polzer, R. J., & Winter, S. M. (2003). The role of absorption, distribution, metabolism, excretion and toxicity in drug discovery. *Current Topics in Medicinal Chemistry*, 3(10), 1125–1154. <https://doi.org/10.2174/156802603452096>
- Lu, J. J., Pan, W., Hu, Y. J., & Wang, Y. T. (2012). Multi-target drugs: The trend of drug research and development. *PLoS One*, 7(6), e40262. <https://doi.org/10.1371/journal.pone.0040262>
- Martínez, L. (2015). Automatic identification of mobile and rigid substructures in molecular dynamics simulations and fractional structural fluctuation analysis. *PLoS One*, 10(3), e0119264. <https://doi.org/10.1371/journal.pone.0119264>
- Mateev, E., Valkova, I., Angelov, B., Georgieva, M., & Zlatkov, A. (2022). Validation through re-docking, cross-docking and ligand enrichment in various well-resolved MAO-B receptors. *International Journal of Pharmaceutical Sciences and Research*, 13, 1099–1107.
- McKinney, W. (2011). pandas: A foundational Python library for data analysis and statistics. *Python for High Performance and Scientific Computing*, 14(9), 1–9.
- Melchionna, S., Ciccotti, G., & Lee Holian, B. (1993). Hoover NPT dynamics for systems varying in shape and size. *Molecular Physics*, 78(3), 533–544. <https://doi.org/10.1080/00268979300100371>
- Mendez, D., Gaulton, A., Bento, A. P., Chambers, J., De Veij, M., Félix, E., Magariños, M. P., Mosquera, J. F., Mutowo, P., Nowotka, M., Gordillo-Marañón, M., Hunter, F., Junco, L., Mugumbate, G., Rodriguez-Lopez, M., Atkinson, F., Bosc, N., Radoux, C. J., Segura-Cabrera, A., Hersey, A., & Leach, A. R. (2019). ChEMBL: Towards direct deposition of bioassay data. *Nucleic Acids Research*, 47(D1), D930–D940. <https://doi.org/10.1093/nar/gky1075>
- Messaad, M., Dhouib, I., Abdelhedi, M., & Khemakhem, B. (2022). Synthesis, bioassay and molecular docking of novel pyrazole and pyrazolone derivatives as acetylcholinesterase inhibitors. *Journal of Molecular Structure*, 1263, 133105. <https://doi.org/10.1016/j.molstruc.2022.133105>
- Milczek, E. M., Binda, C., Rovida, S., Mattevi, A., & Edmondson, D. E. (2011). The 'gating'residues Ile199 and Tyr326 in human monoamine oxidase B function in substrate and inhibitor recognition. *The FEBS Journal*, 278(24), 4860–4869. <https://doi.org/10.1111/j.1742-4658.2011.08386.x>
- Möller, D., Oprzynski, J., Müller, A., & Fischer, J. (1992). Prediction of thermodynamic properties of fluid mixtures by molecular dynamics simulations: Methane-ethane. *Molecular Physics*, 75(2), 363–378. <https://doi.org/10.1080/00268979200100291>
- Murray, R. D. (2002). The naturally occurring coumarins. *Fortschritte der Chemie organischer Naturstoffe/Progress in the Chemistry of Organic Natural Products*, 1–619.
- Ntie-Kang, F. (2013). An in silico evaluation of the ADMET profile of the StreptomeDB database. *Springerplus*, 2(1), 1–11. <https://doi.org/10.1186/2193-1801-2-353>
- O'Boyle, N. M., Banck, M., James, C. A., Morley, C., Vandermeersch, T., & Hutchison, G. R. (2011). Open Babel: An open chemical toolbox. *Journal of Cheminformatics*, 3(1), 1–14. <https://doi.org/10.1186/1758-2946-3-33>
- Pasrija, P., Jha, P., Upadhyaya, P., Khan, M., & Chopra, M. (2022). Machine Learning and Artificial Intelligence: A Paradigm Shift in Big Data-Driven Drug Design and Discovery. *Current Topics in Medicinal Chemistry*, 22(20), 1692–1727. <https://doi.org/10.2174/156802662266220701091339>
- Pires, D. E., Blundell, T. L., & Ascher, D. B. (2015). pkCSM: Predicting small-molecule pharmacokinetic and toxicity properties using graph-based signatures. *Journal of Medicinal Chemistry*, 58(9), 4066–4072. <https://doi.org/10.1021/acs.jmedchem.5b00104>
- Pitchai, A., Rajaretnam, R. K., Mani, R., & Nagarajan, N. (2020). Molecular interaction of human acetylcholinesterase with trans-tephrostachin and derivatives for Alzheimer's disease. *Heliyon*, 6(9), e04930. <https://doi.org/10.1016/j.heliyon.2020.e04930>
- Poewe, W., & Mahlknecht, P. (2020). Pharmacologic treatment of motor symptoms associated with Parkinson disease. *Neurologic Clinics*, 38(2), 255–267. <https://doi.org/10.1016/j.ncl.2019.12.002>
- Poewe, W., Seppi, K., Tanner, C. M., Halliday, G. M., Brundin, P., Volkmann, J., Schrag, A.-E., & Lang, A. E. (2017). Parkinson disease. *Nature Reviews Disease Primers*, 3(1), 1–21. <https://doi.org/10.1038/nrdp.2017.13>
- Pourshojaei, Y., Abiri, A., Eskandari, K., Haghhighijoo, Z., Edraki, N., & Asadipour, A. (2019). phenoxyethyl piperidine/Morpholine Derivatives as pAS and cAS inhibitors of cholinesterases: Insights for future Drug Design. *Scientific Reports*, 9(1), 1–19. <https://doi.org/10.1038/s41598-019-56463-2>
- Radic, Z., Pickering, N. A., Vellom, D. C., Camp, S., & Taylor, P. (1993). Three distinct domains in the cholinesterase molecule confer selectivity for acetyl-and butyrylcholinesterase inhibitors. *Biochemistry*, 32(45), 12074–12084. <https://doi.org/10.1021/bi00096a018>
- Ranjan, A., Kumar, A., Gulati, K., Thakur, S., & Jindal, T. (2015). Role of aromatic amino acids in stabilizing organophosphate and human acetylcholinesterase complex. *Journal of Current Pharma Research*, 5(4), 1632–1639. <https://doi.org/10.33786/JCPR.2015.v05i04.006>
- Sander, T., Freyss, J., von Korff, M., & Rufener, C. (2015). DataWarrior: An open-source program for chemistry aware data visualization and analysis. *Journal of Chemical Information and Modeling*, 55(2), 460–473. <https://doi.org/10.1021/ci500588j>
- Sarker, S. D., & Nahar, L. (2017). Progress in the chemistry of naturally occurring coumarins. *Progress in the Chemistry of Organic Natural Products*, 106, 241–304. https://doi.org/10.1007/978-3-319-59542-9_3
- Shen, T., Tai, K., Henchman, R. H., & McCammon, J. A. (2002). Molecular dynamics of acetylcholinesterase. *Accounts of Chemical Research*, 35(6), 332–340. <https://doi.org/10.1021/ar0100251>
- Shivakumar, D., Williams, J., Wu, Y., Damm, W., Shelley, J., & Sherman, W. (2010). Prediction of absolute solvation free energies using molecular dynamics free energy perturbation and the OPLS force field. *Journal of Chemical Theory and Computation*, 6(5), 1509–1519. <https://doi.org/10.1021/ct900587b>
- Singla, R. K., Agarwal, T., He, X., & Shen, B. (2021). Herbal resources to combat a progressive & degenerative nervous system disorder-Parkinson's disease. *Current Drug Targets*, 22(6), 609–630. <https://doi.org/10.2174/1389450121999201013155202>
- Singla, D., Sharma, A., Kaur, J., Panwar, B., & Raghava, G. P. (2010). BIAbd: A curated database of benzylisoquinoline alkaloids. *BMC Pharmacology*, 10(1), 8. <https://doi.org/10.1186/1471-2210-10-4>

- Soine, T. O. (1964). Naturally occurring coumarins and related physiological activities. *Journal of Pharmaceutical Sciences*, 53(3), 231–264. <https://doi.org/10.1002/jps.2600530302>
- Stefanachi, A., Leonetti, F., Pisani, L., Catto, M., & Carotti, A. (2018). Coumarin: A natural, privileged and versatile scaffold for bioactive compounds. *Molecules*, 23(2), 250. <https://doi.org/10.3390/molecules23020250>
- Sugimoto, H., Yamanishi, Y., Iimura, Y., & Kawakami, Y. (2000). Donepezil hydrochloride (E2020) and other acetylcholinesterase inhibitors. *Current Medicinal Chemistry*, 7(3), 303–339. <https://doi.org/10.2174/0929867003375191>
- Tarasova, O. A., Urusova, A. F., Filimonov, D. A., Nicklaus, M. C., Zakharov, A. V., & Poroikov, V. V. (2015). QSAR modeling using large-scale databases: Case study for HIV-1 reverse transcriptase inhibitors. *Journal of Chemical Information and Modeling*, 55(7), 1388–1399. <https://doi.org/10.1021/acs.jcim.5b00019>
- Tetko, I. V., & Engkvist, O. (2020). From big data to artificial intelligence: Chemoinformatics meets new challenges. *Journal of Cheminformatics*, 12(1), 3. <https://doi.org/10.1186/s13321-020-00475-y>
- Trott, O., & Olson, A. J. (2010). AutoDock Vina: Improving the speed and accuracy of docking with a new scoring function, efficient optimization, and multithreading. *Journal of Computational Chemistry*, 31(2), 455–461. <https://doi.org/10.1002/jcc.21334>
- Van Laar, T., De Deyn, P. P., Aarsland, D., Barone, P., & Galvin, J. E. (2011). Effects of cholinesterase inhibitors in Parkinson's disease dementia: A review of clinical data. *CNS Neuroscience & Therapeutics*, 17(5), 428–441. <https://doi.org/10.1111/j.1755-5949.2010.00166.x>
- Venugopala, K. N., Rashmi, V., & Odhav, B. (2013). Review on Natural Coumarin Lead Compounds for Their Pharmacological Activity. *BioMed Research International*, 2013, 963248. <https://doi.org/10.1155/2013/963248>
- Wang, J., Lai, S., Kong, Y., Yao, W., Chen, X., & Liu, J. (2022). The protonation state of Glu202 in acetylcholinesterase. *Proteins: Structure, Function, and Bioinformatics*, 90(2), 485–492. <https://doi.org/10.1002/prot.26243>
- Wu, Z., Zhu, M., Kang, Y., Leung, E. L.-H., Lei, T., Shen, C., Jiang, D., Wang, Z., Cao, D., & Hou, T. (2021). Do we need different machine learning algorithms for QSAR modeling? A comprehensive assessment of 16 machine learning algorithms on 14 QSAR data sets. *Briefings in Bioinformatics*, 22(4), bbaa321. <https://doi.org/10.1093/bib/bbaa321>
- Xia, R., & Mao, Z. H. (2012). Progression of motor symptoms in Parkinson's disease. *Neuroscience Bulletin*, 28(1), 39–48. <https://doi.org/10.1007/s12264-012-1050-z>
- Yusufzai, S. K., Khan, M. S., Sulaiman, O., Osman, H., & Lamjin, D. N. (2018). Molecular docking studies of coumarin hybrids as potential acetylcholinesterase, butyrylcholinesterase, monoamine oxidase A/B and β -amyloid inhibitors for Alzheimer's disease. *Chemistry Central Journal*, 12(1), 1–57. <https://doi.org/10.1186/s13065-018-0497-z>
- Zhao, L., Ciallella, H. L., Aleksunes, L. M., & Zhu, H. (2020). Advancing computer-aided drug discovery (CADD) by big data and data-driven machine learning modeling. *Drug Discovery Today*, 25(9), 1624–1638. <https://doi.org/10.1016/j.drudis.2020.07.005>
- Zhou, Y., Wang, S., & Zhang, Y. (2010). Catalytic reaction mechanism of acetylcholinesterase determined by Born – Oppenheimer ab initio QM/MM molecular dynamics simulations. *The Journal of Physical Chemistry. B*, 114(26), 8817–8825. <https://doi.org/10.1021/jp104258d>

**CHAPTER IV: EXPLORING NATURAL
PRODUCTS AS MULTI-TARGET-
DIRECTED DRUGS FOR
PARKINSON'S DISEASE: AN IN-
SILICO APPROACH INTEGRATING
QSAR, PHARMACOPHORE
MODELLING, AND MOLECULAR
DYNAMICS SIMULATIONS**

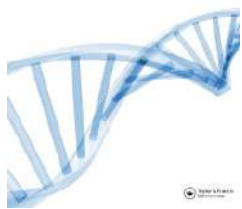
Building upon our initial investigation of COCONUT NP-like caffeine derivatives, we expanded our scope to encompass the entire database, representing the largest collection of NPs currently available. In this study, we utilized *in silico* methods to explore the database and identify potential drug candidates with multi-target activity against PD targets. QSAR models were employed for screening, followed by a hybrid virtual screening approach involving pharmacophore modelling and molecular docking against MAO-B, AA₂AR, and NMDAR. ADME evaluation assessed drug-like properties, revealing twenty-two candidates with desired pharmacophoric features. Notably, CNP0121426 and CNP0242698 exhibited remarkable binding affinities and promising interaction profiles. MD simulations highlighted the curcuminoid: CNP0242698's superior stability with the three targets compared to dihydrochalcones, indicating potential as lead compounds for developing curcuminoids as multi-target remedies for PD. Experimental validation is essential to confirm these findings.

The details of this work are reported in the following publication.

Boulaamane, Y., Touati, I., Goyal, N., Chandra, A., Kori, L., Ibrahim, M. A., ... & Maurady, A. (2023). Exploring natural products as multi-target-directed drugs for Parkinson's disease: an in-silico approach integrating QSAR, pharmacophore modelling, and molecular dynamics simulations. *Journal of Biomolecular Structure and Dynamics*, 1-18. (Reprinted with permission)

Available at: <https://doi.org/10.1080/07391102.2023.2260879>

Conceptualization: Y.B., A.M.; Methodology: Y.B., A.M.; Investigation: Y.B., A.M.; Visualization: Y.B., I.A., H.P.; Supervision: M.R.B., A.M.; Writing—original draft: Y.B.; Writing—review & editing: Y.B., A.M.



Exploring natural products as multi-target-directed drugs for Parkinson's disease: an *in-silico* approach integrating QSAR, pharmacophore modeling, and molecular dynamics simulations

Yassir Boulaamane, Iman Touati, Nainee Goyal, Anshuman Chandra, Lokesh Kori, Mahmoud A. A. Ibrahim, Mohammed Reda Britel & Amal Maurady

To cite this article: Yassir Boulaamane, Iman Touati, Nainee Goyal, Anshuman Chandra, Lokesh Kori, Mahmoud A. A. Ibrahim, Mohammed Reda Britel & Amal Maurady (27 Sep 2023): Exploring natural products as multi-target-directed drugs for Parkinson's disease: an *in-silico* approach integrating QSAR, pharmacophore modeling, and molecular dynamics simulations, Journal of Biomolecular Structure and Dynamics, DOI: [10.1080/07391102.2023.2260879](https://doi.org/10.1080/07391102.2023.2260879)

To link to this article: <https://doi.org/10.1080/07391102.2023.2260879>

 View supplementary material [!\[\]\(586450f125a8cb3be37fbf32f3ec5338_img.jpg\)](#)

 Published online: 27 Sep 2023.

 Submit your article to this journal [!\[\]\(2a43ab231c022f721f599b3726eb8f61_img.jpg\)](#)

 View related articles [!\[\]\(d3462ed9caab158bb29c9d6ee432c4fd_img.jpg\)](#)

 View Crossmark data [!\[\]\(758e046287edfa02db737b047fbb9eba_img.jpg\)](#)



Exploring natural products as multi-target-directed drugs for Parkinson's disease: an *in-silico* approach integrating QSAR, pharmacophore modeling, and molecular dynamics simulations

Yassir Boulaamane^a, Iman Touati^a, Nainee Goyal^b, Anshuman Chandra^c, Lokesh Kori^c, Mahmoud A. A. Ibrahim^{d,e}, Mohammed Reda Britel^a and Amal Maurady^{a,f}

^aLaboratory of Innovative Technologies, National School of Applied Sciences of Tangier, Abdelmalek Essaadi University, Tetouan, Morocco;

^bSchool of Biotechnology, Gautam Buddha University, Greater Noida, India; ^cICMR-National Institute of Malaria Research, Dwarka, New Delhi, India; ^dChemistry Department, Faculty of Science, Computational Chemistry Laboratory, Minia University, Minia, Egypt; ^eSchool of Health Sciences, University of KwaZulu-Natal, Westville, Durban, South Africa; ^fFaculty of Sciences and Techniques of Tangier, Abdelmalek Essaadi University, Tetouan, Morocco

Communicated by Ramaswamy H. Sarma.

ABSTRACT

Parkinson's disease is a neurodegenerative disorder characterized by the progressive loss of dopaminergic neurons in the midbrain. Current treatments provide limited symptomatic relief without halting disease progression. A multi-targeting approach has shown potential benefits in treating neurodegenerative diseases. In this study, we employed *in silico* approaches to explore the COCONUT natural products database and identify novel drug candidates with multi-target potential against relevant Parkinson's disease targets. QSAR models were developed to screen for potential bioactive molecules, followed by a hybrid virtual screening approach involving pharmacophore modeling and molecular docking against MAO-B, AA_{2A}R, and NMDAR. ADME evaluation was performed to assess drug-like properties. Our findings revealed 22 candidates that exhibited the desired pharmacophoric features. Particularly, two compounds: CNP0121426 and CNP0242698 exhibited remarkable binding affinities, with energies lower than -10 kcal/mol and promising interaction profiles with the chosen targets. Furthermore, all the ligands displayed desirable pharmacokinetic properties for brain-targeted drugs. Lastly, molecular dynamics simulations were conducted on the lead candidates, belonging to the dihydrochalcone and curcuminoid class, to evaluate their stability over a 100 ns timeframe and compare their dynamics with reference complexes. Our findings revealed the curcuminoid CNP0242698 to have an overall better stability with the three targets compared to the dihydrochalcone, despite the high ligand RMSD, the curcuminoid CNP0242698 showed better protein stability, implying ligand exploration of different orientations. Similarly, AA_{2A}R exhibited higher stability with CNP0242698 compared to the reference complex, despite the high initial ligand RMSD due to the bulkier active site. In NMDAR, CNP0242698 displayed good stability and less fluctuations implying a more restricted conformation within the smaller active site of NMDAR. These results may serve as lead compounds for the development and optimization of natural products as multi-target disease-modifying natural remedies for Parkinson's disease patients. However, experimental assays remain necessary to validate these findings.

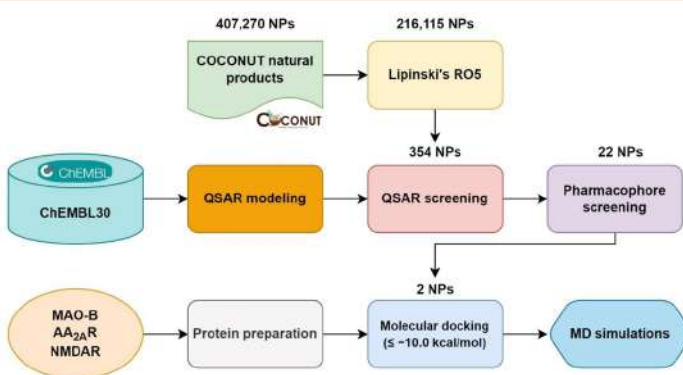
ARTICLE HISTORY

Received 26 April 2023

Accepted 14 September 2023

KEYWORDS

ADME prediction; molecular dynamics simulations; multi-target-directed ligands; natural products; Parkinson's disease; QSAR modeling



1. Introduction

Neurodegenerative disorders are incurable conditions that result in the progressive degeneration of nerve cells in the brain (Barnham et al., 2004). Neurodegenerative diseases such as Alzheimer's, Huntington's, and Parkinson's diseases have complex and multifactorial natures because of the different factors contributing to their progression (Ibrahim & Gabr, 2019). Neurodegenerative diseases lead to increased mortality and morbidity in older patients and are a great burden on society, where there is currently no approved treatment to prevent the progression of these diseases (Van der Schyf, 2011). Parkinson's disease (PD) is considered the second most frequent neurological disorder that is described by the loss of dopaminergic neurons in the midbrain (Dauer & Przedborski, 2003). Current therapeutic approaches for the treatment of PD offer limited symptomatic benefits to patients with no prevention of neuronal loss (Rascol et al., 2003). Accumulating evidence indicates that oxidative damage and mitochondrial imbalance contribute to the cascade of events leading to the degeneration of these dopaminergic neurons (Jenner, 2003). Given the susceptibility of resistance concerning drugs that act on one therapeutic target and the multifactorial nature of neurodegenerative diseases, it has become necessary to develop new treatment strategies. In this regard, scientists have become convinced that the polypharmacological approach targeting multiple proteins linked to the development and progression of the disease should prove to be more beneficial to patients than the current approaches (Lang, 2010; Piau et al., 2011).

Monoamine Oxidase (MAO) is a mitochondrial flavoenzyme that catalyzes the metabolism of some neurotransmitters such as dopamine (Yousdim et al., 2006). It is expressed in two isoforms—namely MAO-A and MAO-B that share about 70% of their sequence identity but differ by their tissue distribution, substrates, and inhibitors preferences (Wang et al., 2013). MAO-A preferentially degrades serotonin while MAO-B preferentially metabolizes 2-phenylethylamine and benzylamine. Dopamine, adrenaline, and noradrenaline are substrates of both isoenzymes (Finberg & Rabey, 2016).

The use of MAO-A inhibitors has been abandoned since the discovery that their use can cause a hypertensive crisis which is related to the metabolism of tyramine (Yamada & Yasuhara, 2004). However, a new generation of selective MAO-B inhibitors proved to be relevant especially when considering that the brain shows an age-related increase in MAO-B activity in patients with PD (Carradori & Silvestri, 2015). During aging, the expression of MAO-B increases in the brain and relates to an enhanced dopamine metabolism which results in an increased reactive oxygen species (ROS) production such as hydrogen peroxide (H_2O_2) inducing oxidative damage and apoptotic signaling events (Lotharius & Brundin, 2002). Given these concerns, MAO-B inhibitors could offer both symptomatic and neuroprotective activities (Tabakman et al., 2004).

Adenosine A_{2A} receptor (AA_{2A}R) is another successful drug target for PD, it represents one of the three subtypes of the adenosine receptor, a G protein-coupled receptor formed by seven transmembrane α -helices (de Lera Ruiz et al., 2014).

The link between AA_{2A}R and PD stems from the link that AA_{2A}R activation counteracts the actions of dopamine, a key neurotransmitter to motor control. Therefore, the blockade of AA_{2A}R through the administration of its antagonists could help with PD motor symptoms. Moreover, oral administration of AA_{2A}R antagonists in experimental models prevented the loss of dopaminergic neurons suggesting their neuroprotective properties (Ikeda et al., 2002).

N-methyl-D-aspartate receptor (NMDAR) is also considered a relevant target for treating PD through receptor-mediated neuroprotection (Hardingham, 2009). NMDAR is a glutamate receptor and ion channel found in neurons, it represents one of three types of ionotropic glutamate receptors, with the other two being AMPA (α -amino-3-hydroxy-5-methyl-4-isoxazolepropionic acid) and kainate receptors (Gonda, 2012). It was demonstrated that the excitatory neurotransmitter, glutamate, contributes to the processes of PD (Iovino et al., 2020). Moreover, it was found that PD patients have higher serum concentrations of glutamate when compared to healthy subjects (Mironova et al., 2018). Whereas NMDAR antagonists display beneficial effects on reversing motor symptoms, reducing levodopa-induced dyskinesia, and slowing progressive neurodegeneration in preclinical PD models (Stoof et al., 1992). Therefore, NMDAR represents a promising target as a therapeutic non-dopaminergic intervention by reversing the severe motor complications that derive from the current dopamine replacement strategies (Zhang et al., 2019).

Recently, there has been a shift of interest in plants and natural products (NPs) when seeking novel remedies for various diseases. NPs and their derivatives have been recognized for many years as a source of therapeutic agents and structural diversity (Kingston, 2011; Shen, 2015).

Several studies revealed strong MAO inhibitory activity from herbal sources such as flavonoids, xanthones, coumarins, caffeine, and alkaloid derivatives, which also became good models for synthetic MAO inhibitors (Erdogan Orhan, 2016). Moreover, it was found that MAO-B inhibitors may as well act as AA_{2A}R antagonists due to the similarity of their binding cavities (Carradori et al., 2014). There is also an increasing body of evidence that safinamide alleviates motor and non-motor PD symptoms through not only MAO-B inhibition which palliates the dopamine deficit in the brain but also by regulating glutamate release through voltage-dependent sodium channels blockade and calcium channels modulation (Stocchi et al., 2022). Furthermore, Ifenprodil, an antagonist of the NMDA receptor, specifically of GluN1 (glycine-binding NMDA receptor subunit 1) and GluN2B (glutamate-binding NMDA receptor subunit 2) subunits was found to possess competitive MAO-A and MAO-B inhibitory activities in the rat brain (Arai et al., 1991). These findings suggest the multi-target potential of these drugs to act on multiple targets implicated in various pathways of PD physiopathology.

The present study aims to search for novel compounds from NPs to act as multitarget drugs against three important targets for the development of antiparkinsonian drugs: MAO-B, AA_{2A}R, and NMDAR. These compounds could potentially provide combined symptomatic relief and neuroprotective activities for patients with PD. A multi-stage virtual

screening approach combining QSAR classification models, pharmacophore screening, molecular docking, and ADME evaluation was conducted to study at the molecular level the interactions of NPs from the COCONUT database, with MAO-B, AA₂AR, and NMDAR (Sorokina et al., 2021). The stability of the lead compounds was further assessed through 100 ns molecular dynamics (MD) simulations and compared to the reference drugs. Active site residues and binding pocket of the reference complexes of MAO-B, AA₂AR and NMDAR are illustrated in Figure S1 in Supporting Information.

2. Materials and methods

2.1. ML and CNN-based QSAR models

Three bioactivity datasets for each target were retrieved from the ChEMBL database (<https://www.ebi.ac.uk/chembl/>), containing chemical structures and their reported bioactivity against human MAO-B, AA₂AR, and NMDAR (GluN1/2B), including 5,066 molecules with reported half maximal inhibitory concentration (IC₅₀) values for hMAO B, 7,813 molecules with reported constant dissociation (k_i) values for hAA₂AR and 699 reported IC₅₀ for NMDAR (GluN1/2B) belonging to homo sapiens and rattus norvegicus since these two organisms express NMDAR (GluN1/2B) with a percent identity matrix of 98.58% based on UniProt sequence alignment tool (Gaulton et al., 2012; The UniProt Consortium, 2021). The datasets were manually curated, and duplicate compounds were removed by taking the mean value when multiple bioactivity values were reported for a given compound. Logarithmic transformation was applied to all the activity

values to better determine the potency of the compounds using the negative logarithm base 10 scale to represent the data in a more interpretable manner (Tarasova et al., 2015). The compounds were then classified as either active or inactive. An activity value >6.5 was used to label active compounds, whereas all compounds displaying an activity value <5 were labeled as inactive as reported in the literature (Burggraaff et al., 2020). Compounds falling within the intermediate range were omitted from the study. The workflow of QSAR modeling is shown in Figure 1.

All investigated compounds from the final datasets were then converted to SMI (Simplified Molecular Input) format, and RDKit cheminformatics software was used to generate chemical structures as graphs, and then as binary molecular descriptors based on the popular Morgan fingerprints, also known as extended-connectivity fingerprints (ECFP4) (Ding et al., 2021; Landrum, 2013).

Finally, three machine learning classification algorithms, namely Random Forest, Extra Trees, and Support Vector Machine were used to generate QSAR models for the selected targets through Scikit-learn machine learning library in Python (Pedregosa et al., 2011; Wu et al., 2021). Convolutional neural networks (CNNs) are a category of neural networks that have proven very effective in areas such as image recognition and classification (Wang et al., 2021). CNNs generally consist of many convolutional layers and one connected layer corresponding to a classic neural network (Figure S2 in Supporting Information). Graph-based and fingerprint-based CNN models were generated to compare their performance with traditional ML algorithms using Keras and TensorFlow libraries in Python (Singh et al., 2020; Gulli & Pal, 2017).

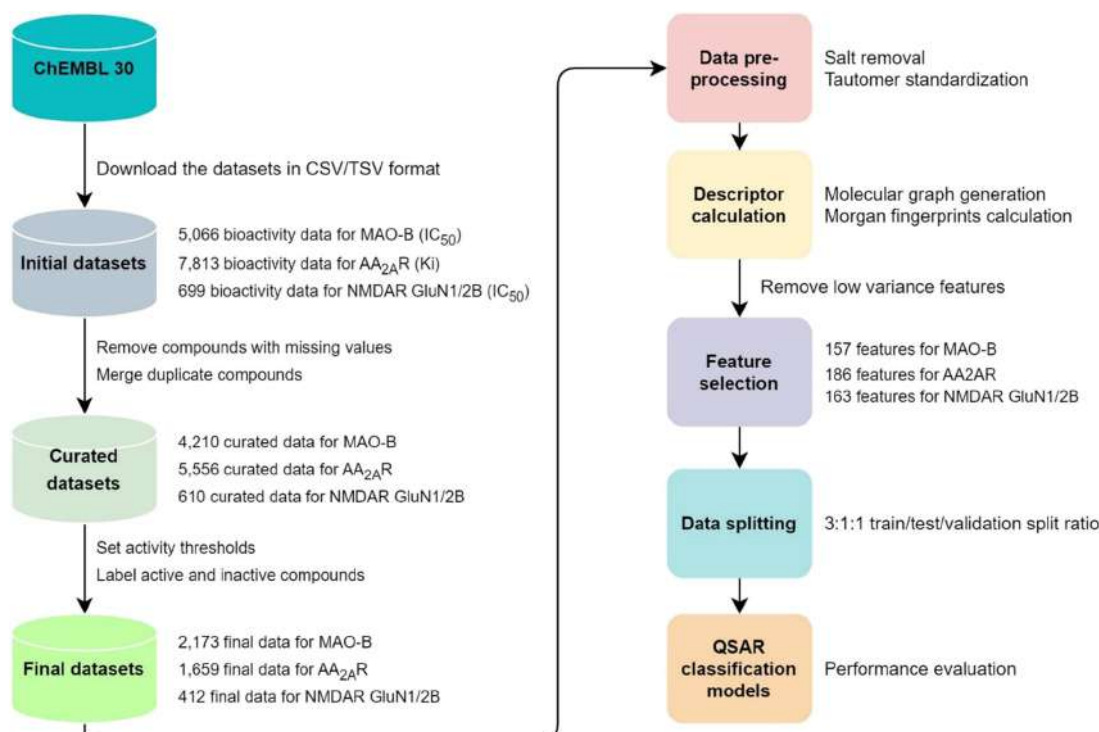


Figure 1. Workflow of QSAR modeling for the prediction of MAO-B, AA₂AR, and NMDAR bioactivity.

Datasets were split into training, testing, and validation sets using a 3:1:1 split ratio (Craft & Leake, 2002). The receiving operating characteristic (ROC) curves were used as a quality parameter to assess the performance of the classification models by plotting the true positive rate (sensitivity) against the false negative rate (specificity), the area under the ROC curve (AUC) values range from 0.5 indicating no discrimination to 1 indicating a perfect separation between the two classes (Hanley & McNeil, 1982; Herrera-Acevedo et al., 2021). Performance metrics were calculated such as sensitivity (SEN) Equation (1), specificity (SPC) Equation (2), false positive rate (FPR) Equation (3), false negative rate (FNR) Equation (4), Matthews Correlation Coefficient (MCC) Equation (5), and accuracy (ACC) Equation (6). Five-fold cross-validation using 100 data splits was also used to evaluate the performance of the selected models. Finally, the validation sets that were not presented to the generated QSAR models yet were used for external validation of the developed QSAR classification models.

$$SEN = \frac{TP}{(TP + FN)} \quad (1)$$

$$SPC = \frac{TN}{(FP + TN)} \quad (2)$$

$$FPR = \frac{FP}{(FP + TN)} \quad (3)$$

$$FNR = \frac{FN}{(FN + TP)} \quad (4)$$

$$ACC = \frac{(TP + TN)}{(P + N)} \quad (5)$$

$$MCC = \frac{(TP \times TN) - (FP \times FN)}{\sqrt{(TP + FP) * (TP + FN) * (TN + FP) * (TN + FN)}} \quad (6)$$

SEN: Number of actual positives correctly identified by a classification model; *SPC*: Number of actual negatives correctly identified by a classification model; *FPR*: Number of negatives incorrectly classified as positives by a classification model; *FNR*: Number of positives incorrectly classified as negatives by a classification model; *ACC*: Overall accuracy of a classification model by calculating the ratio of correct predictions to the total number of predictions; *MCC*: is a statistic that quantifies the quality of binary classification results by considering true and false positives and negatives in a single value, ranging from -1 (perfect disagreement) to $+1$ (perfect agreement). *TP*: Number of true positives; *TN*: Number of true negatives; *FP*: Number of false positives; *FN*: Number of false negatives; *P + N*: Total number of a dataset.

2.2. Ligand database preparation

Chemical structures of the NPs were retrieved in SMILES format from the COCONUT database, the largest NPs database to date (Sorokina et al., 2021). Primary filtration was conducted based on Lipinski's rule of five to eliminate all compounds that present any violation of the five rules of orally active drugs (Lipinski, 2004; Pollastri, 2010). 2D chemical structures and physicochemical properties of all the compounds were computed using the DataWarrior Cheminformatics program to

only retain those with values falling in the recommended range (Sander et al., 2015). Possible ionization states were generated for all ligands at physiological pH of 7.0 ± 2.0 using the Ligprep module of Maestro 12.5 and OPLS3e force field (Roos et al., 2019).

2.3. Pharmacophore modeling

Ligand-based virtual screening was conducted using a pharmacophore model generated from the reference NMDAR antagonist, ifenprodil, and an experimentally evaluated compound, *N*-(4-chloro-1H-benzimidazol-2-yl) benzamide, which displayed an inhibitory activity in the nanomolar range for MAO-B and AA₂AR (Jaiteh et al., 2018; Williams, 2001). Molecular docking was conducted using Glide Extra Precision (XP) mode to identify bioactive conformations for the dual-target reference ligand and the key moieties responsible for the binding with MAO-B and AA₂AR (Friesner et al., 2006). Alternatively, the bioactive conformation of the NMDAR antagonist, ifenprodil was taken from the crystallographic 3D structure from RCSB PDB (<https://www.rcsb.org/>), (PDB ID: 5EWJ) (Stroebel et al., 2016). The alignment of these two ligands was conducted and the Phase module of Maestro 12.5 was used to generate a 3D-pharmacophore model containing the identified pharmacophoric features necessary for the multi-blockade of MAO-B, AA₂AR, and NMDAR (Dixon et al., 2006). The developed 3D-pharmacophore model was then used to further filter the NPs and only retain compounds meeting the proposed pharmacophoric criteria.

2.4. Molecular docking

2AR (PDB ID: 5IU4, resolution = 1.7 Å), and NMDAR (PDB ID: 5EWJ, resolution = 2.7 Å)在与参考抑制剂，safinamide, ZM-241385, 和 ifenprodil，分别，从RCSB PDB (<https://www.rcsb.org/>) (Binda et al., 2007; Segala et al., 2016; Stroebel et al., 2016)。所有结构都使用蛋白准备向导来分配键顺序，添加显式氢，并修复和优化侧链中缺失的原子，使用Prime (Boulaamane et al., 2023; Jacobson et al., 2002, 2004)。质子化状态为残基分配，使用PROPKA程序预测pK_a值，pH = 7.0 (Olsson et al., 2011)。

共晶化的配体用于放置网格盒，使用受体网格生成工具 (Schrödinger Release 2022-3: Maestro, 2020)。网格尺寸选择足够大，以容纳与参考化合物相似大小的配体。分子对接在Maestro 12.5中使用Glide (XP)模式，每配体输出五种构象 (Friesner et al., 2006)。最佳对接姿势根据对接分数和RMSD值选择，以与天然配体对每个目标蛋白的RMSD值。

2.5. ADME properties prediction

Nearly 40% of drug candidates fail in clinical trials due to poor Absorption, Distribution, Metabolism, and Excretion (ADME) properties (Lin et al., 2003). *In silico* ADME prediction is a quick tool to find if a compound is druglike by calculating its pharmacokinetics parameters and physicochemical properties and can considerably reduce the amount of consumed time and resources during the overall drug development process (Bhandari et al., 2022). The selected compounds were analyzed based on common pharmacokinetic parameters including lipophilicity, water solubility, human oral absorption, brain/blood partition coefficient, and human serum albumin binding which were predicted using the Qikprop tool (Ioakimidis et al., 2008). An overview of the virtual screening workflow is represented in Figure S3 in Supporting Information.

2.6. Molecular dynamics simulations

The stability of the most potent compounds complexed with the selected target proteins was evaluated through 100 ns MD simulations using the Desmond module included in Maestro 12.5, Schrödinger's suite (2020-3) (Bowers et al., 2006). The water-soaked solvated system was created in Desmond using the System Builder panel. The OPLS3e force field was selected, and Single Point Charge (SPC) was used as a solvent model with a 10 Å orthorhombic box for both proteins. The system was neutralized by randomly adding enough counter-ions (Na^+ and Cl^-) and an isosmotic state was maintained by adding 0.15 M NaCl. The solvated model

system was subjected to energy minimization using OPLS3e force field parameters as the default protocol associated with Desmond (He et al., 2022). Then, the system was equilibrated throughout the simulation time via Constant Number of Particles, Pressure, and Temperature (NPT) ensemble at a constant 300 K temperature and 1 atm pressure using the Nose-Hoover thermostat algorithm and Martyna-Tobias-Klein Barostat algorithm, respectively (Ke et al., 2022). A total of 100 ns simulations were carried out, during which 1000 frames were recorded. Finally, the MD simulation trajectory was analyzed using the Simulation Interaction Diagram (SID) tool (AlAjmi et al., 2018).

3. Results and discussion

3.1. QSAR models validation

The ROC curve was used to assess the quality of the developed QSAR classification models by plotting the true positive rate against the false positive rate. For all the classification models, AUC values greater than 0.80 were achieved for MAO-B, whereas some classification models for AA_{2A}R displayed lower AUC values as illustrated in Figure 2. The performance of all the built QSAR models was evaluated using different performance metrics as shown in Table 1. Similarly, external validation of the developed QSAR classification models is summarized in Table 2.

Based on the performance of the QSAR classification models on internal and external datasets, the Random Forest model was found to perform the best with an AUC value of 0.93, 0.91, and 0.94 and MCC value for external sets of 0.81,

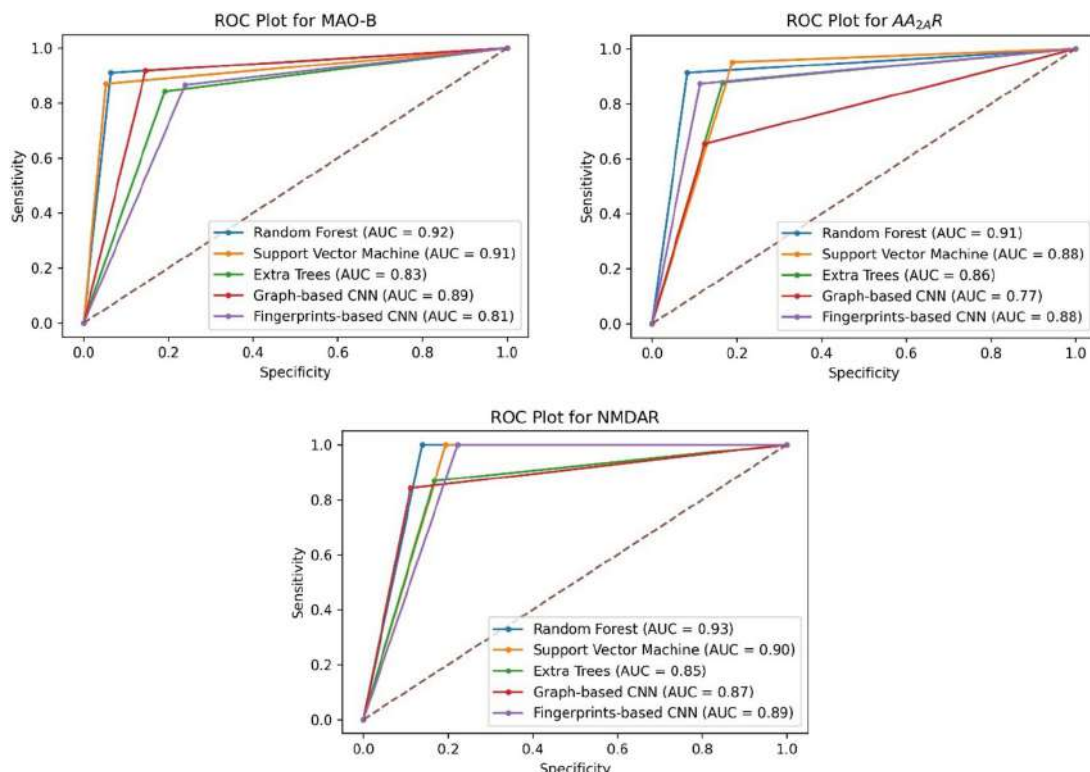


Figure 2. ROC plots of the generated QSAR classification models for MAO-B, AA_{2A}R, and NMDAR.

Table 1. Performance of the developed QSAR classification models.

Target protein	Model	Testing set					5-fold CV ACC
		SEN	SPC	FPR	FNR	MCC	
MAO-B	Random forest	0.92	0.93	0.06	0.07	0.85	0.92
	Support vector machine	0.89	0.93	0.20	0.15	0.82	0.91
	Extra trees	0.84	0.80	0.06	0.10	0.82	0.84
	Graph-based CNN	0.86	0.76	0.23	0.13	0.63	0.81
	Fingerprints-based CNN	0.93	0.87	0.12	0.06	0.80	0.90
AA _{2A} R	Random forest	0.88	0.93	0.06	0.11	0.82	0.91
	Support vector Machine	0.92	0.87	0.12	0.16	0.77	0.89
	Extra trees	0.83	0.87	0.12	0.07	0.85	0.71
	Graph-based CNN	0.65	0.87	0.12	0.34	0.53	0.74
	Fingerprints-based CNN	0.83	0.92	0.07	0.16	0.76	0.88
NMDAR	Random forest	0.97	0.90	0.09	0.02	0.88	0.94
	Support vector machine	0.97	0.87	0.12	0.16	0.84	0.91
	Extra trees	0.84	0.87	0.12	0.02	0.85	0.71
	Graph-based CNN	0.84	0.91	0.08	0.15	0.76	0.87
	Fingerprints-based CNN	0.97	0.86	0.13	0.02	0.82	0.90

SEN: sensitivity (true positive rate); SPC: specificity (true negative rate); FPR: false positive rate; FNR: false negative rate; MCC: Matthews correlation coefficient; ACC: accuracy; 5-fold CV: 5-fold cross-validation.

Table 2. External validation of the developed QSAR classification models.

Target protein	Model	Performance metrics					
		SEN	SPC	FPR	FNR	MCC	ACC
MAO-B	random forest	0.87	0.93	0.06	0.12	0.81	0.90
	Support vector machine	0.85	0.95	0.15	0.14	0.79	0.89
	Extra trees	0.85	0.84	0.04	0.14	0.84	0.69
	Graph-based CNN	0.81	0.80	0.19	0.18	0.61	0.80
	Fingerprints-based CNN	0.84	0.82	0.17	0.15	0.67	0.83
AA _{2A} R	Random forest	0.92	0.93	0.06	0.07	0.85	0.93
	Support vector machine	1.00	0.83	0.13	0.12	0.78	0.88
	Extra trees	0.87	0.86	0.16	0.00	0.87	0.73
	Graph-based CNN	0.72	0.87	0.12	0.27	0.60	0.80
	Fingerprints-based CNN	0.92	0.88	0.11	0.07	0.79	0.90
NMDAR	Random forest	1.00	0.90	0.10	0.00	0.89	0.94
	Support vector machine	1.00	0.86	0.15	0.06	0.84	0.91
	Extra trees	0.93	0.85	0.14	0.00	0.89	0.78
	Graph-based CNN	0.83	0.88	0.12	0.17	0.72	0.86
	Fingerprints-based CNN	1.00	0.82	0.18	0.00	0.79	0.89

SEN: sensitivity (true positive rate); SPC: specificity (true negative rate); FPR: false positive rate; FNR: false negative rate; MCC: Matthews correlation coefficient; ACC: accuracy.

0.85, and 0.89 for MAO-B, AA_{2A}R, and NMDAR, respectively. The model was then selected for target bioactivity prediction against the selected proteins. Out of 216,115 drug-like compounds, 13,996 were predicted as active for MAO-B, among them 1,106 were active for AA_{2A}R and 354 were predicted as actives for all the selected targets. To avoid chemical sampling bias, a wide chemical space diversity of the training sets is mandatory, and it contributes to high prediction accuracy and strong generalization ability of the classification models (Yang et al., 2022). The chemical space diversity of the curated datasets of the selected targets alongside the predicted active NPs were explored using the t-stochastic neighbor embedding (t-SNE) statistical method (Van der Maaten & Hinton, 2008) as shown in Figure 3. Distinct clusters of active compounds, likely signifying diverse scaffolds and chemotypes targeting the same protein were observed. These clusters are clearly separated from inactive compounds. Interestingly, unique clusters emerge from the screened natural products (NPs), potentially representing novel chemical classes absent in the ChEMBL datasets. These NP clusters also exhibit clear separation from inactive compounds (Figure 2).

3.2. Pharmacophore screening

The pharmacophore hypothesis was based on an experimentally validated MAO-B inhibitor/AA_{2A}R antagonist, and on ifenprodil, an NMDAR antagonist as shown in Figure 4(A,B), respectively. The molecular docking study revealed the importance of the nitrogen atom of the furan and the benzene ring to act as a hydrogen bond donor and establish a hydrogen bond with a key residue in the MAO-B entrance cavity of the active site namely Tyr-326. This residue is specific to the MAO-B isoform and acts as a gating residue to allow the binding of selective MAO-B inhibitors (Binda et al., 2011; Milczek et al., 2011). Moreover, this same component is also responsible for the hydrogen bonding with Asn-253 of the active site of AA_{2A}R, a key interaction deemed important for the stability of AA_{2A}R antagonists (Jaakola et al., 2010). In NMDAR, the nitrogen atom is responsible for forming a hydrogen bond with Gln-110B as reported in the literature (Fjelldal et al., 2019). The 3D-pharmacophore model generated using the Phase module consisted of two aromatic rings separated by a distance of 11 Å as shown in Figure 4(C) reflecting the length of the

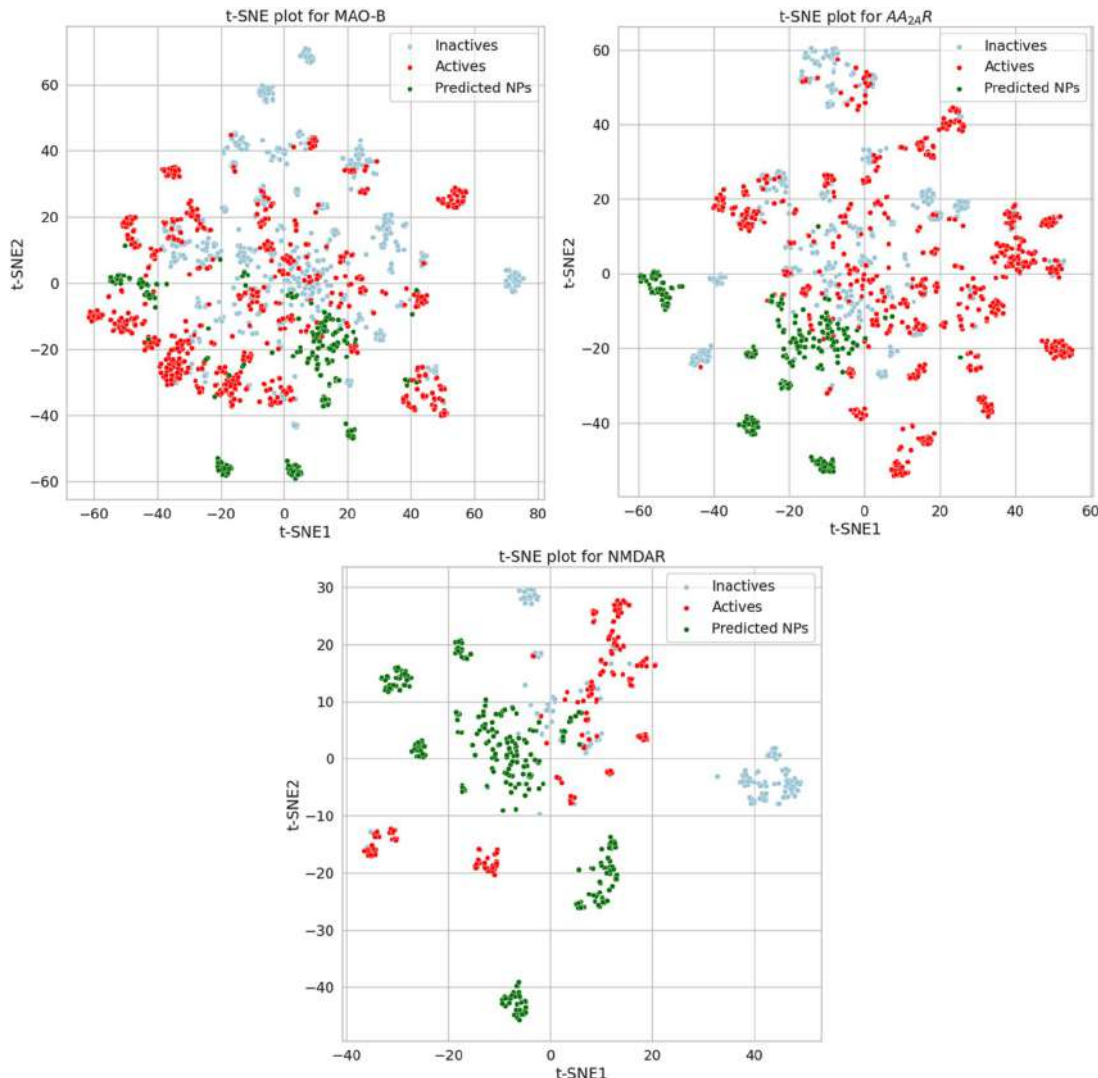


Figure 3. Visual representation of curated ChEMBL datasets for MAO-B, AA₂R, and NMDAR, alongside the predicted active NPs from the QSAR screening using t-SNE method based on Morgan fingerprints.

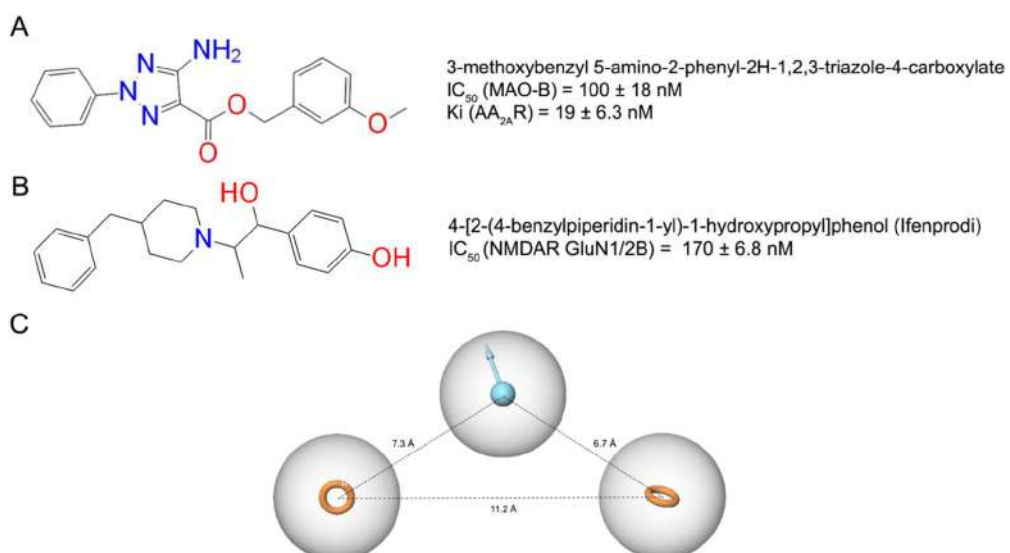


Figure 4. (A) Chemical structure and experimental values of the reference dual MAO-B/AA₂R ligand; (B) chemical structure of the NMDAR reference antagonist, ifenprodil; (C) proposed 3D-pharmacophore model to screen for multi-target drugs, the hypothesis consisted of three pharmacophoric features: one aromatic ring, one hydrogen bond donor, and one aromatic ring.

binding site cavities of the selected targets, and one donor group in the middle which is deemed important for establishing conventional hydrogen bonds with Tyr-326, Asn-253, and Gln-110B of MAO-B, AA_{2A}R, and NMDAR active site, respectively.

3.3. Molecular docking results

The docking protocol implemented in the Glide module was validated by redocking the crystal ligands of human MAO-B, AA_{2A}R, and NMDAR (GluN1/2B). Native ligands were downloaded from the PubChem database with the following CIDs: 131682 for safinamide, 176407 for ZM-24138, and 3689 for ifenprodil (Kim et al., 2021). The Ligprep module was employed for energy minimization using default settings. The root-mean-square deviation (RMSD) was calculated by superposing both docked and native ligands. The results yielded values of 0.12, 0.83, and 0.88 Å for MAO-B, AA_{2A}R, and NMDAR which indicates a good accuracy of the docking program (Figure S4 in Supporting Information). The prepared and filtered compounds were initially screened using the generated pharmacophore model to remove the compounds that do not match the selected pharmacophoric sites. At this stage, 22 of 354 ligands were retained. Subsequently, molecular docking was conducted on the remaining compounds against MAO-B, AA_{2A}R and NMDAR active sites using Glide Extra Precision (XP) mode (Friesner et al., 2006). The chemical structures of the remaining compounds are shown in Figure 5. The docking scores and protein-ligand

interactions are shown in Table 3. The selected binding poses of the two highest-ranking compounds with the selected targets are shown in Figure 6. The chemical space of the 22 compounds highlighting the top two lead compounds, was visualized using t-SNE plots to assess their positioning relative to the reference compounds (Figure S5 in Supporting Information). The two lead compounds exhibited very close proximity, indicating a high degree of similarity. Additionally, in the AA_{2A}R plot, the compounds overlapped with the reference active compounds. However, no similar active compounds were identified in the MAO-B and NMDAR datasets, implying the novelty of these drugs and the need for *in vitro* testing.

3.4. ADME evaluation results

ADME properties results for the selected NPs are shown in Table 4. Qikprop predicted aqueous solubility shows that all the compounds have values within the recommended range (-6.5 to 0.5) where 95% of similar values for known drugs fall inside. Predicted human oral absorption shows that most of the natural compounds have better oral absorption than the reference ligands, and thus greater bioavailability. Brain/blood partition coefficient (QPlogBB) was also predicted, all the values are within the range of recommended values for compounds that penetrate the blood-brain barrier (-3.0 to 1.2) (Boulaamane et al., 2022). Caco-2 cells are a good mimic for the gut-blood barrier, predicted apparent Caco-2 cell permeability cell is considered great if >500 and

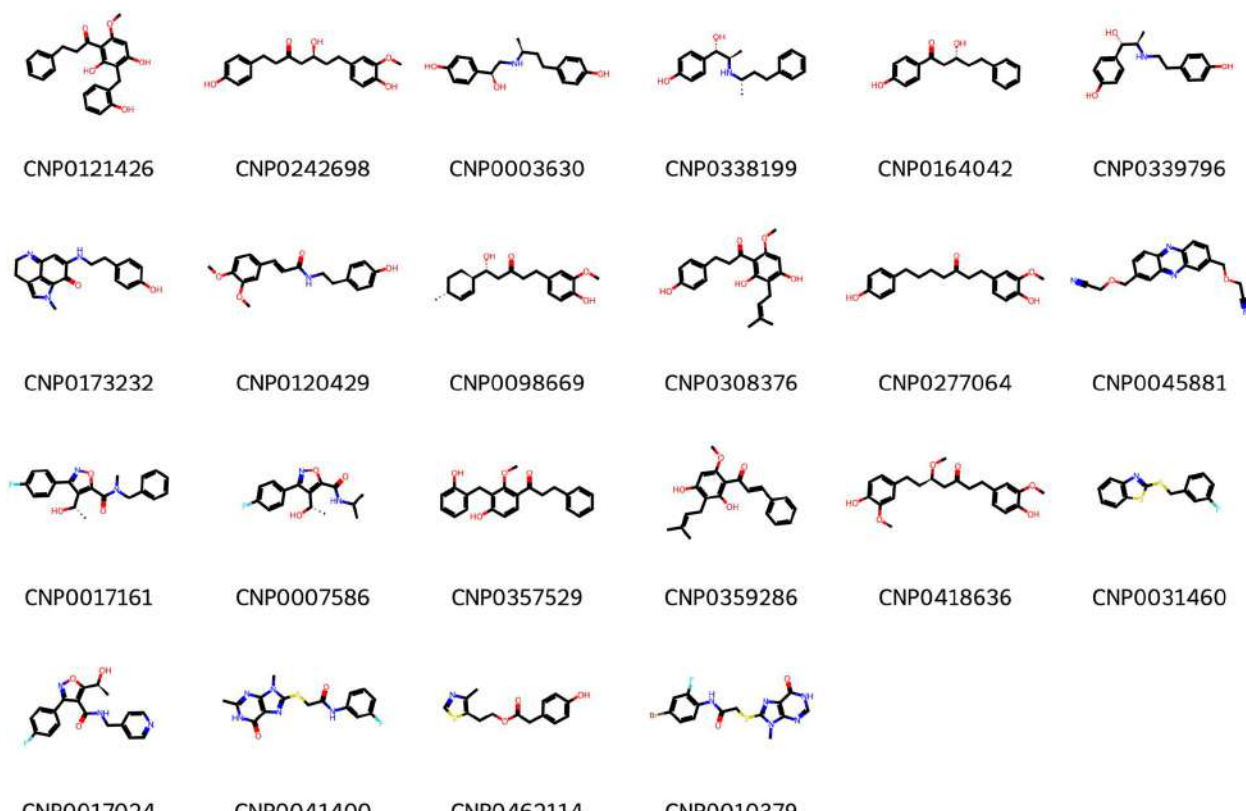
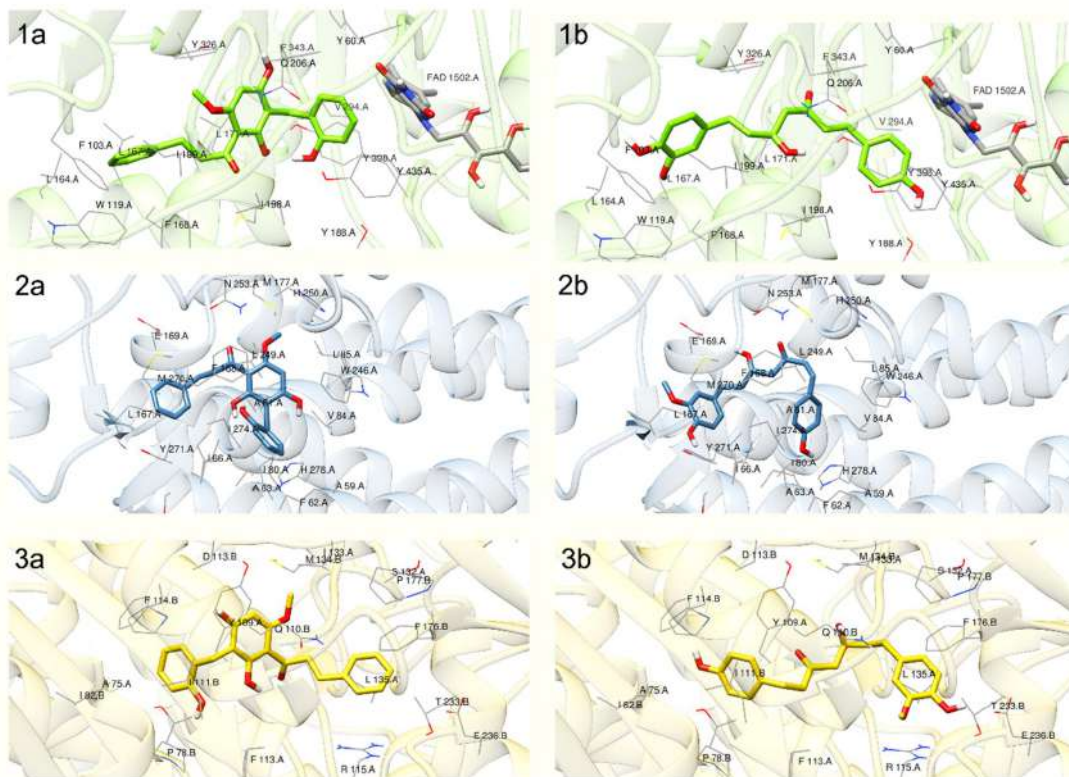


Figure 5. Chemical structures of the remaining 22 compounds selected for molecular docking against MAO-B, AA_{2A}R, and NMDAR.

Table 3. Molecular docking results of the retained NPs against MAO-B, AA₂AR, and NMDAR.

Compound	Glide XP score (kcal/mol)			Hydrogen bonds			$\pi-\pi$ interactions		
	MAO-B	AA ₂ AR	NMDAR	MAO-B	AA ₂ AR	NMDAR	MAO-B	AA ₂ AR	NMDAR
Safinamide	-11.5	-9.1	-9.5	Gln-206	Glu-169	Asp-113Asp-136B	Tyr-326	—	Tyr-109APhe-114B
ZM-241385	-9.9	-10.8	-9.4	Cys-172Tyr-188	Glu-169Asn-253	Tyr-110Alle-133A	Tyr-326	Phe-168Hid-250	Tyr-109A
Ifenprodil	-7.7	-6.5	-11.2	Cys-172Tyr-188	Tyr-271	Gln-110BGl-236B	—	Hid-250	Phe-114BPhe-176B
CNP0121426	-12.0	-12.4	-10.0	Leu-171	Asn-253	Gln-110B	Phe-168Tyr-326	—	Tyr-109APhe-176B
CNP0242698	-12.4	-11.4	-9.5	Ile-198Gly-434	Asn-253Ile-66	Gln-110BArg-115AGlu-236B	Tyr-398Tyr-435	—	Phe-114BPhe-176B
CNP0003630	-10.9	-9.3	-9.3	Ile-198Gly-434Tyr-435	Phe-168Ile-66Ile-80	Gln-110BGl-236B	Tyr-435	—	Phe-176B
CNP0338199	-10.6	-9.1	-9.0	Ile-199	Asn-253Ala-63	Tyr-109A	—	Phe-168	—
CNP0164042	-9.1	-10.3	-9.0	Ile-198Tyr-435	Glu-169Tyr-271	Gln-110BGl-236B	Tyr-435	—	Phe-176B
CNP0339796	-8.4	-8.6	-11.1	Ile-198	Asn-253Ile-66	Tyr-109AThr-110A	—	—	—
CNP0173232	-10.4	-9.8	-7.4	Tyr-398	Glu-169Asn-253	Thr-110Alle-133AGln-110B	Tyr-326Tyr-398	Phe-168	Tyr-109A
CNP0120429	-9.7	-8.9	-8.9	Gly-434	—	Gln-110BGl-236B	Tyr-435	Tyr-271	Phe-176B
CNP0098669	-9.4	-9.7	-8.4	—	Asn-253	Gln-110B	—	Phe-168	Tyr-109A
CNP0308376	-9.6	-9.3	-8.6	—	Ile-80Glu-169	Tyr-109AGln-110B	Tyr-398	Phe-168	Tyr-109A
CNP0277064	-9.8	-9.3	-8.3	Pro-102Gly-434	Asn-253	Glu-106BThr-110A	Tyr-398	—	—
CNP0045881	-9.6	-11.4	-6.5	Gln-65	Asn-253	—	Tyr-326	Phe-168	Tyr-109A
CNP0017161	-10.2	-8.6	-8.5	Ile-66Phe-168Glu-169	Gln-110B	—	—	Phe-114B	—
CNP0007586	-9.2	-9.6	-8.5	—	Asn-253	Gln-110B	Tyr-326	Phe-168	—
CNP0357529	-9.8	-8.8	-8.6	—	Glu-169	Ser-132A	—	Phe-168	—
CNP0359286	-9.7	-8.9	-8.5	—	Asn-253	Gln-110B	—	—	Tyr-109A
CNP0418636	-10.0	-7.5	-9.0	Gly-434Tyr-435	—	—	Tyr-326	Phe-168Tyr-271	Tyr-109A
CNP0031460	-9.2	-8.9	-7.8	—	Asn-253	—	—	Phe-168	Tyr-109APhe-114B
CNP0017024	-7.3	-9.1	-8.9	Gln-206	—	Gln-110B	Tyr-326	Phe-168	Tyr-109A
CNP0041400	-8.6	-7.2	-7.5	—	Asn-253	Glu-236B	Trp-119	—	Phe-176B
CNP0462114	-7.1	-7.2	-6.5	—	Asn-253	Thr-110A	—	Phe-168	—
CNP0010379	-5.8	-8.0	-5.8	—	Asn-253	Gln-110B	Tyr-326	—	Phe-176B

**Figure 6.** Selected binding conformations of the most potent multi-target ligands: CNP0121426 (a) and CNP0242698 (b) with MAO-B (1), AA₂AR (2), and NMDAR (3).

poor if <25. The predicted QPPCaco values show that most compounds have medium-good Caco-2 cell permeability. Finally, the prediction of binding to human serum albumin

(QPlogKhsa) yielded values for the studied compounds within the recommended range (-1.5 and 1.5) for 95% of known drugs.

Table 4. ADME prediction results of the retained NPs from the Hybrid virtual screening study.

Compound	QPlogPo/w	QPlogS	%HOA	QPlogBB	QPPCaco	QPlogKhsa
Safinamide	1.9	-2.1	76.2	-0.4	112.5	-0.2
ZM-241385	1.6	-4.0	73.3	-1.9	108.7	-0.2
Ifenprodil	3.7	-3.9	95.0	-0.3	392.8	0.5
CNP0121426	4.2	-6.3	100.0	-1.1	760.0	0.5
CNP0242698	3.4	-4.9	87.7	-2.1	188.0	0.3
CNP0003630	2.5	-2.9	74.9	-1.2	75.4	-0.1
CNP0164042	3.5	-4.0	95.9	-1.2	526.0	0.2
CNP0338199	3.2	-3.2	90.5	-0.5	321.8	0.2
CNP0173232	3.2	-4.7	100.0	-0.9	791.1	0.3
CNP039796	1.6	-2.6	71.8	-1.0	93.7	-0.2
CNP0120429	3.7	-4.6	100.0	-0.9	1256.8	0.3
CNP0098669	3.9	-5.1	100.0	-1.3	654.6	0.5
CNP0308376	4.0	-4.5	100.0	-1.2	592.7	0.5
CNP0277064	3.9	-5.2	96.2	-1.7	389.7	0.4
CNP0045881	1.2	-3.6	75.6	-1.8	204.7	-0.9
CNP0017161	3.2	-4.4	100.0	-0.6	862.1	0.2
CNP0007586	2.8	-4.3	96.8	-0.6	952.2	0.0
CNP0357529	4.1	-4.7	100.0	-0.9	1146.7	0.6
CNP0359286	4.8	-5.3	100.0	-0.9	1294.1	0.8
CNP0418636	3.9	-5.3	100.0	-1.7	539.3	0.3
CNP0031460	4.9	-5.3	100.0	0.5	6952.4	0.6
CNP0017024	2.4	-4.0	88.4	-0.9	462.7	-0.1
CNP0041400	2.1	-4.8	83.6	-1.2	297.8	-0.1
CNP0462114	3.0	-4.3	94.3	-0.9	621.4	0.1
CNP0010379	2.3	-5.0	84.6	-1.0	292.2	-0.1

QPlogPo/w: Predicted octanol/water partition coefficient; QPlogS: Predicted water solubility; %HOA: Percentage of human oral absorption; QPlogBB: Predicted brain/blood partition coefficient; QPPCaco: Predicted apparent Caco-2 cell permeability in nm/sec; QPlogKhsa: Prediction of binding to human serum albumin.

3.5. Molecular dynamics simulations

The results obtained from the molecular docking study could be further validated using MD simulations to assess the stability of the selected NPs under dynamic conditions. Therefore, to further validate the docking results, CNP0121426 and CNP0242698 in complex with MAO-B, AA_{2A}R, and NMDAR were subjected to 100 ns MD simulations and compared to the reference ligands, safinamide, ZM-241385, and ifenprodil under the same conditions. Several parameters including root mean square deviation (RMSD) of C_α atoms, ligand RMSD with respect to protein, root mean square fluctuation (RMSF) of C_α atoms of the proteins, and protein-ligand interactions were analyzed from the MD simulation trajectories.

3.5.1. Root-mean square deviation

In Figure 7, the RMSD plots for the chosen compounds and reference ligands bound to MAO-B, AA_{2A}R, and NMDAR are presented. RMSD values indicate the degree of movement exhibited by the protein and ligand from their original positions, and hence, the stability of the complex. Notably, the CNP0121426-MAO-B complex demonstrated high RMSD values of C_α atoms, reaching approximately 4.8 Å, while CNP0242698-MAO-B remained stable at around 3 Å by the last 50 ns in similar manner to the reference complex. The ligand RMSD for the reference inhibitor, safinamide was stabilized at 1.2 Å as demonstrated in previous studies (Kurczab et al., 2018). Meanwhile, a higher deviation was observed for CNP0121426 reaching 1.8 Å, while CNP0242698 was stabilized at 2.5 Å. The significant variations observed can be attributed to the remarkable flexibility of CNP0242698, which possesses rotatable bonds that impact the ligand's ability to undergo conformational changes to find the optimal binding pose.

Regarding the reference structure of AA_{2A}R, the C_α atoms exhibited RMSD value of 4.8 Å, whereas CNP0121426 and CNP0242698 showed a more stable RMSD at 4 and 3 Å, respectively. However, the reference antagonist ZM-241385 demonstrated a consistent RMSD of approximately 0.6 Å, while CNP0121426 and CNP0242698 displayed a deviation of 6 Å. The increased variances observed can be explained by the expansive binding pocket of AA_{2A}R, which permits the smaller ligands to undergo diverse conformations throughout the simulation period.

In the case of NMDAR, the three protein-ligand complexes exhibited comparable deviations, ranging from 2 to 3.5 Å, consistent with the findings reported in the literature (Touati et al., 2023). Specifically, the CNP0121426 and CNP0242698 complexes had slightly higher deviations of 3.2 and 3.5 Å, respectively. In contrast, the antagonist ifenprodil demonstrated remarkable stability, exhibiting deviations of less than 1.0 Å when bound to both chains A and B of NMDAR. However, CNP0121426 showed larger deviations of 6 Å, while CNP0242698 exhibited stabilized RMSD values at 1.5 Å, which are considered acceptable for lead compounds.

3.5.2. Root-mean square fluctuation

The RMSF is a useful analytical tool for observing atomic fluctuations in protein chains during MD simulations (Benson & Daggett, 2012). Figure 8 displays RMSF plots that highlight areas of the protein that experience the most movement, with peaks indicating high levels of fluctuation. It is common for the N-terminal and C-terminal ends of the protein to exhibit greater fluctuation compared to other regions. Secondary structure elements, such as α-helices and β-strands, tend to be more rigid and less flexible than loop regions, resulting in lower levels of fluctuation. In Figure 9, the MAO-B

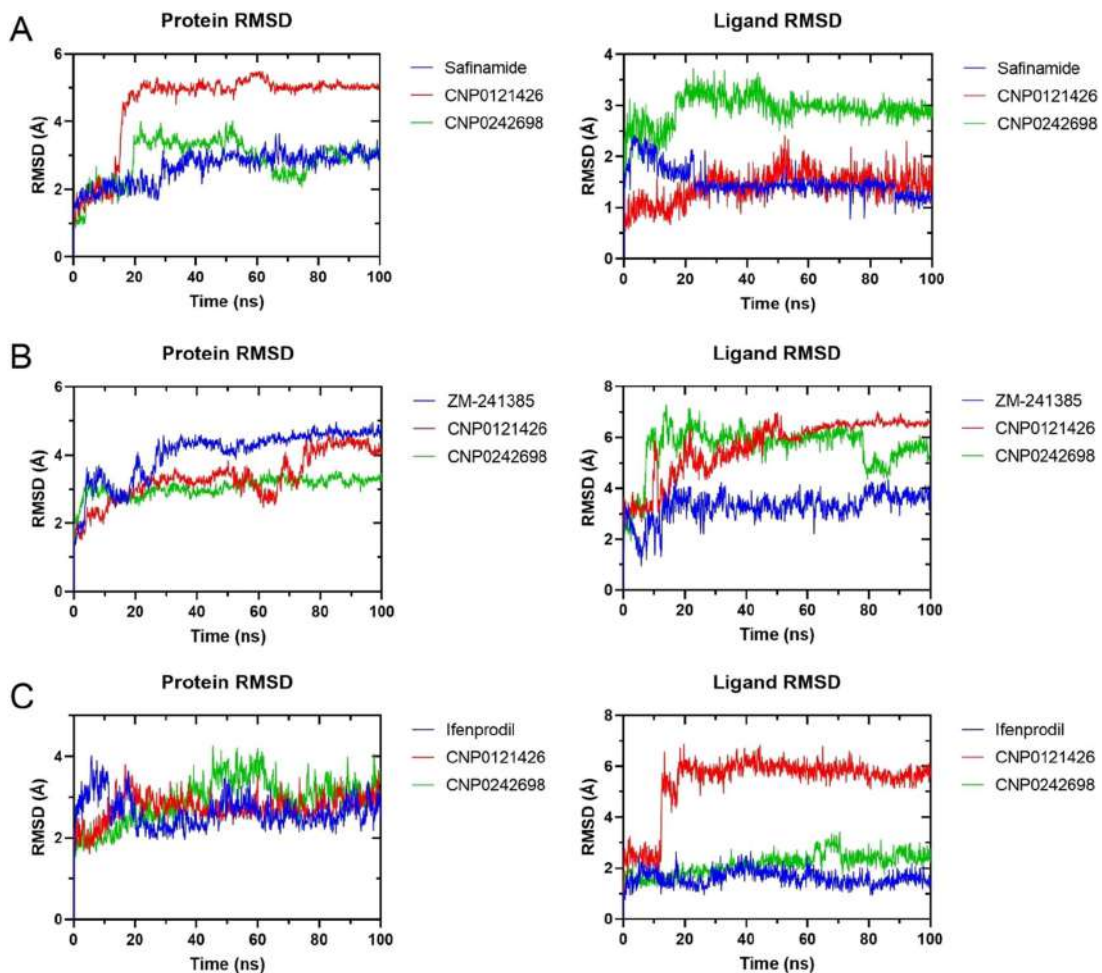


Figure 7. RMSD analysis of C_{α} atoms (Left) and the corresponding ligands (right) of the selected targets: MAO-B (a), AA₂AR (B), and NMDAR (C) in complex with the reference ligands, CNP0121426, and CNP0242698.

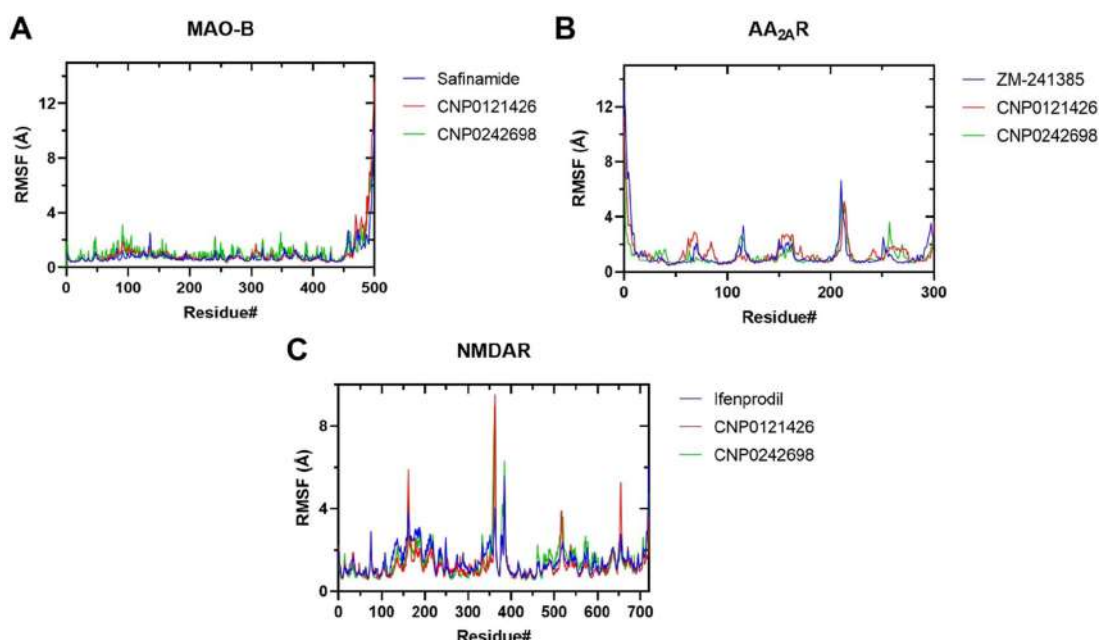


Figure 8. RMSF plots of the selected targets: MAO-B (A), AA₂AR (B), and NMDAR (C) in complex with the reference ligands, CNP0121426, and CNP0242698.

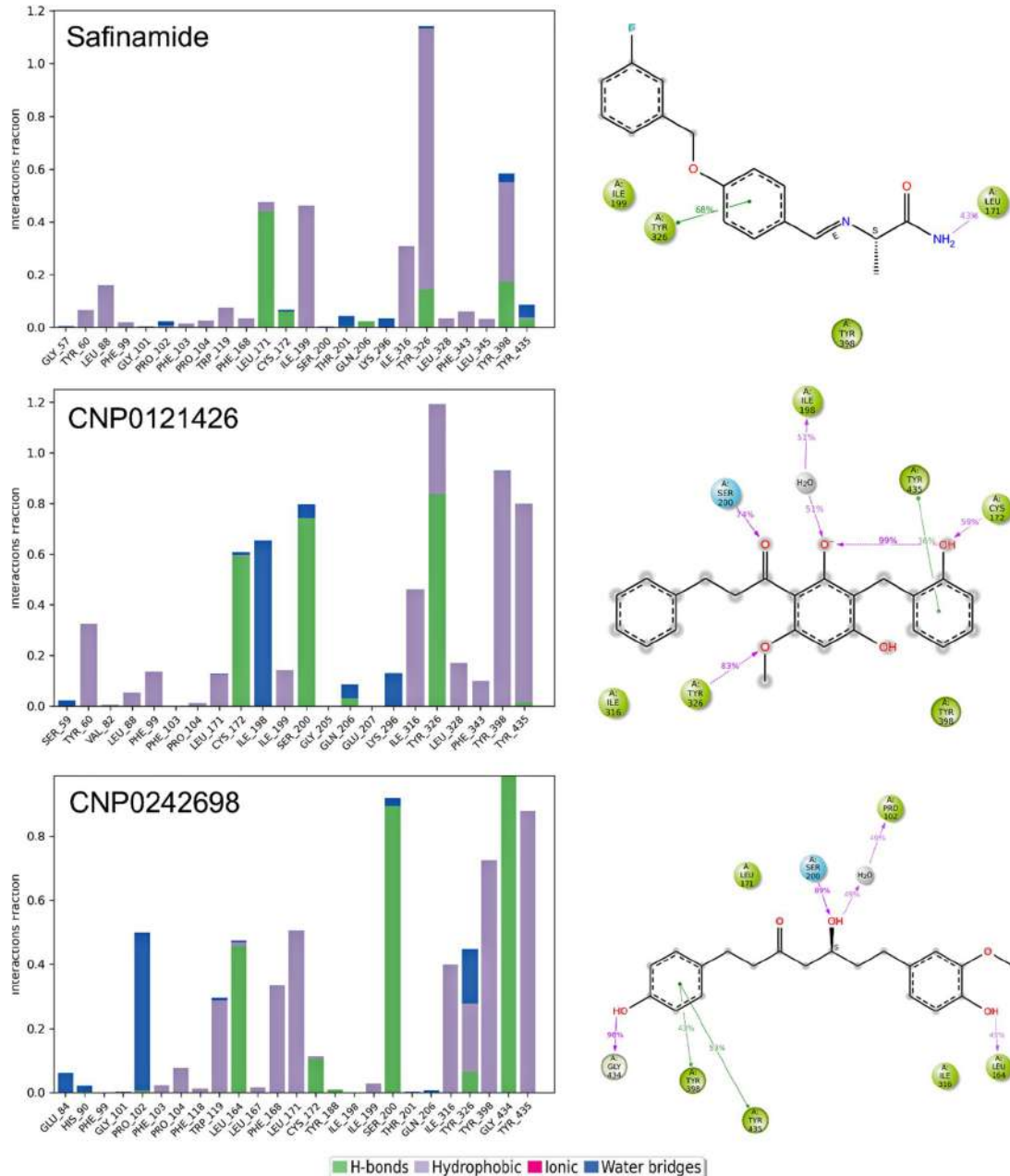


Figure 9. Protein-ligand interaction histograms of safinamide, CNP0121426, and CNP0242698 in complex with MAO-B displaying the fraction of interactions with active amino acids. On the right, schematic representations of the ligands with the percentage of interactions with the protein residues.

enzyme's residues remained consistently stable when bound to the selected compounds, with all fluctuations remaining below 2 Å during the simulation. The study revealed that the highest level of fluctuation observed in all three MAO-B complexes was at 14 Å. However, these residues were not involved in ligand binding, as they were in the C-terminal region. This indicates a slight conformational change in the enzyme rather than any significant impact on ligand binding.

The RMSF analysis of AA_{2A}R revealed significant fluctuations of approximately 4.8 Å in certain regions. Specifically, residues 210–230 showed high flexibility in all three complexes, which is consistent with findings in the literature (Ng et al., 2013). However, the ligand-binding regions experienced less fluctuation, with values of around 2.4 Å in the reference and CNP0121426 complex. In contrast, the same

region exhibited higher fluctuations in the CNP0242698 complex, indicating a potential conformational change due to the ligand's mode of binding.

In the case of NMDAR, the RMSF analysis highlighted high fluctuations of approximately 5 Å in certain regions that were not involved in ligand binding. However, the amino acids within the binding site that made contact with the ligands experienced much lower levels of fluctuation, approximately 1.6 Å, indicating excellent stability of the ligands within their respective binding cavities in all complexes.

3.5.3. Protein-ligand interactions

The role of each amino acid in protein-ligand interactions was unveiled by the simulation results. Figure 9 displays the diagrams

of the molecular interactions with MAO-B, indicating that most of the interactions with the active site of MAO-B are hydrophobic. In the reference complex, Leu-171 formed one preserved hydrogen bond. Due to the hydrophobic nature of the cavity, most other interactions were also hydrophobic. The crucial hydrophobic interactions were primarily formed by Ile-199 and Tyr-326, which serve as the gating residues responsible for substrate and inhibitor specificity (Boulaamane et al., 2023; Milczek et al., 2011). In addition, CNP0121426 formed hydrogen bonds with Cys-172, Ser-200, and Tyr-326. The simulation also highlighted the presence of strong water bridges involving Ile-198. Furthermore, CNP0242698 mainly interacted with Ser-200 and Gly-434 through hydrogen bonds. Other hydrophobic interactions with Ile-316, Tyr-398, and Tyr-435 of the aromatic cage were also observed.

Figure 10 displays the protein-ligand interactions for AA₂AR. The simulation results confirm the presence of a

strong hydrogen bond involving Asn-253 between the antagonist ZM-241385 and AA₂AR, consistent with previous literature (Welihinda et al., 2016). Additionally, another hydrogen bond involving Ala-63 was identified, along with several hydrophobic interactions involving Phe-168, Leu-249, and His-250. In the case of CNP0121426, a hydrogen bond was observed involving Glu-169, and significant hydrophobic interactions were identified with Phe-168 and His-264. However, CNP0242698 exhibited a greater number of interactions, including hydrogen bonds and water bridges with Ala-59, Ile-80, Val-84, His-250, and Asn-253.

Figure 11 illustrates the highlighted interactions between NMDAR and the selected compounds. As per the literature, the reference antagonist consistently binds with B:Gln-110 via hydrogen bonding (Kumar & Patnaik, 2016), while additional hydrogen bonds are observed with B:Glu-106 and B:Glu-236. Several hydrophobic interactions were also

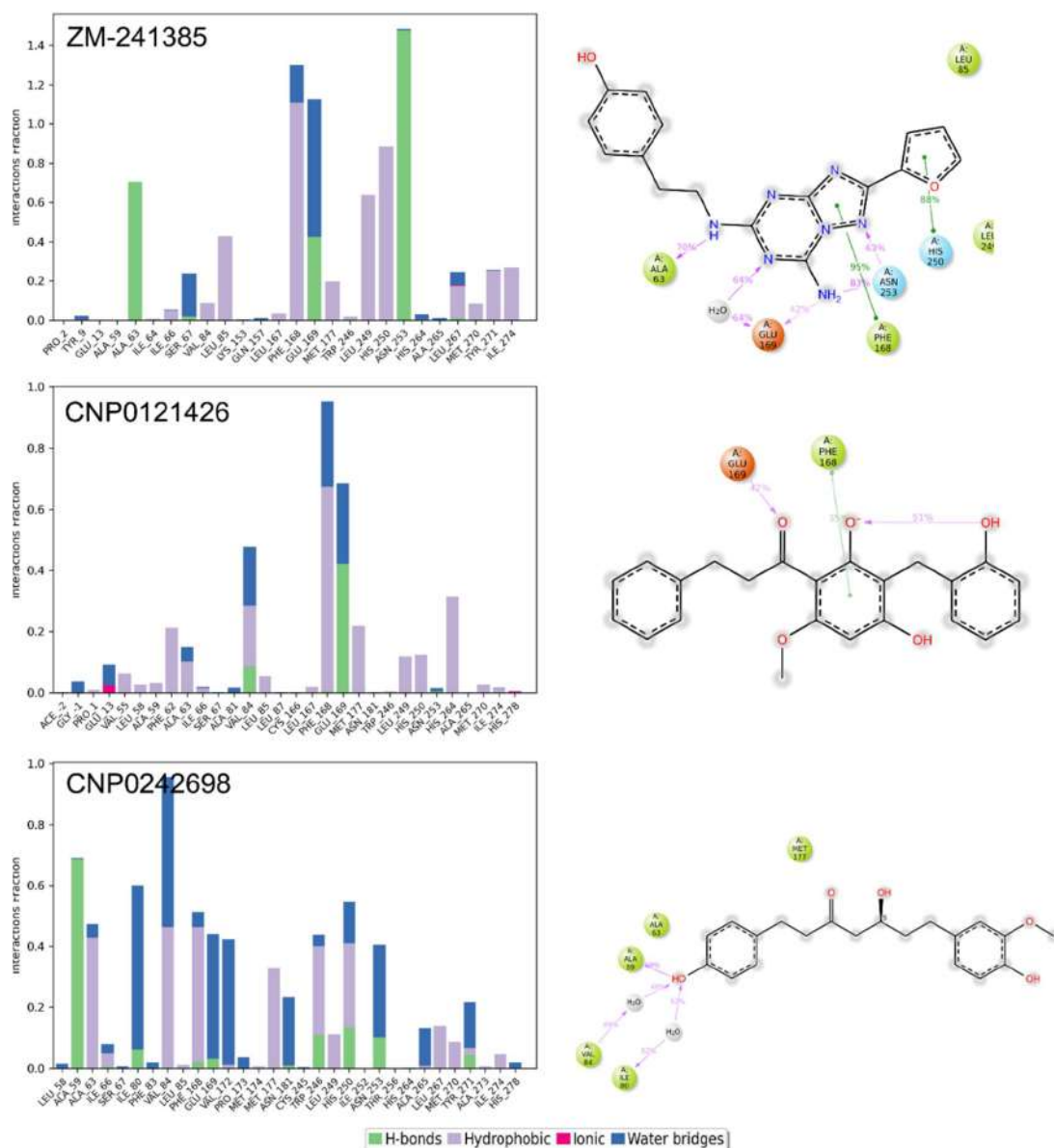
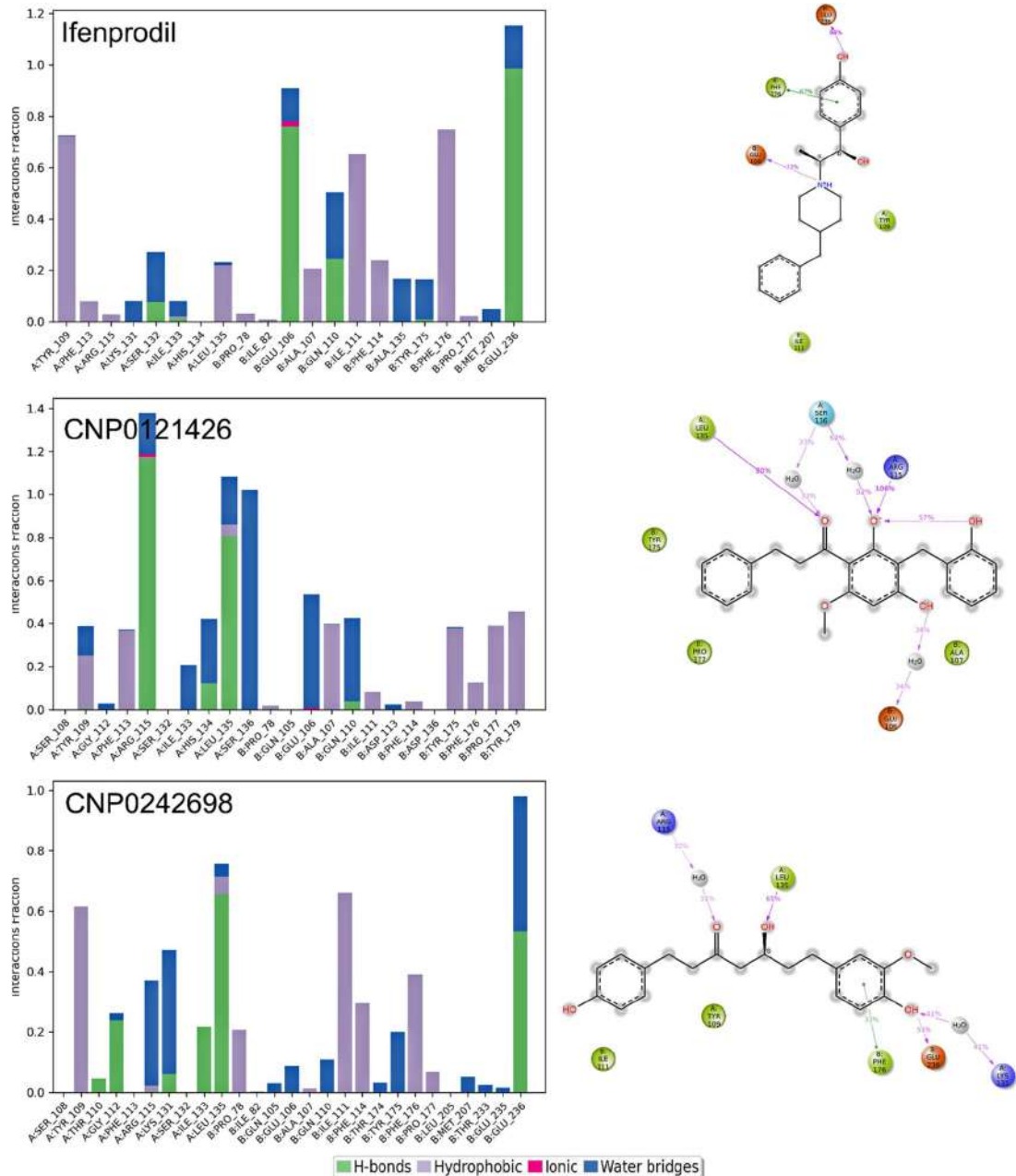


Figure 10. Protein-ligand interaction histograms of ZM-241385, CNP0121426, and CNP0242698 in complex with AA₂AR displaying the fraction of interactions with active amino acids. On the right, schematic representations of the ligands with the percentage of interactions with the protein residues.



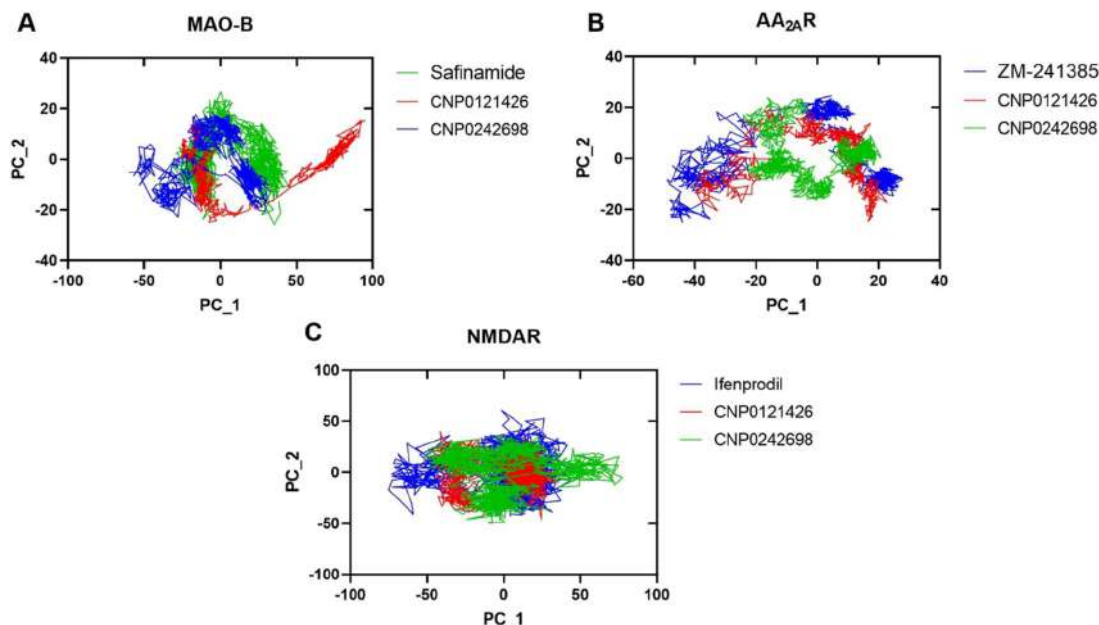


Figure 12. PCA plots for the MD simulations trajectories for MAO-B (A), AA₂AR (B), and NMDAR (C) in complex with the reference ligands, CNP0121426, and CNP0242698.

Table 5. Post-MD simulation binding free energy components of the selected protein-ligand complexes calculated using MM-GBSA approach.

Protein-ligand complexes	MM-GBSA (kcal/mol)					
	ΔG_{Bind}	ΔG_{Coul}	ΔG_{Hbond}	ΔG_{Lipo}	ΔG_{vdW}	
MAO-B	Safinamide	-137.90 ± 6.43	0.97 ± 27.32	-13.50 ± 0.66	-30.65 ± 0.92	-119.10 ± 3.72
	CNP0121426	-139.43 ± 7.23	-2.78 ± 15.27	-11.11 ± 0.43	-31.09 ± 1.41	-111.89 ± 4.01
	CNP0242698	-147.29 ± 4.36	-5.03 ± 21.27	-11.84 ± 0.51	-31.74 ± 0.93	-119.07 ± 2.47
AA ₂ AR	ZM-241385	-61.80 ± 3.61	-12.01 ± 2.26	-0.99 ± 0.23	-18.64 ± 0.84	-49.32 ± 1.84
	CNP0121426	-59.24 ± 3.45	-5.68 ± 2.54	-0.15 ± 0.23	-13.71 ± 1.37	-48.06 ± 3.62
	CNP0242698	-63.92 ± 3.22	-6.24 ± 1.81	-0.02 ± 0.05	-19.14 ± 1.41	-43.62 ± 2.32
NMDAR	Ifenprodil	-36.87 ± 0.34	-24.72 ± 0.23	-3.94 ± 0.12	-4.52 ± 0.28	-32.17 ± 0.41
	CNP0121426	-35.72 ± 0.27	-22.48 ± 0.31	-2.02 ± 0.17	-5.74 ± 0.25	-29.08 ± 0.37
	CNP0242698	-38.98 ± 0.33	-26.19 ± 0.28	-4.79 ± 0.15	-4.39 ± 0.34	-34.65 ± 0.33

ΔG_{Bind} : free energy of binding; ΔG_{Coul} : Coulomb energy; ΔG_{Hbond} : hydrogen bonding energy; ΔG_{Lipo} : hydrophobic energy; ΔG_{vdW} : Van der Waals energy.

exhibiting a non-stable cluster correspond to less stable complexes. In MAO-B, CNP0242698 displayed conformational motions that followed a similar trend to the reference complex. On the other hand, in AA₂AR, CNP0121426 showed the closest resemblance in terms of conformational changes to the reference complex. However, in NMDAR, CNP0121426 exhibited the narrowest range of motions, followed by the reference complex and CNP0242698.

3.5.5. MM-GBSA binding free energy calculation

We conducted MM-GBSA-based binding free energy calculations using the pose viewer file of the docked complexes, and the results are presented in Table 5. The binding free energy values reached values of -147.29, -63.92 and -38.98 kcal/mol for MAO-B, AA₂AR, and NMDAR, respectively. To assess the binding vigor of MAO-B with safinamide, CNP0121426, and CNP0242698, we further decomposed the MM-GBSA binding energies into individual components. It was observed that Van der Waals binding energy played a significant role in the three compounds' interaction with MAO-B, with average binding free energy values of -119.1, -111.9, and -119.1 kcal/mol, respectively. Regarding

AA₂AR, the calculated ΔG_{bind} values for CNP0121426 (-59.24 kcal/mol) and CNP0242698 (-63.92 kcal/mol) were in close proximity, consistent with the earlier molecular docking findings. In the case of NMDAR, CNP0121426 (-35.72 kcal/mol) and CNP0242698 (-38.98 kcal/mol) exhibited similar results to the reference antagonist, ifenprodil. Notably, electrostatic interactions (Coulomb energy) and Van der Waals forces emerged as significant contributors to ligand binding, as indicated by the high ΔG values.

4. Conclusion

Multitargeting strategies are emerging as a promising approach for the management of neurodegenerative diseases. The current study introduces a novel approach integrating data-driven drug discovery and molecular modeling to screen for potential multi-target compounds from the largest available NPs database. QSAR models were developed for three pivotal targets in PD: MAO-B, AA₂AR, and NMDAR. Subsequently, we used the best models for each target to predict the bioactivity of the NPs. The predicted active compounds were then subjected to pharmacophore screening

and molecular docking. Two natural lead candidates, CNP0121426 and CNP0242698, belonging to the dihydrochalcones and curcuminoids chemical classes, respectively, exhibited the highest compound rankings. Further structural analysis revealed favorable interactions within the binding sites of all three targets. The stability of the lead candidates in complex with the selected targets was further assessed through MD simulations. Despite the high RMSD with respect to the protein, curcuminoid demonstrated improved stability in the case of MAO-B. Similarly, the structure of AA_{2A}R complexed with the curcuminoid exhibited higher stability compared to the reference complex. However, the inherent flexibility of the ligand resulted in higher ligand RMSD initially, which eventually stabilized by the end of the simulation, suggesting that it requires more time to accommodate an optimal orientation within the binding pocket. In NMDAR, although more protein deviations were observed, curcuminoid, CNP0242698 exhibited good stability compared to the dihydrochalcone ligand. Overall, the curcuminoid complexed with the studied structures displayed superior stability compared to the dihydrochalcone, indicating its potential as a multitarget agent in combating PD. Results obtained from the current study may generate an increased shift of interest toward developing novel antiparkinsonian drugs with neuroprotective activities from NPs. However, additional experimental studies are needed to further validate these findings.

We would like to thank Prof. Francisco Javier Luque Garriga, University of Barcelona, Spain, for his constructive criticism and Dr. Pankaj Mishra, Neovarsity, Germany for his invaluable knowledge in machine learning and artificial intelligence. Their contribution is sincerely appreciated and gratefully acknowledged. The authors also acknowledge ProteinsInsights, Nangal Raya, New Delhi, India, for providing computational resources essential for the successful completion of this research work. The authors received no financial support for the research, authorship, and/or publication of this article.

Acknowledgment

The authors gratefully acknowledge ProteinsInsights, Nangal Raya, New Delhi, India, for providing the computational resources essential for the successful completion of this research.

Disclosure statement

No potential conflict of interest was reported by the author(s).

References

- AlAjmi, M. F., Rehman, M. T., Hussain, A., & Rather, G. M. (2018). Pharmacoinformatics approach for the identification of Polo-like kinase-1 inhibitors from natural sources as anti-cancer agents. *International Journal of Biological Macromolecules*, 116, 173–181. <https://doi.org/10.1016/ijbiomac.2018.05.023>
- Arai, Y., Nakazato, K., Kinemuchi, H., Tadano, T., Satoh, N., Oyama, K., & Kisara, K. (1991). Inhibition of rat brain monoamine oxidase activity by cerebral anti-ischemic agent, ifenprodil. *Neuropharmacology*, 30(7), 809–812. [https://doi.org/10.1016/0028-3908\(91\)90190-m](https://doi.org/10.1016/0028-3908(91)90190-m)
- Barnham, K. J., Masters, C. L., & Bush, A. I. (2004). Neurodegenerative diseases and oxidative stress. *Nature Reviews. Drug Discovery*, 3(3), 205–214. <https://doi.org/10.1038/nrd1330>
- Benson, N. C., & Daggett, V. (2012). A comparison of multiscale methods for the analysis of molecular dynamics simulations. *The Journal of Physical Chemistry-B*, 116(29), 8722–8731. <https://doi.org/10.1021/jp302103t>
- Bhandari, S., Agrwal, A., Kasana, V., Tandon, S., Boulaamane, Y., & Maurady, A. (2022). β-amino carbonyl derivatives: Synthesis, molecular docking, ADMET, molecular dynamic and herbicidal studies. *ChemistrySelect*, 7(48), e202201572. <https://doi.org/10.1002/slct.202201572>
- Bharadwaj, K. K., Sarkar, T., Ghosh, A., Baishya, D., Rabha, B., Panda, M. K., Nelson, B. R., John, A. B., Sheikh, H. I., Dash, B. P., Edinur, H. A., & Pati, S. (2021). Macrolactin A as a novel inhibitory agent for SARS-CoV-2 M pro: Bioinformatics approach. *Applied Biochemistry and Biotechnology*, 193(10), 3371–3394. <https://doi.org/10.1007/s12010-021-03608-7>
- Binda, C., Mattevi, A., & Edmondson, D. E. (2011). Structural properties of human monoamine oxidases A and B. *International Review of Neurobiology*, 100, 1–11.
- Binda, C., Wang, J., Pisani, L., Caccia, C., Carotti, A., Salvati, P., Edmondson, D. E., & Mattevi, A. (2007). Structures of human monoamine oxidase B complexes with selective noncovalent inhibitors: Safinamide and coumarin analogs. *Journal of Medicinal Chemistry*, 50(23), 5848–5852. <https://doi.org/10.1021/jm070677y>
- Boulaamane, Y., Ahmad, I., Patel, H., Das, N., Britel, M. R., & Maurady, A. (2023). Structural exploration of selected C6 and C7-substituted coumarin isomers as selective MAO-B inhibitors. *Journal of Biomolecular Structure & Dynamics*, 41(6), 2326–2340. <https://doi.org/10.1080/07391102.2022.2033643>
- Boulaamane, Y., Ibrahim, M. A., Britel, M. R., & Maurady, A. (2022). *In silico* studies of natural product-like caffeine derivatives as potential MAO-B inhibitors/AA2AR antagonists for the treatment of Parkinson's disease. *Journal of Integrative Bioinformatics*, 19(4), 20210027. <https://doi.org/10.1515/jib-2021-0027>
- Boulaamane, Y., Kandpal, P., Chandra, A., Britel, M. R., & Maurady, A. (2023). Chemical library design, QSAR modeling and molecular dynamics simulations of naturally occurring coumarins as dual inhibitors of MAO-B and AChE. *Journal of Biomolecular Structure & Dynamics*, 1–18. <https://doi.org/10.1080/07391102.2023.2209650>
- Bowers, K. J., Chow, E., Xu, H., Dror, R. O., Eastwood, M. P., Gregersen, B. A., ... Shaw, D. E. (2006). Scalable algorithms for molecular dynamics simulations on commodity clusters. In Proceedings of the 2006 ACM/IEEE Conference on Supercomputing, November. (pp. 84–es). <https://doi.org/10.1145/1188455.1188544>
- Burggraaff, L., van Vlijmen, H. W. T., IJzerman, A. P., & van Westen, G. J. P. (2020). Quantitative prediction of selectivity between the A1 and A2A adenosine receptors. *Journal of Cheminformatics*, 12(1), 33. <https://doi.org/10.1186/s13321-020-00438-3>
- Carradori, S., D'Ascenzo, M., Chimienti, P., Secci, D., & Bolasco, A. (2014). Selective MAO-B inhibitors: A lesson from natural products. *Molecular Diversity*, 18(1), 219–243. <https://doi.org/10.1007/s11030-013-9490-6>
- Carradori, S., & Silvestri, R. (2015). New frontiers in selective human MAO-B inhibitors: Miniperspective. *Journal of Medicinal Chemistry*, 58(17), 6717–6732. <https://doi.org/10.1021/jm501690r>
- Craft, R. C., & Leake, C. (2002). The Pareto principle in organizational decision making. *Management Decision*, 40(8), 729–733. <https://doi.org/10.1108/00251740210437699>
- Dauer, W., & Przedborski, S. (2003). Parkinson's disease: Mechanisms and models. *Neuron*, 39(6), 889–909. [https://doi.org/10.1016/s0896-6273\(03\)00568-3](https://doi.org/10.1016/s0896-6273(03)00568-3)
- David, C. C., & Jacobs, D. J. (2014). Principal component analysis: A method for determining the essential dynamics of proteins. *Method in Molecular Biology*, 1084, 193–226.
- de Lera Ruiz, M., Lim, Y. H., & Zheng, J. (2014). Adenosine A2A receptor as a drug discovery target. *Journal of Medicinal Chemistry*, 57(9), 3623–3650. <https://doi.org/10.1021/jm4011669>
- Ding, Y., Chen, M., Guo, C., Zhang, P., & Wang, J. (2021). Molecular fingerprint-based machine learning assisted QSAR model development for prediction of ionic liquid properties. *Journal of Molecular Liquids*, 326, 115212. <https://doi.org/10.1016/j.molliq.2020.115212>

- Dixon, S. L., Smondyrev, A. M., & Rao, S. N. (2006). PHASE: A novel approach to pharmacophore modeling and 3D database searching. *Chemical Biology & Drug Design*, 67(5), 370–372. <https://doi.org/10.1111/j.1747-0285.2006.00384.x>
- Erdogan Orhan, I. (2016). Potential of natural products of herbal origin as monoamine oxidase inhibitors. *Current Pharmaceutical Design*, 22(3), 268–276. <https://doi.org/10.2174/138161282266151112150612>
- Finberg, J. P., & Rabey, J. M. (2016). Inhibitors of MAO-A and MAO-B in psychiatry and neurology. *Frontiers in Pharmacology*, 7, 340. <https://doi.org/10.3389/fphar.2016.00340>
- Fjelldal, M. F., Freyd, T., Evenseth, L. M., Sylte, I., Ring, A., & Paulsen, R. E. (2019). Exploring the overlapping binding sites of ifenprodil and EVT-101 in GluN2B-containing NMDA receptors using novel chicken embryo forebrain cultures and molecular modeling. *Pharmacology Research & Perspectives*, 7(3), e00480. <https://doi.org/10.1002/prp2.480>
- Friesner, R. A., Murphy, R. B., Repasky, M. P., Frye, L. L., Greenwood, J. R., Halgren, T. A., Sanschagrin, P. C., & Mainz, D. T. (2006). Extra precision glide: Docking and scoring incorporating a model of hydrophobic enclosure for protein–ligand complexes. *Journal of Medicinal Chemistry*, 49(21), 6177–6196. <https://doi.org/10.1021/jm051256o>
- Gaulton, A., Bellis, L. J., Bento, A. P., Chambers, J., Davies, M., Hersey, A., Light, Y., McGlinchey, S., Michalovich, D., Al-Lazikani, B., & Overington, J. P. (2012). ChEMBL: A large-scale bioactivity database for drug discovery. *Nucleic Acids Research*, 40(Database issue), D1100–D1107. <https://doi.org/10.1093/nar/gkr777>
- Gonda, X. (2012). Basic pharmacology of NMDA receptors. *Current Pharmaceutical Design*, 18(12), 1558–1567. <https://doi.org/10.2174/138161212799958521>
- Gulli, A., & Pal, S. (2017). *Deep learning with Keras*. Packt Publishing Ltd.
- Hanley, J. A., & McNeil, B. J. (1982). The meaning and use of the area under a receiver operating characteristic (ROC) curve. *Radiology*, 143(1), 29–36. <https://doi.org/10.1148/radiology.143.1.7063747>
- Hardingham, G. E. (2009). Coupling of the NMDA receptor to neuroprotective and neurodestructive events. *Biochemical Society Transactions*, 37(Pt 6), 1147–1160. <https://doi.org/10.1042/BST0371147>
- He, X., Walker, B., Man, V. H., Ren, P., & Wang, J. (2022). Recent progress in general force fields of small molecules. *Current Opinion in Structural Biology*, 72, 187–193. <https://doi.org/10.1016/j.sbi.2021.11.011>
- Herrera-Acevedo, C., Perdomo-Madrigal, C., Herrera-Acevedo, K., Coy-Barrera, E., Scotti, L., & Scotti, M. T. (2021). Machine learning models to select potential inhibitors of acetylcholinesterase activity from SistemX: A natural products database. *Molecular Diversity*, 25(3), 1553–1568. <https://doi.org/10.1007/s11030-021-10245-z>
- Ibrahim, M. M., & Gabr, M. T. (2019). Multitarget therapeutic strategies for Alzheimer's disease. *Neural Regeneration Research*, 14(3), 437–440. <https://doi.org/10.4103/1673-5374.245463>
- Ikeda, K., Kurokawa, M., Aoyama, S., & Kuwana, Y. (2002). Neuroprotection by adenosine A2A receptor blockade in experimental models of Parkinson's disease. *Journal of Neurochemistry*, 80(2), 262–270. <https://doi.org/10.1046/j.0022-3042.2001.00694.x>
- Ioakimidis, L., Thoukydidis, L., Mirza, A., Naeem, S., & Reynisson, J. (2008). Benchmarking the reliability of QikProp. Correlation between experimental and predicted values. *QSAR & Combinatorial Science*, 27(4), 445–456. <https://doi.org/10.1002/qsar.200730051>
- Iovino, L., Tremblay, M. E., & Civiero, L. (2020). Glutamate-induced excitotoxicity in Parkinson's disease: The role of glial cells. *Journal of Pharmacological Sciences*, 144(3), 151–164. <https://doi.org/10.1016/j.jphs.2020.07.011>
- Jaakkola, V. P., Lane, J. R., Lin, J. Y., Katritch, V., IJzerman, A. P., & Stevens, R. C. (2010). Ligand binding and subtype selectivity of the human A2A adenosine receptor: Identification and characterization of essential amino acid residues. *The Journal of Biological Chemistry*, 285(17), 13032–13044. <https://doi.org/10.1074/jbc.M109.096974>
- Jacobson, M. P., Friesner, R. A., Xiang, Z., & Honig, B. (2002). On the role of the crystal environment in determining protein side-chain conformations. *Journal of Molecular Biology*, 320(3), 597–608. [https://doi.org/10.1016/s0022-2836\(02\)00470-9](https://doi.org/10.1016/s0022-2836(02)00470-9)
- Jacobson, M. P., Pincus, D. L., Rapp, C. S., Day, T. J., Honig, B., Shaw, D. E., & Friesner, R. A. (2004). A hierarchical approach to all-atom protein loop prediction. *Proteins*, 55(2), 351–367. <https://doi.org/10.1002/prot.10613>
- Jaiteh, M., Zeifman, A., Saarinen, M., Svenssonsson, P., Bréa, J., Loza, M. I., & Carlsson, J. (2018). Docking screens for dual inhibitors of disparate drug targets for Parkinson's disease. *Journal of Medicinal Chemistry*, 61(12), 5269–5278. <https://doi.org/10.1021/acs.jmedchem.8b00204>
- Jenner, P. (2003). Oxidative stress in Parkinson's disease. *Annals of Neurology*, 53(Suppl S3), S26–S38. <https://doi.org/10.1002/ana.10483>
- Ke, Q., Gong, X., Liao, S., Duan, C., & Li, L. (2022). Effects of thermostats/barostats on physical properties of liquids by molecular dynamics simulations. *Journal of Molecular Liquids*, 365, 120116. <https://doi.org/10.1016/j.molliq.2022.120116>
- Kim, S., Chen, J., Cheng, T., Gindulyte, A., He, J., He, S., Li, Q., Shoemaker, B. A., Thiessen, P. A., Yu, B., Zaslavsky, L., Zhang, J., & Bolton, E. E. (2021). PubChem in 2021: New data content and improved web interfaces. *Nucleic Acids Research*, 49(D1), D1388–D1395. <https://doi.org/10.1093/nar/gkaa971>
- Kingston, D. G. (2011). Modern natural products drug discovery and its relevance to biodiversity conservation. *Journal of Natural Products*, 74(3), 496–511. <https://doi.org/10.1021/np100550t>
- Kumar, G., & Patnaik, R. (2016). Exploring neuroprotective potential of *Withania somnifera* phytochemicals by inhibition of GluN2B-containing NMDA receptors: An *in silico* study. *Medical Hypotheses*, 92, 35–43. <https://doi.org/10.1016/j.mehy.2016.04.034>
- Kurczab, R., Ali, W., Łażewska, D., Kotańska, M., Jastrzębska-Więsek, M., Satała, G., Więcek, M., Lubelska, A., Latacz, G., Partyka, A., Starek, M., Dąbrowska, M., Wesołowska, A., Jacob, C., Kieć-Kononowicz, K., & Handzlik, J. (2018). Computer-aided studies for novel arylhydantoin 1, 3, 5-triazine derivatives as 5-HT₆ serotonin receptor ligands with antidepressive-like, anxiolytic and antioesity action *in vivo*. *Molecules*, 23(10), 2529. <https://doi.org/10.3390/molecules23102529>
- Landrum, G. (2013). RDKit: A software suite for cheminformatics, computational chemistry, and predictive modeling. *Greg Landrum*, 8, 31.
- Lang, A. E. (2010). Clinical trials of disease-modifying therapies for neurodegenerative diseases: The challenges and the future. *Nature Medicine*, 16(11), 1223–1226. <https://doi.org/10.1038/nm.2220>
- Lin, J., Sahakian, D. C., De Morais, S. M., Xu, J. J., Polzer, R. J., & Winter, S. M. (2003). The role of absorption, distribution, metabolism, excretion and toxicity in drug discovery. *Current Topics in Medicinal Chemistry*, 3(10), 1125–1154. <https://doi.org/10.2174/1568026033452096>
- Lipinski, C. A. (2004). Lead-and drug-like compounds: The rule-of-five revolution. *Drug Discovery Today. Technologies*, 1(4), 337–341. <https://doi.org/10.1016/j.ddtec.2004.11.007>
- Lotharius, J., & Brundin, P. (2002). Pathogenesis of Parkinson's disease: Dopamine, vesicles and α -synuclein. *Nature Reviews. Neuroscience*, 3(12), 932–942. <https://doi.org/10.1038/nrn983>
- Maestro, S. (2020). Maestro. Schrödinger, LLC, New York, NY, 2020.
- Milczek, E. M., Binda, C., Rovida, S., Mattevi, A., & Edmondson, D. E. (2011). The 'gating' residues Ile199 and Tyr326 in human monoamine oxidase B function in substrate and inhibitor recognition. *The FEBS Journal*, 278(24), 4860–4869. <https://doi.org/10.1111/j.1742-4658.2011.08386.x>
- Mironova, Y. S., Zhukova, I. A., Zhukova, N. G., Alifirova, V. M., Izhboldina, O. P., & Latypova, A. V. (2018). Parkinson's disease and glutamate excitotoxicity. *Zhurnal nevrologii i psichiatrii imeni S.S. Korsakova*, 118(6. Vyp. 2), 50–54. <https://doi.org/10.17116/jnevro201811806250>
- Ng, H. W., Laughton, C. A., & Doughty, S. W. (2013). Molecular dynamics simulations of the adenosine A2a receptor: Structural stability, sampling, and convergence. *Journal of Chemical Information and Modeling*, 53(5), 1168–1178. <https://doi.org/10.1021/ci300610w>
- Olsson, M. H., Søndergaard, C. R., Rostkowski, M., & Jensen, J. H. (2011). PROPKA3: Consistent treatment of internal and surface residues in empirical pKa predictions. *Journal of Chemical Theory and Computation*, 7(2), 525–537. <https://doi.org/10.1021/ct100578z>
- Pedregosa, F., Varoquaux, G., Gramfort, A., Michel, V., Thirion, B., Grisel, O., & Duchesnay, E. (2011). Scikit-learn: Machine learning in Python. *The Journal of Machine Learning Research*, 12, 2825–2830.
- Piau, A., Nourhashemi, F., Hein, C., Caillaud, C., & Vellas, B. (2011). Progress in the development of new drugs in Alzheimer's disease. *The*

- Journal of Nutrition, Health & Aging*, 15(1), 45–57. <https://doi.org/10.1007/s12603-011-0012-x>
- Pollastri, M. P. (2010). Overview on the rule of five. *Current Protocols in Pharmacology*, 9(1), Unit 9.12. <https://doi.org/10.1002/0471141755.ph0912s49>
- Rascol, O., Payoux, P., Ory, F., Ferreira, J. J., Brefel-Courbon, C., & Montastruc, J. L. (2003). Limitations of current Parkinson's disease therapy. *Annals of Neurology*, 53(Suppl. 3), S3–S15. <https://doi.org/10.1002/ana.10513>
- Roos, K., Wu, C., Damm, W., Reboul, M., Stevenson, J. M., Lu, C., Dahlgren, M. K., Mondal, S., Chen, W., Wang, L., Abel, R., Friesner, R. A., & Harder, E. D. (2019). OPLS3e: Extending force field coverage for drug-like small molecules. *Journal of Chemical Theory and Computation*, 15(3), 1863–1874. <https://doi.org/10.1021/acs.jctc.8b01026>
- Sander, T., Freyss, J., von Korff, M., & Rufener, C. (2015). DataWarrior: An open-source program for chemistry aware data visualization and analysis. *Journal of Chemical Information and Modeling*, 55(2), 460–473. <https://doi.org/10.1021/ci500588j>
- Segala, E., Guo, D., Cheng, R. K. Y., Bortolato, A., Deflorian, F., Doré, A. S., Errey, J. C., Heitman, L. H., IJzerman, A. P., Marshall, F. H., & Cooke, R. M. (2016). Controlling the dissociation of ligands from the adenosine A2A receptor through modulation of salt bridge strength. *Journal of Medicinal Chemistry*, 59(13), 6470–6479. <https://doi.org/10.1021/acs.jmedchem.6b00653>
- Shen, B. (2015). A new golden age of natural products drug discovery. *Cell*, 163(6), 1297–1300. <https://doi.org/10.1016/j.cell.2015.11.031>
- Singh, P., Manure, A., Singh, P., & Manure, A. (2020). Introduction to tensorflow 2.0. Learn Tensor Flow 2.0: Implement Machine Learning and Deep Learning Models with Python, 1-24.
- Sorokina, M., Merseburger, P., Rajan, K., Yirik, M. A., & Steinbeck, C. (2021). COCONUT online: Collection of open natural products database. *Journal of Cheminformatics*, 13(1), 2. <https://doi.org/10.1186/s13321-020-00478-9>
- Stocchi, F., Antonini, A., Berg, D., Bergmans, B., Jost, W., Katzenschlager, R., Kulisevsky, J., Odin, P., Valdeoriola, F., & Ray Chaudhuri, K. (2022). Safinamide in the treatment pathway of Parkinson's disease: A European Delphi consensus. *NPJ Parkinson's Disease*, 8(1), 17. <https://doi.org/10.1038/s41531-022-00277-z>
- Stoop, J. C., Booij, J., & Drukarch, B. (1992). Amantadine as N-methyl-D-aspartic acid receptor antagonist: New possibilities for therapeutic applications? *Clinical Neurology and Neurosurgery*, 94, S4–S6. [https://doi.org/10.1016/0303-8467\(92\)90006-o](https://doi.org/10.1016/0303-8467(92)90006-o)
- Stroebel, D., Buhl, D. L., Knafels, J. D., Chanda, P. K., Green, M., Sciabola, S., Mony, L., Paoletti, P., & Pandit, J. (2016). A novel binding mode reveals two distinct classes of NMDA receptor GluN2B-selective antagonists. *Molecular Pharmacology*, 89(5), 541–551. <https://doi.org/10.1124/mol.115.103036>
- Tabakman, R., Lecht, S., & Lazarovici, P. (2004). Neuroprotection by monoamine oxidase B inhibitors: A therapeutic strategy for Parkinson's disease? *BioEssays*, 26(1), 80–90. <https://doi.org/10.1002/bies.10378>
- Tarasova, O. A., Urusova, A. F., Filimonov, D. A., Nicklaus, M. C., Zakharov, A. V., & Poroikov, V. V. (2015). QSAR modeling using large-scale databases: Case study for HIV-1 reverse transcriptase inhibitors. *Journal of Chemical Information and Modeling*, 55(7), 1388–1399. <https://doi.org/10.1021/acs.jcim.5b00019>
- The UniProt Consortium. (2021). UniProt: The universal protein knowledgebase in 2021. *Nucleic Acids Research*, 49(D1), D480–D489. <https://doi.org/10.1093/nar/gkaa1100>
- Touati, I., Abdalla, M., Ali, N. H., AlRuwaili, R., Alruwaili, M., Britel, M. R., & Mraudy, A. (2023). Constituents of Stachys plants as potential dual inhibitors of AChE and NMDAR for the treatment of Alzheimer's disease: A molecular docking and dynamic simulation study. *Journal of Biomolecular Structure & Dynamics*, 1–17. <https://doi.org/10.1080/07391102.2023.2217925>
- Van der Maaten, L., & Hinton, G. (2008). Visualizing data using t-SNE. *Journal of Machine Learning Research*, 9(11), 2579–2605.
- Van der Schyf, C. J. (2011). The use of multi-target drugs in the treatment of neurodegenerative diseases. *Expert Review of Clinical Pharmacology*, 4(3), 293–298. <https://doi.org/10.1586/ecp.11.13>
- Wang, C. C., Billett, E., Borchert, A., Kuhn, H., & Ufer, C. (2013). Monoamine oxidases in development. *Cellular and Molecular Life Sciences*, 70(4), 599–630. <https://doi.org/10.1007/s00018-012-1065-7>
- Wang, M., Hou, S., Wei, Y., Li, D., & Lin, J. (2021). Discovery of novel dual adenosine A1/A2A receptor antagonists using deep learning, pharmacophore modeling and molecular docking. *PLOS Computational Biology*, 17(3), e1008821. <https://doi.org/10.1371/journal.pcbi.1008821>
- Welihinda, A. A., Kaur, M., Greene, K., Zhai, Y., & Amento, E. P. (2016). The adenosine metabolite inosine is a functional agonist of the adenosine A2A receptor with a unique signaling bias. *Cellular Signalling*, 28(6), 552–560. <https://doi.org/10.1016/j.cellsig.2016.02.010>
- Williams, K. (2001). Ifenprodil, a novel NMDA receptor antagonist: Site and mechanism of action. *Current Drug Targets*, 2(3), 285–298. <https://doi.org/10.2174/1389450013348489>
- Wu, Z., Zhu, M., Kang, Y., Leung, E. L.-H., Lei, T., Shen, C., Jiang, D., Wang, Z., Cao, D., & Hou, T. (2021). Do we need different machine learning algorithms for QSAR modeling? A comprehensive assessment of 16 machine learning algorithms on 14 QSAR data sets. *Briefings in Bioinformatics*, 22(4), bbaa321. <https://doi.org/10.1093/bib/bbaa321>
- Yamada, M., & Yasuhara, H. (2004). Clinical pharmacology of MAO inhibitors: safety and future. *Neurotoxicology*, 25(1-2), 215–221.
- Yang, S., Li, S., & Chang, J. (2022). Discovery of Cobimetinib as a novel A-FABP inhibitor using machine learning and molecular docking-based virtual screening. *RSC Advances*, 12(21), 13500–13510. <https://doi.org/10.1039/d2ra01057g>
- Youdim, M. B., Edmondson, D., & Tipton, K. F. (2006). The therapeutic potential of monoamine oxidase inhibitors. *Nature Reviews Neuroscience*, 7(4), 295–309. <https://doi.org/10.1038/nrn1883>
- Zhang, Z., Zhang, S., Fu, P., Zhang, Z., Lin, K., Ko, J. K. S., & Yung, K. K. L. (2019). Roles of glutamate receptors in Parkinson's disease. *International Journal of Molecular Sciences*, 20(18), 4391. <https://doi.org/10.3390/ijms20184391>

**CHAPTER V: PROBING THE
MOLECULAR MECHANISMS OF
A-SYNUCLEIN INHIBITORS UNVEILS
PROMISING NATURAL CANDIDATES
THROUGH MACHINE-LEARNING
QSAR, PHARMACOPHORE
MODELING, AND MOLECULAR
DYNAMICS SIMULATIONS**

The abnormal deposition of α -synuclein fibrils is a neuropathological hallmark to PD. To elucidate the structural requirements for modulating α -synuclein fibril aggregation, we analyzed a dataset of α -synuclein inhibitors from the ChEMBL database. We employed QSAR models to screen the LOTUS NPs database, then designed a pharmacophore from a clinical candidate, Anle138b. The pharmacophore-based screening identified five potential α -synuclein inhibitors. Molecular docking studies revealed binding affinities of -6.0 kcal/mol or lower. ADMET analysis indicated satisfactory properties and BBB penetration. Notably, LTS0078917 displayed superior stability in MD simulations compared to Anle138b. LTS0078917 showed promise in stabilizing the α -synuclein monomer by binding it to its hairpin-like coil in the N-terminal region, potentially inhibiting the formation and aggregation of pathological oligomers. These findings provide valuable insights for developing novel α -synuclein inhibitors from natural sources.

The details of this work are reported in the following publication.

Boulaamane, Y., Jangid, K., Britel, M. R., & Maurady, A. (2023). Probing the molecular mechanisms of α -synuclein inhibitors unveils promising natural candidates through machine-learning QSAR, pharmacophore modelling, and molecular dynamics simulations. Molecular Diversity, 1-17. (Reprinted with permission)

Available at: <https://doi.org/10.1007/s11030-023-10691-x>

Conceptualization: Y.B. A.M.; Methodology: Y.B., A.M.; Investigation: Y.B., A.M.; Visualization: Y.B., I.A., H.P.; Supervision: M.R.B., A.M.; Writing—original draft: Y.B.; Writing—review & editing: Y.B., A.M.



Probing the molecular mechanisms of α -synuclein inhibitors unveils promising natural candidates through machine-learning QSAR, pharmacophore modeling, and molecular dynamics simulations

Yassir Boulaamane¹ · Kailash Jangid² · Mohammed Reda Britel¹ · Amal Maurady^{1,3}

Received: 7 March 2023 / Accepted: 3 July 2023
© The Author(s), under exclusive licence to Springer Nature Switzerland AG 2023

Abstract

Parkinson's disease is characterized by a multifactorial nature that is linked to different pathways. Among them, the abnormal deposition and accumulation of α -synuclein fibrils is considered a neuropathological hallmark of Parkinson's disease. Several synthetic and natural compounds have been tested for their potency to inhibit the aggregation of α -synuclein. However, the molecular mechanisms responsible for the potency of these drugs to further rationalize their development and optimization are yet to be determined. To enhance our understanding of the structural requirements necessary for modulating the aggregation of α -synuclein fibrils, we retrieved a large dataset of α -synuclein inhibitors with their reported potency from the ChEMBL database to explore their chemical space and to generate QSAR models for predicting new bioactive compounds. The best performing QSAR model was applied to the LOTUS natural products database to screen for potential α -synuclein inhibitors followed by a pharmacophore design using the representative compounds sampled from each cluster in the ChEMBL dataset. Five natural products were retained after molecular docking studies displaying a binding affinity of -6.0 kcal/mol or lower. ADMET analysis revealed satisfactory properties and predicted that all the compounds can cross the blood–brain barrier and reach their target. Finally, molecular dynamics simulations demonstrated the superior stability of LTS0078917 compared to the clinical candidate, Anle138b. We found that LTS0078917 shows promise in stabilizing the α -synuclein monomer by specifically binding to its hairpin-like coil within the N-terminal region. Our dynamic analysis of the inhibitor–monomer complex revealed a tendency towards a more compact conformation, potentially reducing the likelihood of adopting an elongated structure that favors the formation and aggregation of pathological oligomers. These findings offer valuable insights for the development of novel α -synuclein inhibitors derived from natural sources.

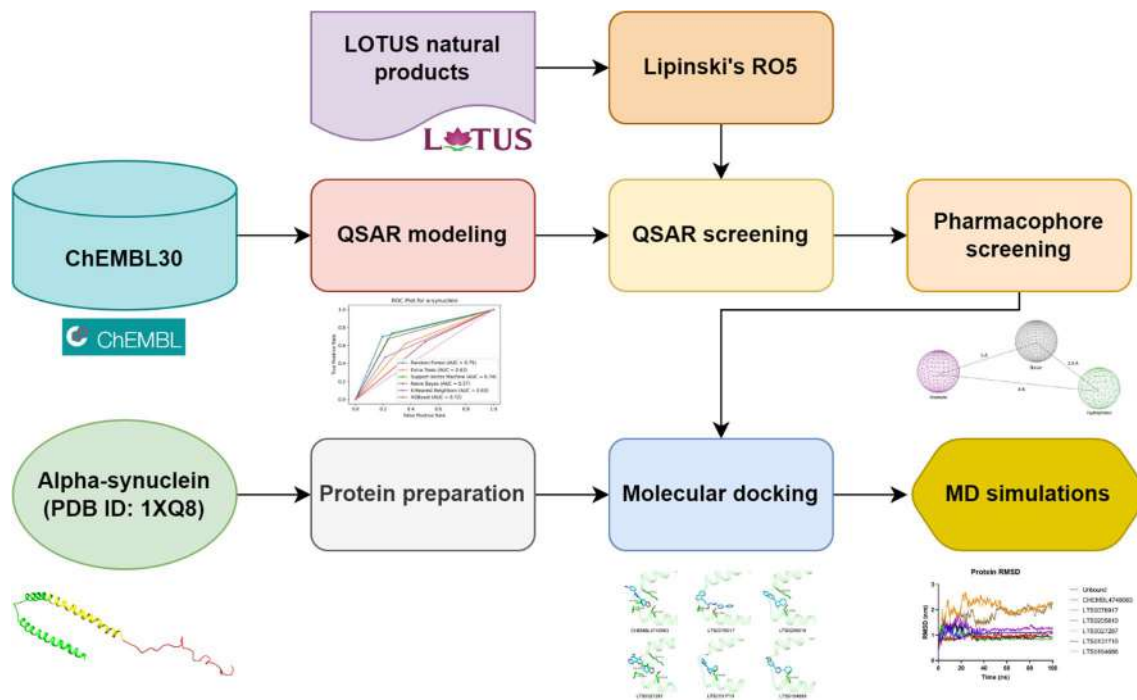
✉ Amal Maurady
amal.maurady.ma@gmail.com

¹ Laboratory of Innovative Technologies, National School of Applied Sciences of Tangier, Abdelmalek Essaadi University, Tetouan, Morocco

² Department of Pharmaceutical Sciences and Natural Products, Central University of Punjab, Ghudda, Bathinda, India

³ Faculty of Sciences and Techniques of Tangier, Abdelmalek Essaadi University, Tetouan, Morocco

Graphical abstract



Keywords α -Synuclein · ADMET prediction · Machine learning · Molecular docking · Molecular dynamics simulations · Natural products · QSAR · Parkinson's disease

Introduction

Neurodegenerative disorders, including Alzheimer's and Parkinson's disease (PD), are among the most common neurological conditions globally [1]. These disorders are characterized by the gradual loss of brain cells due to a variety of factors, including the accumulation of amyloid fibrils, oxidative stress, mitochondrial dysfunction, and metal accumulation [2]. PD is the second most common neurological disorder in the world, characterized by the loss of dopaminergic neurons in the midbrain and resulting in dopamine deficiency in the striatum [3]. It is estimated to affect 6 million people globally, with a projected increase in prevalence of two- to threefold by 2030 [4, 5]. Common motor symptoms of PD include dyskinesia, tremors, and difficulty with movement [6]. Non-motor symptoms, such as depression, insomnia, and constipation, may also occur [7]. Evidence suggests that oxidative damage and mitochondrial imbalance contribute to the degeneration of dopaminergic neurons in PD [8], leading to a need for novel "disease-modifying" therapies [9]. Current treatments for PD include L-DOPA therapy, which is considered the gold standard for controlling motor symptoms, and dopaminergic treatments such as dopamine agonists, monoamine oxidase-B (MAO-B)

inhibitors, and catechol-*O*-methyltransferase (COMT) inhibitors [10, 11]. More recently, non-dopaminergic treatments, including adenosine A_{2A} and *N*-methyl-*D*-aspartate (NMDA) receptor antagonists, have been shown to be effective in relieving PD symptoms and slowing neuronal damage [12, 13]. Many other potential "disease-modifying" therapies are under development for PD, including agents that modulate α -synuclein, neurotrophic factors, inflammation modulators, neuroprotective agents, and multi-target drugs [14–16]. α -synuclein is a protein that is expressed in neurons of the central and peripheral nervous systems [17]. It is a member of the synuclein family of proteins, which are characterized by the presence of a central non-amyloid β component (NAC) domain and an amino-terminal domain that is rich in hydrophobic amino acids [18]. α -synuclein is thought to play a role in the regulation of neurotransmitter release and in the formation and maintenance of presynaptic terminals [19]. In PD, abnormal accumulation and aggregation of α -synuclein in the brain is believed to contribute to the degeneration of dopaminergic neurons and the development of PD symptoms [20]. The aggregation of α -synuclein can also lead to the formation of intracellular inclusions called Lewy bodies, which are a hallmark of PD pathology [21]. The precise mechanisms by which α -synuclein contributes

to the development of PD are not fully understood, but there is evidence suggesting that α -synuclein can affect the function of mitochondria, the integrity of the cytoskeleton, and the ability of cells to respond to stress [22]. A growing body of experimental evidence highlighted the potency of small molecules to inhibit the aggregation of α -synuclein fibrils. Among them, Anle138b and NPT200-11 are currently evaluated in clinical trials for their efficacy and safety. They are thought to reduce α -synuclein aggregation and misfolding, however, the molecular mechanisms behind their activity are yet to be elucidated [23, 24].

The 3D structure of α -synuclein has been resolved through solution NMR (PDB ID: 1XQ8) [25]. The snapshot represents a micelle-bound α -synuclein monomer at atomic resolution as shown in Fig. 1. The monomer is formed by 140 amino acids and has a molecular weight of approximately 14 kDa consisting of a membrane binding N-terminal region, a NAC region and an acidic C-terminal tail [26].

Previous experimental evidence revealed the molecular mechanisms of flavonoids and their anti-aggregation effects on α -synuclein, it was suggested that the binding site for small molecules is in the interhelical loop between the hairpin-like α -helices formed by the residues 30–48 [27, 28]. Several natural mutations that modify the membrane-binding affinity have been identified in this region, such as A30P and E46K, both of which are linked to distinct disease pathology [28]. Furthermore, a recent study examined the favorable binding site between α -synuclein and Quercetin, a flavonoid found in many fruits, vegetables, leaves, seeds, and grains. They found that Quercetin

binds near the lysine-rich region formed by the residues: LYS-32, LYS-43, LYS-45, and VAL-40 [29]. The effectiveness of Quercetin and its oxidized form against α -synuclein fibrillization has been demonstrated in many in vitro assays and neuron-like PC12 cell models [30, 31]. When Quercetin interacts with early-stage aggregates, they result in highly soluble α -synuclein oligomers. This occurs because the polyphenol binds to the lysine side chains located in the N-terminal domain of α -synuclein [32].

In the present study, a dataset of experimentally evaluated α -synuclein inhibitors was retrieved from the ChEMBL database (<https://www.ebi.ac.uk/chembl/>) [33] and was employed to develop quantitative structure–activity relationship (QSAR) models to screen for novel potential α -synuclein inhibitors. Exploratory data analysis was performed to define the chemical space of bioactive inhibitors and cluster similar compounds. The best performing QSAR model was selected to screen for natural products as potential α -synuclein inhibitors. Moreover, a pharmacophore was generated from the representative experimental drugs and was used to further screen our dataset. A molecular docking study was conducted on the remaining compounds to evaluate the molecular interactions involved in the ligand binding. Subsequently, an ADMET analysis was conducted to evaluate the suitability of the compounds to act as central nervous system (CNS) drugs. Finally, 100 ns molecular dynamics (MD) simulations were conducted to assess the stability of α -synuclein in the unbound state and when bound to the reference inhibitor and the selected natural products.

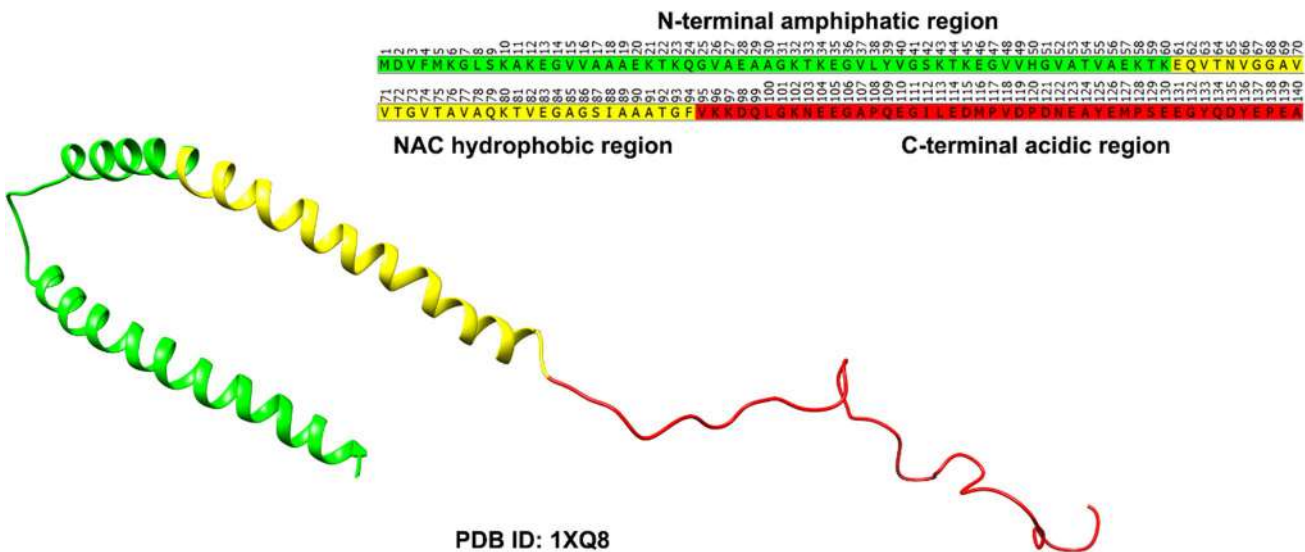


Fig. 1 Micelle-bound α -synuclein monomer solved by solution NMR (PDB ID: 1XQ8) and the corresponding full sequence. The structure is formed by three domains: N-terminal, NAC, and C-terminal region

Materials and methods

Bioactivity dataset preparation

A bioactivity dataset was retrieved from the ChEMBL database containing chemical structures of 10,408 compounds with their reported potency against human α -synuclein [33]. The dataset was curated by removing duplicate compounds. The molecules were classified as either “active” or “inactive” according to the information provided in the ChEMBL dataset. Compounds with “inconclusive” labels were omitted from the study. The processed dataset contained 524 compounds labelled as “active” and 3755 labelled as “inactive”. To obtain a more balanced classification, inactive compounds were clustered using Tanimoto similarity coefficient [34]. The final dataset contained 1124 compounds where 524 are “active” and 600 are “inactive”.

QSAR modelling

The final dataset was used to generate 2048 bits of circular molecular descriptors using Morgan fingerprints included in the RDKit cheminformatics suite with a Radius value of 2 based on the popular extended-connectivity fingerprints (ECFP4) derived from the SMILES representations of the compounds in the dataset [35, 36]. Datasets were split into training and testing sets using the 70/30 rule. The testing set was subject to an additional 80/20 split into testing and validation sets before building the QSAR models as illustrated in Fig. 2. Various statistical metrics were used to assess the performance of the machine learning models. To evaluate the classification ability, parameters such as true positive

rate (TPR) (Eq. 1), true negative rate (TNR) (Eq. 2), false positive rate (FPR) (Eq. 3), false negative rate (FNR) (Eq. 4), accuracy (ACC) (Eq. 5), and Matthews correlation coefficient (MCC) (Eq. 6) were calculated using the following equations:

$$TPR = \frac{TP}{(TP + FN)} \quad (1)$$

$$TNR = \frac{TN}{(FP + TN)} \quad (2)$$

$$FPR = \frac{FP}{(FP + TN)} \quad (3)$$

$$FNR = \frac{FN}{(FN + TP)} \quad (4)$$

$$ACC = \frac{(TP + TN)}{(P + N)} \quad (5)$$

$$MCC = \frac{(TP \times TN) - (FP \times FN)}{\sqrt{(TP + FP) * (TP + FN) * (TN + FP) * (TN + FN)}} \quad (6)$$

Natural products dataset preparation

The chemical structures of natural products were obtained from the LOTUS database in SMILES format. The database contains more than 200,000 distinct compound names and structural elements, as well as over 500,000 records of

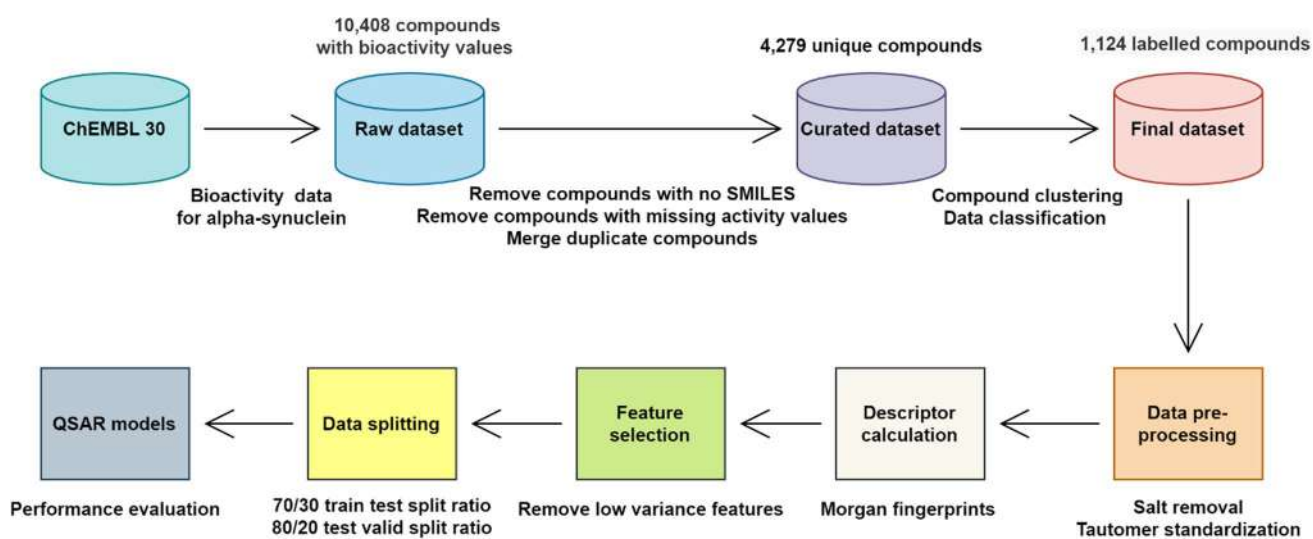


Fig. 2 Machine learning-based QSAR modelling workflow for α -synuclein inhibitors reported in the ChEMBL database

distinct, fully cited structure-organism pairs [37]. The structures were filtered using Lipinski's rule of five to remove any compounds that did not meet the criteria for orally active drugs [38]. The remaining compounds were analyzed using the DataWarrior Cheminformatics program to generate their 2D structures and calculate their physicochemical properties [39]. Only compounds with properties within the recommended range for orally active drugs were retained and saved in a CSV file for subsequent use in QSAR bioactivity prediction.

Pharmacophore modelling

To minimize the number of compounds for molecular docking experiments and ensure that only those meeting the essential pharmacophoric prerequisites present in clinical candidates were considered, we employed the Pharmit web-server (<https://pharmit.csb.pitt.edu/>) [40]. Using the clinical candidate Anle138b as a reference, we constructed our pharmacophore with the help of Pharmit. The pharmacophore was subsequently employed to screen the natural products that had been predicted to be bioactive through our QSAR study. The remaining compounds were then subjected to molecular docking investigations.

Molecular docking

The solution NMR structure of α -synuclein monomer was retrieved from the RCSB PDB (<https://www.rcsb.org/>) with PDB ID: 1XQ8 [25]. Polar hydrogens and Kollman charges were added using AutoDockTools 1.5.6 [41]. The C-terminal

tail was omitted from the study to ease the calculation charge and the resulting protein was used for molecular docking, without any further adjustment. The binding site druggability was assessed using DoGSiteScorer which is a grid-based method that uses a Difference of Gaussian filter to detect potential binding pockets solely based on the 3D structure of the protein [42, 43]. The highest-scoring pocket (Drug Score = 0.55) was found to be in the interhelical loop between the two α -helices as mentioned in the literature [27, 28]. The grid box was centered around this region formed by residues 30–48 of α -synuclein with the coordinates: $-12.29x - 24.50x - 82.36$ in x , y , and z directions respectively with a box size of 24 Å and a spacing of 1 Å. The binding site of α -synuclein and its residues is shown in Fig. 3.

Molecular docking was performed using AutoDock Vina 1.1.2 [44]. Since there is no reference ligand in the protein structure, the best docking poses were chosen according to their binding affinity and molecular interactions [45]. Protein–ligand interactions such as hydrogen bonds and hydrophobic interactions were visualized using the Protein–Ligand Interaction Profiler (PLIP) web tool (<https://plip-tool.biotecl.dresden.de/plip-web/plip/index>) [46].

ADMET analysis

ADMET stands for Absorption, Distribution, Metabolism, Excretion, and Toxicity. These are the key factors that determine the potential of a drug candidate to be developed into a safe and effective medicine [47]. In silico ADMET prediction is the use of computer-based methods to predict the potential of a chemical compound to be absorbed,

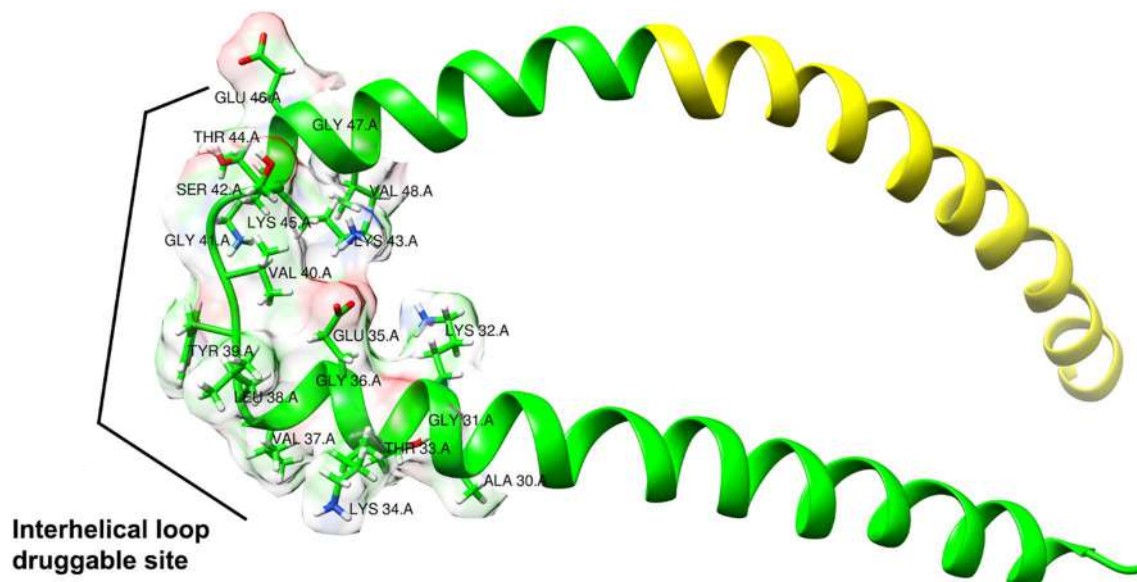


Fig. 3 Binding site of α -synuclein monomer at the interhelical loop located in the N-terminal region (PDB ID: 1XQ8)

distributed within the body, metabolized, excreted, and cause toxicity in living organisms [48]. ADMET prediction is an important tool in the early stages of drug discovery and development, as it allows researchers to identify potential compounds with favorable ADMET properties, reducing the need for costly and time-consuming animal testing [49]. In this study, pkCSM webserver (<https://biosig.lab.uq.edu.au/pkcsms/>) [50] was used to compute various parameters such as water solubility to determine how easily a drug can dissolve in the body and be absorbed into the bloodstream, intestinal absorption which refers to the extent to which a drug is absorbed into the body through the gastrointestinal tract, blood–brain barrier (BBB) permeability refers to the ability of a drug to pass through the BBB and reach the CNS, CYP2D6 interaction refers to the potential of a drug to interact with the enzyme CYP2D6, which is involved in the metabolism of many drugs [51]. Ames toxicity is a type of genotoxicity assessment used to determine the mutagenic potential of a compound, specifically its ability to cause mutations in bacteria whereas hepatotoxicity refers to the potential of a drug to cause injuries to the liver's normal function [45].

Molecular dynamics simulations

The stability of the selected candidates with respect to the binding site of α -synuclein monomer was determined using MD simulations with GROMACS 2021.3 [52, 53]. The protein structure of α -synuclein was prepared using CHARMM-GUI webserver [54]. The CHARMM36 all-atom force field was used to generate the protein topology file with the pdb2gmx module of GROMACS. Meanwhile, the CGENFF server (<https://cgenff.umaryland.edu/>) was used to assign atom types and bonded parameters and charges to the ligands [55]. The generated ligand files were then translated to GROMACS topology files using cgenff_charmm2gmx python script [56]. Subsequently, the TIP3P water model was chosen to solvate the protein–ligand systems in a cubic box of size $150 \times 80 \times 80$ in x , y , and z directions respectively. Na^+ and Cl^- ions were added to neutralize the system charge. All the systems were simulated in the standard biological salt concentration of 0.15 mM. For energy minimization, the steepest descent technique was utilized, with Fmax set to not exceed 1000 kJ/mol/nm. Two successive 1 ns simulation using canonical NVT, and isobaric NPT ensembles were used to equilibrate the system at 300 Kelvin and a pressure of 1 bar. All the simulations were carried out under periodic boundary conditions (PBC), and long-range electrostatic interactions were treated using the particle mesh Ewald method [57]. Finally, 100 ns MD simulations were then performed for data collection [58–60]. Various geometrical properties were calculated using GROMACS program to analyze the dynamic behavior of the selected

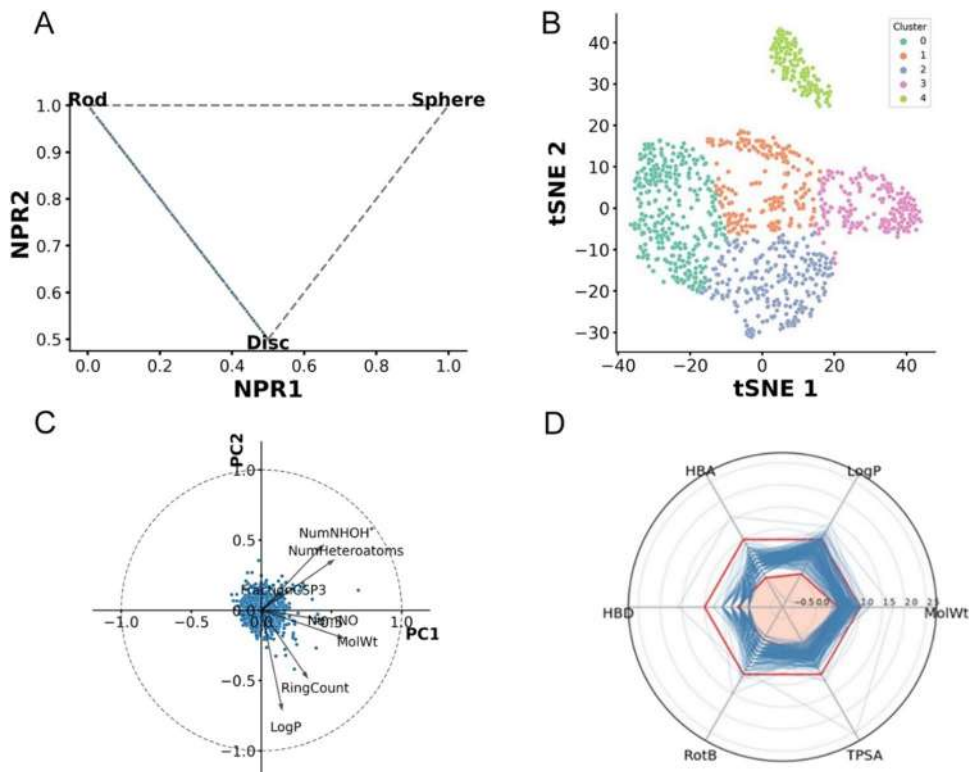
complexes such as root-mean square deviation (RMSD), root-mean square fluctuation (RMSF), radius of gyration (R_g), solvent accessible surface area (SASA), principal component analysis (PCA), and hydrogen bonds [61].

Results and discussion

Chemical space of α -synuclein inhibitors

Chemical space diversity of a dataset is important for the performance of machine learning classification models because a diverse set of compounds helps to prevent chemical sampling bias and leads to higher prediction accuracy and stronger generalization ability of the models. The chemical space diversity of the α -synuclein dataset was analysed using the Normalized principal moment of inertia ratios (NPR) plot to analyse the shape and size of molecules [62]. The normalized PMI ratios were then plotted on a triangular graph, where the vertices $(0,1)$, $(0.5,0.5)$, and $(1,1)$ represent a perfect rod (2-butyne), disc (benzene), and sphere (adamantane), respectively (Fig. 4A). Each molecule is represented by a single point in a three-dimensional space, with the x , y , and z axes corresponding to the normalized principal moment of inertia (PMI) for the three principal axes of the molecule (I_{xx} , I_{yy} , I_{zz}). The distance of the point from the origin of the plot represents the size of the molecule, while the orientation of the point reflects the shape of the molecule. Notably, all the studied α -synuclein inhibitors occupied the rod-disc region of the graph characterized by high values of NPR1 (I_2/I_1) and NPR2 (I_3/I_1). High NPR1 values suggest that the molecules have an elongated or rod-like shape, while high NPR2 values indicate a flattened or disc-like shape. This observation indicates that the molecules exhibit a common structural feature of elongation and a tendency toward planarity. T-Distributed Stochastic Neighbor Embedding (t-SNE) is a popular plot for visualizing high-dimensionality data while preserving the distances between the points as much as possible. In Fig. 4B, t-SNE analysis was used to compare molecules by their structural features based on RDkit's Morgan fingerprints [63]. To identify cluster of compounds with similar features, we employed k-means clustering method [64]. Then, we determined the optimal number of clusters using the silhouette-based algorithm [65]. The silhouette score is a metric commonly used to assess the effectiveness of clustering techniques [66]. Despite the average silhouette score for the five identified clusters was 0.26 which is considerate fair, the selected diverse set of representative compounds for molecular docking from each cluster represent compounds with different scaffolds. The lack of separation could be due to the dimensionality reduction resulting in some overlapping regions between clusters. Finally, principal component analysis (PCA) was performed

Fig. 4 **A** Normalized principal moment of inertia ratios (NPR) plot to describe molecules shapes. **B** t-distributed Stochastic Neighbor Embedding (t-SNE) plot with K-means clustering to describe molecules by their structural features and identify clusters of molecules with similar features. **C** Principal component analysis (PCA) to describe molecules by their physicochemical properties. **D** Radar chart of Beyond Lipinski's Rule of Five (bRo5)



to analyze the physicochemical properties of the molecules (Fig. 4C) [67]. By examining the correlations with PC1 (TPSA, HBA, MolWt) and PC2 (HBD, nRotB, LogP), we can identify the features that have positive and negative associations. Notably, LogP stands out as the “most important” feature (descriptor) due to its vector length. Finally, the radar chart of beyond Lipinski’s rule of five (bRo5) was performed to assess the percentage of the compounds that are unlikely to be suitable for oral administration [68]. Figure 4D illustrates that the majority of compounds in the dataset adhere to the suggested ranges for physicochemical properties as defined by Lipinski’s rule of five.

Validation of the QSAR models

Six machine learning (ML) algorithms that are known to perform well for QSAR modeling such as Random Forest (RF), Support Vector Machine (SVM), k-Nearest Neighbors (kNN), Extra Trees (ET), Gaussian Naïve Bayes (GNB), and XGBoost (XGB) were selected to build our models [69]. The receiving operating characteristic (ROC) curve was used to evaluate the quality of the developed QSAR classification models by comparing the true positive rate to the false positive rate. After evaluating the six QSAR models, we identified that the RF algorithm yielded the highest performance. The QSAR model based on the RF algorithm achieved an area under the ROC curve (AUC) value of 0.75 (Fig. 5) for the testing set and 0.72 for the external validation set for

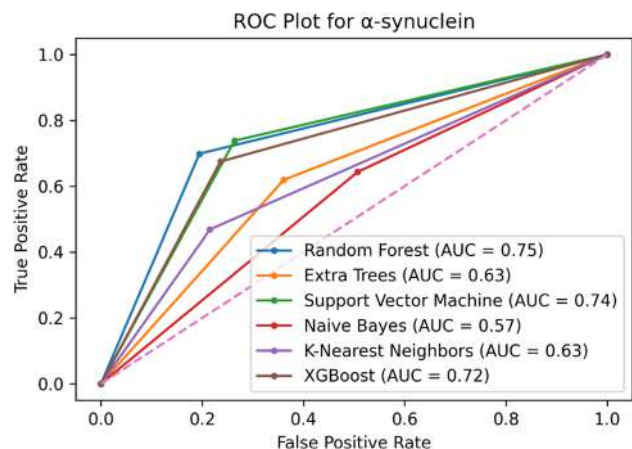


Fig. 5 ROC plot for α -synuclein visualizing the trade-off between true positive and false positive rates

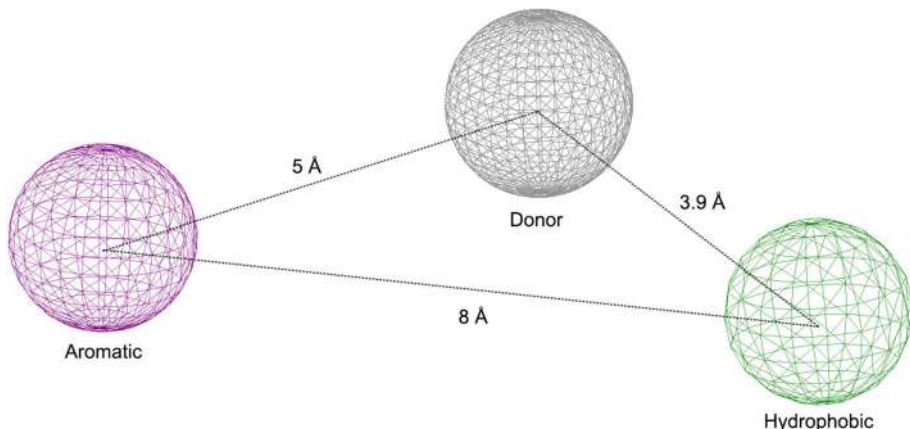
α -synuclein inhibitors. This indicates a reasonably good predictive ability of the model in distinguishing between positive and negative instances. The performance of all the QSAR models was also assessed using various performance metrics, as shown in Table 1.

The best performing QSAR model based on the RF algorithm was then applied to the LOTUS dataset containing 129,557 natural products to screen for potential α -synuclein inhibitors. 40,251 compounds were retained at this stage and were subjected to a pharmacophore-based virtual screening.

Table 1 Comparing the performance of multiple machine learning models using a variety of statistical metrics

ML model	Testing set							Validation set AUC
	TPR	TNR	FPR	FNR	ACC	MCC	AUC	
Random forest	0.75	0.75	0.24	0.24	0.75	0.51	0.75	0.72
Support vector machine	0.76	0.70	0.29	0.23	0.73	0.47	0.74	0.71
k-nearest neighbors	0.62	0.65	0.34	0.37	0.63	0.27	0.62	0.66
Extra trees	0.65	0.60	0.4	0.34	0.62	0.25	0.62	0.65
Gaussian Naïve Bayes	0.61	0.52	0.47	0.38	0.56	0.13	0.56	0.53
XGBoost	0.72	0.71	0.28	0.27	0.72	0.44	0.72	0.71

Fig. 6 Pharmacophoric features selected based on the clinical candidate, Anle138b using Pharmit server



Pharmacophore screening

Prior research has emphasized the significance of the nitrogen atoms located in the imidazole ring of the clinical candidate Anle138b (CHEMBL4748063) in establishing a hydrogen bond with VAL-40 of the interhelical loop in α -synuclein [28]. Using the existing literature and Anle138b's chemical structure, we have devised a pharmacophore model that enables us to narrow down the pool of compounds and only retain those exhibiting the desired pharmacophoric traits as depicted in Fig. 6.

The pharmacophore model we created contained an aromatic ring, a hydrophobic component, and a hydrogen donor group in the center. This is consistent with earlier research that attempted to develop a pharmacophore model for α -synuclein inhibitors [70, 71]. After employing our pharmacophore for screening, we were able to identify 103 compounds that met the proposed criteria out of a total of 40,251 compounds. These compounds were then subjected to molecular docking investigations.

Molecular docking of α -synuclein inhibitors

A molecular docking study was conducted for the experimental α -synuclein inhibitors as well as the remaining natural products against the binding site of the target monomer. The best docking poses were selected according to their

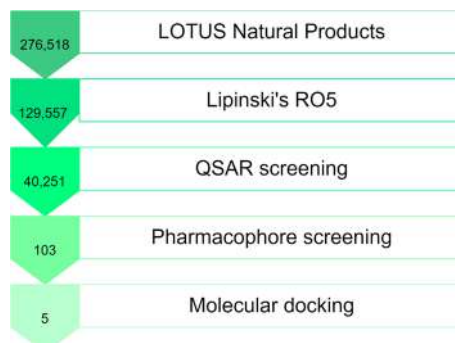
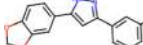
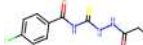
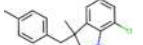
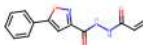
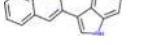
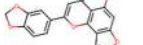
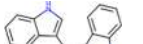
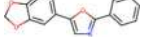


Fig. 7 Virtual screening workflow used in this study to screen for potential α -synuclein inhibitors from natural products

binding affinity and their protein–ligand interactions. Only five compounds were retained displaying a binding energy of -6.0 kcal/mol or lower as illustrated in Fig. 7. The molecular docking results of the highest-ranking candidates, their chemical structures and their molecular interactions are shown in Table 2. The best docking poses were visualized using UCSF Chimera software [72] and are shown in Fig. 8.

The selected compounds showed low binding affinity when docked against the interhelical region of α -synuclein, in contrast to other macromolecules such as enzymes and receptors with well-defined binding cavities. However, the binding scores, ranging from -6.0 to -6.6 kcal/mol, were

Table 2 Molecular docking and protein–ligand interactions of α -synuclein inhibitors and the identified natural products

Compound	Chemical structure	Docking score (kcal/mol)	Hydrogen bonds	Distance (Å)	Hydrophobic interactions
CHEMBL4748063		− 6.2	VAL-40	1.9	TYR-39 VAL-40 LYS-43 THR-44 LYS-45
CHEMBL1544679		− 6.1	LYS-43	2.0	GLU-35 VAL-40 LYS-43
CHEMBL2133766		− 6.0	LYS-45	2.5	GLU-35 VAL-40 LYS-43
CHEMBL1299242		− 5.9	VAL-40	3.3	GLU-35 TYR-39 VAL-40 LYS-43
CHEMBL3392484		− 5.2	VAL-40 LYS-43 LYS-43	2.5 2.4 2.7	GLU-35 VAL-40 LYS-43 VAL-48
LTS0078917		− 6.6	GLU-35 LEU-38 LYS-43	3.4 1.9 3.3	LYS-32 TYR-39
LTS0205810		− 6.5	GLU-35	2.1	GLU-35 TYR-39 LYS-43
LTS0027287		− 6.2	LYS-45	3.5	TYR-39 VAL-40 LYS-43
LTS0131710		− 6.2	GLU-35	2.2	GLU-35 TYR-39 LYS-43 THR-44
LTS0164686		− 6.0	VAL-40 LYS-45	2.5 3.4	GLU-35 TYR-39 LYS-43

consistent with other molecular docking studies against α -synuclein that have been reported in literature [73, 74].

ADMET evaluation results

The studied molecules were subjected to an in silico ADMET analysis to assess their suitability as drugs acting on the brain as shown in Table 3. All the compounds demonstrated a good water solubility with LogS values ranging from − 3.4 to − 4.9, and displayed high intestinal absorption (> 90%). Furthermore, all compounds were predicted to have the ability to cross the BBB. Importantly, none of the compounds were identified as substrates of CYP2D6, an enzyme predominantly expressed in the brain that metabolizes endogenous neural compounds with potential neuroprotective effects [75]. Additionally, based on the Ames toxicity prediction results, five compounds, including four natural products, were predicted to be mutagenic. Furthermore, the assessment of hepatotoxicity indicated that four compounds could potentially cause liver injury and disrupt its normal function. Notably, among the predicted toxic compounds, the clinical candidate Anle138b was included, underscoring

the necessity for experimental toxicity studies to confirm its safety.

Molecular dynamics analysis

Following the analysis of molecular docking results, the clinical candidate Anle138b (CHEMBL4748063) along with the selected natural products were chosen for 100 ns MD simulations. Additionally, the unbound state of the α -synuclein monomer was included to evaluate and compare its stability with the complexes throughout the entire simulation period.

Root-mean square deviation

During the molecular docking study, the protein structure was considered rigid. To better understand the interactions between the protein and the ligands, MD simulations of the docked complexes were conducted in a water environment for a duration of 100 ns. The RMSD was calculated relative to the solution NMR protein of the targeted α -synuclein structure (PDB ID: 1XQ8) in complex with the selected candidates. Figure 9 displays RMSD values for both the protein

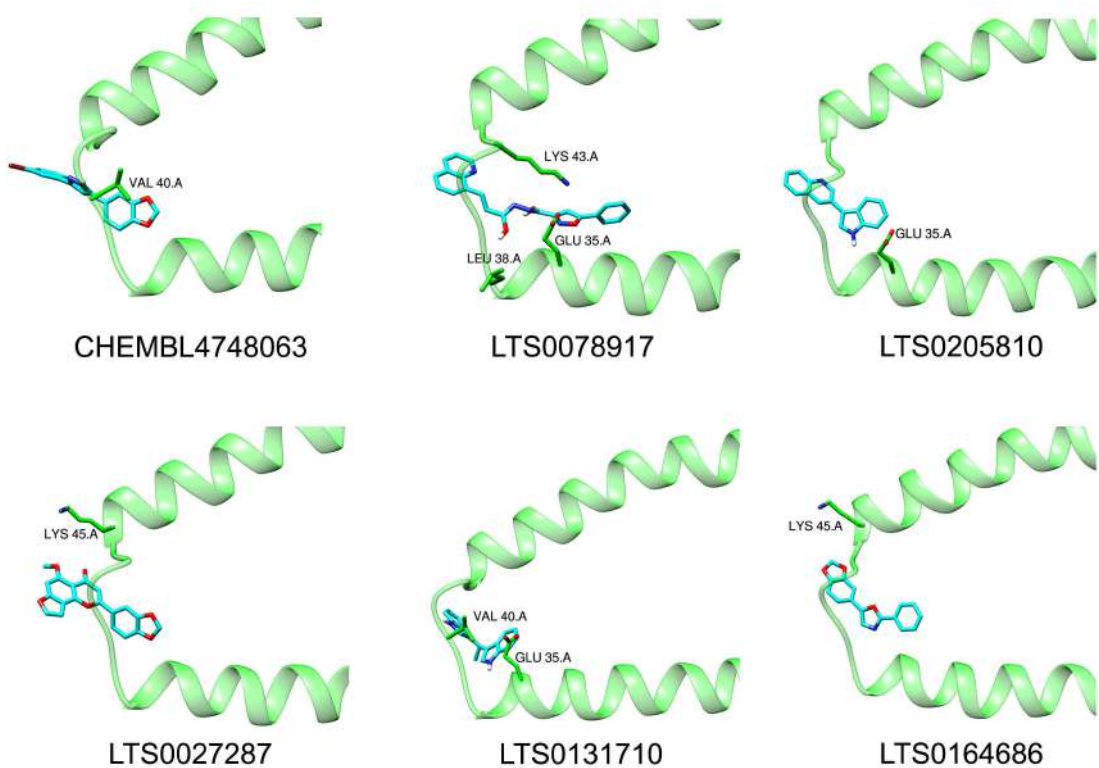


Fig. 8 Molecular docking conformations of the reference inhibitor Anle138b and the selected natural products when bound to α -synuclein

Table 3 ADMET prediction results for the selected compounds

Compound	Water solubility	Intestinal absorption	BBB permeability	CYP2D6 substrate	Ames toxicity	Hepatotoxicity
CHEMBL4748063	-3.4	92.1	0.4	No	No	Yes
CHEMBL1544679	-4.6	90.2	-0.7	No	No	No
CHEMBL2133766	-4.9	91.6	0.6	No	Yes	No
CHEMBL1299242	-3.4	92.6	-0.7	No	No	No
CHEMBL3392484	-4.7	94.5	0.4	No	No	Yes
LTS0078917	-4.7	97.2	-0.8	No	No	Yes
LTS0205810	-4.6	96.0	0.4	No	Yes	Yes
LTS0027287	-4.3	99.7	-0.7	No	Yes	No
LTS0131710	-3.9	92.5	0.7	Yes	Yes	Yes
LTS0164686	-4.0	96.5	0.3	No	Yes	No

Water solubility: Solubility of the molecule in water at 25 °C (log mol/L); Intestinal absorption: Percentage that will be absorbed through the human intestine; BBB permeability: Logarithmic ratio of brain to plasma drug concentrations. (logBB > 0.3 is considered to cross the BBB while molecules with logBB < -1 are poorly distributed to the brain; CYP2D6 substrate: Likelihood of a drug to be metabolized by the cytochrome P450; Ames toxicity: Likeliness of a compound to be mutagenic; Hepatotoxicity: Likeliness of drug-induced liver injury

backbone and the bound ligands, plotted against simulation time for each protein.

The RMSD analysis indicated that the majority of the complexes exhibited deviations ranging from 1 to 2 nm within the first 20 ns of the simulation. By the 40 ns mark,

most complexes had reached equilibrium with RMSD values stabilizing around 1 nm. However, LTS0027287 and LTS0164686 showed larger deviations exceeding 2 nm, suggesting significant conformational changes. Notably, LTS0078917 demonstrated the highest stability throughout

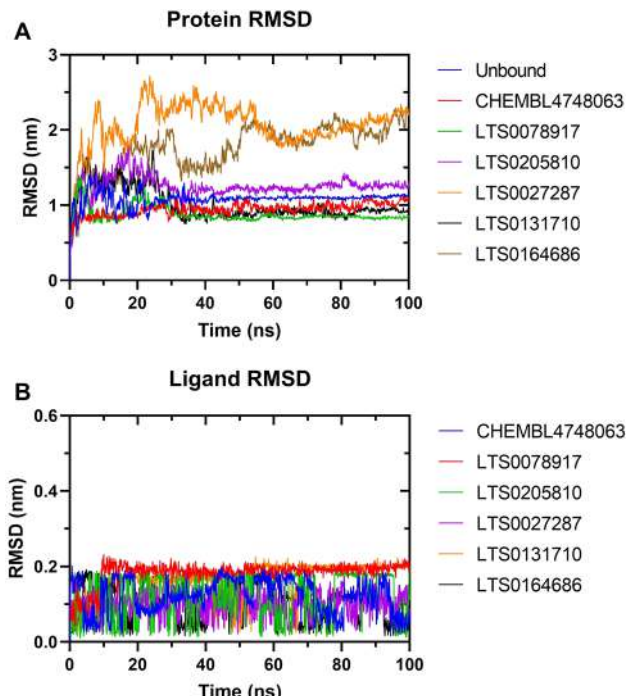


Fig. 9 RMSD graphs of the backbone atoms of α -synuclein in complex with the selected ligands (A) and for the heavy atoms of the selected ligands with respect to the protein (B)

the simulation, maintaining an RMSD value of 0.8 nm over the entire simulation duration.

The ligand RMSD is a measure of the structural variability of a molecule during a simulation [76]. The analyzed natural products exhibited a narrow range of fluctuation in RMSD values, spanning from 0 to 0.2 nm. This implies that these ligands may undergo minor conformational changes due to their inherent flexibility. In contrast, LTS0078917 adopted a stable conformation within the initial 10 ns and maintained a significantly more stable RMSD value of approximately 0.2 nm throughout the remainder of the simulation. These results indicate that LTS0078917 exhibits lower structural variability compared to the other ligands and is likely to retain a consistent conformation throughout the simulation duration.

Root-mean square fluctuation

The RMSF is a measure of a protein's flexibility during molecular simulations, revealing the level of flexibility in different regions of the protein by calculating the motion of each residue around the average position [77]. Figure 10 shows the RMSF profile for the selected complexes, indicating that the binding of these inhibitors has a similar impact on the pattern of residue fluctuations in the protein. The regions with the highest fluctuations were found in residues 0–5 located at the extremity of the N-terminal and

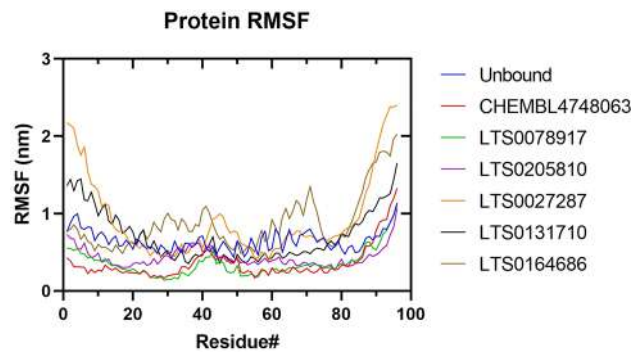


Fig. 10 RMSF graph of the N-terminus region residues for the unbound α -synuclein N-terminus region and when bound to the selected ligands

94–100 representing the beginning of the C-terminal tail, with RMSF values greater than 1 nm for the compounds LTS0027287 and LTS0131710. However, it is noteworthy that these regions exhibit less fluctuation in the unbound α -synuclein structure. In contrast, a considerably more stable RMSF was observed in the presence of the clinical candidate CHEMBL4748063 and LTS0078917. This observation suggests that these compounds potentially exert a stabilizing effect on the protein, reducing the fluctuations in these regions. Furthermore, the RMSF analysis revealed that the residues surrounding the ligand in the binding pocket exhibited RMSF values less than 1 nm, suggesting a stable binding pocket. However, notable peaks in RMSF were observed for residues 40–44, which consist of VAL-40, GLY-41, SER-42, LYS-43, and THR-44. These particular residues are known to be among the most flexible amino acids, indicating their inherent mobility even within the binding pocket.

Radius of gyration

Rg is a metric used to assess the size and shape of biomolecular structures, such as proteins. It is calculated by measuring the root-mean-square distance of all atoms in the structure from the center of mass. In the context of this study, the Rg values for the protein in complex with CHEMBL4748063, LTS0078917, and LTS0131710 were found to be consistently stable, with values approximately 2.4 nm. This is in contrast to the unbound structure, which exhibited an Rg value of 2.8 nm, as depicted in Fig. 11. The observed stability in Rg suggests that the binding of these compounds to the protein may contribute to a more compact and restrained conformation compared to the unbound state. In contrast, when the protein was bound to LTS0205810, fluctuations in the Rg were observed, leading to higher values reaching approximately 2.8 nm. Whereas the protein completely lost its compactness when bound to LTS0027287 resulting in a higher Rg reaching a value of

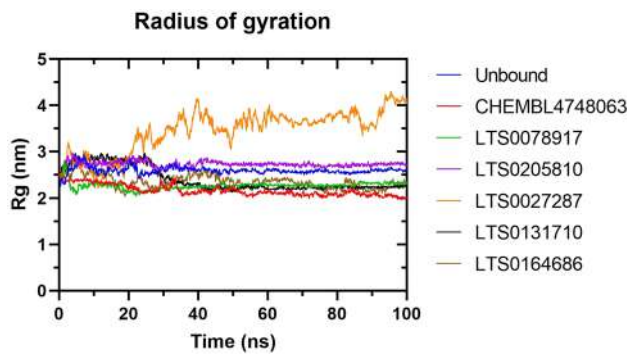


Fig. 11 Radius of Gyration of α -synuclein in unbound and bound states

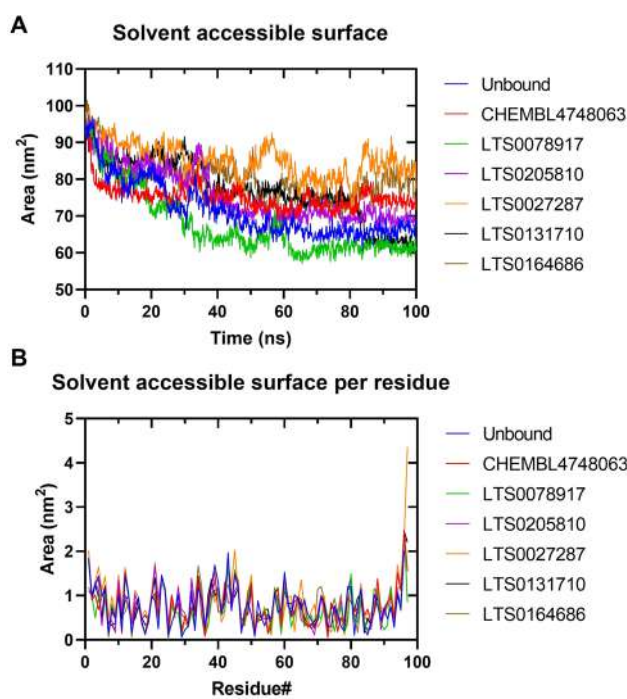


Fig. 12 Solvent accessible surface area for the studied complexes over the simulation time (A) and per residue analysis for each complex (B)

4 nm and still increasing. This suggests that the binding of LTS0027287 causes a change in the shape of the protein leading to a more extended conformation which favors the formation and aggregation of pathologic oligomers.

Solvent accessible surface

The SASA is a measure of the exposed area of proteins that is accessible to solvent molecules, providing information about their relative exposure or burial within the protein structure [78]. In Fig. 12, the SASA plots for the α -synuclein complexes depict changes over the simulation time and on

a per-residue basis. The analysis reveals a consistent trend of decreasing SASA values over time for all complexes. Notably, compared to the unbound state of α -synuclein, the protein–ligand complexes exhibit increased SASA values, indicating greater exposure to solvent molecules. Interestingly, the compound LTS0078917 stands out as it exhibits the lowest SASA value among the complexes, suggesting a more compact or buried conformation with reduced solvent exposure. This could imply stronger interactions or a tighter binding of LTS0078917 with α -synuclein, leading to a more constrained and less exposed protein–ligand complex.

On the other hand, the analysis of SASA per residue consistently demonstrated a similar trend across all the complexes, where the calculated area values ranged from 1 to 2 nm^2 . These values are considered very low, indicating the hydrophobic nature of these regions. Notably, the C-terminal acidic region exhibited the highest solvent exposure among the residues, which is associated to its hydrophilic properties.

Principal component analysis

PCA is a technique used to analyze the motion of biomolecular systems in a molecular dynamics simulation [79]. It identifies the dominant modes of motion by extracting eigenvectors and eigenvalues from the trajectory data. These eigenvectors and eigenvalues describe the principal components and their amplitudes, respectively, capturing the internal motions within a protein [80]. In our study, we employed PCA to investigate conformational changes in the selected complexes. Specifically, we focused on the backbone atoms and analyzed the motions associated with the principal components (PCs).

Since the first few eigenvectors adequately describe most of the internal motions in a protein, we selected the first 40 eigenvectors to calculate the concerted motions in the final 50 ns of the trajectory. Figure 13A illustrates the eigenvalues obtained by diagonalizing the covariance matrix of atomic fluctuations. The eigenvalues are ordered in decreasing magnitude and correspond to their respective eigenvectors. For the last 50 ns of the trajectories, the first ten eigenvectors account for 52.62%, 95.06%, 94.72%, 78.71%, 78.05%, and 72.21% of the motions in CHEMBL4748063, LTS0078917, LTS0205810, LTS0027287, LTS0131710, LTS0164686 complexes, respectively. Another approach to visualizing the dynamics of the complexes is by generating a 2D projection plot using PCA. The first PC1 captures the most variance in the data, followed by PC2 and subsequent components. Therefore, we utilized PC1 and PC2 of the backbone atoms to create a projection of the entire dataset in a lower-dimensional space suitable for 2D visualization. Figure 13B presents the projection of the two selected eigenvectors for all complexes. It is known that complexes occupying a smaller

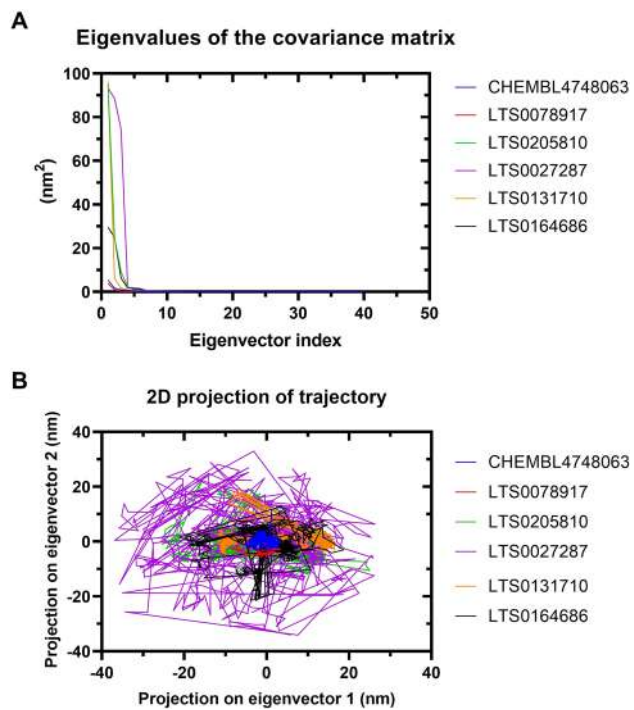


Fig. 13 Plot of the eigenvalues of the covariance matrix against the first 40 eigenvectors (A). 2D motion projection of α -synuclein backbone bound to the selected compounds using first two eigenvectors (B)

phase space and exhibiting a stable cluster represent more stable complexes, while those occupying a larger space and showing a non-stable cluster correspond to less stable complexes. From the plot, it was observed that LTS0027287 complex occupied a larger space, followed by LTS0205810 and LTS0164686, indicating a less stable cluster compared

to other complexes. On the other hand, CHEMBL4748063 and LTS0078917 occupied a smaller phase space and demonstrated a stable cluster.

In Fig. 14, we presented snapshots of the initial conformations superposed with the final conformations at 100 ns, shedding light on the dynamics of the protein–ligand complexes. Our findings reveal that certain complexes underwent significant conformational changes, resulting in the disruption of ligand binding to the interhelical loop region. Notably, LTS0205810, LTS0027287, and LTS0164686 showed the most pronounced alterations in their binding modes. Conversely, the complexes formed by CHEMBL4748063 and LTS0078917 displayed a more compact and stable conformation, suggesting their potential as stabilizers of the α -synuclein monomer. This observation highlights their promising role in mitigating the aggregation and oligomerization of α -synuclein fibrils.

Hydrogen bonds

Hydrogen bonds are crucial interactions that significantly contribute to the stability and specificity of protein–ligand interactions. In MD simulations, analyzing the hydrogen bonds formed between the protein and ligand provides valuable insights into the strength and stability of these interactions. Thus, assessing the number and persistence of hydrogen bonds during MD simulations is essential in evaluating the effectiveness of potential drug candidates.

In our study, we analyzed the hydrogen bonds formed by each ligand and the pairs that remained within a distance of 0.35 nm throughout the simulation time. Figure 15 presents the dynamic changes in the number of hydrogen bonds for all the selected complexes. The first

Fig. 14 Conformation snapshots of the studied complexes at 0 ns (light green) and 100 ns (yellow) after recentering and rewrapping coordinates

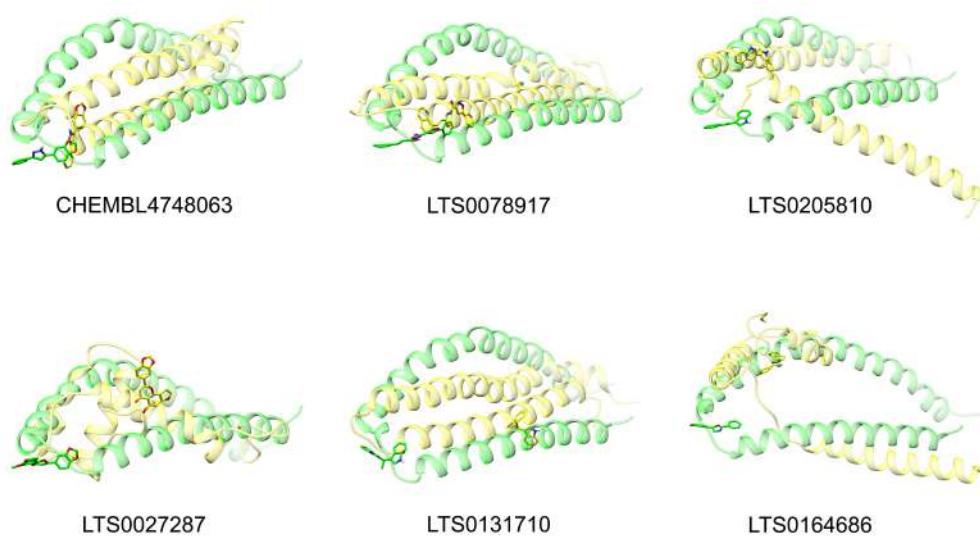
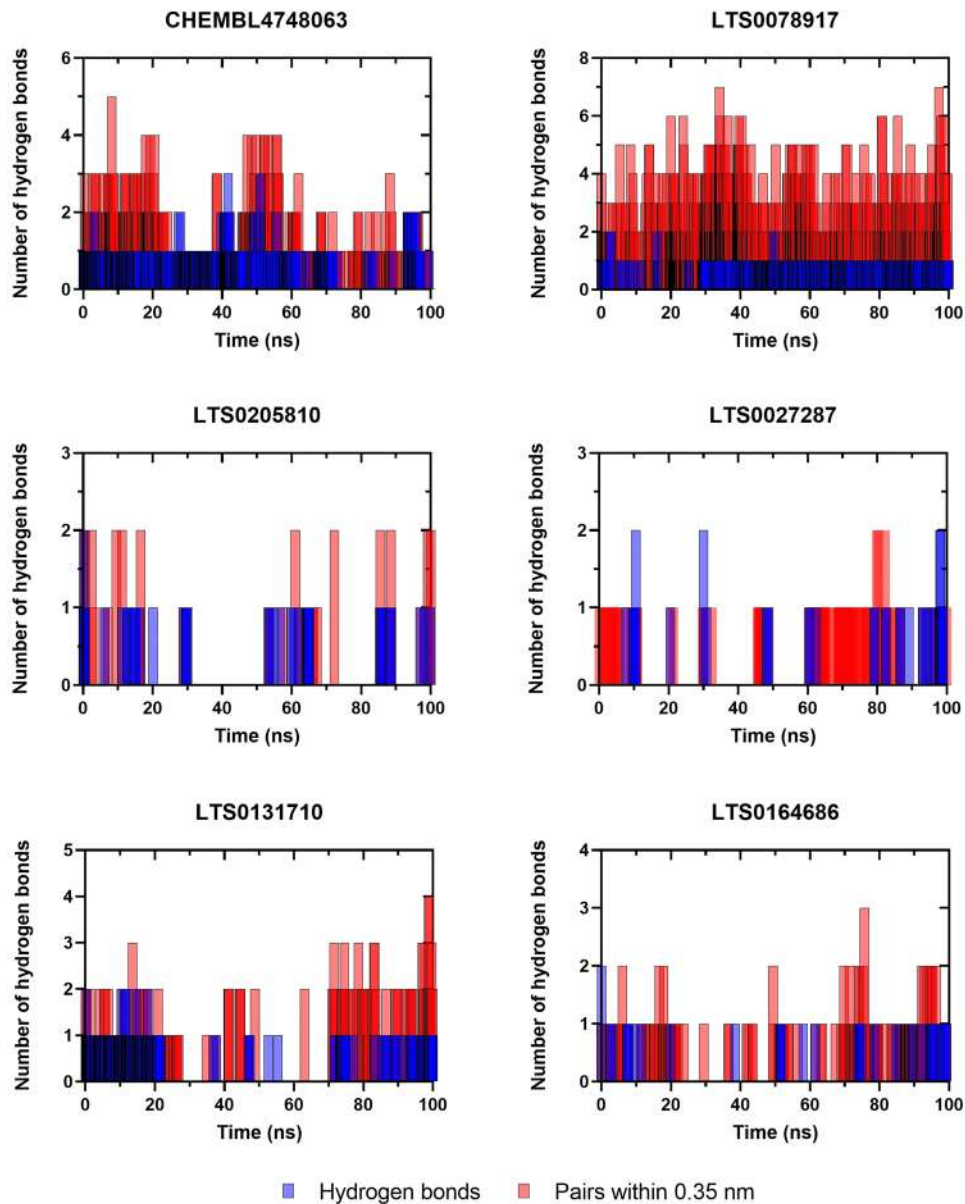


Fig. 15 Number of hydrogen bonds formed for the trajectory of molecular dynamics simulations for the selected ligands in complex with the N-terminus region of α -synuclein



plot reveals that CHEMBL4748063 formed a peak of five hydrogen bonds within the first 20 ns, leading to one persistent pair within 0.35 nm by the end of the simulation. Most compounds formed up to three hydrogen bonds. However, among the ligands investigated, LTS0078917 emerged as the most promising candidate, displaying notable characteristics in comparison to the other ligands. In particular, LTS0078917 demonstrated the formation of up to seven hydrogen bonds, with six consistent pairs maintained within a distance of 0.35 nm throughout the entire duration of the simulation. This suggests strong and stable interactions between LTS0078917 and the target receptor, making it an intriguing candidate for further investigation.

Conclusion

Neurodegenerative diseases are associated with protein misfolding, which leads to the formation of fibrillar amyloids and subsequent damage in the brain and other tissues. In PD, the presence of amyloid fibril aggregates indicates the abnormal accumulation of the fibrillary protein α -synuclein in the brain. This accumulation is believed to contribute to the degeneration of dopamine-producing neurons, resulting in the motor symptoms of PD. Anle138b shows promise as a clinical treatment by preventing the formation of amyloidogenic protein aggregates. In this study, we aimed to gain a deeper understanding of its mechanisms of action, particularly in the N-terminal region of α -synuclein, and identify potential novel candidates based on natural products using

QSAR and pharmacophore design approaches. Through molecular docking and MD simulations, we found that the studied compounds have the ability to bind to the hairpin like coil region that separates the two α -helices of α -synuclein. By binding to this region, these compounds may hinder conformational changes that lead to the adoption of an elongated shape, which is known to promote the formation and deposition of oligomers. Additionally, since the interhelical region of α -synuclein is involved in lipid binding, compounds targeting this region may prevent the protein from associating to the lipid membranes. Our results highlighted LTS0078917 as a promising candidate, displaying strong binding affinity towards the active site of α -synuclein. The identified natural products may pave the way for further investigation, encompassing the determination of their bioactivity and optimization in the quest for effective PD treatments.

Acknowledgements Kailash Jangid gratefully acknowledge NSM for the access to ‘PARAM Seva Facility’ at IIT, Hyderabad, which is implemented by C-DAC and supported by the ministry of Electronics and Information Technology (MeitY) and Department of Science and Technology (DST), Government of India.

Author contributions YB suggested the idea, wrote the main manuscript text and performed the data analysis, KJ performed the MD simulations, MRB and AM supervised the work.

Funding The authors received no financial support for the research, authorship, and/or publication of this article.

Declarations

Competing interests The authors declare no competing interests.

References

- Dugger BN, Dickson DW (2017) Pathology of neurodegenerative diseases. *Cold Spring Harb Perspect Biol* 9(7):a028035
- Hardy J, Gwinn-Hardy K (1998) Genetic classification of primary neurodegenerative disease. *Science* 282(5391):1075–1079
- Goetz CG, Emre M, Dubois B (2008) Parkinson’s disease dementia: definitions, guidelines, and research perspectives in diagnosis. *Ann Neurol* 64(S2):S81–S92
- Dorsey EA, Constantinescu R, Thompson JP, Biglan KM, Holloway RG, Kieburtz K, Tanner CM (2007) Projected number of people with Parkinson disease in the most populous nations, 2005 through 2030. *Neurology* 68(5):384–386
- Wanneveich M, Moisan F, Jacqmin-Gadda H, Elbaz A, Joly P (2018) Projections of prevalence, lifetime risk, and life expectancy of Parkinson’s disease (2010–2030) in France. *Mov Disord* 33(9):1449–1455
- Martinez-Martin P, Rodriguez-Blazquez C, Paz S, Forjaz MJ, Frades-Payo B, Cubo E, ELEP Group (2015) Parkinson symptoms and health related quality of life as predictors of costs: a longitudinal observational study with linear mixed model analysis. *PLoS ONE* 10(12):e0145310
- Chaudhuri KR, Healy DG, Schapira AH (2006) Non-motor symptoms of Parkinson’s disease: diagnosis and management. *Lancet Neurol* 5(3):235–245
- Jenner P (2003) Oxidative stress in Parkinson’s disease. *Ann Neurol* 53(S3):S26–S38
- Kalia LV, Kalia SK, Lang AE (2015) Disease-modifying strategies for Parkinson’s disease. *Mov Disord* 30(11):1442–1450
- Olanow CW, Agid Y, Mizuno Y, Albanese A, Bonuccelli U, Damier P, Stocchi F (2004) Levodopa in the treatment of Parkinson’s disease: current controversies. *Mov Disord* 19(9):997–1005
- Finberg JP (2019) Inhibitors of MAO-B and COMT: their effects on brain dopamine levels and uses in Parkinson’s disease. *J Neural Transm* 126(4):433–448
- Szabo N, Kincses ZT, Vecsei L (2011) Novel therapy in Parkinson’s disease: adenosine A2A receptor antagonists. *Expert Opin Drug Metab Toxicol* 7(4):441–455
- Vanle B, Olcott W, Jimenez J, Bashmi L, Danovitch I, IsHak WW (2018) NMDA antagonists for treating the non-motor symptoms in Parkinson’s disease. *Transl Psychiatry* 8(1):1–15
- Amer DA, Irvine GB, El-Agnaf O (2006) Inhibitors of α -synuclein oligomerization and toxicity: a future therapeutic strategy for Parkinson’s disease and related disorders. *Exp Brain Res* 173(2):223–233
- Rangasamy SB, Soderstrom K, Bakay RA, Kordower JH (2010) Neurotrophic factor therapy for Parkinson’s disease. *Prog Brain Res* 184:237–264
- Boulaamane Y, Ibrahim MA, Britel MR, Maurady A (2022) In silico studies of natural product-like caffeine derivatives as potential MAO-B inhibitors/AA2AR antagonists for the treatment of Parkinson’s disease. *J Integr Bioinform*, 19(4):20210027
- Oliveira L, Gasser T, Edwards R, Zweckstetter M, Melki R, Stefanis L, Outeiro TF (2021) Alpha-synuclein research: defining strategic moves in the battle against Parkinson’s disease. *Npj Parkinson’s Dis* 7(1):1–23
- Das S, Pukala TL, Smid SD (2018) Exploring the structural diversity in inhibitors of α -synuclein amyloidogenic folding, aggregation, and neurotoxicity. *Front Chem* 6:181
- Cheng F, Vivacqua G, Yu S (2011) The role of alpha-synuclein in neurotransmission and synaptic plasticity. *J Chem Neuroanat* 42(4):242–248
- Takeda A, Mallory M, Sundsmo M, Honer W, Hansen L, Masliah E (1998) Abnormal accumulation of NACP/alpha-synuclein in neurodegenerative disorders. *Am J Pathol* 152(2):367
- Gibb WR, Lees A (1988) The relevance of the Lewy body to the pathogenesis of idiopathic Parkinson’s disease. *J Neurol Neurosurg Psychiatry* 51(6):745–752
- Vicario M, Cieri D, Brini M, Cali T (2018) The close encounter between alpha-synuclein and mitochondria. *Front Neurosci* 12:388
- Wagner J, Ryazanov S, Leonov A, Levin J, Shi S, Schmidt F, Giese A (2013) Anle138b: a novel oligomer modulator for disease-modifying therapy of neurodegenerative diseases such as prion and Parkinson’s disease. *Acta Neuropathologica* 125(6):795–813
- Price DL, Koike MA, Khan A, Wräsiglo W, Rockenstein E, Masliah E, Bonhaus D (2018) The small molecule alpha-synuclein misfolding inhibitor, NPT200-11, produces multiple benefits in an animal model of Parkinson’s disease. *Sci Rep* 8(1):1–12
- Ulmer TS, Bax A, Cole NB, Nussbaum RL (2005) Structure and dynamics of micelle-bound human α -synuclein. *J Biol Chem* 280(10):9595–9603
- Cooper AA, Gitler AD, Cashikar A, Haynes CM, Hill KJ, Bhullar B, Lindquist S (2006) α -Synuclein blocks ER-Golgi traffic and Rab1 rescues neuron loss in Parkinson’s models. *Science* 313(5785):324–328

27. Amos SBT, Schwarz TC, Shi J, Cossins BP, Baker TS, Taylor RJ, Sansom MS (2021) Membrane interactions of α -Synuclein revealed by multiscale molecular dynamics simulations, Markov state models, and NMR. *J Phys Chem B* 125(11):2929–2941
28. Kondratyev MS, Rudnev VR, Nikolsky KS, Petrovsky DV, Kulikova LI, Malsagova KA, Kaysheva AL (2022) In silico study of the interactions of anle138b isomer, an inhibitor of amyloid aggregation, with partner proteins. *Int J Mol Sci* 23(24):16096
29. Baul HS, Rajiniraja M (2018) Favorable binding of quercetin to α -synuclein as potential target in Parkinson disease: an insilico approach. *Res J Pharm Technol* 11(1):203–206
30. Zhu M, Han S, Fink AL (2013) Oxidized quercetin inhibits α -synuclein fibrillization. *Biochimica et Biophysica Acta (BBA)* 1830(4):2872–2881
31. Ahn TB, Jeon BS (2015) The role of quercetin on the survival of neuron-like PC12 cells and the expression of α -synuclein. *Neural Regen Res* 10(7):1113
32. Bisi N, Feni L, Peqini K, Pérez-Peña H, Ongeri S, Pieraccini S, Pellegrino S (2021) α -Synuclein: an all-inclusive trip around its structure, influencing factors and applied techniques. *Front Chem* 9:666585
33. Gaulton A, Bellis LJ, Bento AP, Chambers J, Davies M, Hersey A, Overington JP (2012) ChEMBL: a large-scale bioactivity database for drug discovery. *Nucleic acids Res* 40(D1):D1100–D1107
34. Bajusz D, Rácz A, Héberger K (2015) Why is Tanimoto index an appropriate choice for fingerprint-based similarity calculations? *J Cheminform* 7(1):1–13
35. Landrum, G. (2013). RDKit: a software suite for cheminformatics, computational chemistry, and predictive modeling. Greg Landrum
36. Capecchi A, Probst D, Reymond JL (2020) One molecular fingerprint to rule them all: drugs, biomolecules, and the metabolome. *J Cheminform* 12(1):1–15
37. Rutz A, Sorokina M, Galgonek J, Mietchen D, Willighagen E, Gaudry A, Allard PM (2022) The LOTUS initiative for open knowledge management in natural products research. *elife* 11:e70780
38. Lipinski CA (2004) Lead-and drug-like compounds: the rule-of-five revolution. *Drug Discov Today Technol* 1(4):337–341
39. Sander T, Freyss J, von Korff M, Rufener C (2015) DataWarrior: an open-source program for chemistry aware data visualization and analysis. *J Chem Inf Model* 55(2):460–473
40. Sunseri J, Koes DR (2016) Pharmit: interactive exploration of chemical space. *Nucleic Acids Res* 44(W1):W442–W448
41. Huey R, Morris GM, Forli S (2012) Using AutoDock 4 and AutoDock vina with AutoDockTools: a tutorial. *Scripps Res Inst Mol Graphics Lab* 10550:92037
42. Volkamer A, Griebel A, Grömbacher T, Rarey M (2010) Analyzing the topology of active sites: on the prediction of pockets and subpockets. *J Chem Inf Model* 50(11):2041–2052
43. Volkamer A, Kuhn D, Grömbacher T, Rippmann F, Rarey M (2012) Combining global and local measures for structure-based druggability predictions. *J Chem Inf Model* 52(2):360–372
44. Trott O, Olson AJ (2010) AutoDock Vina: improving the speed and accuracy of docking with a new scoring function, efficient optimization, and multithreading. *J Comput Chem* 31(2):455–461
45. Bhakhar KA, Gajjar ND, Bodiwala KB, Sureja DK, Dhameliya TM (2021) Identification of anti-mycobacterial agents against mmpL3: virtual screening, ADMET analysis and MD simulations. *J Mol Struct* 1244:130941
46. Salentin S, Schreiber S, Haupt VJ, Adasme MF, Schroeder M (2015) PLIP: fully automated protein–ligand interaction profiler. *Nucleic Acids Res* 43(W1):W443–W447
47. Norinder U, Bergström CA (2006) Prediction of ADMET properties. *Chem Enab Drug Discov* 1(9):920–937
48. Cheng F, Li W, Liu G, Tang Y (2013) In silico ADMET prediction: recent advances, current challenges and future trends. *Curr Top Med Chem* 13(11):1273–1289
49. Rao VS, Srinivas K (2011) Modern drug discovery process: an in silico approach. *J Bioinform Sequence Anal* 2(5):89–94
50. Pires DE, Blundell TL, Ascher DB (2015) pkCSM: predicting small-molecule pharmacokinetic and toxicity properties using graph-based signatures. *J Med Chem* 58(9):4066–4072
51. Sureja DK, Shah AP, Gajjar ND, Jadeja SB, Bodiwala KB, Dhameliya TM (2022) In-silico computational investigations of antiviral Lignan derivatives as potent inhibitors of SARS CoV-2. *ChemistrySelect* 7(28):e202202069
52. Van Der Spoel D, Lindahl E, Hess B, Groenhof G, Mark AE, Berendsen HJ (2005) GROMACS: fast, flexible, and free. *J Comput Chem* 26(16):1701–1718
53. Abraham MJ, Murtola T, Schulz R, Päll S, Smith JC, Hess B, Lindahl E (2015) GROMACS: high performance molecular simulations through multi-level parallelism from laptops to supercomputers. *SoftwareX* 1:19–25
54. Jo S, Kim T, Iyer VG, Im W (2008) CHARMM-GUI: a web-based graphical user interface for CHARMM. *J Comput Chem* 29(11):1859–1865
55. Vanommeslaeghe K, MacKerell AD Jr (2012) Automation of the CHARMM General Force Field (CGenFF) I: bond perception and atom typing. *J Chem Inf Model* 52(12):3144–3154
56. Baammi S, Daoud R, El Allali A (2023) Assessing the effect of a series of mutations on the dynamic behavior of phosphite dehydrogenase using molecular docking, molecular dynamics and quantum mechanics/molecular mechanics simulations. *J Biomol Struct Dyn* 41(9):4154–4166
57. Gumbart J, Khalili-Araghi F, Sotomayor M, Roux B (2012) Constant electric field simulations of the membrane potential illustrated with simple systems. *Biochimica et Biophysica Acta (BBA)* 1818(2):294–302
58. Bhandari S, Agrawal A, Kasana V, Tandon S, Boulaamane Y, Maurady A (2022) β -amino carbonyl derivatives: synthesis, molecular docking, ADMET, molecular dynamic and herbicidal studies. *ChemistrySelect* 7(48):e202201572
59. Boulaamane Y, Ahmad I, Patel H, Das N, Britel MR, Maurady A (2023) Structural exploration of selected C6 and C7-substituted coumarin isomers as selective MAO-B inhibitors. *J Biomol Struct Dyn* 41(6):2326–2340
60. Vegad UG, Gajjar ND, Nagar PR, Chauhan SP, Pandya DJ, Dhameliya TM (2023) In silico screening, ADMET analysis and MD simulations of phytochemicals of Onosma bracteata wall as SARS CoV-2 inhibitors. *3 Biotech* 13(7):221
61. Dhameliya TM, Nagar PR, Gajjar ND (2022) Systematic virtual screening in search of SARS CoV-2 inhibitors against spike glycoprotein: pharmacophore screening, molecular docking, ADMET analysis and MD simulations. *Mol Divers* 26(5):2775–2792
62. Firth NC, Brown N, Blagg J (2012) Plane of best fit: a novel method to characterize the three-dimensionality of molecules. *J Chem Inf Model* 52(10):2516–2525
63. Sosnin S, Karlov D, Tetko IV, Fedorov MV (2018) Comparative study of multitask toxicity modeling on a broad chemical space. *J Chem Inf Model* 59(3):1062–1072
64. Medina-Franco JL, Martínez-Mayorga K, Giulianotti MA, Houghten RA, Pinilla C (2008) Visualization of the chemical space in drug discovery. *Curr Comput Aided Drug Des* 4(4):322–333
65. Shahapure KR, Nicholas C (2020) Cluster quality analysis using silhouette score. In: 2020 IEEE 7th international conference on data science and advanced analytics (DSAA), pp 747–748. IEEE
66. Rousseeuw PJ (1987) Silhouettes: a graphical aid to the interpretation and validation of cluster analysis. *J Comput Appl Math* 20:53–65

67. Rosén J, Gottfries J, Muresan S, Backlund A, Oprea TI (2009) Novel chemical space exploration via natural products. *J Med Chem* 52(7):1953–1962
68. Pollastri MP (2010) Overview on the rule of five. *Curr Protoc Pharmacol* 49(1):9–12
69. Zhang L, Tan J, Han D, Zhu H (2017) From machine learning to deep learning: progress in machine intelligence for rational drug discovery. *Drug Discov Today* 22(11):1680–1685
70. Yang J, Hu J, Zhang G, Qin L, Wen H, Tang Y (2021) Pharmacophore modeling and 3D-QSAR study for the design of novel α -synuclein aggregation inhibitors. *J Mol Model* 27(9):260
71. Vittorio S, Adornato I, Gitto R, Peña-Díaz S, Ventura S, De Luca L (2020) Rational design of small molecules able to inhibit α -synuclein amyloid aggregation for the treatment of Parkinson's disease. *J Enzyme Inhib Med Chem* 35(1):1727–1735
72. Pettersen EF, Goddard TD, Huang CC, Couch GS, Greenblatt DM, Meng EC, Ferrin TE (2004) UCSF Chimera—a visualization system for exploratory research and analysis. *J Comput Chem* 25(13):1605–1612
73. Vats S, Kondabala R, Saxena S (2022) Identification of alpha-Synuclein disaggregator from Camellia sp. insight of molecular docking and molecular dynamics simulations. *ChemistrySelect* 7(10):e202104131
74. Mohankumar T, Chandramohan V, Lalithamba HS, Jayaraj RL, Kumaradhas P, Sivanandam M, Elangovan N (2020) Design and molecular dynamic investigations of 7, 8-dihydroxyflavone derivatives as potential neuroprotective agents against alpha-synuclein. *Sci Rep* 10(1):599
75. Boulaamane Y, Kandpal P, Chandra A, Britel MR, Maurady A (2023) Chemical library design, QSAR modeling and molecular dynamics simulations of naturally occurring coumarins as dual inhibitors of MAO-B and AChE. *J Biomol Struct Dyn* 1–18
76. Kufareva I, Abagyan R (2012) Methods of protein structure comparison. *Homol Model* 231–257
77. Taidi L, Maurady A, Britel MR (2022) Molecular docking study and molecular dynamic simulation of human cyclooxygenase-2 (COX-2) with selected eutropoids. *J Biomol Struct Dyn* 40(3):1189–1204
78. Durham E, Dorr B, Woetzel N, Staritzbichler R, Meiler J (2009) Solvent accessible surface area approximations for rapid and accurate protein structure prediction. *J Mol Model* 15:1093–1108
79. Haider S, Parkinson GN, Neidle S (2008) Molecular dynamics and principal components analysis of human telomeric quadruplex multimers. *Biophys J* 95(1):296–311
80. David CC, Jacobs DJ (2014) Principal component analysis: a method for determining the essential dynamics of proteins. *Protein Dyn* 193–226

Publisher's Note Springer Nature remains neutral with regard to jurisdictional claims in published maps and institutional affiliations.

Springer Nature or its licensor (e.g. a society or other partner) holds exclusive rights to this article under a publishing agreement with the author(s) or other rightsholder(s); author self-archiving of the accepted manuscript version of this article is solely governed by the terms of such publishing agreement and applicable law.

**CHAPTER VI: ANTIBIOTIC
DISCOVERY WITH ARTIFICIAL
INTELLIGENCE FOR THE
TREATMENT OF *ACINETOBACTER
BAUMANNII* INFECTIONS**

Global challenges presented by MDR *A. baumannii* infections have stimulated the development of new treatment strategies. OmpW is identified as a potential therapeutic target in *A. baumannii*. A library of 11,648 natural compounds underwent primary screening using QSAR models derived from a dataset of over 7,000 compounds with reported MIC values against *A. baumannii*. Structure-based virtual screening against OmpW followed. *In silico* pharmacokinetic evaluation assessed drug-likeness. The top ten compounds, mainly curcuminoids, exhibited binding energy scores ranging from -7.8 to -7.0 kcal/mol. Demethoxycurcumin emerged as the lead compound, showing promising binding stability and favorable pharmacokinetic properties. Experimental validation against a panel of *A. baumannii* strains confirmed antibacterial activity through microdilution and time-kill curve assays. Tests on an OmpW-deficient mutant compared to wild-type confirmed target binding. Demethoxycurcumin, alone and in combination with colistin, displayed activity against all *A. baumannii* strains and reduced bacterial interaction with host cells, indicating anti-virulence properties. This study underscores the potential of machine learning in discovering curcuminoids as antimicrobial agents against *A. baumannii* infections.

The details of this work are reported in the following publication.

Boulaamane, Y., Molina Panadero, I., Hmadcha, A., Atalaya Rey, C., Baammi, S., El Allali, A., ... & Smani, Y. (2024). Antibiotic discovery with artificial intelligence for the treatment of Acinetobacter baumannii infections. *Msystems*, e00325-24.

Available at: <https://doi.org/10.1128/msystems.00325-24>

Conceptualization: Y.B., A.M., Y.S.; Methodology: Y.B., I.M.P., A.H., S.B., A.E.; Investigation: Y.B., Y.S.; Visualization: Y.B., I.M.P.; Supervision: Y.S., A.M.; Writing-original draft: Y.B., Y.S.; Writing-review & editing: Y.B., Y.S.



8 | Open Peer Review | Antimicrobial Chemotherapy | Research Article

Antibiotic discovery with artificial intelligence for the treatment of *Acinetobacter baumannii* infections

Yassir Boulaamane,¹ Irene Molina Panadero,² Abdelkrim Hmadcha,^{3,4} Celia Atalaya Rey,² Soukayna Baammi,⁵ Achraf El Allali,⁵ Amal Maurady,^{1,6} Younes Smani^{2,3}

AUTHOR AFFILIATIONS See affiliation list on p. 14.

ABSTRACT Global challenges presented by multidrug-resistant *Acinetobacter baumannii* infections have stimulated the development of new treatment strategies. We reported that outer membrane protein W (OmpW) is a potential therapeutic target in *A. baumannii*. Here, a library of 11,648 natural compounds was subjected to a primary screening using quantitative structure-activity relationship (QSAR) models generated from a ChEMBL data set with >7,000 compounds with their reported minimal inhibitory concentration (MIC) values against *A. baumannii* followed by a structure-based virtual screening against OmpW. *In silico* pharmacokinetic evaluation was conducted to assess the drug-likeness of these compounds. The ten highest-ranking compounds were found to bind with an energy score ranging from -7.8 to -7.0 kcal/mol where most of them belonged to curcuminoids. To validate these findings, one lead compound exhibiting promising binding stability as well as favorable pharmacokinetics properties, namely demethoxycurcumin, was tested against a panel of *A. baumannii* strains to determine its antibacterial activity using microdilution and time-kill curve assays. To validate whether the compound binds to the selected target, an OmpW-deficient mutant was studied and compared with the wild type. Our results demonstrate that demethoxycurcumin in monotherapy and in combination with colistin is active against all *A. baumannii* strains. Finally, the compound was found to significantly reduce the *A. baumannii* interaction with host cells, suggesting its anti-virulence properties. Collectively, this study demonstrates machine learning as a promising strategy for the discovery of curcuminoids as antimicrobial agents for combating *A. baumannii* infections.

IMPORTANCE *Acinetobacter baumannii* presents a severe global health threat, with alarming levels of antimicrobial resistance rates resulting in significant morbidity and mortality in the USA, ranging from 26% to 68%, as reported by the Centers for Disease Control and Prevention (CDC). To address this threat, novel strategies beyond traditional antibiotics are imperative. Computational approaches, such as QSAR models leverage molecular structures to predict biological effects, expediting drug discovery. We identified OmpW as a potential therapeutic target in *A. baumannii* and screened 11,648 natural compounds. We employed QSAR models from a ChEMBL bioactivity data set and conducted structure-based virtual screening against OmpW. Demethoxycurcumin, a lead compound, exhibited promising antibacterial activity against *A. baumannii*, including multidrug-resistant strains. Additionally, demethoxycurcumin demonstrated anti-virulence properties by reducing *A. baumannii* interaction with host cells. The findings highlight the potential of artificial intelligence in discovering curcuminoids as effective antimicrobial agents against *A. baumannii* infections, offering a promising strategy to address antibiotic resistance.

KEYWORDS *Acinetobacter baumannii*, antimicrobial resistance, QSAR modeling, molecular modeling, antibacterial assays

Editor Neha Garg, Georgia Institute of Technology, Atlanta, Georgia, USA

Ad Hoc Peer Reviewer Simone Zuffa, University of California San Diego, La Jolla, California, USA

Address correspondence to Younes Smani, ysma@upo.es.

The authors declare no conflict of interest.

See the funding table on p. 14.

Received 6 March 2024

Accepted 27 March 2024

Published 3 May 2024

Copyright © 2024 Boulaamane et al. This is an open-access article distributed under the terms of the [Creative Commons Attribution 4.0 International license](#).

Antimicrobial resistance (AMR) in Gram-negative bacteria (GNB) has become a serious problem in recent years, with potentially devastating impacts on the economy and human life (1). The need for more effective and safer antimicrobial compounds has become increasingly urgent in the post-antibiotic era (1). *Acinetobacter baumannii*, one of the six superbug *Enterococcus faecium*, *Staphylococcus aureus*, *Klebsiella pneumoniae*, *Acinetobacter baumannii*, *Pseudomonas aeruginosa*, and *Enterobacter spp.* (ESKAPE) pathogens, is a global priority pathogen for the development of effective antimicrobial therapies, due to rapid changes in the genetic constitution of *A. baumannii* and the plasticity to acquire different resistance mechanisms (2–4). The scarce development of efficient antibiotics against this microorganism has sparked renewed scientific interest in finding effective antimicrobial agents capable of killing, inhibiting growth, or inhibiting the activity of essential virulence factors of *A. baumannii* (5).

The extensive functions of outer membrane proteins (OMPs) in GNB have led to their identification as potential drug targets (6). Among the OMPs, outer membrane protein W (OmpW) is a porin playing a pivotal role in the uptake of nutritional substances such as iron (7). Several studies have highlighted the relevance of OmpW as a potential drug target in GNB. For instance, researchers investigated how *A. baumannii* adapts to low oxygen conditions during infection. They found that OmpW was downregulated in hypoxic conditions. To understand its role as a virulence factor, they studied the effects of OmpW loss in *A. baumannii*. They discovered that the absence of OmpW reduced *in vitro* the bacterium's ability to adhere to and invade host cells, to cause cell death, and to form biofilm without affecting its growth and *in vivo* the pathogenicity of *A. baumannii* (8). Similarly, *Vibrio cholerae* mutant strains lacking OmpW showed reduced colonization in the mouse intestine compared with strains expressing OmpW (9). The collective evidence from these studies strongly suggests that OmpW plays a crucial role in bacterial pathogenesis and could be a promising target for the development of drugs aimed at combating GNB infections.

Natural products have long been a subject of great interest in the development of novel antimicrobial drugs (10). These products, derived from plants, animals, and microorganisms, have been used for centuries by various traditional medicine systems to treat infections (11).

Chemical libraries enable comprehensive virtual drug screening by offering a diverse range of compounds. Large databases enhance the integration of advanced methods like machine learning and artificial intelligence for accurate prediction of drug properties. For example, Massachusetts Institute of Technology (MIT) researchers used artificial intelligence to identify a potent new antibiotic known as halicin. This compound demonstrates efficacy against a wide range of bacteria, including some that exhibit resistance to all known antibiotics. Furthermore, halicin displayed no significant side effects in mice, prompting researchers to plan further development and clinical trials (12). Recently discovered by researchers at the University of Toronto in 2021, abaucin exhibits promising efficacy against the lethal superbug *A. baumannii*. Although still in early development, it holds significant potential in the treatment of drug-resistant infections (13).

Thus, the objective of the present study was to screen a large library of natural products with potential activity against *A. baumannii* using “*in silico*” and “*in vitro*” assays. The screening focused on compounds targeting the function of OmpW. A library of 11,648 natural compounds was retrieved from Ambinter chemical library, and an *in silico* approach combining data-driven and molecular modeling methods for drug discovery was employed. Artificial-based quantitative-structure activity relationship (QSAR) models were developed to predict the bioactivity of the natural products against *A. baumannii*. The retained compounds were subsequently subjected to molecular docking screens and absorption, distribution, metabolism, and excretion (ADME) evaluation to assess their pharmacological and pharmacokinetic profiles. The best compounds, which exhibited a strong affinity for OmpW along with favorable pharmacokinetic properties, were further evaluated through molecular dynamics simulations. Finally, a

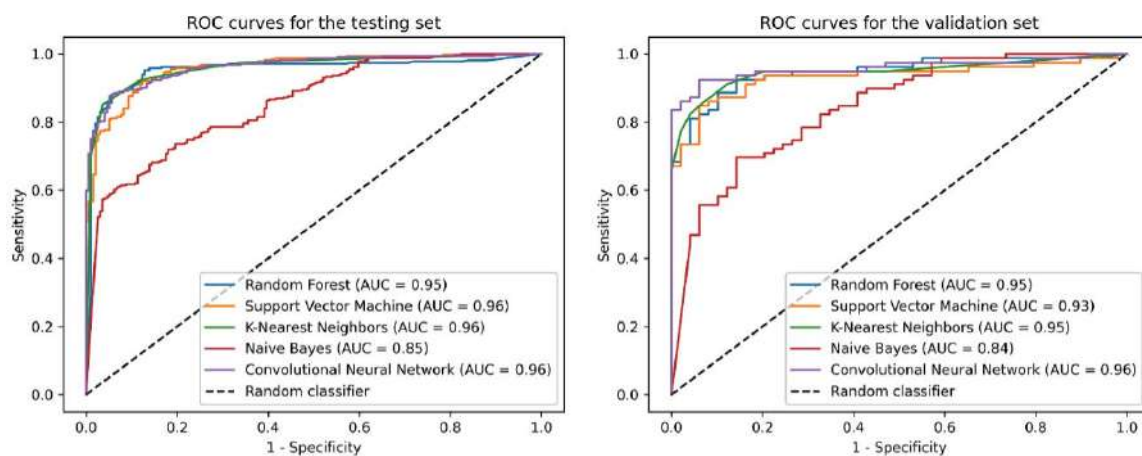


FIG 1 Performance of QSAR classification models on test and validation sets. The ROC curve and AUC values illustrate model performance. The CNN model resulted as the best classifier in the test and validation sets. QSAR: quantitative structure-activity relationship; ROC: receiver-operating characteristic; AUC: area under the curve; CNN: convolutional neural network.

lead candidate was subjected to *in vitro* testing to assess its potential for inhibiting *A. baumannii* growth.

RESULTS

QSAR screening

In this study, four machine learning algorithms known for their efficacy in QSAR modeling were chosen: random forest, support vector machine, k-nearest neighbors, and Gaussian naïve Bayes, based on previous reports of their performance (14). Furthermore, we have developed a convolutional neural network (CNN) using sequential architecture consisting of embedding, convolutional, pooling, flattened, and dense layers. Beginning with an embedding layer mapping input data to dense vectors, the model subsequently utilizes two convolutional layers with rectified linear unit (ReLU) activation for feature extraction, followed by max-pooling layers for dimensionality reduction. The flattened output is fed into dense layers, facilitating non-linear transformations and classification. With a final sigmoid activation layer for binary classification, the model is trained using binary cross-entropy loss and Adam optimizer, aiming to discern compound properties efficiently for screening active compounds against *A. baumannii*. The hyperparameters of the four machine learning classifiers underwent optimization using the GridSearchCV module within Scikit-Learn (v1.2.2) (15).

The performance of the QSAR classification models was evaluated using area under the curve (AUC) scores, with all models demonstrating excellent AUC values, as depicted

TABLE 1 Performance metrics of the generated classification models on the testing and validation sets^a

Data set	Model	SE	SP	Q+	Q-	ACC	F1 score	MCC
Testing set	Random forest	0.89	0.92	0.88	0.94	0.91	0.89	0.82
	Support vector machine	0.88	0.91	0.85	0.93	0.90	0.91	0.78
	k-nearest neighbors	0.88	0.93	0.88	0.92	0.91	0.92	0.80
	Naïve Bayes	0.58	0.96	0.96	0.56	0.72	0.72	0.53
	Convolutional neural network	0.83	0.96	0.95	0.88	0.90	0.92	0.81
Validation set	Random forest	0.86	0.91	0.86	0.91	0.89	0.91	0.77
	Support vector machine	0.81	0.91	0.86	0.87	0.87	0.89	0.72
	k-nearest neighbors	0.79	0.96	0.94	0.85	0.88	0.90	0.77
	Naïve Bayes	0.53	0.93	0.94	0.49	0.66	0.64	0.45
	Convolutional neural network	0.81	0.97	0.96	0.86	0.90	0.91	0.80

^aSE: sensitivity (true positive rate); SP: specificity (false positive rate); Q+: positive predictive value (precision); Q-: negative predictive value; ACC: accuracy; MCC: Matthews' correlation coefficient.

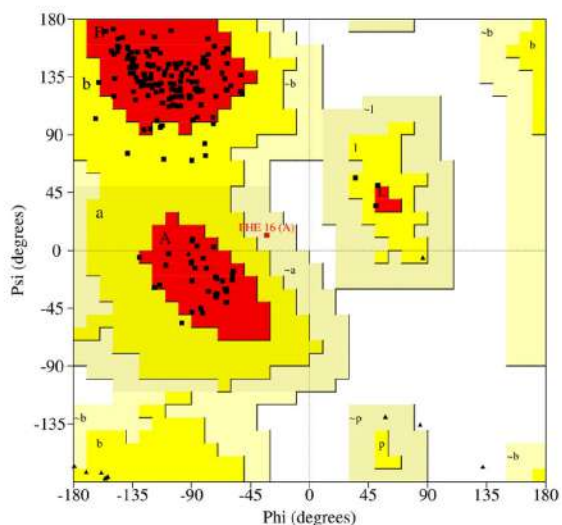
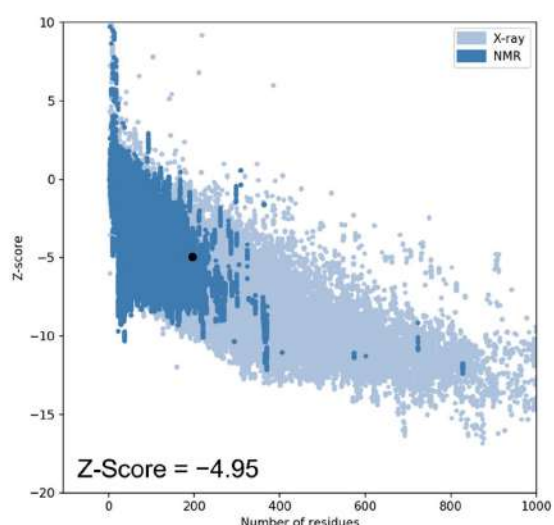
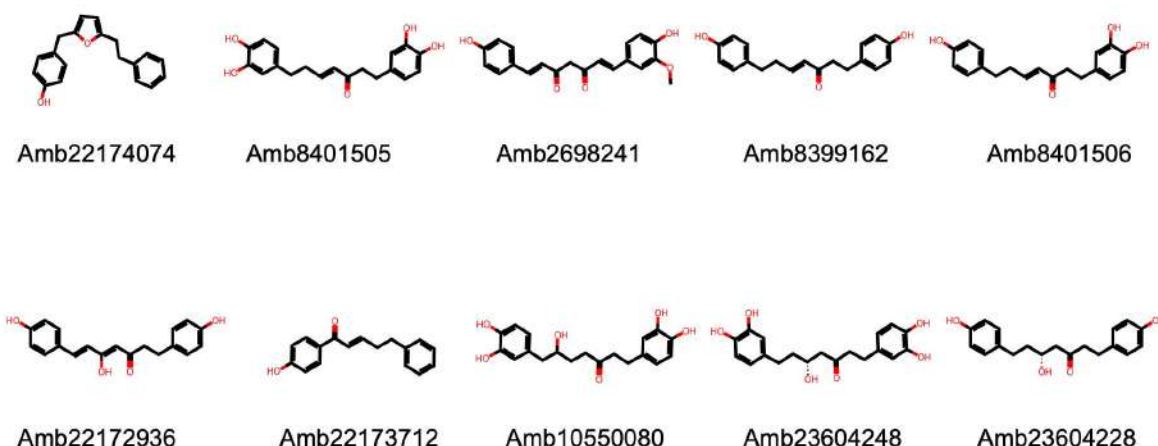
A**B****C**

FIG 2 Ramachandran plot for OmpW displaying the distribution of each amino acid within the favored, allowed, and disallowed regions (A). Scatter plot and Z-score revealing the overall model quality of OmpW (B). Chemical structures of the top ten highest-scoring compounds against OmpW. OmpW: outer membrane protein W (C).

in Fig. 1. Furthermore, the performance of QSAR models was assessed using various metrics such as precision, F1 score, accuracy, and Matthews correlation coefficient (MCC), as outlined in Table 1. Notably, the CNN model exhibited excellent performance on both the test and validation sets, achieving an AUC value of 0.96. Consequently, it was chosen to predict the activity of Ambinter drug-like natural compounds by comparing their molecular descriptors with those in the training data set and leveraging the learned relationships. At this step, 1,193 compounds were identified as active against *A. baumannii* and subsequently selected for the structure-based virtual screening study.

Docking screens of natural products

The quality assessment of the AlphaFold model of OmpW (Uniprot ID: A0A335FU53) (16, 17), according to Ramachandran plot, shows that 92.2% of residues are in the most favorable regions, 7.2% in allowed regions, 0.6% in generously disallowed regions, and 0.0% in disallowed regions. Validation of the OmpW structure using Protein Structure

Analysis-web (ProSA-web) shows a Z-score value of -4.95 , which is within the range of scores typically found for native proteins of similar size (Fig. 2A and B). The predicted active compounds were subjected to molecular docking screens, and their binding affinities were ranked accordingly. Specifically, we observed that the highest-ranking compounds exhibit binding scores ranging from -7.0 to -7.8 kcal/mol and belong to curcuminoids as shown in Fig. 3. The amino acids involved in the ligand binding are presented in Table 2.

Docking poses of the highest-ranking compounds are displayed in Fig. 3. In brief, the structural analysis of the docked compounds reveals consistent hydrogen bond formation between the hydroxyl (-OH) group of the phenyl ring in curcuminoids and the amino acid residue GLN-23. Furthermore, we detected additional hydrogen bond interactions implicating key residues, namely ASN-104, THR-109, and LYS-195, situated within the periplasmic site of OmpW. Additionally, our analysis reveals multiple instances of hydrophobic interactions, with notable involvement of amino acid residues PHE-59, HIS-101, ASN-144, and GLN-146.

ADME evaluation

A significant proportion, approximately 40%, of drug candidates fail during clinical trials primarily due to inadequate ADME properties (18). *In silico* ADME prediction offers a rapid method to assess the drug-likeness of a compound by calculating its physicochemical properties. This approach substantially reduces the time and resources required during the overall drug development process. In this study, SwissADME

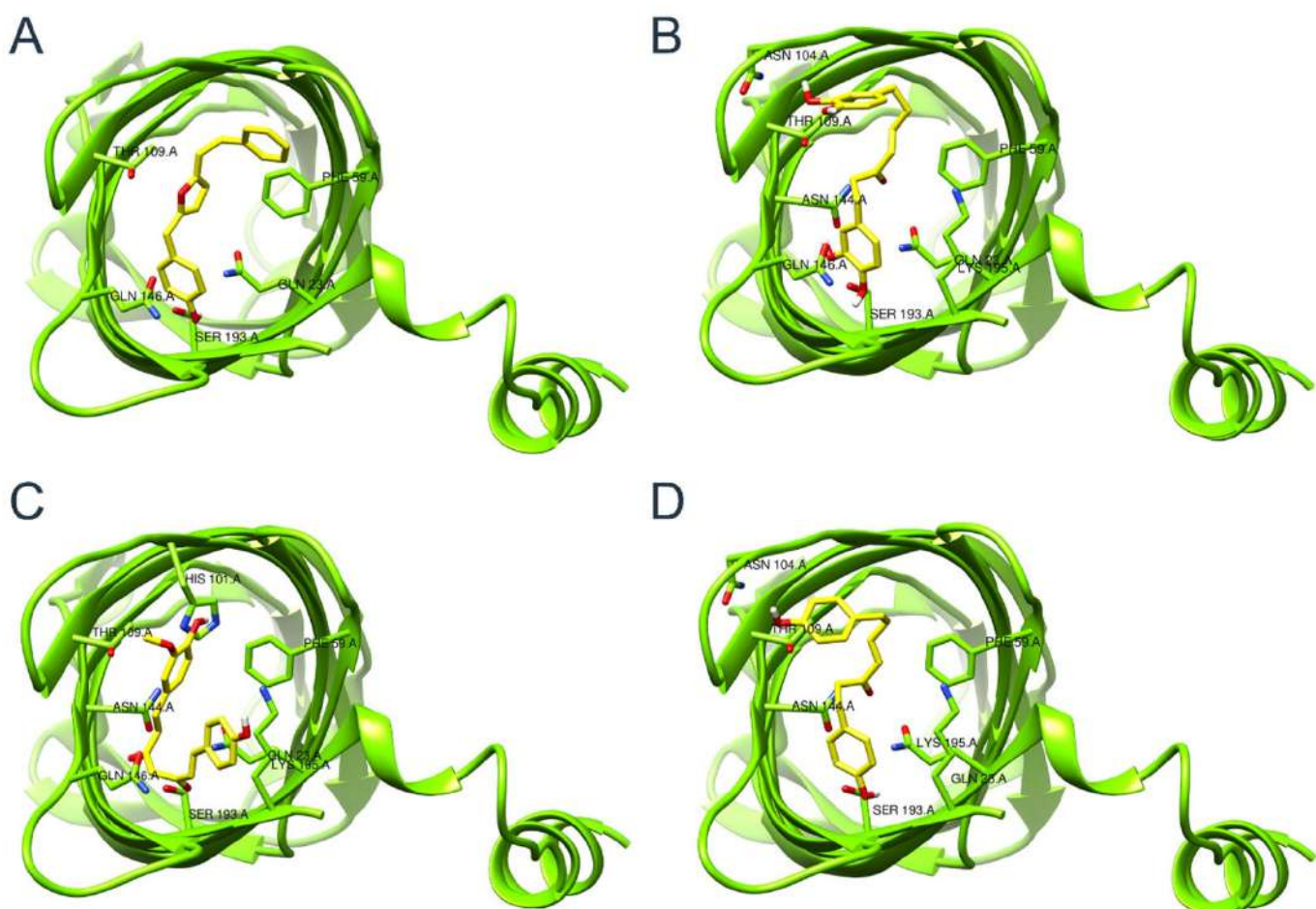


FIG 3 Binding conformations of the top four highest-ranking natural products: Amb22174074 (A), Amb8401505 (B), Amb2698241 (C), and Amb8399162 (D) in complex with OmpW's periplasmic region. OmpW: outer membrane protein W.

TABLE 2 Structure-based virtual screening results of the selected natural compounds against OmpW of *A. baumannii*

Compound	Binding score (kcal/mol)	Hydrogen bonds	Hydrophobic interactions
Amb22174074	-7.8	GLN-23, SER-193, LYS-195	PHE-59, HIS-101, ASN-144, GLN-146, LYS-195
Amb8401505	-7.7	GLN-23, PHE-102, ASN-104, ASN-144, TRP-153, SER-193	PHE-59, HIS-101, LYS-103, ASN-144, LYS-195
Amb2698241	-7.5	GLN-23, HIS-101, SER-193, LYS-195	PHE-59, THR-109, ASN-144, GLN-146, LYS-195
Amb8399162	-7.4	GLN-23, ASN-104, SER-193, LYS-195	PHE-59, LYS-103, THR-109, ASN-144, LYS-195
Amb8401506	-7.4	PHE-102, ASN-104, GLN-146, LYS-195	PHE-59, HIS-101, LYS-103, LYS-195
Amb22172936	-7.4	GLN-23, ARG-107, THR-109, TRP-153, LYS-195	HIS-101, LYS-103, THR-109, ASN-144, GLN-146, LYS-195
Amb22173712	-7.4	GLN-23, THR-109, SER-193, LYS-195	PHE-59, HIS-101, LYS-103, THR-109, ASN-144, GLN-146, LYS-195
Amb10550080	-7.3	GLN-23, ASN-104, THR-109, ASN-152, SER-193	PHE-59, HIS-101, LYS-195
Amb23604248	-7.2	ASN-104, THR-109, ASN-144, GLN-146, SER-193	PHE-59, LYS-103, THR-109
Amb23604228	-7.0	GLN-23, ASN-104, ASN-144, SER-193, LYS-195	GLN-23, ASN-104, ASN-144, SER-193, LYS-195

(<http://www.swissadme.ch/>) was employed to compute various pharmacokinetic properties of the highest-scoring compounds to evaluate their drug-likeness and suitability for further experimental studies (19). ADME properties for the selected compounds are shown in Table 3. The results reveal that all the compounds possess good lipophilicity in accordance with Lipinski's rule of five; moreover, water solubility values were found to be in the recommended range for most drugs. Intestinal absorption was found to be high in all the compounds. Of the top 10 compounds tested for blood-brain barrier (BBB) permeability, only five were found to be unable to penetrate the BBB. This is a crucial finding, as antibacterial compounds should not exert their effects on the central nervous system (CNS). None of the compounds were found to act as a P-glycoprotein substrate; thus, their bioavailability is not impacted by this protein. Finally, the pan-assay interference compounds (PAINS) test has revealed four compounds presenting one alert in their structure due to the presence of the catechol group, which can result in non-specific binding with various target proteins.

Molecular dynamics simulations and binding free energy

In the molecular docking study, the protein structure was treated as rigid. To gain deeper insights into the protein-ligand interactions, molecular dynamics simulations were performed on the docked complexes in a water environment for 100 ns. The root-mean square deviation (RMSD) was measured relative to the OmpW structure bound to the selected candidates. Fig. 4A illustrates the protein RMSD values for the top four complexes, showing a consistently stable RMSD of 0.3 nm during most of the simulation, except for Amb22174074, which displayed higher fluctuations exceeding 0.3 nm in the last 20 ns. The analysis of the ligand RMSD showed values between 0.1 and 0.25 nm for most ligands, suggesting minor conformational changes during the

TABLE 3 ADME properties' prediction results for the selected compounds

Compound	LogS	GI absorption	BBB	P-gp substrate	Bioavailability score	PAINS
Amb22174074	-4.88	High	Yes	No	0.55	0 alert
Amb8401505	-3.73	High	No	No	0.55	Catechol_A
Amb2698241	-3.92	High	No	No	0.56	0 alert
Amb8399162	-4.01	High	Yes	No	0.55	0 alert
Amb8401506	-3.87	High	Yes	No	0.55	Catechol_A
Amb22172936	-4.17	High	Yes	No	0.55	0 alert
Amb22173712	-4.02	High	Yes	No	0.55	0 alert
Amb10550080	-3.11	High	No	No	0.55	Catechol_A
Amb23604248	-3.11	High	No	No	0.55	Catechol_A
Amb23604228	-3.39	High	Yes	No	0.55	0 alert

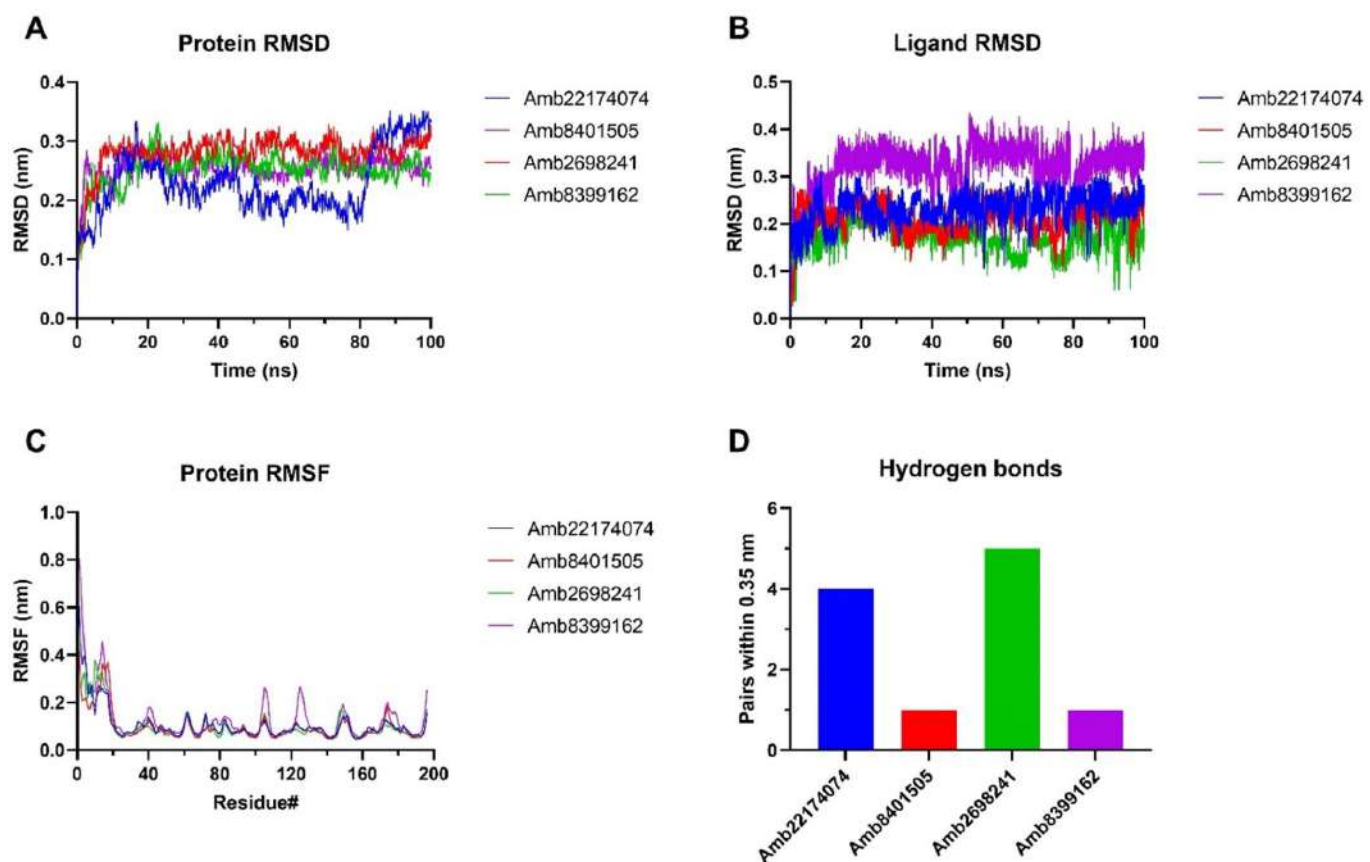


FIG 4 Molecular dynamics simulations analysis through protein RMSD (A), ligand RMSD (B), RMSF (C), and hydrogen bonds at 100 ns (D).

simulation. However, the ligand Amb8399162 deviated from this trend, with an RMSD of 0.35 nm, suggesting a more significant conformational change (Fig. 4B). In Fig. 5C, the graph illustrates the variations observed in each amino acid. Notably, the N-terminal region exhibited the highest fluctuations, which is a common characteristic. For all other residues, minor fluctuations of approximately 0.1 nm were observed, except for Amb8399162, which displayed fluctuations higher than 0.2 nm in certain regions of the periplasm. Finally, hydrogen bonds within a proximity of 0.35 nm were documented. Fig. 4D depicts the hydrogen bonds observed at 100 ns, with Amb2698241 forming four hydrogen bonds, highlighting its stable and consistent binding to the protein. The average free binding energy of the selected complexes was determined using the g_mmpbsa package (v1.6) (20, 21).

The binding energy was computed by combining the scores of Van der Waals energy, electrostatic energy, polar solvation, and SASA energy as presented in Table 4. The highest binding energy was observed in Amb2698241 (-45.23 kJ/mol), suggesting a strong binding to the target protein.

Antibacterial activity

The best compound exhibiting the lowest docking score as well as favorable ADME properties was demethoxycurcumin (Amb2698241). The MIC was then assessed using microdilution assays against different reference *A. baumannii* ATCC 17978 strains, its isogenic mutant deficient in OmpW, and colistin-resistant *A. baumannii* clinical isolates. Demethoxycurcumin inhibited bacterial growth at a concentration of 64 mg/L for all the studied strains (Table 5).

Colistin potentiation is critical for safeguarding this last resort antibiotic as it is often our only treatment option against highly resistant Gram-negative pathogens.

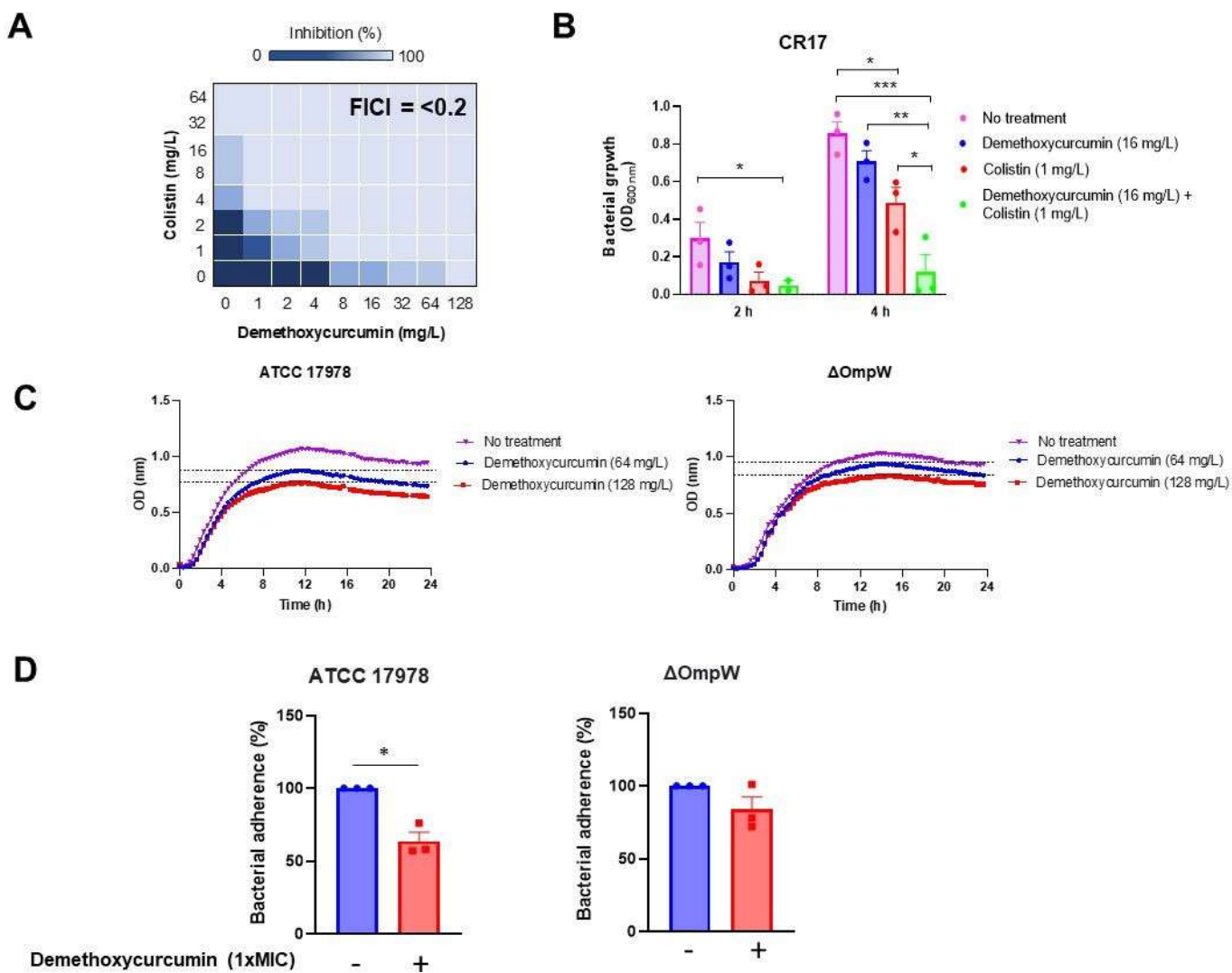


FIG 5 *In vitro* antibacterial activity of demethoxycurcumin. Representative heat plots of microdilution checkerboard assay for the combination of colistin and demethoxycurcumin against colistin-resistant *A. baumannii* CR17 strain (A). Bacterial growth for colistin and demethoxycurcumin monotherapy and combination therapy against colistin-resistant *A. baumannii* CR17 strain during 24 h incubation. The concentrations of colistin and demethoxycurcumin are 1 and 16 mg/L, respectively. The data are presented as means \pm standard errors of the means (SEM), and analysis of variance (ANOVA) test followed by the post hoc Tukey test was used for statistical analysis. * P < 0.05: colistin vs no treatment, demethoxycurcumin plus colistin vs no treatment, and demethoxycurcumin plus colistin vs colistin. ** P < 0.01: demethoxycurcumin plus colistin vs demethoxycurcumin, *** P < 0.001: demethoxycurcumin plus colistin vs no treatment (B). Bacterial growth curve plots of *A. baumannii* ATCC 17978 and *A. baumannii* ΔOmpW in the absence and presence of demethoxycurcumin treatment at different concentrations (C). Analysis of *A. baumannii* ATCC 17978 and ΔOmpW adhesion to HeLa host cells with and without demethoxycurcumin treatment. The data are presented as means \pm SEM, and student t-test was used for statistical analysis. * P < 0.05: treatment vs no treatment (D).

We examined whether demethoxycurcumin can sensitize colistin-resistant clinical strain CR17. Checkerboard assay showed that demethoxycurcumin at ≥ 1 mg/L demonstrated synergy with colistin against CR17 strain. Demethoxycurcumin at ≥ 8 mg/L in

TABLE 4 List of average and standard deviations of all energetic components including the binding energy taken from MM-PBSA analysis

Complex	MM-PBSA (kJ/mol)				
	ΔG_{bind}	ΔG_{vdW}	ΔG_{elec}	ΔG_{solv}	ΔG_{sasa}
Amb22174074	-35.03 ± 20.08	-118.74 ± 16.41	-45.52 ± 24.70	144.30 ± 33.25	-15.10 ± 1.63
Amb8401505	-41.92 ± 17.02	-122.42 ± 15.16	-42.96 ± 15.32	139.20 ± 22.25	-15.74 ± 1.58
Amb2698241	-45.23 ± 17.96	-115.48 ± 18.37	-37.25 ± 11.57	122.31 ± 23.21	-14.81 ± 1.54
Amb8399162	-39.11 ± 16.56	-143.59 ± 18.84	-35.11 ± 16.60	156.61 ± 30.64	-17.01 ± 1.94

TABLE 5 MIC results for the studied compounds against different wild-type, colistin-resistant, and OmpW-deficient *A. baumannii*

<i>A. baumannii</i> strain	MIC (mg/L)	
	Colistin	Demethoxycurcumin
ATCC 17978	0.25	64
ATCC17978 ΔOmpW	0.25	64
Ab11	256	64
Ab20	64	64
Ab21	128	64
Ab22	128	64
Ab99	64	64
Ab113	256	64
CR17	32	64

combination with colistin increased the activity of colistin against CR17 strain, with a fractional inhibitory concentration index (FICI) of <0.2 (Fig. 5A). In addition, the combination between 16 mg/L demethoxycurcumin and 1 mg/L colistin exhibited a synergistic effect during 2 and 4 h, reducing the bacterial growth compared with colistin demethoxycurcumin alone (Fig. 5B).

Using bacterial growth assays, we examined the antibacterial activity of demethoxycurcumin against ATCC 17978 and ΔOmpW strains. Figure 5C reveals that *A. baumannii* ATCC 17978 exhibits rapid growth, reaching 0.5 OD within the first 4 h. However, a noticeable disparity in growth is observed between the control sample and the samples treated with demethoxycurcumin, particularly at higher compound concentrations (2× MIC and 4× MIC). A similar trend of growth inhibition is observed in the ΔOmpW strain, although it demonstrates a higher OD value compared with *A. baumannii* ATCC 17978 in the presence of demethoxycurcumin treatment. This disparity in growth can be attributed to the resistance of the mutant strain to the compound, as the absence of OmpW may hinder the compound's ability to exert its effect, as indicated by the findings of the molecular docking study.

In addition, and to evaluate the effect of demethoxycurcumin on *A. baumannii* interaction with host cells, we studied the adherence of ATCC 17978 and ΔOmpW strains to HeLa cells for 2 h in the presence of demethoxycurcumin. Treatment with demethoxycurcumin at 1× MIC reduced the adherence of ATCC 17978 and ΔOmpW strains to HeLa cells by 36% and 16%, respectively (Fig. 5D).

DISCUSSION

In this study, we present a multi-stage approach for screening bioactive compounds from extensive databases. This approach combines data-driven QSAR models and structure-based virtual screening methods for drug discovery. Our classification models demonstrated strong performance in distinguishing between active and inactive compounds, achieving AUC values ranging from 0.85 to 0.96 for the testing set and 0.84 to 0.96 for the validation set. The results of molecular docking indicated binding affinities spanning from -5.4 to -7.8 kcal/mol. Notably, the top-scoring compounds belong to the curcuminoid chemical class, recognized for their antibacterial activities (22, 23).

Analysis of molecular interactions revealed a consistent hydrogen bond formation with GLN-23 in most of the compounds under study. Additional hydrophobic interactions involved the following amino acids: PHE-59, HIS-101, ASN-144, and GLN-146. Molecular dynamics analysis of the first four complexes displayed remarkable stability throughout the simulation, except for the tricyclic compound Amb22174074, which exhibited some deviations, leading to an RMSD of 0.3 nm. This observation could be attributed to the inherent limited flexibility of this compound, prompting conformational changes in the protein.

Furthermore, our investigation identified van der Waals energy as the primary contributor to the stability of the complexes, as determined by the MMPBSA method. To

validate our *in silico* results, we assessed a lead candidate, demethoxycurcumin, for its *in vitro* activity in monotherapy and in combination with colistin against an extensive range of *A. baumannii* strains, including colistin-resistant strains. This lead candidate presents an antibacterial activity as shown by microdilution and time-kill curve assays. Notably, a reduction in compound activity against OmpW-deficient mutant has been observed in the time-kill curve assay. Li et al. showed that demethoxycurcumin present antibacterial activity in monotherapy and in combination with gentamicin against another pathogen, methicillin-resistant *Staphylococcus aureus* (24).

Our findings suggest the crucial role of the OmpW in facilitating the compound's activity. Previous studies reported the binding of colistin and tamoxifen metabolites to OmpW (25, 26).

Bacterial adhesion to and invasion into host cells are important steps in causing *A. baumannii* infection (27). It is well-known that OmpW plays a key role in host-pathogen interactions. Deletion of OmpW reduced *A. baumannii*'s adherence and invasion into host cells, as well as its cytotoxicity (8). Similarly, in the absence of OprG, which is homologous to OmpW in *P. aeruginosa*, this pathogen was significantly less cytotoxic against human bronchial epithelial cells (28). OmpW is essential for *A. baumannii* to disseminate between organs and to cause the death of mice, as observed for other pathogens such as *V. cholerae* (9). Motley et al. reported an increase in OmpW expression during *E. coli* infection in a murine granulomatous pouch model (29), and OmpW has been shown to protect *E. coli* against host responses, conferring resistance to complement-mediated killing and phagocytosis (30, 31). All these previous studies indicated that OmpW could be a potential drug target in GNB to develop new treatments. However, no data have been reported on the effect of natural products on host-*A. baumannii* interactions. To our knowledge, this study provides the first evidence for the effect of demethoxycurcumin in reducing *A. baumannii*'s adherence to host cells. Moreover, this effect is consistent with time-kill curve data. Further studies are needed, such as animal infection models, to validate the potential use of demethoxycurcumin as monotherapy and in combination with antibiotics used in clinical settings.

In summary, this study demonstrated a multi-step computational and experimental approach to identify natural products as potential therapeutics targeting the OmpW protein of *A. baumannii*. Demethoxycurcumin was validated as an active lead compound both *in vitro* and in reducing bacterial interaction with host cells. Further investigations are necessary, such as testing in animal models of infection, to validate the therapeutic potential of targeting OmpW by demethoxycurcumin and related natural products.

MATERIALS AND METHODS

QSAR modeling

A bioactivity data set from the ChEMBL database, which comprised the chemical structures of 11,014 compounds along with their reported MIC values against *A. baumannii*, was acquired (32). To ensure the reliability of the data, the data set by only keeping those with MIC values of the same unit (mg/L) was carefully curated. For duplicate compounds with multiple reported activities, a mean value was calculated, and only one entry was kept in the study using the Pandas (v2.2.0) library in Python (33). The processed data set consisted of 3,196 compounds. To classify the compounds, molecules with reported MIC values < 32 were labeled as active, whereas molecules with MIC > 64 were labeled as inactive. This resulted in 1,310 active compounds and 816 inactive compounds. For further analysis, the RDKit cheminformatics suite (v2023.09.4) was used to generate 2,048 bits of molecular descriptors using Morgan fingerprints (34, 35). These descriptors were derived from the compounds' Simplified Molecular-Input Line-Entry System (SMILES) representation and were based on the widely used extended-connectivity fingerprints (ECFP4) (36).

To support the training and assessment of our QSAR models, we partitioned the data sets into a unified train/test set (80%) and a distinct validation set (20%). Within the

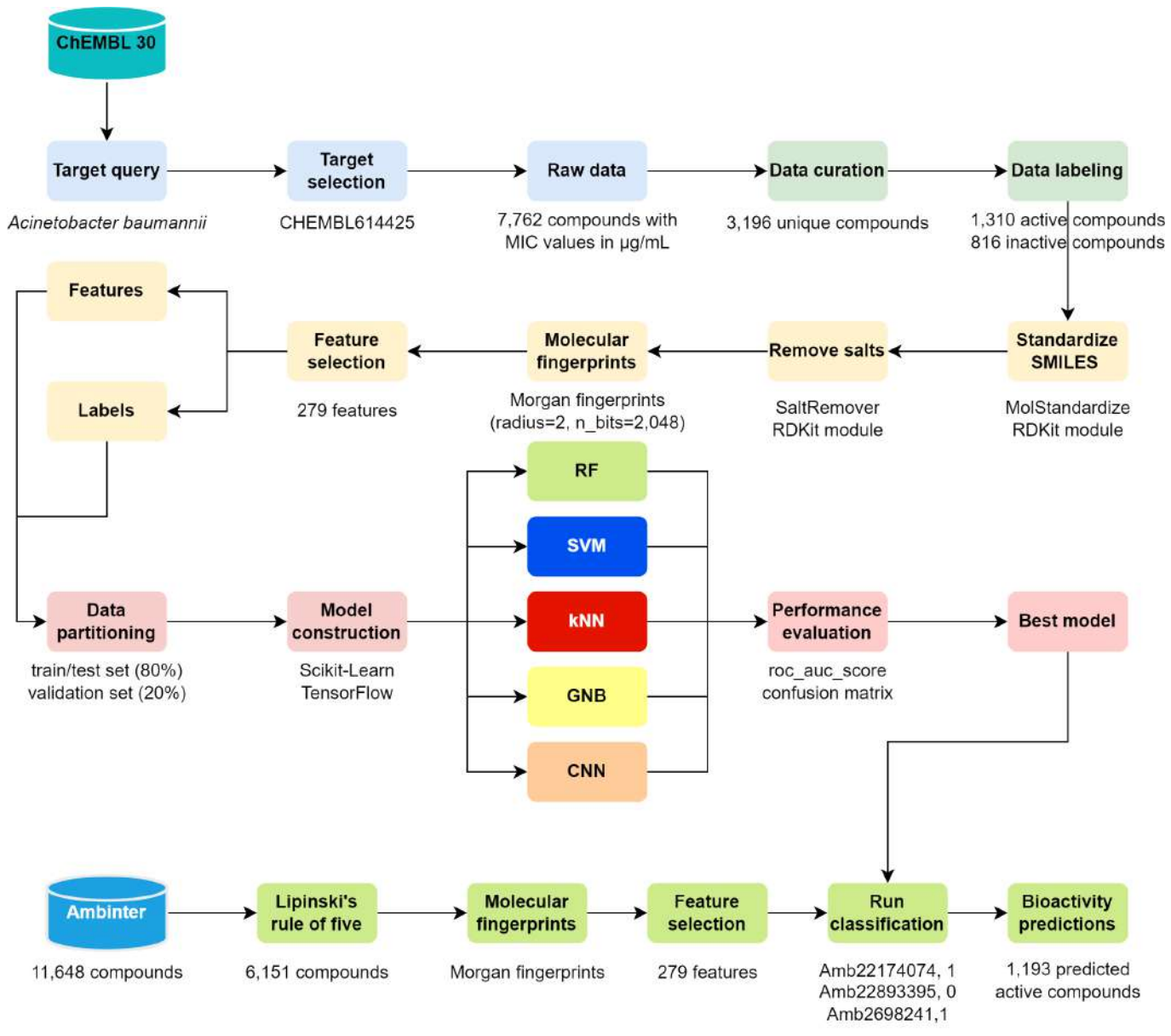


FIG 6 The QSARBioPred workflow outlines the processes involved in constructing QSAR models aimed at predicting the likelihood of a compound being active against *A. baumannii*. This involves generating molecular fingerprints of the compounds and employing machine learning techniques to discern patterns correlated with activity. Subsequently, the model enables the screening of novel compounds for potential activity against *A. baumannii*.

train/test set, an 80/20 split further divided the data into train and test subsets for model training and evaluation, respectively. The validation set was exclusively allocated for the final evaluation of the selected model's performance on unseen data, as depicted in Fig. 6. A standard workflow for our proposed QSAR approach, along with the source code, can be found in the GitHub repository (<https://github.com/yboulaamane/QSARBioPred/>).

Protein structure preparation

To refine and enhance the quality of the 3D protein model, the online server GalaxyRefine (<https://galaxy.seoklab.org/cgi-bin/submit.cgi?type=REFINE>) was used (37). The platform employs a multi-step approach that involves side-chain rebuilding, side-chain repacking, and molecular dynamics simulation to achieve overall structure relaxation. Subsequently, the PROCHECK algorithm was employed through the SAVES webserver

(<https://saves.mbi.ucla.edu/>) (38) to generate Ramachandran plots, whereas ProSA-web was used to assess model accuracy and statistical significance using a knowledge-based potential (39).

Binding site detection

The plausible binding pockets for the selected OmpW protein structure were predicted using PrankWeb ligand binding site prediction webserver (<https://prankweb.cz/>) (40). Fig. S1 depicts the 3D structure of OmpW with their predicted binding pockets shown as residues with different colors. The predicted binding pockets scores, grid coordinates, and residue IDs are shown in Table S1.

Structure-based virtual screening

The natural compounds were retrieved from Ambinter natural compounds library (<https://www.ambinter.com/>). Eleven thousand six hundred forty-eight compounds were evaluated for their drug-likeness by computing their physicochemical properties such as molecular weight, LogP, number of hydrogen bond donors/acceptors, and the number of rotatable bonds DataWarrior (v06.01.00) (41). According to Lipinski's rule of five, only 6,151 compounds were retained for further analysis (42). Structure-based virtual screening was performed using AutoDock Vina (v1.1.2) with a Perl script to automate the molecular docking process as published in our previous study (43, 44). The 3D structure of OmpW was optimized using AutoDockTools (v1.5.6) by adding polar hydrogens and computing Kollman charges (45). The grid box was centered around the coordinates provided by PrankWeb for the best-scoring pockets. The pocket (2) located near the periplasmic of the β-barrel structure was selected for molecular docking as mentioned in the literature (46).

Docking snapshots were generated using UCSF Chimera 1.17.3 (47). Molecular interactions were visualized using Protein-Ligand Interaction Profiler (<https://plip-tool.bioteclab.de/plip-web/plip/index>) (48).

Molecular dynamics simulations and binding free energy calculation

Molecular dynamics simulations were performed using GROMACS (v2019.3) (49, 50) to evaluate the stability of selected candidates in complexes with OmpW. The CHARMM36 force field generated the protein topology file, whereas the CGENFF server assigned parameters to ligands (51). TIP3P water model solvated the protein-ligand systems in a cubic box, with Na⁺ and Cl⁻ ions added for charge neutrality. To optimize the energy, the steepest descent technique was employed, setting Fmax not to exceed 1,000 kJ/mol/nm. Subsequently, two consecutive 1 ns simulations using canonical constant number of molecules, volume and temperature (T) (NVT) and isobaric constant number of molecules, pressure and temperature (NPT) ensembles were performed to equilibrate the systems at 300 Kelvin and 1 bar pressure. All simulations were conducted under periodic boundary conditions (PBC), and long-range electrostatic interactions were handled using the particle mesh Ewald method (52). For data collection, 100 ns molecular dynamics simulations were conducted. To analyze the dynamic behavior of the selected complexes, various geometric properties such as root-mean-square deviation (RMSD), root-mean-square fluctuation (RMSF), and hydrogen bonds were calculated using GROMACS (v2019.3) (53).

The binding free energies of the screened complexes were calculated using the molecular mechanics Poisson–Boltzmann surface area (MM-PBSA) method (54). The binding free energy ($\Delta E_{\text{binding}}$) is determined using the following equations:

$$\Delta E_{\text{binding}} = E_{\text{complex}} - (E_{\text{inhibitor}} + E_{\text{OmpW}}) \quad (1)$$

Equation 1 is the total MMPBSA energy of the protein-ligand complex, where E_{OmpW} and $E_{\text{inhibitor}}$ are the isolated proteins and ligands' total free energies in solution, respectively.

$$\Delta G_{\text{binding}} = \Delta G_{\text{vdW}} + \Delta G_{\text{elec}} + \Delta G_{\text{solv}} + \Delta G_{\text{sasa}} \quad (2)$$

Equation 2 defines the generalized MMPBSA as the sum of four energies: electrostatic (ΔG_{elec}), van der Waals (ΔG_{vdw}), polar (ΔG_{solv}), and SASA (ΔG_{sasa}).

Antibacterial activity assays

Microdilution assay

The MIC of demethoxycurcumin was determined against ATCC 17978 strain, an isogenic mutant deficient in OmpW, and seven colistin-resistant *A. baumannii* clinical strains, along with 24 clinical strains, in two independent experiments using the broth microdilution method, in accordance with the standard guidelines of the European Committee on Antimicrobial Susceptibility Testing (EUCAST) (55). A 5×10^5 CFU/mL inoculum of each strain was cultured in Luria Bertani (LB) and added to U bottom microtiter plates (Deltlab, Spain) containing demethoxycurcumin. The plates were incubated for 18 h at 37°C.

Bacterial growth curve assay

To determine the antibacterial activity, bacterial growth curves of the ATCC 17978 strain and its isogenic deficient in OmpW (ΔE_{OmpW}) and CR17 strain were performed in triplicate in 96-well plate (Deltlab, Spain). An initial inoculum of 5×10^5 CFU/mL was prepared in LB in the presence of 1x MIC, 2x MIC, and 4x MIC of demethoxycurcumin. A drug-free broth was evaluated in parallel as a control. Plates were incubated at 37°C with shaking, and bacterial growth was monitored for 24 h using a microtiter plate reader (Tecan Spark, Austria).

Checkerboard assay

The assay was performed on a 96-well plate in duplicate as previously described (56). Colistin was 2-fold serially diluted along the x axis, whereas demethoxycurcumin was 2-fold serially diluted along the y axis to create a matrix, where each well consists of a combination of both agents at different concentrations. Bacterial cultures grown overnight were then diluted in saline to 0.5 McFarland turbidity, followed by 1:50 further dilution LB and inoculation on each well to achieve a final concentration of approximately 5.5×10^5 CFU/mL. The 96-well plates were then incubated at 37°C for 18 h and examined for visible turbidity. The fractional inhibitory concentration (FIC) of the colistin was calculated by dividing the MIC of colistin in the presence of demethoxycurcumin by the MIC of colistin alone. Similarly, the FIC of demethoxycurcumin was calculated by dividing the MIC of demethoxycurcumin in the presence of colistin by the MIC of rafloxanide alone. The FIC index was the summation of both FIC values. FIC index values of ≤ 0.5 were interpreted as synergistic.

Human cell culture

HeLa cells were grown in 24-well plates in Dulbecco's Modified Eagle medium (DMEM) supplemented with 10% heat-inactivated fetal bovine serum (FBS), vancomycin (50 mg/L), gentamicin (20 mg/L), amphotericin B (0.25 mg/L) (Invitrogen, Spain), and 1% 4-(2-hydroxyethyl)-1-piperazineethanesulfonic acid (HEPES) in a humidified incubator with 5% CO₂ at 37°C. HeLa cells were routinely passaged every 3 or 4 days. Immediately before infection, HeLa cells were washed three times with prewarmed phosphate buffered saline (PBS) and further incubated in DMEM without FBS and antibiotics (57).

Adhesion assay

HeLa cells were infected with 1×10^8 CFU/mL of *A. baumannii* ATCC 17978 and Δ OmpW strains in the absence and presence of 1x MIC of demethoxycurcumin at a multiplicity of infection (MOI) of 100 for 2 h with 5% CO₂ at 37°C. Subsequently, infected HeLa cells were washed five times with prewarmed PBS and lysed with 0.5% Triton X-100. Diluted lysates were plated onto LB agar (Merck, Spain) and incubated at 37°C for 24 h for enumeration of developed colonies and then the determination of the number of bacteria that attached to HeLa cells (8). All experiments were performed in triplicate.

Statistical analysis

The GraphPad Prism 9 (version 9.3.1; GraphPad Software, LLC.) statistical package was used. Group data are presented as bar plots and means \pm standard errors of the means (SEM). To determine differences between means, an ANOVA test followed by the *post hoc* Tukey test and Student *t*-test was used for the bacterial growth assay and the adherence/invasion assay, respectively. *P* value of <0.05 was considered significant.

ACKNOWLEDGMENTS

This work was co-funded by the Consejería de Universidad e Investigación e Innovación de la Junta de Andalucía (grant ProyExcel_00116) and funded by the Instituto de Salud Carlos III, Subdirección General de Redes y Centros de Investigación Cooperativa, Ministerio de Economía, and Industria y Competitividad (grant PI19/01009), cofinanced by the European Development Regional Fund (A way to achieve Europe, Operative Program Intelligent Growth 2014 to 2020). Y.B. is supported by ERASMUS+ Student Mobility for Traineeships.

Conceptualization: Y.B., A.M., and Y.S.; Methodology: Y.B., I.M.P., A.H., C.A.R., S.B., and A.E.A.; Investigation: Y.B. and Y.S.; Visualization: Y.B. and I.M.P.; Supervision: Y.S. and A.M.; Writing-original draft: Y.B. and Y.S.; Writing-review & editing: Y.B. and Y.S.

AUTHOR AFFILIATIONS

¹Laboratory of Innovative Technologies, National School of Applied Sciences of Tangier, Abdelmalek Essaadi University, Tetouan, Morocco

²Centro Andaluz de Biología del Desarrollo, Universidad Pablo de Olavide/CSIC/Junta de Andalucía, Seville, Spain

³Departamento de Biología Molecular e Ingeniería Bioquímica, Universidad Pablo de Olavide, Seville, Spain

⁴Biosanitary Research Institute (IIB-VIU), Valencian International University (VIU), Valencia, Spain

⁵Bioinformatics Laboratory, College of Computing, Mohammed VI Polytechnic University, Benguerir, Morocco

⁶Faculty of Sciences and Techniques of Tangier, Abdelmalek Essaadi University, Tetouan, Morocco

AUTHOR ORCIDs

Abdelkrim Hmadcha  <http://orcid.org/0000-0002-4105-3702>

Younes Smani  <http://orcid.org/0001-9302-8384>

FUNDING

Funder	Grant(s)	Author(s)
Consejería de Universidad, Investigación e Innovación de la Junta de Andalucía	ProyExcel_00116	Younes Smani
Instituto de Salud Carlos III	PI19/01009	Younes Smani

DATA AVAILABILITY

The data that support the findings of this study are available from the corresponding author upon reasonable request.

ADDITIONAL FILES

The following material is available [online](#).

Supplemental Material

Figure S1 (mSystems00325-24-S0001.pdf). 3D structure and protein sequence of OmpW.

Table S1 (mSystems00325-24-S0002.pdf). Predicted binding pockets for OmpW.

Open Peer Review

PEER REVIEW HISTORY (review-history.pdf). An accounting of the reviewer comments and feedback.

REFERENCES

1. World Health Organization Global research agenda for antimicrobial resistance in human health Policy brief. 2023. Available from: https://cdn.who.int/media/docs/default-source/antimicrobial-resistance/amr-spc-npm/who-global-research-agenda-for-amr-in-human-health---policy-brief.pdf?sfvrsn=f86aa073_4&download=true
2. Tacconelli E, Carrara E, Savoldi A, Harbarth S, Mendelson M, Monnet DL, Pulcini C, Kahlmeter G, Kluytmans J, Carmeli Y, Ouellette M, Outterson K, Patel J, Cavalieri M, Cox EM, Houchens CR, Grayson ML, Hansen P, Singh N, Theuretzbacher U, Magrini N, WHO Pathogens Priority List Working Group. 2018. Discovery, research, and development of new antibiotics: the WHO priority list of antibiotic-resistant bacteria and tuberculosis. *Lancet Infect Dis* 18:318–327. [https://doi.org/10.1016/S1473-3099\(17\)30753-3](https://doi.org/10.1016/S1473-3099(17)30753-3)
3. Harding CM, Hennon SW, Feldman MF. 2018. Uncovering the mechanisms of *Acinetobacter baumannii*. *Nat Rev Microbiol* 16:91–102. <https://doi.org/10.1038/nrmicro.2017.148>
4. Theuretzbacher U, Bush K, Harbarth S, Paul M, Rex JH, Tacconelli E, Thwaites GE. 2020. Critical analysis of antibacterial agents in clinical development. *Nat Rev Microbiol* 18:286–298. <https://doi.org/10.1038/s41579-020-0340-0>
5. Theuretzbacher U, Outterson K, Engel A, Karlén A. 2020. The global preclinical antibacterial pipeline. *Nat Rev Microbiol* 18:275–285. <https://doi.org/10.1038/s41579-019-0288-0>
6. Walker SS, Black TA. 2021. Are outer-membrane targets the solution for MDR gram-negative bacteria? *Drug Discov Today* 26:2152–2158. <https://doi.org/10.1016/j.drudis.2021.03.027>
7. Schmitt BL, Leal BF, Leyser M, de Barros MP, Trentin DS, Ferreira CAS, de Oliveira SD. 2023. Increased Ompw and Ompa expression and higher virulence of *Acinetobacter baumannii* Persister cells. *BMC Microbiol* 23:157. <https://doi.org/10.1186/s12866-023-02904-y>
8. Gil-Marqués ML, Pachón J, Smani Y. 2022. iTRAQ-based quantitative proteomic analysis of *Acinetobacter baumannii* under hypoxia and normoxia reveals the role of Ompw as a virulence factor. *Microbiol Spectr* 10:e0232821. <https://doi.org/10.1128/spectrum.02328-21>
9. Nandi B, Nandy RK, Sarkar A, Ghose AC. 2005. Structural features, properties and regulation of the outer-membrane protein W (Ompw) of *Vibrio cholerae*. *Microbiology (Reading)* 151:2975–2986. <https://doi.org/10.1099/mic.0.27995-0>
10. Chassagne F, Samarakoon T, Porras G, Lyles JT, Dettweiler M, Marquez L, Salam AM, Shabih S, Farrokhi DR, Quave CL. 2020. A systematic review of plants with antibacterial activities: a taxonomic and phylogenetic perspective. *Front Pharmacol* 11:586548. <https://doi.org/10.3389/fphar.2020.586548>
11. Anand U, Jacobo-Herrera N, Altemimi A, Lakhssassi N. 2019. A comprehensive review on medicinal plants as antimicrobial therapeutics: potential avenues of biocompatible drug discovery. *Metabolites* 9:258. <https://doi.org/10.3390/metabo9110258>
12. Stokes JM, Yang K, Swanson K, Jin W, Cubillos-Ruiz A, Donghia NM, MacNair CR, French S, Carfrae LA, Bloom-Ackermann Z, Tran VM, Chiappino-Pepe A, Badran AH, Andrews IW, Chory EJ, Church GM, Brown ED, Jaakkola TS, Barzilay R, Collins JJ. 2020. A deep learning approach to antibiotic discovery. *Cell* 180:688–702. <https://doi.org/10.1016/j.cell.2020.01.021>
13. Liu G, Catacutan DB, Rathod K, Swanson K, Jin W, Mohammed JC, Chiappino-Pepe A, Syed SA, Fragis M, Rachwalski K, Magolan J, Surette MG, Coombes BK, Jaakkola T, Barzilay R, Collins JJ, Stokes JM. 2023. Deep learning-guided discovery of an antibiotic targeting *Acinetobacter baumannii*. *Nat Chem Biol* 19:1342–1350. <https://doi.org/10.1038/s41589-023-01349-8>
14. Wu Z, Zhu M, Kang Y, Leung EL-H, Lei T, Shen C, Jiang D, Wang Z, Cao D, Hou T. 2021. Do we need different machine learning Algorithms for QSAR modeling? a comprehensive assessment of 16 machine learning Algorithms on 14 QSAR data SETS. *Brief Bioinform* 22:bbaa321. <https://doi.org/10.1093/bib/bbaa321>
15. Pedregosa F, Varoquaux G, Gramfort A, Michael V, Thirion B, Grisel O, Blondel M, Prettenhofer P, Weiss R, Dubourg V, Vanderplas J, Passos A, Cournapeau D, Brucher M, Perrot M, Duchesnay E. 2011. Scikit-learn: Machine learning in Python. *J Machine Learning Res* 12:2825–2830.
16. Jumper J, Evans R, Pritzel A, Green T, Figurnov M, Ronneberger O, Tunyasuvunakool K, Bates R, Žídek A, Potapenko A, et al. 2021. Highly accurate protein structure prediction with AlphaFold. *Nature* 596:583–589. <https://doi.org/10.1038/s41586-021-03819-2>
17. Varadi M, Anyango S, Deshpande M, Nair S, Natassia C, Yordanova G, Yuan D, Stroe O, Wood G, Laydon A, et al. 2022. AlphaFold protein structure database: massively expanding the structural coverage of protein-sequence space with high-accuracy models. *Nucleic Acids Res* 50:D439–D444. <https://doi.org/10.1093/nar/gkab1061>
18. Gombar VK, Silver IS, Zhao Z. 2003. Role of ADME characteristics in drug discovery and their in Silico evaluation: *in silico* screening of chemicals for their metabolic stability. *Curr Top Med Chem* 3:1205–1225. <https://doi.org/10.2174/1568026033452014>
19. Daina A, Michelin O, Zoete V. 2017. Swissadme: a free web tool to evaluate pharmacokinetics, drug-likeness and medicinal chemistry friendliness of small molecules. *Sci Rep* 7:42717. <https://doi.org/10.1038/srep42717>
20. Baker NA, Sept D, Joseph S, Holst MJ, McCammon JA. 2001. Electrostatics of nanosystems: application to microtubules and the ribosome. *Proc Natl Acad Sci U S A* 98:10037–10041. <https://doi.org/10.1073/pnas.181342398>

21. Kumari R, Kumar R. 2014. Open source drug discovery consortium, Lynn, A. G_Mmpbsa A GROMACS tool for high-throughput MM-PBSA calculations. *J Chem Inf Model* 54:1951–1962. <https://doi.org/10.1021/ci500020m>
22. Betts JW, Wareham DW. 2014. In vitro activity of Curcumin in combination with Epigallocatechin Gallate (EGCG) versus multidrug-resistant *Acinetobacter baumannii*. *BMC Microbiol* 14:1–5. <https://doi.org/10.1186/1471-2180-14-172>
23. Othman AS, Shamekh IM, Abdalla M, Eltayb WA, Ahmed NA. 2023. Molecular modeling study of Micro and nanocurcumin with *in vitro* and *in vivo* Antibacterial validation. *Sci Rep* 13:12224. <https://doi.org/10.1038/s41598-023-38652-2>
24. Li Q-Q, Kang O-H, Kwon D-Y. 2021. Study on demethoxycurcumin as a promising approach to reverse methicillin-resistance of *Staphylococcus aureus*. *Int J Mol Sci* 22:3778. <https://doi.org/10.3390/ijms22073778>
25. Catel-Ferreira M, Marti S, Guillou L, Jara L, Coadou G, Molle V, Bouffartigues E, Bou G, Shalk I, Jouenne T, Vila-Farrés X, Dé E. 2016. The outer membrane porin Ompw of *Acinetobacter baumannii* is involved in iron uptake and Colistin binding. *FEBS Lett* 590:224–231. <https://doi.org/10.1002/1873-3468.12050>
26. Vila-Domínguez A, Molino Panadero I, Pachón J, Jiménez Mejías ME, Smani Y. 2022. Abstr acinetovibes. identification of the outer membrane protein W (Ompw) as the potential target of tamoxifen metabolites in *Acinetobacter baumannii*. a two-day virtual conference on acinetobacter research
27. Smani Y, Docobo-Pérez F, López-Rojas R, Domínguez-Herrera J, Ibáñez-Martínez J, Pachón J. 2012. Platelet-activating factor receptor initiates contact of *Acinetobacter baumannii* expressing phosphorylcholine with host cells. *J Biol Chem* 287:26901–26910. <https://doi.org/10.1074/jbc.M112.344556>
28. McPhee JB, Tamber S, Bains M, Maier E, Gellatly S, Lo A, Benz R, Hancock REW. 2009. The major outer membrane protein Oprg of *Pseudomonas aeruginosa* contributes to cytotoxicity and forms an anaerobically regulated, cation-selective channel. *FEMS Microbiol Lett* 296:241–247. <https://doi.org/10.1111/j.1574-6968.2009.01651.x>
29. Motley ST, Morrow BJ, Liu X, Dodge IL, Vitiello A, Ward CK, Shaw KJ. 2004. Simultaneous analysis of host and pathogen interactions during an *in vivo* infection reveals local induction of host acute phase response proteins, a novel bacterial stress response, and evidence of a host-imposed metal ion limited environment. *Cell Microbiol* 6:849–865. <https://doi.org/10.1111/j.1462-5822.2004.00407.x>
30. Li W, Wen L, Li C, Chen R, Ye Z, Zhao J, Pan J. 2016. Contribution of the outer membrane protein Ompw in *Escherichia coli* to complement resistance from binding to factor H. *Microb Pathog* 98:57–62. <https://doi.org/10.1016/j.micpath.2016.06.024>
31. Wu XB, Tian LH, Zou HJ, Wang CY, Yu ZQ, Tang CH, Zhao FK, Pan JY. 2013. Outer membrane protein Ompw of *Escherichia coli* is required for resistance to phagocytosis. *Res Microbiol* 164:848–855. <https://doi.org/10.1016/j.resmic.2013.06.008>
32. Gaulton A, Bellis LJ, Bento AP, Chambers J, Davies M, Hersey A, Light Y, McGlinchey S, Michalovich D, Al-Lazikani B, Overington JP. 2012. ChEMBL: a large-scale bioactivity database for drug discovery. *Nucleic Acids Res* 40:D1100–7. <https://doi.org/10.1093/nar/gkr777>
33. McKinney W. 2011. Pandas: a foundational Python library for data analysis and statistics. *Python for high performance and scientific computing* 14(9):1–9.
34. Landrum G. 2013. Rdkit: a software suite for cheminformatics, computational chemistry, and predictive modeling. *Greg Landrum* 8
35. Rogers D, Hahn M. 2010. Extended-connectivity fingerprints. *J Chem Inf Model* 50:742–754. <https://doi.org/10.1021/ci100050t>
36. Probst D, Reymond JL. 2018. A probabilistic molecular fingerprint for big data settings. *J Cheminform* 10:1–12. <https://doi.org/10.1186/s13321-018-0321-8>
37. Heo L, Park H, Seok C. 2013. Galaxyrefine: protein structure refinement driven by side-chain repacking. *Nucleic Acids Res* 41:W384–8. <https://doi.org/10.1093/nar/gkt458>
38. Laskowski RA, MacArthur MW, Moss DS, Thornton JM. 1993. PROCHECK: a program to check the stereochemical quality of protein structures. *J Appl Crystallogr* 26:283–291. <https://doi.org/10.1107/S0021889892009944>
39. Wiederstein M, Sippl MJ. 2007. Prosa-web: interactive web service for the recognition of errors in three-dimensional structures of proteins. *Nucleic Acids Res* 35:W407–10. <https://doi.org/10.1093/nar/gkm290>
40. Jendele L, Krivak R, Skoda P, Novotny M, Hoksza D. 2019. Prankweb: a web server for ligand binding site prediction and visualization. *Nucleic Acids Res* 47:W345–W349. <https://doi.org/10.1093/nar/gkz424>
41. Sander T, Freyss J, von Korff M, Rufener C. 2015. Datawarrior: an open-source program for chemistry aware data visualization and analysis. *J Chem Inf Model* 55:460–473. <https://doi.org/10.1021/ci500588j>
42. Lipinski CA. 2004. Lead- and drug-like compounds: The rule-of-five revolution. *Drug Discov Today Technol* 1:337–341. <https://doi.org/10.1016/j.ddtec.2004.11.007>
43. Trott O, Olson AJ. 2010. Autodock vina: improving the speed and accuracy of docking with a new scoring function, efficient optimization, and multithreading. *J Comput Chem* 31:455–461. <https://doi.org/10.1002/jcc.21334>
44. Boulaamane Y, Ibrahim MAA, Britel MR, Maurady A. 2022. *In silico* studies of natural product-like caffeine derivatives as potential MAO-B inhibitors/Aa2Ar antagonists for the treatment of Parkinson's disease. *J Integr Bioinform* 19:20210027. <https://doi.org/10.1515/jib-2021-0027>
45. Huey R, Morris GM. 2008. Using Autodock 4 with Autodocktools: A Tutorial, Vol. 54, p 56. Vol. 54. The Scripps Research Institute, USA.
46. Soojhawon I, Pattabiraman N, Tsang A, Roth AL, Kang E, Noble SM. 2017. Discovery of novel inhibitors of multidrug-resistant *Acinetobacter baumannii*. *Biorganic & Medicinal Chemistry* 25:5477–5482. <https://doi.org/10.1016/j.bmc.2017.08.014>
47. Pettersen EF, Goddard TD, Huang CC, Couch GS, Greenblatt DM, Meng EC, Ferrin TE. 2004. UCSF Chimera - a visualization system for exploratory research and analysis. *J Comput Chem* 25:1605–1612. <https://doi.org/10.1002/jcc.20084>
48. Salentin S, Schreiber S, Haupt VJ, Adasme MF, Schroeder M. 2015. PLIP: fully automated protein-ligand interaction profiler. *Nucleic Acids Res* 43:W443–7. <https://doi.org/10.1093/nar/gkv315>
49. Van Der Spoel D, Lindahl E, Hess B, Groenhof G, Mark AE, Berendsen HJC. 2005. GROMACS: fast, flexible, and free. *J Comput Chem* 26:1701–1718. <https://doi.org/10.1002/jcc.20291>
50. Abraham MJ, Murtola T, Schulz R, Pälli S, Smith JC, Hess B, Lindahl E. 2015. GROMACS: High performance molecular simulations through multi-level parallelism from laptops to supercomputers. *SoftwareX* 1–2:19–25. <https://doi.org/10.1016/j.softx.2015.06.001>
51. Huang J, MacKerell AD. 2013. Charmm36 all-atom additive protein force field: validation based on comparison to NMR data. *J Comput Chem* 34:2135–2145. <https://doi.org/10.1002/jcc.23354>
52. Abraham MJ, Gready JE. 2011. Optimization of parameters for molecular dynamics simulation using smooth Particle - Mesh Ewald in GROMACS 4.5. *J Comput Chem* 32:2031–2040. <https://doi.org/10.1002/jcc.21773>
53. Boulaamane Y, Jangid K, Britel MR, Maurady A. 2023. Probing the molecular mechanisms of A-Synuclein inhibitors unveils promising natural candidates through machine-learning QSAR, Pharmacophore modeling, and molecular Dynamics simulations. *Mol Divers*. <https://doi.org/10.1007/s11030-023-10691-x>
54. Genheden S, Ryde U. 2015. The MM/PBSA and MM/GBSA methods to estimate ligand-binding affinities. *Expert Opin Drug Discov* 10:449–461. <https://doi.org/10.1517/17460441.2015.1032936>
55. European Committee on Antimicrobial Susceptibility Testing. 2023. European antimicrobial breakpoints. Basel EUCAST
56. Miró-Canturri A, Ayerbe-Algabea R, Villodres ÁR, Pachón J, Smani Y. 2020. Repositioning rafloxanide to treat gram-negative bacilli infections. *J Antimicrob Chemother* 75:1895–1905. <https://doi.org/10.1093/jac/dkaa103>
57. Parra-Millán R, Guerrero-Gómez D, Ayerbe-Algabea R, Pachón-Ibáñez ME, Miranda-Vizuete A, Pachón J, Smani Y. 2018. Intracellular trafficking and persistence of *Acinetobacter baumannii* requires transcription factor EB. *mSphere* 3:e00106–18. <https://doi.org/10.1128/mSphere.00106-18>

CHAPTER VII: GENERAL DISCUSSION

The search of effective natural remedies for Parkinson's disease has led to a focus on MAO-B as a promising target. Existing MAO-B inhibitors, however, pose challenges due to selectivity-associated side effects [436]. This requires the development of novel inhibitors that are potent and highly selective. Recent research has uncovered the potential of coumarins, particularly alkynyl-coumarinyl ethers, as potent and selective MAO-B inhibitors [437]. The elongation of the ether chain, resulting in increased molecule length, has been shown to be favorable for MAO-B inhibition. Interestingly, those connected to a hex-5-ynyloxy chain at position C6 exhibited higher selectivity toward MAO-B than their C7-isomers [437].

In-depth investigation into the interaction modes of these coumarin isomers has revealed molecular interactions contributing to MAO-B selectivity (Refer to Annex 1). Molecular docking has unveiled a common π - π stacking interaction with Tyr-326 among the selective C6-isomers which is not found in C7-isomers [438]. The MD simulations further revealed the stability of C7-isomers in both MAO isoforms, while the C6-isomers demonstrated instability in MAO-A, possibly attributed to steric clashes of the ether chain with the bulky Phe-208 residue [438]. This selectivity arising from structural isomerism can be correlated with the inversion of key amino acids in MAO isoforms, wherein aliphatic Ile-199 is substituted with aromatic Phe-208, and conversely, aromatic Tyr-326 is replaced with Ile-335. These findings align with existing literature on the influence of these amino acids on substrate and inhibitor specificity in MAO enzymes [439], [440]. Such insights provide valuable guidance for the development and optimization of coumarin derivatives as potential drugs for Parkinson's disease.

Building upon this foundation, a chemical library was compiled to consolidate information on naturally occurring coumarins [363]. Employing a multi-stage virtual screening approach, including ML-QSAR regression modelling, molecular docking, and ADMET prediction, we identified ten coumarin derivatives as potential dual-target action against MAO-B and AChE with predicted $pIC_{50} > 6$ ($IC_{50} < 1 \mu M$). A notable candidate, such as CDB0738, demonstrated favorable interactions, including a non-bonded interaction with Tyr-326 and multiple hydrogen bonds with tyrosine residues within the substrate cavity of MAO-B. In AChE, diverse hydrogen bonds and hydrophobic interactions were observed in both the peripheral anionic site (PAS) and the catalytic anionic site (CAS). Furthermore, CDB0738 exhibited a favorable ADMET profile, predicting non-mutagenicity in the Ames test and no predicted interaction with CYP2D6—a key enzyme known for drug interactions, particularly abundant in the brain. This is crucial for drugs targeting the brain, as CYP2D6 is involved in metabolizing endogenous

neural compounds, suggesting potential neuroprotective properties. MD simulations supported the stability of CDB0738 as a promising dual inhibitor of MAO-B and AChE.

Expanding the scope beyond coumarins, the entire COCONUT database, representing the largest collection of NPs, was explored. *In silico* methods were employed for screening, utilizing ML and CNN-based QSAR classification models, pharmacophore modelling, and molecular docking against Parkinson's disease targets implicated in oxidative stress. Twenty-two candidates with desired pharmacophoric features were identified, with two diarylheptanoids, CNP0121426 and CNP0242698 standing out for their remarkable binding affinities and promising interaction profiles [349]. MD simulations highlighted the curcuminoid, CNP0242698's superior stability with MAO-B, AA_{2A}R, and NMDAR compared to the dihydrochalcone, Uvaretin, suggesting its potential as a lead compound for developing curcuminoids as multi-target remedies for Parkinson's disease.

Shifting focus to the neuropathological hallmark of Parkinson's disease, the abnormal deposition of α -synuclein fibrils, a dataset of α -synuclein inhibitors from the ChEMBL database was analyzed. ML-QSAR models screened the LOTUS NPs database, and a pharmacophore based on the clinical candidate Anle138b identified potential α -synuclein natural inhibitors. Molecular docking studies evaluated their binding affinities, and ADMET analysis indicated satisfactory properties and BBB penetration [441]. Notably, the cinnamic acid derivative, LTS0078917 displayed superior stability in MD simulations compared to Anle138b, showing promise in stabilizing the α -synuclein monomer by binding to the interhelical loop region separating the two helices. This is particularly relevant since the interhelical region of α -synuclein is involved in lipid binding, thus LTS0078917 may prevent the protein from associating to the lipid membranes and potentially inhibiting the formation and aggregation of pathological oligomers. These findings provide valuable insights for developing novel α -synuclein inhibitors from natural sources, contributing to the ongoing efforts to find effective treatments for Parkinson's disease.

Literature has previously studied some of the effects of the proposed drug candidates as depicted in Table 10. The chemical structures of the lead NPs are illustrated in Figure 28. CDB0738 is found to inhibit inflammation and astrocyte activation in the spinal cord for the treatment of neuropathic pain [442]. Additionally, CDB0738 has demonstrated efficacy in inhibiting neuronal oxidative stress and apoptosis [442]. Notably, it exhibits inhibitory effects on both the lyase and polymerase activities of DNA polymerase β [443]. Furthermore,

CDB0738 has shown the capability to potentiate the inhibitory action of the anticancer drug bleomycin in cultured A549 cells by inhibiting DNA repair synthesis [443]. It's worth noting that while CDB0046 is not reported in the literature, Excavarin-A, an O-terpenoidal coumarin like CDB0046, has been studied for its antifungal activity against 15 fungal strains, including human pathogens such as *Candida tropicalis*, *Rhizoctonia solani*, and *Sclerotinia sclerotiorum* [444]. This additional information further highlights the diverse and potentially valuable pharmacological properties of naturally occurring coumarins, encouraging continued exploration in the context of Parkinson's disease and related disorders.

The diarylheptanoid, Uvaretin, a cytotoxic C-benzylated dihydrochalcone found in plants such as *Uvaria acuminata* and *Uvaria chamae*, has shown significant antitumor activity against several cancer cell lines *in vitro* and *in vivo* [445], [446]. Research has demonstrated that Uvaretin, along with its derivatives, displayed growth inhibitory effects and induced apoptosis in various cancer cell lines, including human promyelocytic leukemia cells [446]. In addition, some chalcones, including Uvaretin, have potent Nrf2-inducing, antioxidant, and anti-inflammatory effects, which are key endogenous cellular defense systems against oxidative stress [446]. Although there is no direct evidence of the effect of Uvaretin on neurodegenerative diseases, some chalcones, including Diuvaretin and Uvaretin, have shown potential in modulating the cannabinoid system, which has been implicated in neurodegenerative diseases [447].

The other diarylheptanoid, CNP0242698, discovered in *Zingiber officinale*, exhibited superior stability with the three selected targets compared to Uvaretin, further highlighting its efficacy in mitigating oxidative stress, as documented in the literature [448], [449]. LTS0078917, identified as a cinnamic acid derivative in the LOTUS NPs database, lacks comprehensive documentation in existing literature. Nevertheless, it exhibits notable activity by targeting DNA gyrase, inducing chemical perturbation in *Streptomyces venezuelae* sporulation [450]. Additionally, it is recognized as a lead inhibitor against extensively resistant Gram-positive pathogens [450].

Table 10. Proposed lead candidates from NPs through in silico approaches for Parkinson's disease and their reported activities from the literature.

ID	Source	Target	Reported activities	Reference
CDB0738	<i>Edgeworthia chrysanthia</i>	MAO-B AChE	Inhibits inflammation and astrocyte activation in the spinal cord for the treatment of neuropathic pain. Inhibits neuronal oxidative stress and apoptosis.	[443], [451], [452]

			Inhibits both the lyase and polymerase activities of DNA pol β . It can potentiate the inhibitory action of the anticancer drug bleomycin in cultured A549 cells via an inhibition of DNA repair synthesis.	
CDB0046	<i>Clausena excavata</i>	MAO-B AChE	Excavarin-A, is an O-terpenoidal coumarin like CDB0046, it exhibits antifungal activity against 15 fungal strains, including human pathogens like <i>Candida tropicalis</i> , <i>Rhizoctonia solani</i> , and <i>Sclerotinia sclerotiorum</i> .	[444], [453]
CNP0121426	<i>Uvaria acuminata</i>	MAO-B AA _{2A} R NMDAR	Uvaretin is a C-benzylated dihydrochalcone with a cyclohexene epoxide ring. It shows significant antitumor activity against several cancer cell lines <i>in vitro</i> and <i>in vivo</i> .	[454]
CNP0242698	<i>Zingiber officinale</i>	MAO-B AA _{2A} R NMDAR	Diarylheptanoids found in ginger can help protect from oxidative stress, they also demonstrate anti-inflammatory properties. Demethoxycurcumin, also found in ginger exhibits antibacterial activity against colistin resistant strains of <i>Acinetobacter baumannii</i> .	[448], [455]
LTS0078917	—	α -synuclein	Lead inhibitor of extensively resistant Gram-positive pathogens. Targets DNA gyrase through chemical perturbation of <i>Streptomyces venezuelae</i> sporulation.	[450]

In the context of infectious diseases, our focus on OmpW's virulence in *A. baumannii* led us to construct QSAR models predicting antimicrobial compounds based on bioactivity data reported in ChEMBL. These models demonstrated robust performance, effectively distinguishing between active and inactive compounds with high AUC values. Molecular docking investigations further revealed promising binding affinities, particularly notable for curcuminoid compounds. Analysis of molecular interactions highlighted consistent hydrogen bond formations and hydrophobic interactions, while MD simulations assessed the stability of most complexes. Notably, van der Waals energy emerged as the primary contributor to complex stability. *In vitro* assays confirmed the antibacterial activity of the lead candidate, Demethoxycurcumin, with MIC values of 64 mg/L outperforming previously evaluated natural small-molecules against *A. baumannii* [294]. Demethoxycurcumin exhibited synergistic effects when combined with the antibiotic colistin against various *A. baumannii* strains, including a colistin-resistant clinical strain (CR17) [456]. Our study also emphasizes the crucial function of OmpW in mediating compound efficacy, as Demethoxycurcumin exhibited reduced activity against mutants lacking the OmpW protein. Additionally, the compound demonstrated efficacy in reducing *A. baumannii* adherence to host cells. Further validation studies, including animal infection models, are imperative to ascertain the therapeutic potential of targeting OmpW with Demethoxycurcumin and related NPs.

Demethoxycurcumin has been reported to exhibit various beneficial properties (Table 11). One of its notable activities is its antioxidant potential, which can protect cells from oxidative stress and damage [457], similar to the diarylheptanoid CNP0242698 from *Zingiber officinale* identified in our previous work on multi-target drugs [349]. Furthermore, studies have shown that Demethoxycurcumin can inhibit the activation of nuclear factor- κ B (NF- κ B), a crucial regulator of inflammation, in human epithelial intestinal cells (Caco-2 cells) [458]. Interestingly, Demethoxycurcumin has also been found to suppress the growth of both androgen-dependent LNCaP and androgen-independent PC3 cells, suggesting a neuroprotective effect. Additionally, Demethoxycurcumin possesses antimicrobial properties, as demonstrated in a study investigating the antifungal activity of turmeric oil, which contains Demethoxycurcumin and other curcuminoids [459].

Table 11. Proposed lead candidate against *A. baumannii* infections and its previously reported activities.

ID	Source	Target	Reported activities	Reference
Amb2698241	<i>Curcuma longa</i>	OmpW	Exhibits antioxidant properties that protect cells from oxidative stress and damage. Inhibits activation of the inflammatory regulator NF- κ B in intestinal epithelial cells. Suppresses growth of both androgen-dependent and androgen-independent prostate cancer cells. Possesses antimicrobial properties, contributing to the antifungal activity of turmeric oil.	[457], [458], [459]

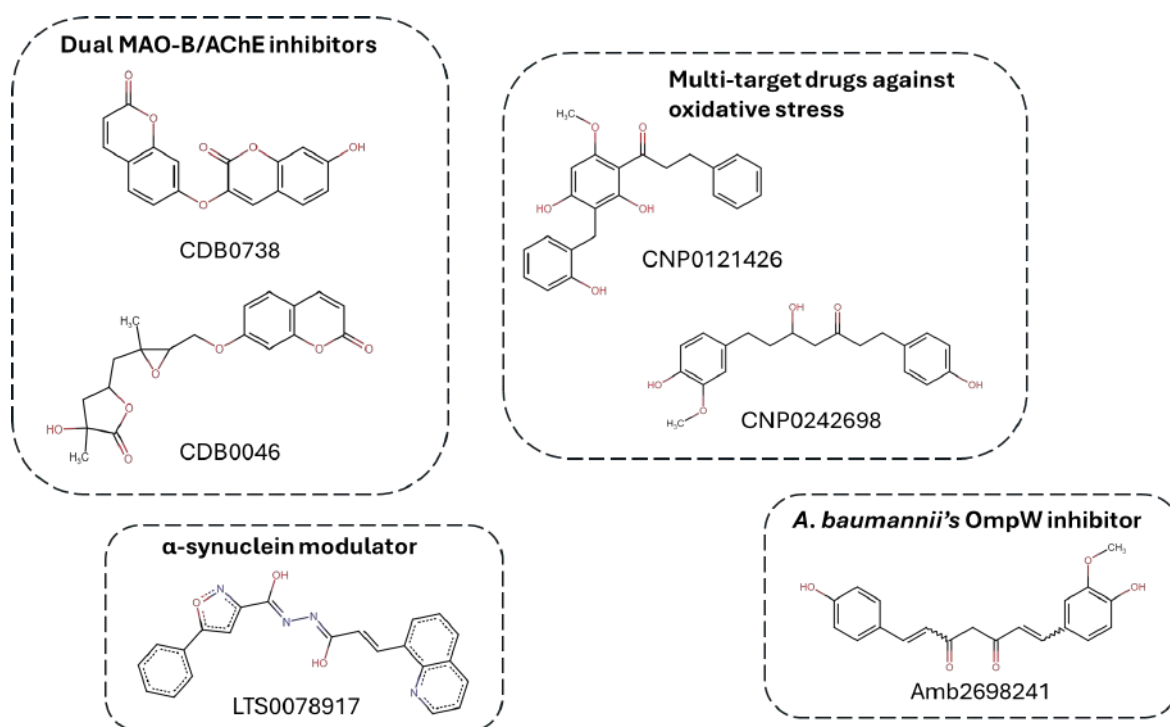


Figure 28. Chemical structures of proposed NPs against Parkinson's disease and *A. baumannii* infections.

CHAPTER VIII: CONCLUSION AND PERSPECTIVES

This doctoral thesis has demonstrated the vast potential of natural products as promising candidates for the treatment of neurodegenerative disorders such as Parkinson's disease and combating infectious diseases like those caused by *Acinetobacter baumannii*. Through a comprehensive exploration employing advanced computational techniques such as QSAR modelling, virtual screening, pharmacophore modelling, and molecular dynamics simulations, several lead natural products candidates were identified with favorable pharmacological profiles.

Notably, the coumarins CDB0738 and CDB0046 exhibited potential as inhibitors of the enzymes MAO-B and AChE, which are relevant targets for developing neuroprotective drugs against Parkinson's and Alzheimer's diseases. The compilation of a chemical library specific to naturally occurring coumarins aims to attract more interest in exploring their potential against various diseases. The curcuminoid CNP0242698 and dihydrochalcone CNP0121426 displayed promising interactions and stability when docked with MAO-B, AA_{2A}R, and NMDAR, suggesting their potential as multi-target agents for Parkinson's disease. Additionally, LTS0078917 emerged as a candidate for preventing protein aggregates of α -synuclein implicated in Parkinson's pathogenesis.

In the area of antimicrobial research, the curcuminoid Demethoxycurcumin was identified as a lead compound targeting the outer membrane protein OmpW of *A. baumannii*. Demethoxycurcumin binds to the periplasmic region of OmpW, potentially reducing the influx of essential nutrients and weakening the bacteria. Targeting a ubiquitous surface protein like OmpW with an inhibitor could make it more challenging for the bacteria to develop resistance through mutation compared to classical antibiotics. Experimental studies on Demethoxycurcumin showed promising antibacterial activity against *A. baumannii* wild-type and colistin-resistant strains.

While these findings are encouraging, further experimental validation through *in vitro* and *in vivo* studies is necessary to confirm the effectiveness and safety of these natural products before considering clinical development. Future work should focus on expanding the chemical space of lead compounds and prioritizing lead optimization to enhance potency, selectivity, and safety profiles. By harnessing the chemical diversity of natural products and employing advanced computational and experimental approaches, this thesis has paved the way for continued progress in the field of pharmacognosy, ultimately contributing to improved healthcare outcomes worldwide.

REFERENCES

- [1] A. Amit Koparde, R. Chandrashekhar Doijad, and C. Shripal Magdum, “Natural Products in Drug Discovery,” in *Pharmacognosy - Medicinal Plants*, S. Perveen and A. Al-Taweel, Eds., IntechOpen, 2019. doi: 10.5772/intechopen.82860.
- [2] D. J. Newman and G. M. Cragg, “Natural Products as Sources of New Drugs over the Nearly Four Decades from 01/1981 to 09/2019,” *J Nat Prod*, vol. 83, no. 3, pp. 770–803, Mar. 2020, doi: 10.1021/acs.jnatprod.9b01285.
- [3] J. Hong, “Role of natural product diversity in chemical biology,” *Curr Opin Chem Biol*, vol. 15, no. 3, pp. 350–354, Jun. 2011, doi: 10.1016/J.CBPA.2011.03.004.
- [4] H. Lachance, S. Wetzel, K. Kumar, and H. Waldmann, “Charting, navigating, and populating natural product chemical space for drug discovery,” *J Med Chem*, vol. 55, no. 13, pp. 5989–6001, Jul. 2012, doi: 10.1021/JM300288G/ASSET/JM300288G.FP.PNG_V03.
- [5] P. Vuorela *et al.*, “Natural Products in the Process of Finding New Drug Candidates,” *Curr Med Chem*, vol. 11, no. 11, pp. 1375–1389, Nov. 2012, doi: 10.2174/0929867043365116.
- [6] I. V. Tetko, O. Engkvist, U. Koch, J. L. Reymond, and H. Chen, “BIGCHEMA: Challenges and Opportunities for Big Data Analysis in Chemistry,” *Mol Inform*, vol. 35, no. 11–12, pp. 615–621, Dec. 2016, doi: 10.1002/MINF.201600073.
- [7] M. H. J. Seifert, K. Wolf, and D. Vitt, “Virtual high-throughput in silico screening,” *BIOSILICO*, vol. 1, no. 4, pp. 143–149, Sep. 2003, doi: 10.1016/S1478-5382(03)02359-X.
- [8] M. Sorokina and C. Steinbeck, “Review on natural products databases: where to find data in 2020,” *Journal of Cheminformatics 2020 12:1*, vol. 12, no. 1, pp. 1–51, Apr. 2020, doi: 10.1186/S13321-020-00424-9.
- [9] W. P. Walters and R. Barzilay, “Critical assessment of AI in drug discovery,” *Expert Opin Drug Discov*, vol. 16, no. 9, pp. 937–947, Sep. 2021, doi: 10.1080/17460441.2021.1915982.
- [10] A. D. Gitler, P. Dhillon, and J. Shorter, “Neurodegenerative disease: models, mechanisms, and a new hope,” *Dis Model Mech*, vol. 10, no. 5, pp. 499–502, 2017.
- [11] D. Kumar, G. M. Ashraf, A. L. Bilgrami, and M. I. Hassan, “Emerging therapeutic developments in neurodegenerative diseases: a clinical investigation,” *Drug Discov Today*, vol. 27, no. 10, p. 103305, 2022.
- [12] L. Morrison and T. R. Zembower, “Antimicrobial Resistance,” *Gastrointest Endosc Clin N Am*, vol. 30, no. 4, pp. 619–635, Oct. 2020, doi: 10.1016/j.giec.2020.06.004.
- [13] R. Vázquez-López *et al.*, “Acinetobacter baumannii Resistance: A Real Challenge for Clinicians,” *Antibiotics 2020, Vol. 9, Page 205*, vol. 9, no. 4, p. 205, Apr. 2020, doi: 10.3390/ANTIBIOTICS9040205.
- [14] I. Kyriakidis, E. Vasileiou, Z. D. Pana, and A. Tragiannidis, “Acinetobacter baumannii Antibiotic Resistance Mechanisms,” *Pathogens 2021, Vol. 10, Page 373*, vol. 10, no. 3, p. 373, Mar. 2021, doi: 10.3390/PATHOGENS10030373.
- [15] K. S. Lam, “New aspects of natural products in drug discovery,” *Trends in Microbiology*, vol. 15, no. 6. 2007. doi: 10.1016/j.tim.2007.04.001.
- [16] D. J. Newman and G. M. Cragg, “Natural Products as Sources of New Drugs from 1981 to 2014,” *Journal of Natural Products*, vol. 79, no. 3. 2016. doi: 10.1021/acs.jnatprod.5b01055.
- [17] J. LI, C. A. Larregieu, and L. Z. Benet, “Classification of natural products as sources of drugs according to the biopharmaceutics drug disposition classification system (BDDCS),” *Chin J Nat Med*, vol. 14, no. 12, pp. 888–897, Dec. 2016, doi: 10.1016/S1875-5364(17)30013-4.
- [18] J. Roberts and M. Caserio, “Basic principles of organic chemistry,” *Basic principles of organic chemistry*. 1977.

REFERENCES

- [19] F. Chassagne, G. Cabanac, G. Hubert, B. David, and G. Marti, “The landscape of natural product diversity and their pharmacological relevance from a focus on the Dictionary of Natural Products ®,” *Phytochemistry Reviews*, vol. 18, no. 3. 2019. doi: 10.1007/s11101-019-09606-2.
- [20] C. L. Prins, I. J. C. Vieira, and S. P. Freitas, “Growth regulators and essential oil production,” *Brazilian Journal of Plant Physiology*, vol. 22, no. 2, pp. 91–102, 2010, doi: 10.1590/S1677-04202010000200003.
- [21] B. M. Abegaz and H. H. Kinfe, “Secondary metabolites, their structural diversity, bioactivity, and ecological functions: An overview,” *Physical Sciences Reviews*, vol. 4, no. 6, Jun. 2019, doi: 10.1515/PSR-2018-0100/XML.
- [22] Z. A. Reshi, W. Ahmad, A. S. Lukatkin, and S. Bin Javed, “From Nature to Lab: A Review of Secondary Metabolite Biosynthetic Pathways, Environmental Influences, and In Vitro Approaches,” *Metabolites*, vol. 13, no. 8, Aug. 2023, doi: 10.3390/METABO13080895.
- [23] Suresh S.S. Raja. and Ramasamy Vijayakumar., “Secondary Metabolites - Sources and Applications,” 2018, Accessed: Dec. 25, 2023. [Online]. Available: https://books.google.com/books/about/Secondary_Metabolites.html?id=xS6RDwAAQBAJ
- [24] A. L. Demain and A. Fang, “The natural functions of secondary metabolites,” *Adv Biochem Eng Biotechnol*, vol. 69, pp. 1–39, 2000, doi: 10.1007/3-540-44964-7_1.
- [25] K. Nawrot-Chorabik, M. Sułkowska, and N. Gumulak, “Secondary Metabolites Produced by Trees and Fungi: Achievements So Far and Challenges Remaining,” *Forests 2022, Vol. 13, Page 1338*, vol. 13, no. 8, p. 1338, Aug. 2022, doi: 10.3390/F13081338.
- [26] C. V. Simoben *et al.*, “Challenges in natural product-based drug discovery assisted with in silico-based methods,” *RSC Adv*, vol. 13, no. 45, p. 31578, Oct. 2023, doi: 10.1039/D3RA06831E.
- [27] A. G. Atanasov *et al.*, “Natural products in drug discovery: advances and opportunities,” *Nature Reviews Drug Discovery 2021 20:3*, vol. 20, no. 3, pp. 200–216, Jan. 2021, doi: 10.1038/s41573-020-00114-z.
- [28] S. Mathur and C. Hoskins, “Drug development: Lessons from nature (Review),” *Biomed Rep*, vol. 6, no. 6, pp. 612–614, Jun. 2017, doi: 10.3892/BR.2017.909.
- [29] J. Lipp, “Possible mechanisms of morphine analgesia,” *Clinical Neuropharmacology*, vol. 14, no. 2. 1991. doi: 10.1097/00002826-199104000-00003.
- [30] P. Madadi and G. Koren, “Pharmacogenetic insights into codeine analgesia: implications to pediatric codeine use,” <http://dx.doi.org/10.2217/14622416.9.9.1267>, vol. 9, no. 9, pp. 1267–1284, Sep. 2008, doi: 10.2217/14622416.9.9.1267.
- [31] N. Kardos and A. L. Demain, “Penicillin: The medicine with the greatest impact on therapeutic outcomes,” *Appl Microbiol Biotechnol*, vol. 92, no. 4, pp. 677–687, Oct. 2011, doi: 10.1007/S00253-011-3587-6/METRICS.
- [32] Y. Tu, “The discovery of artemisinin (qinghaosu) and gifts from Chinese medicine,” *Nature Medicine 2011 17:10*, vol. 17, no. 10, pp. 1217–1220, Oct. 2011, doi: 10.1038/nm.2471.
- [33] P. J. Wysocki *et al.*, “Metronomic Chemotherapy Based on Topotecan or Topotecan and Cyclophosphamide Combination (CyTo) in Advanced, Pretreated Ovarian Cancer,” *Cancers (Basel)*, vol. 15, no. 4, 2023, doi: 10.3390/cancers15041067.
- [34] Y. Liu *et al.*, “Galantamine improves cognition, hippocampal inflammation, and synaptic plasticity impairments induced by lipopolysaccharide in mice,” *J Neuroinflammation*, vol. 15, no. 1, 2018, doi: 10.1186/s12974-018-1141-5.
- [35] M. Brunet *et al.*, “Therapeutic Drug Monitoring of Tacrolimus-Personalized Therapy: Second Consensus Report,” *Ther Drug Monit*, vol. 41, no. 3, 2019, doi: 10.1097/FTD.0000000000000640.
- [36] R. Cencic *et al.*, “Antitumor Activity and Mechanism of Action of the Cyclopenta[b]benzofuran, Silvestrol,” *PLoS One*, vol. 4, no. 4, p. e5223, Apr. 2009, doi: 10.1371/JOURNAL.PONE.0005223.

REFERENCES

- [37] M. De Lourdes Reyes-Escogido, E. G. Gonzalez-Mondragon, and E. Vazquez-Tzompantzi, “Chemical and Pharmacological Aspects of Capsaicin,” *Molecules* 2011, Vol. 16, Pages 1253–1270, vol. 16, no. 2, pp. 1253–1270, Jan. 2011, doi: 10.3390/MOLECULES16021253.
- [38] J. Parkinson, “An essay on the shaking palsy. 1817.,” *J Neuropsychiatry Clin Neurosci*, vol. 14, no. 2, Mar. 2002, doi: 10.1176/jnp.14.2.223.
- [39] F. Viallet, D. Gayraud, B. Bonnefoi, L. Renie, and R. Aurenty, “Maladie de Parkinson idiopathique : aspects cliniques, diagnostiques et thérapeutiques,” *EMC - Neurologie*, vol. 7, no. 2, pp. 1–30, 2010, doi: 10.1016/s0246-0378(10)51548-3.
- [40] M. J. Armstrong and M. S. Okun, “Diagnosis and Treatment of Parkinson Disease: A Review,” *JAMA*, vol. 323, no. 6, pp. 548–560, Feb. 2020, doi: 10.1001/JAMA.2019.22360.
- [41] W. Poewe and P. Mahlknecht, “Pharmacologic Treatment of Motor Symptoms Associated with Parkinson Disease,” *Neurol Clin*, vol. 38, no. 2, pp. 255–267, 2020, doi: 10.1016/j.ncl.2019.12.002.
- [42] H. Khalil *et al.*, “Parkinson’s Disease in the Middle East, North Africa, and South Asia: Consensus from the International Parkinson and Movement Disorder Society Task Force for the Middle East,” *J Parkinsons Dis*, vol. 10, no. 2, pp. 729–741, Jan. 2020, doi: 10.3233/JPD-191751.
- [43] N. Zeghbib, “Synthèse de nouveaux inducteurs chimiques de la maladie de Parkinson : étude relation structure/activité,” Université Paris-Est, 2016. [Online]. Available: <https://theses.hal.science/tel-01459525>
- [44] H. Xu and F. Yang, “The interplay of dopamine metabolism abnormalities and mitochondrial defects in the pathogenesis of schizophrenia,” *Transl Psychiatry*, vol. 12, no. 1, p. 464, 2022, doi: 10.1038/s41398-022-02233-0.
- [45] S. F. Logue and T. J. Gould, “The neural and genetic basis of executive function: Attention, cognitive flexibility, and response inhibition,” *Pharmacology Biochemistry and Behavior*, vol. 123. 2014. doi: 10.1016/j.pbb.2013.08.007.
- [46] O. Hornykiewicz, “Biochemical aspects of Parkinson’s disease,” in *Neurology*, 1998. doi: 10.1212/wnl.51.2_suppl_2.s2.
- [47] A. Björklund and S. B. Dunnett, “Dopamine neuron systems in the brain: an update,” *Trends Neurosci*, vol. 30, no. 5, pp. 194–202, May 2007, doi: 10.1016/j.tins.2007.03.006.
- [48] J. A. Obeso *et al.*, “Past, present, and future of Parkinson’s disease: A special essay on the 200th Anniversary of the Shaking Palsy,” *Movement Disorders*, vol. 32, no. 9. 2017. doi: 10.1002/mds.27115.
- [49] H. Bernheimer, W. Birkmayer, O. Hornykiewicz, K. Jellinger, and F. Seitelberger, “Brain dopamine and the syndromes of Parkinson and Huntington Clinical, morphological and neurochemical correlations,” *J Neurol Sci*, vol. 20, no. 4, 1973, doi: 10.1016/0022-510X(73)90175-5.
- [50] H. C. Cheng, C. M. Ulane, and R. E. Burke, “Clinical progression in Parkinson disease and the neurobiology of axons,” *Annals of Neurology*, vol. 67, no. 6. 2010. doi: 10.1002/ana.21995.
- [51] M. Goedert, M. G. Spillantini, K. Del Tredici, and H. Braak, “100 years of Lewy pathology,” *Nature Reviews Neurology*, vol. 9, no. 1. 2013. doi: 10.1038/nrneurol.2012.242.
- [52] F. R. Cabrero and E. H. Morrison, “Lewy Bodies,” *StatPearls*, Jul. 2023, Accessed: Mar. 15, 2024. [Online]. Available: <https://www.ncbi.nlm.nih.gov/books/NBK536956/>
- [53] H. Fujiwara *et al.*, “ α -Synuclein is phosphorylated in synucleinopathy lesions,” *Nat Cell Biol*, vol. 4, no. 2, pp. 160–164, 2002, doi: 10.1038/ncb748.
- [54] K. Beyer, M. Domingo-Sàbat, and A. Ariza, “Molecular Pathology of Lewy Body Diseases,” *Int J Mol Sci*, vol. 10, no. 3, p. 724, Mar. 2009, doi: 10.3390/IJMS10030724.

REFERENCES

- [55] S. J. Kish, K. Shannak, and O. Hornykiewicz, “Uneven Pattern of Dopamine Loss in the Striatum of Patients with Idiopathic Parkinson’s Disease,” *New England Journal of Medicine*, vol. 318, no. 14, pp. 876–880, Jan. 1988, doi: 10.1056/nejm198804073181402.
- [56] B. Scatton, L. Rouquier, F. Javoy-Agid, and Y. Agid, “Dopamine deficiency in the cerebral cortex in parkinson disease,” *Neurology*, vol. 32, no. 9, pp. 1039–1040, 1982, doi: 10.1212/wnl.32.9.1039.
- [57] A. H. V. Schapira, K. R. Chaudhuri, and P. Jenner, “Non-motor features of Parkinson disease,” *Nature Reviews Neuroscience*, vol. 18, no. 7. Nature Publishing Group, pp. 435–450, Jul. 01, 2017. doi: 10.1038/nrn.2017.62.
- [58] C. H. Hawkes, K. Del Tredici, and H. Braak, “A timeline for Parkinson’s disease,” *Parkinsonism Relat Disord*, vol. 16, no. 2, pp. 79–84, 2010, doi: 10.1016/j.parkreldis.2009.08.007.
- [59] B. Ford, “Pain in Parkinson’s disease,” *Movement Disorders*, vol. 25, no. SUPPL. 1, 2010, doi: 10.1002/mds.22716.
- [60] T. Van Laar, P. P. De Deyn, D. Aarsland, P. Barone, and J. E. Galvin, “Effects of Cholinesterase Inhibitors in Parkinson’s Disease Dementia: A Review of Clinical Data,” *CNS Neurosci Ther*, vol. 17, no. 5, pp. 428–441, Oct. 2011, doi: 10.1111/J.1755-5949.2010.00166.X.
- [61] D. W. Dickson *et al.*, “Neuropathology of non-motor features of Parkinson disease,” *Parkinsonism Relat Disord*, vol. 15, no. SUPPL. 3, pp. S1–S5, Dec. 2009, doi: 10.1016/S1353-8020(09)70769-2.
- [62] C. A. Gautier, O. Corti, and A. Brice, “Mitochondrial dysfunctions in Parkinson’s disease,” *Rev Neurol (Paris)*, vol. 170, no. 5, pp. 339–343, 2014, doi: 10.1016/j.neurol.2013.06.003.
- [63] S. Fahn, “The Case of the Frozen Addicts: How the Solution of an Extraordinary Medical Mystery Spawned a Revolution in the Understanding and Treatment of Parkinson’s Disease,” *N Engl J Med*, vol. 335, no. Libcap 2008, pp. 2002–2003, 1996.
- [64] H. L. Weingarten, “1-Methyl-4-Phenyl-1,2,3,6-Tetrahydropyridine (MPTP): One Designer Drug and Serendipity,” *J Forensic Sci*, vol. 33, no. 2, pp. 588–595, Mar. 1988, doi: 10.1520/JFS11978J.
- [65] G. C. Davis *et al.*, “Chronic parkinsonism secondary to intravenous injection of meperidine analogues,” *Psychiatry Res*, vol. 1, no. 3, pp. 249–254, 1979, doi: 10.1016/0165-1781(79)90006-4.
- [66] M. Ferrucci and F. Fornai, “MPTP Neurotoxicity: Actions, Mechanisms, and Animal Modeling of Parkinson’s Disease,” *Handbook of Neurotoxicity*, pp. 1–41, 2021, doi: 10.1007/978-3-030-71519-9_239-1.
- [67] C. M. Tanner, “Is the cause of Parkinson’s disease environmental or hereditary? Evidence from twin studies.,” *Adv Neurol*, vol. 91, pp. 133–142, 2003.
- [68] K. S. M. Taylor, C. E. Counsell, J. C. Gordon, and C. E. Harris, “Screening for undiagnosed parkinsonism among older people in general practice [3],” *Age Ageing*, vol. 34, no. 5, pp. 501–504, 2005, doi: 10.1093/ageing/afi123.
- [69] F. D. Dick *et al.*, “Environmental risk factors for Parkinson’s disease and parkinsonism: The Geoparkinson study,” *Occup Environ Med*, vol. 64, no. 10, pp. 666–672, Oct. 2007, doi: 10.1136/oem.2006.027003.
- [70] J. M. Gorell *et al.*, “Occupational exposures to metals as risk factors for Parkinson’s disease,” *Neurology*, vol. 48, no. 3, pp. 650–658, 1997, doi: 10.1212/WNL.48.3.650.
- [71] A. Y. Sun and Y.-M. Chen, “Oxidative Stress and Neurodegenerative Disorders,” *J Biomed Sci*, vol. 5, no. 6, pp. 401–414, Dec. 1998, doi: 10.1159/000025354.
- [72] Y. Christen, “Oxidative stress and Alzheimer disease,” *Am J Clin Nutr*, vol. 71, no. 2, 2000, doi: 10.1093/AJCN/71.2.621S.
- [73] O. Hwang, “Role of Oxidative Stress in Parkinson’s Disease,” *Exp Neurobiol*, vol. 22, no. 1, p. 11, Mar. 2013, doi: 10.5607/EN.2013.22.1.11.

REFERENCES

- [74] Y. Nakabeppu, D. Tsuchimoto, H. Yamaguchi, and K. Sakumi, “Oxidative damage in nucleic acids and Parkinson’s disease,” *J Neurosci Res*, vol. 85, no. 5, pp. 919–934, Apr. 2007, doi: 10.1002/JNR.21191.
- [75] G. D. Zeevark, R. Razmpour, and L. P. Bernard, “Glutathione and Parkinson’s disease: Is this the elephant in the room?,” *Biomedicine & Pharmacotherapy*, vol. 62, no. 4, pp. 236–249, Apr. 2008, doi: 10.1016/J.BIOPHA.2008.01.017.
- [76] B. Halliwell, “Reactive Oxygen Species and the Central Nervous System,” *J Neurochem*, vol. 59, no. 5, pp. 1609–1623, Nov. 1992, doi: 10.1111/J.1471-4159.1992.TB10990.X.
- [77] P. J. Kahle, M. Neumann, L. Ozmen, and C. Haass, “Physiology and pathophysiology of α -synuclein cell culture and transgenic animal models based on a Parkinson’s disease-associated protein,” *Ann N Y Acad Sci*, vol. 920, pp. 33–41, 2000, doi: 10.1111/j.1749-6632.2000.tb06902.x.
- [78] R. G. Perez, J. C. Waymire, E. Lin, J. J. Liu, F. Guo, and M. J. Zigmond, “Erratum: ‘A role for α -synuclein in the regulation of dopamine biosynthesis’ The Journal of Neuroscience (April 15, 2002) (3090-3099),” *Journal of Neuroscience*, vol. 22, no. 20, p. 9142, 2002, doi: 10.1523/jneurosci.22-20-09142.2002.
- [79] M. H. Polymeropoulos, “Genetics of Parkinson’s disease,” *Ann N Y Acad Sci*, vol. 920, pp. 28–32, 2000, doi: 10.1111/j.1749-6632.2000.tb06901.x.
- [80] W. Li, C. Lesuisse, Y. Xu, J. C. Troncoso, D. L. Price, and M. K. Lee, “Stabilization of α -synuclein protein with aging and familial Parkinson’s disease-linked A53T mutation,” *Journal of Neuroscience*, vol. 24, no. 33, pp. 7400–7409, 2004, doi: 10.1523/JNEUROSCI.1370-04.2004.
- [81] V. L. Sousa *et al.*, “ α -Synuclein and its A30P mutant affect actin cytoskeletal structure and dynamics,” *Mol Biol Cell*, vol. 20, no. 16, pp. 3725–3739, Aug. 2009, doi: 10.1091/mcb.E08-03-0302.
- [82] J. J. Zarzanz *et al.*, “The New Mutation, E46K, of α -Synuclein Causes Parkinson and Lewy Body Dementia,” *Ann Neurol*, vol. 55, no. 2, pp. 164–173, Feb. 2004, doi: 10.1002/ana.10795.
- [83] L. Qiao *et al.*, “Lysosomal enzyme cathepsin D protects against alpha-synuclein aggregation and toxicity.,” *Mol Brain*, vol. 1, p. 17, 2008, doi: 10.1186/1756-6606-1-17.
- [84] V. Cullen *et al.*, “Cathepsin D expression level affects alpha-synuclein processing, aggregation, and toxicity in vivo,” *Mol Brain*, vol. 2, no. 1, 2009, doi: 10.1186/1756-6606-2-5.
- [85] S. Fahn, “The history of dopamine and levodopa in the treatment of Parkinson’s disease,” *Movement Disorders*, vol. 23, no. S3, pp. S497–S508, Jan. 2008, doi: 10.1002/MDS.22028.
- [86] J. Geyer and R. Bogan, “Identification and treatment of augmentation in patients with restless legs syndrome: practical recommendations,” *Postgrad Med*, vol. 129, no. 7, pp. 667–675, Oct. 2017, doi: 10.1080/00325481.2017.1360747.
- [87] J. KNOLL, “Deprenyl (selegiline): the history of its development and pharmacological action,” *Acta Neurol Scand*, vol. 68, pp. 57–80, 1983, doi: 10.1111/J.1600-0404.1983.TB01517.X.
- [88] C. Caccia *et al.*, “Safinamide: From molecular targets to a new anti-Parkinson drug,” *Neurology*, vol. 67, no. 7 SUPPL. 2, pp. S18–S23, Oct. 2006, doi: 10.1212/wnl.67.7_suppl_2.s18.
- [89] P. T. Männistö and S. Kaakkola, “Catechol-O-methyltransferase (COMT): Biochemistry, Molecular Biology, Pharmacology, and Clinical Efficacy of the New Selective COMT Inhibitors,” *Pharmacol Rev*, vol. 51, no. 4, p. 593, Dec. 1999, [Online]. Available: <http://pharmrev.aspjournals.org/content/51/4/593.abstract>
- [90] L. E. Kiss and P. Soares-Da-Silva, “Medicinal chemistry of catechol O -methyltransferase (COMT) inhibitors and their therapeutic utility,” *J Med Chem*, vol. 57, no. 21, pp. 8692–8717, Nov. 2014, doi: 10.1021/JM500572B/ASSET/IMAGES/MEDIUM/JM-2014-00572B_0022.GIF.
- [91] E. Nissinen, I. B. Lindén, E. Schultz, S. Kaakkola, P. T. Männistö, and P. Pohto, “Inhibition of catechol-O-methyltransferase activity by two novel disubstituted catechols in the rat,” *Eur J Pharmacol*, vol. 153, no. 2–3, pp. 263–269, Aug. 1988, doi: 10.1016/0014-2999(88)90614-0.

REFERENCES

- [92] C. De Santi, P. C. Julianotti, A. Pietrabissa, F. Mosca, and G. M. Pacifici, “Catechol-O-methyltransferase: Variation in enzyme activity and inhibition by entacapone and tolcapone,” *Eur J Clin Pharmacol*, vol. 54, no. 3, pp. 215–219, 1998, doi: 10.1007/S002280050448/METRICS.
- [93] D. J. Brooks *et al.*, “Safety and tolerability of COMT inhibitors,” *Neurology*, vol. 62, no. 1 SUPPL. 1, Jan. 2004, doi: 10.1212/WNL.62.1_SUPPL_1.S39.
- [94] A. Kalda, L. Yu, E. Oztas, and J. F. Chen, “Novel neuroprotection by caffeine and adenosine A2A receptor antagonists in animal models of Parkinson’s disease,” *J Neurol Sci*, vol. 248, no. 1–2, pp. 9–15, Oct. 2006, doi: 10.1016/J.JNS.2006.05.003.
- [95] G. C. Palmer, “Neuroprotection by NMDA Receptor Antagonists in a Variety of Neuropathologies,” *Curr Drug Targets*, vol. 2, no. 3, pp. 241–271, Mar. 2005, doi: 10.2174/1389450013348335.
- [96] M. De Lera Ruiz, Y. H. Lim, and J. Zheng, “Adenosine A2A receptor as a drug discovery target,” *J Med Chem*, vol. 57, no. 9, pp. 3623–3650, May 2014, doi: 10.1021/jm4011669.
- [97] K. Ikeda, M. Kurokawa, S. Aoyama, and Y. Kuwana, “Neuroprotection by adenosine A2A receptor blockade in experimental models of Parkinson’s disease,” *J Neurochem*, vol. 80, no. 2, pp. 262–270, 2002, doi: 10.1046/j.0022-3042.2001.00694.x.
- [98] R. Dungo and E. D. Deeks, “Istradefylline: First global approval,” *Drugs*, vol. 73, no. 8, pp. 875–882, Jun. 2013, doi: 10.1007/s40265-013-0066-7.
- [99] J. F. Chen and R. A. Cunha, “The belated US FDA approval of the adenosine A2A receptor antagonist istradefylline for treatment of Parkinson’s disease,” *Purinergic Signal*, vol. 16, no. 2, pp. 167–174, Jun. 2020, doi: 10.1007/s11302-020-09694-2.
- [100] X. Gonda, “Basic Pharmacology of NMDA Receptors,” *Curr Pharm Des*, vol. 18, no. 12, pp. 1558–1567, Mar. 2012, doi: 10.2174/13816121279958521.
- [101] J. C. Stoof, J. Booij, and B. Drukarch, “Amantadine as N-methyl-d-aspartic acid receptor antagonist: new possibilities for therapeutic applications?,” *Clin Neurol Neurosurg*, vol. 94, no. SUPPL., pp. 4–6, Jan. 1992, doi: 10.1016/0303-8467(92)90006-O.
- [102] Y. S. Mironova, I. A. Zhukova, N. G. Zhukova, V. M. Alifirova, O. P. Izboldina, and A. V. Latypova, “[Parkinson’s disease and glutamate excitotoxicity],” *Zh Nevrol Psichiatr Im S S Korsakova*, vol. 118, no. 6. Vyp. 2, pp. 50–54, Jan. 2018, doi: 10.17116/JNEVRO201811806250.
- [103] L. Iovino, M. E. Tremblay, and L. Civiero, “Glutamate-induced excitotoxicity in Parkinson’s disease: The role of glial cells,” *J Pharmacol Sci*, vol. 144, no. 3, pp. 151–164, Nov. 2020, doi: 10.1016/J.JPHS.2020.07.011.
- [104] Z. Zhang *et al.*, “Roles of Glutamate Receptors in Parkinson’s Disease,” *International Journal of Molecular Sciences 2019, Vol. 20, Page 4391*, vol. 20, no. 18, p. 4391, Sep. 2019, doi: 10.3390/IJMS20184391.
- [105] J. H. Chen, T. W. Huang, and C. T. Hong, “Cholinesterase inhibitors for gait, balance, and fall in Parkinson disease: a meta-analysis,” *npj Parkinson’s Disease* 2021 7:1, vol. 7, no. 1, pp. 1–7, Nov. 2021, doi: 10.1038/s41531-021-00251-1.
- [106] T. B. Stoker, K. M. Torsney, and R. A. Barker, “Emerging Treatment Approaches for Parkinson’s Disease,” *Front Neurosci*, vol. 12, no. OCT, Oct. 2018, doi: 10.3389/FNINS.2018.00693.
- [107] A. Y. Hung and M. A. Schwarzschild, “Approaches to Disease Modification for Parkinson’s Disease: Clinical Trials and Lessons Learned,” *Neurotherapeutics*, vol. 17, no. 4, p. 1393, Oct. 2020, doi: 10.1007/S13311-020-00964-W.
- [108] M. Vicario, D. Cieri, M. Brini, and T. Cali, “The close encounter between alpha-synuclein and mitochondria,” *Front Neurosci*, vol. 12, no. JUN, p. 388, Jun. 2018, doi: 10.3389/FNINS.2018.00388/BIBTEX.

REFERENCES

- [109] J. Wagner *et al.*, “Anle138b: A novel oligomer modulator for disease-modifying therapy of neurodegenerative diseases such as prion and Parkinson’s disease,” *Acta Neuropathol.*, vol. 125, no. 6, pp. 795–813, Jun. 2013, doi: 10.1007/S00401-013-1114-9/FIGURES/9.
- [110] J. Q. Li, L. Tan, and J. T. Yu, “The role of the LRRK2 gene in Parkinsonism,” *Mol Neurodegener.*, vol. 9, no. 1, p. 47, Nov. 2014, doi: 10.1186/1750-1326-9-47/FIGURES/3.
- [111] M. G. Heckman *et al.*, “Fine-mapping of the non-coding variation driving the Caucasian LRRK2 GWAS signal in Parkinson’s disease,” *Parkinsonism Relat Disord.*, vol. 83, pp. 22–30, Feb. 2021, doi: 10.1016/J.PARKRELDIS.2020.12.016.
- [112] J. L. Henderson *et al.*, “Discovery and preclinical profiling of 3-[4-(morpholin-4-yl)-7H-pyrrolo[2,3-d]pyrimidin-5-yl]benzonitrile (PF-06447475), a highly potent, selective, brain penetrant, and in vivo active LRRK2 kinase inhibitor,” *J Med Chem.*, vol. 58, no. 1, pp. 419–432, Jan. 2015, doi: 10.1021/jm5014055.
- [113] E. J. R. Fletcher, T. Kaminski, G. Williams, and S. Duty, “Drug repurposing strategies of relevance for Parkinson’s disease,” *Pharmacol Res Perspect.*, vol. 9, no. 4, p. e00841, Aug. 2021, doi: 10.1002/PRP2.841.
- [114] A. Elkouzi, V. Vedam-Mai, R. S. Eisinger, and M. S. Okun, “Emerging therapies in Parkinson disease—repurposed drugs and new approaches,” *Nature Reviews Neurology* 2019 15:4, vol. 15, no. 4, pp. 204–223, Mar. 2019, doi: 10.1038/s41582-019-0155-7.
- [115] C. A. Mulvaney *et al.*, “GLP-1 receptor agonists for Parkinson’s disease,” *Cochrane Database of Systematic Reviews*, vol. 2020, no. 7, Jul. 2020, doi: 10.1002/14651858.CD012990.PUB2/INFORMATION/EN.
- [116] S. Gua, H. Huang, J. Bia, Y. Yao, and T. Wen, “Combined treatment of neurotrophin-3 gene and neural stem cells is ameliorative to behavior recovery of Parkinson’s disease rat model,” *Brain Res.*, vol. 1257, pp. 1–9, Feb. 2009, doi: 10.1016/J.BRAINRES.2008.12.016.
- [117] T. J. Collier and C. E. Sortwell, “Therapeutic potential of nerve growth factors in Parkinson’s disease,” *Drugs Aging*, vol. 14, no. 4, pp. 261–287, Aug. 1999, doi: 10.2165/00002512-199914040-00003/METRICS.
- [118] R. Morphy and Z. Rankovic, “Designed multiple ligands. An emerging drug discovery paradigm,” *J Med Chem.*, vol. 48, no. 21, pp. 6523–6543, Oct. 2005, doi: 10.1021/JM058225D/ASSET/IMAGES/LARGE/JM058225DF00041.JPG.
- [119] R. Morphy and Z. Rankovic, “Designing Multiple Ligands – Medicinal Chemistry Strategies and Challenges,” *Curr Pharm Des.*, vol. 15, no. 6, pp. 587–600, 2009, doi: 10.2174/138161209787315594.
- [120] C. J. Van Der Schyf, “The use of multi-target drugs in the treatment of neurodegenerative diseases,” <https://doi.org/10.1586/ecp.11.13>, vol. 4, no. 3, pp. 293–298, May 2014, doi: 10.1586/ECP.11.13.
- [121] D. Charvin, R. Medori, R. A. Hauser, and O. Rascol, “Therapeutic strategies for Parkinson disease: Beyond dopaminergic drugs,” *Nat Rev Drug Discov.*, vol. 17, no. 11, pp. 804–822, Nov. 2018, doi: 10.1038/nrd.2018.136.
- [122] M. Cieślak, M. Komoszyński, and A. Wojtczak, “Adenosine A2A receptors in Parkinson’s disease treatment,” *Purinergic Signalling*, vol. 4, no. 4. 2008. doi: 10.1007/s11302-008-9100-8.
- [123] P. Jenner, A. Mori, S. D. Aradi, and R. A. Hauser, “Istradefylline—a first generation adenosine A2A antagonist for the treatment of Parkinson’s disease,” *Expert Review of Neurotherapeutics*, vol. 21, no. 3. 2021. doi: 10.1080/14737175.2021.1880896.
- [124] M. M. Essa, R. K. Vijayan, G. Castellano-Gonzalez, M. A. Memon, N. Braidy, and G. J. Guillemin, “Neuroprotective effect of natural products against Alzheimer’s disease,” *Neurochemical Research*, vol. 37, no. 9. 2012. doi: 10.1007/s11064-012-0799-9.

REFERENCES

- [125] P. J. Houghton and M. J. Howes, “Natural products and derivatives affecting neurotransmission relevant to Alzheimer’s and Parkinson’s disease,” *NeuroSignals*, vol. 14, no. 1–2. 2005. doi: 10.1159/000085382.
- [126] C. N. Metz and V. A. Pavlov, “Treating disorders across the lifespan by modulating cholinergic signaling with galantamine,” *Journal of Neurochemistry*, vol. 158, no. 6. 2021. doi: 10.1111/jnc.15243.
- [127] D. P. Hong, A. L. Fink, and V. N. Uversky, “Structural Characteristics of α -Synuclein Oligomers Stabilized by the Flavonoid Baicalein,” *J Mol Biol*, vol. 383, no. 1, pp. 214–223, Oct. 2008, doi: 10.1016/j.jmb.2008.08.039.
- [128] K. Rezai-Zadeh *et al.*, “Apigenin and luteolin modulate microglial activation via inhibition of STAT1-induced CD40 expression,” *J Neuroinflammation*, vol. 5, Sep. 2008, doi: 10.1186/1742-2094-5-41.
- [129] Y. Cui *et al.*, “Anti-neuroinflammatory activity of nobiletin on suppression of microglial activation,” *Biol Pharm Bull*, vol. 33, no. 11, pp. 1814–1821, Nov. 2010, doi: 10.1248/bpb.33.1814.
- [130] N. Haleagrahara, C. J. Siew, N. K. Mitra, and M. Kumari, “Neuroprotective effect of bioflavonoid quercetin in 6-hydroxydopamine-induced oxidative stress biomarkers in the rat striatum,” *Neurosci Lett*, vol. 500, no. 2, pp. 139–143, Aug. 2011, doi: 10.1016/j.neulet.2011.06.021.
- [131] F. Islam *et al.*, “Rutin protects dopaminergic neurons from oxidative stress in an animal model of parkinson’s disease,” *Neurotox Res*, vol. 22, no. 1, pp. 1–15, Jul. 2012, doi: 10.1007/s12640-011-9295-2.
- [132] K. B. Magalingam, A. Radhakrishnan, and N. Haleagrahara, “Protective effects of flavonol isoquercitrin, against 6-hydroxy dopamine (6-OHDA) - Induced toxicity in PC12 cells,” *BMC Res Notes*, vol. 7, no. 1, pp. 1–8, Jan. 2014, doi: 10.1186/1756-0500-7-49/FIGURES/7.
- [133] G. Filomeni *et al.*, “Neuroprotection of kaempferol by autophagy in models of rotenone-mediated acute toxicity: Possible implications for Parkinson’s disease,” *Neurobiol Aging*, vol. 33, no. 4, pp. 767–785, Apr. 2012, doi: 10.1016/j.neurobiolaging.2010.05.021.
- [134] V. Zbarsky, K. P. Datla, S. Parkar, D. K. Rai, O. I. Aruoma, and D. T. Dexter, “Neuroprotective properties of the natural phenolic antioxidants curcumin and naringenin but not quercetin and fisetin in a 6-OHDA model of Parkinson’s disease,” *Free Radic Res*, vol. 39, no. 10, pp. 1119–1125, Oct. 2005, doi: 10.1080/10715760500233113.
- [135] X. Wang, S. Chen, G. Ma, M. Ye, and G. Lu, “Genistein protects dopaminergic neurons by inhibiting microglial activation,” *Neuroreport*, vol. 16, no. 3, pp. 267–270, Feb. 2005, doi: 10.1097/00001756-200502280-00013.
- [136] A. Carotti *et al.*, “Natural and synthetic geiparvarins are strong and selective MAO-B inhibitors. Synthesis and SAR studies,” *Bioorg Med Chem Lett*, vol. 12, no. 24, pp. 3551–3555, Dec. 2002, doi: 10.1016/S0960-894X(02)00798-9.
- [137] X. Ren and J. F. Chen, “Caffeine and Parkinson’s Disease: Multiple Benefits and Emerging Mechanisms,” *Front Neurosci*, vol. 14, Dec. 2020, doi: 10.3389/fnins.2020.602697.
- [138] K. Kieburz and K. B. Wunderle, “Parkinson’s disease: Evidence for environmental risk factors,” *Movement Disorders*, vol. 28, no. 1, pp. 8–13, Jan. 2013, doi: 10.1002/MDS.25150.
- [139] K. W. Lee *et al.*, “Neuroprotective and Anti-inflammatory Properties of a Coffee Component in the MPTP Model of Parkinson’s Disease,” *Neurotherapeutics*, vol. 10, no. 1, pp. 143–153, Jan. 2013, doi: 10.1007/S13311-012-0165-2/METRICS.
- [140] R. Voelker, “Add-on Drug Approved for ‘Off’ Episodes of Parkinson Disease,” *JAMA*, vol. 322, no. 13, pp. 1246–1246, Oct. 2019, doi: 10.1001/JAMA.2019.15403.
- [141] E. El Nebris, “Neuroprotective Activities of Curcumin in Parkinson’s Disease: A Review of the Literature,” *International Journal of Molecular Sciences 2021, Vol. 22, Page 11248*, vol. 22, no. 20, p. 11248, Oct. 2021, doi: 10.3390/IJMS222011248.

REFERENCES

- [142] R. A. Sharma, A. J. Gescher, and W. P. Steward, “Curcumin: The story so far,” *Eur J Cancer*, vol. 41, no. 13, pp. 1955–1968, Sep. 2005, doi: 10.1016/J.EJCA.2005.05.009.
- [143] P. Dadgostar, “Antimicrobial resistance: implications and costs,” *Infection and Drug Resistance*, vol. 12. 2019. doi: 10.2147/IDR.S234610.
- [144] E. Christaki, M. Marcou, and A. Tofarides, “Antimicrobial Resistance in Bacteria: Mechanisms, Evolution, and Persistence,” *Journal of Molecular Evolution*, vol. 88, no. 1. 2020. doi: 10.1007/s00239-019-09914-3.
- [145] A. Y. Peleg, H. Seifert, and D. L. Paterson, “Acinetobacter baumannii: Emergence of a successful pathogen,” *Clinical Microbiology Reviews*, vol. 21, no. 3. 2008. doi: 10.1128/CMR.00058-07.
- [146] S. Santajit and N. Indrawattana, “Mechanisms of Antimicrobial Resistance in ESKAPE Pathogens,” *BioMed Research International*, vol. 2016. 2016. doi: 10.1155/2016/2475067.
- [147] L. C. S. Antunes, P. Visca, and K. J. Towner, “Acinetobacter baumannii: Evolution of a global pathogen,” *Pathogens and Disease*, vol. 71, no. 3. 2014. doi: 10.1111/2049-632X.12125.
- [148] M. Sarshar, P. Behzadi, D. Scribano, A. T. Palamara, and C. Ambrosi, “Acinetobacter baumannii: An ancient commensal with weapons of a pathogen,” *Pathogens*, vol. 10, no. 4, 2021, doi: 10.3390/pathogens10040387.
- [149] R. Gyawali and S. A. Ibrahim, “Natural products as antimicrobial agents,” *Food Control*, vol. 46. 2014. doi: 10.1016/j.foodcont.2014.05.047.
- [150] Y. Jalali, M. Jalali, and J. Payer, “Acinetobacter baumannii : Emergence of a Superbug, Past, Present, and Future ,” in *The Global Antimicrobial Resistance Epidemic - Innovative Approaches and Cutting-Edge Solutions*, 2022. doi: 10.5772/intechopen.104124.
- [151] L. C. Kuo, L. J. Teng, C. J. Yu, S. W. Ho, and P. R. Hsueh, “Dissemination of a Clone of Unusual Phenotype of Pandrug-Resistant Acinetobacter baumannii at a University Hospital in Taiwan,” *J Clin Microbiol*, vol. 42, no. 4, 2004, doi: 10.1128/JCM.42.4.1759-1763.2004.
- [152] R. J. Worthington, J. J. Richards, and C. Melander, “Small molecule control of bacterial biofilms,” *Organic and Biomolecular Chemistry*, vol. 10, no. 37. 2012. doi: 10.1039/c2ob25835h.
- [153] J. Yeom, J. H. Shin, J. Y. Yang, J. Kim, and G. S. Hwang, “¹H NMR-Based Metabolite Profiling of Planktonic and Biofilm Cells in Acinetobacter baumannii 1656-2,” *PLoS One*, vol. 8, no. 3, 2013, doi: 10.1371/journal.pone.0057730.
- [154] C. Nejjari, Y. El Achhab, A. Benaouda, and C. Abdelfattah, “Antimicrobial resistance among GLASS pathogens in Morocco: an epidemiological scoping review,” *BMC Infect Dis*, vol. 22, no. 1, 2022, doi: 10.1186/s12879-022-07412-4.
- [155] U. J. Kim, H. K. Kim, J. H. An, S. K. Cho, K.-H. Park, and H.-C. Jang, “ Update on the Epidemiology, Treatment, and Outcomes of Carbapenem-resistant Acinetobacter infections ,” *Chonnam Med J*, vol. 50, no. 2, 2014, doi: 10.4068/cmj.2014.50.2.37.
- [156] C. R. Lee *et al.*, “Biology of Acinetobacter baumannii: Pathogenesis, antibiotic resistance mechanisms, and prospective treatment options,” *Front Cell Infect Microbiol*, vol. 7, no. MAR, 2017, doi: 10.3389/fcimb.2017.00055.
- [157] S. Skariyachan, N. Taskeen, M. Ganta, and B. Venkata Krishna, “Recent perspectives on the virulent factors and treatment options for multidrug-resistant Acinetobacter baumannii,” *Critical Reviews in Microbiology*, vol. 45, no. 3. 2019. doi: 10.1080/1040841X.2019.1600472.
- [158] S. E. Rollauer, M. A. Soreshjani, N. Noinaj, and S. K. Buchanan, “Outer membrane protein biogenesis in Gram-negative bacteria,” *Philosophical Transactions of the Royal Society B: Biological Sciences*, vol. 370, no. 1679. 2015. doi: 10.1098/rstb.2015.0023.

REFERENCES

- [159] J. W. Fairman, N. Noinaj, and S. K. Buchanan, “The structural biology of β -barrel membrane proteins: A summary of recent reports,” *Current Opinion in Structural Biology*, vol. 21, no. 4. 2011. doi: 10.1016/j.sbi.2011.05.005.
- [160] Y. Smani, A. Fabrega, I. Roca, V. Saánchez-Encinales, J. Vila, and J. Pachón, “Role of OmpA in the multidrug resistance phenotype of *Acinetobacter baumannii*,” *Antimicrob Agents Chemother*, vol. 58, no. 3, 2014, doi: 10.1128/AAC.02101-13.
- [161] S. G. J. Smith, V. Mahon, M. A. Lambert, and R. P. Fagan, “A molecular Swiss army knife: OmpA structure, function and expression,” *FEMS Microbiology Letters*, vol. 273, no. 1. 2007. doi: 10.1111/j.1574-6968.2007.00778.x.
- [162] S. Krishnan and N. V. Prasad Rao, “Outer membrane protein A and OprF: Versatile roles in Gram-negative bacterial infections,” *FEBS Journal*, vol. 279, no. 6. 2012. doi: 10.1111/j.1742-4658.2012.08482.x.
- [163] M. Catel-Ferreira, “The outer membrane porin OmpW of *Acinetobacter baumannii* is involved in iron uptake and colistin binding,” *FEBS Lett*, vol. 590, pp. 224–231, 2016.
- [164] H. Pilsl, D. Šmajc, and V. Braun, “Characterization of colicin S4 and its receptor, OmpW, a minor protein of the *Escherichia coli* outer membrane,” *J Bacteriol*, vol. 181, no. 11, 1999, doi: 10.1128/jb.181.11.3578-3581.1999.
- [165] F. Gil *et al.*, “The *ompW* (porin) gene mediates methyl viologen (paraquat) efflux in *Salmonella enterica* serovar *Typhimurium*,” *Res Microbiol*, vol. 158, no. 6, 2007, doi: 10.1016/j.resmic.2007.05.004.
- [166] F. Fernández-Cuenca *et al.*, “Attenuated virulence of a slow-growing pandrug-resistant *Acinetobacter baumannii* is associated with decreased expression of genes encoding the porins CarO and OprD-like,” *International Journal of Antimicrobial Agents*, vol. 38, no. 6. 2011. doi: 10.1016/j.ijantimicag.2011.08.002.
- [167] E. Geisinger and R. R. Isberg, “Antibiotic Modulation of Capsular Exopolysaccharide and Virulence in *Acinetobacter baumannii*,” *PLoS Pathog*, vol. 11, no. 2, 2015, doi: 10.1371/journal.ppat.1004691.
- [168] M. L. Liou, P. C. Soo, S. R. Ling, H. Y. Kuo, C. Y. Tang, and K. C. Chang, “The sensor kinase BfmS mediates virulence in *Acinetobacter baumannii*,” *Journal of Microbiology, Immunology and Infection*, vol. 47, no. 4, 2014, doi: 10.1016/j.jmii.2012.12.004.
- [169] T. A. Russo *et al.*, “The Response Regulator BfmR Is a Potential Drug Target for *Acinetobacter baumannii*,” *mSphere*, vol. 1, no. 3, 2016, doi: 10.1128/mSphere.00082-16.
- [170] J. H. Moffatt *et al.*, “Colistin resistance in *Acinetobacter baumannii* is mediated by complete loss of lipopolysaccharide production,” *Antimicrob Agents Chemother*, vol. 54, no. 12, 2010, doi: 10.1128/AAC.00834-10.
- [171] J. J. Kenyon and R. M. Hall, “Variation in the Complex Carbohydrate Biosynthesis Loci of *Acinetobacter baumannii* Genomes,” *PLoS One*, vol. 8, no. 4, 2013, doi: 10.1371/journal.pone.0062160.
- [172] J. J. Kenyon, S. J. Nigro, and R. M. Hall, “Variation in the OC locus of *Acinetobacter baumannii* genomes predicts extensive structural diversity in the lipooligosaccharide,” *PLoS One*, vol. 9, no. 9, 2014, doi: 10.1371/journal.pone.0107833.
- [173] M. Flores-Díaz, L. Monturiol-Gross, C. Naylor, A. Alape-Girón, and A. Flieger, “Bacterial Sphingomyelinases and Phospholipases as Virulence Factors,” *Microbiology and Molecular Biology Reviews*, vol. 80, no. 3, 2016, doi: 10.1128/mmbr.00082-15.
- [174] S. M. Kareem, I. M. S. Al-Kadmy, M. H. Al-Kaabi, S. N. Aziz, and M. Ahmad, “*Acinetobacter baumannii* virulence is enhanced by the combined presence of virulence factors genes phospholipase C (*plcN*) and elastase (*lasB*),” *Microb Pathog*, vol. 110, 2017, doi: 10.1016/j.micpath.2017.08.001.
- [175] S. E. Fieste *et al.*, “Iron-Regulated phospholipase C Activity contributes to the cytolytic activity and virulence of *acinetobacter baumannii*,” *PLoS One*, vol. 11, no. 11, 2016, doi: 10.1371/journal.pone.0167068.

REFERENCES

- [176] J. Zhang, L. L. Xu, D. Gan, and X. Zhang, “In Vitro study of bacteriophage AB3 Endolysin LysAB3 Activity Against Acinetobacter baumannii Biofilm and Biofilm-Bound A. baumannii,” *Clin Lab*, vol. 64, no. 6, 2018, doi: 10.7754/Clin.Lab.2018.180342.
- [177] E. G. Di Domenico *et al.*, “Biofilm is a major virulence determinant in bacterial colonization of chronic skin ulcers independently from the multidrug resistant phenotype,” *Int J Mol Sci*, vol. 18, no. 5, 2017, doi: 10.3390/ijms18051077.
- [178] A. H. K. Choi, L. Slamti, F. Y. Avci, G. B. Pier, and T. Maira-Litrán, “The pgaABCD locus of *Acinetobacter baumannii* encodes the production of poly- β -1-6-N-acetylglucosamine, which is critical for biofilm formation,” *J Bacteriol*, vol. 191, no. 19, 2009, doi: 10.1128/JB.00647-09.
- [179] C. M. Harding, S. W. Hennon, and M. F. Feldman, “Uncovering the mechanisms of *Acinetobacter baumannii* virulence,” *Nature Reviews Microbiology*, vol. 16, no. 2. 2018. doi: 10.1038/nrmicro.2017.148.
- [180] M. López *et al.*, “Quorum sensing network in clinical strains of *A. baumannii*: AidA is a new quorum quenching enzyme,” *PLoS One*, vol. 12, no. 3, 2017, doi: 10.1371/journal.pone.0174454.
- [181] L. Fernandez-Garcia *et al.*, “Relationship between the Quorum network (sensing/quenching) and clinical features of pneumonia and bacteraemia caused by *A. Baumannii*,” *Front Microbiol*, vol. 9, 2018, doi: 10.3389/fmicb.2018.03105.
- [182] N. Bhargava, P. Sharma, and N. Capalash, “Quorum sensing in *Acinetobacter*: An emerging pathogen,” *Critical Reviews in Microbiology*, vol. 36, no. 4. 2010. doi: 10.3109/1040841X.2010.512269.
- [183] C. Mayer, A. Muras, M. Romero, M. López, M. Tomás, and A. Otero, “Multiple quorum quenching enzymes are active in the nosocomial pathogen *Acinetobacter baumannii* ATCC17978,” *Front Cell Infect Microbiol*, vol. 8, no. SEP, 2018, doi: 10.3389/fcimb.2018.00310.
- [184] R. Saha, N. Saha, R. S. Donofrio, and L. L. Bestervelt, “Microbial siderophores: A mini review,” *J Basic Microbiol*, vol. 53, no. 4, 2013, doi: 10.1002/jobm.201100552.
- [185] J. A. Gaddy, L. A. Actis, B. A. Arivett, M. J. Mcconnell, L. R. Rafael, and J. Pachón, “Role of *Acinetobactin*-mediated iron acquisition functions in the interaction of *Acinetobacter baumannii* strain ATCC 19606T with human lung epithelial cells, *Galleria mellonella* caterpillars, and mice,” *Infect Immun*, vol. 80, no. 3, 2012, doi: 10.1128/IAI.06279-11.
- [186] D. L. Zimbler *et al.*, “Stress response and virulence functions of the *Acinetobacter baumannii* NfuA Fe-S scaffold protein,” *J Bacteriol*, vol. 194, no. 11, 2012, doi: 10.1128/JB.00213-12.
- [187] B. D. Corbin *et al.*, “Metal chelation and inhibition of bacterial growth in tissue abscesses,” *Science (1979)*, vol. 319, no. 5865, 2008, doi: 10.1126/science.1152449.
- [188] M. I. Hood *et al.*, “Identification of an *Acinetobacter baumannii* Zinc Acquisition System that Facilitates Resistance to Calprotectin-mediated Zinc Sequestration,” *PLoS Pathog*, vol. 8, no. 12, 2012, doi: 10.1371/journal.ppat.1003068.
- [189] A. Kulp and M. J. Kuehn, “Biological Functions and biogenesis of secreted bacterial outer membrane vesicles,” *Annual Review of Microbiology*, vol. 64. 2010. doi: 10.1146/annurev.micro.091208.073413.
- [190] T. N. Ellis and M. J. Kuehn, “Virulence and Immunomodulatory Roles of Bacterial Outer Membrane Vesicles,” *Microbiology and Molecular Biology Reviews*, vol. 74, no. 1, 2010, doi: 10.1128/mmbr.00031-09.
- [191] J. S. Jin *et al.*, “*Acinetobacter baumannii* secretes cytotoxic outer membrane protein a via outer membrane vesicles,” *PLoS One*, vol. 6, no. 2, 2011, doi: 10.1371/journal.pone.0017027.
- [192] C. M. Harding, R. L. Kinsella, L. D. Palmer, E. P. Skaar, and M. F. Feldman, “Medically Relevant *Acinetobacter* Species Require a Type II Secretion System and Specific Membrane-Associated Chaperones for the Export of Multiple Substrates and Full Virulence,” *PLoS Pathog*, vol. 12, no. 1, 2016, doi: 10.1371/journal.ppat.1005391.

REFERENCES

- [193] M. Basler, B. T. Ho, and J. J. Mekalanos, “Tit-for-tat: Type VI secretion system counterattack during bacterial cell-cell interactions,” *Cell*, vol. 152, no. 4, 2013, doi: 10.1016/j.cell.2013.01.042.
- [194] L. V. Bentancor, A. Camacho-Peiro, C. Bozkurt-Guzel, G. B. Pier, and T. Maira-Litrán, “Identification of Ata, a multifunctional trimeric autotransporter of *Acinetobacter baumannii*,” *J Bacteriol*, vol. 194, no. 15, 2012, doi: 10.1128/JB.06769-11.
- [195] F. P. Nocera, A. R. Attili, and L. De Martino, “*Acinetobacter baumannii*: Its clinical significance in human and veterinary medicine,” *Pathogens*, vol. 10, no. 2. 2021. doi: 10.3390/pathogens10020127.
- [196] H. Yu, R. Hu, X. Hu, Y. Lu, Y. Yao, and J. Su, “Risk factors for bacteremia and mortality due to multidrug-resistant *Acinetobacter baumannii*: a retrospective study,” *Lett Appl Microbiol*, vol. 77, no. 2, Feb. 2024, doi: 10.1093/LAMBIO/OVAE006.
- [197] Y. Zheng *et al.*, “Colonization With Extensively Drug-Resistant *Acinetobacter baumannii* and Prognosis in Critically Ill Patients: An Observational Cohort Study,” *Front Med (Lausanne)*, vol. 8, 2021, doi: 10.3389/fmed.2021.667776.
- [198] J. Uwingabiye *et al.*, “Intensive care unit-acquired *Acinetobacter baumannii* infections in a Moroccan teaching hospital: Epidemiology, risk factors and outcome,” *Germs*, vol. 7, no. 4, 2017, doi: 10.18683/germs.2017.1126.
- [199] S. S. Long, C. G. Prober, and M. Fischer, *Principles and Practice of Pediatric Infectious Diseases*. 2017. doi: 10.1086/516117.
- [200] D. R. Chung *et al.*, “High prevalence of multidrug-resistant nonfermenters in hospital-acquired pneumonia in Asia,” *Am J Respir Crit Care Med*, vol. 184, no. 12, 2011, doi: 10.1164/rccm.201102-0349OC.
- [201] C. Dananché *et al.*, “Trends of incidence and risk factors of ventilator-associated pneumonia in elderly patients admitted to French ICUs between 2007 and 2014,” *Crit Care Med*, vol. 46, no. 6, 2018, doi: 10.1097/CCM.00000000000003019.
- [202] A. Martínez-Pellús, J. Ruiz Gómez, F. Jaime Sánchez, E. Simarro Córdoba, and J. A. Fernández Lozano, “Incidence of colonization and infection by *Acinetobacter baumannii* in an endemic setting (ICU). Analysis of risk factors,” *Enferm Infecc Microbiol Clin*, vol. 20, no. 5, 2002, doi: 10.1016/s0213-005x(02)72788-2.
- [203] A. Rodríguez, P. Póvoa, S. Nseir, J. Salluh, D. Curcio, and I. Martín-Loeches, “Incidence and diagnosis of ventilator-associated tracheobronchitis in the intensive care unit: An international online survey,” *Crit Care*, vol. 18, no. 1, 2014, doi: 10.1186/cc13725.
- [204] E. Bergogne-Bérénin and K. J. Towner, “*Acinetobacter* spp. as nosocomial pathogens: Microbiological, clinical, and epidemiological features,” *Clinical Microbiology Reviews*, vol. 9, no. 2. 1996. doi: 10.1128/cmrx.9.2.148-165.1996.
- [205] A. Tabah *et al.*, “Characteristics and determinants of outcome of hospital-acquired bloodstream infections in intensive care units: The EUROBACT International Cohort Study,” *Intensive Care Med*, vol. 38, no. 12, 2012, doi: 10.1007/s00134-012-2695-9.
- [206] T. Chopra *et al.*, “Risk factors and outcomes for patients with bloodstream infection due to *Acinetobacter baumannii*-calcoaceticus complex,” *Antimicrob Agents Chemother*, vol. 58, no. 8, 2014, doi: 10.1128/AAC.02441-14.
- [207] H. Y. Zhou, Z. Yuan, and Y. P. Du, “Prior use of four invasive procedures increases the risk of *Acinetobacter baumannii* nosocomial bacteremia among patients in intensive care units: A systematic review and meta-analysis,” *International Journal of Infectious Diseases*, vol. 22, 2014, doi: 10.1016/j.ijid.2014.01.018.
- [208] M. Castanheira, R. E. Mendes, and A. C. Gales, “Global Epidemiology and Mechanisms of Resistance of *Acinetobacter baumannii*-calcoaceticus Complex,” *Clinical Infectious Diseases*, vol. 76, 2023, doi: 10.1093/cid/ciad109.

REFERENCES

- [209] E. Tacconelli, “Discovery, research, and development of new antibiotics: the WHO priority list of antibiotic-resistant bacteria and tuberculosis,” *Lancet Infect. Dis.*, vol. 18, pp. 318–327, 2018.
- [210] R. E. Mendes, D. J. Farrell, H. S. Sader, and R. N. Jones, “Comprehensive assessment of tigecycline activity tested against a worldwide collection of *Acinetobacter* spp. (2005–2009),” *Diagn Microbiol Infect Dis*, vol. 68, no. 3, 2010, doi: 10.1016/j.diagmicrobio.2010.07.003.
- [211] European Centre for Disease Prevention and Control, *Annual Epidemiological Report 2012. Reporting on 2010 surveillance data and 2011 epidemic intelligence data*. 2013.
- [212] J. Nowak *et al.*, “High incidence of pandrug-resistant *Acinetobacter baumannii* isolates collected from patients with ventilator-associated pneumonia in Greece, Italy and Spain as part of the MagicBullet clinical trial,” *Journal of Antimicrobial Chemotherapy*, vol. 72, no. 12, 2017, doi: 10.1093/jac/dkx322.
- [213] I. Abbott, G. M. Cerqueira, S. Bhuiyan, and A. Y. Peleg, “Carbapenem resistance in *Acinetobacter baumannii*: Laboratory challenges, mechanistic insights and therapeutic strategies,” *Expert Review of Anti-Infective Therapy*, vol. 11, no. 4. 2013. doi: 10.1586/eri.13.21.
- [214] P. C. S. Ribeiro *et al.*, “Phenotypic and molecular detection of the bla KPC gene in clinical isolates from inpatients at hospitals in São Luis, MA, Brazil,” *BMC Infect Dis*, vol. 16, no. 1, 2016, doi: 10.1186/s12879-016-2072-3.
- [215] L. J. V. Piddock, “Clinically relevant chromosomally encoded multidrug resistance efflux pumps in bacteria,” *Clinical Microbiology Reviews*, vol. 19, no. 2. 2006. doi: 10.1128/CMR.19.2.382-402.2006.
- [216] L. Huang, L. Sun, G. Xu, and T. Xia, “Differential susceptibility to carbapenems due to the AdeABC efflux pump among nosocomial outbreak isolates of *Acinetobacter baumannii* in a Chinese hospital,” *Diagn Microbiol Infect Dis*, vol. 62, no. 3, 2008, doi: 10.1016/j.diagmicrobio.2008.06.008.
- [217] S. Coyne, P. Courvalin, and B. Périchon, “Efflux-mediated antibiotic resistance in *Acinetobacter* spp.,” *Antimicrobial Agents and Chemotherapy*, vol. 55, no. 3. 2011. doi: 10.1128/AAC.01388-10.
- [218] M. Catel-Ferreira *et al.*, “Structure-function relationships of CarO, the carbapenem resistance-associated outer membrane protein of *Acinetobacter baumannii*,” *Journal of Antimicrobial Chemotherapy*, vol. 66, no. 9, 2011, doi: 10.1093/jac/dkr267.
- [219] M. D. M. Tomás *et al.*, “Cloning and functional analysis of the gene encoding the 33- to 36-kilodalton outer membrane protein associated with carbapenem resistance in *Acinetobacter baumannii*,” *Antimicrob Agents Chemother*, vol. 49, no. 12, 2005, doi: 10.1128/AAC.49.12.5172-5175.2005.
- [220] A. Pormohammad *et al.*, “Global prevalence of colistin resistance in clinical isolates of *Acinetobacter baumannii*: A systematic review and meta-analysis,” *Microb Pathog*, vol. 139, 2020, doi: 10.1016/j.micpath.2019.103887.
- [221] F. A. Gogry, M. T. Siddiqui, I. Sultan, and Q. M. R. Haq, “Current Update on Intrinsic and Acquired Colistin Resistance Mechanisms in Bacteria,” *Frontiers in Medicine*, vol. 8. 2021. doi: 10.3389/fmed.2021.677720.
- [222] N. Tafreshi, L. Babaekhou, and M. Ghane, “Antibiotic resistance pattern of *acinetobacter baumannii* from burns patients: Increase in prevalence of blaOXA-24-like and blaOXA-58-like genes,” *Iran J Microbiol*, vol. 11, no. 6, 2019, doi: 10.18502/ijm.v11i6.2222.
- [223] G. Mancuso, S. De Gaetano, A. Midiri, S. Zummo, and C. Biondo, “The Challenge of Overcoming Antibiotic Resistance in Carbapenem-Resistant Gram-Negative Bacteria: ‘Attack on Titan.’” *Microorganisms*, vol. 11, no. 8. 2023. doi: 10.3390/microorganisms11081912.
- [224] L. L. Maragakis and T. M. Perl, “*Acinetobacter baumannii*: Epidemiology, antimicrobial resistance, and treatment options,” *Clinical Infectious Diseases*, vol. 46, no. 8. 2008. doi: 10.1086/529198.
- [225] T. W. Cooper, S. E. Pass, S. D. Brouse, and R. G. Hall, “Can pharmacokinetic and pharmacodynamic principles be applied to the treatment of multidrug-resistant *Acinetobacter*?,” *Annals of Pharmacotherapy*, vol. 45, no. 2. 2011. doi: 10.1345/aph.1P187.

REFERENCES

- [226] M. Castanheira, R. N. Jones, and D. M. Livermore, “Antimicrobial activities of doripenem and other carbapenems against *Pseudomonas aeruginosa*, other nonfermentative bacilli, and *Aeromonas* spp.,” *Diagn Microbiol Infect Dis*, vol. 63, no. 4, 2009, doi: 10.1016/j.diagmicrobio.2009.01.026.
- [227] I. Roca, P. Espinal, X. Vila-Fanés, and J. Vila, “The *Acinetobacter baumannii* oxymoron: Commensal hospital dweller turned pan-drug-resistant menace,” *Front Microbiol*, vol. 3, no. APR, 2012, doi: 10.3389/fmicb.2012.00148.
- [228] S. Martí, J. Sánchez-Céspedes, V. Alba, and J. Vila, “In vitro activity of doripenem against *Acinetobacter baumannii* clinical isolates,” *Int J Antimicrob Agents*, vol. 33, no. 2, 2009, doi: 10.1016/j.ijantimicag.2008.08.015.
- [229] P. J. Bergen, J. Li, C. R. Rayner, and R. L. Nation, “Colistin methanesulfonate is an inactive prodrug of colistin against *Pseudomonas aeruginosa*,” *Antimicrob Agents Chemother*, vol. 50, no. 6, 2006, doi: 10.1128/AAC.00035-06.
- [230] D. Yahav, L. Farbman, L. Leibovici, and M. Paul, “Colistin: New lessons on an old antibiotic,” *Clinical Microbiology and Infection*, vol. 18, no. 1. 2012. doi: 10.1111/j.1469-0691.2011.03734.x.
- [231] W. Yau *et al.*, “Colistin hetero-resistance in multidrug-resistant *Acinetobacter baumannii* clinical isolates from the Western Pacific region in the SENTRY antimicrobial surveillance programme,” *Journal of Infection*, vol. 58, no. 2, 2009, doi: 10.1016/j.jinf.2008.11.002.
- [232] K. H. Luepke and J. F. Mohr, “The antibiotic pipeline: reviving research and development and speeding drugs to market,” *Expert Review of Anti-Infective Therapy*, vol. 15, no. 5. 2017. doi: 10.1080/14787210.2017.1308251.
- [233] J. Garnacho-Montero and J. F. Timsit, “Managing *Acinetobacter baumannii* infections,” *Current Opinion in Infectious Diseases*, vol. 32, no. 1. 2019. doi: 10.1097/QCO.0000000000000518.
- [234] R. L. Nation *et al.*, “Updated US and European Dose Recommendations for Intravenous Colistin: How Do They Perform?,” *Clinical Infectious Diseases*, vol. 62, no. 5, 2016, doi: 10.1093/cid/civ964.
- [235] K. Z. Vardakas, A. D. Mavroudis, M. Georgiou, and M. E. Falagas, “Intravenous colistin combination antimicrobial treatment vs. monotherapy: a systematic review and meta-analysis,” *International Journal of Antimicrobial Agents*, vol. 51, no. 4. 2018. doi: 10.1016/j.ijantimicag.2017.12.020.
- [236] D. R. Bowers *et al.*, “Assessment of minocycline and polymyxin B combination against *Acinetobacter baumannii*,” *Antimicrob Agents Chemother*, vol. 59, no. 5, 2015, doi: 10.1128/AAC.04110-14.
- [237] G. E. Stein and T. Babinchak, “Tigecycline: An update,” *Diagnostic Microbiology and Infectious Disease*, vol. 75, no. 4. 2013. doi: 10.1016/j.diagmicrobio.2012.12.004.
- [238] F. F. Tuon, C. H. Yamada, A. P. de Andrade, L. N. V. S. Arend, D. dos Santos Oliveira, and J. P. Telles, “Oral doxycycline to carbapenem-resistant *Acinetobacter baumannii* infection as a polymyxin-sparing strategy: results from a retrospective cohort,” *Brazilian Journal of Microbiology*, vol. 54, no. 3, 2023, doi: 10.1007/s42770-023-01015-0.
- [239] S. L. Greig and L. J. Scott, “Intravenous Minocycline: A Review in *Acinetobacter* Infections,” *Drugs*, vol. 76, no. 15, 2016, doi: 10.1007/s40265-016-0636-6.
- [240] G. C. Wood, S. D. Hanes, B. A. Boucher, M. A. Croce, and T. C. Fabian, “Tetracyclines for treating multidrug-resistant *Acinetobacter baumannii* ventilator-associated pneumonia,” *Intensive Care Med*, vol. 29, no. 11, 2003, doi: 10.1007/s00134-003-1811-2.
- [241] S. Shakil, M. Akram, and A. U. Khan, “Tigecycline: A critical update,” *Journal of Chemotherapy*, vol. 20, no. 4. 2008. doi: 10.1179/joc.2008.20.4.411.
- [242] J. Vila and J. Pachón, “Therapeutic options for *Acinetobacter baumannii* infections: An update,” *Expert Opinion on Pharmacotherapy*, vol. 13, no. 16. 2012. doi: 10.1517/14656566.2012.729820.

REFERENCES

- [243] L. Principe, S. D'Arezzo, A. Capone, N. Petrosillo, and P. Visca, "In vitro activity of tigecycline in combination with various antimicrobials against multidrug resistant *Acinetobacter baumannii*," *Ann Clin Microbiol Antimicrob*, vol. 8, 2009, doi: 10.1186/1476-0711-8-18.
- [244] J. Vouillamoz, P. Moreillon, M. Giddey, and J. M. Entenza, "In vitro activities of tigecycline combined with other antimicrobials against multiresistant Gram-positive and Gram-negative pathogens," *Journal of Antimicrobial Chemotherapy*, vol. 61, no. 2, 2008, doi: 10.1093/jac/dkm459.
- [245] L. E. López-Cortés *et al.*, "Monotherapy versus combination therapy for sepsis due to multidrug-resistant *Acinetobacter baumannii*: Analysis of a multicentre prospective cohort," *Journal of Antimicrobial Chemotherapy*, vol. 69, no. 11, 2014, doi: 10.1093/jac/dku233.
- [246] Q. Liu, W. Li, Y. Feng, and C. Tao, "Efficacy and safety of polymyxins for the treatment of *Acinetobacter baumannii* infection: A systematic review and meta-analysis," *PLoS ONE*, vol. 9, no. 6. 2014. doi: 10.1371/journal.pone.0098091.
- [247] A. Batirel *et al.*, "Comparison of colistin-carbapenem, colistin-sulbactam, and colistin plus other antibacterial agents for the treatment of extremely drug-resistant *Acinetobacter baumannii* bloodstream infections," *European Journal of Clinical Microbiology and Infectious Diseases*, vol. 33, no. 8, 2014, doi: 10.1007/s10096-014-2070-6.
- [248] R. Sirijatuphat and V. Thamlikitkul, "Preliminary study of colistin versus colistin plus fosfomycin for treatment of carbapenem-resistant *Acinetobacter baumannii* infections," *Antimicrob Agents Chemother*, vol. 58, no. 9, 2014, doi: 10.1128/AAC.02435-13.
- [249] T. Niu, Q. Luo, Y. Li, Y. Zhou, W. Yu, and Y. Xiao, "Comparison of Tigecycline or Cefoperazone/Sulbactam therapy for bloodstream infection due to Carbapenem-resistant *Acinetobacter baumannii*," *Antimicrob Resist Infect Control*, vol. 8, no. 1, 2019, doi: 10.1186/s13756-019-0502-x.
- [250] F. Temocin *et al.*, "Synergistic effects of sulbactam in multi-drug-resistant *acinetobacter baumannii*," *Brazilian Journal of Microbiology*, vol. 46, no. 4, 2015, doi: 10.1590/S1517-838246420140101.
- [251] B. Liu *et al.*, "In vitro activity of tigecycline in combination with cefoperazone–sulbactam against multidrug-resistant *acinetobacter Baumannii*," *Journal of Chemotherapy*, vol. 27, no. 5, 2015, doi: 10.1179/1973947814Y.0000000203.
- [252] M. Abdallah, O. Olafisoye, C. Cortes, C. Urban, D. Landman, and J. Quale, "Activity of eravacycline against Enterobacteriaceae and *Acinetobacter baumannii*, including multidrug-resistant isolates, from New York City," *Antimicrob Agents Chemother*, vol. 59, no. 3, 2015, doi: 10.1128/AAC.04809-14.
- [253] Y. Li, L. Cui, F. Xue, Q. Wang, and B. Zheng, "Synergism of eravacycline combined with other antimicrobial agents against carbapenem-resistant Enterobacteriaceae and *Acinetobacter baumannii*," *J Glob Antimicrob Resist*, vol. 30, 2022, doi: 10.1016/j.jgar.2022.05.020.
- [254] E. Rando *et al.*, "Cefiderocol for severe carbapenem-resistant *a. Baumannii* pneumonia: Towards the comprehension of its place in therapy," *Antibiotics*, vol. 11, no. 1, 2022, doi: 10.3390/antibiotics1101003.
- [255] S. M. Smoke *et al.*, "Evolution and Transmission of Cefiderocol-Resistant *Acinetobacter baumannii* during an Outbreak in the Burn Intensive Care Unit," *Clinical Infectious Diseases*, vol. 76, no. 3, 2023, doi: 10.1093/cid/ciac647.
- [256] C. H. Rodriguez, A. Brune, M. Nastro, C. Vay, and A. Famiglietti, "In vitro synergistic activity of the sulbactam/avibactam combination against extensively drug-resistant *Acinetobacter baumannii*," *J Med Microbiol*, vol. 69, no. 7, 2020, doi: 10.1099/JMM.0.001211.
- [257] M. Sabet, Z. Tarazi, and D. C. Griffith, "Activity of Meropenem-Vaborbactam against *Pseudomonas aeruginosa* and *Acinetobacter baumannii* in a Neutropenic Mouse Thigh Infection Model," *Antimicrob Agents Chemother*, vol. 63, no. 1, 2019, doi: 10.1128/AAC.01665-18.

REFERENCES

- [258] G. Poulakou *et al.*, “Daptomycin as adjunctive treatment for experimental infection by *Acinetobacter baumannii* with resistance to colistin,” *Int J Antimicrob Agents*, vol. 53, no. 2, 2019, doi: 10.1016/j.ijantimicag.2018.10.024.
- [259] M. G. Smith *et al.*, “New insights into *Acinetobacter baumannii* pathogenesis revealed by high-density pyrosequencing and transposon mutagenesis,” *Genes Dev*, vol. 21, no. 5, 2007, doi: 10.1101/gad.1510307.
- [260] N. M. Elhosseiny and A. S. Attia, “*Acinetobacter*: An emerging pathogen with a versatile secretome review-article,” *Emerging Microbes and Infections*, vol. 7, no. 1. 2018. doi: 10.1038/s41426-018-0030-4.
- [261] R. López-Rojas, Y. Smani, and J. Pachón, “Treating multidrug-resistant *Acinetobacter baumannii* infection by blocking its virulence factors,” *Expert Review of Anti-Infective Therapy*, vol. 11, no. 3. 2013. doi: 10.1586/eri.13.11.
- [262] D. A. Rasko and V. Sperandio, “Anti-virulence strategies to combat bacteria-mediated disease,” *Nature Reviews Drug Discovery*, vol. 9, no. 2. 2010. doi: 10.1038/nrd3013.
- [263] H. M. Wexler, “Outer-membrane pore-forming proteins in gram-negative anaerobic bacteria,” in *Clinical Infectious Diseases*, 2002. doi: 10.1086/341923.
- [264] M. J. Kuehn and N. C. Kesty, “Bacterial outer membrane vesicles and the host-pathogen interaction,” *Genes and Development*, vol. 19, no. 22. 2005. doi: 10.1101/gad.1299905.
- [265] X. Vila-Farrés *et al.*, “Combating virulence of Gram-negative bacilli by OmpA inhibition,” *Sci Rep*, vol. 7, no. 1, 2017, doi: 10.1038/s41598-017-14972-y.
- [266] R. Parra-Millán *et al.*, “Synergistic activity of an OmpA inhibitor and colistin against colistin-resistant *Acinetobacter baumannii*: Mechanistic analysis and in vivo efficacy,” *Journal of Antimicrobial Chemotherapy*, vol. 73, no. 12, 2018, doi: 10.1093/jac/dky343.
- [267] I. Soojhawon, N. Pattabiraman, A. Tsang, A. L. Roth, E. Kang, and S. M. Noble, “Discovery of novel inhibitors of multidrug-resistant *Acinetobacter baumannii*,” *Bioorg. Medicinal Chem*, vol. 25, pp. 5477–5482, 2017.
- [268] D. Wong, T. B. Nielsen, R. A. Bonomo, P. Pantapalangkoor, B. Luna, and B. Spellberg, “Clinical and pathophysiological overview of *Acinetobacter* infections: A century of challenges,” *Clin Microbiol Rev*, vol. 30, no. 1, 2017, doi: 10.1128/CMR.00058-16.
- [269] L. Lin *et al.*, “Inhibition of LpxC protects mice from resistant *Acinetobacter baumannii* by modulating inflammation and enhancing phagocytosis,” *mBio*, vol. 3, no. 5, 2012, doi: 10.1128/mBio.00312-12.
- [270] J. Badger *et al.*, “Structure determination of LpxA from the lipopolysaccharide-synthesis pathway of *Acinetobacter baumannii*,” *Acta Crystallogr Sect F Struct Biol Cryst Commun*, vol. 68, no. 12, 2012, doi: 10.1107/S174430911204571X.
- [271] J. Badger *et al.*, “Structure determination of LpxD from the lipopolysaccharide-synthesis pathway of *Acinetobacter baumannii*,” *Acta Crystallogr Sect F Struct Biol Cryst Commun*, vol. 69, no. 1, 2013, doi: 10.1107/S1744309112048890.
- [272] P. Nidadavolu, W. Amor, P. L. Tran, J. Dertien, J. A. Colmer-Hamood, and A. N. Hamood, “Garlic ointment inhibits biofilm formation by bacterial pathogens from burn wounds,” *J Med Microbiol*, vol. 61, no. 5, 2012, doi: 10.1099/jmm.0.038638-0.
- [273] I. Sulemankhil, J. G. Ganopolsky, C. A. Dieni, A. F. Dan, M. L. Jones, and S. Prakash, “Prevention and treatment of virulent bacterial biofilms with an enzymatic nitric oxide-releasing dressing,” *Antimicrob Agents Chemother*, vol. 56, no. 12, 2012, doi: 10.1128/AAC.01173-12.
- [274] P. V. Gawande, K. P. Leung, and S. Madhyastha, “Antibiofilm and antimicrobial efficacy of Dispersin®-KSL-w peptide-based wound gel against chronic wound infection associated bacteria,” *Curr Microbiol*, vol. 68, no. 5, 2014, doi: 10.1007/s00284-014-0519-6.

REFERENCES

- [275] R. J. Thompson *et al.*, “Identification of BfmR, a response regulator involved in biofilm development, as a target for a 2-aminoimidazole-based antibiofilm agent,” *Biochemistry*, vol. 51, no. 49, 2012, doi: 10.1021/bi3015289.
- [276] C. de la Fuente-Núñez, F. Reffuveille, E. F. Haney, S. K. Straus, and R. E. W. Hancock, “Broad-Spectrum Anti-biofilm Peptide That Targets a Cellular Stress Response,” *PLoS Pathog*, vol. 10, no. 5, 2014, doi: 10.1371/journal.ppat.1004152.
- [277] R. Gopal *et al.*, “Synergistic effects and antibiofilm properties of chimeric peptides against multidrug-resistant *Acinetobacter baumannii* strains,” *Antimicrob Agents Chemother*, vol. 58, no. 3, 2014, doi: 10.1128/AAC.02473-13.
- [278] D. M. Stacy, M. A. Welsh, P. N. Rather, and H. E. Blackwell, “Attenuation of quorum sensing in the pathogen *Acinetobacter baumannii* using non-native N -acyl homoserine lactones,” *ACS Chem Biol*, vol. 7, no. 10, 2012, doi: 10.1021/cb300351x.
- [279] M. Nicol *et al.*, “Unsaturated fatty acids affect quorum sensing communication system and inhibit motility and biofilm formation of *Acinetobacter baumannii*,” *Int J Mol Sci*, vol. 19, no. 1, 2018, doi: 10.3390/ijms19010214.
- [280] M. G. Thompson, B. W. Corey, Y. Si, D. W. Craft, and D. V. Zurawski, “Antibacterial activities of iron chelators against common nosocomial pathogens,” *Antimicrob Agents Chemother*, vol. 56, no. 10, 2012, doi: 10.1128/AAC.01197-12.
- [281] C. R. Chitambar, “Gallium and its competing roles with iron in biological systems,” *Biochimica et Biophysica Acta - Molecular Cell Research*, vol. 1863, no. 8. 2016. doi: 10.1016/j.bbamcr.2016.04.027.
- [282] L. De Léséleuc, G. Harris, R. KuoLee, and W. Chen, “In Vitro and in Vivo biological activities of iron chelators and gallium nitrate against *Acinetobacter baumannii*,” *Antimicrob Agents Chemother*, vol. 56, no. 10, 2012, doi: 10.1128/AAC.00778-12.
- [283] L. C. S. Antunes, F. Imperi, F. Minandri, and P. Visca, “In Vitro and In Vivo antimicrobial activities of gallium nitrate against multidrug-resistant *Acinetobacter baumannii*,” *Antimicrob Agents Chemother*, vol. 56, no. 11, 2012, doi: 10.1128/AAC.01519-12.
- [284] Y. S. Cheng *et al.*, “Repurposing screen identifies unconventional drugs with activity against multidrug resistant *Acinetobacter baumannii*,” *Front Cell Infect Microbiol*, vol. 9, no. JAN, 2019, doi: 10.3389/fcimb.2018.00438.
- [285] A. Miró-Canturri, R. Ayerbe-Algaba, A. Vila-Domínguez, M. E. Jiménez-Mejías, J. Pachón, and Y. Smani, “Repurposing of the tamoxifen metabolites to combat infections by multidrug-resistant gram-negative bacilli,” *Antibiotics*, vol. 10, no. 3, Mar. 2021, doi: 10.3390/antibiotics10030336.
- [286] L. N. Jeffreys *et al.*, “Remdesivir–ivermectin combination displays synergistic interaction with improved in vitro activity against SARS-CoV-2,” *Int J Antimicrob Agents*, vol. 59, no. 3, 2022, doi: 10.1016/j.ijantimicag.2022.106542.
- [287] K. M. Carlson-Banning, A. Chou, Z. Liu, R. J. Hamill, Y. Song, and L. Zechiedrich, “Toward Repurposing Ciclopirox as an Antibiotic against Drug-Resistant *Acinetobacter baumannii*, *Escherichia coli*, and *Klebsiella pneumoniae*,” *PLoS One*, vol. 8, no. 7, 2013, doi: 10.1371/journal.pone.0069646.
- [288] S. Thangamani, W. Younis, and M. N. Seleem, “Repurposing celecoxib as a topical antimicrobial agent,” *Front Microbiol*, vol. 6, no. JUL, 2015, doi: 10.3389/fmicb.2015.00750.
- [289] M. Masadeh, N. Mhaidat, K. Alzoubi, S. Al-azzam, and Z. Alnasser, “Antibacterial activity of statins: A comparative study of Atorvastatin, Simvastatin, and Rosuvastatin,” *Ann Clin Microbiol Antimicrob*, vol. 11, 2012, doi: 10.1186/1476-0711-11-13.
- [290] J. A. Andersson *et al.*, “Combating multidrug-resistant pathogens with host-directed nonantibiotic therapeutics,” *Antimicrob Agents Chemother*, vol. 62, no. 1, 2018, doi: 10.1128/AAC.01943-17.

REFERENCES

- [291] L. Dijkshoorn, A. Nemec, and H. Seifert, “An increasing threat in hospitals: Multidrug-resistant *Acinetobacter baumannii*,” *Nature Reviews Microbiology*, vol. 5, no. 12. 2007. doi: 10.1038/nrmicro1789.
- [292] W. H. Elwakil, S. S. Rizk, A. M. El-Halawany, M. E. Rateb, and A. S. Attia, “Multidrug-Resistant *Acinetobacter baumannii* Infections in the United Kingdom versus Egypt: Trends and Potential Natural Products Solutions,” *Antibiotics*, vol. 12, no. 1. 2023. doi: 10.3390/antibiotics12010077.
- [293] I. Assaf, N. Al Hakawati, and J. Borjac, “In-silico study of Lebanese herbal compounds against carbapenem-resistant *Acinetobacter baumannii* proteins,” *Inform Med Unlocked*, vol. 43, p. 101409, Jan. 2023, doi: 10.1016/J.IMU.2023.101409.
- [294] V. Tiwari, R. Roy, and M. Tiwari, “Antimicrobial active herbal compounds against *Acinetobacter baumannii* and other pathogens,” *Front Microbiol*, vol. 6, no. JUN, 2015, doi: 10.3389/fmicb.2015.00618.
- [295] H. Becker, J. M. Scher, J. B. Speakman, and J. Zapp, “Bioactivity guided isolation of antimicrobial compounds from *Lythrum salicaria*,” *Fitoterapia*, vol. 76, no. 6, 2005, doi: 10.1016/j.fitote.2005.04.011.
- [296] E. Guclu, “Antibacterial Activity of *Lythrum salicaria* against Multidrug-resistant *Acinetobacter baumannii* and *Pseudomonas aeruginosa*,” *Annu Res Rev Biol*, vol. 4, no. 7, 2014, doi: 10.9734/arrb/2014/7357.
- [297] Y. Miyasaki *et al.*, “Isolation and Characterization of Antimicrobial Compounds in Plant Extracts against Multidrug-Resistant *Acinetobacter baumannii*,” *PLoS One*, vol. 8, no. 4, 2013, doi: 10.1371/journal.pone.0061594.
- [298] B. Chan, C. B. Lau, and C. Jolivalt, “Chinese medicinal herbs against antibiotic-resistant bacterial pathogens,” *formatex.info*, 2011.
- [299] A. Montagu, P. Saulnier, V. Cassissa, E. Rossines, M. Eveillard, and M. L. Joly-Guillou, “Aromatic and terpenic compounds loaded in lipidic nanocapsules: Activity against multi-drug resistant *acinetobacter baumannii* assessed in vitro and in a murine model of sepsis,” *J Nanomed Nanotechnol*, vol. 5, no. 3, 2014, doi: 10.4172/2157-7439.1000206.
- [300] A. K. Johny, M. J. Darre, A. M. Donoghue, D. J. Donoghue, and K. Venkitanarayanan, “Antibacterial effect of trans-cinnamaldehyde, eugenol, carvacrol, and thymol on salmonella enteritidis and *Campylobacter jejuni* in chicken cecal contents in vitro,” *Journal of Applied Poultry Research*, vol. 19, no. 3, 2010, doi: 10.3382/japr.2010-00181.
- [301] I. C. da S. Cirino *et al.*, “Comparative transcriptomics analysis of multidrug-resistant *Acinetobacter baumannii* in response to treatment with the terpenic compounds thymol and carvacrol,” *Biomedicine and Pharmacotherapy*, vol. 165, 2023, doi: 10.1016/j.bioph.2023.115189.
- [302] R. Pelletier, “Effect of Plant-Derived Molecules on *Acinetobacter baumannii* Biofilm on Abiotic Surfaces,” *Honors Scholar Theses*, May 2012, Accessed: Apr. 04, 2024. [Online]. Available: https://digitalcommons.lib.uconn.edu/srhonors_theses/257
- [303] J. W. Betts, S. M. Kelly, and S. J. Haswell, “Antibacterial effects of theaflavin and synergy with epicatechin against clinical isolates of *Acinetobacter baumannii* and *Stenotrophomonas maltophilia*,” *Int J Antimicrob Agents*, vol. 38, no. 5, 2011, doi: 10.1016/j.ijantimicag.2011.07.006.
- [304] M. A. and G. A., “Effect of some natural plant extracts against gram negative bacteria in Njran Area, Saudi Arabia,” *Egyptian Academic Journal of Biological Sciences, G. Microbiology*, vol. 4, no. 1, 2012, doi: 10.21608/eajbsg.2012.16663.
- [305] R. Lawrence, P. Tripathi, and E. Jeyakumar, “Isolation, purification and evaluation of antibacterial agents from *Aloe Vera*,” *Brazilian Journal of Microbiology*, vol. 40, no. 4, 2009, doi: 10.1590/S1517-83822009000400023.
- [306] X. Lu, B. A. Rasco, J. M. F. Jabal, D. Eric Aston, M. Lin, and M. E. Konkel, “Investigating antibacterial effects of garlic (*Allium sativum*) concentrate and garlic-derived organosulfur compounds on

REFERENCES

- Campylobacter jejuni by using fourier transform infrared spectroscopy, Raman spectroscopy, and electron microscopy,” *Appl Environ Microbiol*, vol. 77, no. 15, 2011, doi: 10.1128/AEM.02845-10.
- [307] N. Singh, P. Vayer, S. Tanwar, J.-L. Poyet, K. Tsaioun, and B. O. Villoutreix, “Drug discovery and development: introduction to the general public and patient groups,” *Frontiers in Drug Discovery*, vol. 3, p. 1201419, May 2023, doi: 10.3389/FDDSV.2023.1201419.
- [308] W. Yu and A. D. Mackerell, “Computer-Aided Drug Design Methods,” *Methods Mol Biol*, vol. 1520, p. 85, 2017, doi: 10.1007/978-1-4939-6634-9_5.
- [309] J. P. Hughes, S. S. Rees, S. B. Kalindjian, and K. L. Philpott, “Principles of early drug discovery,” *Br J Pharmacol*, vol. 162, no. 6, p. 1239, Mar. 2011, doi: 10.1111/J.1476-5381.2010.01127.X.
- [310] P. Sharma, K. Sharma, and M. Nandave, “Computational approaches in drug discovery and design,” *Computational Approaches in Drug Discovery, Development and Systems Pharmacology*, pp. 53–93, Jan. 2023, doi: 10.1016/B978-0-323-99137-7.00009-5.
- [311] N. Brown, “Chemoinformatics—An Introduction for Computer Scientists,” *ACM Comput Surv*, vol. 41, no. 2, 2009, doi: 10.1145/1459352.1459353.
- [312] R. Guha and A. Bender, *Computational Approaches in Cheminformatics and Bioinformatics*. 2011. doi: 10.1002/9781118131411.
- [313] H. M. Patel *et al.*, “Quantitative structure-activity relationship (QSAR) studies as strategic approach in drug discovery,” *Medicinal Chemistry Research*, vol. 23, no. 12, pp. 4991–5007, Jun. 2014, doi: 10.1007/S00044-014-1072-3/METRICS.
- [314] S. Kwon, H. Bae, J. Jo, and S. Yoon, “Comprehensive ensemble in QSAR prediction for drug discovery,” *BMC Bioinformatics*, vol. 20, no. 1, pp. 1–12, Oct. 2019, doi: 10.1186/S12859-019-3135-4/FIGURES/4.
- [315] C. Nantasesamat, “Best practices for constructing reproducible QSAR models,” *Methods in Pharmacology and Toxicology*, pp. 55–75, 2020, doi: 10.1007/978-1-0716-0150-1_3/COVER.
- [316] D. S. Wigh, J. M. Goodman, and A. A. Lapkin, “A review of molecular representation in the age of machine learning,” *Wiley Interdiscip Rev Comput Mol Sci*, vol. 12, no. 5, p. e1603, Sep. 2022, doi: 10.1002/WCMS.1603.
- [317] M. Yamada and M. Sugiyama, “Molecular Graph Generation by Decomposition and Reassembling,” *ACS Omega*, vol. 8, no. 22, pp. 19575–19586, Jun. 2023, doi: 10.1021/ACSOMEKA.3C01078/ASSET/IMAGES/LARGE/AO3C01078_0011.JPG.
- [318] L. David, A. Thakkar, R. Mercado, and O. Engkvist, “Molecular representations in AI-driven drug discovery: a review and practical guide,” *Journal of Cheminformatics 2020 12:1*, vol. 12, no. 1, pp. 1–22, Sep. 2020, doi: 10.1186/S13321-020-00460-5.
- [319] S. N. Illemo, D. Barth, O. David, F. Quesette, M. A. Weisser, and D. Watel, “Improving graphs of cycles approach to structural similarity of molecules,” *PLoS One*, vol. 14, no. 12, p. e0226680, Dec. 2019, doi: 10.1371/JOURNAL.PONE.0226680.
- [320] A. Veselinovic, J. Veselinovic, J. Zivkovic, and G. Nikolic, “Application of SMILES Notation Based Optimal Descriptors in Drug Discovery and Design,” *Curr Top Med Chem*, vol. 15, no. 18, pp. 1768–1779, Jun. 2015, doi: 10.2174/1568026615666150506151533.
- [321] M. Hirohara, Y. Saito, Y. Koda, K. Sato, and Y. Sakakibara, “Convolutional neural network based on SMILES representation of compounds for detecting chemical motif,” *BMC Bioinformatics*, vol. 19, no. 19, pp. 83–94, Dec. 2018, doi: 10.1186/S12859-018-2523-5/FIGURES/7.
- [322] C. Ehrt, B. Krause, R. Schmidt, E. S. R. Ehmki, and M. Rarey, “SMARTS.plus – A Toolbox for Chemical Pattern Design,” *Mol Inform*, vol. 39, no. 12, Dec. 2020, doi: 10.1002/MINF.202000216.

REFERENCES

- [323] A. Dalby *et al.*, “Description of several chemical structure file formats used by computer programs developed at Molecular Design Limited,” *J Chem Inf Model*, vol. 32, no. 3, p. 244, Feb. 1992, doi: 10.1021/ci00007a012.
- [324] S. Sahoo, C. Adhikari, M. Kuanar, and B. Mishra, “A Short Review of the Generation of Molecular Descriptors and Their Applications in Quantitative Structure Property/Activity Relationships,” *Curr Comput Aided Drug Des*, vol. 12, no. 3, pp. 181–205, May 2016, doi: 10.2174/1573409912666160525112114.
- [325] L. Xue and J. Bajorath, “Molecular Descriptors in Chemoinformatics, Computational Combinatorial Chemistry, and Virtual Screening,” *Comb Chem High Throughput Screen*, vol. 3, no. 5, pp. 363–372, Oct. 2012, doi: 10.2174/138620700331454.
- [326] E. Bielska, X. Lucas, A. Czerwoniec, J. M. Kasprzak, K. H. Kaminska, and J. M. Bujnicki, “Virtual screening strategies in drug design—methods and applications,” *journals.pan.pl*, vol. 92, pp. 249–264, 2011, Accessed: Feb. 09, 2023. [Online]. Available: <https://journals.pan.pl/Content/82320/mainfile.pdf>
- [327] J. L. Durant, B. A. Leland, D. R. Henry, and J. G. Nourse, “Reoptimization of MDL Keys for Use in Drug Discovery,” *J Chem Inf Comput Sci*, vol. 42, no. 6, pp. 1273–1280, Nov. 2002, doi: 10.1021/CI010132R.
- [328] D. Rogers and M. Hahn, “Extended-connectivity fingerprints,” *J Chem Inf Model*, vol. 50, no. 5, pp. 742–754, May 2010, doi: 10.1021/CI100050T/ASSET/IMAGES/MEDIUM/CI-2010-00050T_0018.GIF.
- [329] G. Peyrat, “Conception d'inhibiteurs de protéines kinases à partir de méthodes in silico basées sur les fragments,” 2021. Accessed: Feb. 11, 2023. [Online]. Available: <https://theses.hal.science/tel-03921639/>
- [330] Z. Wu *et al.*, “Do we need different machine learning algorithms for QSAR modeling? A comprehensive assessment of 16 machine learning algorithms on 14 QSAR data sets,” *Brief Bioinform*, vol. 22, no. 4, Jul. 2021, doi: 10.1093/BIB/BBAA321.
- [331] L. Breiman, “Random forests,” *Mach Learn*, vol. 45, no. 1, pp. 5–32, Oct. 2001, doi: 10.1023/A:1010933404324/METRICS.
- [332] J. Ali, R. Khan, N. Ahmad, and I. Maqsood, “Random Forests and Decision Trees,” 2012, Accessed: Dec. 28, 2023. [Online]. Available: www.IJCSI.org
- [333] T. K. Ho, “The random subspace method for constructing decision forests,” *IEEE Trans Pattern Anal Mach Intell*, vol. 20, no. 8, pp. 832–844, 1998, doi: 10.1109/34.709601.
- [334] W. S. Noble, “What is a support vector machine?,” *Nature Biotechnology* 2006 24:12, vol. 24, no. 12, pp. 1565–1567, Dec. 2006, doi: 10.1038/nbt1206-1565.
- [335] V. Vapnik and R. Izmailov, “Reinforced SVM method and memorization mechanisms,” *Pattern Recognit*, vol. 119, p. 108018, Nov. 2021, doi: 10.1016/J.PATCOG.2021.108018.
- [336] K. Q. Weinberger, J. Blitzer, and L. K. Saul, “Distance Metric Learning for Large Margin Nearest Neighbor Classification,” *Adv Neural Inf Process Syst*, vol. 18, 2005.
- [337] X. Hu, J. Wang, L. Wang, and K. Yu, “K-Nearest Neighbor Estimation of Functional Nonparametric Regression Model under NA Samples,” *Axioms* 2022, Vol. 11, Page 102, vol. 11, no. 3, p. 102, Feb. 2022, doi: 10.3390/AXIOMS11030102.
- [338] G. Guo, H. Wang, D. Bell, Y. Bi, and K. Greer, “KNN model-based approach in classification,” *Lecture Notes in Computer Science (including subseries Lecture Notes in Artificial Intelligence and Lecture Notes in Bioinformatics)*, vol. 2888, pp. 986–996, 2003, doi: 10.1007/978-3-540-39964-3_62/COVER.
- [339] S. Zhang, X. Li, M. Zong, X. Zhu, and D. Cheng, “Learning k for kNN Classification,” *ACM Transactions on Intelligent Systems and Technology (TIST)*, vol. 8, no. 3, Jan. 2017, doi: 10.1145/2990508.
- [340] H. Kamel, D. Abdulah, and J. M. Al-Tuwaijri, “Cancer Classification Using Gaussian Naive Bayes Algorithm,” *Proceedings of the 5th International Engineering Conference, IEC 2019*, pp. 165–170, Jun. 2019, doi: 10.1109/IEC47844.2019.8950650.

REFERENCES

- [341] S. Alkhushayni, D. Al-Zaleq, L. Andradi, and P. Flynn, “The Application of Differing Machine Learning Algorithms and Their Related Performance in Detecting Skin Cancers and Melanomas,” *J Skin Cancer*, vol. 2022, 2022, doi: 10.1155/2022/2839162.
- [342] T. Chen and C. Guestrin, “XGBoost: A scalable tree boosting system,” *Proceedings of the ACM SIGKDD International Conference on Knowledge Discovery and Data Mining*, vol. 13-17-August-2016, pp. 785–794, Aug. 2016, doi: 10.1145/2939672.2939785.
- [343] V. Kotu and B. Deshpande, “Deep Learning,” *Data Science*, pp. 307–342, 2019, doi: 10.1016/B978-0-12-814761-0.00010-1.
- [344] H. Askri, E. Elgeldawi, H. Aboul Ella, Y. A. M. M. Elshaier, M. M. Gomaa, and A. E. Hassanien, “Deep learning in drug discovery: an integrative review and future challenges,” *Artif Intell Rev*, vol. 56, no. 7, pp. 5975–6037, Jul. 2023, doi: 10.1007/S10462-022-10306-1/FIGURES/3.
- [345] D. Jiang *et al.*, “Could graph neural networks learn better molecular representation for drug discovery? A comparison study of descriptor-based and graph-based models,” *J Cheminform*, vol. 13, no. 1, pp. 1–23, Dec. 2021, doi: 10.1186/S13321-020-00479-8/FIGURES/6.
- [346] P. Karpov, G. Godin, and I. V. Tetko, “Transformer-CNN: Swiss knife for QSAR modeling and interpretation,” *J Cheminform*, vol. 12, no. 1, pp. 1–12, Mar. 2020, doi: 10.1186/S13321-020-00423-W/FIGURES/9.
- [347] C. Zhang, Y. Lu, and T. Zang, “CNN-DDI: a learning-based method for predicting drug–drug interactions using convolution neural networks,” *BMC Bioinformatics*, vol. 23, no. 1, pp. 1–11, Jan. 2022, doi: 10.1186/S12859-022-04612-2/FIGURES/3.
- [348] C. Hung and G. Gini, “QSAR modeling without descriptors using graph convolutional neural networks: the case of mutagenicity prediction,” *Mol Divers*, vol. 25, no. 3, pp. 1283–1299, Aug. 2021, doi: 10.1007/S11030-021-10250-2/METRICS.
- [349] Y. Boulaamane *et al.*, “Exploring natural products as multi-target-directed drugs for Parkinson’s disease: an in-silico approach integrating QSAR, pharmacophore modeling, and molecular dynamics simulations,” *J Biomol Struct Dyn*, 2023, doi: 10.1080/07391102.2023.2260879.
- [350] J. Jiménez-Luna, F. Grisoni, and G. Schneider, “Drug discovery with explainable artificial intelligence,” *Nature Machine Intelligence* 2020 2:10, vol. 2, no. 10, pp. 573–584, Oct. 2020, doi: 10.1038/s42256-020-00236-4.
- [351] Y. Xu, X. Li, H. Yao, and K. Lin, “Neural networks in drug discovery: current insights from medicinal chemists,” <https://doi.org/10.4155/fmc-2019-0118>, vol. 11, no. 14, pp. 1669–1672, Jul. 2019, doi: 10.4155/FMC-2019-0118.
- [352] V. Mandlik, P. R. Bejugam, and S. Singh, “Application of Artificial Neural Networks in Modern Drug Discovery,” *Artificial Neural Network for Drug Design, Delivery and Disposition*, pp. 123–139, Jan. 2016, doi: 10.1016/B978-0-12-801559-9.00006-5.
- [353] D. Paul, G. Sanap, S. Shenoy, D. Kalyane, K. Kalia, and R. K. Tekade, “Artificial intelligence in drug discovery and development,” *Drug Discov Today*, vol. 26, no. 1, p. 80, Jan. 2021, doi: 10.1016/J.DRUDIS.2020.10.010.
- [354] M. H. S. Segler, T. Kogej, C. Tyrchan, and M. P. Waller, “Generating focused molecule libraries for drug discovery with recurrent neural networks,” *ACS Cent Sci*, vol. 4, no. 1, pp. 120–131, Jan. 2018, doi: 10.1021/ACSCENTSCI.7B00512/SUPPL_FILE/OC7B00512_SI_002.ZIP.
- [355] N. Suresh, N. C. A. Kumar, S. Subramanian, and G. Srinivasa, “Memory augmented recurrent neural networks for de-novo drug design,” *PLoS One*, vol. 17, no. 6, Jun. 2022, doi: 10.1371/JOURNAL.PONE.0269461.

REFERENCES

- [356] O. Silakari and P. K. Singh, “Fundamentals of molecular modeling,” *Concepts and Experimental Protocols of Modelling and Informatics in Drug Design*, pp. 1–27, 2021, doi: 10.1016/B978-0-12-820546-4.00001-5.
- [357] J.-L. Rivail, “Molecular Modelling. Semi-Empirical and Empirical Methods of Theoretical Chemistry,” *Computational Advances in Organic Chemistry: Molecular Structure and Reactivity*, pp. 229–259, 1991, doi: 10.1007/978-94-011-3262-6_4.
- [358] R. Iftimie, P. Minary, and M. E. Tuckerman, “Ab initio molecular dynamics: Concepts, recent developments, and future trends,” *Proc Natl Acad Sci U S A*, vol. 102, no. 19, pp. 6654–6659, May 2005, doi: 10.1073/PNAS.0500193102/SUPPL_FILE/00193FIG5.JPG.
- [359] R. J. Bartlett, V. F. Lotrich, and I. V. Schweigert, “Ab initio density functional theory: the best of both worlds?,” *J Chem Phys*, vol. 123, no. 6, Aug. 2005, doi: 10.1063/1.1904585.
- [360] M. Hoffmann and J. Rychlewski, “Density Functional Theory (DFT) and Drug Design,” *Reviews of Modern Quantum Chemistry*, pp. 1767–1803, Dec. 2002, doi: 10.1142/9789812775702_0058.
- [361] “Fundamental Principles of Molecular Modeling,” *Fundamental Principles of Molecular Modeling*, 1996, doi: 10.1007/978-1-4899-0212-2.
- [362] M. Sorokina, P. Merseburger, K. Rajan, M. A. Yirik, and C. Steinbeck, “COCONUT online: Collection of Open Natural Products database,” *J Cheminform*, vol. 13, no. 1, pp. 1–13, Dec. 2021, doi: 10.1186/S13321-020-00478-9/FIGURES/4.
- [363] Y. Boulaamane, P. Kandpal, A. Chandra, M. R. Britel, and A. Maurady, “Chemical library design, QSAR modeling and molecular dynamics simulations of naturally occurring coumarins as dual inhibitors of MAO-B and AChE,” *J Biomol Struct Dyn*, 2023, doi: 10.1080/07391102.2023.2209650.
- [364] B. A. P. Wilson, C. C. Thornburg, C. J. Henrich, T. Grkovic, and B. R. O’Keefe, “Creating and screening natural product libraries,” *Nat Prod Rep*, vol. 37, no. 7, pp. 893–918, Jul. 2020, doi: 10.1039/C9NP00068B.
- [365] H. Koeppen, J. Kriegl, U. Lessel, C. S. Tautermann, and B. Wellenzohn, “Ligand-Based Virtual Screening,” pp. 61–85, May 2011, doi: 10.1002/9783527633326.CH3.
- [366] D. Bajusz, A. Rácz, and K. Héberger, “Why is Tanimoto index an appropriate choice for fingerprint-based similarity calculations?,” *J Cheminform*, vol. 7, no. 1, pp. 1–13, Dec. 2015, doi: 10.1186/S13321-015-0069-3/FIGURES/7.
- [367] O. F. Güner and J. P. Bowen, “Setting the record straight: The origin of the pharmacophore concept,” *J Chem Inf Model*, vol. 54, no. 5, pp. 1269–1283, Apr. 2014, doi: 10.1021/CI5000533/ASSET/IMAGES/MEDIUM/CI-2014-000533_0002.GIF.
- [368] X. Qing *et al.*, “Pharmacophore modeling: advances, limitations, and current utility in drug discovery,” *Journal of Receptor, Ligand and Channel Research*, vol. 7, pp. 81–92, Jan. 2014, doi: 10.2147/JRLCR.S46843.
- [369] A. H. Beckett, N. J. Harper, and J. W. Clitherow, “The Importance of Stereoisomerism in Muscarinic Activity,” *Journal of Pharmacy and Pharmacology*, vol. 15, no. 1, pp. 362–371, Apr. 2011, doi: 10.1111/J.2042-7158.1963.TB12799.X.
- [370] L. B. Kier, “Molecular Orbital Calculation of Preferred Conformations of Acetylcholine, Muscarine, and Muscarone,” *Mol Pharmacol*, vol. 3, no. 5, 1967.
- [371] D. R. Buckle *et al.*, “Glossary of terms used in medicinal chemistry. Part II (IUPAC recommendations 2013),” *Pure and Applied Chemistry*, vol. 85, no. 8, pp. 1725–1758, Jul. 2013, doi: 10.1351/PAC-REC-12-11-23/MACHINEREADABLECITATION/RIS.
- [372] F. R. Makhouri and J. B. Ghasemi, “Combating Diseases with Computational Strategies Used for Drug Design and Discovery,” *Curr Top Med Chem*, vol. 18, no. 32, pp. 2743–2773, Mar. 2019, doi: 10.2174/1568026619666190121125106.

REFERENCES

- [373] L. Maveyraud and L. Mourey, “Protein X-ray Crystallography and Drug Discovery,” *Molecules*, vol. 25, no. 5, Feb. 2020, doi: 10.3390/MOLECULES25051030.
- [374] A. Kouranov *et al.*, “The RCSB PDB information portal for structural genomics,” *Nucleic Acids Res*, vol. 34, no. suppl_1, pp. D302–D305, Jan. 2006, doi: 10.1093/NAR/GKJ120.
- [375] J. Jumper *et al.*, “Highly accurate protein structure prediction with AlphaFold,” *Nature* 2021 596:7873, vol. 596, no. 7873, pp. 583–589, Jul. 2021, doi: 10.1038/s41586-021-03819-2.
- [376] F. Stanzione, I. Giangreco, and J. C. Cole, “Use of molecular docking computational tools in drug discovery,” *Prog Med Chem*, vol. 60, pp. 273–343, Jan. 2021, doi: 10.1016/BS.PMCH.2021.01.004.
- [377] “Molecular docking towards drug discovery - Gschwend - 1996 - Journal of Molecular Recognition - Wiley Online Library.” Accessed: Dec. 11, 2023. [Online]. Available: [https://onlinelibrary.wiley.com/doi/10.1002/\(SICI\)1099-1352\(199603\)9:2%3C175::AID-JMR260%3E3.0.CO;2-D](https://onlinelibrary.wiley.com/doi/10.1002/(SICI)1099-1352(199603)9:2%3C175::AID-JMR260%3E3.0.CO;2-D)
- [378] N. Sauton, D. Lagorce, B. O. Villoutreix, and M. A. Miteva, “MS-DOCK: Accurate multiple conformation generator and rigid docking protocol for multi-step virtual ligand screening,” *BMC Bioinformatics*, vol. 9, no. 1, pp. 1–12, Apr. 2008, doi: 10.1186/1471-2105-9-184/FIGURES/3.
- [379] M. McGann, “FRED pose prediction and virtual screening accuracy,” *J Chem Inf Model*, vol. 51, no. 3, pp. 578–596, Mar. 2011, doi: 10.1021/CI100436P/SUPPL_FILE/CI100436P_SI_001.PDF.
- [380] J. Fan, A. Fu, and L. Zhang, “Progress in molecular docking,” *Quantitative Biology*, vol. 7, no. 2, pp. 83–89, Jun. 2019, doi: 10.1007/S40484-019-0172-Y/METRICS.
- [381] F. Ding, S. Yin, and N. V. Dokholyan, “Rapid flexible docking using a stochastic rotamer library of ligands,” *J Chem Inf Model*, vol. 50, no. 9, pp. 1623–1632, Sep. 2010, doi: 10.1021/CI100218T/ASSET/IMAGES/MEDIUM/CI-2010-00218T_0010.GIF.
- [382] C. N. Cavasotto, J. A. Kovacs, and R. A. Abagyan, “Representing receptor flexibility in ligand docking through relevant normal modes,” *J Am Chem Soc*, vol. 127, no. 26, pp. 9632–9640, Jul. 2005, doi: 10.1021/JA042260C/SUPPL_FILE/JA042260CSI20050608_024422.PDF.
- [383] R. Rosenfeld, S. Vajda, and C. DeLisi, “Flexible Docking and Design,” <http://dx.doi.org/10.1146/annurev.bb.24.060195.003333>, vol. 24, pp. 677–700, Nov. 2003, doi: 10.1146/ANNUREV.BB.24.060195.003333.
- [384] M. Totrov and R. Abagyan, “Flexible ligand docking to multiple receptor conformations: a practical alternative,” *Curr Opin Struct Biol*, vol. 18, no. 2, pp. 178–184, Apr. 2008, doi: 10.1016/J.SBI.2008.01.004.
- [385] Y. Pak and S. Wang, “Application of a Molecular Dynamics Simulation Method with a Generalized Effective Potential to the Flexible Molecular Docking Problems,” *Journal of Physical Chemistry B*, vol. 104, no. 2, pp. 354–359, Jan. 1999, doi: 10.1021/JP993073H.
- [386] N. S. Pagadala, K. Syed, and J. Tuszyński, “Software for molecular docking: a review,” *Biophysical Reviews* 2017 9:2, vol. 9, no. 2, pp. 91–102, Jan. 2017, doi: 10.1007/S12551-016-0247-1.
- [387] O. Trott and A. J. Olson, “AutoDock Vina: Improving the speed and accuracy of docking with a new scoring function, efficient optimization, and multithreading,” *J Comput Chem*, vol. 31, no. 2, pp. 455–461, Jan. 2010, doi: 10.1002/JCC.21334.
- [388] T. J. A. Ewing, S. Makino, A. G. Skillman, and I. D. Kuntz, “DOCK 4.0: Search strategies for automated molecular docking of flexible molecule databases,” *J Comput Aided Mol Des*, vol. 15, no. 5, pp. 411–428, 2001, doi: 10.1023/A:1011115820450/METRICS.
- [389] M. L. Verdonk, J. C. Cole, M. J. Hartshorn, C. W. Murray, and R. D. Taylor, “Improved protein–ligand docking using GOLD,” *Proteins: Structure, Function, and Bioinformatics*, vol. 52, no. 4, pp. 609–623, Sep. 2003, doi: 10.1002/PROT.10465.

REFERENCES

- [390] R. A. Friesner *et al.*, “Glide: A New Approach for Rapid, Accurate Docking and Scoring. 1. Method and Assessment of Docking Accuracy,” *J Med Chem*, vol. 47, no. 7, pp. 1739–1749, Mar. 2004, doi: 10.1021/JM0306430/SUPPL_FILE/JM0306430_S.PDF.
- [391] C. C. G. Inc., “Molecular operating environment (MOE).” Chemical Computing Group Inc. Montreal, QC, Canada, 2016.
- [392] G. M. Morris *et al.*, “AutoDock4 and AutoDockTools4: Automated docking with selective receptor flexibility,” *J Comput Chem*, vol. 30, no. 16, pp. 2785–2791, Dec. 2009, doi: 10.1002/JCC.21256.
- [393] B. Kramer, M. Rarey, and T. Lengauer, “Evaluation of the FLEXX Incremental Construction Algorithm for Protein-Ligand Docking”, doi: 10.1002/(SICI)1097-0134(19991101)37:2.
- [394] M. McGann, “FRED pose prediction and virtual screening accuracy,” *J Chem Inf Model*, vol. 51, no. 3, pp. 578–596, Mar. 2011, doi: 10.1021/CI100436P/SUPPL_FILE/CI100436P_SI_001.PDF.
- [395] A. N. Jain, “Surflex-Dock 2.1: Robust performance from ligand energetic modeling, ring flexibility, and knowledge-based search,” *J Comput Aided Mol Des*, vol. 21, no. 5, pp. 281–306, Mar. 2007, doi: 10.1007/S10822-007-9114-2/METRICS.
- [396] G. Bitencourt-Ferreira and W. F. de Azevedo, “Molegro virtual docker for docking,” *Methods in Molecular Biology*, vol. 2053, pp. 149–167, 2019, doi: 10.1007/978-1-4939-9752-7_10/COVER.
- [397] H. Kubinyi, “Drug research: myths, hype and reality,” *Nature Reviews Drug Discovery* 2003 2:8, vol. 2, no. 8, pp. 665–668, 2003, doi: 10.1038/nrd1156.
- [398] M. J. Waring *et al.*, “An analysis of the attrition of drug candidates from four major pharmaceutical companies,” *Nature Reviews Drug Discovery* 2015 14:7, vol. 14, no. 7, pp. 475–486, Jun. 2015, doi: 10.1038/nrd4609.
- [399] L. L. G. Ferreira and A. D. Andricopulo, “ADMET modeling approaches in drug discovery,” *Drug Discov Today*, vol. 24, no. 5, pp. 1157–1165, May 2019, doi: 10.1016/J.DRUDIS.2019.03.015.
- [400] R. Thelingwani, “Integration of In Silico and In Vitro ADMET properties in lead identification and optimization of compounds for the treatment of parasitic diseases,” 2012.
- [401] S. Kar and J. Leszczynski, “Open access in silico tools to predict the ADMET profiling of drug candidates,” *Expert Opin Drug Discov*, vol. 15, no. 12, pp. 1473–1487, Dec. 2020, doi: 10.1080/17460441.2020.1798926.
- [402] Y. Wang *et al.*, “In silico ADME/T modelling for rational drug design,” *Q Rev Biophys*, vol. 48, no. 4, pp. 488–515, Jul. 2015, doi: 10.1017/S0033583515000190.
- [403] G. Xiong *et al.*, “ADMETlab 2.0: an integrated online platform for accurate and comprehensive predictions of ADMET properties,” *Nucleic Acids Res*, vol. 49, no. W1, pp. W5–W14, Jul. 2021, doi: 10.1093/NAR/GKAB255.
- [404] A. Daina, O. Michelin, and V. Zoete, “SwissADME: a free web tool to evaluate pharmacokinetics, drug-likeness and medicinal chemistry friendliness of small molecules,” *Scientific Reports* 2017 7:1, vol. 7, no. 1, pp. 1–13, Mar. 2017, doi: 10.1038/srep42717.
- [405] D. E. V. Pires, T. L. Blundell, and D. B. Ascher, “pkCSM: Predicting small-molecule pharmacokinetic and toxicity properties using graph-based signatures,” *J Med Chem*, vol. 58, no. 9, pp. 4066–4072, May 2015, doi: 10.1021/ACS.JMEDCHEM.5B00104/SUPPL_FILE/JM5B00104_SI_001.PDF.
- [406] M. De Vivo, M. Masetti, G. Bottegoni, and A. Cavalli, “Role of Molecular Dynamics and Related Methods in Drug Discovery,” *J Med Chem*, vol. 59, no. 9, pp. 4035–4061, May 2016, doi: 10.1021/ACS.JMEDCHEM.5B01684/ASSET/IMAGES/LARGE/JM-2015-016843_0006.JPG.
- [407] D. N. Theodorou, “Progress and outlook in Monte Carlo simulations,” *Ind Eng Chem Res*, vol. 49, no. 7, pp. 3047–3058, Apr. 2010, doi: 10.1021/IE9019006/ASSET/IE9019006.FP.PNG_V03.

REFERENCES

- [408] R. Iftimie, P. Minary, and M. E. Tuckerman, “Ab initio molecular dynamics: Concepts, recent developments, and future trends,” *Proc Natl Acad Sci U S A*, vol. 102, no. 19, pp. 6654–6659, May 2005, doi: 10.1073/PNAS.0500193102/SUPPL_FILE/00193FIG5.JPG.
- [409] D. Frenkel and B. Smit, *Understanding molecular simulation: From algorithms to applications*. 1996. doi: 10.1063/1.881812.
- [410] J. R. Valverde, “Molecular Modelling: Principles and Applications,” *Brief Bioinform*, vol. 2, no. 2, 2001, doi: 10.1093/bib/2.2.199.
- [411] J. W. Ponder and D. A. Case, “Force fields for protein simulations,” *Adv Protein Chem*, vol. 66, 2003, doi: 10.1016/S0065-3233(03)66002-X.
- [412] P. S. Nerenberg and T. Head-Gordon, “New developments in force fields for biomolecular simulations,” *Current Opinion in Structural Biology*, vol. 49. 2018. doi: 10.1016/j.sbi.2018.02.002.
- [413] J. A. Maier, C. Martinez, K. Kasavajhala, L. Wickstrom, K. E. Hauser, and C. Simmerling, “ff14SB: Improving the Accuracy of Protein Side Chain and Backbone Parameters from ff99SB,” *J Chem Theory Comput*, vol. 11, no. 8, pp. 3696–3713, Jul. 2015, doi: 10.1021/ACS.JCTC.5B00255/SUPPL_FILE/CT5B00255_SI_001.PDF.
- [414] J. Wang, R. M. Wolf, J. W. Caldwell, P. A. Kollman, and D. A. Case, “Development and testing of a general amber force field,” *J Comput Chem*, vol. 25, no. 9, pp. 1157–1174, Jul. 2004, doi: 10.1002/JCC.20035.
- [415] J. Huang and A. D. Mackerell, “CHARMM36 all-atom additive protein force field: Validation based on comparison to NMR data,” *J Comput Chem*, vol. 34, no. 25, pp. 2135–2145, Sep. 2013, doi: 10.1002/JCC.23354.
- [416] N. Schmid *et al.*, “Definition and testing of the GROMOS force-field versions 54A7 and 54B7,” *European Biophysics Journal*, vol. 40, no. 7, pp. 843–856, Jul. 2011, doi: 10.1007/S00249-011-0700-9/METRICS.
- [417] E. Harder *et al.*, “OPLS3: A Force Field Providing Broad Coverage of Drug-like Small Molecules and Proteins,” *J Chem Theory Comput*, vol. 12, no. 1, pp. 281–296, Jan. 2016, doi: 10.1021/ACS.JCTC.5B00864/SUPPL_FILE/CT5B00864_SI_001.ZIP.
- [418] S. J. Marrink, H. J. Risselada, S. Yefimov, D. P. Tieleman, and A. H. De Vries, “The MARTINI Force Field: Coarse Grained Model for Biomolecular Simulations,” *Journal of Physical Chemistry B*, vol. 111, no. 27, pp. 7812–7824, Jul. 2007, doi: 10.1021/JP071097F.
- [419] C. Zhang *et al.*, “AMOEBA Polarizable Atomic Multipole Force Field for Nucleic Acids,” *J Chem Theory Comput*, vol. 14, no. 4, p. 2084, Apr. 2018, doi: 10.1021/ACS.JCTC.7B01169.
- [420] R. Zadorozhnyi *et al.*, “Determination of Histidine Protonation States in Proteins by Fast Magic Angle Spinning NMR,” *Front Mol Biosci*, vol. 8, p. 767040, Dec. 2021, doi: 10.3389/FMOLB.2021.767040/BIBTEX.
- [421] S. Horowitz and R. C. Trievel, “Carbon-oxygen hydrogen bonding in biological structure and function,” *Journal of Biological Chemistry*, vol. 287, no. 50, pp. 41576–41582, Dec. 2012, doi: 10.1074/jbc.R112.418574.
- [422] S. Genheden and U. Ryde, “The MM/PBSA and MM/GBSA methods to estimate ligand-binding affinities,” *Expert Opin Drug Discov*, vol. 10, no. 5, p. 449, May 2015, doi: 10.1517/17460441.2015.1032936.
- [423] C. Mulakala and V. N. Viswanadhan, “Could MM-GBSA be accurate enough for calculation of absolute protein/ligand binding free energies?,” *J Mol Graph Model*, vol. 46, pp. 41–51, Nov. 2013, doi: 10.1016/J.JMGM.2013.09.005.
- [424] P. A. Kollman *et al.*, “Calculating Structures and Free Energies of Complex Molecules: Combining Molecular Mechanics and Continuum Models,” *Acc Chem Res*, vol. 33, no. 12, pp. 889–897, 2000, doi: 10.1021/AR000033J.

REFERENCES

- [425] H. Gohlke and D. A. Case, “Converging free energy estimates: MM-PB(GB)SA studies on the protein–protein complex Ras–Raf,” *J Comput Chem*, vol. 25, no. 2, pp. 238–250, Jan. 2004, doi: 10.1002/JCC.10379.
- [426] I. Massova and P. A. Kollman, “Combined molecular mechanical and continuum solvent approach (MM-PBSA/GBSA) to predict ligand binding,” *Perspectives in Drug Discovery and Design*, vol. 18, no. 1, pp. 113–135, 2000, doi: 10.1023/A:1008763014207/METRICS.
- [427] N. Homeyer and H. Gohlke, “Free Energy Calculations by the Molecular Mechanics Poisson–Boltzmann Surface Area Method,” *Mol Inform*, vol. 31, no. 2, pp. 114–122, Feb. 2012, doi: 10.1002/MINF.201100135.
- [428] J. Weiser, P. S. Shenkin, and W. C. Still, “Approximate atomic surfaces from linear combinations of pairwise overlaps (LCPO),” *J Comput Chem*, vol. 20, no. 2, 1999, doi: 10.1002/(SICI)1096-987X(19990130)20:2<217::AID-JCC4>3.0.CO;2-A.
- [429] L. Dong, X. Qu, Y. Zhao, and B. Wang, “Prediction of Binding Free Energy of Protein-Ligand Complexes with a Hybrid Molecular Mechanics/Generalized Born Surface Area and Machine Learning Method,” *ACS Omega*, vol. 6, no. 48, pp. 32938–32947, Dec. 2021, doi: 10.1021/ACSOMEKA1C04996/ASSET/IMAGES/LARGE/AO1C04996_0006.JPG.
- [430] F. Fogolari, A. Brigo, and H. Molinari, “The Poisson–Boltzmann equation for biomolecular electrostatics: a tool for structural biology,” *Journal of Molecular Recognition*, vol. 15, no. 6, pp. 377–392, Nov. 2002, doi: 10.1002/JMR.577.
- [431] D. Van Der Spoel, E. Lindahl, B. Hess, G. Groenhof, A. E. Mark, and H. J. C. Berendsen, “GROMACS: Fast, flexible, and free,” *J Comput Chem*, vol. 26, no. 16, pp. 1701–1718, Dec. 2005, doi: 10.1002/JCC.20291.
- [432] D. A. Case *et al.*, “The Amber biomolecular simulation programs,” *J Comput Chem*, vol. 26, no. 16, pp. 1668–1688, Dec. 2005, doi: 10.1002/JCC.20290.
- [433] K. J. Bowers *et al.*, “Scalable algorithms for molecular dynamics simulations on commodity clusters,” *Proceedings of the 2006 ACM/IEEE Conference on Supercomputing, SC’06*, 2006, doi: 10.1145/1188455.1188544.
- [434] A. P. Thompson *et al.*, “LAMMPS - a flexible simulation tool for particle-based materials modeling at the atomic, meso, and continuum scales,” *Comput Phys Commun*, vol. 271, p. 108171, Feb. 2022, doi: 10.1016/J.CPC.2021.108171.
- [435] J. C. Phillips *et al.*, “Scalable molecular dynamics with NAMD,” *J Comput Chem*, vol. 26, no. 16, pp. 1781–1802, Dec. 2005, doi: 10.1002/JCC.20289.
- [436] D. Robakis and S. Fahn, “Defining the Role of the Monoamine Oxidase-B Inhibitors for Parkinson’s Disease,” *CNS Drugs*, vol. 29, no. 6, pp. 433–441, Jun. 2015, doi: 10.1007/S40263-015-0249-8/METRICS.
- [437] M. D. Mertens, S. Hinz, C. E. Müller, and M. Gütschow, “Alkynyl-coumarinyl ethers as MAO-B inhibitors,” *Bioorg Med Chem*, vol. 22, no. 6, pp. 1916–1928, Mar. 2014, doi: 10.1016/J.BMC.2014.01.046.
- [438] Y. Boulaamane, I. Ahmad, H. Patel, N. Das, M. R. Britel, and A. Maurady, “Structural exploration of selected C6 and C7-substituted coumarin isomers as selective MAO-B inhibitors,” *J Biomol Struct Dyn*, vol. 41, no. 6, pp. 2326–2340, 2023, doi: 10.1080/07391102.2022.2033643.
- [439] R. M. Geha, I. Rebrin, K. Chen, and J. C. Shih, “Substrate and inhibitor specificities for human monoamine oxidase A and B are influenced by a single amino acid,” *J Biol Chem*, vol. 276, no. 13, pp. 9877–9882, Mar. 2001, doi: 10.1074/JBC.M006972200.

REFERENCES

- [440] E. M. Milczek, C. Binda, S. Rovida, A. Mattevi, and D. E. Edmondson, “The ‘gating’ residues Ile199 and Tyr326 in human monoamine oxidase B function in substrate and inhibitor recognition,” *FEBS J*, vol. 278, no. 24, pp. 4860–4869, Dec. 2011, doi: 10.1111/J.1742-4658.2011.08386.X.
- [441] Y. Boulaamane, K. Jangid, M. R. Britel, and A. Maurady, “Probing the molecular mechanisms of α -synuclein inhibitors unveils promising natural candidates through machine-learning QSAR, pharmacophore modeling, and molecular dynamics simulations,” *Mol Divers*, pp. 1–17, Jul. 2023, doi: 10.1007/S11030-023-10691-X/METRICS.
- [442] T. Zhang, W. Liang, W. Ou, M. Zhang, S. Cui, and S. Zhang, “Daphnetin alleviates neuropathic pain in chronic constrictive injury rats via regulating the NF- κ B dependent CXCL1/CXCR2 signaling pathway,” *Pharm Biol*, vol. 61, no. 1, p. 746, 2023, doi: 10.1080/13880209.2023.2198560.
- [443] Z. Gao, D. J. Maloney, L. M. Dedkova, and S. M. Hecht, “Inhibitors of DNA polymerase beta: activity and mechanism,” *Bioorg Med Chem*, vol. 16, no. 8, pp. 4331–4340, Apr. 2008, doi: 10.1016/J.BMCC.2008.02.071.
- [444] R. Kumar, A. Saha, and D. Saha, “A new antifungal coumarin from Clausena excavata,” *Fitoterapia*, vol. 83, no. 1, pp. 230–233, Jan. 2012, doi: 10.1016/J.FITOTE.2011.11.003.
- [445] T. D. Popoola *et al.*, “Potent Nrf2-inducing, antioxidant, and anti-inflammatory effects and identification of constituents validate the anti-cancer use of Uvaria chamae and Olax subscorpioides,” *BMC Complement Med Ther*, vol. 21, no. 1, Dec. 2021, doi: 10.1186/S12906-021-03404-0.
- [446] M. Stompor, D. Broda, and A. Bajek-Bil, “Dihydrochalcones: Methods of Acquisition and Pharmacological Properties—A First Systematic Review,” *Molecules*, vol. 24, no. 24, Dec. 2019, doi: 10.3390/MOLECULES24244468.
- [447] B. Salehi *et al.*, “Pharmacological Properties of Chalcones: A Review of Preclinical Including Molecular Mechanisms and Clinical Evidence,” *Front Pharmacol*, vol. 11, Jan. 2020, doi: 10.3389/FPHAR.2020.592654.
- [448] J. Ma, X. Jin, L. Yang, and Z. L. Liu, “Diarylheptanoids from the rhizomes of Zingiber officinale,” *Phytochemistry*, vol. 65, no. 8, pp. 1137–1143, Apr. 2004, doi: 10.1016/J.PHYTOCHEM.2004.03.007.
- [449] H. Fang *et al.*, “Dimeric diarylheptanoids with anti-inflammatory activity from Zingiber officinale,” *Phytochemistry*, vol. 219, p. 113975, Mar. 2024, doi: 10.1016/J.PHYTOCHEM.2024.113975.
- [450] S. McAuley, A. Huynh, A. Howells, C. Walpole, A. Maxwell, and J. R. Nodwell, “Discovery of a Novel DNA Gyrase-Targeting Antibiotic through the Chemical Perturbation of Streptomyces venezuelae Sporulation,” *Cell Chem Biol*, vol. 26, no. 9, pp. 1274–1282.e4, Sep. 2019, doi: 10.1016/j.chembiol.2019.06.002.
- [451] S. S. Li, Z. Gao, X. Feng, and S. M. Hecht, “Biscoumarin Derivatives from Edgeworthia gardneri that Inhibit the Lyase Activity of DNA Polymerase β ,” *J Nat Prod*, vol. 67, no. 9, pp. 1608–1610, Sep. 2004, doi: 10.1021/NP040127S.
- [452] T. Zhang, W. Liang, W. Ou, M. Zhang, S. Cui, and S. Zhang, “Daphnetin alleviates neuropathic pain in chronic constrictive injury rats via regulating the NF- κ B dependent CXCL1/CXCR2 signaling pathway,” *Pharm Biol*, vol. 61, no. 1, p. 746, 2023, doi: 10.1080/13880209.2023.2198560.
- [453] I. A. Arbab *et al.*, “Clausena excavata Burm. f. (Rutaceae): A review of its traditional uses, pharmacological and phytochemical properties,” *Journal of Medicinal Plants Research*, vol. 5, no. 33, pp. 7177–7184, Dec. 2011, doi: 10.5897/JMPRX11.013.
- [454] J. R. Cole, S. J. Torrance, R. M. Wiedhopf, S. K. Arora, and R. B. Bates, “Uvaretin, a New Antitumor Agent from Uvaria acuminata (Annonaceae),” *Journal of Organic Chemistry*, vol. 41, no. 10, pp. 1852–1855, May 1976, doi: 10.1021/JO00872A037/SUPPL_FILE/JO00872A037_SI_001.PDF.
- [455] Y. Smani *et al.*, “Antibiotic discovery with artificial intelligence for the treatment of Acinetobacter baumannii infections,” Nov. 2023, doi: 10.21203/RS.3.RS-3664762/V1.

REFERENCES

- [456] Y. Boulaamane *et al.*, “Antibiotic discovery with artificial intelligence for the treatment of *Acinetobacter baumannii* infections,” *mSystems*, May 2024, doi: 10.1128/MSYSTEMS.00325-24.
- [457] R. Mishra and A. K. Gupta, “Biological Activities of Curcuminoids,” *Food Chemistry, Function and Analysis*, vol. 2021-January, no. 25, pp. 172–195, Oct. 2020, doi: 10.1039/9781788015936-00172.
- [458] S. K. Sandur *et al.*, “Curcumin, demethoxycurcumin, bisdemethoxycurcumin, tetrahydrocurcumin and turmerones differentially regulate anti-inflammatory and anti-proliferative responses through a ROS-independent mechanism,” *Carcinogenesis*, vol. 28, no. 8, pp. 1765–1773, Aug. 2007, doi: 10.1093/CARCIN/BGM123.
- [459] A. Amalraj, A. Pius, S. Gopi, and S. Gopi, “Biological activities of curcuminoids, other biomolecules from turmeric and their derivatives – A review,” *J Tradit Complement Med*, vol. 7, no. 2, p. 205, Apr. 2017, doi: 10.1016/J.JTCME.2016.05.005.

LIST OF PUBLICATIONS

The work conducted during this thesis has led to the following publications:

Boulaamane, Y., Ahmad, I., Patel, H., Das, N., Britel, M. R., & Maurady, A. (2022). Structural exploration of selected C6 and C7-substituted coumarin isomers as selective MAO-B inhibitors. *Journal of Biomolecular Structure and Dynamics*, 1-15. DOI: <https://doi.org/10.1080/07391102.2022.2033643>

Boulaamane, Y., Ibrahim, M. A., Britel, M. R., & Maurady, A. (2022). In silico studies of natural product-like caffeine derivatives as potential MAO-B inhibitors/AA2AR antagonists for the treatment of Parkinson's disease. *Journal of Integrative Bioinformatics*. DOI: <https://doi.org/10.1515/jib-2021-0027>

Boulaamane, Y., Kandpal, P., Chandra, A., Britel, M. R., & Maurady, A. (2023). Chemical library design, QSAR modeling and molecular dynamics simulations of naturally occurring coumarins as dual inhibitors of MAO-B and AChE. *Journal of Biomolecular Structure and Dynamics*, 1-18. DOI: <https://doi.org/10.1080/07391102.2023.2209650>

Boulaamane, Y., Jangid, K., Britel, M. R., & Maurady, A. (2023). Probing the molecular mechanisms of α -synuclein inhibitors unveils promising natural candidates through machine-learning QSAR, pharmacophore modeling, and molecular dynamics simulations. *Molecular Diversity*, 1-17. DOI : <https://doi.org/10.1007/s11030-023-10691-x>

Boulaamane, Y., Touati, I., Goyal, N., Chandra, A., Kori, L., Ibrahim, M. A., ... & Maurady, A. (2023). Exploring natural products as multi-target-directed drugs for Parkinson's disease: an in-silico approach integrating QSAR, pharmacophore modeling, and molecular dynamics simulations. *Journal of Biomolecular Structure and Dynamics*, 1-18. DOI: <https://doi.org/10.1080/07391102.2023.2260879>

Boulaamane, Y., Molina Panadero, I., Hmadcha, A., Atalaya Rey, C., Baammi, S., El Allali, A., ... & Smani, Y. (2024). Antibiotic discovery with artificial intelligence for the treatment of *Acinetobacter baumannii* infections. *Msystems*, e00325-24. DOI: <https://doi.org/10.1128/msystems.00325-24>

LIST OF COMMUNICATIONS

Throughout the course of my thesis, I have taken part in multiple conferences, presenting my research through both oral and poster communications:

Docking-based virtual screening and ADME evaluation of caffeine-based phytochemicals as inhibitors of Monoamine Oxidase B, June 23, 2021, oral communication at the 1st International Bioinformatics Conference (iABC2021), Istanbul, Turkey. Link: <https://iabconference.com/>

Machine Learning model to predict potential Monoamine Oxidase B inhibitors from Cannabis Compound Database, December 27, 2021, poster presentation at the International Bioinformatics Conference IBC'2021, Hotel Solazur, Tangier, Morocco. Link: <https://sites.google.com/view/ibc2021>

Computational studies of African Natural Products Databases to identify natural dual-target-directed antiparkinsonian drugs, December 27, 2021, oral communication at the International Bioinformatics Conference IBC'2021, Hotel Solazur, Tangier, Morocco. Link: <https://sites.google.com/view/ibc2021>

QSAR and molecular modelling studies for the discovery of natural products as multi-target-directed drugs for Parkinson's disease, October 09, 2022, oral communication at the International Bioinformatics Conference IBC'2022, Hotel Solazur, Tangier, Morocco. Link: <https://sites.google.com/view/ibc2022>

Enhanced accuracy in predicting drug blood-brain barrier permeability with a Machine Learning Ensemble model, October 06, 2023, oral communication at the International Bioinformatics Conference IBC'2023, Hotel Solazur, Tangier, Morocco. Link: <https://sites.google.com/view/ibc2023>

DECLARATION OF AUTHORSHIP

Statement of Authorship

I, Yassir BOULAAMANE, declare that this thesis titled “Data-driven discovery of bioactive natural products: Application to neurodegenerative and infectious diseases”, and the work presented in it are my own and has been generated by me as the result of my own original research.

I confirm that:

1. This work was done wholly or mainly while in candidature for a Ph.D. degree at Abdelmalek Essaadi University.
2. Where any part of this thesis has previously been submitted for a degree or any other qualification at this University or any other institution, this has been clearly stated.
3. Where I have consulted the published work of others, this is always clearly attributed.
4. Where I have quoted from the work of others, the source is always given. With the exception of such quotations, this thesis is entirely my own work.
5. I have acknowledged all main sources of help.
6. Where the thesis is based on work done by myself jointly with others, I have made clear exactly what was done by others and what I have contributed myself.

Date: 23/04/2024

Yassir Boulaamane

ANNEXES

ANNEX 1: STRUCTURAL EXPLORATION OF SELECTED C6 AND C7 SUBSTITUTED COUMARIN ISOMERS AS SELECTIVE MAO-B INHIBITORS

MAO-B is a promising target for antiparkinsonian drugs; however, existing MAO-B inhibitors have selectivity-associated side effects, necessitating the development of novel, potent, and highly selective inhibitors. Recent research indicates that coumarins, particularly those connected to a hex-5-ynyloxy chain at position C6, exhibit higher selectivity toward MAO-B than MAO-A compared to their C7-isomers. In this study, we have investigated the interaction modes of C6 and C7-substituted coumarin isomers to elucidate the structural components and molecular interactions contributing to MAO-B selectivity. Molecular docking revealed a common π - π stacking interaction with Tyr-326 among the selective C6-isomers. Molecular dynamics simulations further demonstrated the stability of the C7-isomer in both MAO isoforms, while the C6-isomer exhibited instability in MAO-A, due to the bulky Phe-208 residue. These findings provide insights for the development and optimization of coumarin derivatives as potential drugs for PD.

The details of this work are reported in the following publication.

Boulaamane, Y., Ahmad, I., Patel, H., Das, N., Britel, M. R., & Maurady, A. (2022). Structural exploration of selected C6 and C7-substituted coumarin isomers as selective MAO-B inhibitors. *Journal of Biomolecular Structure and Dynamics*, 1-15. (Reprinted with permission)

Available at: <https://doi.org/10.1080/07391102.2022.2033643>

Conceptualization: Y.B. A.M.; Methodology: Y.B., A.M.; Investigation: Y.B., A.M.; Visualization: Y.B., I.A., H.P.; Supervision: M.R.B., A.M.; Writing—original draft: Y.B.; Writing—review & editing: Y.B., A.M.



Structural exploration of selected C6 and C7-substituted coumarin isomers as selective MAO-B inhibitors

Yassir Boulaamane, Iqrar Ahmad, Harun Patel, Niloy Das, Mohammed Reda Britel & Amal Maurady

To cite this article: Yassir Boulaamane, Iqrar Ahmad, Harun Patel, Niloy Das, Mohammed Reda Britel & Amal Maurady (2022): Structural exploration of selected C6 and C7-substituted coumarin isomers as selective MAO-B inhibitors, *Journal of Biomolecular Structure and Dynamics*, DOI: [10.1080/07391102.2022.2033643](https://doi.org/10.1080/07391102.2022.2033643)

To link to this article: <https://doi.org/10.1080/07391102.2022.2033643>



Published online: 15 Feb 2022.



Submit your article to this journal [↗](#)



Article views: 109



View related articles [↗](#)



View Crossmark data [↗](#)

RESEARCH ARTICLE



Structural exploration of selected C6 and C7-substituted coumarin isomers as selective MAO-B inhibitors

Yassir Boulaamane^a , Iqrar Ahmad^b , Harun Patel^b , Niloy Das^c , Mohammed Reda Britel^a  and Amal Maurady^{a,d} 

^aLaboratory of Innovative Technologies, National School of Applied Sciences of Tangier, Abdelmalek Essaadi University, Tetouan, Morocco;

^bDivision of Computer Aided Drug Design, Department of Pharmaceutical Chemistry, R. C. Patel Institute of Pharmaceutical Education and Research, Shirpur, India; ^cDepartment of Pharmacy, BGC Trust University Bangladesh, Chittagong, Bangladesh; ^dLaboratory of Innovative Technologies, Faculty of Sciences and Techniques of Tangier, Abdelmalek Essaadi University, Tetouan, Morocco

Communicated by Ramaswamy H. Sarma

ABSTRACT

Monoamine Oxidase B is considered a successful target for developing antiparkinsonian drugs. Due to the side effects of current MAO-B inhibitors, there's an urgent need for novel potent and highly selective MAO-B inhibitors. A recent study has shown that coumarins tend to be more selective towards MAO-B than MAO-A when connected to a hex-5-ynyoxy chain at position 6 in contrast to their C7-isomers. The present study describes the mode of interaction of the C6 and C7-substituted coumarin isomers characterized by their difference in selectivity towards MAO-B through molecular docking and molecular dynamics simulations in an effort to elucidate the structural components and molecular interactions that may be responsible for MAO-B selectivity. Three isomeric coumarin pairs connected to ether chain at position 6 or 7 were taken from the literature and modelled according to their IUPAC nomenclature. Molecular docking study revealed one π - π stacking interaction with Tyr-326 in common between the selective coumarin C6-isomers. Resulting complexes of one isomeric coumarin pair that displayed the highest selectivity shift towards MAO-B were subject to 100 ns molecular dynamics simulations study to analyze the stability of the docked complexes. Molecular dynamics revealed that the C7-isomer is relatively stable in both MAO isoforms through the simulation duration, whereas the C6-isomer deemed unstable for MAO-A which may be due to the bulky Phe-208 residue in MAO-A. Our results might be applied for further development and optimization of coumarin derivatives into a successful drug against Parkinson's disease.

ARTICLE HISTORY

Received 12 August 2021

Accepted 10 January 2022

KEYWORDS

Coumarin; selectivity; monoamine oxidase A; monoamine oxidase B; molecular docking; Parkinson's disease; ADME; drug likeness; Lipinski's rule of five; molecular dynamics simulation

1. Introduction

Parkinson's disease (PD) is a neurodegenerative disorder defined by the progressive loss of dopaminergic neurons in the substantia nigra pars compacta (SNpc) of the mid brain (Noda et al., 2020). It is estimated to affect 6 million people worldwide with a prevalence of 150 in every 100 000 people which is expected to further increase by 2- to 3-fold until 2030 (Poewe & Mahlknecht, 2020). It is considered the second most frequent neurodegenerative disorder after Alzheimer's disease (Dorsey et al., 2018). Current available drugs for treating PD include levodopa, which remains the most used therapy, dopamine agonists and catechol-O-methyl transferase (COMT)/monoamine oxidase (MAO) inhibitors (Youdim et al., 2006). Monoamine Oxidase (MAO) (EC 1.4.3.4) is a flavoenzyme attached to the outer mitochondrial membrane of the neurons, it is responsible for the oxidative deamination of monoamine neurotransmitters such as dopamine, adrenaline and noradrenaline in the central nervous system (CNS) (Shih et al., 1999). The MAO enzyme exists in two forms namely MAO-A and MAO-B that share about 70%

of their amino acid identity, but differ in their tissue distribution, substrate and inhibitor preferences (Youdim et al., 2006). Development of the first MAO inhibitors was abandoned since the discovery that their use potentiates a 'cheese effect' related to the metabolism of tyramine, which causes a cardiovascular crisis (Culpepper, 2013; Youdim et al., 2006). However, a new class of selective MAO-B inhibitors has proven to be efficient in treating PD symptoms. It was also shown that this new class of MAO inhibitors are devoid of the tyramine related side effects. Furthermore, they may act as neuroprotective agents by limiting the release of free radical species and hence may decrease the progression of the disease (Tetrud & Koller, 2004; Youdim et al., 2006).

MAO-A has serotonin as its preferred substrate while MAO-B preferentially deaminates 2-phenylethylamine and benzylamine. Dopamine, norepinephrine, and epinephrine are metabolized by both isoforms in most animal tissues (Finberg & Rabey, 2016).

During aging, the expression of MAO-B increases in the brain and is connected with an enhanced dopamine metabolism that produce reactive oxygen species (ROS) such as

hydrogen peroxide (H_2O_2) resulting in oxidative damage and apoptotic signaling events (Mallajosyula et al., 2008).

Previously approved MAO-B inhibitors are selegiline and rasagiline which irreversibly inhibits MAO-B with an IC_{50} value of 6.8 nM and 14 nM respectively (Youdim et al., 2001). The latest approved MAO-B inhibitor was safinamide which reversibly inhibits MAO-B with an IC_{50} value of 450 nM and a selectivity index ($\text{SI} = \text{IC}_{50} \text{ MAO-A}/\text{IC}_{50} \text{ MAO-B}$) of over 700 (Binda et al., 2007).

Crystal structure of MAO-A has a monopartite substrate cavity of $\sim 550 \text{ \AA}^3$ volume while crystal structure of MAO-B contains a dipartite cavity structure with an entrance cavity of $\sim 290 \text{ \AA}^3$ and a substrate cavity of $\sim 400 \text{ \AA}^3$ (De Colibus et al., 2005). Ile-199 and Tyr-326 side chains separate these two cavities in MAO-B (Binda et al., 2003). Mutagenesis studies of mutant Ile-199Phe in MAO-B show that the bulky side chain of Phenylalanine limits conformational flexibility of this residue in MAO-B, and hence prevents larger cavity-spanning inhibitors from binding to both cavities (Mostert et al., 2015). The smaller side chain of Ile-199 is more flexible and may exhibit conformational changes to merge both cavities and allow the binding of larger inhibitors. Tyr-326 is also another key residue that plays a role in the selectivity mechanism of MAO-B, the bulky side chain of this residue restricts the binding of certain inhibitors such as harmine (Mostert et al., 2015). The corresponding residue in MAO-A is Ile-335, which is smaller and allows the binding of harmine. Thus, Ile-199 and Tyr-326 serves as 'gating' residues and a structural determinant for substrate and inhibitor recognition by MAO-B (Edmondson et al., 2007). MAO-A and MAO-B structures and active site cavities are shown in Figure 1.

Structural study revealed that MAO-B (PDB ID: 2V61) is formed by two monomers consisting of a globular domain anchored to the membrane through a C-terminal helix (Binda et al., 2002). The active site is located in the substrate fixing domain located near the FAD cofactor binding domain and is formed by the residues: Tyr-60, Pro-102, Pro-104, Leu-164, Phe-168, Leu-171, Cys-172, Ile-198, Ile-199, Gln-206, Ile-316, Tyr-326, Phe-343, Tyr-398 and Tyr-435 (Binda et al., 2007). Meanwhile, MAO-A (PDB ID: 2Z5Y) is expressed as a monomer consisting of a C-terminal domain that forms helical tails which are responsible for attaching the protein to the membrane. Structural analysis revealed that the active site of MAO-A is located in the substrate cavity near the FAD cofactor cavity and is formed by the residues: Tyr-69, Asn-181, Phe-208, Val-210, Gln-215, Cys-323, Ile-325, Ile-335, Leu-337, Phe-352, Tyr-407, Tyr-444 (Binda et al., 2011).

Coumarin is a highly flexible scaffold that has been extensively studied for developing new MAO inhibitors displaying a wide range of selectivity for MAO-B (Rempel et al., 2012). In a previous study conducted by Mertens et al. (2014), it was reported that alkynyl coumarinyl ethers are able to inhibit MAO-B at nanomolar concentrations ranging from 0.58 nM to 1790 nM with a selectivity for MAO-B reaching a value of over 3400-fold (Mertens et al., 2014). The compounds were found to be reversible inhibitors and it was concluded that the triple bond doesn't form a covalent bond

with the propargyl group as noted in the irreversible inhibitors, selegiline and rasagiline (Mertens et al., 2014).

In an effort to develop new potent and highly selective MAO-B inhibitors, we used molecular modelling techniques to get an insight on the possible molecular mechanisms of three isomeric coumarin pairs in which the inhibitory activity and selectivity for MAO-B were previously evaluated *in vitro* (Mertens et al., 2014).

Molecular docking study was carried out to investigate the structural conformations of these compounds with crystallographic structures of MAO-A and MAO-B and to identify key interactions that may enhance the selectivity for MAO-B. Furthermore, *in silico* ADME properties were evaluated in order to evaluate the drug likeness of the selected compounds.

Finally, two isomeric coumarins that displayed the highest selectivity shift towards MAO-B were subject to 100 ns molecular dynamics in order to compare their stability over time and to investigate the key residues that are involved during the protein-ligand interaction.

2. Materials and methods

2.1. Preparation of the target proteins

http://www.rcsb.org/)，分辨率最高的结构 (PDB ID: 2Z5Y, 分辨率 = 2.1 Å) 与已知抑制剂 harmine (HRM) 结合的结构被选中 (Son et al., 2008)。MAO-B 结构与 coumarin 衍生物 (C18) 结合的分辨率最高的结构 (PDB ID: 2V61, 分辨率 = 1.7 Å) 被选择，该结构中的 coumarin 框架被用来叠加 docked 蛋白质，并选择与天然配体结合位点最相似的结合方式 (Binda et al., 2007)。共结晶的配体和水分子被删除，因为它们不参与结合，因此删除它们以使计算更容易并清楚结合口袋中可能的水分子，这些水分子会扭曲结合位点 (Wang et al., 2019)。FAD 脱辅基蛋白在催化 monoamines 的脱氨基作用时发挥重要作用，并且为了研究它是否参与配体结合到蛋白在分子对接研究中被保留 (Gaweska & Fitzpatrick, 2011)。蛋白准备向导 (PPW) 在 Maestro 12.5 中使用，以分配键级数、添加显式氢原子、固定并优化缺少原子的侧链并使用 Prime (Schrödinger Release: Maestro, 2021; Jacobson et al., 2004; Jacobson et al., 2002; Greenwood et al., 2010)。蛋白残基的质子化状态根据 PROPKA 程序预测 pH = 7.0 时的 pKa 值 (Olsson et al., 2011)。结合的天然配体被用于定义活性位点残基。

2.2. Preparation of ligands

选定的 coumarin 同系物从 Mertens et al. (2014) 的实验研究中检索并转换为化学结构，从它们的 IUPAC 命名使用 2D Sketcher

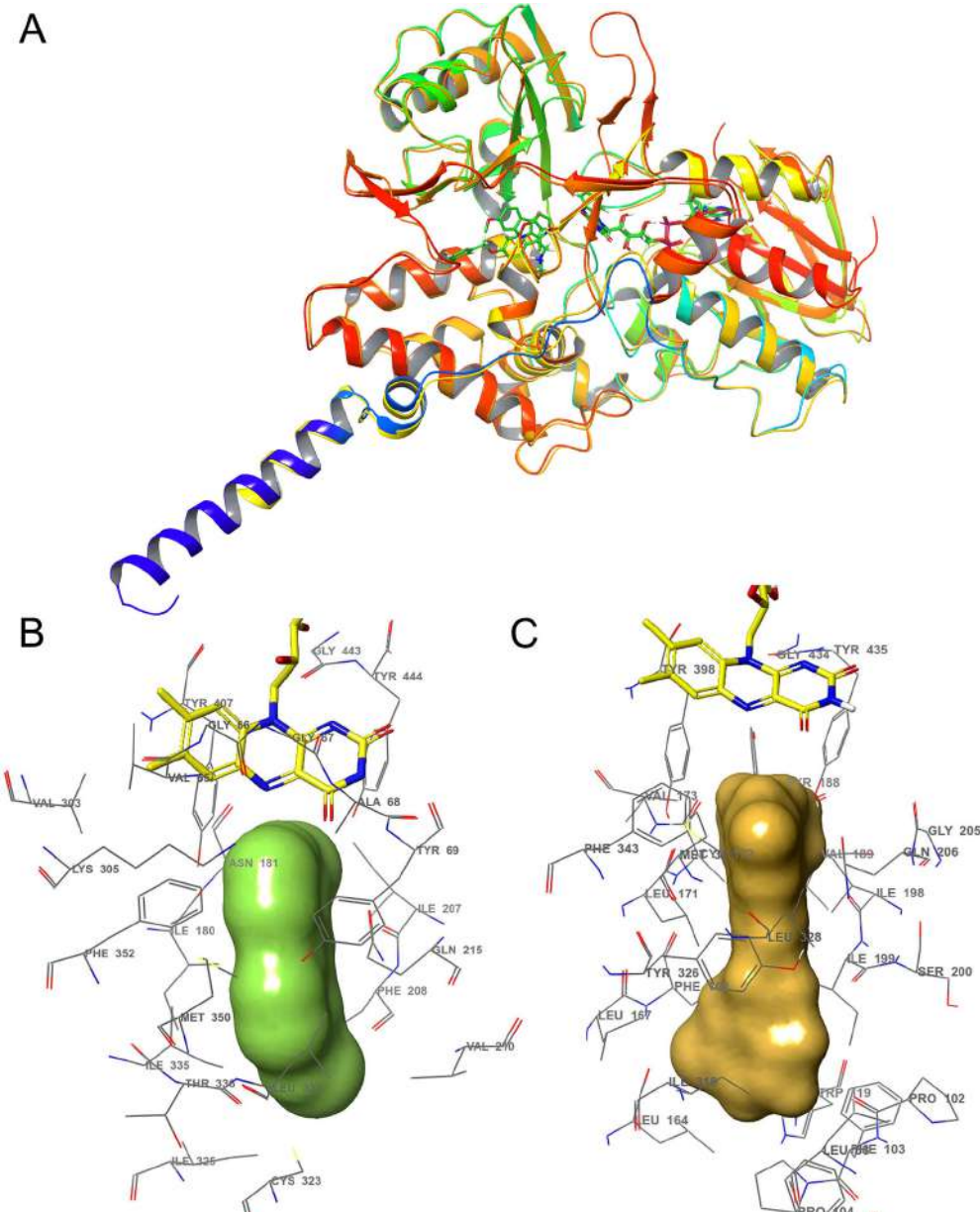


Figure 1. Superposition of crystal structures of MAO-A (PDB ID: 2Z5Y) and MAO-B (PDB ID: 2V61) (A). Binding surfaces and active site residues of MAO-A (B) and MAO-B (C).

module included in Maestro 12.5 (Mertens et al., 2014; Schrödinger Release: Maestro, 2021). Explicit hydrogens and 3D coordinates were also generated. Ligprep module was used for energy minimization using Optimized Potentials for Liquid Simulations (OPLS3e) force field, ionization states and other parameters were kept unchanged (Roos et al., 2019). Chemical structures of coumarin isomers and their respective MAO-B selectivity are reported in Table 1.

2.3. Molecular docking study and binding free energy calculations

Molecular docking was used for analysis of interactions between the coumarin isomers and the active site of MAO-B and MAO-A. Ligand docking was performed by employing Glide program in Maestro 12.5 (Schrödinger Release: Maestro,

2021). Co-crystallized ligands were used for grid box placing with a spacing of 1 Å using receptor grid generation tool of Maestro 12.5 (Schrödinger Release: Maestro, 2021). Grid dimensions were chosen large enough ($24 \times 24 \times 24$ Å) in x, y and z directions, respectively, to fit the following amino acids of the active sites of the proteins: Tyr-60, Pro-102, Pro-104, Leu-164, Phe-168, Leu-171, Cys-172, Ile-198, Ile-199, Gln-206, Ile-316, Tyr-326, Phe-343, Tyr-398 and Tyr-435 for MAO-B and Tyr-69, Asn-181, Phe-208, Val-210, Gln-215, Cys-323, Ile-325, Ile-335, Leu-337, Phe-352, Tyr-407, Tyr-444 for MAO-A. The grid box was positioned in a way to cover the entire binding site and to allow larger molecules to dock properly ($51.2 \times 155.5 \times 28.7$ Å for MAO-B and $-40.6 \times -26.7 \times -14.9$ Å for MAO-A) in x, y and z directions, respectively. Ligand docking was performed using Glide Extra Precision (XP) mode included in Maestro 12.5 (Friesner et al., 2006; Halgren et al., 2004; Schrödinger Release:

Table 1. Chemical structures of coumarin isomers and their MAO-B selectivity [20].

Compound	Nomenclature	Chemical structure	SI
1	Methyl 2-oxo-7-(hex-5-nyloxy)-2H-chromene-3-carboxylate		6.8
2	Methyl 6-(hex-5-nyloxy)-2-oxo-2H-chromene-3-carboxylate		81.3
3	Methyl 7-(4-chlorophenoxy)-2-oxo-2H-chromene-3-carboxylate		53
4	Methyl 6-(4-chlorophenoxy)-2-oxo-2H-chromene-3-carboxylate		>83.3
5	N-(2-Oxo-7-(hex-5-nyloxy)-2H-chromen-3-yl) acetamide		1.6
6	N-(2-Oxo-6-(hex-5-nyloxy)-2H-chromen-3-yl) acetamide		>404.8

SI: Selectivity index (IC_{50} MAO-A/ IC_{50} MAO-B).

Maestro, 2021). Conformations of docked ligands were chosen according to their binding energy and their conformation similarity to the native ligands. Finally, binding free energy calculations were performed by employing Prime MM-GBSA approach using Variable Dielectric Surface Generalized Born (VSGB) as an implicit solvent model and OPLS3e force field for the resulting protein-ligand complexes to estimate ligand-binding affinities (Genheden & Ryde, 2015; Li et al., 2011). The values were calculated based on the following equation (Das et al., 2009; Lyne et al., 2006):

$$\Delta G_{bind} = \Delta E_{mm} + \Delta G_{solv} + \Delta G_{sa}$$

$$\Delta E_{mm} = E_{complex} - (E_{protein} + E_{ligand})$$

Where, ΔE_{mm} is the difference in the minimized energies between the obtained protein-ligand complexes and the sum of the protein and ligand energies individually. ΔG_{solv} is the difference in the GBSA solvation energy of the protein-ligand complex and the sum of the solvation energies of protein and ligand in the unbound state. ΔG_{sa} is the difference between the surface area energies for the complex and the sum of the surface area energies for the free protein and ligand.

$E_{complex}$, $E_{protein}$, and E_{ligand} are the minimized energies of the protein-ligand complex, free protein, and ligand, respectively.

2.4. ADME properties prediction

It has been estimated that nearly 40% of drug candidates fail in clinical trials due to poor Absorption, Distribution, Metabolism and Excretion (ADME) properties (Lin et al., 2003). *In silico* ADME prediction is a cost-efficient approach to find if a compound is druglike by calculating its pharmacokinetics parameters and physicochemical properties and can considerably reduce the amount of consumed time and resources during the overall drug development process. The selected compounds were analyzed based on Lipinski's' Rule of Five' which allows the evaluation of physicochemical properties that would make it likely for a drug to be orally active in humans (Congreve et al., 2003; Lipinski, 2004). Pharmacokinetic parameters including water solubility, human oral absorption, blood-brain barrier permeability, human colon adenocarcinoma (Caco-2) and Madin-Darby Canine Kidney (MDCK) cell permeability were predicted using Qikprop tool in Maestro 12.5 (Schrödinger Release: Maestro, 2021).

2.5. Molecular dynamics simulation

Two coumarin isomers **5** and **6** characterized by their highest selectivity shift towards MAO-B in complex with MAO-A and MAO-B were taken from the molecular docking study. The

docked complexes were prepared using the protein preparation wizard (PPW) in Maestro 12.5 in order to fix structural defects. Non-standard residues such as FAD cofactor were removed because they weren't directly involved in the ligand binding to crystal structures of MAO-B (PDB ID: 2V61) and MAO-A (PDB ID: 2Z5Y) despite its catalytic role in the proper functioning of the protein (Binda et al., 2007; Son et al., 2008). Moreover, the FAD cofactor didn't display any type of interaction with coumarin derivatives during the molecular docking study, therefore we removed FAD cofactor from MD simulation study. Missing side chains and loops were fixed using Prime. Desmond module was used to run a MD simulation to investigate the change in protein structure within the solvent system (D. E. Shaw Research, Schrödinger Release, 2020-3). The water-soaked solvated system was created in Desmond using the System Builder panel. For the simulations, the complex was centered in an orthorhombic cubic box with periodic boundary conditions and filled with Single Point Charge (SPC) water molecules buffered at a distance of minimum 10 Å between a protein atom and box edges (Ahmad et al., 2021; Zrieq et al., 2021). The system was neutralized by randomly adding a sufficient number of counter-ions (Na^+ and Cl^-) and isosmotic state was maintained by adding 0.15 M NaCl. Then, the solvated built system was minimized and relaxed utilizing OPLS3e force field parameters as the default protocol associated with Desmond (Jorgensen et al., 1996; Pawara et al., 2021). A constant 300 K temperature and 1 atm pressure was maintained during the simulation using the Nose-Hoover thermostat algorithm and Martyna-Tobias-Klein Barostat algorithm, respectively (Mehta et al., 2019). A total of 100 ns simulations were conducted, during which 1000 trajectories were saved. Lastly, MD simulation trajectory was analyzed using the Simulation Interaction Diagram (SID) tool (Lee et al., 2021; Martyna, 1994).

3. Results

3.1. Validation of the docking protocol

The docking protocol implemented in Glide module was validated by redocking the crystal ligands of human MAO-B (PDB ID: 2V61) and MAO-A (PDB ID: 2Z5Y). Co-crystallized ligands were modelled using 2D Sketcher module included

in Maestro 12.5, explicit hydrogens and 3D coordinates were generated, Ligprep was employed for energy minimization using default settings (Gaweska & Fitzpatrick, 2011). The root-mean-square deviation (RMSD) was calculated by superimposing both docked and native ligands, the later was used as a reference. The results yielded values of 1.81 Å for MAO-B and 1.47 Å for MAO-A which indicates a good accuracy of the docking program (Figure 2).

3.2. Molecular docking of coumarin isomers with MAO-B and MAO-A

Molecular docking study was performed using Glide module included in Maestro 12.5 with extra precision (XP) mode (Friesner et al., 2004; 2006; Halgren et al., 2004; Wang et al., 2019). Conformations of docked compounds were ranked by their energies and then selected based on their similarity to the co-crystallized ligands by mean of superposition.

Hydrogen bonds and nearby interacting hydrophobic amino acids were identified using Ligand interaction diagram of Maestro 12.5 (Schrödinger Release: Maestro, 2021). Molecular docking results of coumarin isomers with MAO-B and MAO-A and MM-GBSA binding free energy of the resulting protein-ligand complexes are shown in Table 2 and Table 3 respectively. Protein-ligand interactions diagrams of the selected ligands with MAO-B and MAO-A are shown in Figures 3 and 4 respectively.

Molecular docking study revealed that coumarin derivatives and their isomers bind more optimally within MAO-B active site than MAO-A active site regardless of their selectivity. The docking scores of Glide XP mode varied from -8.96 to -10.47 kcal/mol for MAO-B. The compound 3 which displayed the lowest binding energy (-10.47 kcal/mol) is considered the most potent MAO-B inhibitor among the selected coumarin derivatives which is in correlation with the experimental study ($\text{IC}_{50} = 1.41 \text{ nM}$) (Mertens et al., 2014).

Structural analysis demonstrated that all coumarin derivatives bind to MAO-B with the coumarin scaffold directed towards the aromatic cage consisting of Tyr-398, Tyr-435 and FAD-1502. Compound **2**, **4** and **5** established a hydrogen bond with the aromatic residue Tyr-188 which is located at the

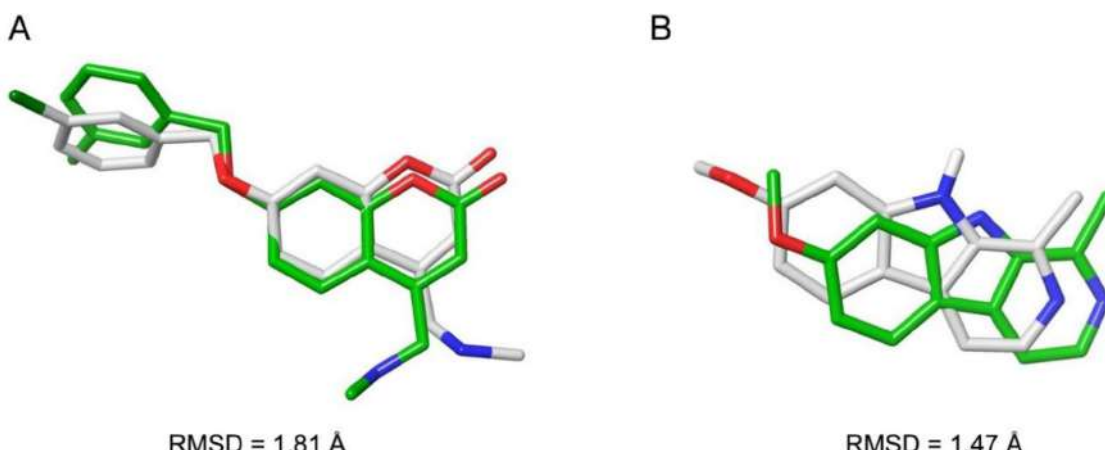


Figure 2. RMSD values and superimposition of native co-crystallized and docked ligands for MAO-B (A) and MAO-A (B).

Table 2. Docking results and MM-GBSA binding free energy of the selected ligands with MAO-B.

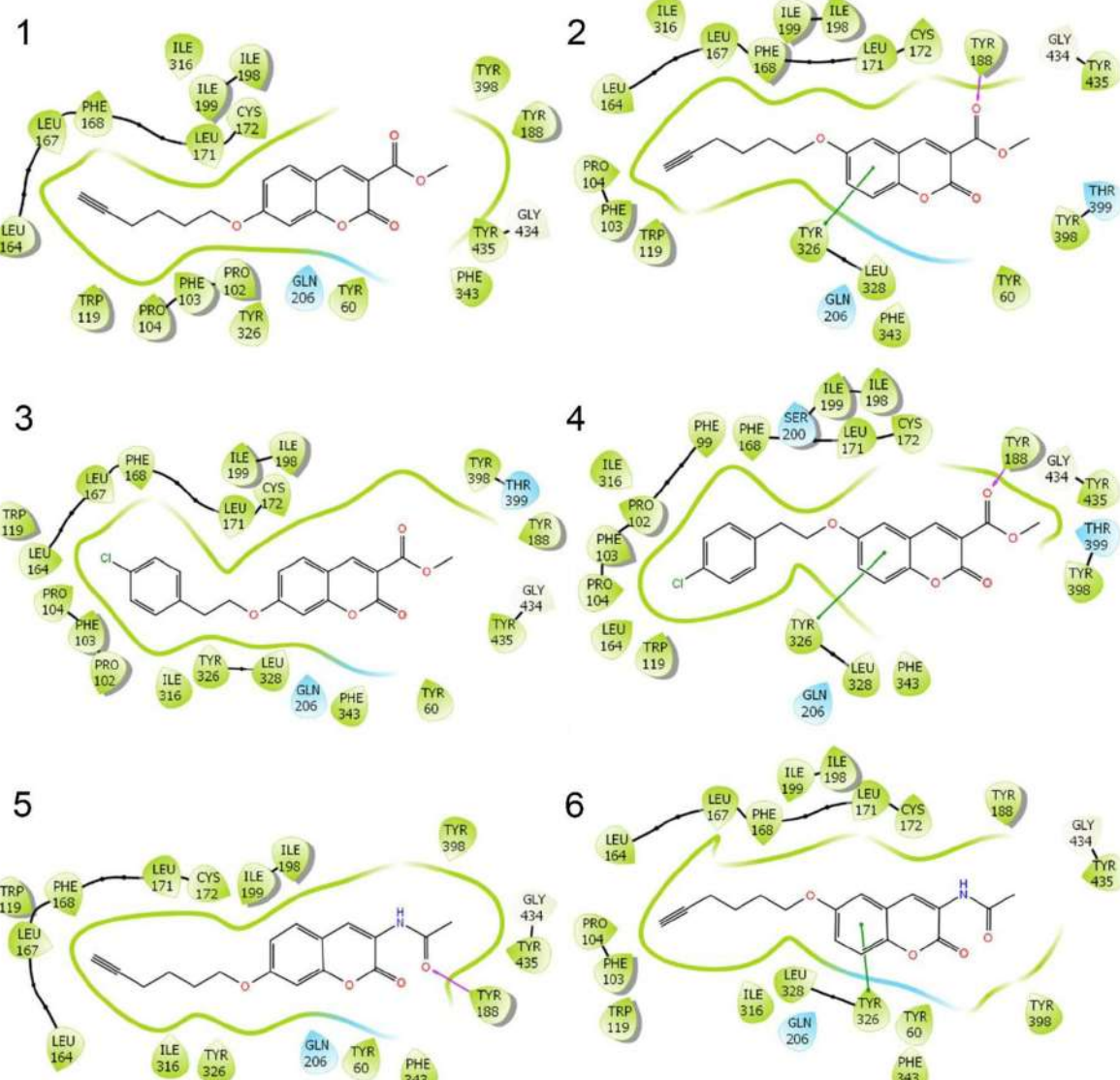
Compound	Glide XP score (kcal/mol)	MM-GBSA binding free energy (kcal/mol)
1	-10.22	-66.47
2	-9.24	-64.18
3	-10.47	-69.83
4	-8.96	-54.75
5	-9.45	-54.70
6	-9.76	-45.23

bottom of the substrate cavity. This residue may play a role in anchoring inhibitors within MAO-B active site and thus increasing their stability. However, this residue doesn't seem to be involved in the MAO-B selectivity mechanism as it is not interacting with the most selective coumarin isomer (**6**). On the other hand, the comparison of the C6-substituted coumarin isomers has revealed a common interaction between those compounds which is a π - π stacking interaction between the coumarin ring and the gating residue Tyr-326. This residue is replaced by the aliphatic amino acid Ile-335 in MAO-A and thus

Table 3. Docking results and MM-GBSA binding free energy of the selected ligands with MAO-A.

Compound	Glide XP score (kcal/mol)	MM-GBSA binding free energy (kcal/mol)
1	-7.93	-34.23
2	-4.97	-29.49
3	-4.14	-17.81
4	1.66	-52.60
5	-4.40	-41.60
6	-2.39	-35.32

might have a role in the selectivity of the selected coumarin isomers towards MAO-B. MM-GBSA binding free energy calculations were performed in order to assess the ligand-binding affinities, the results show that the C6-substituted coumarin isomers in complex with MAO-B tend to be slightly less stable when compared to the C7-substituted coumarin isomers. We note that those results correlate well with the experimental data which demonstrated that C6-substituted coumarins are slightly less potent towards MAO-B regardless of their selectivity (Mertens et al., 2014).

**Figure 3.** Protein-ligand interactions of the selected ligands with MAO-B.

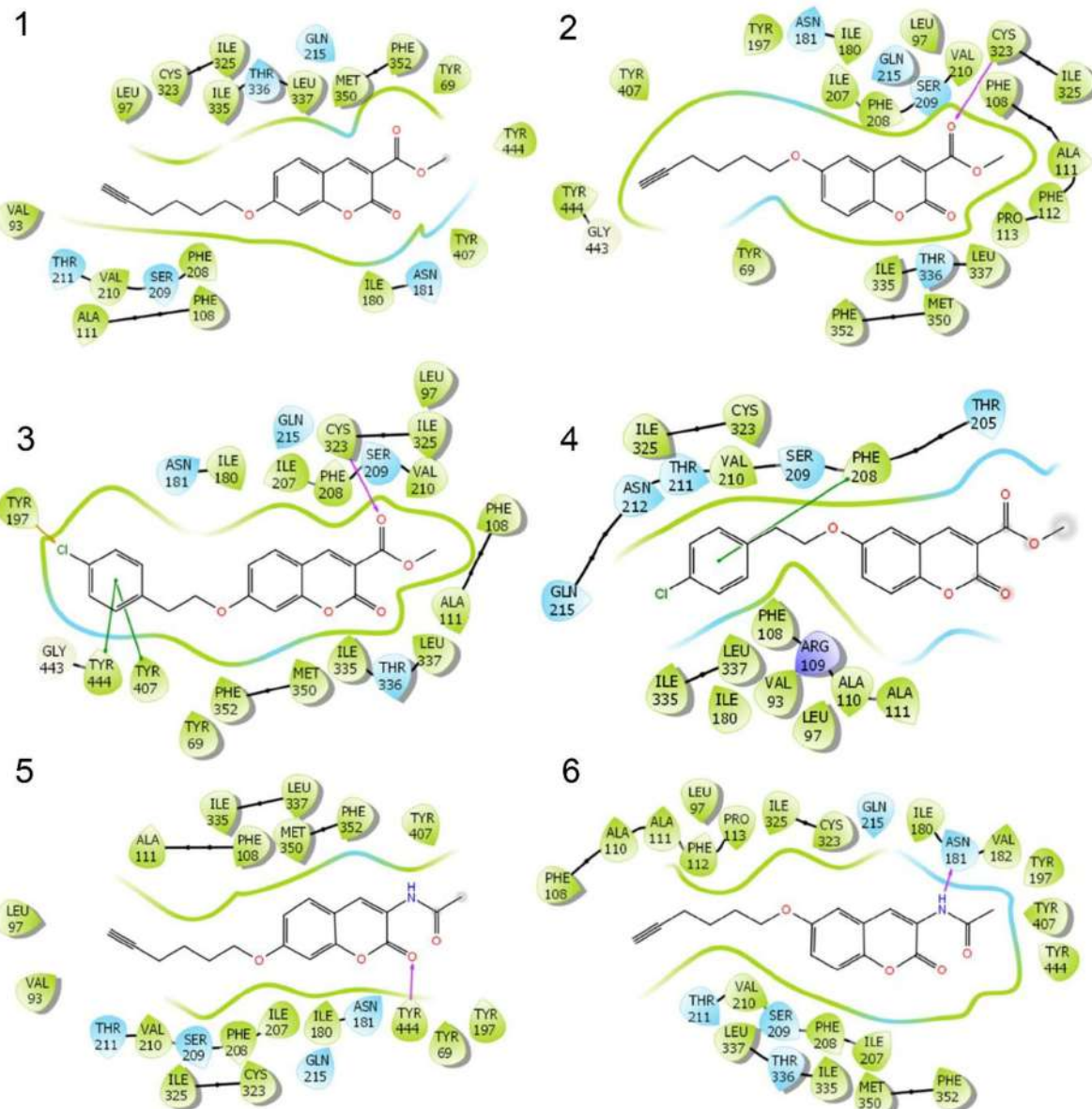


Figure 4. Protein-ligand interactions of the selected ligands with MAO-A.

Molecular docking study of coumarin derivatives and their isomers with MAO-A active site yielded docking scores ranging from 1.66 to -7.93 kcal/mol . The C6-substituted coumarin isomers are showing high binding scores compared to their C7-isomers, this is in accordance with the previously reported experimental data which demonstrated that the C6-isomers of coumarin derivatives tend to lose inhibitory activity for MAO-A (Mertens et al., 2014). MMGBSA binding free energy calculations showed relatively lower affinities when compared to coumarin isomers in complex with MAO-B.

Binding conformations of coumarin isomers with MAO-B and MAO-A are shown in Figures 5 and 6 respectively. Docking poses analysis show that all the compounds bind to MAO-B with the coumarin scaffold directed towards the

substrate cavity with either the hex-5-ynoate chain or the 4-chlorophenoxy moiety occupying the entrance cavity and forming various hydrophobic interactions with nearby residues such as Pro-102, Pro-103, Pro-104, Leu-164, Leu-167, Phe-168 and Leu-171. Docking analysis of coumarin isomers with MAO-A has yielded different poses due to the smaller cavity of MAO-A, the hex-5-ynoate chain doesn't fit well inside MAO-A cavity and thus adopt different conformations which are less stable than those of MAO-B complexes. Furthermore, the coumarin isomer (**4**) bearing the 4-chlorophenoxy at C6 doesn't seem to fit well inside the MAO-A active site pocket which might be due to the bulkier chlorophenyl ring, this result is in accordance with the experimental data ($\text{IC}_{50}\text{ MAO-A} > 10\text{ }\mu\text{M}$) which further emphasize our hypothesis (Mertens et al., 2014).

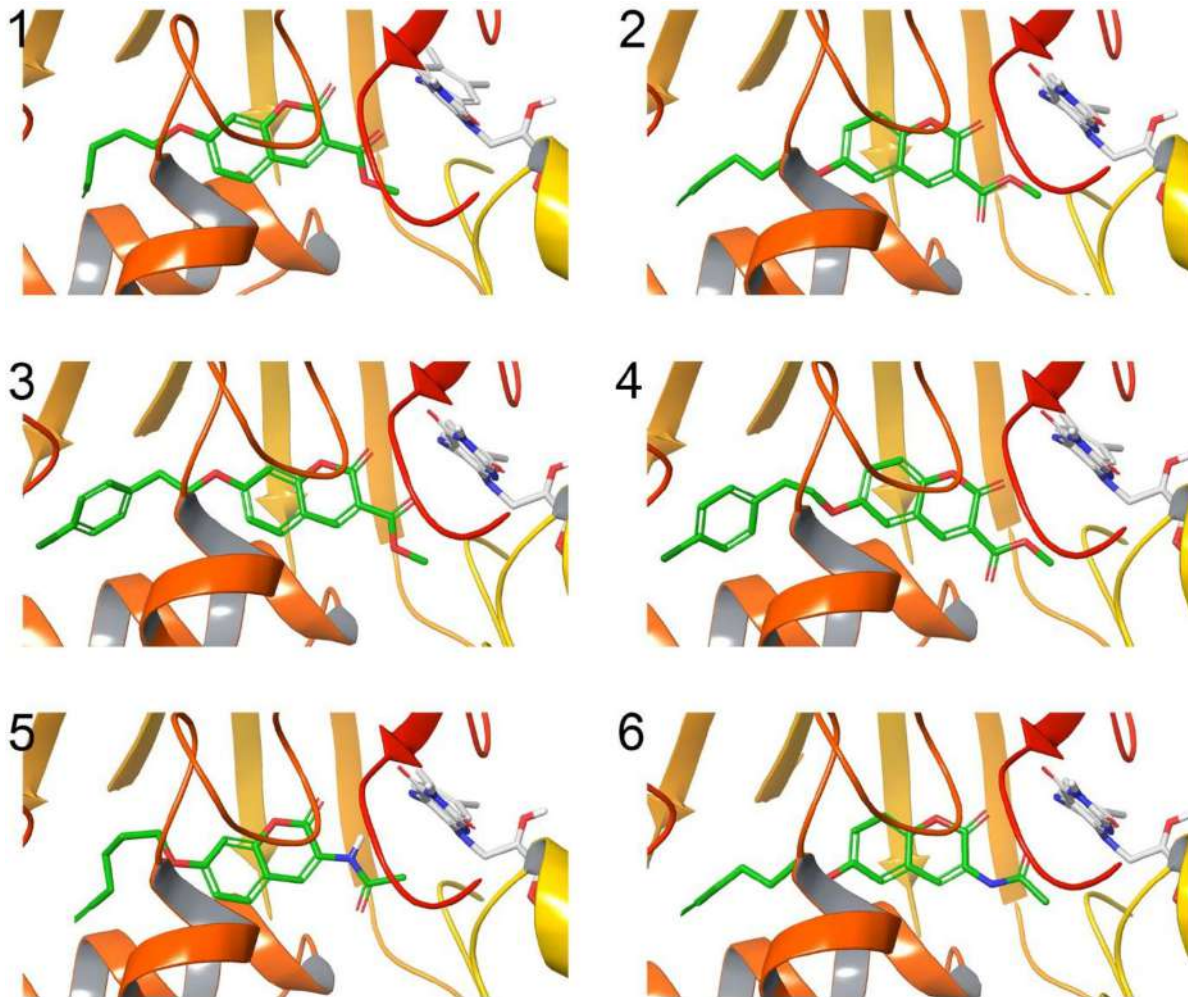


Figure 5. Docking poses of coumarin isomers with MAO-B active site. Binding conformations of coumarins are shown in green color, the C7-isomers are shown in 1,3,5 and their respective C6-isomers are shown in 2,4,6. FAD cofactor is shown in white color.

3.3. ADME properties prediction results

ADME properties and the 'Rule of Five' results for the selected coumarin isomers are shown in Table 4. All compounds were predicted as drug-like without any violations to the five rules. Qikprop predicted aqueous solubility show that all the compounds have values within the recommended range (-6.5 to 0.5) where 95% of similar values for known drugs fall inside. Predicted human oral absorption shows that all the selected coumarins have great oral absorption and thus greater bioavailability. Predicted apparent Caco-2 cell permeability yielded values greater than 500 which indicates a good cell permeability for the selected coumarins. Predicted brain/blood partition coefficient showed values greater than -3.0 and less than 1.2 which falls into the recommended range for drugs acting on the CNS. MDCK cells are considered to be a good mimic for the blood-brain barrier, predicted apparent MDCK cell permeability is considered great if >500 and poor if <25. The predicted MDCK values show that isomers 3 and 4 have great MDCK cell permeability, meanwhile it's considered to be moderate for the other compounds.

3.4. Molecular dynamics analysis

Molecular dynamics simulation was carried out in order to enumerate the structural stability of MAO enzyme variants in the presence of C6- and C7- coumarin isomers, as this could give a first-hand clue into their perturbing effects on protein structural integrity (Figure 7).

a) Root-mean square deviation (RMSD)

The stability of the two coumarin isomers in complex with MAO-A and MAO-B was evaluated according to different parameters. Protein RMSD of C-alpha atoms was used to measure the conformational changes of given complexes over time and describes whether the simulation has equilibrated and if its fluctuations towards the end of the simulation are around some thermal average structure with respect to the initial structure obtained from the molecular docking study of 0 ns as a reference structure. For all the complexes, the time-evolution of the RMSD profiles for C-alpha atoms of the protein and the ligand were determined and are shown in Figure 8.

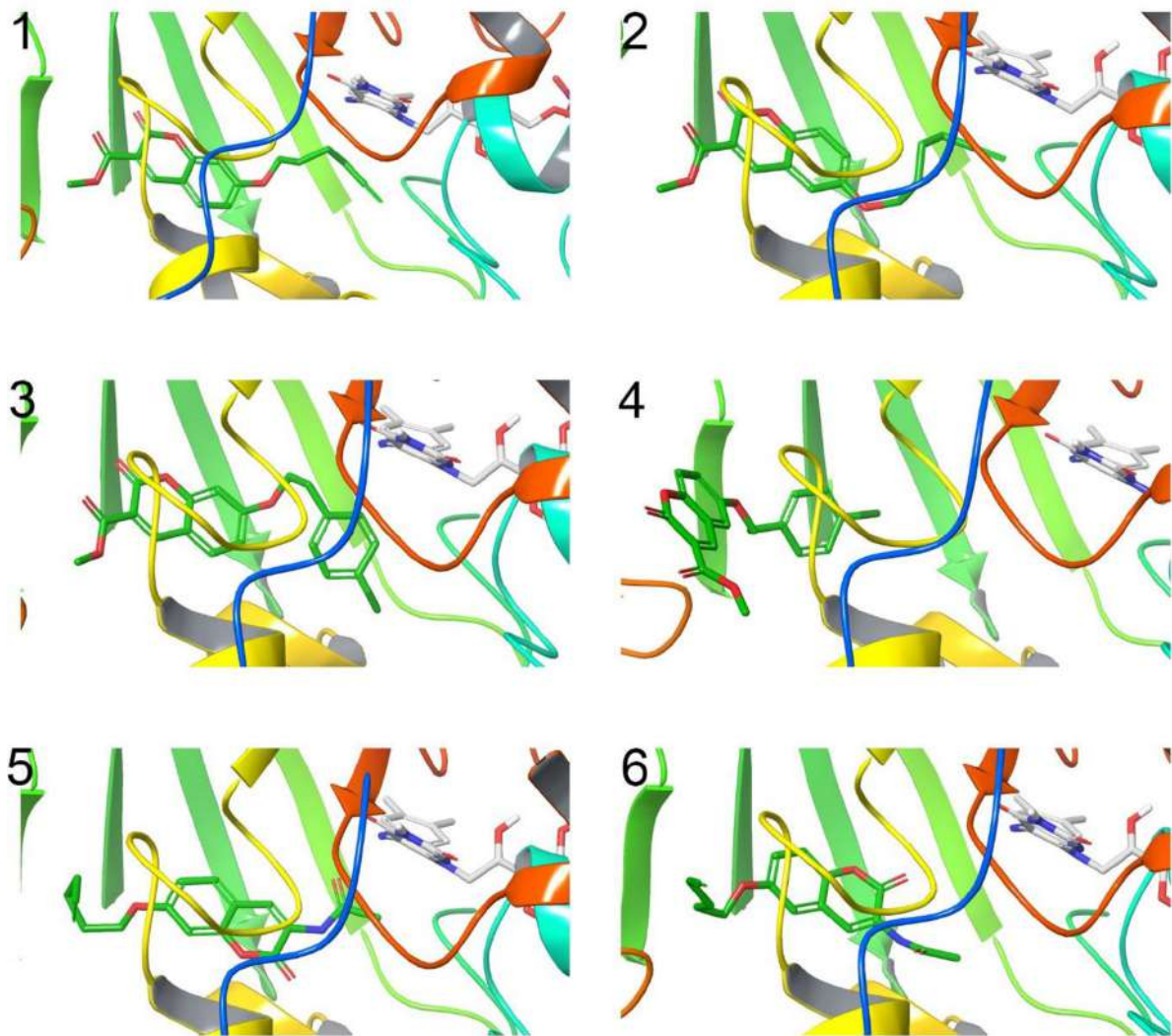


Figure 6. Docking poses of coumarin isomers with MAO-A active site. Binding conformations of coumarins are shown in green color, the C7-isomers are shown in 1,3,5 and their respective C6-isomers are shown in 2,4,6. FAD cofactor is shown in white color.

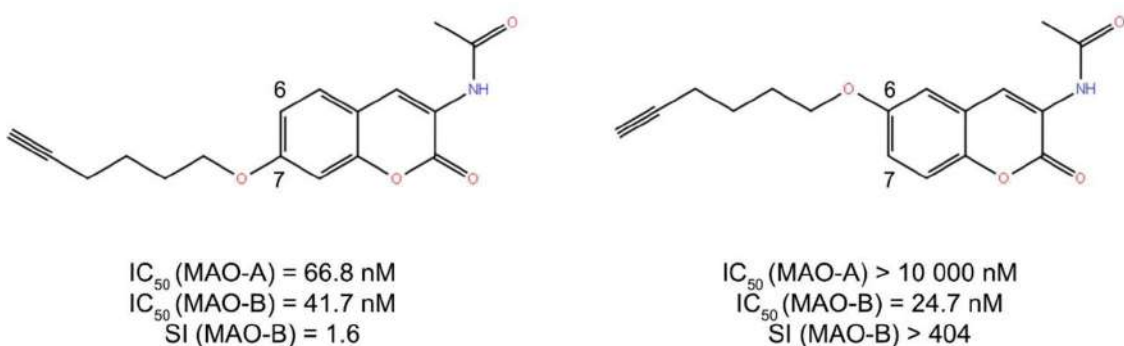


Figure 7. Chemical structures, IC₅₀ values and selectivity index of the selected coumarins for MD simulation: C6-isomer (right) and C7-isomer (left).

The RMSD analysis of the C-alpha atoms of MAO-A and MAO-B in complex with C7-substituted coumarin displayed an increase in the RMSD for the first 20 ns up to 4.5 Å for MAO-A and 2.5 Å for MAO-B, whereas it remained stable with only small fluctuations averaging around 2.0 and 3.0 Å for the rest of the trajectory. On the other hand, the ligand RMSD seems to be stable in MAO-A for the MD simulation

duration and only fluctuates around 1.5 Å and 2.5 Å which is in the acceptable range. However, in MAO-B the ligand seems to reach higher RMSD values in the beginning of the simulation and peaks at 8 Å. However, it seems to be decreasing at the end of the trajectory which implies that the C7-isomer needed longer time to reach a stable state within the protein.

Table 4. ADME properties prediction results of the selected coumarin isomers.

Compound	QPlogS	%HOA	QPPCaco	QPlogBB	QPPMDCK	Rule of Five
1	-4.5	96.7	803.7	-1.0	390.6	0
2	-4.5	96.7	803.5	-1.0	390.5	0
3	-5.4	100.0	802.6	-0.7	961.3	0
4	-5.4	100.0	803.6	-0.7	962.6	0
5	-4.6	96.1	715.3	-1.1	344.4	0
6	-4.5	96.1	718.7	-1.1	346.2	0

QPlogS: Predicted aqueous solubility; %HOA: Percentage of human oral absorption; QPPCaco: Predicted apparent Caco-2 cell permeability; QPlogBB: Predicted brain/blood partition coefficient; QPPMDCK: Predicted apparent MDCK cell permeability; Rule of Three: Molecular weight (MW) \leq 500 g/mol; Number of hydrogen bond acceptors (HBA) \leq 10; Number of hydrogen bond donors (HBD) \leq 5; Number of rotatable bonds (nRotb) \leq 10 and lipophilicity clogPo/w \leq 5.

As for the C6-substituted coumarin, the RMSD analysis of MAO-A backbone shows a noticeable fluctuation in RMSD especially in the first 20 ns which reached 8 Å before starting to equilibrate after 39 ns around 6 Å for the rest of the simulation. The high deviation in backbone atoms of the protein could be linked to the bulky residue Phe-208 in MAO-A which doesn't allow the binding of long inhibitors, this could be more specific to the placement of the hex-5-ynyoxy in position 6 of the coumarin scaffold which is directed towards the bottom of the cavity and might be constrained by the residue Phe-208. The corresponding C7-isomer was found to be more stable as the hex-5-ynyoxy chain is more directed towards the flexible residue Ile-335 of the entrance cavity. For MAO-B, the backbone RMSD analysis shows a slight increase in RMSD in contrast with MAO-A which is stabilized around 3 Å, this difference in stability between the two

isoforms may well be due to the entrance cavity residues, the flexible Ile-199 residue in MAO-B better tolerate longer inhibitors to fit inside the substrate cavity by undergoing a conformational change which serves as a gate for MAO-B inhibitors.

On the other hand, ligand RMSD was calculated to indicate how stable the ligand is with respect to the protein and its active site cavity. The C6-substituted coumarin isomer in complex with MAO-A shows slight fluctuations around 3 Å. However, for MAO-B these fluctuations are less important as they average around 2.5 Å at the end of the trajectory.

The information obtained from the RMSD analysis could provide a clue into the dual inhibitory activity of the C7-isomer towards MAO-A and MAO-B when compared to the C6-isomer.

b) Root-mean square fluctuation (RMSF)

RMSF is useful for characterizing local changes along the protein chain. It is calculated from the motion of each residue around the average position along the trajectory revealing the flexibility of a certain region of the protein during the MD simulation. RMSF plots of the C-alpha atoms for the chosen complexes are shown in Figure 9.

The RMSF graphs indicate the flexibility and mobility of each amino acid throughout the simulation. Higher RMSF values imply greater flexibility during the MD simulation, whereas lower RMSF values interpret the good stability of the system. It is calculated from the motion of each residue around the average position along the trajectory revealing the flexibility of a certain region of the protein during the

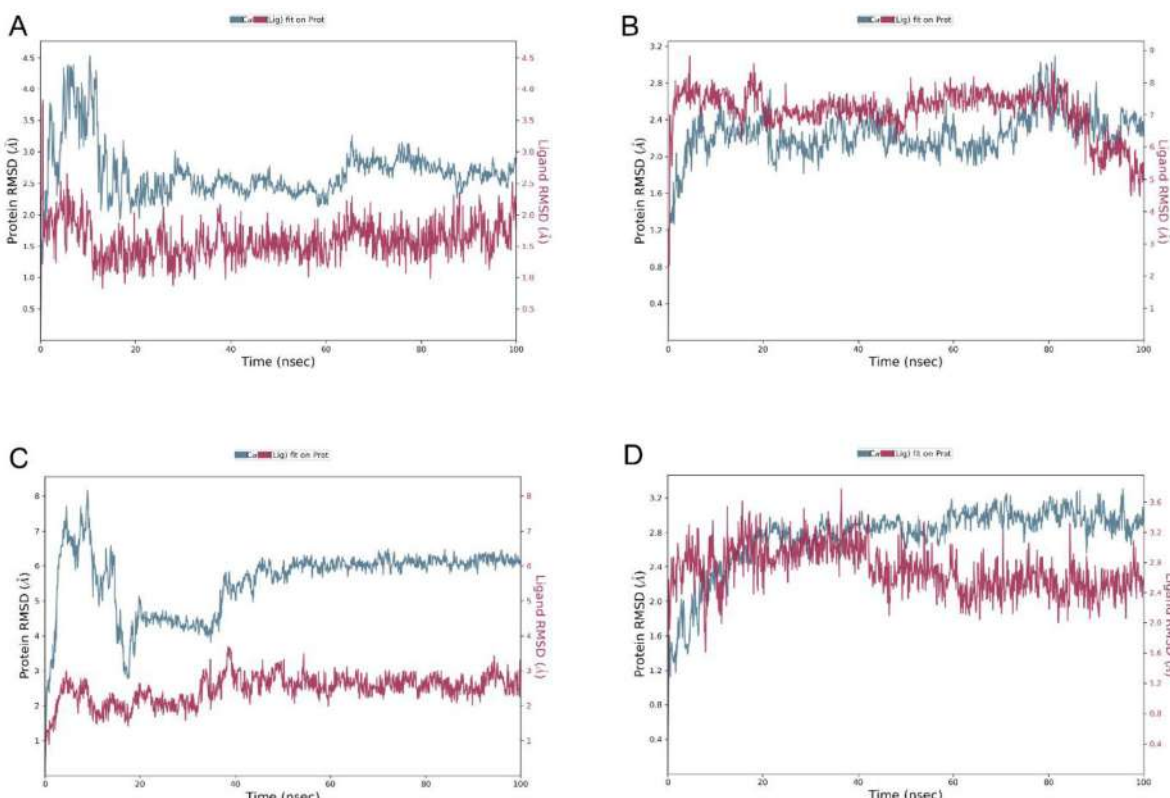


Figure 8. RMSD analysis of C-alpha atoms and ligand during MD simulation of C7-isomer with MAO-A (A) and MAO-B (B) and C6-isomer with MAO-A (C) and MAO-B (D).

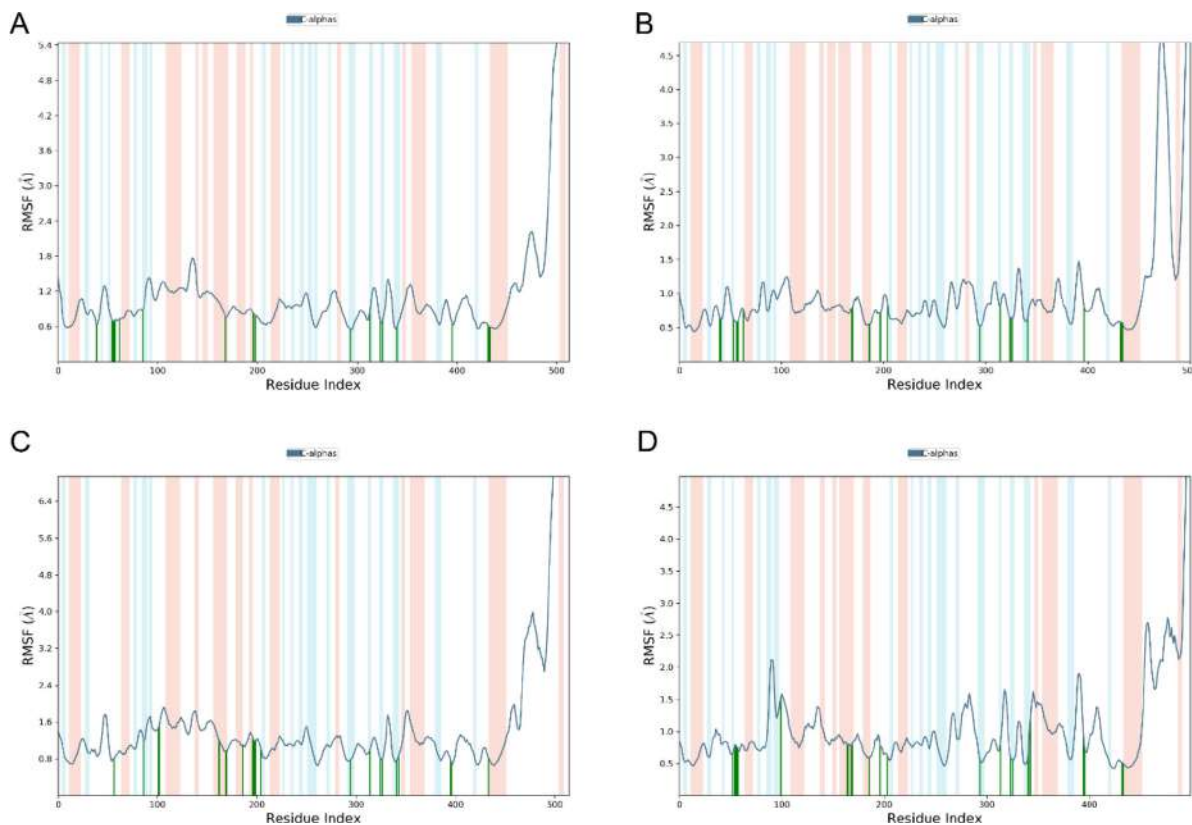


Figure 9. RMSF plots of C7-isomer with MAO-A (A) and MAO-B (B) and C6-isomer with MAO-A (C) and MAO-B (D) during MD simulation.

MD simulation. In this graph, the amino acids that make contacts with the ligand are represented by green vertical lines, secondary structural components such as α - helices and β -strands regions are represented by red and blue backgrounds, respectively, while the loop region is represented by a white background. Typically, α - helices and β -strands regions are rigid than the unstructured part of the protein, and hence fluctuate less than the loop regions. Compared to other parts of the protein, the N- and C-terminal regions showed the most fluctuations. The slight fluctuation of the active site and the main chain atoms indicates that the conformational change was minor (Martyna, 1994; Pawara et al., 2021; Zrieq et al., 2021). The RMSF graph of the C7-isomer and the C6-isomer with MAO-A and MAO-B enzymes complex yielded little fluctuations with less than 3 Å for residues in contact with ligands which is perfectly acceptable for small globular proteins (Vora et al., 2019).

c) Protein-ligand interactions analysis

Protein-ligand contacts were monitored throughout the simulation in order to clearly highlights the contribution of each residue of the binding site of each ligand-protein complex. The protein-ligand interactions diagrams are shown in Figure 10.

The C7-isomer was shown to establish a hydrogen bond with Tyr-69 of MAO-A and hydrophobic contacts mainly with Tyr-407 and Tyr-444 of the aromatic cage. Meanwhile the C7-isomer interacted with MAO-B through hydrogen bonding with Gly-434 and Met-436, stronger hydrophobic contacts

were observed between the ligand and Tyr-398 and Tyr-435 of the aromatic cage.

On the other hand, C6-isomer interacted with MAO-A through a hydrogen bond with Tyr-444, various hydrophobic interactions were noticed involving the residues: Ile-180, Phe-208, Ile-335, Phe-352 and Tyr-407. Meanwhile the C6-isomer in complex with MAO-B established three hydrogen bonds involving Ser-59, Tyr-60 and Gln-206, many hydrophobic contacts were observed with the residues: Tyr-389, Tyr-435, Phe-343, Tyr-326 and Ile-199. The results obtained from this analysis further emphasizes the role and implication of Ile-199 and Tyr-326 on shifting MAO-B selectivity as these two residues contribute largely in the binding of the C6-isomer to MAO-B in contrast with its respective C7-isomer.

d) MM-GBSA binding free energy calculations

The MD complexes were subjected to a post-MD MM-GBSA analysis in order to estimate their binding free energy. As noted in Table 5, among the four studied protein-ligand complexes, the C6-substituted coumarin in complex with MAO-B is showing the most negative value which indicates a stronger binding affinity (-71.05 kcal/mol), whereas it's estimated to -57.94 kcal/mol in the C7-isomer in complex with MAO-B which is in correlation with the experimental data. However, the large difference in potency for C6-isomer upon binding to MAO-A is not reflected in the GBSA binding free energy which suggests that certain residues in the binding pocket might suffer important rearrangements, which could have a conformational penalty not accounted for in the GBSA method.

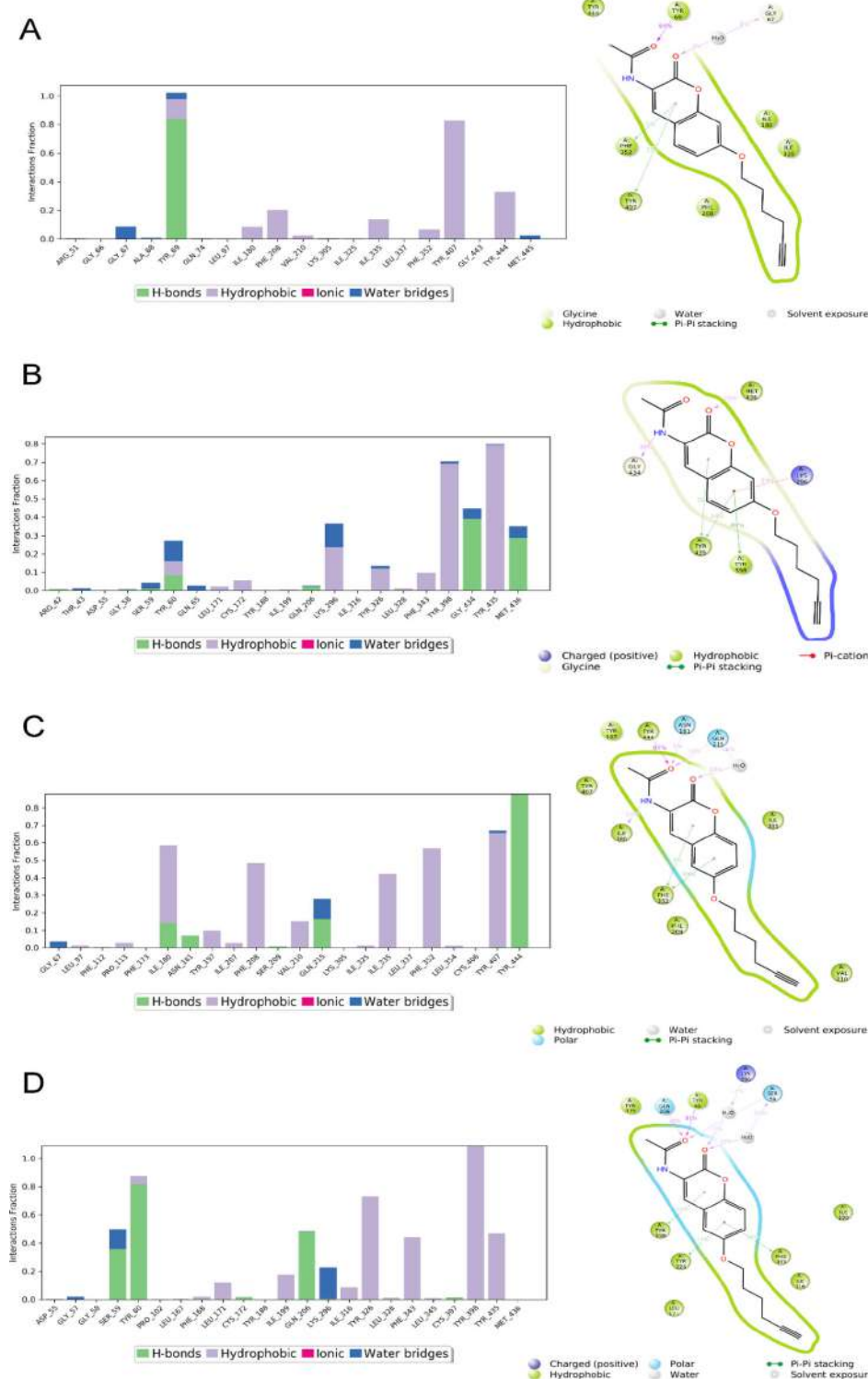


Figure 10. Protein-ligand interactions diagrams and 2 D representation of the C7-isomer with MAO-A (A) and MAO-B (B) and the C6-isomer with MAO-A (C) and MAO-B (D) throughout the MD simulation.

4. Discussion

Based on previously reported experimental data, it was confirmed that the C7-isomers of coumarins tend to be more potent towards MAO-B, meanwhile the C6-isomers are slightly less potent but tend to be more selective towards MAO-B isoform (Mertens et al., 2014). We noticed that this

hypothesis is applied to the selected coumarin derivatives: **1**, **3** and **5** and their respective C6-isomers: **2**, **4** and **6** which displayed a MAO-B selectivity shift of approximately 80, 80 and 400-fold respectively. Structural analysis revealed that the C6-substituted coumarin isomers form a π - π stacking interaction with Tyr-326 which is not present in the C7-substituted isomers.

Table 5. Post-MD MM-GBSA binding free energy results of C7-isomer with MAO-A (A) and MAO-B (B) and the C6-isomer with MAO-A (C) and MAO-B (D).

Protein-ligand complex	MM-GBSA binding free energy after MD (kcal/mol)
A	-59.63
B	-57.94
C	-69.95
D	-71.05

Furthermore, the positioning of the hex-5-ynyoxy moiety plays a role in the selectivity mechanism as the differences between MAO-A and MAO-B are mainly related to the shape and the flexibility of their active site cavities (Knez et al., 2020). The long and narrow cavity of MAO-B makes it preferentially bind long inhibitors which forces a conformational change of the gating residue Ile-199 and fuses the two cavities into one (Finberg & Rabey, 2016). The absence of this mechanism in MAO-A isoform further emphasize this hypothesis and could explain why such inhibitors tend to be more selective towards MAO-B.

Moreover, the molecular docking study confirmed that all coumarin derivatives bind non-covalently to MAO-B active site and the triple bond of the hex-5-ynyoxy chain doesn't bind to the FAD cofactor as such in irreversible inhibitors.

ADME properties prediction has shown that all the studied compounds are druglike, able to cross the blood-brain barrier and have values within recommended ranges where 95% of known drugs fall inside.

Lastly, a molecular dynamics simulation was conducted in order to assess and compare the stability of two coumarin isomers that displayed the highest selectivity shift towards MAO-B isoform (>404-fold). Analysis was conducted based on the RMSD of the protein backbone and ligands throughout the simulation, RMSF of the protein and protein-ligand interactions. The results showed favorable interactions and better stability regarding the C6-isomer with MAO-B isoform by establishing various hydrophobic interactions especially with Ile-199 and Tyr-326 which are known to play a role in substrate and inhibitors specificity (Edmondson et al., 2007). These residues are replaced with the bulky Phe-208 and Ile-335 in MAO-A which may hinder C6-substituted isomers from binding inside its active site cavity. Moreover, the selective C6-isomer was found to be unstable within MAO-A isoform in contrast to the non-selective C7-isomer which is in accordance with the experimental data.

5. Conclusion

The present study aimed to investigate the mode of interaction of previously reported alkynyl coumarinyl ethers at the molecular level. It was found that C7-isomers tend to be more potent towards MAO-A and MAO-B while the C6-isomers tend to be more selective towards MAO-B. Molecular docking analysis revealed that the loss of activity towards MAO-A of these compounds may be due to the bulky side chain of Phe-208 which is replaced by the gating residue Ile-199 that displays a conformational change depending on the nature of the inhibitor. Among the studied coumarin isomers, the compound **6** is considered the best drug-candidate

which needs more focus for the development of new anti-parkinsonian drugs in respect to its drug likeness, potency and selectivity for MAO-B. In conclusion, the computational investigation through molecular docking and molecular dynamics simulation helped elucidate not only the mechanism of MAO-B inhibition but also provide valuable insight for the rational improvements of selectivity of coumarin derivatives to be explored as novel drug candidates against Parkinson's disease.

Acknowledgments

We would like to thank Francisco Javier Luque Garriga, Professor in the Department of Chemical Physics, University of Barcelona, Spain, for his assistance. His contribution is sincerely appreciated and gratefully acknowledged.

Disclosure statement

No potential conflict of interest was reported by the authors.

Funding

The author(s) reported there is no funding associated with the work featured in this article.

ORCID

- Yassir Boulaamane  <http://orcid.org/0000-0002-2939-7772>
 Iqrar Ahmad  <http://orcid.org/0000-0002-7697-9572>
 Harun Patel  <http://orcid.org/0000-0003-0920-1266>
 Niloy Das  <http://orcid.org/0000-0001-6848-3502>
 Mohammed Reda Britel  <http://orcid.org/0000-0002-9918-5767>
 Amal Mauandy  <http://orcid.org/0000-0001-9298-717X>

References

- Ahmad, I., Jadhav, H., Shinde, Y., Jagtap, V., Girase, R., & Patel, H. (2021). Optimizing Bedaquiline for cardiotoxicity by structure based virtual screening, DFT analysis and molecular dynamic simulation studies to identify selective MDR-TB inhibitors. *In Silico Pharmacology*, 9(1), 23. <https://doi.org/10.1007/s40203-021-00086-x>
- Binda, C., Li, M., Hubálek, F., Restelli, N., Edmondson, D. E., & Mattevi, A. (2003). Insights into the mode of inhibition of human mitochondrial monoamine oxidase B from high-resolution crystal structures. *Proceedings of the National Academy of Sciences*, 100(17), 9750–9755. <https://doi.org/10.1073/pnas.1633804100>
- Binda, C., Mattevi, A., & Edmondson, D. E. (2011). Structural properties of human monoamine oxidases A and B. *International Review of Neurobiology*, 100, 1–11.
- Binda, C., Newton-Vinson, P., Hubálek, F., Edmondson, D. E., & Mattevi, A. (2002). Structure of human monoamine oxidase B, a drug target for the treatment of neurological disorders. *Nature Structural Biology*, 9(1), 22–26.
- Binda, C., Wang, J., Pisani, L., Caccia, C., Carotti, A., Salvati, P., Edmondson, D. E., & Mattevi, A. (2007). Structures of human monoamine oxidase B complexes with selective noncovalent inhibitors: Safinamide and coumarin analogs. *Journal of Medicinal Chemistry*, 50(23), 5848–5852.
- Congreve, M., Carr, R., Murray, C., & Jhoti, H. (2003). A 'rule of three' for fragment-based lead discovery? *Drug Discovery Today*, 8(19), 876–877.
- Culpepper, L. (2013). Reducing the burden of difficult-to-treat major depressive disorder: Revisiting monoamine oxidase inhibitor therapy. *The Primary Care Companion for CNS Disorders*, 15(5), 27220. <https://doi.org/10.4088/PCC.13r01515>

- D. E. Shaw Research, Schrödinger Release. (2020–3). Desmond molecular dynamics system. Maestro-Desmond interoperability tools.
- Das, D., Koh, Y., Tojo, Y., Ghosh, A. K., & Mitsuya, H. (2009). Prediction of potency of protease inhibitors using free energy simulations with polarizable quantum mechanics-based ligand charges and a hybrid water model. *Journal of Chemical Information and Modeling*, 49(12), 2851–2862. <https://doi.org/10.1021/ci900320p>
- De Colibus, L., Li, M., Binda, C., Lustig, A., Edmondson, D. E., & Mattevi, A. (2005). Three-dimensional structure of human monoamine oxidase A (MAO A): Relation to the structures of rat MAO A and human MAO B. *Proceedings of the National Academy of Sciences*, 102(36), 12684–12689. <https://doi.org/10.1073/pnas.0505975102>
- Dorsey, E. R., Elbaz, A., Nichols, E., Abbasi, N., Abd-Allah, F., Abdelalim, A., Adsuar, J. C., Ansha, M. G., Brayne, C., Choi, J.-Y. J., Collado-Mateo, D., Dahodwala, N., Do, H. P., Edessa, D., Endres, M., Fereshtehnejad, S.-M., Foreman, K. J., Gankpe, F. G., Gupta, R., ... Murray, C. J. L. (2018). Global, regional, and national burden of Parkinson's disease, 199–2016: A systematic analysis for the Global Burden of Disease Study 2016. *The Lancet Neurology*, 17(11), 939–953. [https://doi.org/10.1016/S1474-4422\(18\)30295-3](https://doi.org/10.1016/S1474-4422(18)30295-3)
- Edmondson, D. E., Binda, C., & Mattevi, A. (2007). Structural insights into the mechanism of amine oxidation by monoamine oxidases A and B. *Archives of Biochemistry and Biophysics*, 464(2), 269–276. <https://doi.org/10.1016/j.abb.2007.05.006>
- Finberg, J. P., & Rabey, J. M. (2016). Inhibitors of MAO-A and MAO-B in psychiatry and neurology. *Frontiers in Pharmacology*, 7, 340.
- Friesner, R. A., Banks, J. L., Murphy, R. B., Halgren, T. A., Klicic, J. J., Mainz, D. T., Repasky, M. P., Knoll, E. H., Shelley, M., Perry, J. K., Shaw, D. E., Francis, P., & Shenvi, P. S. (2004). Glide: A new approach for rapid, accurate docking and scoring. 1. Method and assessment of docking accuracy. *Journal of Medicinal Chemistry*, 47(7), 1739–1749.
- Friesner, R. A., Murphy, R. B., Repasky, M. P., Frye, L. L., Greenwood, J. R., Halgren, T. A., Sanschagrin, P. C., & Mainz, D. T. (2006). Extra precision glide: Docking and scoring incorporating a model of hydrophobic enclosure for protein–ligand complexes. *Journal of Medicinal Chemistry*, 49(21), 6177–6196. <https://doi.org/10.1021/jm051256o>
- Gaweska, H., & Fitzpatrick, P. F. (2011). Structures and mechanism of the monoamine oxidase family, 2(5), 365–377. <https://doi.org/10.1515/BMC.2011.030>
- Genheden, S., & Ryde, U. (2015). The MM/PBSA and MM/GBSA methods to estimate ligand-binding affinities. *Expert Opinion on Drug Discovery*, 10(5), 449–461. <https://doi.org/10.1517/17460441.2015.1032936>
- Greenwood, J. R., Calkins, D., Sullivan, A. P., & Shelley, J. C. (2010). Towards the comprehensive, rapid, and accurate prediction of the favorable tautomeric states of drug-like molecules in aqueous solution. *Journal of Computer-Aided Molecular Design*, 24(6–7), 591–604.
- Halgren, T. A., Murphy, R. B., Friesner, R. A., Beard, H. S., Frye, L. L., Pollard, W. T., & Banks, J. L. (2004). Glide: A new approach for rapid, accurate docking and scoring. 2. Enrichment factors in database screening. *Journal of Medicinal Chemistry*, 47(7), 1750–1759.
- Jacobson, M. P., Friesner, R. A., Xiang, Z., & Honig, B. (2002). On the role of the crystal environment in determining protein side-chain conformations. *Journal of Molecular Biology*, 320(3), 597–608.
- Jacobson, M. P., Pincus, D. L., Rapp, C. S., Day, T. J., Honig, B., Shaw, D. E., & Friesner, R. A. (2004). A hierarchical approach to all-atom protein loop prediction. *Proteins: Structure, Function, and Bioinformatics*, 55(2), 351–367. <https://doi.org/10.1002/prot.10613>
- Jorgensen, W. L., Maxwell, D. S., & Tirado-Rives, J. (1996). Development and testing of the OPLS all atom force field on conformational energetics and properties of organic liquids. *Journal of the American Chemical Society*, 118(45), 11225–11236. <https://doi.org/10.1021/ja9621760>
- Knez, D., Coletti, N., Iacovino, L. G., Sova, M., Pišlar, A., Konc, J., Lešnik, S., Higgs, J., Kamecki, F., Mangialavori, I., Dolsák, A., Žakelj, S., Trontelj, J., Kos, J., Binda, C., Marder, M., & Gobec, S. (2020). Stereoselective activity of 1-propargyl-4-styrylpiperidine-like analogues that can discriminate between monoamine oxidase isoforms A and B. *Journal of Medicinal Chemistry*, 63(3), 1361–1387. <https://doi.org/10.1021/acs.jmedchem.9b01886>
- Lee, H. Y., Cho, D. Y., Ahmad, I., Patel, H. M., Kim, M. J., Jung, J. G., Jeong, E. H., Haque, M. A., & Cho, K. M. (2021). Mining of a novel esterase (est3S) gene from a cow rumen metagenomic library with organophosphorus insecticides degrading capability: Catalytic insights by site directed mutations, docking, and molecular dynamic simulations. *International Journal of Biological Macromolecules*, 190, 441–455.
- Li, J., Abel, R., Zhu, K., Cao, Y., Zhao, S., & Friesner, R. A. (2011). The VSGB 2.0 model: A next generation energy model for high resolution protein structure modeling. *Proteins: Structure, Function, and Bioinformatics*, 79(10), 2794–2812. <https://doi.org/10.1002/prot.23106>
- Lin, J., Sahakian, D. C., De Morais, S. M., Xu, J. J., Polzer, R. J., & Winter, S. M. (2003). The role of absorption, distribution, metabolism, excretion and toxicity in drug discovery. *Current Topics in Medicinal Chemistry*, 3(10), 1125–1154.
- Lipinski, C. A. (2004). Lead- and drug-like compounds: The rule-of-five revolution. *Drug Discovery Today. Technologies*, 1(4), 337–341. <https://doi.org/10.1016/j.ddtec.2004.11.007>
- Lyne, P. D., Lamb, M. L., & Saeh, J. C. (2006). Accurate prediction of the relative potencies of members of a series of kinase inhibitors using molecular docking and MM-GBSA scoring. *Journal of Medicinal Chemistry*, 49(16), 4805–4808.
- Mallajosyla, J. K., Kaur, D., Chinta, S. J., Rajagopalan, S., Rane, A., Nicholls, D. G., Di Monte, D. A., MacArthur, H., & Andersen, J. K. (2008). MAO-B elevation in mouse brain astrocytes results in Parkinson's pathology. *PLoS ONE*, 3(2), e1616. <https://doi.org/10.1371/journal.pone.0001616>
- Martyna, G. J. (1994). Remarks on "Constant-temperature molecular dynamics with momentum conservation". *Physical Review E, Statistical Physics, Plasmas, Fluids, and Related Interdisciplinary Topics*, 50(4), 3234–3236. <https://doi.org/10.1103/physreve.50.3234>
- Mehta, C. H., Narayan, R., Aithal, G., Pandiyani, S., Bhat, P., Dengale, S., Shah, A., Nayak, U. Y., & Garg, S. (2019). Molecular simulation driven experiment for formulation of fixed dose combination of Darunavir and Ritonavir as anti-HIV nanosuspension. *Journal of Molecular Liquids*, 293, 111469. <https://doi.org/10.1016/j.molliq.2019.111469>
- Mertens, M. D., Hinz, S., Müller, C. E., & Gütschow, M. (2014). Alkynyl-coumarinyl ethers as MAO-B inhibitors. *Bioorganic & Medicinal Chemistry*, 22(6), 1916–1928. <https://doi.org/10.1016/j.bmc.2014.01.046>
- Mostert, S., Petzer, A., & Petzer, J. P. (2015). Indanones as high-potency reversible inhibitors of monoamine oxidase. *ChemMedChem*, 10(5), 862–873. <https://doi.org/10.1002/cmdc.201500059>
- Noda, S., Sato, S., Fukuda, T., Tada, N., Uchiyama, Y., Tanaka, K., & Hattori, N. (2020). Loss of Parkin contributes to mitochondrial turnover and dopaminergic neuronal loss in aged mice. *Neurobiology of Disease*, 136, 104717. <https://doi.org/10.1016/j.nbd.2019.104717>
- Olsson, M. H., Søndergaard, C. R., Rostkowski, M., & Jensen, J. H. (2011). PROPKA3: Consistent treatment of internal and surface residues in empirical pKa predictions. *Journal of Chemical Theory and Computation*, 7(2), 525–537. <https://doi.org/10.1021/ct100578z>
- Pawara, R., Ahmad, I., Surana, S., & Patel, H. (2021). Computational identification of 2,4-disubstituted amino-pyrimidines as L858R/T790M-EGFR double mutant inhibitors using pharmacophore mapping, molecular docking, binding free energy calculation, DFT study and molecular dynamic simulation. *In Silico Pharmacol*, 9 (1), 54. <https://doi.org/10.1007/s40203-021-00113-x>
- Poewe, W., & Mahlknecht, P. (2020). Pharmacologic treatment of motor symptoms associated with Parkinson disease. *Neurologic Clinics*, 38(2), 255–267. <https://doi.org/10.1016/j.ncl.2019.12.002>
- Rempel, V., Volz, N., Hinz, S., Karcz, T., Meliciani, I., Nieger, M., Wenzel, W., Bräse, S., & Müller, C. E. (2012). 7-Alkyl-3-benzylcoumarins: A versatile scaffold for the development of potent and selective cannabinoid receptor agonists and antagonists. *Journal of Medicinal Chemistry*, 55(18), 7967–7977.
- Roos, K., Wu, C., Damm, W., Reboul, M., Stevenson, J. M., Lu, C., Dahlgren, M. K., Mondal, S., Chen, W., Wang, L., Abel, R., Friesner, R. A., & Harder, E. D. (2019). OPLS3e: Extending force field coverage for drug-like small molecules. *Journal of Chemical Theory and Computation*, 15(3), 1863–1874. <https://doi.org/10.1021/acs.jctc.8b01026>
- Schrödinger Release: Maestro. (2021). Schrödinger, LLC.
- Shih, J. C., Chen, K., & Ridd, M. J. (1999). Monoamine oxidase: From genes to behavior. *Annual Review of Neuroscience*, 22(1), 197–217.

- Son, S. Y., Ma, J., Kondou, Y., Yoshimura, M., Yamashita, E., & Tsukihara, T. (2008). Structure of human monoamine oxidase A at 2.2-Å resolution: The control of opening the entry for substrates/inhibitors. *Proceedings of the National Academy of Sciences*, 105(15), 5739–5744. <https://doi.org/10.1073/pnas.0710626105>
- Tetrud, J. W., & Koller, W. C. (2004). A novel formulation of selegiline for the treatment of Parkinson's disease. *Neurology*, 63(7 Suppl 2), S2–S6. suppl
- Vora, J., Patel, S., Athar, M., Sinha, S., Chhabria, M. T., Jha, P. C., & Srivastava, N. (2019). Pharmacophore modeling, molecular docking and molecular dynamics simulation for screening and identifying anti-dengue phytocompounds. *Journal of Biomolecular Structure and Dynamics*, 38(6), 1726–1740. <https://doi.org/10.1080/07391102.2019.1615002>
- Wang, D., Hong, R. Y., Guo, M., Liu, Y., Chen, N., Li, X., & Kong, D. X. (2019). Novel C7-substituted coumarins as selective monoamine oxidase inhibitors: Discovery, synthesis and theoretical simulation. *Molecules*, 24(21), 4003. <https://doi.org/10.3390/molecules24214003>
- Youdim, M. B., Gross, A., & Finberg, J. P. (2001). Rasagiline [N-propargyl-1R (+)-aminoindan], a selective and potent inhibitor of mitochondrial monoamine oxidase B. *British Journal of Pharmacology*, 132(2), 500–506.
- Youdim, M. B., Edmondson, D., & Tipton, K. F. (2006). The therapeutic potential of monoamine oxidase inhibitors. *Nature Reviews. Neuroscience*, 7(4), 295–309.
- Zrieg, R., Ahmad, I., Snoussi, M., Noumi, E., Iriti, M., Algahtani, F. D., Patel, H., Saeed, M., Tasleem, M., Sulaiman, S., Aouadi, K., & Kadri, A. (2021). Tomatidine and Patchouli alcohol as inhibitors of SARS-CoV-2 enzymes (3CLpro, PLpro and NSP15) by molecular docking and molecular dynamics simulations. *International Journal of Molecular Sciences*, 22(19), 10693. <https://doi.org/10.3390/ijms221910693>

ANNEX 2: *IN SILICO STUDIES OF NATURAL PRODUCT-LIKE CAFFEINE DERIVATIVES AS POTENTIAL MAO-B INHIBITORS/AA_{2A}R ANTAGONISTS FOR THE TREATMENT OF PARKINSON'S DISEASE*

Following our work on MAO-B, we have directed our efforts towards NPs, specifically caffeine derivatives, as potential candidates for novel antiparkinsonian drugs. We explored NP-like caffeine derivatives as potential dual MAO-B inhibitors/AA_{2A}R antagonists for PD. Two top hits, CNP0202316 and CNP0365210, identified from COCONUT NPs, exhibited properties conducive to brain-targeted drugs. MD simulations confirmed their stability with MAO-B. This research highlights the potential of natural-based compounds, specifically caffeine derivatives, for optimizing dual-target-directed drugs to manage and prevent neuronal damage in PD patients.

The details of this work are reported in the following publication.

Boulaamane, Y., Ibrahim, M. A., Britel, M. R., & Maurady, A. (2022). In silico studies of natural product-like caffeine derivatives as potential MAO-B inhibitors/AA_{2A}R antagonists for the treatment of Parkinson's disease. *Journal of Integrative Bioinformatics*, 19(4), 20210027.

Available at: <https://doi.org/10.1515/jib-2021-0027>

Conceptualization: Y.B., A.M.; Methodology: Y.B., A.M.; Investigation: Y.B., A.M.; Visualization: Y.B., I.A., H.P.; Supervision: M.R.B., A.M.; Writing—original draft: Y.B.; Writing—review & editing: Y.B., A.M.



Yassir Boulaamane, Mahmoud A. A. Ibrahim, Mohammed Reda Britel and Amal Maurady*

In silico studies of natural product-like caffeine derivatives as potential MAO-B inhibitors/AA_{2A}R antagonists for the treatment of Parkinson's disease

<https://doi.org/10.1515/jib-2021-0027>

Received August 28, 2021; accepted June 24, 2022; published online September 19, 2022

Abstract: Parkinson's disease is considered the second most frequent neurodegenerative disease. It is described by the loss of dopaminergic neurons in the mid-brain. For many decades, L-DOPA has been considered as the gold standard for treating Parkinson's disease motor symptoms, however, due to the decrease of efficacy, in the long run, there is an urgent need for novel antiparkinsonian drugs. Caffeine derivatives have been reported several times for their neuroprotective properties and dual blockade of monoamine oxidase (MAO) and adenosine A_{2A} receptors (AA_{2A}R). Natural products are currently attracting more focus due to structural diversity and safety in contrast to synthetic drugs. In the present work, computational studies were conducted on natural product-like caffeine derivatives to search for novel potent candidates acting as dual MAO-B inhibitors/AA_{2A}R antagonists for Parkinson's disease. Our findings revealed two natural products among the top hits: CNP0202316 and CNP0365210 fulfill the requirements of drugs acting on the brain. The selected lead compounds were further studied using molecular dynamics simulation to assess their stability with MAO-B. Current findings might shift the interest towards natural-based compounds and could be exploited to further optimize caffeine derivatives into a successful dual-target-directed drug for managing and halting the neuronal damage in Parkinson's disease patients.

Keywords: ADMET prediction; caffeine; molecular dynamics simulation; natural products; neuroprotection; structure-based virtual screening.

1 Introduction

Neurodegenerative diseases and brain-associated diseases are major concerns among aging populations across the world [1]. Neurodegenerative diseases such as Parkinson's and Alzheimer's diseases have a multi-factorial nature that is characterized by the progressive loss of neurons in the brain [2]. Parkinson's disease

*Corresponding author: Amal Maurady, Laboratory of Innovative Technologies, National School of Applied Sciences of Tangier, Abdelmalek Essaadi University, Tetouan, Morocco; and Faculty of Sciences and Techniques of Tangier, Abdelmalek Essaadi University, Tetouan, Morocco, E-mail: amaurady@uae.ac.ma. <https://orcid.org/0000-0001-9298-717X>

Yassir Boulaamane and Mohammed Reda Britel, Laboratory of Innovative Technologies, National School of Applied Sciences of Tangier, Abdelmalek Essaadi University, Tetouan, Morocco, E-mail: boulaamane.yassir@etu.uae.ac.ma (Y. Boulaamane), mbritel@uae.ac.ma (M.R. Britel). <https://orcid.org/0000-0002-2939-7772> (Y. Boulaamane). <https://orcid.org/0000-0002-9918-5767> (M.R. Britel)

Mahmoud A. A. Ibrahim, Computational Chemistry Laboratory, Chemistry Department, Faculty of Science, Minia University, Minia, 61519, Egypt, E-mail: m.ibrahim@compchem.net. <https://orcid.org/0000-0003-4819-2040>

(PD) is defined especially by the progressive loss of dopaminergic neurons in the substantia nigra pars compacta (SNpc) of the midbrain [3]. More than six million people in the world are affected today with a prevalence of 150 in every 100,000 people which is further increasing with age and affects 1% of the population over 60 years [4]. Current pharmaceutical treatments for PD include levodopa or levodopa plus dopa-decarboxylase inhibitors, dopamine agonists, and catechol-O-methyl transferase (COMT)/monoamine oxidase B (MAO-B) inhibitors [5]. Recently, other non-dopaminergic drugs have shown promising efficacy to relieve PD symptoms such as adenosine A_{2A} receptor (AA_{2A}R) antagonists [6].

Monoamine Oxidase (MAO) (EC 1.4.3.4) belongs to a family of flavin adenine dinucleotide (FAD)-dependant enzymes that are expressed in the outer mitochondrial membrane of neuronal cells. The MAO enzymes are responsible for the oxidative deamination of monoamine neurotransmitters such as dopamine, adrenaline, and noradrenaline in the central nervous system (CNS) [5, 7]. The MAO enzymes exist in two isoforms, MAO-A and MAO-B that share sequence similarities of 70% but differ in tissue distribution, substrate, and inhibitor preferences [5]. The development of the first MAO inhibitors was abandoned due to side effects related to the metabolism of tyramine, which causes a cardiovascular crisis [8]. However, a new class of selective MAO-B inhibitors has been proven to be efficient in treating PD symptoms. It was also shown that this new class of selective MAO-B inhibitors is devoid of tyramine-related side effects. Furthermore, the selective MAO-B inhibitors may act as neuroprotective agents by limiting the release of free radical species and hence may decrease the progression of the disease [5, 9].

MAO-A preferentially metabolizes serotonin while MAO-B preferentially deaminates 2-phenylethylamine and benzylamine. Dopamine, norepinephrine, and epinephrine are substrates of both isoforms in most animal tissues [10].

During aging, the expression of MAO-B increases in the brain and is connected with an enhanced dopamine metabolism which results in an increased reactive oxygen species (ROS) production such as hydrogen peroxide (H_2O_2) inducing oxidative damage and apoptotic signaling events [11].

Previously approved MAO-B inhibitors are selegiline and rasagiline which irreversibly inhibit MAO-B with an IC_{50} value of 6.8 and 14 nM respectively [12]. The latest approved MAO-B inhibitor is safinamide which reversibly inhibits MAO-B with an IC_{50} value of 450 nM [13]. Istradefylline, a caffeine-based inhibitor that was approved in Japan in 2013 and also approved for medical use in the United States in 2019 acts as a dual inhibitor of MAO-B and AA_{2A}R [14, 15]. However, istradefylline was found to be a weak inhibitor of MAO-B ($IC_{50} = 28 \mu M$) which encourages further research on new substitutions to the caffeine core [16]. The chemical structures of MAO-B inhibitors are shown in Figure 1.

The crystal structure of MAO-A (PDB ID: 2Z5Y) has a monopartite substrate cavity of $\sim 550 \text{ \AA}^3$ volume while the crystal structure of MAO-B contains a bipartite cavity structure with an entrance cavity of $\sim 290 \text{ \AA}^3$ and a substrate cavity of $\sim 400 \text{ \AA}^3$ [17]. ILE-199 and TYR-326 separate these two cavities in MAO-B serving as

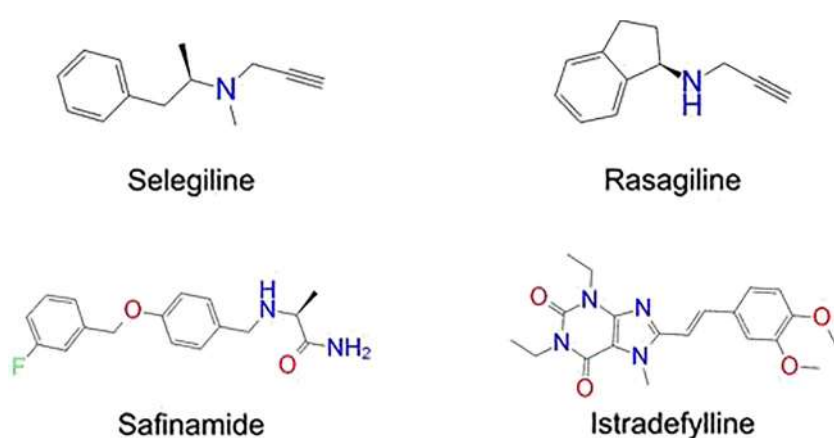


Figure 1: Chemical structures of monoamine oxidase B inhibitors.

“gating” residues and a structural determinant for substrate and inhibitor recognition by MAO-B [18, 19]. The superposition of MAO-A and MAO-B and their active site residues are shown in Figure 2.

The structural study revealed that MAO-B (PDB ID: 2V5Z) is formed by two monomers consisting of a globular domain anchored to the membrane through a C-terminal helix [20]. MAO-B active site residues that share similarities to MAO-A active site are TYR-60, LEU-164, PHE-168, GLN-206, ILE-198, ILE-316, PHE-343, TYR-398, and TYR-435. Meanwhile, the amino acids that are specific to MAO-B are located in the hydrophobic pocket which is formed by LEU-171, CYS-172, ILE-199, TYR-326 [13].

There is a great deal of literature supporting the use and efficacy of natural products (NP) in PD such as flavonoids, xanthones, phenolic derivatives, alkaloids, and caffeine [21, 22]. These natural resources and their derivatives have been reported for their potential to selectively inhibit MAO-B and may offer a safer alternative compared to conventional drugs [23]. Furthermore, caffeine has been used in several studies as a scaffold for the design of dual MAO inhibitors/AA_{2A}R antagonists. Pretorius et al. synthesized a series

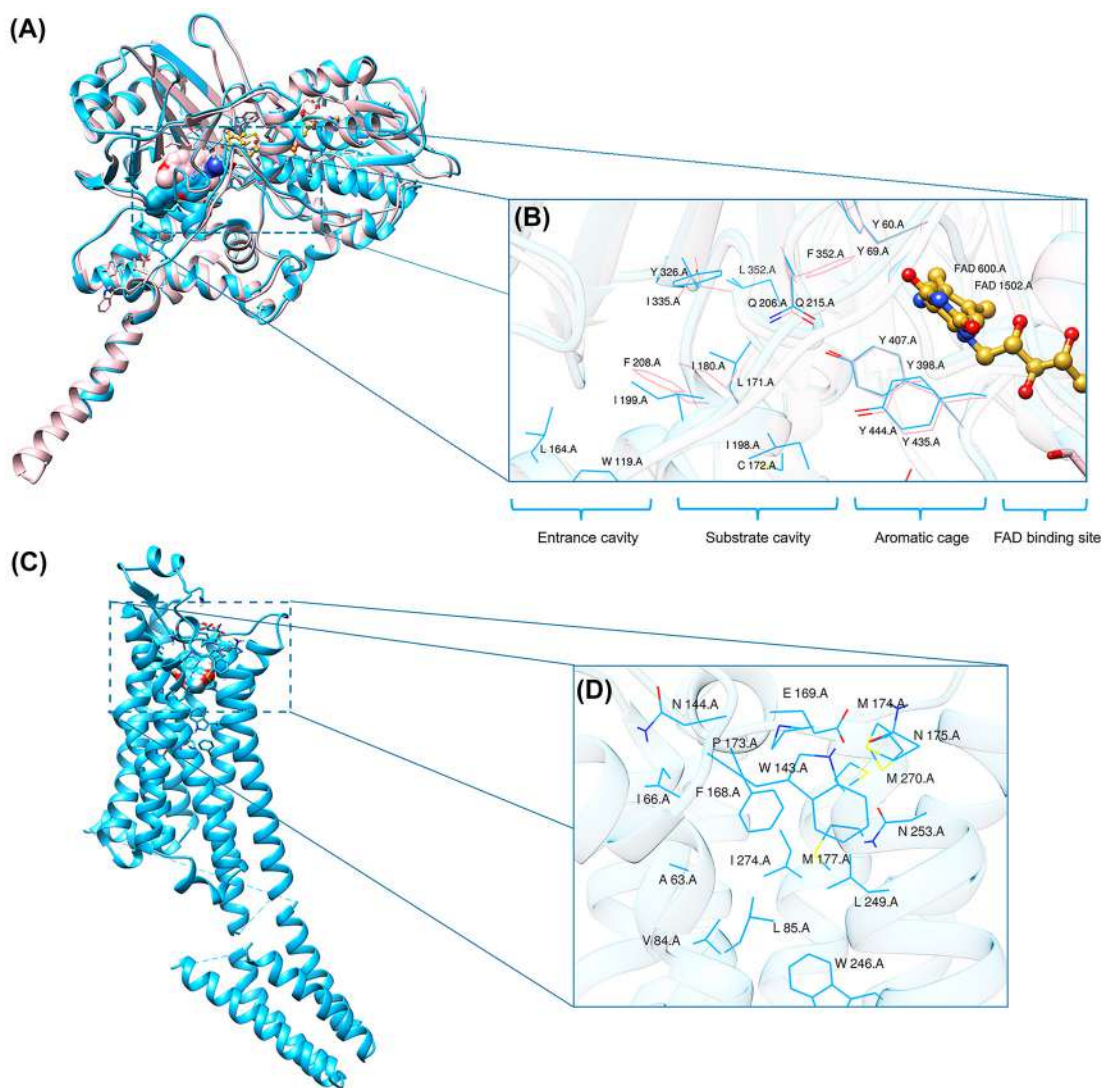


Figure 2: (A) Superposition of crystal structures of MAO-A (pink color) and MAO-B (deep sky-blue color). (B) Superposition of active site residues of MAO-A (pink color) and MAO-B (deep sky-blue color), FAD (goldenrod color) is shown in ball & stick representation. (C) Crystal structure of AA_{2A}R in complex with caffeine. (D) Active site residues of AA_{2A}R.

of C-8 substituted caffeinyl analogues and it was found that the compound bearing a 4-phenylbutadien moiety is the most potent candidate for MAO-B and AA_{2A}R [24]. On the other hand, Azam et al. explored numerous caffeine derivatives from the literature bearing multiple substitutions through molecular docking and structure-activity relationship studies, it was found that the placement of hydrophobic moieties at C8 is essential for both MAO-B inhibition and AA_{2A}R antagonism, whereas replacements occurring at C1 and C3 are optimal for AA_{2A}R but not detrimental for MAO-B [25]. Although research on caffeine is underway for decades, its naturally occurring derivatives are yet to be investigated in detail [26].

NPs and NP-based compounds are an ideal choice for scientists and researchers due to the broad-spectrum activity of NPs with their minimal or no toxic effect on human health [27]. The literature has indicated that caffeine among other NPs is a potent compound that has neuroprotective properties [28]. Considering the link between neurodegeneration and oxidative stress due to the mitochondrial imbalance and the accumulation of reactive oxygen species (ROS), MAO-B was and still is, considered a valid therapeutic target for slowing down the progression of Parkinson's disease.

In the present study, a substructure search was conducted on natural products databases to retrieve caffeine-containing natural products since it is known for its neuroprotective properties and its potency to act as an antagonist of AA_{2A}R, a validated target for PD [29]. Structure-based virtual screening was employed to evaluate the affinity of the selected natural compounds towards MAO-B and AA_{2A}R. ADMET properties were evaluated using *in silico* methods. Finally, molecular dynamics simulations were performed to study the interactions and the stability between the selected compounds and MAO-B over the simulation time.

2 Material and methods

2.1 Data sources

To retrieve all the available natural compounds based on the caffeine scaffold, we used the COCONUT database (<https://coconut.naturalproducts.net/>); the largest open-source natural products (NP) database to date containing more than 400 000 unique NP from over 50 sources [30]. The search was conducted using the Ulmann algorithm for the substructure search with the caffeine scaffold as a pharmacophore [31]. The search results revealed 144 caffeine-containing natural products. These compounds were downloaded in SDF format for further analysis.

2.2 Protein preparation and grid generation

Crystal structure of MAO-B (PDB ID: 2V5Z, resolution = 1.7 Å) in complex with safinamide and crystal structure of AA_{2A}R (PDB ID: 5MZP, resolution = 2.1 Å) in complex with caffeine were retrieved from the RCSB Protein Data Bank (<https://www.rcsb.org/>) [13]. Residues with missing atoms were fixed using the CHARMM-GUI web server [32]. Water molecules were removed since they are not involved in the ligand binding. Since MAO-B is expressed as a dimer, only one chain was kept along with the FAD cofactor for the molecular modeling studies to ease the computational cost [33]. Finally, polar hydrogens and Kollman charges were added using AutoDockTools 1.5.6 [34]. The grid box was placed near the FAD cofactor with a spacing of 1 Å. Grid dimensions were chosen large enough (24 × 24 × 24 Å in x, y, and z directions, respectively) to fit all the residues forming both cavities of the active site in the protein. The grid box was positioned in a way to cover the entire binding site and to allow larger molecules to dock properly: 53 × 155 × 27 Å for MAO-B and -21.6 × 6.1 × 17.5 for AA_{2A}R in x, y, and z directions, respectively. Lastly, the generated coordinates for the grid box were saved in a text file.

2.3 Preparation of ligands

The selected caffeine derivatives were split into multiple files, with each file containing a single ligand. The 3D conformations were generated for all the compounds, geometrical optimization was performed using Merck molecular force field (MMFF94) implemented in the Open Babel chemical toolbox [35]. The minimized ligands were then prepared for the molecular docking study using the prepare_ligand4.py package of AutoDockTools 1.5.6. Partial charges, atomic types, and polar hydrogens were added to all compounds and then converted to PDBQT format.

2.4 Structure-based virtual screening workflow

Structure-based virtual screening was performed using a Perl script for the automated execution of AutoDock Vina 1.1.2 [36]. The proposed methodology is detailed in Figure 3, a text file containing all the names of the prepared ligands was created to serve as a single input file for the docking screens. To facilitate the analysis of the virtual screening results, all the generated output log files were concatenated into a single output text file. All procedures were performed in respect of good practices using state-of-the-art virtual screening approaches for natural products bioprospecting as shown in Figure 4. The standard virtual screening consists mainly of target identification, selection of the chemical library, molecular docking studies, ADMET evaluation, molecular dynamics simulations, and finally experimental validation of the lead compounds [37].

2.5 Visualization and analysis

The ligands were ranked by their binding affinities. The compounds displaying a binding score of -8.0 kcal/mol or less were subject to further analysis. The conformations of the selected compounds were visualized using UCSF Chimera visualization software and superposed to the ligand of reference [38]. Discovery Studio Visualizer program was used to identify hydrogen bonds and other hydrophobic interactions [39].

2.6 *In silico* ADMET prediction

The profiling of compound pharmacokinetics is very essential in drug discovery. As of today, many online tools are available to predict the ADMET profiles of drugs based on their chemical properties [40]. *In silico* ADMET profiling can be useful to speed up the drug development process by limiting the number of compounds for experimental testing. In this study, physicochemical properties and pharmacokinetic parameters were evaluated using SwissADME online calculation toolkit (<http://www.swissadme.ch/>) [41]. Lipinski's rule of five was taken into account to assess the ability of the compounds to be active for orally administrated drugs [42]. Other parameters such as water solubility, gastrointestinal absorption, and blood-brain barrier permeability were predicted. Pain-assay interference compounds (PAINS) are chemical molecules that often give false-positive results in high-throughput

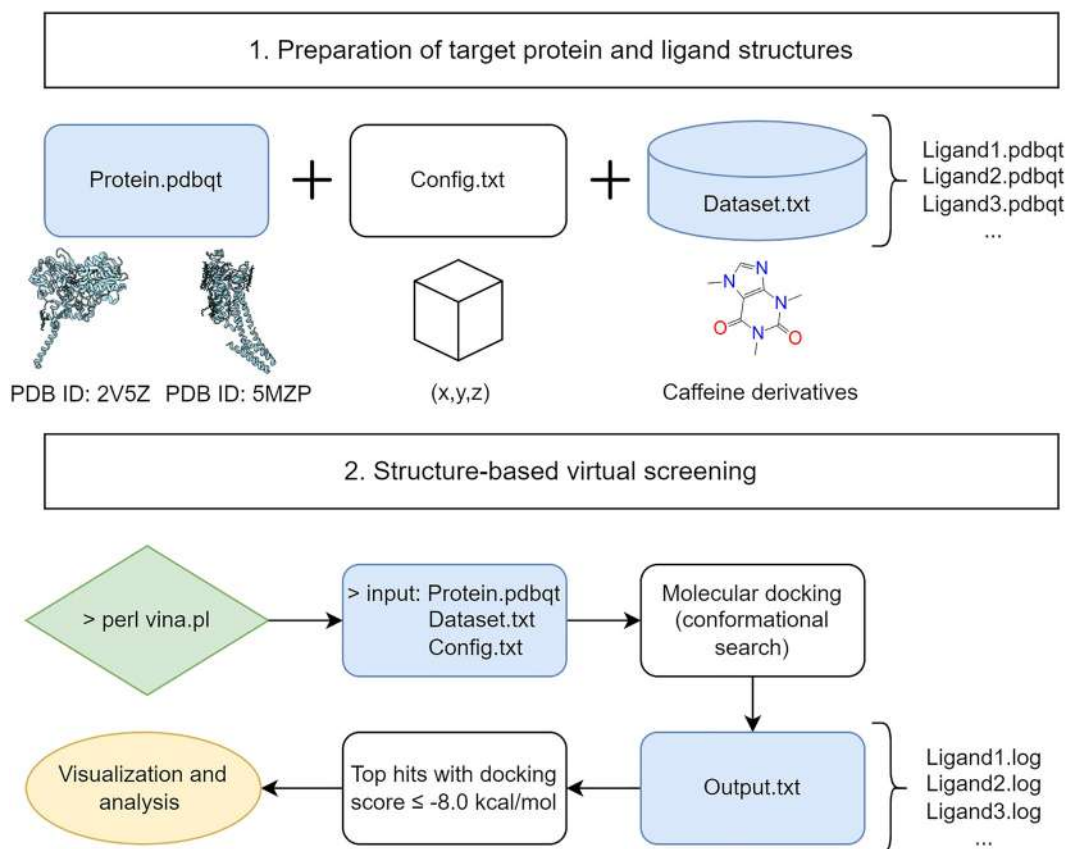


Figure 3: Proposed workflow for structure-based virtual screening using AutoDock Vina.

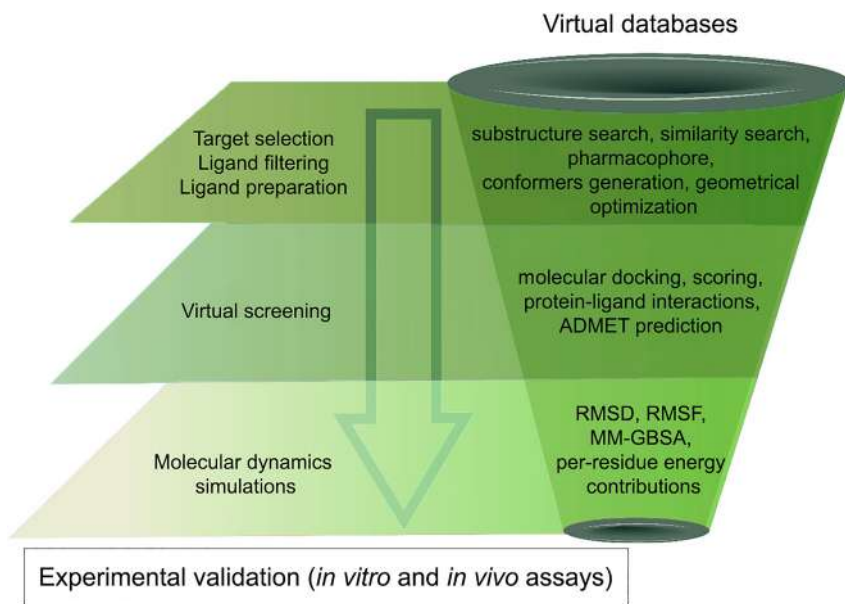


Figure 4: State-of-the-art virtual screening methodology to select and study natural products.

screens due to the presence of several disruptive functional groups that interact nonspecifically with various biological targets rather than selectively affecting the therapeutic target of interest [43]. Hepatotoxicity was predicted using the ProTox-II web server (https://tox-new.charite.de/prototx_II/) [44].

2.7 Molecular dynamics simulations

AMBER16 software [45] was employed to conduct molecular dynamics simulations on the most potent compounds in complex with MAO-B. AMBER force field 14SB [46] and the general AMBER force field (GAFF2) [47] were used to parametrize the protein and the identified inhibitors, respectively. The TIP3P water model with a margin of 15.0 Å (1.5 nm) in each direction from the solute was used to construct a water-solvated cubic box. The specifics of the used MD simulations are elucidated in Ref. [48–55]. In synopsis, energy minimization was initially used on the investigated inhibitors in complex with MAO-B for 5000 steps using the combined steepest and conjugate gradient algorithms. Thereafter, the minimized systems were progressively heated from 0 k to 300 k over 50 ps. The complexes were equilibrated to a free simulation for 1000 ps. Ultimately, a production run for 100 ns was subsequently carried out utilizing an NPT ensemble at 300 K with 1.0 atm pressure. All the periodic boundary PME (Particle Mesh Ewald) simulations were conducted using the “pmemd.cuda” implementation in AMBER for GPU-accelerated simulations on the CompChem hybrid GPU/CPU cluster.

2.8 MM-GBSA binding energy

The molecular mechanics-generalized Born surface area (MM-GBSA) approach was applied to estimate the binding free energies ($\Delta G_{\text{binding}}$) of the investigated inhibitors in complex with MAO-B [56]. Thus, the total binding free energies were evaluated according to IGB value of 2. For each system, the binding free energy calculations were executed for 10,000 snapshots recorded throughout 100 ns MD simulations. For each snapshot, the MM-GBSA ($\Delta G_{\text{binding}}$) binding energy was calculated by the standard formula:

$$\Delta G_{\text{binding}} = G_{\text{complex}} - (G_{\text{inhibitor}} + G_{\text{MAO-B}})$$

3 Results

Developing efficient therapies against neurodegenerative diseases such as Parkinson’s disease remains a great challenge. The use of natural products has been known for a long time to offer great promise and they’re often a safer alternative compared to synthesized drugs. Currently, *in silico* studies are providing much-needed preliminary data about potential drugs, which can be a great help in conducting additional *in vitro* and *in vivo* studies [57].

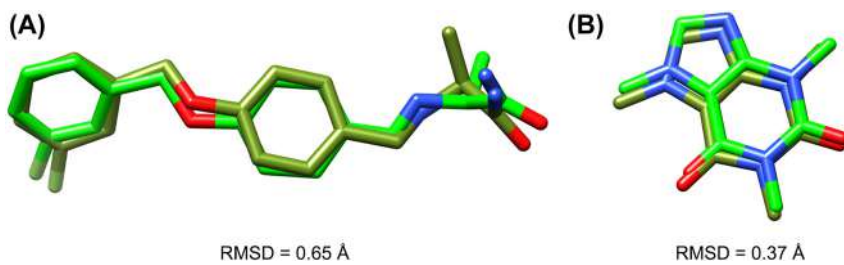


Figure 5: (A) Superposition and RMSD of crystal (green) and docked (olive green) structure of safinamide. (B) Superposition and RMSD of crystal (green) and docked (olive green) structure of caffeine.

3.1 Validation of molecular docking accuracy

Molecular docking protocol was first validated by cross-docking the co-crystallized ligands using the same parameters that were applied for the studied compounds against different crystallographic structures (PDB ID: 2V61 for MAO-B and PDB ID: 5IU4 for AA_{2A}R) [13, 58]. Computed root-mean-square deviation (RMSD) was calculated by mean of superposition; the obtained values are below 2 Å which indicates a good quality of the docking program (Figure 5).

Additionally, molecular docking accuracy was further validated using two datasets of 10 caffeine derivatives with reported half-maximal inhibitory concentrations (IC₅₀) for MAO-B and dissociation constants (Ki) for AA_{2A}R respectively [24, 59]. A good correlation was established between the docking results and the experimental values for MAO-B and AA_{2A}R, which confirms the reliability of the molecular docking approach to study the natural product-like caffeine derivatives with MAO-B. The correlation charts, correlation coefficients, and slopes are shown in Figure 6.

3.2 Natural product-like caffeine derivatives screening

In the present study, we screened 144 natural product-like caffeine derivatives against MAO-B using structure-based virtual screening. The compounds were ranked by their binding affinities (kcal/mol). The highest-ranking molecules displaying a docking score of -8.0 kcal/mol or less were further analyzed based on their interactions with the MAO-B active site cavity. Molecular docking results and protein-ligand interactions are shown in Table 1.

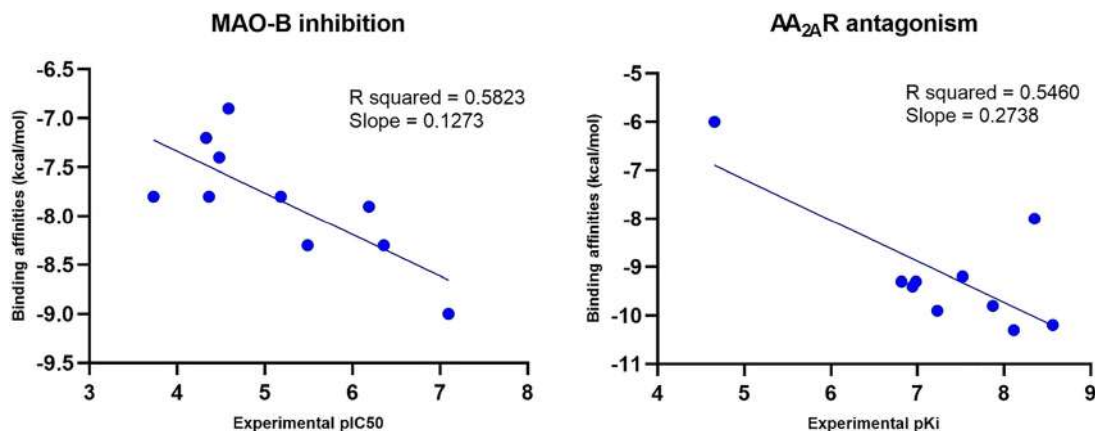


Figure 6: Correlation chart between molecular docking results and experimental pIC50 for MAO-B (left) and experimental pKi for AA_{2A}R (right).

Table 1: Docking results and protein-ligand interactions between the highest-scoring compounds and MAO-B.

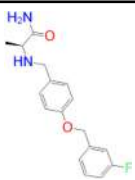
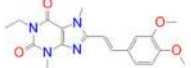
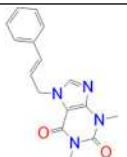
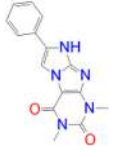
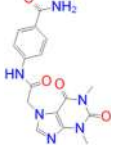
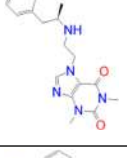
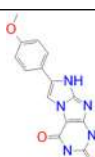
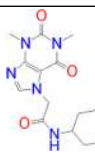
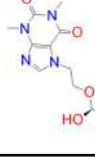
Compound	Chemical structure	Docking score (kcal/mol)	H bonds	Hydrophobic interactions
Safinamide		-9.9	GLN-206	TRP-119, TYR-60, LEU-164, LEU-171, TYR-326, PHE-168, GLN-206, TYR-398, TYR-435
Istradefylline		-9.3	FAD-1502	TYR-60, PRO-102, TYR-326, MET-341, LEU-328, GLN-206, ILE-199, TYR-398, TYR-435
CNP0202316		-10.1	CYS-172	TYR-60, LEU-328, TYR-326, PHE-343, TYR-398, ILE-316, LEU-171, ILE-198, ILE-199, CYS-172, PHE-168
CNP0298322		-9.8	ILE-199, TYR-435	PHE-168, ILE-164, ILE-316, ILE-198, CYS-172, TYR-398, TYR-60, PHE-343, LEU-328
CNP0369093		-9.8	CYS-172	ILE-199, LEU-171, ILE-199, ILE-316, TYR-326, FAD-1502, TYR-60, PHE-343
CNP0365210		-9.7	TYR-435	ILE-198, CYS-172, LEU-171, ILE-316, ILE-199, TYR-326, PHE-343, LEU-328, TYR-398
CNP0366822		-9.7	CYS-172	TYR-60, TYR-398, TYR-435, PHE-343, LEU-171, TYR-326, ILE-199, ILE-316, ILE-198
CNP0352436		-9.6	TYR-326	TYR-60, LEU-171, ILE-316, TYR-398, TYR-435, CYS-172, ILE-199
CNP0349562		-9.5	TYR-435, FAD-1502	ILE-199, ILE-316, LEU-171, PHE-168, TYR-326, LEU-328, PHE-343, TYR-60

Table 1: (continued).

Compound	Chemical structure	Docking score (kcal/mol)	H bonds	Hydrophobic interactions
CNP0006822		-9.4	CYS-172, TYR-435, PRO-102, FAD-1502	TYR-60, PHE-343, LEU-328, LEU-171, ILE-199, TYR-398, GLN-206
CNP0074857		-9.2	GLN-206, LEU-171	TRP-119, LEU-167, TYR-398, TYR-326, ILE-199, ILE-316, PHE-168
CNP0390050		-9.1	GLN-206, TYR-435, LEU-171	TRP-119, ILE-199, ILE-316, CYS-172, PHE-343, TYR-60, TYR-398, PHE-168
CNP0089299		-9.0	GLN-206, TYR-435, FAD-1502	TYR-60, TYR-326, ILE-316, LEU-164, TRP-119, LEU-328, PHE-343, LEU-171, TYR-398
CNP0370968		-9.0	GLN-206, TYR-435, FAD-1502	PHE-343, TYR-60, TYR-326, ILE-316, LEU-164, LEU-328, LEU-171, CYS-172
CNP0338201		-8.9	ILE-198, TYR-435, FAD-1502	ILE-199, TYR-326, TYR-398, LEU-328, ILE-316, LEU-164, TYR-60, PHE-343, LEU-171
CNP0074614		-8.8	LEU-164, TYR-326, TYR-435, FAD-1502	ILE-198, TYR-398, LEU-171, TYR-60, PHE-343, LEU-328, CYS-172, ILE-199, ILE-316, LEU-167
CNP0212890		-8.7	ILE-199, FAD-1502	TYR-60, TYR-435, PHE-343, LEU-171, TYR-398, CYS-172, ILE-198
CNP0010096		-8.4	CYS-172	ILE-316, LEU-171, TYR-326, ILE-199, PHE-168, TYR-398, TYR-326, LEU-167

Table 1: (continued).

Compound	Chemical structure	Docking score (kcal/mol)	H bonds	Hydrophobic interactions
CNP0276217		-8.3	—	LEU-167, TYR-326, LEU-164, ILE-316, PRO-102, ILE-199, LEU-171, CYS-172, PHE-343, TYR-398
CNP0370378		-8.2	—	TRP-119, ILE-316, TYR-326, TYR-398, TYR-435, LEU-171, ILE-199, FAD-1502
CNP0224039		-8.2	TYR-435, FAD-1502	LEU-171, TYR-326, TYR-60, LEU-326, PHE-168
CNP0383986		-8.0	CYS-172	TYR-60, LEU-328, PHE-343, TYR-435, ILE-316

3.3 *In silico* ADMET prediction results

In silico pharmacokinetics, toxicity, and drug-likeness prediction results are shown in Table 2. All compounds were predicted as either soluble or highly soluble. Furthermore, most of the molecules are showing high gastro-intestinal absorption which indicates a good oral bioavailability. However, the blood-brain barrier permeability parameter revealed only two compounds besides safinamide that may readily cross the blood-brain barrier and act on the central nervous system. Moreover, all compounds, excluding safinamide, were identified as non-inhibitors of CYP2D6, which is particularly necessary for drugs acting on the brain since the expression of CYP2D6 is higher in the brain and is involved in metabolizing endogenous neural compounds that suggest its neuroprotective effects [60]. Moreover, the inhibition of CYP enzymes can decrease drug efficacy leading to therapeutic failure or increased drug side effects and toxicity [61–63]. Organ toxicity predicted using the ProTox-II webserver revealed that all the compounds are safe for the liver and do not disrupt its normal function. Physicochemical properties profiling of the selected compounds revealed that all the compounds are drug-like according to Lipinski's rule of five. Finally, Pain-assay interference compounds (PAINS) alerts calculations indicated that all the compounds do not contain any disruptive functional groups except CNP0074614 displaying one PAINS alert due to the catecholamine group.

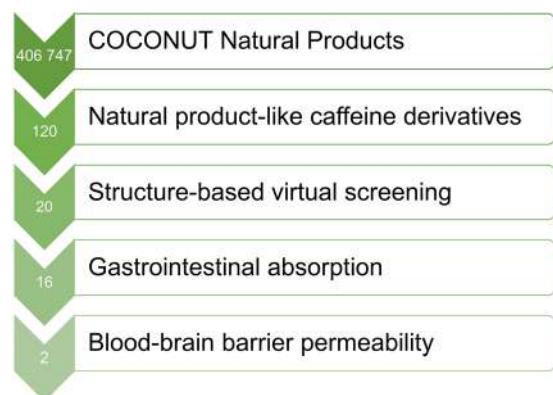
3.4 Interaction analysis of lead compounds with MAO-B and AA_{2A}R

According to the molecular docking and ADMET-based screening as summarized in Figure 7, two compounds were identified as potential drug candidates that possess the desired pharmacokinetics properties for drugs acting on the central nervous system: CNP0202316 and CNP0365210 superposed to the reference inhibitor, safinamide in complex with MAO-B are illustrated in Figure 8. The binding scores of these molecules were -10.1 and -9.7 kcal/mol for MAO-B respectively and are comparable to the reference inhibitor, safinamide

Table 2: Pharmacokinetics, toxicity prediction and drug likeness of the selected compounds.

Compound	Water solubility	GI absorption	BBB	CYP2D6 inhibitor	Hepatotoxicity	Lipinski violation	PAINS alert
Safinamide	-3.04	High	Yes	Yes	Inactive	0	0
Istradefylline	-3.83	High	No	No	Inactive	0	0
CNP0202316	-3.28	High	Yes	No	Inactive	0	0
CNP0298322	-3.67	High	No	No	Inactive	0	0
CNP0369093	-3.31	High	No	No	Inactive	0	0
CNP0365210	-3.28	High	Yes	No	Inactive	0	0
CNP0366822	-2.75	Low	No	No	Inactive	0	0
CNP0352436	-4.46	High	No	No	Inactive	0	0
CNP0349562	-2.75	Low	No	No	Inactive	0	0
CNP0006822	-3.72	High	No	No	Inactive	0	0
CNP0074857	-3.52	High	No	No	Inactive	0	0
CNP0390050	-4.07	High	No	No	Inactive	0	0
CNP0089299	-2.90	High	No	No	Inactive	0	0
CNP0370968	-3.20	High	No	No	Inactive	0	0
CNP0338201	-1.98	High	No	No	Inactive	0	0
CNP0074614	-2.33	Low	No	No	Inactive	0	1
CNP0212890	-3.67	High	No	No	Inactive	0	0
CNP0010096	-0.80	Low	No	No	Inactive	0	0
CNP0276217	-3.32	High	No	No	Inactive	0	0
CNP0370378	-3.79	High	No	No	Inactive	0	0
CNP0224039	-2.30	High	No	No	Inactive	0	0
CNP0383986	-2.15	High	No	No	Inactive	0	0

Water solubility, insoluble < -10 < poorly < -6 < moderately < -4 < soluble < -2 < very < 0 < highly; **GI absorption**, gastrointestinal absorption; **BBB**, blood-brain barrier permeability; **CYP2D6 inhibitor**, Likeliness of a drug to act as inhibitor of cytochrome P450 CYP2D6; **Hepatotoxicity**, prediction of drug-induced liver injury; **Lipinski violation**, number of violations to the rule of five ($\log P_{o/w} \leq 5$; MW ≤ 500 g/mol; HBA ≤ 10 ; HBD ≤ 5 ; RB ≤ 10); **PAINS alert**, number of disruptive functional groups shared by many PAINS (Pan-assay interference compounds).

**Figure 7:** Step-wise structure and ADMET-based screening of the selected natural product-like caffeine derivatives.

which displayed a binding score of -9.9 kcal/mol. However, molecular docking of istradefylline revealed a low binding affinity (-9.3 kcal/mol) compared to the aforementioned compounds.

Safinamide was found to interact through hydrogen bonding with GLN-206 which is known to be a hydrogen bond acceptor for the majority of MAO-B inhibitors and is by the literature [13]. Structural analysis shows that both compounds share a phenyl ring linked to the caffeine scaffold with a pentane group. The phenyl ring seems to be favorable for the stability of the ligands within the MAO-B active site by establishing numerous hydrophobic interactions with the nearby residues of the entrance cavity. Meanwhile, the caffeine

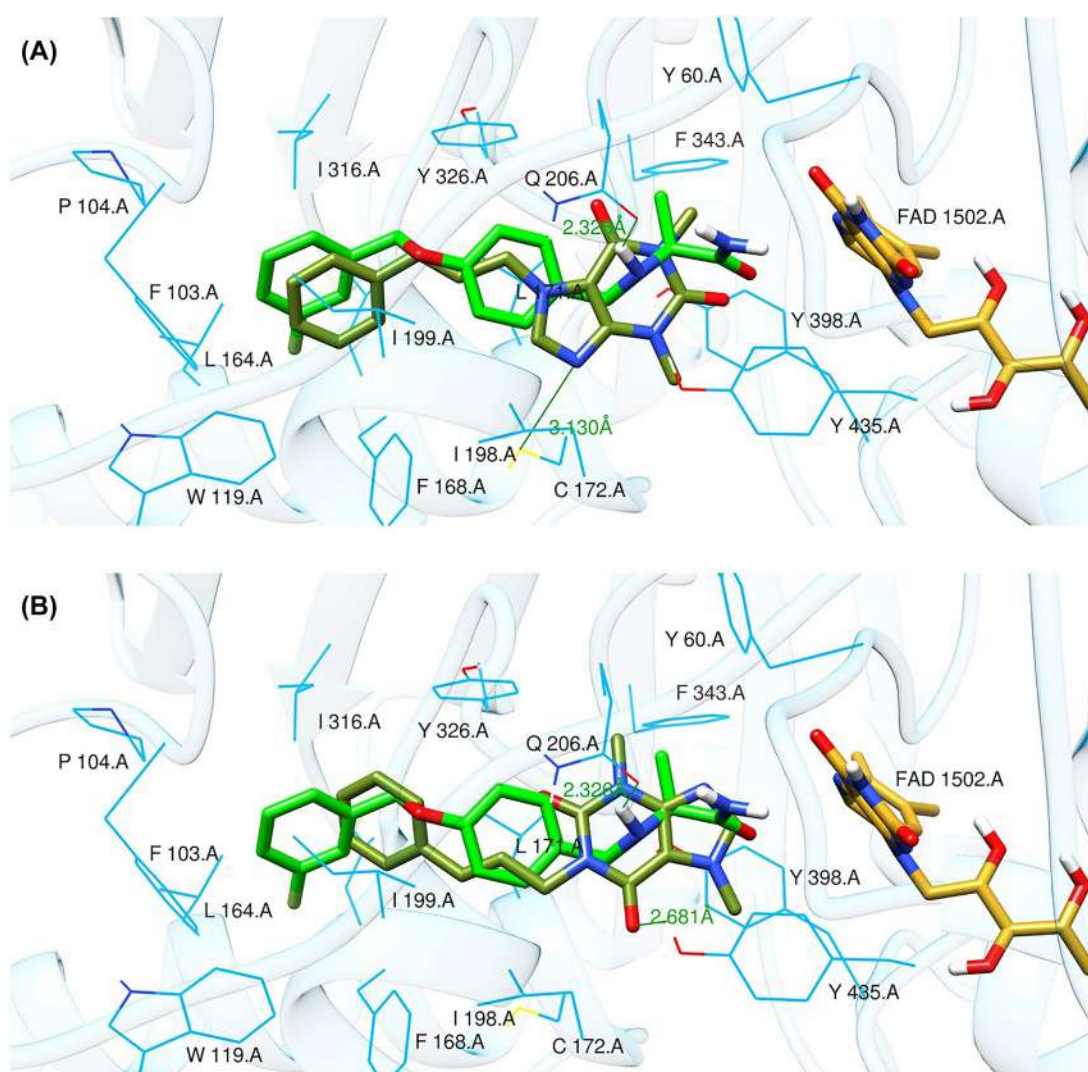


Figure 8: Binding poses of selected lead compounds: CNP0202316 (A) and CNP0365210 (B) (shown in olive green color) with MAO-B and superposed to safinamide (shown in green color).

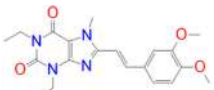
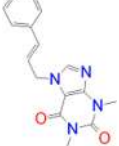
scaffold is directed towards the FAD cofactor and interacts with CYS-172 in CNP0202316 and TYR-435 of the aromatic cage in CNP0365210 through hydrogen bonding.

It has been shown in previous studies that hydrophobic interactions through the phenyl ring are vital for establishing MAO-B binding and are more favorable than all other interactions such as hydrogen or halogen bonds [64]. However, CNP0202316 where the phenyl ring is placed at C7 of the xanthine core seems to be more stable than the second compound implying that the presence of hydrophilic interaction with CYS-172 contributes more to the anchoring and the stability of this compound in the active site cavity of MAO-B.

Alternatively, the selected compounds were analyzed through molecular docking studies with AA_{2A}R to assess their binding affinities with the AA_{2A}R active site and compare their binding conformations to istradefylline. Molecular docking results and protein-ligand interactions are shown in Table 3.

The binding poses of the selected compounds and istradefylline were superposed to the co-crystallized structure of caffeine (Figure 9). The structural analysis indicates that both compounds were able to interact with a key polar residue, ASN-253 through the formation of hydrophilic hydrogen bonds, similarly to istradefylline and other potent AA_{2A}R antagonists [65]. A large network of hydrophobic interactions was also

Table 3: Molecular docking results and protein-ligand interactions of selected lead compounds with AA_{2A}R.

Compound	Chemical structure	Docking score (kcal/mol)	H bonds	Hydrophobic interactions
Istradefylline		-8.0	ASN-253	ALA-81, PHE-168, GLU-169, MET-174, LEU-249, TYR-271
CNP0202316		-8.7	ASN-253	LEU-85, ILE-66, LEU-167, PHE-168, GLU-169, TRP-246, LEU-249, ILE-274, LEU-267, TYR-271
CNP0365210		-8.0	ASN-253	LEU-85, ILE-66, PHE-168, GLU-169, TRP-246, LEU-267, TYR-271

observed, where key residues namely PHE-168 and GLU-169 were found to make a consistent appearance. Since all compounds share the same core that characterizes the caffeine molecule, this would entail a somewhat similar disposition inside the binding pocket. This holds especially for CNP0202316 where the xanthine core was found to be positioned similarly to istradefylline. Moreover, the propylbenzene moiety at position C7 in CNP0202316 might be more favorable to the hydrophobic pocket of the receptor suggesting its affinity potential which may be on par or better than istradefylline.

3.5 Molecular dynamics simulations and binding energy calculations

Molecular dynamics (MD) simulations were applied to probe the stability of the selected ligand-protein complexes, structural specifics, conformational flexibilities, and realize reliable inhibitor-enzyme binding affinities [66, 67]. The most promising compounds in complex with the MAO-B enzyme were further inspected via MD throughout 100 ns simulation time. According to the gathered inhibitor-enzyme snapshots over the production run of 100 ns, the MM-GBSA approach was used to calculate the binding free energies ($\Delta G_{\text{binding}}$) and are illustrated in Figure 10. From the data in Figure 10, it is apparent that the CNP0202316 and CNP0365210 demonstrated auspicious binding affinities with values of -36.7 and -34.5 kcal/mol, respectively, and are comparable to the reference inhibitor, safinamide ($\Delta G_{\text{binding}} = -37.9$ kcal/mol). The comparison of safinamide with CNP0202316 and CNP0365210 unveiled competing for binding affinities proposing the *in silico* prospectivity of the two molecules as MAO-B inhibitors.

The calculated MM-GBSA binding energies were then decomposed into separate components to recognize the vigor in the binding of MAO-B with CNP0202316, CNP0365210, and safinamide (Figure 10). The van der Waals (ΔE_{vdw}) energy was a considerable contributor to CNP0202316, CNP0365210, and safinamide-MAO-B binding affinities with average values of -50.9, -46.8, and -47.3 kcal/mol, respectively. ΔE_{ele} was effectual with average values of -5.2, -11.1, and -25.3 kcal/mol for the CNP0202316, CNP0365210, and safinamide-MAO-B binding affinities, respectively.

The binding energies of CNP0202316, CNP0365210, and safinamide in complex with MAO-B were further decomposed at the per-residue level, and the amino acid residues with free energy contribution <-0.50 kcal/mol were depicted (Figure 11). LEU-171, GLN-206, and TYR-326 in the MAO-B complex appropriately share with CNP0202316, CNP0365210, and safinamide. There was significant participation by LEU-171 to the

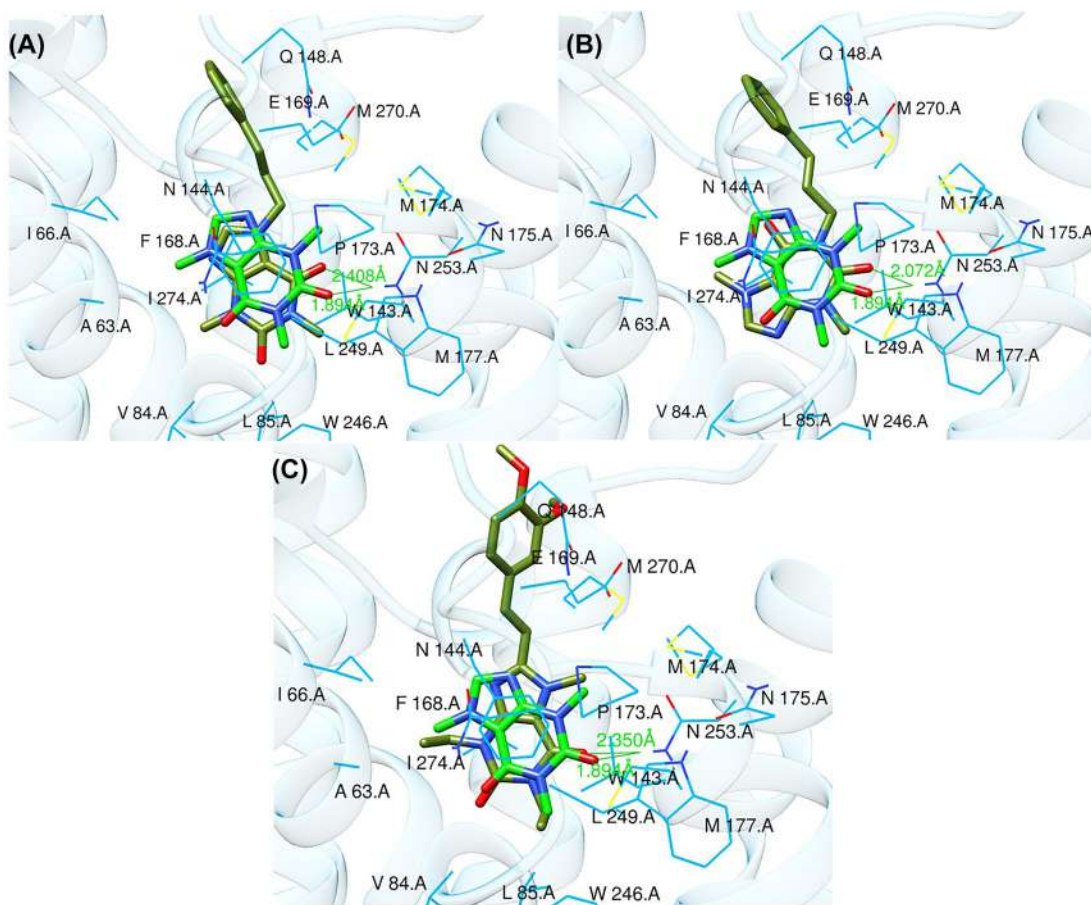


Figure 9: Binding poses of CNP0202316 (A), CNP0365210 (B), and istradefylline (C) (shown in olive green color) with AA₂AR and superposed to the crystal structure of caffeine (shown in green color).

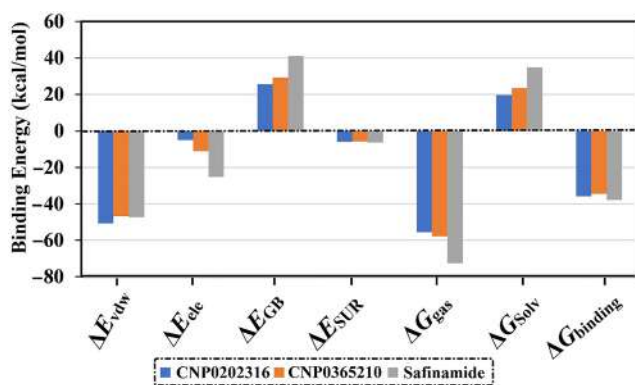


Figure 10: Decomposition of MM-GBSA binding energies for the investigated inhibitors in complex with MAO-B throughout 100 ns MD simulations.

total binding free energy with values of -2.0, -3.0, and -2.2 kcal/mol for CNP0202316-, CNP0365210- and safinamide-MAO-B complexes, respectively.

3.6 Post-MD simulations analysis

Molecular docking calculations, and MD simulations combined with MM-GBSA binding energy calculations, unveiled the most potent molecules as potential MAO-B inhibitors. The MD-based analysis could be required

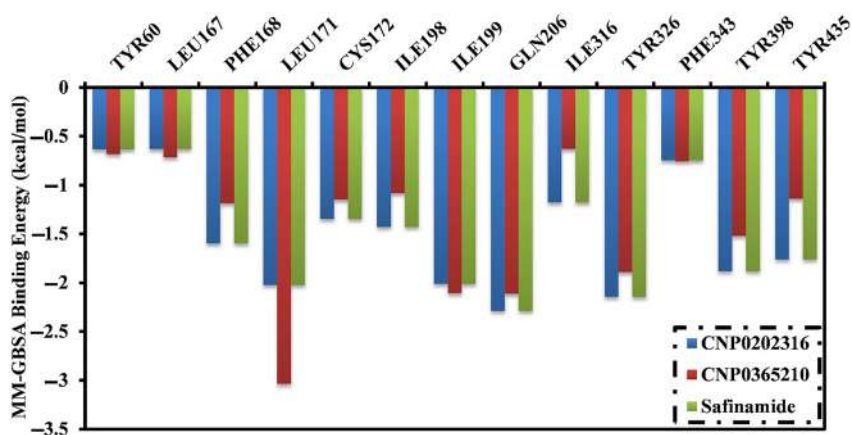


Figure 11: Energy contributions (kcal/mol) for MAO-B amino acid residues to the binding free energy of CNP0202316, CNP0365210, and safinamide.

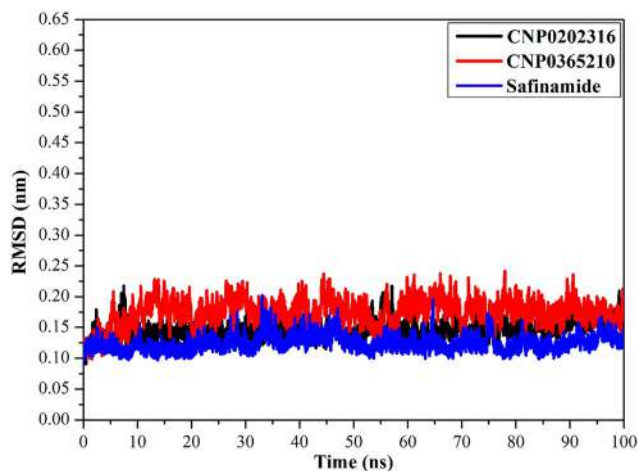


Figure 12: Root-mean-square deviation (RMSD) of the backbone atoms from the starting structure of CNP0202316 (in black), CNP0365210 (in red), and safinamide (in blue) with MAO-B during the 100 ns MD simulations.

to demonstrate structural and energetic stabilities for the scrutinized inhibitors in complex with MAO-B. The structural and energetical analysis included root-mean-square deviation (RMSD), Center-of-Mass (CoM) distance, and binding energy per-frame.

3.6.1 Root-mean-square deviation (RMSD)

The root-mean-square deviation (RMSD) values of the backbone atoms within the whole complex throughout the simulation time were estimated to monitor the structural stability of the CNP0202316, CNP0365210, and safinamide in complex with MAO-B. The RMSD of the backbone atoms as a function of time following the initial structure of the three investigated systems is displayed in Figure 12. The platform in RMSD curves emphasizes that all three inspected systems attain an equilibrium within 1000–10,000 ps throughout MD simulations, exposing that the three investigated systems are converged over the simulation window. These findings suggest that all the compounds are tightly bound and not influenced by the topology of the protein. This is especially true for CNP0202316, which displayed very slight deviations somewhat similar to safinamide suggesting its high stability compared to CNP0365210.

3.6.2 Center-of-mass distance

To get a more in-depth insight into the stability of the selected compounds throughout the MD simulation time, center-of-mass (CoM) distances were evaluated (Figure 13). The most interesting aspect of this graph is

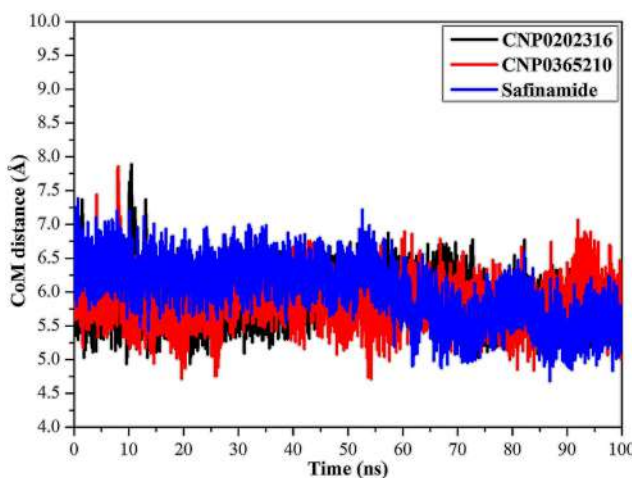


Figure 13: Center-of-mass (CoM) distances (in Å) between CNP0202316 (in black), CNP0365210 (in red), and safinamide (in blue) and TYR324 of MAO-B throughout a 100 ns MD simulation.

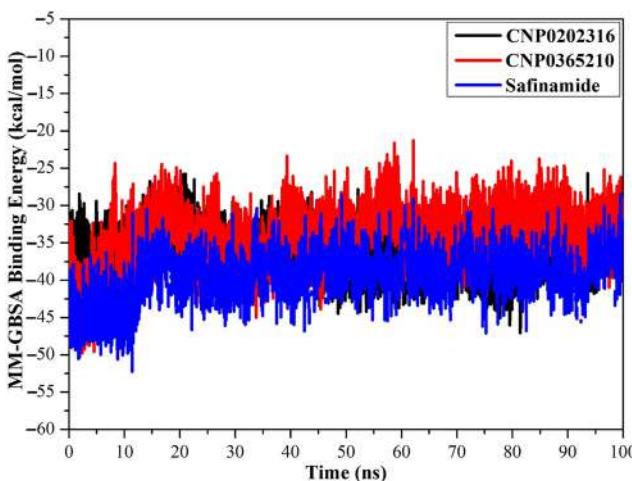


Figure 14: Estimated MM-GBSA binding energy per frame for CNP0202316 (in black), CNP0365210 (in red), and safinamide (in blue) with MAO-B over a 100 ns MD simulation.

that CoM distances were consistent for the CNP0202316- and CNP0365210 in complex with MAO-B compared to safinamide-MAO-B complex, with average values of 5.7, 5.8, and 6.1 Å, respectively. The most obvious finding to emerge from this analysis is that CNP0202316 and CNP0365210 bound more tightly to the MAO-B complex than the reference inhibitor, safinamide.

3.6.3 Binding energy per frame

The comprehensive structural stability of CNP0202316, CNP0365210, and safinamide complexed with MAO-B was evaluated throughout a 100 ns MD simulation via inspecting the correlation between the binding energy per frame and time (Figure 14). Overall stabilities for CNP0202316, CNP0365210, and safinamide were noticed with average binding energies ($\Delta G_{\text{binding}}$) of -36.6 , -34.5 , and -37.9 kcal/mol, respectively. Based on this analysis, all investigated complexes preserved their stability over the 100 ns MD simulations.

4 Discussion

The results obtained from the molecular docking study with MAO-B were further analyzed through molecular dynamics simulations and binding free energy calculations. MM-GBSA binding energies further confirmed that van der Waals (ΔE_{vdw}) energy is a considerable contributor to the stability of MAO-B inhibitors. This

finding confirms that hydrophobic interactions outweigh any other interactions in terms of MAO-B inhibition, and is also supported by the literature [65]. Post-MD simulations analysis confirmed the stability of the three compounds and revealed that all the complexes achieve equilibrium within 1–10 ns throughout the simulation time. These results suggest that the proposed natural products may be on par or better than the inhibitor of reference, safinamide regarding MAO-B inhibition. The key residues involved in MAO-B inhibition were found to be LEU-171, ILE-199, TYR-326, and GLN-206, these residues contribute the most to the stability of the inhibitors when bound to MAO-B. LEU-171, ILE-199, and TYR-326 are specific residues to MAO-B isoform, they are located in the entrance cavity and play a role in substrate and inhibitor specificity [68, 69]. Meanwhile, GLN-206 is recognized as a hydrogen bond acceptor for most MAO-B inhibitors and is responsible for their stability in the substrate cavity [17]. Moreover, the identified compounds may confer neuroprotective properties linked to the xanthine core as reported in the literature [70]. For MAO-B, the orientation of the phenyl ring linked to the xanthine core was found to be similar to safinamide especially in CNP0202316, and is favorable to the entrance hydrophobic cavity. On the other hand, this molecule adopted a similar conformation to istradefylline when bound to AA_{2A}R. The propylbenzene moiety attached to the imidazole of the caffeine in CNP0202316 at position C7 is more favorable to the hydrophobic pocket of AA_{2A}R, whereas the oxygen atom of the xanthine core maintained a hydrogen bond with ASN-253 that is deemed crucial to the binding of most AA_{2A}R antagonists [71]. Thus, the identified compounds might offer a dual-target activity in the context of a polypharmacological approach and might represent a more efficient alternative for treating and slowing down the neuronal damage in Parkinson's disease patients.

5 Conclusions

The present study aimed to find novel natural product-like caffeine derivatives as potential dual MAO-B inhibitors/AA_{2A}R antagonists. Structure-based virtual screening and ADMET analysis revealed two natural products that fulfill the requirements for drugs acting on the brain. The selected compounds in complex with MAO-B were subject to molecular dynamics simulations to assess their stability over the simulation time along with the inhibitor of reference, safinamide. Our findings show that the presence of the phenyl ring in the selected compounds is crucial for the ligands to fill the long-shaped cavity of the MAO-B active site and is a major contributor to various van der Waals interactions responsible for the stability and the tight-binding of these compounds to MAO-B. Similarly, the propylbenzene moiety was found to be more favorable for the hydrophobic pocket of AA_{2A}R especially when linked at position C7 of the xanthine core which allowed the caffeine core to adopt a similar conformation to istradefylline suggesting the dual-target properties of the identified natural products. In conclusion, the structure-based virtual screening helped provide valuable insight on the studied natural product-like caffeine derivatives and our findings may attract more focus for the development of novel antiparkinsonian drugs with dual-targeting properties. However, *in vitro* experiments such as bioactivity assays for MAO-B and AA_{2A}R, membrane permeability and cell viability assays remains necessary to further validate these findings.

Acknowledgments: We would like to thank Prof. Phillip E. Barnes, University of South Carolina, Columbia, for proofreading the manuscript, and Prof. Francisco Javier Luque Garriga, University of Barcelona, Spain, for his constructive criticism. Their contribution is sincerely appreciated and gratefully acknowledged.

Author contribution: All the authors have accepted responsibility for the entire content of this submitted manuscript and approved submission.

Research funding: The computational work was completed with resources supported by the Science and Technology Development Fund, STDF, Egypt, Grants No. 5480 & 7972 (Granted to Dr. Mahmoud A. A. Ibrahim).

Conflict of interest statement: The authors declare that they have no conflict of interest.

Ethical Approval: This article does not contain any studies with animals performed by any of the authors.

References

1. Barnham KJ, Masters CL, Bush AI. Neurodegenerative diseases and oxidative stress. *Nat Rev Drug Discov* 2004;3:205–14.
2. Moya-Alvarado G, Gershoni-Emek N, Perlson E, Bronfman FC. Neurodegeneration and Alzheimer's disease (AD). What can proteomics tell us about the Alzheimer's brain? *Mol Cell Proteomics* 2016;15:409–25.
3. Noda S, Sato S, Fukuda T, Tada N, Uchiyama Y, Tanaka K, et al. Loss of Parkin contributes to mitochondrial turnover and dopaminergic neuronal loss in aged mice. *Neurobiol Dis* 2020;136:104717.
4. Davie CA. A review of Parkinson's disease. *Br Med Bull* 2008;86:109–27.
5. Youdim MB, Edmondson D, Tipton KF. The therapeutic potential of monoamine oxidase inhibitors. *Nat Rev Neurosci* 2006;7:295–309.
6. Hickey P, Stacy M. Adenosine A2A antagonists in Parkinson's disease: what's next? *Curr Neurol Neurosci Rep* 2012;12:376–85.
7. Shih JC, Chen K, Ridd MJ. Monoamine oxidase: from genes to behavior. *Annu Rev Neurosci* 1999;22:197–217.
8. Culpepper L. Reducing the burden of difficult-to-treat major depressive disorder: revisiting monoamine oxidase inhibitor therapy. *Prim Care Companion CNS Disord* 2013;15:27220.
9. Tetrud JW, Koller WC. A novel formulation of selegiline for the treatment of Parkinson's disease. *Neurology* 2004;63(7 Suppl 2):S2–6.
10. Finberg JP, Rabey JM. Inhibitors of MAO-A and MAO-B in psychiatry and neurology. *Front Pharmacol* 2016;7:340.
11. Mallajosyula JK, Kaur D, Chinta SJ, Rajagopalan S, Rane A, Nicholls DG, et al. MAO-B elevation in mouse brain astrocytes results in Parkinson's pathology. *PLoS One* 2008;3:e1616.
12. Youdim MB, Gross A, Finberg JP. Rasagiline [N-propargyl-1R (+)-aminoindan], a selective and potent inhibitor of mitochondrial monoamine oxidase B. *Br J Pharmacol* 2001;132:500–6.
13. Binda C, Wang J, Pisani L, Caccia C, Carotti A, Salvati P, et al. Structures of human monoamine oxidase B complexes with selective noncovalent inhibitors: safinamide and coumarin analogs. *J Med Chem* 2007;50:5848–52.
14. Dungo R, Deeks ED. Istradefylline: first global approval. *Drugs* 2013;73:875–82.
15. Chen JF, Cunha RA. The belated US FDA approval of the adenosine A2A receptor antagonist istradefylline for treatment of Parkinson's disease. *Purinergic Signal* 2020;16:167–74.
16. Preti D, Baraldi PG, Moorman AR, Borea PA, Varani K. History and perspectives of A2A adenosine receptor antagonists as potential therapeutic agents. *Med Res Rev* 2015;35:790–848.
17. Binda C, Li M, Hubálek F, Restelli N, Edmondson DE, Mattevi A. Insights into the mode of inhibition of human mitochondrial monoamine oxidase B from high-resolution crystal structures. *Proc Natl Acad Sci USA* 2003;100:9750–5.
18. Mostert S, Petzer A, Petzer JP. Indianones as high-potency reversible inhibitors of monoamine oxidase. *ChemMedChem* 2015;10:862–73.
19. Edmondson DE, Binda C, Mattevi A. Structural insights into the mechanism of amine oxidation by monoamine oxidases A and B. *Arch Biochem Biophys* 2007;464:269–76.
20. Binda C, Newton-Vinson P, Hubálek F, Edmondson DE, Mattevi A. Structure of human monoamine oxidase B, a drug target for the treatment of neurological disorders. *Nat Struct Biol* 2002;9:22–6.
21. Carradori S, D'Ascenzo M, Chimenti P, Secci D, Bolasco A. Selective MAO-B inhibitors: a lesson from natural products. *Mol Divers* 2014;18:219–43.
22. Khanam S, Subitsha AJ, Sabu S. Plants as a promising source for the treatment of parkinson disease: a systemic review. *IP Int J Compr Adv Pharmacol* 2021;5:158–66.
23. Pitsillou E, Liang J, Karagiannis C, Ververis K, Darmawan KK, Ng K, et al. Interaction of small molecules with the SARS-CoV-2 main protease in silico and in vitro validation of potential lead compounds using an enzyme-linked immunosorbent assay. *Comput Biol Chem* 2020;89:107408.
24. Pretorius J, Malan SF, Castagnoli N Jr, Bergh JJ, Petzer JP. Dual inhibition of monoamine oxidase B and antagonism of the adenosine A2A receptor by (E, E)-8-(4-phenylbutadien-1-yl) caffeine analogues. *Bioorg Med Chem* 2008;16:8676–84.
25. Azam F, Madi AM, Ali HI. Molecular docking and prediction of pharmacokinetic properties of dual mechanism drugs that block MAO-B and adenosine A2A receptors for the treatment of Parkinson's disease. *J Young Pharm* 2012;4:184–92.
26. Petzer A, Pierna A, Petzer JP. The interactions of caffeine with monoamine oxidase. *Life Sci* 2013;93:283–7.
27. Mathur R, Velpandian T. Medicinal plant-based health products: where is the medicinal constituent? *Indian J Pharmacol* 2009;41:205.
28. Essa MM, Braidy N, Bridge W, Subash S, Manivasagam T, Vijayan RK, et al. Review of natural products on Parkinson's disease pathology. *J Aging Res Clin Pract* 2014;3:1–8.
29. Fisone G, Borgkvist A, Usiello A. Caffeine as a psychomotor stimulant: mechanism of action. *Cell Mol Life Sci CMLS* 2004;61:857–72.
30. Sorokina M, Merseburger P, Rajan K, Yirik MA, Steinbeck C. COCONUT online: collection of open natural products database. *J Cheminf* 2021;13:1–3.

31. Agrafiotis DK, Lobanov VS, Shemanarev M, Rassokhin DN, Izrailev S, Jaeger EP, et al. Efficient substructure searching of large chemical libraries: the ABCD chemical cartridge. *J Chem Inf Model* 2011;51:3113–30.
32. Jo S, Kim T, Iyer VG, Im W. CHARMM-GUI: a web-based graphical user interface for CHARMM. *J Comput Chem* 2008;29:1859–65.
33. Boulaamane Y, Ahmad I, Patel H, Das N, Britel MR, Maurady A. Structural exploration of selected C6 and C7-substituted coumarin isomers as selective MAO-B inhibitors. *J Biomol Struct Dyn* 2022;24:1–5.
34. Morris GM, Huey R, Lindstrom W, Sanner MF, Belew RK, Goodsell DS, et al. AutoDock4 and AutoDockTools4: automated docking with selective receptor flexibility. *J Comput Chem* 2009;30:2785–91.
35. O’Boyle NM, Banck M, James CA, Morley C, Vandermeersch T, Hutchison GR. Open Babel: an open chemical toolbox. *J Cheminf* 2011;3:1–4.
36. Trott O, Olson AJ. AutoDock Vina: improving the speed and accuracy of docking with a new scoring function, efficient optimization, and multithreading. *J Comput Chem* 2010;31:455–61.
37. Santana K, do Nascimento LD, Lima e Lima A, Damasceno V, Nahum C, Braga RC, et al. Applications of virtual screening in bioprospecting: facts, shifts, and perspectives to explore the chemo-structural diversity of natural products. *Front Chem* 2021;9:155.
38. Pettersen EF, Goddard TD, Huang CC, Couch GS, Greenblatt DM, Meng EC, et al. UCSF Chimera—a visualization system for exploratory research and analysis. *J Comput Chem* 2004;25:1605–12.
39. Bovia DS. Discovery studio visualizer. San Diego, CA, USA: Dassault Systèmes; 2017:936 p.
40. Kar S, Leszczynski J. Open access in silico tools to predict the ADMET profiling of drug candidates. *Expert Opin Drug Discov* 2020;15:1473–87.
41. Daina A, Michielin O, Zoete V. SwissADME: a free web tool to evaluate pharmacokinetics, drug-likeness and medicinal chemistry friendliness of small molecules. *Sci Rep* 2017;7:1–3.
42. Lipinski CA. Lead-and drug-like compounds: the rule-of-five revolution. *Drug Discov Today Technol* 2004;1:337–41.
43. Baell JB. Feeling nature’s PAINS: natural products, natural product drugs, and pan assay interference compounds (PAINS). *J Nat Prod* 2016;79:616–28.
44. Banerjee P, Eckert AO, Schrey AK, Preissner R. ProTox-II: a webserver for the prediction of toxicity of chemicals. *Nucleic Acids Res* 2018;46:W257–63.
45. Case DA, Betz RM, Cerutti DS, Cheatham T, Darden T, Duke RE, et al. Amber 16, University of California, San Francisco. San Francisco: University of California; 2016.
46. Maier JA, Martinez C, Kasavajhala K, Wickstrom L, Hauser KE, Simmerling C. ff14SB: improving the accuracy of protein side chain and backbone parameters from ff99SB. *J Chem Theor Comput* 2015;11:3696–713.
47. Wang J, Wolf RM, Caldwell JW, Kollman PA, Case DA. Development and testing of a general amber force field. *J Comput Chem* 2004;25:1157–74.
48. Ibrahim MA, Abdelrahman AH, Hassan AM. Identification of novel *Plasmodium falciparum* PI4KB inhibitors as potential anti-malarial drugs: homology modeling, molecular docking and molecular dynamics simulations. *Comput Biol Chem* 2019;80:79–89.
49. Ibrahim MA, Abdeljawad KA, Abdelrahman AH, Hegazy ME. Natural-like products as potential SARS-CoV-2 Mpro inhibitors: in-silico drug discovery. *J Biomol Struct Dyn* 2020;39:5722–34.
50. Ibrahim MA, Abdelrahman AH, Hegazy ME. In-silico drug repurposing and molecular dynamics puzzled out potential SARS-CoV-2 main protease inhibitors. *J Biomol Struct Dyn* 2021;39:5756–67.
51. Ibrahim MA, Abdelrahman AH, Hussien TA, Badr EA, Mohamed TA, El-Seedi HR, et al. In silico drug discovery of major metabolites from spices as SARS-CoV-2 main protease inhibitors. *Comput Biol Med* 2020;126:104046.
52. Ibrahim MA, Abdelrahman AH, Allemailem KS, Almatroudi A, Moustafa MF, Hegazy ME. In silico evaluation of prospective anti-COVID-19 drug candidates as potential SARS-CoV-2 main protease inhibitors. *Protein J* 2021;40:296–309.
53. Ibrahim MA, Abdelrahman AH, Mohamed TA, Atia MA, Al-Hammady MA, Abdeljawad KA, et al. In silico mining of terpenes from red-sea invertebrates for SARS-CoV-2 main protease (Mpro) inhibitors. *Molecules* 2021;26:2082.
54. Ibrahim MA, Badr EA, Abdelrahman AH, Almansour NM, Shawky AM, Mekhemer GA, et al. Prospective drug candidates as human multidrug transporter ABCG2 inhibitors: an in silico drug discovery study. *Cell Biochem Biophys* 2021;79:189–200.
55. Ibrahim MA, Mohamed EA, Abdelrahman AH, Allemailem KS, Moustafa MF, Shawky AM, et al. Rutin and flavone analogs as prospective SARS-CoV-2 main protease inhibitors: in silico drug discovery study. *J Mol Graph Model* 2021;105:107904.
56. Massova I, Kollman PA. Combined molecular mechanical and continuum solvent approach (MM-PBSA/GBSA) to predict ligand binding. *Perspect Drug Discov Des* 2000;18:113–35.
57. Singh R, Gautam A, Chandel S, Ghosh A, Dey D, Roy S, et al. Protease inhibitory effect of natural polyphenolic compounds on SARS-CoV-2: an in silico study. *Molecules* 2020;25:4604.
58. Segala E, Guo D, Cheng RK, Bortolato A, Deflorian F, Dore AS, et al. Controlling the dissociation of ligands from the adenosine A2A receptor through modulation of salt bridge strength. *J Med Chem* 2016;59:6470–9.

59. Petzer A, Grobler P, Bergh JJ, Petzer JP. Inhibition of monoamine oxidase by selected phenylalkylcaffeine analogues. *J Pharm Pharmacol* 2014;66:677–87.
60. Da Prada M, Zürcher G, Wüthrich I, Haefely WE. On tyramine, food, beverages and the reversible MAO inhibitor moclobemide. *J Neural Transm Suppl* 1988;26:31–56.
61. Guengerich FP. Cytochrome p450 and chemical toxicology. *Chem Res Toxicol* 2008;21:70–83.
62. Lin JH, Lu AY. Inhibition and induction of cytochrome P450 and the clinical implications. *Clin Pharmacokinet* 1998;35:361–90.
63. Pelkonen O, Turpeinen M, Hakkola J, Honkakoski P, Hukkanen J, Raunio H. Inhibition and induction of human cytochrome P450 enzymes: current status. *Arch Toxicol* 2008;82:667–715.
64. Rauhamäki S, Postila PA, Niinivehmas S, Kortet S, Schildt E, Pasanen M, et al. Structure-activity relationship analysis of 3-phenylcoumarin-based monoamine oxidase B inhibitors. *Front Chem* 2018;6:41.
65. de Lera Ruiz M, Lim YH, Zheng J. Adenosine A2A receptor as a drug discovery target. *J Med Chem* 2014;57:3623–50.
66. De Vivo M, Masetti M, Bottegoni G, Cavalli A. Role of molecular dynamics and related methods in drug discovery. *J Med Chem* 2016;59:4035–61.
67. Kerrigan JE. Molecular dynamics simulations in drug design. In: Kortagere S, editors. *In silico models for drug discovery*. Totowa, NJ: Humana Press; 2013; vol. 993: 95–113 pp.
68. Geha RM, Rebrin I, Chen K, Shih JC. Substrate and inhibitor specificities for human monoamine oxidase A and B are influenced by a single amino acid. *J Biol Chem* 2001;276:9877–82.
69. Milczek EM, Binda C, Rovida S, Mattevi A, Edmondson DE. The ‘gating’ residues Ile199 and Tyr326 in human monoamine oxidase B function in substrate and inhibitor recognition. *FEBS J* 2011;278:4860–9.
70. Kasabova-Angelova A, Tzankova D, Mitkov J, Georgieva M, Tzankova V, Zlatkov A, et al. Xanthine derivatives as agents affecting non-dopaminergic neuroprotection in Parkinson’s disease. *Curr Med Chem* 2020;27:2021–36.
71. Jaakola VP, Lane JR, Lin JY, Katritch V, IJzerman AP, Stevens RC. Ligand binding and subtype selectivity of the human A2A adenosine receptor: identification and characterization of essential amino acid residues. *J Biol Chem* 2010;285:13032–44.